

# **Geotechnical, Geological, and Seismological (GG&S) Evaluations for the Bellefonte Site, North Alabama**

PREPARED FOR  
**Tennessee Valley Authority**

MARCH 2006

PREPARED BY

**CH2MHILL**

AND

 **Geomatrix**

**VOLUME I OF II**



# **Geotechnical, Geological, and Seismological (GG&S) Evaluations for the Bellefonte Site, North Alabama**

PREPARED FOR  
**Tennessee Valley Authority**

MARCH 2006

PREPARED BY

**CH2MHILL**

AND



**VOLUME II OF II**

#### DISCLAIMER

This report was prepared as an account of work sponsored by an agency of the United States Government. Neither the United States Government nor any agency thereof, nor any of their employees, make any warranty, express or implied, or assumes any legal liability or responsibility for the accuracy, completeness, or usefulness of any information, apparatus, product, or process disclosed, or represents that its use would not infringe privately owned rights. Reference herein to any specific commercial product, process, or service by trade name, trademark, manufacturer, or otherwise does not necessarily constitute or imply its endorsement, recommendation, or favoring by the United States Government or any agency thereof. The views and opinions of authors expressed herein do not necessarily state or reflect those of the United States Government or any agency thereof.

# Contents

---

Section	Page
<b>Acronyms and Abbreviations</b> .....	<b>xi</b>
<b>1. Introductory Information</b> .....	<b>1-1</b>
1.0 Introduction.....	1-1
1.1 Purpose and Scope .....	1-1
1.2 Regulatory Guidance .....	1-2
1.3 Background .....	1-2
1.3.1 Existing Facilities and TVA Plans .....	1-3
1.3.2 Available Information.....	1-4
1.4 Geotechnical, Geological, and Seismological Program Description.....	1-5
1.5 Report Organization.....	1-6
1.6 Section 1 References .....	1-7
<b>2. 5 Geology, Seismology, and Geotechnical Engineering</b> .....	<b>2.5.1-1</b>
2.5 Geology, Seismology, and Geotechnical Engineering.....	2.5.1-1
2.5.1 Basic Geologic and Seismic Information .....	2.5.1-1
2.5.1.1 Regional Geology .....	2.5.1-2
2.5.1.2 Site Geology.....	2.5.1-29
2.5.2 Vibratory Ground Motion .....	2.5.2-1
Existing Guidance in Regulatory Guide 1.165.....	2.5.2-1
Regulatory Basis for the Performance-Based Approach.....	2.5.2-2
2.5.2.1 Seismicity .....	2.5.2-3
2.5.2.2 Geologic Structures and Seismic Source Models .....	2.5.2-12
2.5.2.3 Correlation of Earthquake Activity with Seismic Sources.....	2.5.2-15
2.5.2.4 Probabilistic Seismic Hazard Analysis and Controlling Earthquakes .....	2.5.2-15
2.5.2.5 Seismic Wave Transmission Characteristics of the Site .....	2.5.2-45
2.5.2.6 Safe Shutdown Earthquake Ground Motions.....	2.5.2-45
2.5.3 Surface Faulting .....	2.5.3-1
2.5.3.1 Geological, Seismological, and Geophysical Investigations.....	2.5.3-1
2.5.3.2 Geological Evidence, or Absence of Evidence, for Surface Deformation.....	2.5.3-3

<b>Section</b>	<b>Page</b>
2.5.3.3	Correlation of Earthquakes with Capable Tectonic Sources .....2.5.3-7
2.5.3.4	Ages of Most Recent Deformation .....2.5.3-7
2.5.3.5	Relationship of Tectonic Structures in the Site Area to Regional Tectonic Structures .....2.5.3-7
2.5.3.6	Characterization of Capable Tectonic Structures .....2.5.3-7
2.5.3.7	Designation of Zones of Quaternary Deformation in Site Region.....2.5.3-8
2.5.3.8	Potential for Surface Tectonic Deformation at the Site.....2.5.3-9
2.5.4	Stability of Subsurface Materials and Foundations .....2.5.4-1
2.5.4.1	Geologic Features.....2.5.4-1
2.5.4.2	Properties of Subsurface Materials.....2.5.4-4
2.5.4.3	Bellefonte Site Explorations.....2.5.4-6
2.5.4.4	Geophysical Surveys .....2.5.4-11
2.5.4.5	Excavation and Backfill.....2.5.4-17
2.5.4.6	Groundwater .....2.5.4-19
2.5.4.7	Response of Soil and Rock to Dynamic Loading .....2.5.4-20
2.5.4.8	Liquefaction Potential .....2.5.4-20
2.5.4.9	Earthquake Design Basis .....2.5.4-23
2.5.4.10	Static Stability .....2.5.4-23
2.5.4.11	Design Criteria .....2.5.4-25
2.5.4.12	Techniques to Improve Subsurface Conditions .....2.5.4-26
2.5.4.13	Subsurface Instrumentation .....2.5.4-27
2.5.4.14	Construction Notes.....2.5.4-27
2.5.5	Stability of Slopes .....2.5.5-1
2.5.5.1	Compaction Specifications .....2.5.5-1
2.5.6	Embankments and Dams .....2.5.6-1
2.5.7	Section 2 References .....2.5.7-1

## Appendixes

A	Borehole and Rock Core Logs, Piezometer Construction Logs, Photographs, Water Level Data
B	CPT Report
C	Technos Reports
	C.1 Technos Final Report – March 18, 2005
	C.2 Technos Final Report – August 19, 2005
D	GeoVision Report
E	Surveying Report
F	Laboratory Data Report
G	Photographs
H	Slug Testing Memorandum
I	Catalog Listing

## Tables

- 2.5.1-1. Summary of New Information for New Madrid Seismic Zone
- 2.5.1-2. Magnitude Comparisons for New Madrid 1811-1812 Earthquake Sequence
- 2.5.1-3. Characteristic Magnitudes from Rupture Areas for Fault Segments in the NMSZ
- 2.5.1-4. Summary of Age Constraints for New Madrid Seismic Zone Earthquakes
- 2.5.1-5. Timing and Source of Liquefaction Events in the Southern Atlantic Coastal Plain
- 2.5.1-6. Estimated Magnitudes and Peak Ground Accelerations of Prehistoric Earthquake Episodes in South Carolina Coastal Plain
  
- 2.5.2-1. Earthquake Catalogs for the Central and Southeastern U.S. Used in Development of TVA Dam Safety Earthquake Catalog
- 2.5.2-2. New Seismicity Data for the Central and Southeastern U.S. Used in Development of Bellefonte GG&S Earthquake Catalog
- 2.5.2-3a. Bechtel Seismic Sources
- 2.5.2-3b. Dames and Moore Seismic Sources
- 2.5.2-3c. Law Engineering Seismic Sources
- 2.5.2-3d. Roundout Associates Seismic Sources
- 2.5.2-3e. Weston Geophysical Seismic Sources
- 2.5.2-3f. Woodward-Clyde Consultants Seismic Sources
- 2.5.2-4. Description of the Minimum Set Zones for the LLNL-TIP Study
- 2.5.2-5. Earthquake Counts for Region within 200 Miles of the Bellefonte Site
- 2.5.2-6. Verification of Repeatability of EPRI- (1989) PSHA results
- 2.5.2-7. Source Contributions to Mean Hazard in EPRI-SOG Seismic Hazard Model
- 2.5.2-8. Magnitude Distributions for Repeating Large Magnitude New Madrid Earthquakes
- 2.5.2-9. Earthquake Frequencies for Repeating Large Magnitude Earthquakes
- 2.5.2-10. Magnitude Comparisons for 1886 Charleston Earthquake in Charleston Region
- 2.5.2-11. Recurrence Scenarios for Charleston Repeating Large Magnitude Earthquakes
- 2.5.2-12. Controlling Earthquakes
- 2.5.2-13. Mean Seismic CDF for Plants Performing Seismic PRA
- 2.5.2-14. Computation of SSE Spectra
- 2.5.2-15. SEE Spectra (5 percent damping) for the Bellefonte Site
  
- 2.5.4-1. Summary of Rock Unconfined Compression Strength Test Results
- 2.5.4-2. Summary of Soil Test Results
- 2.5.4-3. Summary of Borehole Observations
- 2.5.4-4. Summary of Cavities Observed in GG&S Rock Cores
- 2.5.4-5. Summary of CPT Sounding Observations
- 2.5.4-6. CPT Soil Shear Wave Velocity Results
- 2.5.4-7. Piezometer Construction Data
- 2.5.4-8. Groundwater Elevation Measurements
- 2.5.4-9. Summary of Bedrock S-wave and P-wave Velocity from Field Tests – Bellefonte and BLNP Sites
- 2.5.4-10. Results of Hydraulic Conductivity from Slug Tests at GG&S Site Piezometers

## Figures

- 1-1 Vicinity Map of the Bellefonte Site
- 1-2 Site Map Showing the GG&S Evaluation Location
  
- 2.5.1-1 Regional Physiographic Map (200-Mile Radius) (Source: <http://water.usgs.gov/GIS/dsdl/physio.e00.gz>; base map ESRI, 2004)
- 2.5.1-2 Deformation-thermal Events Affecting the U.S. Appalachians and Possibly Related Plate Tectonic Processes (From Hatcher, 1989a)
- 2.5.1-3 Tectonic Evolution of the Southern and Central Appalachian Orogen (From Hatcher, 1989b)
- 2.5.1-4 Paleogeographic Reconstructions of Phases in the Tectonic Evolution of the Appalachian-Ouachita Orogen (From Thomas, 1989a)
- 2.5.1-5 Regional Geologic Map (200-mile radius) (Source: Schruben et al., 2005; <http://pubs.usgs.gov/dds/dds11>; base map ESRI, 2004)
- 2.5.1-6 Stratigraphic Column in the Appalachian Thrust Belt in Alabama (Modified from Thomas, 2001)
- 2.5.1-7 Geologic Map of Northeastern Alabama (Source: modified from Osborne et al., 1988; <http://www.gsa.state.al.us/gsa/GIS/geologydetails.html>) (Note: see Figure 2.5.1-8 for explanation of geologic map units and symbols)
- 2.5.1-8 Explanation of Geologic Map Units and Symbols (Source: Osborne et al., 1988; <http://www.gsa.state.al.us/gsa/GIS/geologydetails.html>)
- 2.5.1-9 Regional Tectonic Map (200-mile radius) (From Figure 2.5-4, TVA, 1986)
- 2.5.1-10 Tectonic Map of the Appalachian-Ouachita Orogen (From Thomas, 1989b)
- 2.5.1-11 Tectonic Map of the Southern Appalachians Showing Locations of Regional Cross-sections A-A' and B-B' (From Hatcher et al., 1989d) (Note: see Figure 2.5.1-12 for cross-sections AA' and BB'')
- 2.5.1-12 Regional Structural Cross-sections A-A' and B-B' (From Hatcher et al., 1989d) (Note: see Figure 2.5.1-11 for legend and location of cross-sections)
- 2.5.1-13 Major Geologic and Tectonic Features and Terrane Boundaries of the Southern Appalachians (From Hatcher et al., 1989b)
- 2.5.1-14 Structural Geology Map of Appalachian Orogen in Alabama and Georgia (From Thomas and Bayona, 2002)
- 2.5.1-15 Geologic Map of the Anniston Transverse Zone in the Appalachian Thrust Belt in Alabama (From Thomas and Bayona, 2002)
- 2.5.1-16 Structural Cross-sections, Appalachian Thrust Belt, Alabama (From Thomas and Bayona, 2002) (Note: Locations of cross-sections are shown in Figure 2.5.1-15)
- 2.5.1-17 Map Showing Tectonic and Geophysical Elements of Central and Eastern North America with Independent Seismicity Catalog (References: Wheeler and Bolinger, 1984; Williams and Hatcher, 1983; King and Zeitz, 1978; Nelson and Zeitz, 1983; Wheeler, 1995; Bollinger and Wheeler, 1988; Marple and Talwani, 1993, 2000); Hildenbrand and Hendricks, 1995; Wheeler, 1997; Langenheim and Hildenbrand, 1997; Braile et al., 1984; Van Schmus et al., 1996)
- 2.5.1-18 Structure Contour Map of the Top of Basement in the Southern Appalachian Orogen (From Hatcher and Lemiszki, 1998)



## Figures (continued)

- 2.5.1-19 Map of Depth to Basement, Subdetachment Basement Faults, and Transverse Zones in the Foreland Thrust Belt, Alabama and Georgia (From Bayona et al., 2003)
- 2.5.1-20 Map of Magnetic Anomalies (top) and Bouger Gravity Anomalies (bottom) With and Without Relocated Earthquakes (1983-1994) (Modified from Vlahovic et al., 1998)
- 2.5.1-21 Cross-section of East Tennessee Seismic Zone (From Vlahovic et al., 1998)
- 2.5.1-22 Map of New Madrid Seismic Zone and Northern Mississippian Embayment Region (From Hildenbrand and Hendricks, 1995)
- 2.5.1-23 Schematic Map of the Reelfoot Scarp and Selected Features in the Area of the New Madrid Seismic Zone (Modified from Crone and Wheeler, 2000; location of Farrenburg lineaments from Baldwin et al., 2002)
- 2.5.1-24 Central Fault System of New Madrid Seismic Zone (From Johnston and Schweig, 1996)
- 2.5.1-25 Map Showing Location of New Madrid Seismic Zone as Illuminated by Seismicity Between 1974 and 1996 (From Hough and Martin, 2002)
- 2.5.1-26 Map of New Madrid Seismic Zone Showing Estimated Ages and Measured Sizes of Liquefaction Features (From Tuttle et al., 2002)
- 2.5.1-27 Earthquake Chronology for NMSZ from Dating and Correlation of Liquefaction Features at Sites Along NE-SW Transect Across Region (From Tuttle et al., 2002)
- 2.5.1-28 Timing and Recurrence Intervals of New Madrid Events (From Tuttle et al., 2002)
- 2.5.1-29 Subsurface Structures Mapped in Paleozoic and Basement Rocks in Northeastern Mississippi Embayment (From Cox et al., 2001b) (Note: Based on Hildenbrand et al., 1982; Johnson et al., 1994)
- 2.5.1-30 Schematic Figure Showing Seismotectonic Elements in the Epicentral Region of the 1886 Earthquake (Talwani, 2000) (References: Marple and Talwani, 2000; Weems and Lewis, 2002)
- 2.5.1-31 Location of the East Coast Fault System (ECFS) (Modified from Marple and Talwani, 2000)
- 2.5.1-32 Distribution of Potential Liquefaction Sites Evaluated Along the Atlantic Coast Plain (Modified from Amick et al., 1990) (References: Marple and Talwani, 2000; Amick et al., 1990)
- 2.5.1-33 Distribution of Paleoliquefaction Sites in South Carolina and North Carolina (Source: Hu et al., 2002b)
- 2.5.1-34 Maps Showing the Distribution of Liquefaction Sites for the 1886 Earthquake and the Distribution of Paleoliquefaction Sites Associated with Paleoearthquake Episodes A to G (From Talwani and Schaefer, 2001)
- 2.5.1-35 Geologic Map of the Site Vicinity (25-Mile Radius) and Site Area (5-Mile Radius) (Source: modified from Osborne et al., 1988; <http://www.gsa.state.al.us/gsa/GIS/geologydetails.html>) (Note: see Figure 2.5.1-8 for explanation of the geologic map units and symbols)
- 2.5.1-36 Geologic Map of the Site (0.6-Mile Radius) and Surrounding Area (Source: Modified from Figure 2.5-7, TVA, 1986)
- 2.5.1-37 Geologic Map of the Footprint and Surrounding Area (Note: Geologic data from Figure 2.5.9 (TVA, 1986))
- 2.5.1-38 Soil Map of the Site Area (Source: Modified from Figure 3.1.3-1, TVA, 1997)
- 2.5.1-39 Photograph of Small-Scale Dissolution Cavity in Chicamauga (Limestone at the Bellefonte Site)

## Figures (continued)

- 2.5.2-1 Independent Earthquake Catalog for Study Region (1758-2005)
- 2.5.2-2 Independent Earthquake Catalog for Study Region Showing EPRI-SOG (1758-1985) and Added Historical Events
- 2.5.2-3 Independent Earthquake Catalog for Study Region Showing EPRI-SOG (1758-1985) and Post-EPRI-SOG (1985-2005) Events
- 2.5.2-4 Bechtel EPRI-SOG Source Map
- 2.5.2-5 Dames and Moore EPRI-SOG Source Map
- 2.5.2-6 Law Engineering EPRI-SOG Source Map
- 2.5.2-7 Roundout Associates EPRI-SOG Source Map
- 2.5.2-8 Weston Geophysical EPRI-SOG Source Map
- 2.5.2-9 Woodward-Clyde Consultants EPRI-SOG Source Map
- 2.5.2-10 LLNL TIP Seismic Source Zones (Savy et al., 2002)
- 2.5.2-11 USGS National Seismic Hazard Mapping Project Source Model (Frankel et al., 2002)
- 2.5.2-12 (a) TVA Dam Safety Seismic Hazard Analysis Seismotectonic Source Zones (Geomatrix, 2004)  
(b) TVA Dam Safety Seismic Hazard Analysis Seismotectonic Source Zones (Geomatrix, 2004)  
(c) TVA Dam Safety Seismic Hazard Analysis Seismotectonic Source Zones (Geomatrix, 2004)  
(d) TVA Dam Safety Seismic Hazard Analysis Seismotectonic Source Zones (Geomatrix, 2004)
- 2.5.2-13 (a) Composite of EPRI-SOG Seismic Sources Representing the East Tennessee Seismic Zone  
(b) Composite of Post EPRI-SOG Seismic Sources Representing the East Tennessee Seismic Zone
- 2.5.2-14 Histogram of the Difference between  $m_b^*$  in the Updated Catalog and  $m_b^*$  Defined in the EPRI-SOG (1988) Catalog for Earthquakes Within 200 Miles of the Bellefonte Site
- 2.5.2-15 Earthquakes in the Updated Catalog ( $m_b^* \geq 3.3$ ) and EPRI-SOG (1988) Completeness Regions Covering the Area within 200 Miles of the Bellefonte Site
- 2.5.2-16 “Stepp” Plots for 200-Mile Radius Region Around the Bellefonte Site
- 2.5.2-17 Earthquake Recurrence Rates Estimated for the “Equivalent Period of Completeness” for the Portions of EPRI-SOG Completeness Regions 3 and 4 within 200 Miles of the Bellefonte ESP Site
- 2.5.2-18 Earthquake Recurrence Rates for New Madrid Seismic Sources
- 2.5.2-19 Maximum Magnitude Distributions for Sources Representing the East Tennessee Seismic Zone. (top) Composite EPRI-SOG Distribution in Terms of  $m_b$ . (bottom) Composite EPRI-SOG Distribution in Terms of  $M$  Compared to More Recent Assessments
- 2.5.2-20 Maximum Magnitude Distributions for Sources Representing the Host/Background Seismic Source for the Bellefonte Site. (top) Composite EPRI-SOG Distribution in Terms of  $m_b$ . (bottom) Composite EPRI-SOG Distribution in Terms of  $M$  Compared to More Recent Assessments
- 2.5.2-21 Maximum Magnitude Distributions for Sources Representing the New Madrid Seismic Zone. (top) Composite EPRI-SOG Distribution in Terms of  $m_b$ . (bottom) Composite EPRI-SOG Distribution in Terms of  $M$  Compared to More Recent Assessments

## Figures (continued)

- 2.5.2-22 Maximum Magnitude Distributions for Sources Representing the Source of the 1886 Charleston Earthquake. (top) Composite EPRI-SOG Distribution in Terms of mb. (bottom) Composite EPRI-SOG Distribution in Terms of  $M$  Compared to More Recent Assessments
- 2.5.2-23 Comparison of the EPRI-SOG (1988) and EPRI (2004) Median Ground Motion Models
- 2.5.2-24 Uncertainty Range for the EPRI (2004) Ground Motion Models Compared to the EPRI-SOG (1988) Median Models
- 2.5.2-25 Comparison of the EPRI-SOG (1988) and EPRI (2004) Models for Aleatory Variability in Ground Motions
- 2.5.2-26 Effect on Hazard of the “Correction” to the 99 Percent Hazard Source List for the Bellefonte Site in the EPRI-SOG (1988) Seismic Hazard Model
- 2.5.2-27 Disaggregation of Hazard from the EPRI-SOG (1988) Seismic Source Model
- 2.5.2-28 Effect of Adding Sources of Repeating Large Magnitude New Madrid and Charleston Earthquakes on the Site Hazard
- 2.5.2-29 Effect of Including Repeating Large Magnitude New Madrid and Charleston Earthquakes with Adjustments for Double-Counting on the Site Hazard
- 2.5.2-30 Effect of Use of the EPRI (2004) Ground Motion Model on Site Hazard
- 2.5.2-31 New Madrid (Inset A) and Charleston (Inset B) Repeating Large Magnitude Earthquake Sources
- 2.5.2-32 Source Characterization Logic Tree for Repeating Large Magnitude New Madrid Earthquakes
- 2.5.2-33 Distributions for Mean Repeat Time for New Madrid Repeating Large Magnitude Earthquakes
- 2.5.2-34 Earthquake Rupture Sequences for Repeating Large Magnitude New Madrid Earthquakes (From Tuttle et al., 2002)
- 2.5.2-35 Source Characterization Logic Tree for Repeating Large Magnitude Charleston Earthquakes
- 2.5.2-36 (a) Distributions for Mean Repeat Time for Charleston Repeating Large Magnitude Earthquakes  
(b) Distributions for Mean Repeat Time for Charleston Repeating Large Magnitude Earthquakes
- 2.5.2-37 Logic Tree for Ground Motion Models
- 2.5.2-38 Mean and Fractile Hazard Curves from Updated PSHA
- 2.5.2-39 Seismic Source Contributions to Mean Hazard
- 2.5.2-40 Uniform Hazard Spectra
- 2.5.2-41 Disaggregation of Mean Hazard
- 2.5.2-42 Development of Smoothed Response Spectrum for Mean 10-4 Ground Motions
- 2.5.2-43 Development of Smoothed Response Spectrum for Mean 10-5 Ground Motions
- 2.5.2-44 SSE Spectra (5 percent damping) for the Bellefonte Site

## Figures (continued)

- 2.5.3.1 1970 Aerial Photograph of the Bellefonte Site Showing Features Used to Define Lineaments
- 2.5.3-2 Interpreted Lineaments at the Bellefonte Site
- 2.5.3-3 Aerial and Field Reconnaissance (Base map: Osborne et al., 1988; <http://www.gsa.state.al.us/gsa/GIS/geologydetails.html>) (Note: see Figure 2.5.1-8 for explanation of units and symbols.)
- 2.5.3-4 Seismicity Relative to Mapped Basement Faults (Modified from Bayona et al., 2003)
  
- 2.5.4-1 (a) Borehole and Piezometer Locations  
(b) CPT Sounding Locations  
(c) Seismic Refraction Survey Line Locations
- 2.5.4-2 (a) Cross-section A-A'  
(b) Cross-section B-B'
- 2.5.4-3 Top of Bedrock Elevations
- 2.5.4-4 Cavity Distribution with Depth - Bellefonte and BLNP Site Boreholes
- 2.5.4-5 (a) P-Wave Velocity Model Profiles - Lines 12000 and 23000  
(b) P-Wave Velocity Model Profile - Line 2001  
(c) P-Wave Velocity Model Profile - Line 25000  
(d) P-Wave Velocity Model Profiles - Lines 9000 and 17001
- 2.5.4-6 (a) Top of L2 Layer - P-Wave Velocity Model  
(b) Top of L3 Layer - P-Wave Velocity Model  
(c) Thickness of L2 Layer - P-Wave Velocity Model
- 2.5.4-7 Bedrock S-Wave Velocity with Depth - Bellefonte and BLNP Site Boreholes
- 2.5.4-8 (a) Microgravity and Seismic Refraction Model Profile - Line 2000  
(b) Microgravity and Seismic Refraction Model Profile - Line 2001  
(c) Microgravity and Seismic Refraction Model Profile - Line 9000  
(d) Microgravity and Seismic Refraction Model Profile - Line 12000  
(e) Microgravity and Seismic Refraction Model Profile - Line 25000
- 2.5.4-9 (a) Potentiometric Surface Map - March 2, 2005  
(b) Potentiometric Surface Map - May 4, 2005  
(c) Potentiometric Surface Map - July 8, 2005  
(d) Potentiometric Surface Map - September 2005
- 2.5.4-10 Graph of Bellefonte Site Groundwater Elevations - 2005

## Acronyms and Abbreviations

AASHTO	American Association of State Highway and Transportation Officials
ABWR	Advanced Boiling Water Reactor
AD	anno domini (after Christ) – used to denote specified calendar date
amsl	above mean seal level
ANSS	Advanced National Seismograph System
ASCE	American Society of Civil Engineers
ASTM	American Society for Testing and Materials
BA	Blytheville arch
BC	before Christ – used to denote specified calendar date
BCFZ	Big Creek fault zone
BFZ	Blytheville fault zone
bgs	below ground surface
BL	Bootheel lineament
BLNP	Bellefonte Nuclear Plant
BP	before present
BRP	Blue Ridge-Piedmont
CAMS	Center for Accelerator Mass Spectrometry
CCFZ	Crittenden County Fault Zone
CERI	Center for Earthquake Research and Information
CEUS	Central and Eastern U.S.
CFR	<i>Code of Federal Regulations</i>
CGL	Commerce geophysical lineament
cm/s	cubic meters per second
COCORP	Consortium for Continental Reflection Profiling
COL	Construction and Operating License
COLA	Construction and Operating License Application
CPT	cone penetrometer testing
CRR	normalized liquefaction resistance ratio
CSR	cyclic shearing stress ratio
DF	design factor
DNAG	Decade of North American Geology

DOE	U.S. Department of Energy
DRS	design response spectrum
ECFS	East Coast fault system
EIS	Environmental Impact Statement
ENA	Eastern North America
ENE	east-northeast
EPRI	Electric Power Research Institute
EPRI-SOG	Electric Power Research Institute-Seismicity Owners Group
ESBWR	Economic Simplified Boiling Water Reactor
ETSZ	Eastern Tennessee Seismic Zone
EWD	elastic weight drop
FA	Felt Area
FEIS	Final Environmental Impact Statement
FOS	factor of safety
fps	feet per second
FSAR	Final Safety Analysis Report
Ga	billion years before present
GCVSZ	Giles County, Virginia, Seismic Zone
GG&S	Geotechnical, Geological, and Seismological
GPS	Global Positioning System
HCLPF	High Confidence of Low Probability of Failure
IPG	Independent Peer Group
ka	thousand years before present
LLNL	Lawrence Livermore National Laboratory
<b>M</b>	<b>Moment magnitude</b>
Ma	million years before present
$m_b$	body-wave magnitude
$m_{bLg}$	Lg-wave magnitude
$M_{max}$	Maximum magnitude
MMI	Modified Mercalli Intensity
MPSSZ	Middleton Place-Summerville seismic zone
MSF	magnitude scaling factor
msl	mean sea level

my	million years
NCEER	National Center for Earthquake Engineering Research
NE	Northeast
NEHRP	National Earthquake Hazard Reduction Program
NEIC	National Earthquake Information Center
NGCC	Natural Gas Combined Cycle
NGCC	natural gas combined cycle
NMSZ	New Madrid seismic zone
NN	New Madrid North fault
NNE	New Madrid North Extension
NS	New Madrid South fault
NW	New Madrid West fault
NY-AL	New York – Alabama
OBE	Operating Basis Earthquake
PDE	Preliminary Determination of Epicenters
PF	performance goals
pga	peak ground acceleration
PI	plasticity index
PRA	probabilistic risk analysis
PSHA	Probabilistic Seismic Hazard Analysis
PVC	polyvinyl chloride
p-wave	compression wave
RF	Reelfoot fault
RG	Regulatory Guide
RQD	rock quality designation
RS	Reelfoot south
SA	spectral acceleration
SAR	Safety Analysis Report
SDB	Seismic Design Basics
SDC	Seismic Design Criteria
SEI	Structural Engineering Institute
SEUSSN	Southeast U.S. Seismic Network
SF	safety factor

SH <sub>max</sub>	maximum horizontal shear
SOG	Seismicity Owners Group
SP	spectral velocity
SPT	standard penetration test
SSC	seismic source characterization
SSE	safe shutdown earthquake
SSHAC	Senior Seismic Hazard Analysis Committee
ST	Shelby tube
S-wave	shear waves
TFI	Technical/Facilitator/Integrator
TIP	Trial Implementation Project
TOC	top of casing
TOR	top of rock
TVA	Tennessee Valley Authority
TZ	Transverse zone
UC	unconsolidated-undrained
UHRS	Uniform Hazard Response Spectrum
UHS	Uniform hazard spectra
USCS	Unified Soil Classification System
USGS	U.S. Geological Survey
USNRC	U.S. Nuclear Regulatory Commission
UU	unconsolidated-undrained
V/H	vertical to horizontal
ybp	years before present
ZIT	zone of intense thinning
ZRA	zone of river anomalies
ZRA-C	zone of river anomalies-central segment
ZRA-N	zone of river anomalies-northern segment
ZRA-S	zone of river anomalies-southern segment



## 1.0 Introduction

This report presents results from *Geotechnical, Geological, and Seismological (GG&S) Evaluations for the Bellefonte Site, North Alabama*. The GG&S evaluation was conducted to assess the suitability of the Tennessee Valley Authority (TVA) Bellefonte Nuclear Plant (BLNP) site for siting of a new nuclear power generating facility. The information presented in this GG&S evaluation may also be used by TVA at a later date to support preparation of a combined (construction and operating) license (COL) application (COLA) to the U.S. Nuclear Regulatory Commission (USNRC). This work was carried out by CH2M HILL in accordance with TVA Agreement Number 42134.

## 1.1 Purpose and Scope

The primary purpose of this report was to determine whether geotechnical, geological, and seismological conditions at the proposed Bellefonte Site are suitable for the future development of a nuclear power generating facility. A site is considered to be “suitable” if it meets the following criteria:

- There are no geologic hazards that could affect the successful construction and operation of the facility. These geologic hazards could include potentially unstable slopes, active faults, or underground cavities.
- The safe shutdown earthquake (SSE) has been established in accordance with current USNRC regulatory requirements and is found to be within acceptable design limits.
- Relevant geotechnical site characteristics, such as static and dynamic soil properties, liquefaction potential, bearing capacity, and shear wave velocity, have been established and are found to be within limits that will result in safe facilities performance during non-seismic and seismic loading.

The following scope of activities was implemented to gather and evaluate GG&S information for the Bellefonte Site:

- Geologic, geotechnical, and seismic literature available in engineering and environmental reports for the Bellefonte Site and in scientific publications for the general region were reviewed. This available information includes the Final Safety Analysis Report (FSAR) that was prepared for the nearly completed facilities at the site.
- Field explorations consisting of soil drilling, rock coring, sampling of soil and rock, cone penetrometer test (CPT) soundings, surface seismic refraction geophysical surveys, a microgravity survey, and shear wave velocity measurements using CPT and in-hole geophysical logging methods were carried out.

- Laboratory tests were conducted to evaluate physical properties of representative soil and rock samples from the site;
- New information related to rock site ground motion models (e.g., the recurrence of New Madrid and Charleston earthquakes) was evaluated and a probabilistic seismic hazard analysis (PSHA) sensitivity analyses was performed. Based on this analysis, it was concluded that the PSHA required updating. Controlling earthquakes were identified in terms of magnitude and source to site distance. Appropriate spectral shapes for the controlling earthquakes and for rock site conditions were developed.
- Seismic studies were conducted to determine the SSE Ground Motion for the site, the potential for surface tectonic and non-tectonic deformations, and other design conditions.
- Engineering assessments of typical foundation design conditions such as bearing capacity, settlement characteristics, and lateral earth pressures were performed.

## 1.2 Regulatory Guidance

The primary licensing and siting processes for nuclear power plants are specified in 10 *Code of Federal Regulations* (CFR) 50, “Domestic Licensing of Production and Utilization Facilities,” and 10 CFR 52, “Early site permits; standard design certifications; and combined licenses for nuclear power plants.”

Within this broad regulatory framework, two regulatory guides have been specifically developed for use in the planning of subsurface investigations for the design and licensing of nuclear power plants:

- *Site Investigations for Foundations of Nuclear Power Plants, Regulatory Guide (RG)-1.132* (USNRC, 2004b).
- *Laboratory Investigations of Soils for Engineering Analysis and Design of Nuclear Power Plants, RG-1.138* (USNRC, 2004a).

The geotechnical investigations for the Bellefonte Site were planned and performed in general accordance with the previous guides as applicable to evaluate site suitability.

Seismic investigations at the Bellefonte Site were based on the requirements of 10 CFR 100.23, “Geologic and Seismic Siting Criteria,” which cites Appendix S of 10 CFR 50, “Earthquake Engineering Criteria for Nuclear Power Plants,” and identifies the principal seismic issues that must be addressed by the site studies. In accordance with these criteria, the GG&S collected seismic information for the Bellefonte Site and then assessed (1) the SSE for the site; (2) the potential for surface tectonic deformation; and (3) the effects of vibratory ground motion on the stability of the site.

## 1.3 Background

The USNRC’s evaluation of the suitability of a proposed site considers the site’s geological, seismological, and engineering characteristics. Before a COL can be issued by the USNRC, research and investigation into a number of geologic and seismic site factors that influence facility design – vibratory ground motion, tectonic surface deformation, and earthquake

recurrence rates, for example—must demonstrate that the construction and operation of a nuclear power plant at the proposed site will not pose undue risk to the health and safety of the public. The following subsection provides background information relevant to assessing the suitability of the Bellefonte Site and obtaining data needed for a COLA.

### 1.3.1 Existing Facilities and TVA Plans

The GG&S was performed in an area south of TVA's existing facilities at Bellefonte. The site is located near the cities of Hollywood and Scottsboro in northeast Alabama (Figure 1-1) in Jackson County on the right bank of Guntersville Reservoir at river mile 391.5.

In the early 1970s, projections of increasing demands on the TVA's power system led to the USNRC's 1974 issuance of a construction permit for a nuclear power plant at the Bellefonte Site. TVA began construction of two units, and by 1988, was nearing completion of the first and more than halfway complete on the second. At that time, TVA reassessed whether the operation of the facility as a nuclear power facility was indeed a viable approach to meeting future demands. By December 1994, TVA concluded that comprehensive evaluations of TVA's power needs were needed before construction could resume. A year later, TVA published their *Energy Vision 2020--Integrated Resource Plan and Environmental Impact Statement* (USNRC, 1995). This analysis considered multiple alternatives for the site's path forward and evaluated each alternative's potential for providing flexible and competitive energy choices for the future. The document presented two key conclusions and recommendations: (1) continue to defer the completion of the site as a nuclear-powered facility unless partners could be found to share in the investment, or (2) convert the unfinished facilities to a fossil-fueled power plant that could produce the additional 6,250 megawatts of energy resources projected to be needed by 2005.

To explore possible conversion options, TVA prepared an Environmental Impact Statement (EIS) to evaluate the costs, technical challenges, and environmental impacts of different conversion approaches (FEIS, 1997). The option of a natural gas combined cycle (NGCC) plant was preferred, and in 1997, TVA proposed to complete the unfinished facility as an NGCC plant.

However, when the U.S. Department of Energy's (DOE's) Nuclear Power 2010 program was presented in 2003, the availability of possible new funding suggested a different solution for the site. The DOE Nuclear Power 2010 program wished to have a COLA prepared for at least one new nuclear power plant that could begin commercial operation early in the next decade. The GG&S evaluation is being performed in partnership with DOE in an effort to realize the 2010 goal of preparing a COLA.

The area evaluated at the Bellefonte Site is located southwest of the existing cooling towers in the lay-down area for the original construction (Figure 1-2). The area is approximately 1,800 feet by 2,000 feet in size and is relatively flat. The geology typically consists of 10 to 20 feet of residuum over rock. The GG&S evaluation was performed within this location to build on the existing environmental and geological database of information that has been collected over the years.

Three potential generating facility designs were identified during the GG&S evaluation as: (1) the Advanced Boiling Water Reactor (ABWR), (2) the General Electric Economic Simplified Boiling Water Reactor (ESBWR), and (3) the Westinghouse AP1000 reactor. Each of these

reactors would require different foundation depths. The approximate foundation depths below ground surface (bgs) for safety-related structures for the ABWR, ESBWR, and AP1000 facility designs are approximately 84, 69, and 39.5 feet, respectively. It is anticipated that these facilities will be constructed on mat foundations placed on either engineered fill or directly on bedrock, as were the structures for the adjacent structures.

The range in potential foundation depth among the three facility designs, and the suitability of the Bellefonte Site to support this range of foundation depths, is considered in detail in this report.

### 1.3.2 Available Information

The approach taken during the GG&S involved building on the extensive database of information that had been developed for the site during previous environmental and engineering studies. This information was provided in the following documents:

- FEIS published in 1974 for the completion of Bellefonte (TVA, 1974)
- Bellefonte Nuclear Plant Final Safety Analysis Report (BLNP FSAR) (TVA, 1986)
- FEIS prepared in 1997 for the Bellefonte Conversion Project (TVA, 1997)
- Various construction documents from the original Bellefonte construction provided by TVA
- Energy Vision 2020 (TVA, 1995)

The FSAR served as the key starting point for all studies during the GG&S. Information in the FSAR included regional and local geological conditions, results of geotechnical drilling and sampling, seismic studies, and engineering analyses. This information was reviewed and updated where appropriate during the GG&S evaluation. The existing information also was used to directly compare information obtained from this evaluation of the Bellefonte Site to previous conditions elsewhere at the Bellefonte Site where applicable, such as for field and laboratory tests.

The FSAR included a detailed discussion of seismic sources; however, much of these data had been collected in the mid-1970s to early 1980s and have been superseded as the understanding of local seismic sources and regional seismic conditions has improved. The starting points for updating seismic conditions for the site were work completed by the Electric Power Research Institute (EPRI) for the Seismicity Owners Group (SOG) in the 1980s (EPRI-SOG, 1988; EPRI, 1989) documenting the seismic hazard at the Bellefonte Site, as well as other central and eastern U.S. (CEUS) nuclear facilities. Procedures given in the EPRI Report are referenced in USNRC RG-1.165 as providing an acceptable method of defining the SSE for a site – although the USNRC regulatory guide requires that the EPRI results be updated where significant changes in the understanding or results of seismic hazard analyses are found to occur.

The archives for the Bellefonte Site also served as a key resource for existing information. The archives included aerial photographs before the site was developed, construction records prepared during development of the existing Bellefonte facilities, groundwater records for the area, and performance observations made by site personnel. This archival information helped in establishing information about the project area.

## 1.4 Geotechnical, Geological, and Seismological Program Description

To ensure that the GG&S evaluations provided the highest quality data and most defensible information on the local and regional GG&S characteristics of the site, and therefore fully satisfied the regulations and requirements of the COLA process, the TVA GG&S evaluation was composed of four key tasks:

- Task 1 – Geotechnical Evaluation
- Task 2 – Geological Mapping and Characterization of Seismic Sources
- Task 3 – PSHA and Sensitivity Analysis
- Task 4 – Peer Group Review

Brief descriptions of these tasks, and the activities associated with each, appear as follows.

### Task 1 – Geotechnical Evaluation

Task 1 focused on evaluating the suitability of geotechnical properties of soil and rock at the GG&S for future development of a nuclear generating facility. An extensive amount of preexisting geotechnical data are available for the Bellefonte Site (adjacent and northeast of the Bellefonte Site), as reported in the BLNP FSAR. These data were considered to form part of the database of information for the Bellefonte Site. New field and laboratory investigations were performed to collect additional data on the Bellefonte Site to develop a database sufficient to make a conclusion on site suitability for a future generating facility.

Task 1 included the following activities:

- Obtain and review existing information (i.e., the FSAR and other information).
- Prepare the field and laboratory workplans.
- Perform subsurface investigations and support work including boreholes (soil and rock), soil and rock sample collection, downhole geophysics, seismic refraction geophysics, a microgravity survey, cone penetrometer testing, and piezometer installation.
- Conduct laboratory testing program (soil and rock samples).
- Interpret field and laboratory information.
- Conduct engineering evaluations.
- Document results of work in this report.

### Task 2 – Geologic Mapping and Characterization of Seismic Sources

The focus of the Task 2 work was on developing an up-to-date, site-specific earth science database that supplemented information used to support previous seismic source characterization models. This work included evaluating new and previous data to identify both seismogenic sources and capable tectonic sources and to determine their potential for generating earthquakes and causing surface deformation. Task 2 also involved assessing whether the new data and their interpretation were consistent with information used as the basis for source interpretations.

Task 2 included the following activities:

- Obtain and review existing site information regarding geology and seismology.
- Compile and review new data.
- Update seismicity catalog and describe significant earthquakes.
- Identify tectonic features, seismic sources, and pre-field investigations.
- Perform ground and aerial field reconnaissance.
- Review and evaluate existing Seismic Source Characterization (SSC) models.
- Document results of work in this report.

### **Task 3 – PSHA and Sensitivity Analysis**

Task 3 consisted of evaluating new information related to rock site ground motion models, performing the necessary PSHA sensitivity analyses, updating the PSHA for the site, and identifying the controlling earthquakes – all of which serve to provide the studies required by regulations.

Task 3 included the following activities:

- Perform sensitivity analysis using updated ground motion models.
- Perform sensitivity analysis using updated sources.
- Conduct PSHA analysis for the site.
- Identify controlling earthquakes and develop site-specific rock motions.
- Develop SSE spectra.
- Document results of work in this report.

### **Task 4 – Independent Peer Group Review**

An Independent Peer Group (IPG) performed reviews of work after completion of Tasks 1, 2, and 3. This approach ensured that experts in multiple disciplines – regional and local geology, regulations, geotechnical engineering, as well as procedures for conducting PSHA, site response analyses, and seismic source characterization – were participating in the oversight of data collection, confirming the suitability and quality of the data, and reviewing the conclusions or recommendations formed on the basis of the information.

## **1.5 Report Organization**

The GG&S information in this report is organized to reflect the structure suggested by NUREG-0800, “Standard Review Plan for the Review of Safety Analysis Reports for Nuclear Power Plants” (USNRC, 1987), in addition to meeting the requirements of RG 1.70, *Standard Format and Content of Safety Analysis Reports for Nuclear Power Plants* (USNRC, 1978). The report is presented such that the introductory section can be omitted and the Section 2.5 material easily inserted into Section 2.5 of a Safety Analysis Report (SAR) document if the BNLP site moves forward to a COLA.

**Section 1, *Introductory Information***, includes the three previous sections summarizing the purpose and scope, regulatory guidance, and background information for the GG&S evaluation. In addition to outlining the report organization, the end of Chapter 1 includes references for the chapter.

**Section 2.5, *Geology, Seismology, and Geotechnical Engineering***, includes seven main subsections. The format of these subsections was selected for consistency with the contents of a SAR, as described in RG 1.70. The contents of the subsections were also prepared in general accordance with RG 1.70, to the extent possible without available detailed design information for the future facility. If a nuclear generating facility design is selected in the future, the contents of these sections can be incorporated into a SAR (with additional amendment to support detailed design) for submittal as part of the COLA:

- Section 2.5.1, *Basic Geologic and Seismic Information*, contains fundamental information on the geology of both the site and the surrounding region.
- Section 2.5.2, *Vibratory Ground Motion*, addresses seismicity, associated geologic structures, and correlations between earthquakes and seismic sources, presenting pertinent discussions regarding seismic wave transmission, Operating Basis Earthquake (OBE), and the development of SSE ground motions.
- Section 2.5.3, *Surface Faulting*, discusses a range of investigative findings, exploring such topics as surface deformation, tectonic sources and structures, zones of quaternary deformation in the region, and potential surface tectonic deformation.
- Section 2.5.4, *Stability of Surface Materials and Foundations*, presents descriptions of the geological features and subsurface materials for the site, discusses explorations and surveys, and evaluates numerous site conditions that influence design, including but not limited to such topics as excavation and backfill, response of soil and rock to dynamic loading, liquefaction potential, earthquake design basis, design criteria techniques to improve subsurface conditions, and construction considerations.
- Section 2.5.5, *Stability of Slopes*, provides a qualitative discussion of slope stability issues associated with facility construction.
- Section 2.5.6, *Embankments and Dams*, identifies the potential hazards from failures of dams and embankments located near or upstream of the site.
- Section 2.5.7, *Section 2 References*, lists full information for all sources cited within the Section 2.5 text.

## 1.6 Section 1 References

10 CFR Part 50. Volume 51. No. 149. Code of Federal Regulations. "Safety Goals for the Operation of Nuclear Plants: Policy Statement."

10 CFR Part 52. Code of Federal Regulations. "Early Site Permits; Standard Design Certification; and Combined Licenses for Nuclear Power Plants."

EPRI. 1989. *Probabilistic Seismic Hazard Evaluations at Nuclear Power Plant Sites in the Central and Eastern United States*. Technical Report NP-6395-D. Electric Power Research Institute. Palo Alto, California.

EPRI-SOG. 1988. *Seismic Hazard Methodology for the Central and Eastern United States*. Technical Report NP-4726-A. Electric Power Research Institute. Palo Alto, California. Vols. 1-10.

- TVA. 1974. Final Environmental Impact Statement, Bellefonte Nuclear Plant, Units 1 and 2. Volumes 1 and 2. May 24, 1974.
- TVA. 1995. Energy Vision 2020, Integrated Resource Plan Environmental Impact Statement. Volumes 1 through 3. Tennessee Valley Authority. December 21, 1995.
- TVA. 1997. Final Environmental Impact Statement for the Bellefonte Conversion Project. Volumes 1 and 2. Tennessee Valley Authority.
- USNRC. 1973. Design Response Spectra for Seismic Design of Nuclear Power Plants. Regulatory Guide 1.60. U.S. Nuclear Regulatory Commission, Washington, DC.
- USNRC. 1978a. Laboratory Investigations of Soils for Engineering Analysis and Design of Nuclear Power Plants. Regulatory Guide 1.138. U.S. Nuclear Regulatory Commission, Washington, DC.
- USNRC. 1978b. Standard Format and Content of Safety Analysis Reports for Nuclear Power Plants. Regulatory Guide 1.70. Revision 3. U.S. Nuclear Regulatory Commission, Washington, DC.
- USNRC. 1979. Site Investigations for Foundations of Nuclear Power Plants. Regulatory Guide 1.132. U.S. Nuclear Regulatory Commission, Washington, DC.
- USNRC. 1987. Standard Review Plan for the Review of Safety Analysis Reports for Nuclear Power Plants. NUREG-0800. Office of Nuclear Regulatory Research.
- USNRC. 1997. Identification and Characterization of Seismic Sources and Determination of Safe Shutdown Earthquake Ground Motion. Regulatory Guide 1.165. U.S. Nuclear Regulatory Commission, Washington, DC.
- USNRC. 1998. "White Paper on Risk-Informed, Performance-Based Regulation." SECY-98-144. U.S. Nuclear Regulatory Commission, Washington, DC. June 22, 1998.
- USNRC. 2001a. Site Investigations for Foundations of Nuclear Power Plants. Draft Regulatory Guide 1101, proposed revised Regulatory Guide 1.132. U.S. Nuclear Regulatory Commission, Washington, DC.
- USNRC. 2001b. Procedures and Criteria for Assessing Seismic Soil Liquefaction at Nuclear Power Plant Sites. Draft Regulatory Guide 1105. U.S. Nuclear Regulatory Commission, Washington, DC.
- USNRC. 2001c. Laboratory Investigations of Soils and Rocks for Engineering Analysis and Design of Nuclear Power Plants. Draft Regulatory Guide 1109, proposed Revision 1 of Regulatory Guide 1.138. U.S. Nuclear Regulatory Commission, Washington, DC.
- USNRC. 2002. "Update of the Risk-Informed Regulation Implementation Plan." SECY-02-0131. U.S. Nuclear Regulatory Commission, Washington, DC.
- USNRC. 2004a. Laboratory Investigations of Soils for Engineering Analysis and Design of Nuclear Power Plants, RG-1.138.
- USNRC. 2004b. Site Investigations for Foundations of Nuclear Power Plants, Regulatory Guide (RG)-1.132.



fig1-1\_site\_location.mxd

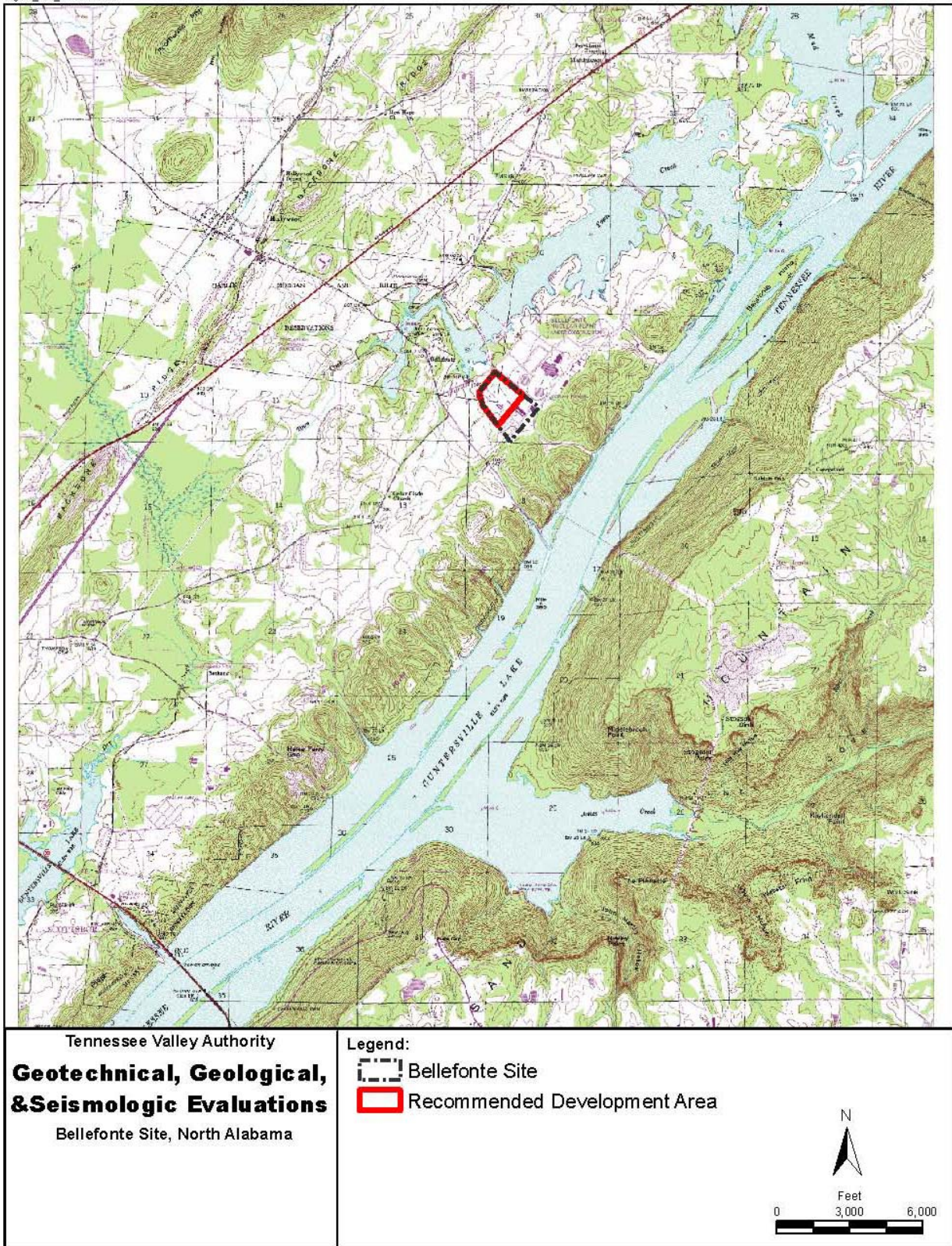


Figure 1-1. Vicinity Map of the Bellefonte Site

fig1-2\_GGS\_site.mxd

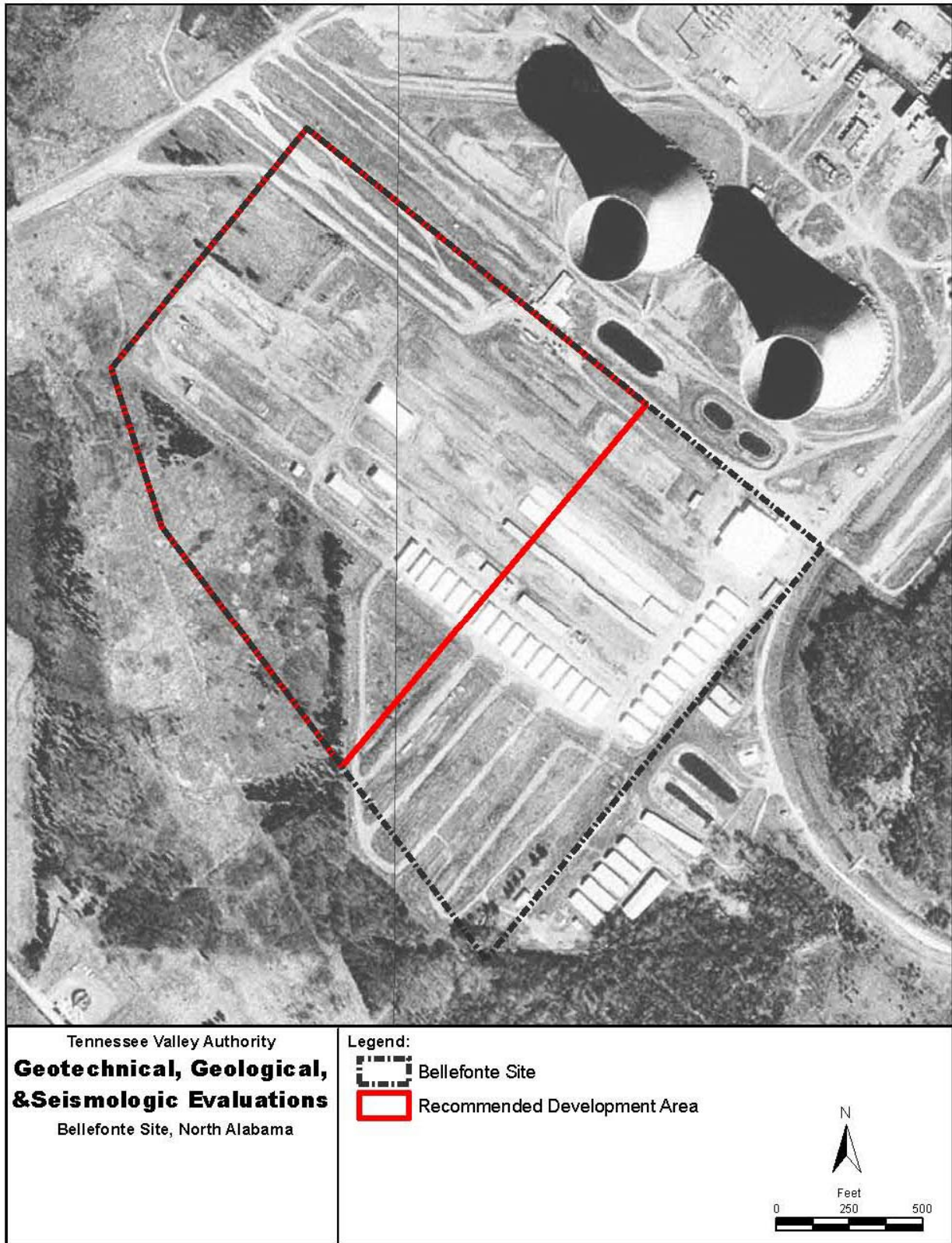


Figure 1-2. Site Map Showing the GG&S Evaluation Location

## 2.5 Geology, Seismology, and Geotechnical Engineering

### 2.5.1 Basic Geologic and Seismic Information

This section describes information on the geological and seismological setting of the TVA Bellefonte Site and region. Regulatory Guide 1.165 (USNRC, 1997) describes the regions around a proposed site for a nuclear facility and the level of investigation needed to confirm the suitability of the site. The guidance outlines four levels of investigation that generally increase in detail with proximity to the site. These include the region within a radius of 200 miles; the site vicinity within a radius of 25 miles, the site area within a radius of 5 miles, and the site within 0.6 mile.

The information described in this section is organized in accordance with these guidelines and emphasizes new information that would suggest significant differences from the information used to develop the EPRI-SOG source model (EPRI-SOG, 1988), which forms the starting point for the assessment of seismic hazard at sites in the CEUS (see discussion in Section 2.5.2). The EPRI-SOG study involved an extensive evaluation of the scientific knowledge concerning earthquake hazards in the CEUS by multi-discipline teams of experts in geology, seismology, geophysics, and earthquake ground motions. Regulatory Guide 1.165 specifies that the adequacy of the EPRI-SOG hazard results must be evaluated in light of more recent data and evolving knowledge pertaining to seismic hazard evaluation in the CEUS.

Section 2.5.1.1 describes the regional geologic and tectonic setting, focusing primarily on the region within a 200-mile radius. The EPRI-SOG seismic hazard analysis for the TVA Bellefonte Site identified significant seismic sources at distances greater than 200 miles, particularly the New Madrid and Charleston seismic zones that were the source of large, geologically recent earthquakes. Recent information regarding the location, magnitude, and recurrence of these more distant, but significant seismic sources also is described. Section 2.5.1.2 describes the geology and structural setting of the site vicinity (25-mile radius) and site area (5-mile radius). This section also addresses site (0.6-mile radius) geologic conditions and potential geologic hazards (e.g., karst).

Several sources of information were used to develop the information summarized in this chapter. Bellefonte Site-specific reports and documents including the BLNP FSAR issued in June 1986 (TVA, 1986), a Final Environmental Impact Statement (FEIS) prepared in 1997 for the Bellefonte Conversion Project (TVA, 1997), and various construction documents were reviewed as part of the initial compilation effort. Extensive new data sets that have been compiled and interpreted for numerous site-specific and regional studies throughout the CEUS in the time since completion of the EPRI-SOG study in the late 1980s also were reviewed. These studies have used a variety of techniques to characterize the location, extent, and activity of tectonic features; the location, magnitude, and rates of seismic activity; and the general characteristics of the continental crust throughout the CEUS. The information summarized in this chapter incorporates the information and findings of these studies as well as recent reports, maps, and articles published by state and federal agencies and in professional/academic journals.

Additional unpublished data and information were obtained through communications with individual researchers at university and state agencies.

## 2.5.1.1 Regional Geology

This section describes the physiography, geologic history, and tectonic setting of the TVA Bellefonte Site within a 200-mile radius region of the site. In addition, relevant new information on potential seismic sources of significant more distant, large magnitude earthquakes in the New Madrid, Missouri, and Charleston, South Carolina, areas also is discussed.

### 2.5.1.1.1 Regional Physiography and Topography

The TVA Bellefonte Site is located in the Browns Valley-Sequatchie valley segment of the Cumberland Plateau section of the Appalachian Plateaus Province of the Appalachian Highlands Division (Fenneman, 1938). The area within a 200-mile radius includes parts of five other physiographic provinces. These are: the Valley and Ridge Province, Blue Ridge Province, and Piedmont Province within the Appalachian Highlands to the east; the Interior Low Plateaus Province to the northwest; and the Coastal Plain Province to the southwest, south, and east (Figure 2.5.1-1). The following descriptions of the major physiographic provinces within the region is taken in part from the BLNP FSAR (TVA, 1986), which relied extensively on descriptions provided by Fenneman (1938) and Thornbury (1965). A more detailed discussion of the Browns Valley-Sequatchie valley segment and physiography in the site vicinity and site area is provided in Section 2.5.1.2.1.

#### 2.5.1.1.1.1 Appalachian Plateaus Physiographic Province

The Appalachian Plateaus Physiographic Province extends from northwestern New York to northwestern Alabama. From its maximum width of more than 200 miles, it begins to narrow in eastern Kentucky until it is barely 30 miles wide in Tennessee. The width in Alabama is 50 miles. This province is essentially a broad syncline in rocks of Late Paleozoic age, bounded on all sides by escarpments that reflect the regional synclinal structure. The rock formations are nearly horizontal, a typical plateau structure, but the formations are so elevated and dissected that the landforms are in large part mountainous (Hunt, 1967).

The Appalachian Plateaus Physiographic Province is divided into seven sections, three of which are within the 200-mile-radius region boundary. Portions of the Kanawha, or unglaciated Allegheny Plateau, and the Cumberland Mountain sections are present in Kentucky and northern Tennessee. The Cumberland Plateau section, which includes the Bellefonte Site, is the southwestern most of the seven sections comprising the Appalachian Plateaus Province. In Tennessee and Alabama, the Cumberland Plateau section is generally underlain by the resistant Pottsville Formation of Pennsylvanian age, which consists of alternating beds of sandstone, siltstone, and shale with coal seams. In the vicinity of the Bellefonte Site, the plateau is approximately 1,400 feet mean sea level (msl). Elevations increase to the north, and approach 2,000 feet msl near the Tennessee-Alabama border, and exceed 3,000 feet msl central and northern Tennessee, and 4,000 feet msl in Virginia.

The Cumberland Plateau section is bounded on the west by the Highland Rim section of the Interior Low Plateaus Physiographic Province. An escarpment that descends from 1,500 to 1,000 feet elevation separates the two. This escarpment is approximately 1,000 feet high in Tennessee but gradually diminishes in height in Alabama south of Huntsville. The Cumberland

Plateau section is bounded on the southwest by the Gulf Coastal Plain. Hills in the plateau may be capped by remnants of Coastal Plain sediment. On the east, the Cumberland Plateau section is bounded by the Valley and Ridge Physiographic Province. The eastern boundary of the Cumberland Plateau section is the Cumberland escarpment (described as follows), which marks the change from the broad open folds in the Cumberland Plateau to the close folding with marked faulting in the Valley and Ridge to the east. The straightness of the eastern Cumberland escarpment is in strong contrast with the dissected character of the scarp on the west side of the Plateau.

#### 2.5.1.1.1.2 Valley and Ridge Physiographic Province

The Valley and Ridge Physiographic Province to the east of the Appalachian Plateaus Physiographic Province extends for 1,200 miles, from eastern New York to central Alabama. It ranges from 14 to 80 miles in width, and is 40 to 50 miles wide in Alabama and northwestern Georgia. The boundary between the Appalachian Plateaus and the Valley and Ridge is an abrupt topographic rise known as the Allegheny front in Pennsylvania and the Cumberland escarpment in Tennessee and Virginia. This escarpment is breached by the Pine Mountain thrust fault and the Sequatchie Valley fault and anticline, which are the westernmost of the Valley and Ridge thrust faults. Anticlinal valleys, anticlinal ridges, synclinal valleys, synclinal ridges, homoclinal valleys, and homoclinal ridges are six possible topographic expressions of the geologic structure commonly encountered in the Valley and Ridge Province (Thornbury, 1965). Folds are strongly compressed and the amount of faulting increases southward. This province is underlain by Paleozoic sedimentary formations totaling from 30,000 to 40,000 feet in thickness. Drainage in this province mainly shows a northeast-southwest flow. The physiographic boundary between the Valley and Ridge and the Blue Ridge coincides approximately with the northwestern limit of Precambrian basement rocks and late Precambrian rift-fill sedimentary and volcanic rocks in the hanging walls of Alleghanian thrust faults. In Alabama, ridges are generally approximately 1,000 feet msl in elevation and sometimes reach 1,500 feet msl; elevations in the northern part of the province sometimes exceed 4,000 feet msl.

#### 2.5.1.1.1.3 Blue Ridge Physiographic Province

The Blue Ridge Physiographic Province is bounded on the east by the Piedmont Physiographic Province and on the west by the Valley and Ridge Physiographic Province. The Blue Ridge Physiographic Province is a deeply dissected mountainous area of numerous steep mountain ridges, intermontane basins, and trench valleys that intersect at all angles and give the area its rugged mountain character. The Blue Ridge contains the highest elevations and the most rugged topography in the Appalachian Mountain system of eastern North America. The North Carolina portion of the Blue Ridge, a part of which lies within the region, is about 200 miles long and ranges from 15 to 55 miles wide (Physiographic Provinces in North Carolina <http://gw.ehnr.state.nc.us/blue.htm>). Within North Carolina, 43 peaks exceed 6,000 feet in elevation and 82 peaks are between 5,000 and 6,000 feet.

The Blue Ridge is composed of complexly folded and faulted igneous (granitic) and metamorphic rocks. These rocks date to the Precambrian and Paleozoic and represent parts of the basement rock of the North American continent. Thomas (1991) describes the Blue Ridge as an elongate external basement massif along which late Precambrian syn-rift sedimentary and volcanic rocks, as well as older basement rocks, have been translated and deformed by younger

Appalachian compressional structures, especially large-scale Alleghanian (late Paleozoic) thrust faults (Thomas, 1991).

#### **2.5.1.1.1.4 Piedmont Physiographic Province**

The Piedmont Province lies between the Coastal Plain and the Blue Ridge Mountains. The Piedmont is characterized by gently rolling, well-rounded hills and long, low ridges. Along the border between the Piedmont and the Coastal Plain, elevations range from 500 to 800 feet above sea level. To the west, elevations gradually rise to about 1,700 feet above sea level at the foot of the Blue Ridge. Most of the rocks in the Piedmont Province are gneiss and schist, with some marble and quartzite, and were derived by metamorphism of older sedimentary and volcanic rocks. Granite also is present. Some less intensively metamorphosed rocks, including considerable slate, occur along the eastern part of the province from southern Virginia to Georgia.

#### **2.5.1.1.1.5 Interior Low Plateaus Physiographic Province**

Northwest of the Appalachian Plateaus is the Interior Low Plateaus Province, which is about 300 by 300 miles in size and covers most of central Tennessee and central Kentucky. Along its border with the Appalachian Plateaus Province (in Kentucky and Tennessee) is a west-facing escarpment that is underlain by sandstones of early Pennsylvanian age. Toward the center of this province are two large shallow basins called the Nashville Basin and the Lexington Plain. These two basins were formed by breaching and erosion of the Nashville and Jessamine Domes, respectively, along the Cincinnati Arch. From the Cincinnati Arch, the rocks dip gently toward the Appalachian Plateaus on the east and the Illinois Basin on the west (Thornbury, 1965). This province is underlain predominantly by Ordovician and Mississippian limestones on which a moderate karst topography is developed.

#### **2.5.1.1.1.6 Coastal Plain Physiographic Province**

South and southwest of the Appalachian Plateaus Physiographic Province is the East Gulf Coastal Plain Physiographic Province, which may be described largely in terms of its underlying rocks (Cretaceous and Eocene series). The inner boundary of the Coastal Plain Physiographic Province with the Appalachian Plateaus Physiographic Province is commonly called the Fall Line, but few rapids are produced where the central Alabama Coastal Plain rocks abut against Paleozoic sedimentary rocks (Thornbury, 1965). Geologically, it is the contact between the Cretaceous and younger sediments of the Coastal Plain and the older, crystalline rocks of the Piedmont. The Fall Line Hills is the belt of the East Gulf Coastal Plain that borders the Appalachian Plateaus Physiographic Province. Maximum elevations range from approximately 760 feet in the western part to approximately 250 feet along the southeastern boundary of the Fall Line Hills.

#### **2.5.1.1.2 Regional Geologic History**

The Bellefonte Site is located within the southern Appalachian orogen. Information from stratigraphic assemblages, the known timing of the major faults, and times of the plutonic intrusion and metamorphism have been used to reconstruct the plate tectonic history of the central and southern Appalachians. Details of these data sets and interpretations of the geologic history of the region are presented in a series of papers that describe the Appalachian-Ouachita orogen in the U.S. (Hatcher et al., 1989b). Additional discussions of the tectonic framework and structural evolution of the Appalachian orogen in Alabama are outlined by Thomas

(1982). These papers and other recent publications as noted in the following text provide the basis for the following summary of the regional geologic framework.

The Appalachian orogen was built on the late Precambrian-early Paleozoic continental margin of North America. The Proterozoic Grenvillian crystalline rocks form the basement upon which many of the late Precambrian and younger stratigraphic packages that were ultimately involved in the Appalachian orogenies were deposited (Hatcher, 1987). Laurentian (Proterozoic North America) basement rocks underwent a granulite or at least an amphibolite metamorphism about 1.0 to 1.1 Ga (Rankin et al., 1989) during the Grenville orogeny.

Hatcher (1987; 1989b) describes the history of the orogen as a type example of one or more cycles of opening and closing of ocean basins. The process began following a period of crustal extension and rifting during the late Proterozoic that caused the separation of the North America and African plates and created the Iapetus (proto-Atlantic) Ocean. During rifting, the newly formed continental margin began to subside and an eastward thickening wedge of clastic sediments accumulated on the passive margin. Stratigraphic and sedimentologic analyses indicate that the Appalachian region subsequently experienced several compressional events: the Avalonian, Penobscotian, Taconic, Acadian, and Alleghanian orogenies (Figures 2.5.1-2 and 2.5.1-3). The processes of accretion of suspect and exotic terranes, together with terrane collision and ultimately continent-continent collision, resulted in construction of the Appalachian orogen. The major deformational events in the region are summarized as follows and are illustrated schematically in Figure 2.5.1-3. Additional details regarding the sequence of depositional and deformational events in northern Alabama are presented in Figure 2.5.1-4 and are summarized in Section 2.5.1.2.2.

The rifted margin of North America that formed as the Iapetus and Theic-Rheic Oceans opened in the late Precambrian resulting in an irregular rift-transform margin in which basins of various depths developed (Figure 2.5.1-4). Iapetan rifting along the Blue Ridge dates from the interval 730 to 680 Ma (Rankin et al., 1989). Ultimately this rifting led to the formation of oceanic crust and the opening of the Iapetus (proto-Atlantic) Ocean. The western rifted margin of Iapetus has been identified along the western side of the Appalachian orogen (Wheeler, 1995). The block-faulted basins to the west influenced the later configurations of thrusts that transported these deposits onto the North American craton. Deposition of the passive margin sequence followed breakup.

The Avalonian orogeny was a compressional episode in the late Proterozoic that produced calcalkaline plutonic rocks and a volcanic suite commonly described as an island arc. Late Proterozoic rifting during the Avalonian orogeny occurred between 650 and 570 Ma and was accompanied by deposition of non-marine to shallow marine sediments and volcanic deposits in grabens west of the Blue Ridge axis; while thick sequences of Precambrian turbidites and volcanics were deposited in listric fault-bounded basins on attenuated crust to the east (Rankin et al., 1989). The Avalonian rocks in the southern Appalachians are found in the eastern part of the Piedmont Province and in the pre-Mesozoic basement beneath the Coastal Plain (Rankin et al., 1989).

The early Cambrian-early Ordovician Penobscot orogeny represents the initial collision event in the Paleozoic that marks the beginning of the convergent phase in the closing of the Iapetus Ocean. Crustal convergence and accretion of micro-continent and intra-oceanic island-arc

terrane that had developed in the proto-Atlantic ocean as a result of east-directed oceanic subduction and initial closing of the ocean basin occurred during this deformational episode.

The Taconic orogeny was a complex deformation episode that began earlier in the southern Appalachians than in the central and northern Appalachians (Rankin et al., 1989). This early to middle Ordovician orogeny represents a major compressive episode caused by one stage of the closing of the Iapetus Ocean (Rankin et al., 1989). The age of the Taconic event is estimated to be 450 to 480 Ma in the southern Appalachians (Hatcher, 1989b). Uplift at a converging margin is indicated by the development of a prograding clastic wedge derived from orogenic uplift in Tennessee reentrant southwestward onto Alabama promontory (Figure 2.5.1-4). Hatcher (1987) notes that a regional unconformity that developed on top of the Middle Ordovician carbonate bank may be the external vestige of the Taconic/Penobscot orogeny to the east, where thrust sheets loaded the continental margin and caused subsidence, forming a foredeep basin about 450 Ma in the southern Appalachians. Granitic plutons were formed during this deformational episode, probably above an eastward-dipping subduction zone, represented in remnant form by the Hayesville thrust sheet (Hatcher, 1987).

Later Acadian convergence and suturing of the Avalon (Carolina) terrane to North America in the Devonian Period to early Carboniferous Period produced another suite of granitic and mafic plutons and a large fault, the Central Piedmont suture, that welded the Carolina terrane to the ancient North American margin (Hatcher, 1987). This event resulted in a metamorphic event that spread across the Inner Piedmont and into the eastern Blue Ridge.

The Alleghanian orogeny occurred during the late Carboniferous Period and extended into the Permian Period. This orogeny is the most pervasive event to affect the central and southern Appalachians. This mountain building episode marks the collision of North America with Africa and represents the final convergent phase in the closing of the proto-Atlantic ocean. Alleghanian deformation and uplift of the southern and central Appalachians produced a large molasses deposit from Alabama to Pennsylvania, and folds and faults of the Valley and Ridge, and finally deformation of the molasses deposits of the Valley and Ridge and Cumberland-Allegheny Plateau (Hatcher, 1989b). During this orogeny, the southern and central Appalachians were transported toward the North American craton as a huge composite crystalline thrust sheet – the Blue Ridge-Piedmont thrust sheet – that drove the foreland deformation in front of it (Hatcher et al., 1989b). This collision resulted in a detachment of the ductile-brittle transition zone of the crust, propagating a thrust from the collision zone, which is probably under the Coastal Plain (Hatcher, 1987). The thrust sheet ramped into the rift-drift facies and platform sedimentary rocks along the leading edge and faults then propagated westward into the platform and early to late Paleozoic foreland sedimentary rocks (Hatcher et al., 1989c). The master detachment in the frontal fold-thrust belt in the southern Appalachians is the Lower Cambrian Rome Formation. Toward the west, faults propagated into higher detachments in the Ordovician, Mississippian, and Pennsylvanian rocks in parts of the southern Appalachians (Hatcher et al., 1989c). The final phase of the Alleghanian deformation resulted in the development of dextral shear zones in the eastern Piedmont (Horton et al., 1991).

Crustal extension during early Mesozoic (late Triassic) time marked the opening of the Gulf of Mexico and Atlantic oceans. The early Mesozoic extensional episode gave rise to the Cenozoic Mid-Atlantic spreading center and development of the present passive trailing divergent continental margin along the Atlantic seaboard. This extensional period resulted in normal faulting and reactivation of structures and associated igneous activity within the Eastern



continental margin south and east of the Bellefonte Site, but did not significantly affect the site (Miller, 1974).

Mesozoic and Cenozoic downwarping of the Gulf Coastal Plain has been imposed upon the Paleozoic structures of the Appalachian-Ouachita orogen (Thomas, 1989a). Post-Early Jurassic deposition along the present Atlantic Coast records transgression until late Cretaceous and possibly Paleocene time, followed by regression (complicated by smaller cycles of transgression) until the present (Hatcher, 1989b). Tertiary regression is probably related to a change in the fundamental stress configuration in the crust along the continental margin, from dominant extension during the Mesozoic to compression related to ridge-push during the Tertiary to Recent (Hatcher, 1989a). Within the study region, extensive areas of Cretaceous sediments were deposited in the Coastal Plain of Alabama, Tennessee, and Kentucky.

After the late Paleozoic, much of the eastern interior of the North American continent was above sea level, never to be inundated to the present time. There began a long episode of erosion, lasting into Cretaceous time in the Coastal Plains Province and up to the present throughout physiographic provinces of the Appalachian Highlands and Interior Plains Divisions (Figure 2.5.1-1). The present mountains result from Tertiary uplift and continued differential erosion of dissected Mesozoic and Tertiary surfaces as the crust readjusted isostatically to erosional unloading (Hatcher, 1989a).

### 2.5.1.1.3 Regional Stratigraphy

Geologic formations within the 200-mile-radius region are sedimentary rocks of Tertiary to Precambrian age and igneous and metamorphic rocks of Paleozoic to Precambrian age. A map showing the generalized stratigraphy within the 200-mile-radius region is shown in Figure 2.5.1-5. A description of the general stratigraphy within the physiographic provinces in the region is provided as follows.

#### 2.5.1.1.3.1 Appalachian Plateaus Physiographic Province

The Appalachian Plateaus Physiographic Province is underlain by Paleozoic sedimentary rocks (predominantly Mississippian and Pennsylvanian in age) that are nearly horizontal or gently folded. Rocks within this province generally are little deformed and have not been metamorphosed. Older rocks generally are exposed only in the crests of eroded anticlinal folds in the Cumberland Plateau section (e.g., the Sequatchie Valley and Big Wills Valley anticlines).

The following summary of the bedrock stratigraphy within this province is primarily from the BLNP FSAR (TVA, 1986). A more detailed description of the stratigraphy in the site vicinity is provided in Section 2.5.1.2.3. A stratigraphic column in the Appalachian thrust belt in Alabama (including the Cumberland Plateaus and Valley and Ridge Provinces) is shown in Figure 2.5.1-6.

Sedimentary rocks from Permian to Cambrian in age are found within the Appalachian Plateaus Province. In Alabama, the Knox Group, the Chickamauga Formation, the Red Mountain Formation, the Bangor Limestone, and the Pottsville Formation comprise the majority of the bedrock in this province.

The Knox Group, which is 2,500 to 3,000 feet thick, consists mostly of dolomite with some limestone and is late Cambrian to early Ordovician in age (TVA, 1986).

The Chickamauga Limestone of Middle Ordovician age is mainly alternating layers of limestone, siltstone, and shale, and is approximately 1,400 feet thick.

The Red Mountain Formation of Silurian age is a shallow-marine clastic sequence that is composed of resistant sandstone, shale, and limestone. The formation is 200 or more feet thick in northeastern Alabama. Overlying the Red Mountain Formation is a sequence of discontinuous variable shallow-marine facies and internal unconformities that includes the Devonian Frog Mountain Sandstone and Chattanooga Shale, and another resistant unit, the Mississippian Fort Payne Chert (Thomas, 1982).

The Bangor Limestone of Mississippian age in most of the region consists of thick-bedded, dark-bluish gray, crystalline and oolitic limestone. It ranges in thickness from about 100 to 700 feet (TVA, 1986).

The Pottsville Formation of Pennsylvanian age consists of alternating beds of sandstone, siltstone, and shale with coal seams. In Tennessee and Alabama, the entire width of the Cumberland Plateau is underlain by resistant Pottsville strata. In Alabama, the Pottsville Formation reaches a thickness of about 1,200 feet (TVA, 1986).

Surficial deposits in the Appalachians including the Cumberland Plateau section generally are only a few meters thick, patchy, and difficult to date (Mills et al., 2005). Mills and Kaye (2001) report occurrences of gravel on severely eroded remnants of high terraces that likely are of Quaternary age, but the age of these deposits is not well constrained. Inundation of many of the larger rivers by a system of large reservoirs (e.g., the Guntersville Reservoir in the site vicinity) has obscured lower fluvial deposits and terrace surfaces. Many of the channels of the present drainages are eroded into bedrock. The Quaternary cover chiefly is composed of residual soils and soils modified from or derived from locally derived parent material accumulated as alluvium and hillslope colluvium.

As noted in the BLNP FSAR (TVA, 1986), the present course of the Tennessee River, the major drainage within the study region, includes a number of deflections that suggest adjustments by stream capture. Mills and Kaye (2001) review previous hypotheses and present information on gravel locations that may provide constraints on possible former courses of the Tennessee River in the study region. The major course changes described in both the BLNP FSAR (TVA, 1986) and Mills and Kaye (2001) include: (1) west of Chattanooga, Tennessee, where the river leaves the Valley and Ridge Province and cuts through Walden Ridge; (2) near Guntersville, Alabama, where it leaves the southwestward-trending Sequatchie anticlinal valley and assumes a northwesterly course; and (3) near the juncture of the Alabama, Mississippi, and Tennessee borders, where it turns north to cross Tennessee and join the Ohio River. Mills and Kaye (2001) cite studies that relate the northward diversion of the lower reaches of the river to crustal tilting caused by isostatic adjustment due to sea level change or crustal loading due to glaciation that could be as young as 1.13 Ma and other studies that suggest a minimum age of 5 to 6 Ma for the capture. They conclude, however, that there is not sufficient information on the distribution of Plio-Pleistocene deposits to decipher the detailed drainage history of the Tennessee River.

#### **2.5.1.1.3.2 Valley and Ridge Physiographic Province**

The Valley and Ridge Province is underlain primarily by Paleozoic sedimentary rocks that have been intensely folded and thrust faulted. The total thickness of Paleozoic sedimentary formations, which range in age from Cambrian to Permian, ranges from 30,000 to 40,000 feet.

The Paleozoic section includes four major divisions: a basal, transgressive Cambrian clastic unit; a thick, extensive Cambrian-Ordovician carbonate-shelf facies; a thin, laterally variable shelf sequence of Ordovician to Lower Mississippian carbonate rocks, chert, and thin clastic units; and Upper Mississippian-Pennsylvanian synorogenic clastic-wedge rocks and Mississippian carbonate facies (Thomas, 1989a) (Figure 2.5.1-6).

The Quaternary record in the Valley and Ridge, like the rest of the Appalachians is thin, discontinuous, and difficult to date (Mills, 2005b). Quaternary deposits include alluvial stream and fan deposits, and hillslope colluvium (Mills, 2005b). Higher, older stream terraces are recognized and have been dated in this physiographic province to the north of the study region (e.g., the New River terraces in Virginia [Granger et al., 1997]). Chapman (1977) and Whisner et al. (2003) provide descriptions of stream terrace deposits at varying locations within the Valley and Ridge Province. Along some rivers, the areal extent of old, highly weathered alluvium far exceeds the younger alluvium, suggesting that floodplains and low terraces were formerly more extensive than at present (Mills, 2005b).

In northern Alabama, extensive alluvial terrace deposits are mapped in the Coosa River Valley in the Gadsden to Weiss Reservoir area (Etowah and Cherokee Counties) (Osborne et al., 1988) (Figure 2.5.1-7). The alluvial and terrace deposits are preserved within a broad valley underlain by the Cambrian Conasauga Formation. Structural cross-sections and maps indicate that the Cambrian unit beneath the valley is a near horizontal thrust sheet, referred to as the Rome thrust (Thomas and Bayona, 2002) (see discussion in Section 2.5.1.1.4.2a). The meandering river morphology is prominent where the widest part of the Rome thrust sheet is preserved. Downstream of the confluence of Big Canoe Creek and the Coosa River (about 10 miles southwest of Gadsden), the valley narrows and the Coosa River takes a sharp bend to the south and cuts across the regional structural grain. Quaternary deposits are not shown on the State Geologic Map of Alabama (Osborne et al., 1988) downstream of this confluence. On the State Geologic Map of Alabama (Osborne et al., 1988), the deposits are differentiated into alluvial and low terrace (Qalt) and high terrace (Qt) map units. The Qalt deposits are described as consisting of varicolored fine to coarse quartz sand containing clay lenses and gravel in places. Gravel is composed of quartz and chert pebbles and assorted metamorphic and igneous rock fragments in streams near the Piedmont. In areas of the Valley and Ridge Province, gravel is composed of angular to subrounded chert, quartz, and quartzite pebbles. The Qt deposits are described as varicolored lenticular beds of poorly sorted sand, ferruginous sand, silt, clay, and gravelly sand. Sand consists primarily of very fine to very coarse, poorly sorted quartz grains. The gravel is composed of quartz, quartzite, and chert pebbles.

Based on observations made during field reconnaissance investigations for this study, both the Qt and Qalt units appear to include multiple terrace surfaces. The highest surfaces as mapped between Gadsden and the Weiss Reservoir range from elevations of about 600 feet to 670 feet msl (based on contours shown on 1:100,000 and 1:250,000 scale maps). The most prominent surfaces appear to be at about 600 feet elevation, approximately 100 feet above the present river level. Exposures of the high terrace gravels observed in and near Gadsden showed strong soil development with significant clay accumulation, strong mottling, and localized iron cementation. The age of these deposits is not known. Based on the regional denudation rate (100 feet (30 meters)/my) (Mills, 2005b) and the strong soil development, it is likely that the older terraces are on the order of hundreds of thousands to a million years old.

At one location in Gadsden (Field Stop KH9, Figure 2.5.1-7) subvertical features characterized by subvertical bands of alternating red and light brownish gray color were observed in the lower, more clay-rich, strongly mottled part of the soil. The features appeared to flare upward and become less distinct in the upper part of the mottled horizon and could not be traced into the upper 2 feet of the soil. The contact between the mottled unit and gravelly sand does not show any apparent vertical displacement across the features. These features resemble non-tectonic soil weathering features (cutans) seen elsewhere in the Coastal Plain region of the southeastern U.S. (Abbott et al., 1999).

### 2.5.1.1.3.3 Blue Ridge Physiographic Province

The Blue Ridge Physiographic Province consists of an allochthonous belt involving Precambrian (1.0 to 1.1 Ga) basement and younger rocks (Taylor, 1989). The Blue Ridge is separated by a major fault system (Hayesville-Fries fault) into a western and an eastern block (Taylor, 1989). The western block consists mainly of Grenville basement non-conformably overlain by Ocoee Series rocks, a cover sequence of Upper Proterozoic to Lower Cambrian sedimentary and rift-related rocks (Hatcher et al., 1989c). The Ocoee basin was restricted to Tennessee. The Ocoee is conformably succeeded by the Chilhowee Group, a sequence of clean sandstones and shales that are more widespread than the Ocoee. These rocks overlap the basement along much of its extent and it is concluded to have been deposited in a post-rift environment (Hatcher, 1989c). The eastern block consists of coveval metamorphosed turbidite sequences intercalated with mafic and ultramafic igneous rocks that are the same as those of the Inner Piedmont (Hatcher, 1978). Two small Grenville basement inliers – on the Tallulah Falls and Toxaway domes – also are present in the eastern Blue Ridge in the Carolinas and northeastern Georgia (Hatcher et al., 1989c).

The Talladega belt in Alabama, which lies within the western block, was initially defined as a suspect terrane by Williams and Hatcher (1982, 1983). It has since been shown to represent a more eastern (offshore) facies assemblage of the late Proterozoic to Devonian platform sequence that may have been deposited as fill in a strike-slip rhomb-graben basin near the North American shelf edge, and is, therefore, not an exotic terrane (Hatcher, 1989c). The same rock assemblage may be present in the Murphy syncline farther northeast in southwest North Carolina.

The late Precambrian and Paleozoic metasedimentary and metavolcanic rocks become more intensely metamorphosed from west to east across the Blue Ridge Province, which separates platform rocks of the Valley and Ridge Province to the west from metavolcanic and metasedimentary rocks and intrusives of the Piedmont Province.

Surficial deposits in the unglaciated Blue Ridge Physiographic Province include alluvial stream terrace deposits, alluvial and debris-flow deposits, and hillslope colluvium (Mills, 2005). Relative-age mapping of alluvial fans in the Blue Ridge and adjacent Piedmont produces a map pattern of older and younger fan surfaces that has been used to infer the sequence of fan development (Mills, 2005). This mapping also shows that the relative abundance of young, intermediate, and old fan surfaces greatly vary from one area, suggesting episodic development. Comparison of data on fan surface heights and weathering rind thickness in two areas of the region suggest that downcutting and abandonment may take place at different rates. However, this preliminary conclusion is based on the assumption that the rate of

weathering rind thickening on amphibolite is the same in the studied areas. Further numerical dating is needed to confirm this preliminary hypothesis.

#### 2.5.1.1.3.4 Piedmont Physiographic Province

In the Piedmont Province to the east, beyond the Blue Ridge Province, the underlying rocks are mainly metamorphic (schists, gneisses, quartzites, and slates) and plutonic (granites, granodiorites, gabbros, peridotites, and dunites). The Piedmont Province can be subdivided into a number of different zones based on differences in metamorphic grade and dominant lithology (Inner Piedmont, Charlotte belt, Carolina slate belt) (Taylor, 1989). The Inner Piedmont is bounded by the Brevard zone to the west and the Central Piedmont suture to the east. Rocks of the Inner Piedmont consist of late Precambrian to early Paleozoic highly deformed sedimentary and mafic volcanic sequences regionally metamorphosed from upper greenschist to upper amphibolite facies. Small areas of Grenvillian rocks are exposed in windows through the thrust sheet (e.g., Pine Mountain) (Williams and Hatcher, 1983). The Charlotte and Carolina slate belts, to the east, are grouped as part of the late Precambrian-early Paleozoic Avalon terrane by Williams and Hatcher (1982). Both belts contain a thick sequence of volcanic rocks and associated sedimentary rocks metamorphosed to greenschist grade in the slate belt and upper amphibolite grade in the Charlotte belt (Taylor, 1989). The Kiokee belt is a belt of medium- to high-grade metamorphic and associated plutonic rocks between the Carolina slate belt on the northwest and the Belair belt on the southeast (Hatcher et al., 1989c).

#### 2.5.1.1.3.5 Interior Low Plateaus Province

In the Interior Low Plateaus Province to the west of the Appalachians Plateaus Province, the strata are relatively flat-lying and consist of sandstones, shales, and smaller amounts of limestones and dolomites, ranging in age from Ordovician to Cretaceous. The rock strata dip gently off the Jessamine and Nashville Domes, which developed along the axis of the Cincinnati Arch.

#### 2.5.1.1.3.6 Coastal Plain Province

To the southwest lies the Coastal Plain Province, in which Cretaceous and Eocene formations predominate. The Post-Paleozoic strata of the Atlantic and Gulf Coastal Plains are post-orogenic with respect to the Appalachian-Ouachita orogen and belong to two different tectonic regimes (Thomas et al., 1989). The older Mesozoic rocks constitute fill of extensional fault-bounded basins and include sedimentary and volcanic components. These rocks of Triassic and early Jurassic age that are associated with rift-stage evolution of the present Atlantic and Gulf margin generally lie outside the 200-mile-radius region. Younger Mesozoic and Cenozoic strata that overstep the graben-boundary faults are regionally continuous and represent shallow-marine onlap of the post-rift passive margin (Thomas et al., 1989). The latter deposits are present within the study region (Figure 2.5.1-5).

#### 2.5.1.1.4 Regional Tectonic Setting

The seismotectonic framework—the basic understanding of existing tectonic features and their relationship to the contemporary stress regime and seismicity—provides the basic underpinnings for assessments of seismic sources. In the EPRI-SOG study completed in 1988, seismic source models were developed based on the tectonic setting, the identification and characterization of “feature-specific” source zones, and the occurrence, rates, and distribution of historical seismicity. The EPRI models reflected the general state of knowledge of the geoscience

community in the mid- to late-1980s. The original seismic sources identified in the EPRI-SOG study are discussed in detail in the EPRI-SOG (1988) report and are summarized in Section 2.5.2.2.1.

A second study conducted by Lawrence Livermore National Laboratory (LLNL) (Savy et al., 2002), which was a trial implementation project (TIP) of general guidance given in Senior Seismic Hazard Analysis Committee (SSHAC; 1997) for conducting a Level IV PSHA, provided updated information for some of the seismic sources significant to the Bellefonte Site. A brief summary of the TIP study is provided in Section 2.5.2.2.2.

Subsequent to the EPRI-SOG and TIP studies, additional geological, seismological, and geophysical research has been completed at and in the vicinity of the Bellefonte Site. This section presents a summary of the current state of knowledge on the regional tectonic setting and highlights the more recent information that is relevant to the identification of seismic sources for the Bellefonte Site. The following sections describe the region in terms of the contemporary stress environment (2.5.1.1.4.1), the primary tectonic features and seismic sources (2.5.1.1.4.2), and significant seismic sources at distances greater than 200 miles (2.5.1.1.4.3). Historical seismicity is described in Section 2.5.1.3.1.

#### 2.5.1.1.4.1 Contemporary Tectonic Stress

The Bellefonte Site lies within a compressive midplate stress province characterized by a relatively uniform compressive stress field with a maximum horizontal shear (SHmax) direction oriented northeast to east-northeast (NE to ENE) based on earthquake focal mechanisms, in situ stress measurements, borehole breakout data, and recent geologic features (Zoback and Zoback, 1989; 1991). Zoback and Zoback (1989) note that although localized stresses may be important in places, the overall uniformity in the midplate stress pattern suggests a far-field source and that the orientation range coincides with both absolute plate motion and ridge push directions for North America. Richardson and Reding (1991) also concluded, based on modeling of various tectonic processes using an elastic finite element analysis that distributed ridge forces are capable of accounting for the dominant ENE trend for maximum compression throughout much of the North American plate east of the Rocky Mountains.

In contrast to the stress domain map published by Zoback and Zoback (1980), which was a primary reference used by the EPRI-SOG teams, the 1989 compilation shows general ENE compression to extend all the way to the Atlantic continental margin. Zoback and Zoback (1989) concluded that a distinct Atlantic Coastal Plain stress province (characterized by northwest compression as inferred from the orientations of post-Cretaceous reverse faults in the Coastal Plain region and focal mechanisms in the northeastern U.S.) is not supported or justified by the available data.

Based on analysis of well-constrained focal mechanisms of North American midplate earthquakes, Zoback (1992) concluded that earthquakes in the CEUS occur primarily on strike-slip faults dipping between 43° and 80°, with most in the 60° to 75° range. This analysis demonstrated that the CEUS earthquakes occur primarily in response to a strike-slip stress regime.

#### 2.5.1.1.4.2 Regional Structures (Within 200-Mile Radius)

A tectonic map showing structures within a 200-mile radius of the Bellefonte Site known at the time of the BNP licensing studies (TVA, 1986) and the EPRI-SOG study is shown in Figure 2.5.1-9. The concepts of suspect (allochthons) and exotic terranes, which were recognized at that time, have been more widely employed to decipher the accretionary history and tectonic evolution of the Appalachian orogen (see discussion in Section 2.5.1.1.2) and to define lithotectonic units (Williams and Hatcher, 1983; Hatcher, 1987; Hatcher et al., 1989b and 1989c). More recent tectonic maps and structural cross-sections at a regional scale for the Appalachian-Ouachita orogen and southern Appalachians are shown in Figures 2.5.1-10, 2.5.1-11, and 2.5.1-12, respectively. A map showing the major geologic and tectonic features and terrane boundaries of the southern Appalachians is shown in Figure 2.5.1-13.

Hatcher (1989a) defines lithotectonic subdivisions within the region. The westernmost lithotectonic province of the Appalachians as defined by Hatcher (1989a) is the Appalachian foreland, which includes the Cumberland-Allegheny Plateau and Valley and Ridge physiographic provinces. It is made up of two subdivisions: the Appalachian basin and a gently eastward-thickening miogeoclinal wedge of platform sedimentary rocks and syn-orogenic clastic wedges. The Appalachian basin may have formed as thrusts loaded the crust farther east, producing the basin and also the Cincinnati arch. Eastward, the Appalachian foreland fold-thrust belt in the region consists of a belt of Alleghanian imbricate thrusts and folds. East of the fold-thrust belt is the metamorphic core of the Appalachian orogen. Precambrian basement rocks, transported in external basement massifs, are present, along with continental margin or slope and rise sedimentary rocks in the western Blue Ridge. Farther east is the internal core of the Appalachians that includes the eastern Blue Ridge and Inner Piedmont physiographic provinces. Williams and Hatcher (1982, 1983) refer to this belt as the Piedmont terrane. In more recent publications, it is shown as the Inner Piedmont belt (Figure 2.5.1-11). Metamorphic rocks of the northwestern part of the Inner Piedmont exhibit no Alleghanian deformation—except in the Brevard and Brookneal fault zones—but were translated northwestward on the Blue Ridge-Piedmont sole thrust and various splays (such as the Brevard fault) (Hatcher, 1987) (Figures 2.5.1-3 and 2.5.1-12). Metamorphism and plutonism accompanied Alleghanian faulting and penetrative deformation in the eastern Piedmont. The Carolina terrane (previously referred to as the Avalon terrane by Williams and Hatcher, 1983) includes the Charlotte and Carolina slate belts that are considered to be exotic or suspect terranes. These belts are interpreted to be island-arcs of that were accreted to ancestral North America during the Acadian orogeny (Figure 2.5.1-3), but experienced regional metamorphism and presumably ductile deformation during the Taconic orogeny (Drake et al., 1989). The boundary structure between the Piedmont and Carolina terrane is referred to as the Central Piedmont suture (Hatcher, 1987). Along the eastern edge of the Piedmont in the Carolinas and Georgia is the Alleghanian Kiokee-Raleigh belt anticlinorium composed of middle to upper amphibolite-facies metamorphic rocks that contrasts with the older higher-grade rocks toward the west (Hatcher 1989a) (Figure 2.5.1-11).

During collision of North America with Africa during the Alleghanian orogeny, the southern and central Appalachians were transported toward the North America craton as a huge composite crystalline thrust sheet—the Blue Ridge-Piedmont thrust sheet—that drove the foreland deformation in front of it (Hatcher et al., 1989c). Evidence for the extent of the Alleghanian detachment beneath the Blue Ridge and Piedmont is derived from both

geophysical and structural data. The acquisition and interpretation of the Consortium for Continental Reflection Profiling (COCORP) seismic reflection profiles across the southern Appalachians in the late 1970s to early 1980s (Cook et al., 1979; 1983) and subsequent interpretation of industry seismic data provided significant subsurface information to support a model for the development of the Appalachian thrust belt above a master décollement or detachment (Hatcher et al., 1989b and papers therein) (Figure 2.5.1-12).

In central Alabama, the Paleozoic orogen plunges southwestward beneath postorogenic Mesozoic-Cenozoic strata of the Gulf Coast Plain (Figure 2.5.1-10). Data from oil wells drilled through the Coastal Plain sediment indicate that the orogenic belt curves westward through Mississippi and continues northwestward to the exposed Paleozoic structures in the Ouachita Mountains in Arkansas (Thomas, 1982). The geometry and basin fill of the Black Warrior basin in the southwest part of the region (Figures 2.5.1-6 and 2.5.1-10) indicates a foreland basin related to the Ouachita fold-thrust belt rather than the Appalachian fold-thrust belt (Thomas, 1989a).

Comparison of Figure 2.5.1-9 to Figures 2.5.1-10 and 2.5.1-11 shows that the overall tectonic framework of the Appalachian region known at the time of the EPRI-SOG study has not changed with respect to the location of major mapped structural features. Additional information and analysis of subsurface data (e.g., industry seismic reflection profiles, deep wells) and seismicity data, however, provide an improved understanding of structures within the Bellefonte Site (200-mile-radius), particularly with regard to the foreland Appalachian fold-thrust belt and possible relationships to subdetachment basement faults. The following sections: Section (a) Appalachian Thrust Belt and Section (b) Subdetachment Basement Faults describe these structures. More distant structures within the 200-mile-radius region are described in Section (c); Section (d) presents a description of the characteristics of seismicity zones that may be associated with subdetachment faults within the Appalachian thrust belt region.

#### **(a.) Appalachian Foreland Thrust Belt**

The Bellefonte Site lies near the cratonward limit of the Appalachian detachment that underlies the Appalachian foreland thrust belt (Figures 2.5.1-11 and 2.5.1-12). The Appalachian Plateau (Cumberland Plateau Section), Valley and Ridge, and frontal part of the Blue Ridge physiographic provinces encompass the Appalachian foreland thrust belt (also referred to as the Alleghanian foreland thrust belt, the Appalachian fold-thrust belt, or Appalachian fold-and-thrust belt) and foreland basins (Hatcher et al., 1989c). The southern Appalachian foreland thrust belt consists of a stack of mostly thin-skinned thrusts in an unconfined wedge configuration located above the Proterozoic basement and an eastern confined segment below the base of the Blue Ridge-Piedmont composite crystalline thrust (BRP) sheet that served as a rigid indenter that drove the foreland deformation (Hatcher et al., 1998).

In Alabama and Georgia, this thrust belt consists of late Paleozoic (Alleghanian), large-scale, northeast-striking, northwest-vergent thrust faults and associated folds bounded by undeformed strata in the Black Warrior foreland basin on the northwest and by the Talladega slate belt and Appalachian Piedmont on the southeast (Figure 2.5.1-14). The structural geometry and evolution of the thrust belt in Alabama and northeast Georgia is described by Thomas (2001), Thomas and Bayona (2002), and Bayona et al. (2003). Using outcrop data from published geologic maps, detailed local mapping in key areas, and interpretation of seismic reflection profiles (contributed by sources in the petroleum industry), deep well data, and paleomagnetic data, they developed a series of strike-perpendicular balanced cross-sections and strike-parallel



cross-sections (Figure 2.5.1-15). Representative strike-perpendicular cross-sections across the thrust belt in northern Alabama are shown in Figure 2.5.1-16. For cross-section development, the Paleozoic strata are divided into four units: Unit 1, a basal weak unit (Lower and Middle Cambrian strata dominated by fine-grained clastic rocks, mostly Rome and Conasauga Formations); Unit 2, a regionally dominant stiff layer (Knox Group); Unit 3, a heterogeneous carbonate-siliciclastic Middle Ordovician-Lower Mississippian succession (this unit includes the Greensport-Sequatchie Formations); and Unit 4, Upper Mississippian-Pennsylvanian synorogenic foreland deposits. The regional detachment (décollement) is within the basal weak layer above Precambrian crystalline basement.

As illustrated in these cross-sections, the northwestern (frontal) part of the thrust belt is dominated by broad, flat-bottomed synclines and large-scale, northeast-trending asymmetric anticlines. The top of basement beneath the leading imbricate faults is shallow and flat, but it abruptly drops southeastward across basement faults into the Birmingham graben. The depth of the regional detachment as well as the amplitude of thrust ramps, increases abruptly southeast of the Big Canoe Valley fault and Peavine anticline, which are positioned over the down-to-the-southeast boundary fault system of the Birmingham graben. The two major structures closest to the Bellefonte Site, the Sequatchie Valley thrust and the Big Wills Valley thrust, are shallow imbricate faults with relatively small displacement compared to the structures to the southeast. The fold-and-thrust belt is bordered to the southeast by the large-scale, low-angle Talladega Front fault at the northwest boundary of Piedmont metamorphic rocks.

Surficial traces of the generally persistent strike-parallel structures in the overlying thrust sheet southeast of the frontal fault-related folds are interrupted by four distinct northwest-trending transverse zones (TZ), which are referred to from north to south as the Rising Fawn TZ, the Anniston TZ, the Harpersville TZ, and the Bessemer TZ (Thomas, 1982) (Figure 2.5.1-14). Thomas (1991), Thomas and Bayona (2002), and Bayona et al. (2003) describe the changes in deformation styles along-strike across the TZs. These include along-strike termination of structures, abrupt curve or offset in strike, abrupt change in plunge angle or direction, abrupt along-strike change in dip, abrupt along-strike changes in stratigraphic level of a thrust fault, and abrupt along-strike change in structural style. Thomas (1982) notes that the cross-strike structural discontinuities that define the TZs are not lines, but rather are narrow bands (generally less than 12.5 miles wide) that encompass observations across several different northeast-trending Appalachian structures. Bayona et al. (2003) conclude that the along-strike changes in the thrust belt geometry are closely related to basement structural relief beneath the thrust belt. For example, tectonic thickening of graben-fill strata controls deformation southwest of the Anniston TZ (Gladsden mushroom in Sections D and E, Figure 2.5.1-16), whereas ramp and flat geometry is prevalent northeast of this TZ (Sections A, B, and C, Figure 2.5.1-15). Shallow, imbricate faults dominate the thrust belt in Georgia, where the top of basement dips gently to the southeast (Bayona et al., 2003).

The culmination of the Alleghanian orogeny occurred in the late Paleozoic. There is no new information to suggest that the thrust faults within the Appalachian foreland thrust belt are capable tectonic structures as defined by Regulatory Guide 1.165 (Appendix A) (USNRC, 1997). Seismicity in the region occurs primarily within basement rocks below the regional detachment and first motion analyses indicate predominantly strike-slip focal mechanisms (see discussion in Section (d)). Evidence for post-Cenozoic faulting or geomorphic evidence for Quaternary

deformation in the region is not reported in the published literature (Crone and Wheeler, 2000; Powell in Manspeizer et al., 1989).

### **(b.) Subdetachment Basement Faults**

It was recognized at the time of the EPRI-SOG study that potential seismic sources may be present below the Appalachian detachment or décollement (Figure 2.5.1-12). Subsequent studies have focused on better defining the location and geometry of basement structures. Of significance in the southern Appalachian region are known or inferred large normal faults that originally formed along the passive margin of the late Proterozoic to early Paleozoic Iapetus Ocean. Compressional reactivation of favorably oriented Iapetan faults has been suggested as the causal mechanism for several seismically active regions in the southern Appalachians including Giles County, Virginia, and eastern Tennessee (Bollinger and Wheeler, 1988; Wheeler, 1995) (see discussion in Section (d)). Bollinger and Wheeler (1988) suggest that the steep eastward rise in the unfiltered Bouguer anomaly field is the eastern limit for the Iapetan normal faults and that most of the faults occur in the relatively intact continental crust of North America west of the gravity rise. This gravity rise, referred to as the Appalachian (Piedmont) gravity gradient, is interpreted to mark the transition from thick continental to less thick, and possibly more mafic (transitional), crust to the east (Kean and Long, 1981; Hatcher and Zietz, 1980; Hutchinson et al., 1983).

Based on published interpretations of deep seismic reflection profiles across parts of the Appalachians and the Coastal Plain, Wheeler (1994) infers the southeastern boundary of preserved Iapetan faults to coincide with a narrow zone of intense thinning (ZIT) of Grenville crust that extends along the Appalachians coincident with the Appalachian gravity gradient. Wheeler (1996) notes that reflection profiles within the ZIT and farther southeast show structures that disrupted or destroyed the Grenville crust and any Iapetan faults within it during Paleozoic compressional and Mesozoic extensional deformation. Bollinger and Wheeler (1988) note that Iapetan normal faults likely decrease in size, abundance, and slip gradually and irregularly northwestward into the North American craton over a distance of perhaps 100 to 200 kilometers. The northwest boundary to Iapetan normal faults is based on the northwesternmost locations of known Iapetan faults, both seismic and currently aseismic (Wheeler, 1995). This boundary coincides approximately with the northwestward transition from a more seismically active continental rim to a generally less active cratonic interior (Figure 2.5.1-17).

Hatcher and Lemiszki (1998) and Hatcher et al. (1998) present a regional structure contour map on the basement surface beneath the Valley and Ridge and Blue Ridge and Piedmont of Alabama, Georgia, Tennessee, the Carolinas, and southwest Virginia (Figure 2.5.1-18). The basement surface is inferred from industry, academic, and U.S./state geological survey seismic reflection and surface geologic data, along with crustal seismic lines in the more internal parts of the orogen. The basement surface in this reconstruction dips gently southeast in the Tennessee embayment from Virginia to Georgia and contains several previously unrecognized rift-related large and small displacement Neoproterozoic-earliest Cambrian normal faults (Hatcher et al., 1988).

In Alabama and Georgia, more recent interpretation and analysis of industry data has provided a more detailed picture of the top of basement surface and sub-detachment basement faults (Thomas and Bayona, 2002; Bayona et al., 2003). The general depth to basement and the major basement structures that are interpreted from these data are shown in Figure 2.5.1-19. They note

that (1) along- and across-strike changes in thrust belt geometry are closely related to basement structural relief beneath the thrust belt; and (2) along-strike changes of the structural configuration of the top of basement are concentrated at northwest-striking basement faults, which offset northeast-striking basement faults (Bayona et al., 2003). The northwest-striking basement fault separates domains of contrasting structural profiles of basement fault systems, differing elevation of top of basement, and differing thicknesses of the regional décollement-host weak layer in the lower part of the sedimentary succession above basement rocks (Thomas and Bayona, 2002).

### (c.) Other Major Structures Within the Site Region (200-Mile Radius)

The major mapped faults and tectonic structures within the region (200-mile radius) represent deformation that occurred most recently in the Paleozoic. Except for minor faults reported in Miocene deposits in Tennessee (Whisner et al., 2003, see discussion in Section 2.5.1.1.2(d) Eastern Tennessee Seismic Zone), there is no reported evidence to indicate that any of these tectonic structures displace or deform late Cenozoic deposits or exhibit evidence for Quaternary deformation. Powell (in Manspeizer et al., 1989) describes evidence for Cretaceous faulting and Cenozoic tectonism in the Appalachians of the eastern U.S. Cretaceous and younger faults are recognized within the Coastal Plain, Piedmont, Blue Ridge, and Valley and Ridge physiographic provinces, but none lie within the 200-mile-radius region of the Bellefonte Site (Powell in Manspeizer et al., 1989). The Paleozoic structures in the region, therefore, are not considered to be capable tectonic sources, as defined in Regulatory Guide 1.165, Appendix A. A description of the principal structures in each of the physiographic provinces, excepting the structures in the Cumberland Plateaus, Valley, and Ridge Provinces that are described in detail in Section 2.5.1.1.2a, is provided as follows.

#### 1. Appalachian Plateaus Physiographic Province

The Plateaus of the southern Appalachians consists of a few large structures. The largest of these are the Pine Mountain thrust sheet and Sequatchie anticline-Cumberland Plateau overthrust (Figure 2.5.1-6). Important other smaller Plateau structures are the Lookout Valley (Peavine), Murphree Valley, and Wills Valley anticlines (Figure 2.5.1-12). These structures, which lie within the northwestern (frontal) part of the Appalachian fold-thrust belt (see discussion in Section 2.5.1.1.2(a)), are explained in terms of a connected system of ramps and flats (Wilson and Stearns, 1958). Faults and folds are connected, in that steps in basal detachments give rise to ramp anticlines. In the Plateaus, these large-scale, northeast-trending asymmetric anticlines are separated by broad, flat-bottomed synclines (Wiltschko in Hatcher et al., 1989c; Bayona et al., 2003). The Sequatchie Valley and Big Wills Valley anticlines and associated faults, which lie within the site vicinity (25-mile radius), are described in more detail in Section 2.5.1.2.4.

Three broad areas of the southern Appalachian Plateau are virtually undeformed. As described by Wiltschko in Hatcher et al. (1989) these are: (1) the broad region southeast of the Sequatchie Valley anticline but northwest of the Lookout Valley, Wills Valley, and Murphrees Valley anticlines that is macroscopically undeformed at the surface except for joints, although it is underlain by the basal detachment in the Rome Formation; (2) the area between the Pine Mountain thrust sheet and the Sequatchie anticline, which also is likely allochthonous, but is essentially undeformed except for jointing; and (3) the region northeast of the Pine Mountain thrust sheet, which exhibits minimal folding and no faulting.

## **2. Blue Ridge Physiographic Province**

The Blue Ridge Province is allochthonous; estimates of translation of the southern Appalachian Blue Ridge range from 156 miles to 175 miles (Cook et al., 1979; and Harris and Bayer, 1979, respectively), placing the external massif onto platform or platform margin sediments. The Blue Ridge is differentiated from the Valley and Ridge on the basis of the appearance of Cambrian and Precambrian rocks in the thrust sheets, metamorphism southeast of the frontal thrust zone, and increased complexity of deformation (Wiltschko and Geiser in Hatcher et al., 1989c). Blue Ridge rocks are mostly metamorphosed with grade increasing toward the southeast, and have been affected by more than one orogeny. The Blue Ridge may be divided into three subregions on the basis of the nature of exposed lithologies and bounding faults (Hatcher, 1978): (1) a western subregion of imbricate thrusts involving unmetamorphosed to low-grade rocks and some basement, transitional in structural style and degree of deformation to the Valley and Ridge Province on the west; (2) a central subregion containing most of the basement rocks, as well as metamorphic rocks of higher grade to the west; and (3) an eastern subregion bounded on the west by the Hayesville and Fries faults and involving medium- to high-grade metasedimentary and metavolcanic rocks (Wiltschko in Hatcher et al., 1989c).

In the southern Appalachians, the boundary between the Valley and Ridge and the Blue Ridge is a single fault or zone of faults. Westward-directed thrust faults of large displacement characterize the southern part of the Blue Ridge. There is considerable internal folding (e.g., Murphy syncline, Toxaway, Ela, and Bryson City domes) in addition to the thrusting. Much of the metamorphism, folding, and some of the faulting (Greenbrier, Allatoona-Hayesville faults, Shope, and others) clearly predate the Alleghanian orogeny (Hatcher et al., 1989c). Several of the structures formed during earlier orogenies have been reactivated to various degrees during the Alleghanian orogeny. The Alleghanian BRP thrust sheet is bounded on the west by the Blue Ridge fault system, which comprises the Talladega (Alabama), Cartersville (Georgia), Great Smoky (northern Georgia-southern Tennessee), and Holston Mountain (northeastern Tennessee), and Blue Ridge (Virginia) faults (Hatcher in Hatcher et al., 1989c).

The time of last motion of the Alleghanian faults of the Blue Ridge is younger than Mississippian, the youngest rock cut by any frontal Blue Ridge fault. Most of the internal deformation within the Blue Ridge attributed to the Alleghanian orogeny is brittle in nature; the thermal peak occurred earlier during the Taconic (Ordovician) orogeny (Wiltschko in Hatcher et al., 1989b).

## **3. Piedmont Physiographic Province**

Major structures within the Piedmont Physiographic Province include the Brevard fault, the Central Piedmont suture, and the Towaliga, Ocmulgee, and Modoc faults (Figure 2.5.1-11).

The Brevard fault defines the western boundary of the Piedmont Physiographic Province. The Brevard fault, a complex fault zone having a possible earlier history of dip-slip motion and an Alleghanian history of both dip- and strike-slip motion, is a major Alleghanian structure within the BRP thrust sheet (Hatcher in Hatcher et al., 1989c). A summary of earlier studies and models for the origin and structure of the Brevard fault zone is provided by Hatcher in Hatcher et al. (1989c).

The boundary structure between the Piedmont and Carolina terrane, which is recognized in potential field data as well as surface geology, is referred to as the Central Piedmont suture (Hatcher, 1987). It is interpreted to have formed when the Carolina volcanic arc terrane

was joined to North America during either the Taconic or Acadian orogenies, and was tightly folded during either the same or a later event, then suitably oriented segments were reactivated by dextral slip (i.e., the Towaliga, the Ocmulgee, and the Goat Rock fault zones) during the Alleghanian orogeny (Hatcher, 1989b; Hatcher in Hatcher et al., 1989b).

Along the eastern edge of the Piedmont in the Carolinas and Georgia is the Alleghanian Kiokee-Raleigh belt anticlinorium composed of middle to upper amphibolite-facies metamorphic rocks that contrasts with the older higher-grade rocks toward the west (Hatcher 1989a). This belt is interpreted to be a micro-continent that was accreted to ancestral North America during the Taconic orogeny. The western boundary of the Kiokee belt is the Modoc zone, an east-northeast-trending plastic shear zone. The southeast-dipping, east-northeast-trending August fault borders the southeast flank of the Kiokee belt. Alleghanian dextral strike-slip has been documented on the Modoc and the Augusta faults in the eastern Piedmont (Hatcher, 1989c).

#### **4. Interior Low Plateaus Physiographic Province**

Faults within the Interior Low Plateaus Physiographic Province within the northwestern part of the 200-mile-radius study region are part of the Rough Creek graben. Faults associated with the Rough Creek graben show strong evidence for initiation during Cambrian Iapetan phase rifting and reactivation during the mid-late Paleozoic Appalachian-Ouachita orogeny (Kolata and Nelson, 1991; Potter et al., 1995) (Figure 2.5.1-4). Mesozoic activity on the Rough Creek graben faults also is suggested by post-Permian displacements and regional correlation of extensional deformation associated with post-Permian to pre-Cretaceous rifting of the Pangea continental landmass (Kolata and Nelson, 1991). However, a lack of Mesozoic sediments in the Rough Creek graben and restriction of evidence for post-Permian deformation to the western portion of the Rough Creek graben, and a complex but moderately well-defined structural boundary limiting Mesozoic deformation to the west in the Fluorspar area are cited by Wheeler (1997) as a paucity of evidence for Mesozoic reactivation of the Rough Creek graben.

#### **5. Coastal Plain Physiographic Province**

Late Paleozoic orogenic structures exposed in the Appalachian Mountains of Alabama and the Ouachita Mountains of Arkansas extend beneath a cover of post-orogenic Mesozoic-Cenozoic strata in the Gulf Coastal Plain (Figure 2.5.1-10). In the eastern part of the region, post-Paleozoic erosion surface dips eastward beneath an eastward-thickening prism of post-orogenic Mesozoic and Cenozoic strata, and the strike of the post-Paleozoic surface approximately parallels the Appalachian strike (Thomas et al., 1989). To the south, the overlap limit as well as the strike of the post-Paleozoic surface, curves west and northwest and crosses the Appalachian strike at a large angle. The post-Paleozoic surface dips generally toward the Gulf of Mexico beneath a thickening prism of Mesozoic and Cenozoic strata. In the Mississippian embayment of the Gulf Coastal Plain, Mesozoic-Cenozoic strata extend entirely across the Paleozoic Appalachian-Ouachita orogenic belt and cover Paleozoic rocks in the Black Warrior basin (Figure 2.5.1-5).

The Paleozoic Black Warrior basin is defined by a homocline dipping away from the craton and extending beneath the cratonward-directed frontal structures of the Appalachian-Ouachita fold-thrust belt (Thomas, 1989a). The Black Warrior basin is bordered on the cratonward (north) side by the Nashville dome. A northwest-trending system of normal faults displaces the homocline down-to-southwest (Thomas, 1989a). On the southeast, the fault system intersects the front of the Appalachian fold-thrust belt at approximately 90°, and lateral ramps in some thrusts apparently are related genetically to the intersecting faults. The youngest rocks preserved in the Black Warrior basin (early Middle Pennsylvanian) are displaced by the faults.

#### (d.) Seismicity Zones

Higher rates of low- to moderate-magnitude earthquakes that are recognized in two regions of the Valley and Ridge Province of the southern Appalachians are referred to as the Giles County, Virginia, and the East Tennessee seismic zones (ETSZ). These two seismic zones, the Giles County, Virginia, and ETSZ were identified by several of the EPRI-SOG evaluation teams as distinct seismic source zones. Detailed studies of seismicity and potential field data that have been conducted since completion of the EPRI-SOG study provide new information regarding the characterization of these zones.

##### 1. Giles County, Virginia, Seismic Zone (GCVSZ)

Earthquake foci at Giles County in southwestern Virginia define a tabular zone that strikes N44°E and dips steeply to the southeast within Precambrian basement beneath Appalachian thrust sheets (Bollinger and Wheeler, 1983, 1988). This zone, referred to as the Giles County, Virginia, seismic zone (GCVSZ), is about 25 miles long, 6 miles wide, and from 3 to 16 miles deep (Bollinger and Wheeler, 1983; Bollinger et al., 1991). The zone is oriented at an angle of about 20° counter-clockwise to the east-northeasterly trend of the overlying, detached southern Appalachian structures (Valley and Ridge Province) and subparallel to the northeasterly trend of the central Appalachian structures in the northern part of the state (Bollinger et al., 1991). The largest known shock in the state, the 1897 Giles County earthquake (MMI = VIII, mb = 5.7), occurred within this zone near the Virginia-West Virginia border (Bollinger and Hopper, 1971). This event has been reassessed as an mb = 5 in the National Center for Earthquake Engineering Research (NCEER)-91 (Seeber and Armbruster, 1991) and the U.S. Geological Survey (USGS) (Mueller et al., 1997) earthquake catalogs. However, this magnitude is not consistent with the general felt effects of the earthquake (J. Munsey, TVA, personal communication, January 2004). EPRI (Johnston et al., 1994) concluded that the moment magnitude was **M** 5.9; this estimate was selected as the magnitude for the final catalog for the TVA dam safety seismic hazard assessment study (Geomatrix, 2004) and this study.

The seismic energy released by the GCVSZ appears to be released by predominantly strike-slip faulting that lies below the Appalachian detachment. Focal mechanisms of recent earthquakes exhibit mainly strike-slip motions on steeply dipping (>70°) planes that are right-lateral on the northerly striking nodal planes or left-lateral on the easterly striking nodal planes. The P-axes (maximum compressive stress axes) estimates are uniformly of a northeasterly (NNE to ENE) trend with subhorizontal inclination and are similar to the orientation of P-axes estimates elsewhere in the region. Based on an evaluation of the late Proterozoic and Phanerozoic structural history of the surrounding region, Bollinger and Wheeler (1988) concluded that only Iapetan rifting could have produced a fault with an orientation and depth like those of the tabular zone of foci. From seismic reflection profile data, Gresko (1985) interpreted a series of down-on-the-east, subdetachment faults, consistent with this hypothesis. Bollinger et al. (1991) also state that it is likely that the release of seismic energy within the GCVSZ is the result of reactivation of one or more faults formed initially by extensional stresses during Precambrian time.

No capable tectonic sources have been identified within the GCVSZ, but evidence for possible differential uplift of Quaternary terraces near Pearlsburg (Mills, 1986) and a zone of small late Pliocene to early Quaternary age faults have been identified in southwestern Virginia in the area of the GCVSZ, near Pembroke (Law et al., 1993, 1994, 1997; Crone and Wheeler, 2000).

These high-angle faults (the Pembroke faults) and a broad antiformal fold exposed in apparently young unconsolidated fluvial deposits have raised questions regarding the possibility of geologically recent tectonic faulting that may be related to seismic activity in this region (Bollinger et al., 1992; Law et al., 1993; Robinson et al., 1993). The deformation is of latest Pliocene or Quaternary age based on the age of the deformed sediments that have been dated using cosmogenic  $^{26}\text{Al}$  and  $^{10}\text{Be}$  analysis (Law et al., 1997). Law et al. (1994) present three models to explain the formation of the fold and fault structures at this site: landsliding, solution collapse, and basement faulting of tectonic origin. Although some researchers have noted that the correlation between surface faults and sub-detachment seismogenic structures may be tenuous or completely lacking (Chapman and Krimgold, 1994), Law et al. (1994, 1997) have concluded that a tectonic origin cannot be precluded based on the available data and interpretations. Crone and Wheeler (2000) rate the faults as Class B<sup>1</sup> because it has not yet been determined whether the faults are tectonic or the result of solution collapse.

More recent geophysical and subsurface investigations of these structures (Robinson et al., 2000; Williams et al., 2000; Law et al., 2000) provide additional constraints on the origin of the fold and faults. Robinson et al. (2000) show that voids occur in the terrace sediments that may result from cavity collapse in the underlying limestone, and that no features occur in the limestone basement that correspond to the fold and graben structure in the terrace deposits. Williams et al. (2000) map a linear depression in the limestone bedrock surface that corresponds to the graben in the terrace deposits, and they note that the fold and graben structure has a linear nature that is not consistent with formation due to a subcircular sinkhole. Law et al. (2000) show that the nature of fine structure in some of the terrace deposits is consistent with sedimentation in a depression formed by limestone solution, followed by inversion to form the anticlinal structure. These observations appear to indicate that some or all of the observed deformation is non-tectonic (probably related to solution collapse) in origin. Surficial mapping by Anderson and Spotilla (2001) of fractures in bedrock outcrops shows that the orientation of many small fractures is not consistent with topography or with karst-related subsidence. They note that one set of northeast-trending fractures cross-cuts the regional structural trend, is oriented consistent with the trend of the underlying seismic zone, and may be a surface manifestation of rupture in the seismic zone. However, this field evidence does not provide any direct evidence for Quaternary displacement on these fractures (Dr. J. Spotilla, personal communication, November, 2003). Therefore, definitive evidence for a capable tectonic source and for the recurrence of large earthquakes similar or larger than the 1897 Giles County earthquake is lacking.

## 2. Eastern Tennessee Seismic Zone (ETSZ)

The Eastern Tennessee seismic zone (ETSZ) is a well defined, northeasterly trending, 187-mile-long by less than 60-mile-wide belt of seismicity within the Valley and Ridge and Blue Ridge physiographic provinces of eastern Tennessee and parts of North Carolina, Georgia, and Alabama (Johnston et al., 1985; Bollinger et al., 1991; Powell et al., 1994; Chapman et al., 2002). This area, which lies within the 200-mile-radius region, is one of the most active seismic regions.

---

<sup>1</sup> Crone and Wheeler (2000) define Class A features as those where geologic evidence demonstrates the existence of a Quaternary fault of tectonic origin; Class B features as those where the fault may not extend deeply enough to be a potential source of significant earthquakes, or the currently available geologic evidence is not definitive to assign the feature to Class C or to Class A; and Class C features are those where geologic evidence is insufficient to demonstrate the existence of tectonic fault, or Quaternary slip, or deformation associated with the feature.

The largest recorded earthquakes in this zone are the 1973 MS 4.6 Maryville, Tennessee, earthquake (Stover and Coffman, 1993) (mb 4.6, Bollinger et al., 1991) and the recent April 2003 M 4.6 Fort Payne earthquake that occurred in northeast Alabama near the Georgia border (see discussion in Section 2.5.2.1). Focal depths of most earthquakes range from 3 to 14 miles, beneath detached Alleghanian thrust sheets (Vlahovic et al., 1998; Chapman et al., 2002). Focal mechanisms indicate strike-slip faulting on steeply dipping planes and a uniform regional stress field with horizontal maximum compression trending N70°E (Chapman et al., 2002). Most mechanisms involve either right-lateral motion on north-south planes or left-lateral slip on east-west planes (Chapman et al., 1997). Chapman et al. (2002) also note that a smaller population shows right-lateral motion on northeasterly trending planes, parallel to the overall trend of the seismicity. They note that the seismicity is not uniformly distributed; rather epicenters form northeasterly trending en-echelon segments.

The earthquakes are associated with major potential field anomalies (King and Zietz, 1978; Johnston et al., 1985; Bollinger et al., 1991; Powell et al., 1994; Kaufmann and Long, 1996; Vlahovic et al., 1998; Chapman et al., 2002) (Figure 2.5.1-20). The western margin of the ETSZ is associated with a prominent gradient in the total intensity magnetic field, the New York-Alabama (NY-AL) geophysical lineament (Chapman et al., 2002). Alternative structural models have been postulated to explain the association of seismicity with these anomalies. Powell et al. (1994) proposed that the ETSZ is an evolving seismic zone in which slip on north- and east-striking surfaces is slowly coalescing into a northeast-trending zone. They suggested that the ETSZ represents seismic activity that results from the regional stress field and is coalescing near the juncture between a relatively weak, seismogenic block (referred to as the Ocoee block by Johnston et al., 1985) and the relatively strong crust to the northwest that may be strengthened by the presence of mafic rocks associated with an inferred Keweenaw-age (1,100 million years old) rift (Keller et al., 1982). They note that the densest seismicity and the largest of the instrumentally located epicenters in the ETSZ generally lie close to and east of the NY-AL aeromagnetic lineament between latitudes 34.3°N and 36.5°N and west of the Clingman aeromagnetic lineament. They postulated that deformation within the ETSZ may evolve eventually into a thoroughgoing, strike-slip fault running along or near the entire northwest boundary of the Ocoee block in eastern Tennessee. Strike-slip motion would be consistent with both the sharp, apparently near-vertical nature of the boundary, as inferred from the aeromagnetic signature, and the orientation of the boundary in the contemporary stress field.

Based on detailed analyses of the pattern and focal mechanisms of earthquakes in the ETSZ, Chapman (1996) and Chapman et al. (1997) present a more refined picture of the nature of faulting in the region. Using a revised velocity structure model (Vlahovic et al., 1996), focal mechanisms and hypocentral locations were updated. Statistical analysis of trends in the earthquake focal mechanisms suggests that earthquakes occur primarily by left-lateral strike-slip on east-west-trending faults and to a lesser degree by right-lateral slip on north- and northeast-trending faults. The hypocenters suggest possible east-west-trending fault sources are up to 30 to 60 miles long and lie east of and adjacent to the NY-AL lineament. The analyses are consistent with a tectonic model in which seismogenic faulting is localized along a sharp contrast in crustal strength (competency) represented by the NY-AL lineament (Figures 2.5.1-20 and 2.5.1-21).

The faults inferred from the alignments of seismicity within the ETSZ as shown by Chapman et al. (1997) were used to localize seismicity as one alternative seismic source model in the LLNL



TIP study (Savy et al., 2002; see discussion of this study in Section 2.5.2.2.2). Based on more recent discussions with Dr. Chapman, who participated in the TVA Dam Safety Seismic Hazard Assessment (Geomatrix, 2004), it was concluded that the available data do not adequately constrain the locations of specific faults within the ETSZ and fault-specific sources were therefore not included in this study.

An alternative model to explain the localization of seismicity in the eastern Tennessee region is given by Long and Kaufmann (1994). Based on an analysis of the velocity structure of the region, they conclude that the seismically active areas are not apparently constrained by the crustal blocks as defined by the NY-AL lineament, but rather their locations are determined by low-velocity regions at mid-crustal depths. They suggest that the data support the conjecture that intraplate earthquakes occur in crust that may be weakened by the presence of anomalously high fluid pressures. Their data suggest that only a portion of the NY-AL lineament is consistent with the contact between two crustal blocks having different properties.

Chapman et al. (2002) conclude that the linear segments, and the locations of their terminations, may reflect the basement fault structure that is being reactivated in the modern stress field. They state that physical processes for reactivation of basement faults could involve a weak lower crust and/or increased fluid pressures with the upper to middle crust. There may be a marginal correlation between the seismicity and major drainage pattern and general topography of the region, suggesting a possible hydrological element linkage.

Detailed geologic studies focused on locating paleoseismic evidence of large magnitude prehistoric events have only been conducted in limited areas. Whisner et al. (2003) investigated a 300-square-kilometer (117-square-mile) area within the most active part of the ETSZ and found no concrete evidence of large prehistoric earthquakes. They noted, however, two other sites that would warrant further study. At the Gray fossil site in northeastern Tennessee, fractures and joints with little offset exist throughout Miocene clay units that are not inconsistent with the late Tertiary to Holocene stress field. Also, in the same region, apparent dewatering features, in particular a clay- and gravel-filled fracture in Miocene clay, are observed. Deformation is postulated to be related to either strong ground motion, or more likely, sinkhole collapse. At a site in Tellico Plains, Tennessee, disturbed and folded sediments in an older landslide or terrace deposit beneath younger Tellico River alluvium were recently discovered. Deformation at this site may be the result of soft-sediment deformation and liquefaction related to a prehistoric earthquake, or alternatively, it could be the result of dewatering and folding at the toe of a prehistoric landslide. Based on the extent of weathering in cobbles, Whisner et al. (2003) suggest that the older alluvium may be late Pleistocene or early Holocene in age.

#### **2.5.1.1.4.3 Significant Seismic Sources At Distances Greater than 200 miles**

The EPRI-SOG evaluation indicated that the seismic sources in the New Madrid, Missouri, and to a lesser degree, Charleston, South Carolina, regions were significant contributors to the hazard at the Bellefonte Site. The following summarizes new information regarding the characterization of these seismic sources.

##### **(a.) Seismic Sources in the New Madrid Region**

The New Madrid region is the source of the 1811-1812 New Madrid earthquakes, which include the three largest earthquakes to have occurred in historical time in the CEUS. Extensive geologic, geophysical, and seismologic studies have been conducted to characterize the location

and extent of the likely causative faults of each of these earthquakes and to assess the maximum magnitude and recurrence of earthquakes in this region. Table 2.5.1-1 provides a summary of recent publications pertinent to the identification and characterization of seismic sources in this region.

Kenner and Segall (2000) present a time-dependent model for the generation of repeated intraplate earthquakes that incorporates a weak lower crustal zone within an elastic lithosphere. Relaxation of this weak zone after tectonic perturbations transfers stress to the overlying crust, generating a sequence of earthquakes that continues until the zone relaxes fully. Model predictions mostly are consistent with earthquake magnitude, coseismic slip, recurrence intervals, cumulative offset, and surface deformation rates in the New Madrid seismic zone (NMSZ). In particular, the computed interseismic strain rates may be undetectable with available geodetic data, implying that low observed rates of strain accumulation cannot rule out future large-magnitude earthquakes. Modeling studies by Grollmund and Zoback (2001) show that the removal of the Laurentide ice sheet approximately 20 ka changed the stress field in the vicinity of New Madrid, causing seismic strain rates to increase by about three orders of magnitude. Their modeling predicts that the high rate of seismic energy release observed during late Holocene time is likely to continue for the next few thousand years.

Recent analysis of geodetic measurements from a permanent GPS array in mid-America that was installed in the mid- to late 1990s provides evidence for rapid strain rates in the NMSZ (Smalley et al., 2005). Rates of strain are of the order of  $10^{-7}$  per year, comparable in magnitude to those across active plate boundaries, and are consistent with known active faults in the region. Relative convergence across the Reelfoot fault (RF) is  $\sim 2.7 \pm 1.6$  mm/year. Relative fault-parallel, right-lateral motion of  $\sim 1$  mm/year is measured across the southern right lateral strike-slip fault zone, which is highlighted by a prominent northeast-trending and vertical zone of microseismicity and right-lateral focal mechanisms. Surface velocities at distances beyond a few fault dimensions (far-field) from active faults do not differ significantly from zero. It is not certain whether the driving force behind the current surface velocities is related to post-1811-1812 postseismic processes or to the accumulation of a locally sourced strain. The data indicate, however, that aseismic slip is almost certainly required across faults (or shear zones) within the upper few kilometers of the surface.

### **1. Central Fault System**

Van Arsdale and Johnston (1999) summarize the major structures within the Mississippi embayment that show evidence for Quaternary activity. The principal seismic activity within the upper Mississippi embayment is interior to the Reelfoot rift along the NMSZ. The NMSZ consists of three principal trends of seismicity; two northeast-trending arms with a connecting northwest-trending arm. This seismicity pattern has been interpreted as a northeast-trending, right-lateral strike-slip fault system with a compressional left-stepover zone (Russ, 1982; Schweig and Ellis, 1994). The southern arm is coincident with the subcrop Blytheville arch (BA); the central arm is coincident with the subcrop Pascola arch and surface Lake Country uplift; and the northern arm trends at a low angle to the western margin of the Reelfoot rift (Figures 2.5.1-22 and 2.5.1-23). Johnston and Schweig (1996) identify the following fault segments within the central fault system of the NMSZ: BA; Blytheville fault zone (BFZ); Bootheel lineament (BL); New Madrid west (NW); New Madrid North (NN); RF; Reelfoot south (RS) (Figure 2.5.1-24). They outline three rupture scenarios associating each of the three 1811-1812 earthquakes with fault segments (individually or in various combinations) using historical

accounts and geologic evidence (Figure 2.5.1-24). Their interpretation is consistent with the spatial distribution and source characteristics of contemporary NMSZ seismicity (Figure 2.5.1-25).

The December 16, 1811, earthquake (referred to by different authors as either the D1 or NM1 earthquake), is believed to have occurred on the southern arm of seismicity (possibly the Cottonwood Grove-Ridgley fault system) associated with the BA, a major crustal transpressional fault structure identified from seismic-reflection data. Mueller et al. (2004) and Bakun and Hopper (2004a) both infer a location for this event on the northern end of the BA (just south of the intersection of the BL and the BFZ (also referred to as the Cottonwood Grove fault)). Two alternative geometries for the main fault rupture are outlined by Johnston and Schweig (1996): BA/BL (preferred) or BA/BFZ (Figure 2.5.1-24).

The causative fault for the January 23, 1812, earthquake (referred to by different authors as either the J1 or NM2 earthquake) is generally inferred to be the northern seismicity arm of the NMSZ (segment NN) (Figure 2.5.1-24). Toro and Silva (2001) following Van Arsdale and Johnston (1999) refer to this fault as the East Prairie fault. Baldwin et al. (2002) suggest that the North Farrenburg lineament may be associated with the NN and may represent the surface expression of coseismic rupture from the January 23, 1812, earthquake. Johnston and Schweig (1996) also consider an alternative scenario (S#3, Figure 2.5.1-24) in which the source for the January 23, 1812, event is fault NW (the west-trending zone of seismicity that lies along trend of the RF) (Figure 2.5.1-24). In this alternative model, both the NN and RFs ruptured in the February 7, 1812, event.

A possible northward continuation of the NN fault is suggested by a second-order seismicity pattern that is emerging slowly from the regional seismic network data. Braile et al. (1997) have identified two parallel trends of concentrated seismicity ~60 miles long that extend north-northeast from the central NMSZ to within 9 miles of the Illinois/Kentucky border (Wheeler, 1997; Woolery and Street, 2002).

Mueller et al. (2004) and Hough et al. (2005) infer that the NM2 mainshock may have been a remotely triggered earthquake with a location some 200 to 250 kilometers (120 to 150 miles) north of the New Madrid earthquake in the Wabash Valley of southern Illinois and Indiana. Bakun and Hopper (2004a) discount more northerly locations based on the absence of 1811-1812 liquefaction features that would indicate a source in that region. They follow Johnston and Schweig (1996) in assigning the NM2 event to the NN.

The February 7, 1812, earthquake occurred on the RF, which connects the two other fault zones through the stepover region (Johnston and Schweig, 1996). The Reelfoot scarp is the surface expression of a west-dipping reverse fault that lies within the left-stepping restraining bend between two dextral strike-slip arms of the NMSZ (Russ, 1982; Sexton and Jones, 1986; Kelson et al., 1992, 1996; Schweig and Ellis, 1994). The fault and associated fold are defined by microearthquakes (Pujol et al., 1997); seismic-reflection profiles (Sexton and Jones, 1986; Odum et al., 1998; Van Arsdale et al., 1999); surface topography; shallow trench excavations (Russ, 1982; Kelson et al., 1992, 1996; Mueller et al., 1999); and borehole data (Milhills and Van Arsdale, 1999; Champion et al., 2001). Using the constraints on fault geometry derived from interpretation of microearthquakes and seismic-reflection profiles and the amounts of surface deformation based on geomorphic and trenching investigations, the slip rate for the RF is estimated (Mueller et al., 1999; Van Arsdale, 2000; Champion et al., 2001) (see Table 2.5.1-1).

Mueller and Pujol (2001) use these constraints on geometry, slip rate, and displacement during historical and prehistoric events to estimate the rate of late Holocene moment release and the magnitudes of earthquakes for the two most recent strain cycles.

Maximum magnitudes in the New Madrid region are based largely on the analysis of intensity data from the 1811-1812 earthquake sequence (Johnston, 1996b; Johnston and Schweig, 1996; Hough et al., 2000; Mueller et al., 2004; Bakun and Hopper, 2004a) and to a lesser degree on magnitude assessments inferred from paleoliquefaction features (Tuttle et al., 2001, 2002) (Table 2.5.1-2). Cramer (2001) calculates the range of characteristic magnitudes for fault segments that capture the range of uncertainty in the dimensions of the segment rupture (length and width of the seismogenic crust) and choice of magnitude/area relationship (Table 2.5.1-3). Mueller and Pujol (2001) provide an additional assessment of past earthquake magnitudes through detailed mapping of the geometry and area of the RF, combined with estimates of fault slip rate, recurrence, and displacement in individual events to estimate the rate of late Holocene moment release.

Constraints on the recurrence of large-magnitude earthquakes in the NMSZ come from paleoliquefaction studies (Saucier, 1991; Tuttle, 1993, 1999, 2001a; Tuttle and Schweig, 2001; Craven, 1995; Li et al., 1998; Tuttle and Schweig, 1996, 2000; Tuttle et al., 1998, 1999, 2000, 2002; and Tuttle and Wolf, 2003) and from evaluation of fault-related deformation along the Reelfoot scarp (Kelson et al., 1992, 1996). The age constraints for these events are summarized in Table 2.5.1-4. Findings from these studies indicate that major earthquakes occurred in the New Madrid region in AD 1450 ± 150 year and AD 900 ± 100 year (Figures 2.5.1-26 and 2.5.1-27) (Tuttle and Schweig, 2001; Tuttle et al., 2002). Saucier (1991) presents evidence for a significant earthquake in the northern part of the New Madrid region in about AD 490 ± 50 year. Tuttle and Schweig (2001) document evidence for two major earthquakes in the same area, about AD 300 ± 200 year and BC 1370 ± 970 year. Given uncertainties in dating liquefaction events, Tuttle et al. (2002) note that the time between any pair of the past three New Madrid events may have been as short as 200 years or as long as 800, with an average of 500 years (Figure 2.5.1-28). Tuttle (2001a) notes that similarities in the size and spatial distributions of historical (1811-1812) and paleoliquefaction features indicate the NMSZ was the likely source of the two paleoearthquakes that are recognized regionally. Tuttle et al. (2002) document evidence that prehistoric sand blows, like those formed during the 1811-1812 earthquakes, probably are compound structures resulting from multiple earthquakes closely clustered in time (earthquake sequences).

## **2. Reelfoot Rift Marginal Faults**

Other faults located at or near the southeast and northwest margins of the Reelfoot rift are thought to be rift-bounding normal faults that have been reactivated as oblique thrusts or transpressional strike-slip faults in the current stress regime. Faults located on the northwest margin of the Reelfoot rift, including the faults in the Benton Hills and English Hills are not significant sources for the Bellefonte Site. Faults on the southeast margin, which are closer to the Bellefonte Site, are discussed as follows.

Several recent studies have concluded that the southeastern Reelfoot rift margin is a fault zone characterized by recurrent movement in the Quaternary, with the most recent event occurring within the Holocene. The Crittenden County fault zone (CCFZ), located 25 kilometers northwest of Memphis, Tennessee, was initially identified as a potential source of damaging earthquakes (Crone, 1992; Williams et al., 1995) (Figure 2.5.1-23). The CCFZ is a down-to-the-

east reverse fault (Luzietti et al., 1992). High-resolution seismic reflection and refraction data show that the 32-kilometer-long CCFZ in northeastern Arkansas has deformed and faulted beds of Pleistocene (and possibly Holocene) age and that recurrent movement may have occurred on the fault zone in the Quaternary (Williams et al., 1995). Mihills and Van Arsdale (1999) also suggest that Holocene uplift may be associated with the CCFZ. The CCFZ roughly coincides with the southeastern margin of the northeast-trending Reelfoot rift (Figure 2.5.2-23). Based on this coincidence, Crone (1992) suggests that pre-existing normal faults within the rift may have been re-activated as reverse faults during the late Miocene and Tertiary.

Chiu et al. (1997) reported a distinct seismicity lineation appears to be associated with the southeastern Reelfoot rift margin approximately 25 kilometers to the northeast of the CCFZ. They noted that focal mechanisms suggest that minor faulting on this margin is characterized by right-lateral, strike-slip with high-angle thrust faulting. The faulting is generally consistent with an east-west oriented, maximal, horizontal, compressional stress, similar to the regional stress regime. Based on analysis of intensity data, Hough and Martin (2002) conclude that a large aftershock of the December 11, 1811, New Madrid earthquake ( $M 6.1 \pm 0.2$ ), occurred within the southwestern one-third to one-half of this band of seismicity. Cox et al. (2001a) suggest that a fault system along the southeastern margin of the Reelfoot rift (referred to as the Big Creek fault zone by Cox et al., 2001b; Figure 2.5.1-29) is currently accommodating right-lateral strain along the boundary of the hanging wall of the Reelfoot thrust. They note that little if any strain is accumulating on the principal (southern) arm of the central New Madrid fault system and that earthquakes defining this fault are primarily aftershocks of an event that occurred on that arm during the 1811-1812 sequence. The southeastern rift margin coincides with a 150-kilometer-long linear topographic scarp from near Memphis to the Tennessee-Kentucky line, and S-wave reflection profiles, auger data, and a trench excavation reveal late Wisconsin-Holocene surface faulting and late Holocene liquefaction associated with this fault-line scarp. Based on variation in sense of throw along-strike and flower-structure geometry observed in seismic profiles, they conclude that this fault is a strike-slip fault. Cox et al. (2001a) suggest that lateral slip on the southeastern rift margin is greatest southwest of the restraining bend (adjacent to the Reelfoot thrust hanging wall). In this area, 25 meters of reverse separation underlies the bluff along the southern part of the margin. On the northern segment, the rift margin is characterized by a less prominent scarp (9 meters high) and a lack of seismicity. Evidence for latest Pleistocene to Holocene activity is noted for the CCFZ at the southern end of the fault zone (Williams et al., 1995) and along the Big Creek fault zone (BCFZ) at the Meeman-Shelby and Proctor Gap sites (Cox et al., 2001a and 2002; Figure 2.5.1-29). Cox et al. (2001a) present evidence for a faulting event between approximately 18 ka and 9.68 ka. Cox et al. (2002) present evidence for 8 to 15 meters of offset of a late Wisconsin paleo-channel (~20 ka) at a site near Porter Gap (Figure 2.5.1-29), suggesting an average slip rate of between 0.85 mm/year and 0.37 mm/year. They also present evidence for an earthquake circa 2500 to 2000 years before present (ybp) on the southeastern Reelfoot rift margin that ruptured  $\geq 80$  kilometers from Shelby County (15 to 25 kilometers north of Memphis metropolitan area) to Porter Gap. The recurrence data indicate two events occurring in the past 18 to 20 ka.

#### **(b.) Seismic Source in the Charleston, South Carolina, Region**

The 1886 Charleston, South Carolina, earthquake was the largest earthquake occurring in historical time in the eastern U.S., and is considered to have a moment magnitude in the range of 6.8 to 7.5 (Bakun and Hopper, 2004a; Johnston, 1996b; Martin and Clough, 1994; Nuttli et al., 1979). Based on the felt intensity reports defining the meizoseismal area (area of maximum

damage) and the occurrence of continuing seismic activity (the Middleton Place Summerville seismic zone), the epicentral region of the 1886 earthquake is considered to be centered northwest of Charleston. Recent published and unpublished studies for information on the potential location and extent of the Charleston source and the maximum characteristic earthquake expected to occur on it are described as follows.

Several types of data provide constraints on the location and extent of the source fault(s) for Charleston-type earthquakes in the Atlantic Coastal Plain. Bollinger (1977) reviewed the original interpretation of the meizoseismal area by Dutton (1889) and concluded that the meizoseismal area of the 1886 Charleston earthquake forms an elliptical zone roughly 20 miles wide (northwest-southeast) by 30 miles long (northeast-southwest). This zone is centered northwest of Charleston near Middleton Place, and extends from Charleston to Jedbarg, South Carolina. This region is characterized by ongoing seismicity in the so-called Middleton Place-Summerville seismic zone (MPSSZ) (Figure 2.5.1-30). Possible causative source faults for the Charleston earthquake within the meizoseismal region include the Woodstock and Ashley River faults, and Woodstock lineament (Talwani, 1982; Marple and Talwani, 1992; Marple et al., 1994). Talwani (2000) indicates that the northeast-trending Woodstock fault is cut and offset approximately 5 to 7 kilometers near Summerville by the northwest-trending Ashley River fault (Figure 2.5.1-30). Talwani also suggests that the 1886 earthquake was associated with right-lateral strike-slip movement along the offset segments of the Woodstock fault and uplift along the Ashley River fault.

Marple and Talwani (2000) and Talwani (1999) describe a potential causative source for the earthquake that extends beyond the 1886 epicentral region. One possible extended source is the southern segment of the zone of river anomalies (ZRA) (ZRA-S in South Carolina) of the East Coast fault system (ECFS; Figure 2.5.1-31; Marple and Talwani, 2000). The ECFS is a 600-kilometer-long north-northeast-trending inferred fault system that is based on a series of anomalous changes in fluvial geomorphology (ZRA), coincident with linear aeromagnetic anomalies and buried and surficial faults (Marple and Talwani, 2000). The ECFS is divided into three segments, with the strongest geomorphic evidence for tectonic activity associated with the southernmost segment, ZRA-S (Figure 2.5.1-32).

Other features in the vicinity of the meizoseismal region of the 1886 earthquake that are considered potential sources of large-magnitude earthquakes include strike-slip faults that bound Mesozoic rift basins and inferred/mapped faults bounding regions of tectonic warping. Behrendt and Yuan (1986, 1987) and Tarr et al. (1981) note the association of the MPSSZ (and the meizoseismal region of the Charleston earthquake) with a buried Mesozoic basin in South Carolina. No specific evidence for reactivation of basin-boundary faults has been identified, except where those faults are coincident with the ZRA-S. Weems and Lewis (2002) evaluate tectonic warping in the Charleston area from stratigraphic data and suggest that two northwest-trending faults (the Adams Run and Charleston faults) accommodate tectonic movement in a hinge zone (Figure 2.5.1-30). These authors indicate that slip on these inferred boundary faults and on the Ashley River and Woodstock faults may have caused the 1886 Charleston earthquake.

The spatial distribution of seismically induced liquefaction features along the Atlantic seaboard has been used to assess the location and timing of pre-1886 earthquakes (Obermeier et al., 1985, 1990; Amick et al., 1990; Amick and Gelinas, 1991; Rajendran and Talwani, 1993; Talwani and Cox, 1985; Talwani et al., 1999) (Figures 2.5.1-32 and 2.5.1-33). These studies suggest that during

the past 2,000 to ~6,000 years, large earthquakes ( $m_b \geq 5.8 \pm 0.4$ ) have been restricted to South Carolina (Figure 2.5.1-33).

Talwani et al. (1999) and Talwani and Schaefer (2001) established a more precise chronology for paleoliquefaction events observed in the coastal plain sediments of South Carolina. Eight paleoliquefaction events have been identified during the past 5,800 years (Table 2.5.1-5). Six of these events appear to have resulted from earthquakes occurring on the same source as the Charleston earthquake. These six events (including the two most recent prehistoric events) appear to have been of similar magnitude to the 1886 earthquake, based on the similarities in the spatial distribution of generated liquefaction features (Amick et al., 1990; Talwani et al., 1999; Talwani and Schaefer, 2001) (Figure 2.5.1-34).

Maximum magnitudes in the Charleston region are based largely on the analysis of intensity data from the 1886 earthquake sequence and to a lesser degree on magnitude assessments inferred from paleoliquefaction features. Johnston (1996b) suggested a preferred value of  $M 7.3 \pm 0.26$  for the 1886 earthquake. Earlier magnitude estimates (Bollinger, 1977; Nuttli et al., 1979) gave an  $m_b$ , ranging from 6.6 to 6.9. In a recent approach, Bakun and Hopper (2004a) developed a method to directly invert intensity observations. They obtained an estimate of  $M 6.9$  (6.4 to 7.2 at the 95<sup>th</sup> percent confidence level) for the 1886 earthquake.

An alternative approach for estimating the magnitude of the 1886 earthquake relies on back-calculation of ground motions from the liquefaction evidence (Martin and Clough, 1994; Hu et al., 2002a, b). Martin and Clough (1994) conclude that the liquefaction evidence from the 1886 earthquake is consistent with an earthquake no larger than  $M 7.5$ , and possibly as small as  $M 7.0$ . Hu et al. (2002b) estimate magnitudes in the range of  $M 6.8$  to  $7.8$  for paleoearthquakes attributed to the Charleston source. Leon et al. (August 2005) reevaluated the prehistoric earthquake magnitudes and peak ground acceleration (pga) (g) from the spatial distribution of paleoliquefaction features and in situ geotechnical data corrected for aging effects and estimated that the magnitude estimates for prehistoric events should be lowered about 0.9 magnitude units. They estimate that the prehistoric earthquakes that occurred during the past 6,000 years in the South Carolina Coastal Plain had moment magnitudes between approximately 5 and 7 and peak ground accelerations between about 0.15 and 0.30g when aging factors are considered (Table 2.5.1-6).

## 2.5.1.2 Site Geology

The following sections present a summary of geologic conditions of the Bellefonte Site and site area. They provide information concerning the physiography, geologic history, stratigraphy, engineering geology, and groundwater conditions relative to the Bellefonte Site. The information presented is based on a review of previous BLNP reports and documents, review of geologic literature, communications with TVA personnel who are familiar with previous BLNP studies and other researchers, and the results of geotechnical and geologic field investigations conducted at and in the vicinity of the Bellefonte Site.

### 2.5.1.2.1 Site Physiography and Topography

The Bellefonte Site is located in the Browns Valley-Sequatchie Valley segment of the Cumberland Plateau section of the Appalachian Plateaus Physiographic Province (Figure 2.5.1-1). The regional physiography has been discussed in Section 2.5.1.1.1.

The Bellefonte Site lies on the southeast side of the valley that separates Sand Mountain from the Cumberland Plateau (Figure 2.5.1-35). It is known as Browns Valley in Alabama. To the northeast in Tennessee it is known as the Sequatchie Valley. The Browns Valley-Sequatchie Valley extends northeast-southwest for approximately 140 miles, from Crab Orchard, Tennessee, to the vicinity of Blount Springs, Alabama. This valley was formed from erosion of the Sequatchie anticline. Where erosion breached the arch of thick sandstone and exposed the dolomite and limestone, an axial valley was developed. The valley is regionally bounded on the southeast by the prominent flank of Sand Mountain, which rises to about 1,400 feet above msl. The highly dissected and irregular edge of the Cumberland Plateau, which rises to similar elevations, forms the northwestern flank of the valley. The present valley floor is in all respects like those of the folded Valley and Ridge Province to the east. As a result of the easier weathering of the weaker rocks below the sandstone cover, the valley walls, which are bounded by escarpments, remain steep. The straightness of the valley merely reflects the straightness of the structural contours. Base-leveling of the upturned hard rocks on the flanks was never completed and these remain as low monoclinical ridges that are interrupted at intervals by gaps cut down to general level.

The site is on the right bank of Guntersville Reservoir at river mile 391.5 in Jackson County, Alabama. At the site, the valley is approximately 8 kilometers (5 miles) wide, and the Tennessee River flows southwestward, forming the upper reaches of the Guntersville Reservoir (Figures 2.5.1-35 and 2.5.1-36). The river had entrenched its course to about 570 feet msl before impoundment of the reservoir. The Bellefonte Site occupies the gently rolling terrain of the river valley (around 610 feet msl). Directly southeast of the plant, a low ridge is developed in the more resistant beds of the southeastward-dipping Red Mountain Formation (Figure 2.5.1-36). The ridge separates the site from the Tennessee River by a distance of about 3,000 feet and stands at an elevation of about 800 feet msl. Gaps in the ridge are due to erosional development along normal dip joint systems, and no cross faulting is evident (BLNP FSAR, 1986).

Northwest of the site, the land slopes gently downward to a linear depression known as the Town Creek embayment. Quite typical of the area, the Town Creek embayment as well as the Dry Creek embayment to the southwest and the Mud Creek embayment to the northeast, show erosional development along the more soluble belts of the Lower Chickamauga and Upper Knox. The Knox Group underlies the Chickamauga and outcrops to the northwest near the reservation boundary.

Similar to the existing BLNP Site, the Bellefonte Site is underlain by limestone of the Chickamauga Formation of Middle Ordovician age. At the site, the Chickamauga is primarily overlain by a relatively thin (0 to 40 feet) regolith of residual silts and clays derived from in-place weathering of the underlying rock. As shown in Figure 2.5.1-37, overburden has been disturbed by plant construction activities. In many undisturbed areas, there is no sharp interface between residuum and sound rock (Julian, 1993). Drilling and excavation experience at the site and in adjacent areas shows that the residual soil transition through weathered rock to hard, unweathered bedrock can be gradual in the natural shallow subsurface profile in some places, or consist of soil in direct contact with hard bedrock in other places. Most of the Bellefonte Site lies in areas disturbed by construction activities of the BLNP. Those areas are covered with placed fill, gravel roadways and parking areas, and concrete building foundation pads. The Bellefonte Site is relatively flat to very gently sloping toward local drainages. Relief across the Bellefonte Site is generally less than about 10 feet. Surface drainage within the



Bellefonte footprint is toward the Town Creek embayment to the northwest via shallow ditches that transect the site. A shallow divide just east of the Bellefonte footprint separates this northwest drainage from an easterly flowing stream that flows toward the Tennessee River through a water gap in the ridge.

### 2.5.1.2.2 Site Area Geologic History

The geologic history presented herein is an overview of the geologic history of the site area and vicinity. The overall tectonic framework of the region is outlined in Sections 2.5.1.1.2 and 2.5.1.1.4. Generally, current understandings and thoughts on the geologic history of the area around the Bellefonte Site have not changed significantly since the BLNP FSAR (1986) report was prepared. Changes in geologic thought and interpretation of past events deal more with the inferred details of the mechanics of the thrust faulting and folding of the bedrock units, and not with the ages of deformation or mapped positions of the bedrock units and structural features (see discussion in Section 2.5.1.1.4(a)). Changes in interpretation that have occurred in the interim include the differentiation of the Ordovician limestones at the site into as many as three or four separate formations by some workers, and the general recognition of the Chattanooga Shale as being of Devonian rather than Mississippian age. There is no compelling reason to follow this differentiation, however, and the Ordovician system nomenclature used in the original BLNP FSAR (TVA, 1986) will be retained. Those limestones underlying the Bellefonte Site footprint will be referred to as the Chickamauga Limestone. The Chattanooga Shale assignment to the Devonian system will be followed. The stratigraphic column in the Appalachian thrust-belt region of Alabama is presented in Figure 2.5.1-6.

The earliest history of the area is recorded in the basement complex of metamorphosed rock that lies more than 1.5 miles below land surface. Those rocks have been dated by K-Ar dating techniques and are reported as being from 750 to 1,000 million years old (Neathery and Copeland, 1983, as reported by Raymond, et. al., 1988). There is a gap in the geologic record between when the basement rocks were formed and when the near-surface sedimentary rocks exposed in the area were deposited or placed on them. The oldest rocks visible at the surface or projected into the area from regional studies are of early Cambrian age. These rocks are about 500 million years old.

The geologic history of this area for the past half billion years can be generally broken into two primary episodes: the early history when marine and near-shore deposits of limestones, shales, and sandstones of Paleozoic age were deposited on top of the basement complex rocks, and the more recent history when the site generally was well above sea level and subjected to mostly erosional geologic conditions during the Mesozoic and Cenozoic Eras. There is a gap in the geologic record in north Alabama between the youngest Paleozoic rocks in the area, the Pottsville Formation of Pennsylvanian age, and the present. Elsewhere in Alabama, deposits assignable to the time represented by the later part of this gap are present. There are no deposits in Alabama or eastern Tennessee of Permian through early Cretaceous age other than a few intrusive igneous rocks assignable to Triassic age in east Alabama. The time represented by this gap in the record in northeast Alabama adjacent to the Bellefonte Site covers many millions of years and includes the period when the Paleozoic rocks at the site were thrust upward and westward to their present positions. The period of time since the last period of thrust faulting and mountain building in the early Mesozoic has been primarily one of erosion of the current land surfaces in north Alabama. Most deposits that might have been formed there during that time have been subsequently removed by erosion.

Episodes of uplift and erosion also periodically occurred during the Paleozoic Era, but the geologic record in this area for that time is mainly represented by marine rocks deposited in marine or near-shore marine environments. The periods of uplift and erosion are represented by erosional surfaces or unconformities in the stratigraphic record. The most significant of these unconformities roughly coincide with the breaks between the various geologic formations mapped in the area, although minor unconformities also occur within some of the rock units.

During early Paleozoic time, the part of North Alabama in which the Bellefonte Site lies was often covered by a shallow inland sea. The oldest rocks on top of the basement complex are shales and marine carbonate rocks such as limestones and dolomites that were deposited here in the Cambrian and Ordovician Periods. Unconformities developed between rocks of Cambrian and early Ordovician age (Knox Group) and Middle Ordovician age (Chickamauga Limestone equivalent beds) suggest intervals of uplift and sub aerial erosion occurred. Volcanic activity in the Ordovician released ash and these formed thin beds of bentonite clay within the Chickamauga limestone. These clays are laterally continuous and widespread throughout north Alabama, Georgia, and Tennessee in rocks of this age. Toward the later part of the Ordovician Period and into the Silurian, continental uplift and mountain building was associated with the uplift and erosion of the Nashville Dome and adjacent land masses, which in turn resulted in clay and sand being washed into and deposited within the area. These events are represented in the stratigraphic record by shales and sandstones. Unconformities between the rocks of differing age deposited during this time indicate periods of additional uplift and erosion accompanied by relative, local sea level rise and fall. Iron-rich sediments deposited here during the Silurian Period (i.e., the Red Mountain Formation) indicate local environmental conditions changed significantly enough to allow primary deposition of iron-rich deposits in near-shore marine conditions. Following the time when the Silurian system rocks were deposited here, significant uplift occurred and a regional unconformity developed before the deposition of the Devonian rocks. Sandstones and shales (i.e., the Frog Mountain Sandstone and Chattanooga Shale) deposited at this time indicate further inundation and adjacent landmass erosion. In places the deposition apparently continued relatively unabated into the Mississippian Period and less erosion of adjacent land occurred, as evidenced by thick deposits of Mississippian age limestones. Some apparently primary chert deposition in the middle Mississippian Period (Fort Payne Chert) indicates that environmental conditions were again altering and relatively unique, at least for some period of time. Cleaner limestones, containing less clastic material, overlying the Fort Payne indicate that the marine environments typical of shallow seas like those of the Cambrian and Ordovician Periods returned to the area. Shales and sandstones deposited elsewhere in north Alabama in the late Mississippian Period (i.e., the Floyd and Parkwood shales and Hartselle and Pride Mountain sandstones) indicate the relative sea level was beginning to drop and that significant erosion of nearby land masses was occurring. Beginning at the end of the Mississippian Period and extending throughout the Pennsylvanian Period, the entire area of northeast Alabama and eastern Tennessee occupied the shore line area at the edge of the sea. Deposits represented here include sandstones typical of beach deposition altering with stream deposits, near-shore muds and clays, and occasional coal beds. Apparently, the rise and fall of relative sea level in the area occurred in a cyclic pattern with altering periods of submergence and subsequent uplift and vegetation. This resulted in the layering of sandstones, shales, and coal beds typical of the Pottsville Formation.

Following the Pennsylvanian Period, there is no record of significant deposition of geologic units occurring in northeast Alabama through the present time. At that time, the Alleghanian

orogeny was causing the thrusting and faulting observed today in the northeast to southwest trending valley and ridge system common to this part of the country. Associated mountain building caused the Appalachians to rise again. As the mountains rose, erosion began and that resulted in the beginning of Gulf and Atlantic Coastal Plain clastic deposition. This deposition began in the Mesozoic Era and generally continued through to today, although the general deposition was interrupted by periods of uplift and erosion and some gaps occur in the coastal plain record.

No geologic depositional evidence of the time between the Pennsylvanian through the Quaternary is preserved near the Bellefonte Site. The primary geologic processes during this time in the Bellefonte area were erosional in nature. In the major river channels, erosion cut down to bedrock in most places and scoured the unconsolidated alluvial deposits away, leaving little geologic record for the last 135 to 150 million years of the earth's history. Away from the streams, thick residual soils developed in place over the carbonate units as a result of chemical weathering. Colluvial deposits developed to cover most hill slopes as the uppermost rock layers (generally sandstones that are resistant to weathering in this climate) slowly broke down or were undercut by erosion of softer underlying beds, and migrated down the slopes. As local base levels controlling the groundwater system dropped, karst processes began to dissolve deeper channels in some of the soluble bedrock units and caves, and sinkholes formed in some places. A few of these karst features were sites for very localized deposition, like the Gray Fossil Site in eastern Tennessee (Whisner et al., 2003). The Gray Fossil Site preserved a late Miocene or Pliocene vertebrate fauna indicative of a forested ecosystem. More commonly, the karst features that developed on some bedrock units continued to enlarge and were significant factors in the erosional process. Over the Knox Group deposits northwest of the site footprint, large shallow closed depressions in the land surface, or sinkholes, show where significant karst development has occurred. On other units, like the Chickamauga Limestone, no closed depressions are present, indicating that much less karst development occurred in that stratum. Differences in lithology and bedrock susceptibility to groundwater movement and dissolution account for the different rates of karst feature development on the different rock units.

### 2.5.1.2.3 Site Area Stratigraphy

The general stratigraphy of the bedrock units present in the Sequatchie Valley has been understood for many years. While changes in the rock formation names or differences in correlations between rocks there and in adjacent parts of Alabama, Tennessee, and Georgia may have changed slightly, the basic understanding of the relative ages and relationships between the individual rock units has changed little since the first detailed State Geologic Map of Alabama was produced in 1894 by E. A. Smith. The description of the area stratigraphy as understood and generally accepted today is little changed from the description in the BLNP FSAR (TVA, 1986) for the original BLNP site permitting. The only differences are current practice at the state level of breaking the Chickamauga Formation into several other formations, is discussed as follows. This discussion follows the Alabama Geological Survey's correlations and lithologic descriptions as contained in the Geologic Map of Alabama: Northeast Sheet (Osborne et al., 1988) and Alabama Stratigraphy (Raymond et al., 1988).

The stratigraphic units present in the Bellefonte Site area include bedrock formations ranging in age from Cambrian to Pennsylvanian, and unconsolidated sands and gravels of alluvial origin of Quaternary age. No record of deposition from the Permian through the Tertiary Periods is known in this immediate area. The stratigraphic column includes those sedimentary rocks that

crop out in the area or are likely expected to crop out nearby and are projected under the site. Several thousands of feet of bedrock are present at and underlying the site. In outcrop, the bedrock units underlying the area form generally parallel outcrop belts that strike northeast to southwest in the Sequatchie Valley. The alluvial deposits overlie bedrock along the larger streams in the area and are generally thin and of limited areal extent.

Cambrian to Ordovician – Undifferentiated Knox Group rocks are the oldest sedimentary rocks exposed at the site. The Knox Group here consists of dolomitic, siliceous, cherty limestones, which are extensively weathered and covered in the area with thick cherty, red clay residuum that developed in place. In the vicinity of the Bellefonte Site, the Knox Group rocks consist of the Copper Ridge Dolomite and Chepultepec Dolomite formations, which together are more than 2,000 feet thick. As a result of the extreme weathering of the dolomites here, the formations cannot be distinguished in outcrop. Rocks assignable to the Knox Group crop out northwest of the Bellefonte Site along the axis of the Sequatchie anticlinal fold. Little bedrock assignable to the Knox Group is visible in outcrop. Exposures consist mostly of deeply weathered residuum – consisting of reddish-brown clay with chert fragments and cobbles as much as tens of feet thick. Sinkhole features – closed depressions with internal drainage, occur commonly throughout the Knox Group outcrop belt – one relatively recent/apparently active small sinkhole or collapse feature was observed southwest of the site on adjacent land owner’s property during an aerial reconnaissance of the area. All other sinkholes noted from topographic maps of the area appear to be relatively inactive insofar as collapse is concerned – but they are directing surface water into the ground and subterranean groundwater flow is being induced in those areas.

The Knox Group is unconformably overlain by the Chickamauga Limestone of Ordovician age. Historically, all Ordovician Limestones occurring between the Knox Group dolomites and the Silurian age Red Mountain Formation were assigned to the Chickamauga Limestone formation. However, in recent years the Chickamauga has been raised in classification and is sometimes referred to as a Super Group. These rocks in northeast Alabama are now divided into the Nashville Group, Stones River Group, and Sequatchie Formation. Total thickness of the Chickamauga limestones at the Bellefonte Site is more than 1,400 feet. At the site and within the new plant footprint lie the Nashville Group on the northwest and the Stones River Group to the southeast, as mapped by the Alabama Geological Survey (Osborne et al., 1988). The limestones immediately southeast of the site’s footprint on the northwest-facing slopes of the hill, have been mapped as the Sequatchie Formation. Ordovician Limestones assignable to the Chickamauga also crop out northwest of the Knox Group dolomites and cherty residuum on the far side of the Sequatchie anticline. Because the detailed mapping of the BLNP property by TVA for the BLNP FSAR (TVA, 1986) called all the limestones lying between the Knox Group and the Red Mountain Formation, Chickamauga Limestone, that nomenclature is followed here. Also, because the differentiation of these units is subtle and based in large part on fossil assemblages and age rather than significant differences in lithology, the original TVA usage will be retained. Typically, the Chickamauga Limestones are thin- to thick-bedded limestones, argillaceous in part, with occasional thin beds of bentonite or bentonitic shale. The uppermost part of the Chickamauga (likely assignable to the Sequatchie Formation) is composed of calcareous mudstones and shales interbedded with thin, fossiliferous limestones that may be sandy and/or fossiliferous.

The Silurian Red Mountain Formation unconformably overlies the Chickamauga Formation rocks at the site. The Red Mountain Formation consists of dark, reddish-brown siltstone, sandstone, and shale beds, with hematite (i.e., iron ore) beds from 5 to 30 feet thick. The entire formation is as much as 200 feet thick in northeast Alabama. In the Bellefonte Site area, the Red Mountain crops out on the small hills just southeast of the new plant footprint and about 2 miles northwest of the site on the east side of Backbone Ridge.

The Devonian Chattanooga Shale has been mapped through the site area by the Alabama Geological Survey (Osborne et al., 1988), and detailed mapping by TVA geologists for the FSAR (1986) reported a small amount on the facility property, but none was observed onsite during field reconnaissance for this effort. The unit consists of dark-colored organic shales and has occasional sandstone beds near its base. Chattanooga Shale was observed in outcrops near the site elsewhere in Jackson County and its presence here is inferred and likely. In outcrop, the thin, dark gray to black shale comprising the unit is often weathered and covered by colluvium from overlying ridge-forming rock units. The Chattanooga is thin, generally less than about 40 feet (and sometimes less than 2 feet) thick, and on weathering is hard to tell from shales in the lower part of the overlying Fort Payne Chert. Similarly, the sandstones that occur near the base of the Chattanooga are similar to the sandstones in the upper part of the Red Mountain Formation. The outcrop belt of the projected Chattanooga Shale lies southeast of the site footprint in the series of hills along and parallel to the river, and it also occurs on Backbone Ridge northwest of the site, where several outcrops were observed.

The Mississippian Fort Payne Chert consists of several hundred feet of light gray, finely crystalline siliceous limestone and chert that occurs in irregular bed and nodules. In outcrop, the relative amount of chert observed increases with weathering, the freshest outcrops appearing like limestone and the most weathered areas consisting of reddish-brown chert and clay reminiscent of the Knox Group residuum. The more clay-like Fort Payne deposits can be differentiated from the Knox Group residuum by the tabular-shaped cobbles and often bedded nature of much of the Fort Payne Chert. Also, the Fort Payne Chert is very fossiliferous with fossil echinoid molds being common. The Knox Group cherts are relatively non-fossiliferous and do not contain echinoids. In the Bellefonte Site area, the Fort Payne Chert crops out to the southeast on the east-facing side of the hills adjacent to the river and on Backbone Ridge about 2 miles northwest of the site, on the far side of the Sequatchie anticline.

The Mississippian Tuscumbia Limestone overlies the Fort Payne Chert. The Tuscumbia Limestone crops out on some of the small islands in the Tennessee River southeast of the site, most of its outcrop belt having been inundated when the river was dammed. The Tuscumbia Limestone is more than 100 feet thick in this part of the state. The unit consists of thick-bedded micritic to oolitic limestones and, except for being much less siliceous, is similar in appearance to the Fort Payne Chert. In fresh outcrops, the two units are hard to distinguish. In weathered outcrops, the clayey residuum that develops on both in this climate is relatively chert-free over the Tuscumbia Limestone.

The Tuscumbia Limestone is overlain by the Mississippian Monteagle Limestone, consisting of thick-bedded oolitic, argillaceous, bioclastic, micritic, and/or dolomitic limestones and shale. The Monteagle Limestone crops out east of the Tennessee River and west of Backbone Ridge in the project area. It is from 200 to 300 feet thick.

The Mississippian Bangor Limestone overlies the Tuscumbia Limestone. The Bangor Limestone is composed of as much as 700 feet of medium-bedded bioclastic and oolitic limestones with interbeds of shale and mudstone. The Bangor Limestone crops out east of the Tennessee River and west of Backbone Ridge in the project area.

The Mississippian Pennington Formation overlies the Bangor Limestone and consists of more than 150 feet of clay shale with interbeds of mudstone, limestone, dolostones, sandstones, and coal. Near the site area, it is found east of the Tennessee River on hill slopes above the Bangor outcrop and west of Backbone Ridge on the slopes of the small hills there.

The Pennsylvanian Pottsville Formation consists of more than 9,000 feet of alternating beds of sandstone, shale, siltstone, conglomerate, and coal. The base of the Pottsville Formation is typically a massive, conglomeratic, orthoquartzitic sandstone that is a prominent ridge forming bed. The basal Pottsville sandstone is found at the top of the mountain ridge east of the Tennessee River and capping the flat topped hills west of Backbone Ridge northwest of the site.

Quaternary alluvium and colluvium occur along the major streams across north Alabama. These deposits are typically thin and of limited areal extent and generally have so small an outcrop area that they are not mapped. These deposits may be difficult to differentiate from soil and generally consist of 1 or 2 feet of silty, clayey, sandy unconsolidated material derived from the underlying rocks and residuum. The only substantial deposits of Quaternary deposits in north Alabama not inundated by the dams on the Tennessee River occur more than 40 miles southeast of the site in the upper Coosa River watershed. A review of historical aerial photographs of the area near the Bellefonte Site indicated that, prior to the construction of Guntersville Dam, there were few, if any, Quaternary deposits along the Tennessee River near the site. The stream channel was apparently too steep and incised here to allow for significant alluvial deposits to form.

The soils in Jackson County in the site area generally are grouped according to their topographic position (USDA SCS, 1954) as: (1) soils of limestone valley uplands; (2) soils of sandstone plateaus; (3) soils of colluvial slopes; (4) soils of stream terraces; and (5) soils of first bottoms<sup>2</sup>. The areas classified as uplands and plateaus lie above the stream bottoms and consist of materials derived directly from the weathering and decay of the underlying rocks. Strictly residual soils are not common in the limestone valley uplands, as most soils are modified by or derived from parent material accumulated as alluvium or colluvium. Stream terraces are underlain by fluvial deposits that form benches adjacent to stream bottoms, but are not subject to flooding. Many of the higher terraces are severely eroded and mantled chiefly by residuum.

The soils underlying the site and within the adjoining Town Creek valley and embayment region are formed on stream terraces (Etowah, Capshaw, Tupelo, and Cumberland series) or limestone valley uplands (Talbot, Colbert, Fullerton, Tellico, and Armuchee series) (Figure 2.5.1-38). The highest terrace remnants (mapped as Cumberland series) occur at an elevation ranging from 630 to 640 feet msl, approximately 40 feet above the present level of the Guntersville Reservoir in the Town Creek embayment and 60 to 70 feet above the pre-impoundment base level of the Tennessee River. Based on an average regional denudation rate of 100 feet (30 meters)/my (Mills, 2005), this suggests the highest surfaces were developed on the order of 400 thousand years (kyr) to 600 kyr ago. Descriptions of soils mapped on these

---

<sup>2</sup> First bottoms are bottom lands along drainages that are underlain by fluvial deposits and are subject to overflow.

surfaces and observations in the excavations for the Bellefonte Site, indicate that the original deposits and soils have been eroded and these surfaces are mantled by a relatively thin veneer of alluvium or residual soil formed from weathering of the in-place bedrock. Younger terraces have formed along incised drainages cut into the older surfaces. The parent material for these terrace soils is alluvial in origin and consists of material derived mainly from weathered limestone and, to some extent, weathered sandstone and shale. Pebbles and sand are present to some extent.

#### 2.5.1.2.4 Site Area Structural Geology

The Bellefonte Site lies within the northwestern (frontal) part of the Appalachian fold-thrust belt as described in Section 2.5.1.1.4.2(a). Two bedrock faults, the Sequatchie Valley and Big Wills Valley faults, are mapped within the site vicinity (within a 25-mile radius), and one of these, the Sequatchie Valley fault, lies within the site area (within a 5-mile radius) (Figure 2.5.1-35).

Neither of these faults is considered to be a capable tectonic source, as defined in Regulatory Guide 1.165, Appendix A (USNRC, 1997) (see discussion in Section 2.5.3.6).

The structural geology of the site and site area as described in this section is based on a review of existing site licensing documents (TVA, 1986) and more recent published information for the primary structural feature within the site area, the Sequatchie Valley thrust fault and associated anticline. A general site reconnaissance was performed to verify general structural interpretations of the area presented in the literature describing this part of Alabama and observations made on that trip also are included herein.

The geologic mapping and cross-section for the site area presented in the BNP FSAR (1986) is shown in Figure 2.5.1-36. This map incorporated geologic observations made as part of the original site characterization activities for the BLNP licensing studies as well as TVA file maps of the Bellefonte area available at that time (TVA, 1986). This map is consistent with the most recent geologic map of the state (Osborne et al., 1988) except for some modifications to the subdivisions and nomenclature of some geologic units as noted in Section 2.5.1.2.3.

The Bellefonte Site is located on the gently dipping, i.e., about 15° to 25° dip, southeast limb of the Sequatchie anticline, shown in Figure 2.5.1-36. This asymmetrical anticline has a gently dipping southeast limb and a steeply dipping northwest limb. The axis of the Sequatchie Valley anticline lies approximately 1.4 miles northwest of the site. As documented in the BLNP FSAR (TVA, 1986), there is no intense folding or major faulting within the foundation bedrock of the adjacent existing Bellefonte units. The strata strike N39°-40°E and dip 17° to the southeast at the Bellefonte Site. The dip decreases to 14° southeast at the ERCW intake pumping station and to 10° to 12° at locations adjacent to the Tennessee River.

The Sequatchie anticline is broken on the west by the Sequatchie Valley thrust fault, which at its closest point is 2.1 miles northwest of the site (Figure 2.5.1-36). The fault dips to the southeast and is projected to be about 5,000 feet below the surface of the site (TVA, 1986). Additional data on the regional characteristics of the Sequatchie Valley thrust fault are presented in Section 2.5.3. In the site area, the fault juxtaposes the Chickamauga Formation of Middle Ordovician age and the Fort Payne Chert of Mississippian age (TVA, 1986). No exposures of the main Sequatchie thrust fault in the BLNP site area were described in the BLNP FSAR (TVA, 1986), and none were observed during the field reconnaissance studies for the GG&S evaluation. Backbone Ridge, which is formed by the near-vertical resistant beds of Silurian and Mississippian age, marks the northwest limb of the Sequatchie Valley anticline in the site area.

At one location along Backbone Ridge, approximately 3.2 miles northwest of the site, steeply west-dipping beds and numerous small faults that appear to be minor splays or backthrusts off the primary thrust fault are visible in a large landfill excavation (Field Stop KH2, Figure 2.5.1-36). These faults, which have apparent displacements of only a few feet, are all in the hanging wall less than 0.1 mile from the mapped trace of the Sequatchie Valley thrust fault.

No evidence of faulting or shearing in the Chickamauga Limestone was observed in excavations for the Reactor, Auxiliary, and Control Building areas of the Bellefonte Site (TVA, 1986). Minor displacement that was observed in the northwest corner of Unit 1 QA Records Storage Vault was investigated by core drilling and recorded by surface mapping (TVA, 1977). The joints showed 3 inches of vertical offset with a strike of N89°E and an average dip of 64 degrees. Three vertical coreholes and two inclined coreholes were drilled into the feature. The fault is described as 1/16- to 1/2-inch-thick, sinuous in shape, and calcite filled. It terminates at a vertical joint. TVA concluded that the feature is not a significant fault, but is a joint that received minor displacement as part of the process that resulted in the entire joint set (TVA, 1977).

Three prominent joint sets have been mapped in the site area. One nearly parallels the strike north 30° to 50° east and dips steeply 70° to 80° to the northwest, another set strikes N80°E with dips ranging from 70° to the northwest to near vertical, and the other set strikes N50° to 80°W and is near vertical (TVA, 1986). Joints and fractures are present in the bedrock underlying the Bellefonte Site as observed in core samples. Joints and fractures in the site area likely formed as a result of the thrusting and mountain building forces that created the Sequatchie Valley anticline in late Paleozoic time. Most joints in the Appalachian Plateau rocks formed as a result of the primary compression forces with shortening in the NW-SE direction (Wiltschko in Hatcher et al., 1989b). Joints have two major trends in the southern Appalachian Plateau, one across and one parallel to the strike of major structures; two minor sets trend north-south and east-west (Wiltschko in Hatcher et al., 1989c). The joint trends observed at the site are consistent with these trends.

Joints and fractures represent planes of weakness within the bedrock mass and form zones of higher porosity and permeability along which groundwater can more readily move. Occasionally, groundwater moving along the bedrock joints and fractures can create solutionally enlarged voids and channels. Evidence of deep weathering and dissolution in the Chickamauga formation was observed in surface geophysical and borehole data only in the eastern part of the site along a strike-oriented zone. No large voids or deep weathering profiles were observed outside this zone (see Section 2.5.4.4). One solutionally enlarged void of 1 foot or more in size was observed in outcrops at the site (Field Stop KH5, Figures 2.5.1-37 and 2.5.1-38). A small number of enlarged joints or voids were indicated on logs of borings advanced in the BLNP and Bellefonte Sites or on the descriptive logs of the excavations of the Bellefonte Site foundation areas. Those voids were generally all less than 1 foot in maximum dimension and their occurrence decreased with depth below the top of bedrock. There appeared to be no clear correlation between enlarged joint or void presence and stratigraphic unit or location within the site, although they were observed less frequently as boring depth increased. These features are described in more detail in the geotechnical engineering section of this document (Section 2.5.4).

A few prominent photo lineaments were identified on aerial photographs of the site (see discussion in Section 2.5.3.1). These lineaments appear to be related to bedrock structures and jointing and most, but not all, trend parallel or perpendicular to bedding at the site (see



discussion in Section 2.5.3.1). Field investigations consisting of surface geophysical surveys and drilling and coring along and adjacent to these lineaments indicated the following:

- Some of the lineaments coincide with zones of increased depth of weathering of the bedrock surface.
- Some lineaments do not coincide with zones of thick soil or deeper top of rock.
- The lineaments may represent surface expressions of deeper seated geologic structures, but no direct physical evidence for this has been observed.
- The lineaments may indicate the presence and location of areas where increased groundwater flow is concentrated in the near-surface bedrock.
- Some lineaments may be related to subtle lithologic differences in the southeasterly dipping Chickamauga bedrock
- Some southeast-northwest lineaments align with drainage features and erosional gaps through the ridge that borders the site to the east. These appear to be part of a regional topographic fabric probably related to jointing caused by large-scale deformation.
- There is no geomorphic evidence to suggest differential uplift across any of the lineaments that intersect the site.
- There is no geomorphic evidence to indicate that any of the lineaments identified are associated with a capable tectonic source as defined by Regulatory Guide 1.165, Appendix A (USNRC, 1987).

#### 2.5.1.2.5 Site Area Geologic Hazard Evaluation

As part of the evaluation of geologic features, the potential for geologic hazards at the Bellefonte Site was reviewed. The review of geologic hazards was performed through a search of published maps and reports, by visual reconnaissance of the area, and based on discussions with TVA about geologic conditions and types of current and past industries in the area.

Based on review of the site geology, it is concluded that:

- Earthquake activity with its resulting ground motion effects is judged to be the primary geologic hazard to the Bellefonte Site. The potential for tectonic surface deformation is judged to be negligible. A detailed discussion of vibratory ground motion and potential for surface faulting at the Bellefonte Site is provided in Sections 2.5.2 and 2.5.3, respectively.
- The closest water reservoir, the impounded Town Creek embayment of the Tennessee River, is 1,100 feet away and located 15 to 35 feet below and, therefore, is not judged to be a hazard from flooding. The property on which the facility will be constructed is generally above the flood elevation of the impounded Tennessee River and no other significant streams are present in the area. The site footprint is generally at about elevation 610 to 630 msl and the normal pool elevation of the Tennessee River adjacent the site is at about 595 feet msl. The computed maximum flood elevation from any cause is 624.8 feet msl (BLNP FSAR, Section 2.4.2.2). While slight artesian conditions were identified from groundwater data at some locations, there are no groundwater springs within the project limits.

- Slopes in the vicinity of the project are generally flat except on the eastern boundary where very gentle slopes exist (Figures 2.5.1-36 and 2.5.1-37). Existing slopes in and proximal to the recommended development area exhibit no evidence of landslides, nor would landslides be expected, given the slope angles.
- No groundwater withdrawal, petroleum production, or subsurface mining operations that could lead to subsidence are located near the site. There is no evidence of past subsurface mining activities at or near the Bellefonte Site. Coal mining in the region is primarily focused on the Pottsville Formation and occurs well to the northwest of the site (Raymond et al., 1988). Quarry operations that remove limestone from several locations along the Sequatchie Valley do not affect the Bellefonte Site. The closest quarry is approximately 3 miles from the site.

The only other potential geologic hazard that was identified was the potential dissolution of the limestone rock. The potential for this geologic hazard is described in detail in Sections 2.5.4.1 and 2.5.4.4. As stated in Section 2.5.4.1.2, the hazard from karst formation is considered to be low for the recommended development area, based on the results of the field explorations, the groundwater flow regime, and the nature of the limestone at the site.

These conclusions indicate that no geologic conditions were found at the site that result in a hazard that could affect construction or operation of the proposed facility.

The updated earthquake catalog includes a number of newly identified earthquakes for the time period covered by the EPRI-SOG catalog as well as earthquakes that have occurred after completion of the EPRI-SOG evaluation. Most of these newly identified earthquakes within 200 miles of the Bellefonte Site are for time periods identified in the EPRI-SOG evaluation as periods of incomplete catalog reporting ( $P^D < 1.0$ ). Comparisons of the earthquake counts for these time periods suggest that inclusion of the newly identified earthquakes in the estimation of catalog completeness would likely yield values of  $P^D$  near unity for the period post-1860 within completeness regions 3 and 4 for the two lowest magnitude intervals:  $3.3 \geq m_b^* > 3.9$  and  $3.9 \geq m_b^* > 4.5$ . This effect is illustrated by constructing so call "Stepp" plots (Stepp, 1972) that show the variation of earthquake rate with time for specific magnitude intervals. The computation of rate starts at the end of the catalog and moves backward in time. At any point in time, the earthquake rate is defined as the number of earthquakes in the catalog from that point forward to the end of the catalog divided by the length of time from that point to the end of the catalog.

Figure 2.5.2-16 shows "Stepp" plots for the portions of EPRI-SOG completeness regions 3 and 4 that lie within 200 miles of the Bellefonte Site. The plot on the left shows the time variation of earthquake occurrence rates based on the EPRI-SOG catalog, and the plot on the right shows the occurrence rates based on the updated catalog. The observed rate of magnitude  $m_b$  3.3 to 3.9 earthquakes begins to steadily decrease approximately 15 years before the end of the EPRI-SOG catalog and the rate for  $m_b$  3.9 to 4.5 earthquakes begins to decrease approximately 75 years before the end of the EPRI-SOG catalog. In contrast, the occurrence rates remain relatively constant back to approximately 1860 for these two magnitude intervals using the updated catalog. The time variation of the rate for earthquakes larger than  $m_b$  4.5 shows somewhat erratic behavior due to the limited number of events.

The effect of the updated earthquake catalog on earthquake occurrence rates was assessed by computing earthquake recurrence parameters for the portions of EPRI-SOG completeness regions 3 and 4 that lie within 200 miles of the site. The truncated exponential recurrence model was fit to the seismicity data using maximum likelihood. Earthquake recurrence parameters were computed using the EPRI-SOG catalog and equivalent periods of completeness and using the updated catalog and the updated equivalent periods of completeness. It was assumed that the probability of detection for all magnitudes is unity for the time period of March 1985 to March 2005. The resulting earthquake recurrence rates are compared in Figure 2.5.2-17. For completeness region 3, essentially the same earthquake recurrence parameters are obtained using the EPRI-SOG and updated catalog and equivalent periods of completeness. For completeness region 4, use of the updated earthquake catalog and equivalent periods of completeness result in lower earthquake occurrence rates.

On the basis of the comparisons shown in Figures 2.5.2-14 and 2.5.2-17, it is concluded that the earthquake occurrence rate parameters developed in the EPRI-SOG evaluation adequately represent the seismicity rates within 200 miles of the Bellefonte Site based on more recent information.

The earthquake recurrence rate for the New Madrid and Charleston regions was also evaluated using results of paleoliquefaction studies. The results of studies of paleoliquefaction in the NMSZ (summarized in Section 2.5.1.1.4.3) have indicated that large earthquakes are more frequent than suggested by extrapolating the observed seismicity rates for small-to-moderate earthquakes up to large magnitudes ( $m_b \geq 7$ ). Figure 2.5.2-18 compares the seismicity rates estimated from the updated earthquake catalog to the rate for large magnitude events estimated from paleoliquefaction data. The error bars attached to the updated catalog rates represent 90 percent confidence intervals estimated by relative likelihood from the observed earthquake counts within the Bechtel team source zone 30 (Figure 2.5.2-4), a typical EPRI-SOG New Madrid source. The hatched box represents the 90 percent confidence interval for the paleoliquefaction rate based on three earthquake sequences post 300 AD (e.g., Tuttle et al., 2005) and the solid circle indicates the rate used by Frankel et al. (2002) in the USGS National Hazard Mapping project (500-year repeat time). The recurrence relationships shown in the figure indicate the mean and 15<sup>th</sup> to 85<sup>th</sup> percentile recurrence rates for New Madrid sources computed from the EPRI-SOG seismic source models. As shown in the figure, the EPRI-SOG recurrence rates are very consistent with the seismicity rates estimated from the updated earthquake catalog but underestimate the rate based on paleoliquefaction data by approximately an order of magnitude. Based on a similar comparison, Exelon (2003) concluded that the EPRI-SOG recurrence rates for large earthquakes in the NMSZ should be revised for PSHA calculations.

As discussed in Section 2.5.1.1.4.3, paleoliquefaction studies also have been conducted in the region of the 1886 Charleston, South Carolina, earthquake. The results of these studies have led to estimated repeat times for large earthquakes in the Charleston region of approximately 550 years (Frankel et al., 2002; Dominion, 2003; Geomatrix, 2004). This repeat time represents higher occurrence rates than obtained from the EPRI-SOG seismic hazard model (Dominion, 2003).

TABLE 2.5.1-1. Summary of New Information for New Madrid Seismic Zone

Author(s) (Year)	Title	Significance
<b>GEOLOGIC STRUCTURES INTERPRETED FROM GRAVITY, MAGNETIC, AND SEISMIC-PROFILE DATA</b>		
McKeown et al. (1990)	“Diapiric origin of the Blytheville and Pascola arches in the Reelfoot rift, east-central U.S.: Relation to New Madrid seismicity”	Earthquakes in the NMSZ correlate spatially with the BA and part of the Pascola arch, which are interpreted to be the same structure. Both arches were formed by diapirism. The rocks in the arch are more highly deformed, and therefore weaker, than adjacent rocks. Seismicity is hypothesized to be localized in these weaker rocks.
Nelson and Zhang (1991)	“A COCORP deep reflection profile across the buried Reelfoot rift, south-central United States”	Deep reflection profile line reveals features of the late Precambrian (?)/early Paleozoic Reelfoot rift. The BA, an axial antiformal feature, as well as lesser structures indicative of multiple episodes of fault reactivation are evident on profile.
Hildenbrand and Hendricks (1995)	“Geophysical setting of the Reelfoot rift and relations between rift structures and the NMSZ”	Provides discussion of several potential-field features inferred from magnetic and gravity data that may focus earthquake activity in the northern Mississippi embayment and surrounding region. Summarizes complex tectonic and magmatic history of the rift.
Braile et al. (1997)	“New Madrid seismicity, gravity anomalies, and interpreted ancient rift structures”	Epicentral patterns, correlative geophysical data, and historical seismic energy release indicate the significance of New Madrid area seismicity, both within the Reelfoot segment of the rift structures and in areas outside of this segment, particularly to the north. Deep structure of the crust, including thickness variations in the upper crust and the presence of a high-density lower crustal layer, is a controlling factor in New Madrid seismicity.
Hildenbrand et al. (2001)	“Geologic structures related to New Madrid earthquakes near Memphis, Tennessee, based on gravity and magnetic interpretations”	Defines boundaries of regional structures and igneous complexes in the region north of Memphis, Tennessee, and south of latitude 36° that may localize seismicity.
<b>NORTHERN TERMINUS OF REELFOOT RIFT</b>		
Pratt et al. (1989)	“Major Proterozoic basement features of the eastern Midcontinent of North America revealed by recent COCORP profiling”	Interpretation of deep seismic reflection data from southern Illinois and southern Indiana indicates an absence of a thick section of rift-related sedimentary rocks.
Heigold and Kolata (1993)	“Proterozoic crustal boundary in the southern part of the Illinois basin”	Conclude that structures associated with the NMSZ may be distinct from structures to the northeast (in the Wabash Valley zone), as evidenced by the east-southeast-trending geophysical anomaly that separates two areas of distinctly different crust.

TABLE 2.5.1-1. Summary of New Information for New Madrid Seismic Zone

Author(s) (Year)	Title	Significance
Hildenbrand and Hendricks (1995)	“Geophysical setting of the Reelfoot rift and relations between rift structures and the NMSZ”	Inspection of regional magnetic and gravity anomaly maps suggests that the northwest margin does not continue northeastward into southern Indiana. A preferred geometry is that both the northwest and southeast margins bend to the east and merge with the Rough Creek graben.
Bear et al. (1997)	“Seismic interpretation of the deep structure of the Wabash Valley fault system”	Interpretation of recently compiled seismic reflection data suggests that structures associated with the Wabash Valley fault system may not be directly linked to northeast-trending structures in the New Madrid area.  The authors note that a graben may exist within the southern Indiana arm (Braile et al., 1982), but it is limited in geographic extent and is not structurally continuous with the Reelfoot rift-Rough Creek graben.
Hildenbrand and Ravat (1997)	“Geophysical setting of the Wabash Valley fault system”	Concludes from high-resolution aeromagnetic data and the lack of regional potential-field features extending south from the Wabash Valley that the Wabash Valley fault system apparently is not structurally connected to the faults related to the NMSZ.
Kolata and Hildenbrand (1997)	“Structural underpinnings and neotectonics of the southern Illinois basin: An overview”	Summarizes geologic and geophysical information suggesting that the cause of earthquakes in the NMSZ is unrelated to that in the region north of the Reelfoot rift system.
Wheeler (1997)	“Boundary separating the seismically active Reelfoot rift from the sparsely seismic Rough Creek graben”	Concludes that the structural boundary between the relatively high hazard of the Reelfoot rift and low hazard of the Rough Creek graben is marked by bends and ends of large faults, a Cambrian transfer zone, and the geographic extent of alkaline igneous rocks.
<b>SEISMOGENIC FAULTS</b>		
Sexton and Jones (1986)	“Evidence for recurrent faulting in the NMSZ from mini-sosie high-resolution reflection data”	Interpretation and integration of three seismic reflection data sets provides evidence for recurrent movement along the RF, the major reverse fault associated with the Reelfoot scarp. Estimated displacements vary from 200 feet (60 ms) for late Paleozoic rocks to 50 feet (20 ms) for late Eocene sedimentary units. A graben structure is interpreted to be caused by tensional stresses resulting from uplift and folding of the sediments. The location of the graben coincides with normal faults in Holocene sediments observed in trenches. These features are interpreted to be related and caused by reactivation of the RF.
Harrison and Schultz (1994)	“Strike-slip faulting at Thebes Gap, Missouri and Illinois: Implications for New Madrid tectonism”	Documents evidence for Quaternary faulting in trenches in the Benton Hills of southeast Missouri.

TABLE 2.5.1-1. Summary of New Information for New Madrid Seismic Zone

Author(s) (Year)	Title	Significance
Johnston and Schweig (1996)	"The Enigma of the New Madrid earthquakes of 1811-1812"	Associated each of three 1811-1812 earthquakes with a specific fault by using historical accounts and geologic evidence:  Event D1—BA/CDF or BL  Event J1—East Prairie fault  Event F1—RF
Schweig and Van Arsdale (1996)	"Neotectonics of the upper Mississippi embayment"	Summarizes geologic and geophysical evidence of neotectonic activity, including faulting in Benton Hills and Thebes Gap, paleoliquefaction in Western Lowlands, subsurface faulting beneath and tilting of Crowley's Ridge, subsurface faulting along the CCFZ, and numerous indicators of historical and prehistoric large earthquakes in NMSZ.
Pujol et al. (1997)	"Refinement of thrust faulting models for the central NMSZ"	Seismicity cross-sections define the downdip geometry of the Reelfoot thrust.
Palmer et al. (1997)	"Seismic evidence of Quaternary faulting in the Benton Hills area, southeast Missouri"	Seismic profiles show the English Hill area to be tectonic in origin. Individual faults have near-vertical displacements with maximum offsets on the order of 50 feet. Faults are interpreted as flower structures with north northeast-striking, vertically dipping, right-lateral oblique-slip faults. These data suggest previously mapped faults at English Hill are deep-seated and tectonic in origin.
Chiu et al. (1997)	"Seismicity of the southeastern margin of Reelfoot rift, Central United States"	Coincidence of seismicity along the southeastern flank of the Reelfoot rift suggest that this rift flank is seismically active but at a lower level than the main intra-rift NMSZ. The style of faulting as inferred from the seismicity is complex, with the dominant pattern being right-lateral strike-slip with reverse movement. It is concluded that there are sufficient data to show that the southeastern margin of the Reelfoot rift does contain seismically active faults and that it has the potential of producing a major ( $M \sim 7$ ) earthquake.
Odum et al. (1998)	"Near-surface structural model for deformation associated with the February 7, 1812, New Madrid, Missouri, earthquake"	Integrates geomorphic data and documentation of differential surficial deformation (supplemented by historical accounts) with interpretation of seismic reflection data to develop a tectonic model of the near-surface structures in the New Madrid area. Model consists of two primary components: a north-northwest-trending thrust fault (RF), and a series of northeast-trending, strike-slip tear faults.  The authors estimate an overall length of at least 30 kilometers (18 miles) and a dip of $\sim 31^\circ$ for the RF.

TABLE 2.5.1-1. Summary of New Information for New Madrid Seismic Zone

Author(s) (Year)	Title	Significance
Crone (1998)	“Defining the southwestern end of the BA, northeastern Arkansas: Delimiting a seismic source zone in the New Madrid region”	Interprets vibroseis seismic-reflection profiles to document the southwesterly extent of the BA and the length (134 kilometers [80 miles]) of a fault zone that coincides with the arch.
Harrison et al. (1999)	“An example of neotectonism in a continental interior—Thebes Gap, midcontinent, United States”	Documents evidence for four episodes of Quaternary faulting: one in late- to post-Sangamonon, pre- to early Roxana time (~60 to 50 ka), one in syn- or post Roxana, pre-Peoria time (~35-25 ka), and two in Holocene time (middle to late Holocene, and possibly during the 1811-1812 earthquake sequence). The overall style of neotectonic deformation is interpreted as right-lateral strike-slip faulting.
Stephenson et al., 1999	“Deformation and Quaternary faulting in southeast Missouri across the Commerce geophysical lineament (CGL)”	High-resolution seismic-reflection data at three sites along the CGL reveal post-Cretaceous faulting extending into the Quaternary. At Qulin site, ~20 meters of apparent Quaternary vertical displacement is observed. At Idalia Hill, a series of reverse and possibly right-lateral strike-slip faults with Quaternary displacement are imaged. At Benton Hills, a complicated series of anticlinal and synclinal fault-bounded blocks occur directly north of the CGL.
Mihills and Van Arsdale (1999)	“Late Wisconsin to Holocene deformation in the NMSZ”	Interprets a structure contour map of the unconformity between the Eocene strata and overlying Quaternary Mississippi River alluvium as representing the Late Wisconsin to present strain field of the NMSZ. Areas of Holocene uplift include the Lake County uplift, BA, and Crittenden fault. Areas of Holocene subsidence include Reelfoot Lake, historical Lake Obion, the Sunklunds of northeast Arkansas, and possibly areas east and west of the Crittenden County fault.
Mueller et al. (1999)	“Fault slip rates in the modern NMSZ”	Based on structural and geomorphic analysis of late Holocene sediments deformed by fault-related folding above the blind Reelfoot thrust fault, a slip rate of $6.1 \pm 0.7$ mm/year is estimated for the past $2,300 \pm 100$ years. Using an alternative method based on the structural relief across the scarp and the estimated dip of the underlying blind thrust, a slip rate of $4.8 \pm 0.2$ mm/year is calculated. Geometric relations suggest that the right-lateral slip rate on the NMSZ is 1.8 to 2.0 mm/year.  The onset of shortening across the Lake County uplift is estimated to be between 9.3 ka and 16.4 ka, with a preference for the younger age.
Van Arsdale et al. (1999)	“Southeastern extension of the RF”	This evaluation of microseismicity, seismic-reflection profile data, and geomorphic anomalies indicates that prehistoric and 1811-1812 coseismic uplift in the hanging wall of the RF has produced subtle surface warping that extends from Reelfoot Lake to Dyersburg, a total distance of 70 kilometers (42 miles).

TABLE 2.5.1-1. Summary of New Information for New Madrid Seismic Zone

Author(s) (Year)	Title	Significance
Van Arsdale (2000)	"Displacement history and slip rate on the RF of the NMSZ"	<p>Develops a displacement history and slip rates for the RF in the NMSZ from a seismic-reflection profile and trench data.</p> <p>Average slip rate estimates—seismic profile:</p> <p>0.0009 mm/year (past 80 Ma)</p> <p>0.0007 mm/year (late Cretaceous)</p> <p>0.002 mm/year (Paleocene Midway Group)</p> <p>0.001 mm/year (Paleocene-Eocene Wilcox Form.)</p> <p>0.0003 mm/year (post-Wilcox/pre-Holocene)</p> <p>1.8 mm/year (Holocene)</p> <p>Average slip rate estimates—trench data</p> <p>4.4 mm/year (past 2,400 years based on 10 meters of topographic relief and a fault dip of 73°)</p> <p>6.2 mm/year (maximum; estimated 5.4 meters cumulative displacement for two events between AD 900 and AD 1812).</p>
Champion et al. (2001)	"Geometry, numerical models, and revised slip rate for the RF and trishear fault-propagation fold, NMSZ"	<p>Analysis of trench excavations, shallow borings, a digital elevation model of topography, and bathymetry shows that Reelfoot monocline is a forelimb on a fault-propagation fold that has accommodated relatively little shortening. RF is a reactivated Paleozoic structure. A late Holocene fault slip rate of <math>3.9 \pm 0.1</math> mm/year is based on 9 meters of structural relief, the <math>2,290 \pm 60</math> years BP age of folded sediment, and a 75° dip for the fault. The fault tip is 1,016 meters beneath the surface. The thrust is flatter at deeper levels (5 to 14 kilometers) based on the location of earthquake hypocenters (~40°SW for northern segment, ~35°W for central segment, ~45°SW for southern segment).</p>



TABLE 2.5.1-1. Summary of New Information for New Madrid Seismic Zone

Author(s) (Year)	Title	Significance
Mueller and Pujol (2001)	“Three-dimensional geometry of the Reelfoot blind thrust: Implications for moment release and earthquake magnitude in the NMSZ”	Based on seismicity data and structural analysis, the Reelfoot blind thrust is a complex fault that changes in geometry along-strike. The thrust is bound to the north by an east-trending strike-slip fault. The south end is defined by seismicity; it is not truncated by a known transverse fault. The north part of the thrust steepens to 75° to 80° at shallow depths (within the upper 4 kilometers), forming a listric shape. The center of the central part of this thrust segment strikes north-south; the north and south segments strike between N10°W and N22°W, respectively. This segment dips between 31° and 35°W. The southeast fault segment is oriented N28°W and dips 48° to 51°SW. Available data suggest that the thrust flattens to <35° between about 2- and 4-kilometer depth (possibly at the Precambrian basement-Paleozoic cover contact at about 3-kilometer depth). (Magnitude estimates are discussed as follows in this table.)
Cox et al. (2001a)	“Neotectonics of the southeastern Reelfoot rift zone margin, central United States, and implications for regional strain accommodation”	Suggests that the 90-mile- (150-kilometer)-long southeastern Reelfoot rift margin fault system may be accommodating significant northeastward transport as a right-lateral fault that is capable of producing earthquakes of $M \geq 7$ . Results of paleoseismological investigations show:  Union City site (north of intersection with RF)—no Holocene movement.  Porter Gap site (south of intersection with RF) $\geq 3$ meters vertical displacement of ~Peoria loess (~20 ka). ~9.68 ka deposits post-date main events; minor liquefaction post ~4.3 ka.
Cox et al. (2002)	“Paleoseismology of the southeastern margin of the Reelfoot rift in the vicinity of Memphis, Tennessee”	Confirms that the southeastern Reelfoot rift margin is a fault zone with multiple high-angle faults and associated folding based on shallow seismic profiles and paleoseismological investigations. Documents evidence for 8 to 15 meters of right-lateral offset of a late Wisconsin paleo-channel (~20 ka) at a site near Porter Gap, suggesting an average slip rate of between 0.85 mm/year and 0.37 mm/year.  Evidence for an earthquake circa 2500 to 2000 BP on the southeastern Reelfoot rift margin that ruptured $\geq 80$ kilometers from Shelby County (15 to 25 kilometers north of Memphis metropolitan area) to Porter Gap (just south of the intersection with the RF).

TABLE 2.5.1-1. Summary of New Information for New Madrid Seismic Zone

Author(s) (Year)	Title	Significance
Baldwin et al. (2002)	“Preliminary paleoseismic and geophysical investigation of the North Farrenburg lineament: Primary tectonic deformation associated with the NN?”	Presents geomorphic, geologic, seismic-reflection, trench, and microtextural data that strongly suggest that the North Farrenburg lineament, as well as the South Farrenburg lineament, may be the surface expression of an underlying tectonic fault that ruptured in the January 23, 1812, earthquake. Northeast-trending contemporary microseismicity beneath Sikeston Ridge and previously inferred NN locations aligns partly with the lineaments.
Harrison and Schultz (2002)	“Tectonic framework of the southwestern margin of the Illinois basin and its influence on neotectonism and seismicity”	Describes neotectonism along the CGL:
Odum et al. (2002)	“Near-surface faulting and deformation overlying the CGL in southern Illinois”	Seismic reflection and microgravity data demonstrates post-Devonian displacement associated with the CGL in the Tamms area of southern Illinois. Several faults are imaged to the Paleozoic/Quaternary interface, and at one site, deformed Quaternary strata may have been faulted 5 to 10 meters.
Van Arsdale et al.(2002)	“Investigation of faulting beneath the city of Memphis and Shelby County, Tennessee”	Two north northeast-trending faults marked by 20 meter steps, referred to as the Memphis and Ellendale faults, are identified from structure contour maps on Plio-Pleistocene to Eocene datums. Quaternary activity on both faults is indicated from analysis of the structure contour maps and topographic, drainage, and paleodrainage analyses. An anticlinal fold in floodplain sands is observed along the Ellendale fault. Radiocarbon dates indicate the folding occurred between 390 AD and 450 AD and liquefaction observed in the crest of the anticline occurred post 450 AD. Modeling of the fold, which appears to be tectonic, is consistent with 5 meters of right lateral offset.
McBride et al. (2003)	“Variable post-Paleozoic deformation detected by seismic reflection profiling across the northwestern “prong” of NMSZ”	High-resolution shallow seismic reflection profiles in the vicinity of the Olmstead fault (which is close to and parallel with the straight segment of the Ohio River) on trend with the westernmost of two groups of northeast-aligned prongs of epicenters) show Tertiary reactivations of complex Cretaceous deformations (including normal graben faults). A possible fault-propagation fold associated with one of these faults, appears to affect Holocene sediments near the ground surface.

TABLE 2.5.1-1. Summary of New Information for New Madrid Seismic Zone

Author(s) (Year)	Title	Significance
Parrish and Van Arsdale (2004)	“Faulting along the southeastern margin of the Reelfoot rift in northwestern Tennessee revealed in deep seismic-reflection profiles”	Deep seismic-reflection profiles in northwest Tennessee reveal structure of the southeastern margin of the Reelfoot rift. Rift margin consists of at least two major down-to-the-west late Precambrian to Cambrian normal faults. Dominantly reverse faulting, folding, and positive flower structures in the shallow section indicate Eocene and younger transpression. Numerous faults displace the youngest reflectors and therefore the age of most recent faulting is not known. The southeastern rift margin is subject to right-lateral movement and transpression within current stress field.
<b>MAGNITUDE ESTIMATES</b>		
Atkinson and Hanks (1995)	“A high-frequency magnitude scale”	Based on a high-frequency magnitude scale (m), the magnitude of the 1812 New Madrid event is estimated to be <b>M</b> 7.7 ± 0.3.
Johnston (1996b)	“Seismic moment assessment of earthquakes in stable continental regions—III. New Madrid 1811-1812, Charleston 1886, and Lisbon 1755”	Estimates magnitudes for the 1811-1812 earthquake sequence based on intensity data. Estimated magnitudes for the three largest events are: D1 (December 16, 1811): <b>M</b> 8.1 ± 0.3 J1 (January 23, 1812): <b>M</b> 7.8 ± 0.3 F1 (February 7, 1812): <b>M</b> 8.0 ± 0.3
Johnston and Schweig (1996)	“The enigma of the New Madrid earthquakes of 1811-1812”	This review paper focuses on the 1811-1812 earthquakes, their geophysical setting, fault rupture scenarios, and magnitude estimates based on intensity data. Using historical accounts and geologic evidence, the three main 1811-1812 earthquakes are associated with specific structures.
Hough et al. (2000)	“On the Modified Mercalli intensities and magnitudes of the 1811-1812 New Madrid, central United States, earthquakes”	Re-interprets intensity data, obtaining maximum magnitude estimates from 7.0 to 7.5 for the main three events in the 1811-1812 earthquake sequence: December 16, 1811: <b>M</b> 7.2-7.3 January 23, 1812: <b>M</b> 7.0 February 7, 1812: <b>M</b> 7.4-7.5 (thrust event)

TABLE 2.5.1-1. Summary of New Information for New Madrid Seismic Zone

Author(s) (Year)	Title	Significance
Tuttle (2001a)	"The use of liquefaction features in paleoseismology: Lessons learned in the NMSZ, central United States"	<p>Uses two approaches:</p> <p>Magnitude-bound—estimates minimum magnitude for AD 1450 and AD 900 events of <b>M</b> 6.7 and <b>M</b> 6.9, respectively, based on Ambraseys' (1988) relationship between <b>M</b> and epicentral distance to surface manifestations of liquefaction.</p> <p>Energy stress—estimates <b>M</b> 7.5 to 8.3 from in situ geotechnical properties similar to <b>M</b> <math>\geq</math>7.6 from Ambraseys' relation for the largest 1811-1812 earthquakes.</p>
Mueller and Pujol (2001)	"Three-dimensional geometry of the Reelfoot blind thrust: implications for moment release and earthquake magnitude in the NMSZ"	<p>The area of the blind thrust (1,301 square kilometers), coupled with estimates of displacement in the February 7, 1812, event, is used to estimate values of MO from 6.8 by 1,026 to 1.4 by 1,027 dyne-centimeters, with preferred values between 6.8 by 1,026 and 8.7 by 1,026 dyne-centimeters. Computed MW for this event ranges from MW 7.2 to 7.4, with preferred values between MW 7.2 and 7.3. The moment magnitude for the AD 1450 event is computed as MW 7.3.</p>
Tuttle et al. (2002)	"The earthquake potential of the NMSZ"	<p>The size, internal stratigraphy, and spatial distributions of prehistoric sand blows indicate that the AD 900 and AD 1450 earthquakes had source zones and magnitudes similar to those of the three largest shocks in the 1811-1812 sequence.</p>
Hough and Martin (2002)	"Magnitude estimates of two large aftershocks of the 16 December 1811 New Madrid earthquake"	<p>Estimated locations and magnitudes for two large aftershocks:</p> <p>NM1-A- <b>M</b> ~7, thrust mechanism on a southeastern limb of the RF.</p> <p>NM1-B- <b>M</b> 6.1 <math>\pm</math> 0.2, location of event not well constrained, but probably beyond the southern end of the NMSZ, near Memphis, Tennessee (within the southwestern one-third to one-half of the band of seismicity identified by Chiu et al. (1997).</p>

TABLE 2.5.1-1. Summary of New Information for New Madrid Seismic Zone

Author(s) (Year)	Title	Significance
Bakun and Hopper (2004a)	“Magnitudes and locations of the 1811-12 New Madrid, Missouri, and the 1886 Charleston, South Carolina, earthquakes”	<p>Estimated <b>M</b> for the three largest events in the 1811-1812 New Madrid sequence. (MI is intensity magnitude based on inverting observations of intensity).</p> <p>MI 7.6 (<b>M</b> 6.8 to 7.9 at the 95% confidence level) for the December 16, 1811, event (NM1) that occurred in the NMSZ on the Bootheel lineament or on the Blytheville seismic zone.</p> <p>MI 7.5 (<b>M</b> 6.8 to 7.8 at the 95% confidence level) for the January 23, 1812, event (NM2) for a location on the New Madrid north zone of the NMSZ.</p> <p>MI 7.8 (<b>M</b> 7.0 to 8.1 at the 95% confidence level) for the February 7, 1812, event (NM3) that occurred on the Reelfoot blind thrust of the NMSZ.</p>
Mueller et al. (2004)	“Analyzing the 1811-1812 New Madrid earthquakes with recent instrumentally recorded aftershocks”	<p>Instrumentally recorded aftershock locations and models of elastic strain change are used to develop a kinematically consistent rupture scenario for three of the four largest earthquakes of the 1811-1812 earthquake sequence. Three of the events (NM1, NM1-A, and NM3) likely occurred on two contiguous faults (the strike-slip Cottonwood Grove fault and the Reelfoot thrust fault). The third mainshock (NM2), which occurred on January 23, 1812, is inferred to be a more distant triggered event that may have occurred as much as 200 kilometers to the north in the Wabash Valley of southern Illinois-southern Indiana. The magnitudes assigned to each of these events are NM 1 (<b>M</b> 7.3), NM1-A (<b>M</b> 7.0), NM 2 (<b>M</b> 6.8), and NM3 (<b>M</b> 7.5).</p>
Hough et al. (2005)	“Wagon Loads of Sand Blows in White County, Illinois”	<p>Based on anecdotal accounts of possible liquefaction that occurred at several sites in southern Illinois during the 1811-1812 New Madrid sequence, they conclude that (1) either large NMSZ events triggered substantial liquefaction at distances greater than hitherto realized, or (2) at least one large ‘New Madrid’ event occurred significantly north of the NMSZ. Neither can be ruled out, but the following lines of evidence suggest that the January 23, 1812, mainshock occurred in White County, Illinois, near the location of the <math>m_b</math> 5.5 1968 southern Illinois earthquake and recent microearthquake activity. Descriptions report substantial liquefaction (sand blows) as well as a 2-mile-long east-west trending “crack” along which 2 feet of south-side down displacement occurred. A modest offset in the Paleozoic strata is observed in seismic-reflection survey data at this location. Additional field investigations are needed to further document the extent and size of paleoliquefaction features and demonstrate the presence or absence of a east-west fault.</p>

TABLE 2.5.1-1. Summary of New Information for New Madrid Seismic Zone

Author(s) (Year)	Title	Significance
<b>RECURRENCE</b>		
Tuttle (2001a)	“The use of liquefaction features in paleoseismology: Lessons learned in the NMSZ, central United States”	<p>Major earthquakes occurred in the New Madrid region in:</p> <p>AD 1450 ± 150 years</p> <p>AD 900 ± 100 years</p> <p>Consistent with other paleoliquefaction studies in the region and with studies of fault-related deformation along Reelfoot scarp (Kelson et al., 1996).</p> <p>Evidence for earlier events, but age estimates and areas affected are poorly constrained.</p> <p>Based on similarities in size and spatial distribution of paleoliquefaction features from these events and close spatial correlation to historical features, NMSZ was the probable source of two earlier events.</p>
Cramer (2001)	“A seismic hazard uncertainty analysis for the NMSZ”	<p>A 498-year mean recurrence interval is obtained based on a Monte Carlo sampling of 1,000 recurrence intervals and using the Tuttle and Schweig (2000) uncertainties as a range of permissible dates (± two standard deviations). From these results, the 68% confidence limits range from 267 to 725 years; the 95% confidence limits range from 162 to 1,196 years (one and two standard deviation ranges, respectively).</p>
Tuttle et al. (2002)	“The earthquake potential of the NMSZ”	<p>Recurrence—Based on studies of hundreds of earthquake-induced paleoliquefaction features at more than 250 sites, the fault system responsible for New Madrid seismicity generated very large earthquakes temporally clustered in AD 900 ±100 and AD 1450 ±150, years as well as 1811-1812. Given uncertainties in dating liquefaction features, the time between the past three events may be as short as 200 years or as long as 800 years, with an average of 500 years. Evidence suggests that prehistoric sand blows probably are compound structures, resulting from multiple earthquakes closely clustered in time, or earthquake sequences.</p>

TABLE 2.5.1-1. Summary of New Information for New Madrid Seismic Zone

Author(s) (Year)	Title	Significance
<b>GEODETIC AND MODELING STUDIES</b>		
Newman et al. (1999)	"Slow deformation and lower seismic hazard at the NMSZ"	<p>Recent geodetic measurements indicate that the rate of strain accumulation is less than the current detection threshold. Global positioning system (GPS) data show no significant differences in velocities on either side of the southern arm of the NMSZ. Near-field and intermediate-field (primarily hard-rock sites) yield measurements of <math>0.6 \pm 3.2</math> and <math>-0.9 \pm 2.2</math> mm/year, respectively. They are consistent with both 0 and 2 mm/year at 2-sigma.</p> <p>GPS data for the upper Mississippi embayment show that the interior of the Reelfoot rift is moving northeast relative to the North American plate. Modeling stable North America as a single rigid plate fits the site velocities, with a mean residual of 1.0 mm/year.</p> <p>The authors conclude that the present GPS data imply that 1811-1812-size earthquakes are either much smaller or far less frequent than previously assumed (i.e., smaller than <b>M</b> 8 [5 to 10 meter slip/event], or longer than a recurrence interval of 400 to 600 years).</p>
Kenner and Segall (2000)	"A mechanical model for intraplate earthquakes: Application to the NMSZ"	<p>Postulates a time-dependent model for the generation of repeated intraplate earthquakes in which seismic activity is driven by localized transfer of stress from a relaxing lower crustal weak body. Given transient perturbation to the stress field, the seismicity is also transient, but can have a significantly longer duration. This model suggests that interseismic strain rates computed between damaging slip events would not be geodetically detectable.</p>
Grollimund and Zoback (2001)	"Did deglaciation trigger intraplate seismicity in the NMSZ?"	<p>Modeling of the removal of the Laurentide ice sheet ca. 20 ka changed the stress field in the vicinity of New Madrid and caused seismic strain to increase by about three orders of magnitude. The high rate of seismic energy release observed during late Holocene is likely to remain essentially unchanged for the next few thousand years.</p>

TABLE 2.5.1-1. Summary of New Information for New Madrid Seismic Zone

Author(s) (Year)	Title	Significance
Smalley et al. (2005)	"Space geodetic evidence for rapid strain rates in the NMSZ of central USA"	Recent analysis of geodetic measurements from a permanent GPS array in mid-America that was installed in the mid- to late 1990s provides evidence for rapid strain rates in the NMSZ (Smalley et al., 2005). Rates of strain are of the order of $10^{-7}$ per year, comparable in magnitude to those across active plate boundaries, and are consistent with known active faults in the region. Relative convergence across the RF is $\sim 2.7 \pm 1.6$ mm/year. Relative fault-parallel, right-lateral motion of $\sim 1$ mm/year is measured across the southern right lateral strike-slip fault zone, which is highlighted by a prominent northeast-trending and vertical zone of microseismicity and right-lateral focal mechanisms. Surface velocities at distances beyond a few fault dimensions (far-field) from active faults do not differ significantly from zero. It is not certain whether the driving force behind the current surface velocities is related to post-1811-1812 postseismic processes or to the accumulation of a locally sourced strain. The data indicate, however, that aseismic slip is almost certainly required across faults (or shear zones) within the upper few kilometers of the surface.

**SEISMIC SOURCE CHARACTERIZATION MODELS**

Cramer (2001)	"A seismic hazard uncertainty analysis for the NMSZ"	Develops a logic tree of possible alternative parameters to characterize earthquake sources in the NMSZ. Source model alternatives include "fictional" faults from Frankel et al. (1996), actual faults (Boothel lineament, eastern rift boundary, northeast arm, southwest arm, RF, west arm, and western rift boundary).
Frankel et al. (2002)	"Documentation for the 2002 update of the national seismic hazard maps"	Identifies three alternative fault sources: a fault trace matching recent microearthquake activity, and two adjacent sources situated near borders of the Reelfoot rift. The center fault is given twice the weight of the other two. Mean recurrence interval = 500 years:  <b>M 7.3:</b> (0.15 wt) <b>M 7.5:</b> (0.20 wt) <b>M 7.7:</b> (0.50 wt) <b>M 7.9:</b> (0.15 wt)



TABLE 2.5.1-1. Summary of New Information for New Madrid Seismic Zone

Author(s) (Year)	Title	Significance
Toro and Silva (2001)	"Scenario earthquakes for Saint Louis, MO, and Memphis, TN, and seismic hazard maps for the Central United States region including the effect of site conditions."	Develops alternative geometries for NMSZ. Uses fault sources identified by Johnston and Schweig (1996), augmented by alternative fault source model to the north (East Prairie extension), to represent more diffuse patterns of seismicity. Assumes that a large seismic-moment release in the region involves events on all three NMSZ faults occurring within a short interval. Occurrences of large earthquakes in the NMSZ are not independent in time. Uses mean recurrence intervals of 500 to 1,000 years.

TABLE 2.5.1-2. Magnitude Comparisons for New Madrid 1811-1812 Earthquake Sequence

<b>Study</b>	<b>NM1</b>	<b>NM2</b>	<b>NM3</b>
Johnston (1996b)	<b>M</b> 8.1 ± 0.3	<b>M</b> 7.8 ± 0.3	<b>M</b> 8.0 ± 0.3
Hough et al. (2000)	<b>M</b> 7.2 to 7.3	<b>M</b> ~7.0 <sup>a</sup> (located on the NN)	<b>M</b> 7.4 to 7.5
Mueller and Pujol (2001)	-	-	<b>M</b> 7.2 to 7.4 (preferred <b>M</b> 7.2 to 7.3)
Bakun and Hopper (2004a)	<b>M<sub>I</sub></b> 7.6 ( <b>M</b> 7.2 to 7.9) (preferred model 3)	<b>M<sub>I</sub></b> 7.5 ( <b>M</b> 7.1 to 7.8) (preferred model 3)	<b>M<sub>I</sub></b> 7.8 ( <b>M</b> 7.4 to 8.1) (preferred model 3)
	<b>M<sub>I</sub></b> 7.2 ( <b>M</b> 6.8 to 7.9) (model 1)	<b>M<sub>I</sub></b> 7.2 ( <b>M</b> 6.8 to 7.8) (model 1)	<b>M<sub>I</sub></b> 7.4 ( <b>M</b> 7.0 to 8.1) (model 1)
Mueller et al. (2004)	<b>M</b> 7.3	<b>M</b> 6.8 (located within the Wabash Valley of southern Illinois/ southern Indiana)	<b>M</b> 7.5
Johnston (written communication, August 31, 2004)	<b>M</b> 7.8-7.9	<b>M</b> 7.5-7.6	<b>M</b> 7.7-7.8

a. The estimated location and magnitude of this earthquake are revised in Mueller et al. (2004).

TABLE 2.5.1-3. Characteristic Magnitudes from Rupture Areas for Fault Segments in the NMSZ

Segment	Length	W = 10	W = 14	W = 15	W = 19	W = 28	W = 32
<i>Wells and Coppersmith (1994) magnitude-area relation (median): <math>M = 4.07 + 0.98 \log(\text{Area})</math></i>							
Southwest arm	117	7.1	7.2	7.3	7.4	7.5	7.6
Reelfoot fault	60	7.0	7.1	7.2	7.3	7.4	7.5
Bootheel lineament	70	6.9	7.0	7.0	7.1	7.3	7.4
Northeast arm	59	6.8	6.9	7.0	7.1	7.2	7.3
West arm	33	6.5	6.7	6.7	6.8	7.0	7.0
East Rift Boundary	99	7.0	7.1	7.2	7.3	7.4	7.5
West Rift Boundary	137	7.1	7.3	7.3	7.4	7.6	7.6
Bootheel + southern SW arm	133	7.1	7.3	7.3	7.4	7.6	7.6
Remaining (northern) SW arm	54	6.7	6.9	6.9	7.0	7.2	7.2
Bootheel + NE arm	129	7.1	7.3	7.3	7.4	7.6	7.6
<i>Somerville and Saikia (2000) magnitude-area relation (median): <math>M = 4.35 + \log(\text{Area})</math></i>							
Southwest arm	117	7.4	7.6	7.6	7.7	7.9	7.9
Reelfoot fault	60	7.3	7.5	7.5	7.6	7.8	7.8
Bootheel Lineament	70	7.2	7.3	7.4	7.5	7.6	7.7
Northeast arm	59	7.1	7.3	7.3	7.4	7.6	7.6
West arm	33	6.9	7.0	7.0	7.1	7.3	7.4
East Rift Boundary	99	7.3	7.5	7.5	7.6	7.8	7.9
West Rift Boundary	137	7.5	7.6	7.7	7.8	7.9	8.0
Bootheel + southern SW arm	133	7.5	7.6	7.6	7.8	7.9	8.0
remaining (northern) SW arm	54	7.1	7.2	7.3	7.4	7.5	7.6
Bootheel + NE arm	129	7.5	7.6	7.6	7.7	7.9	8.0

a. Rupture lengths and widths (W) in kilometers. Length uncertainty not included; weighting on magnitudes used in the uncertainty analysis are evenly distributed among widths and magnitude-area relations.

Source: Cramer (2001)



TABLE 2.5.1-4. Summary of Age Constraints for New Madrid Seismic Zone Earthquakes

Name of Site	Lab Sample Number <sup>a</sup>	Material	Time Relationship of Sample to Liquefaction	14C Age, years BP ± 1-sigma	Calibrated Age 2-sigma (95% Probability) <sup>b</sup>	Age Estimate Based on Ceramics and Points	Maximum Age Range (published correlation, comments)	Estimated Event Correlation	Reference	
Amanda	Beta-133004 (T1-C2)	Charcoal	Preliquefaction (event 2)	100 ± 40	AD 1680 to 1780 AD 1800 to 1940 AD 1950 to 1955	NA	Event in trench T2, followed by event in trench T1, occurred during or soon after AD 1000 to 1400 (Middle Mississippian)	Two events: 1811-1812 and event Y 1450 ± 150 year	Tuttle et al. (2000)	
	Beta-133006 (T2-C14)	Charcoal (top of lower sand blow)	Preliquefaction (event 2) Postliquefaction (event 1)	240 ± 50	AD 1520 to 1590 AD 1620 to 1690 AD 1740 to 1810 AD 1930 to 1950	NA				
	Beta-133005 (T2-C13)	Charcoal (19 centimeters below sand blow)	Preliquefaction (event 1)	920 ± 40	AD 1020 to 1210	NA				
	Beta-171216 (FSN27)	Nutshell Ceramics	Artifacts on surface and within plow zone	Reworked	NA	NA	Presence of Mississippian archeological site	Close maximum age	Confirms correlation of event 1 to event Y: 1450 ± 150 year	Tuttle and Wolf (2003)
			Artifacts, including diagnostic ceramics	Preliquefaction (event 1)	NA	NA	AD 800 to 1400 (Early and Middle Mississippian)			
Archway	Beta-166245 (C1)	Charcoal	Postliquefaction	200 ± 40	AD 1640 to 1690 AD 1730 to 1810 AD 1920 to 1950	NA		Event X 900 ± 100 year	Tuttle and Wolf (2003)	
	Beta-166246 (C5)	Charcoal	Anomalous result unless root grew into horizon from above	920 ± 40	AD 1020 to 1210	NA				
	Beta-171219 (FSN6)	Hickory nutshell collected 0-10 centimeters below sand blow  Ceramics	Preliquefaction	1310 ± 40	AD 660 to 780	NA	Sand blow formed < 200 year after this time			
			Preliquefaction	NA	NA	AD 400 to 800, Middle to Late Woodland	Sand blow directly above cultural horizon			
Brooke	Beta-102497	Soil	Preliquefaction	1960 ± 40	40 BC to AD 130	NA	Unweathered sand blow, 15 to 20 centimeters thick; A horizon developed post-occupation and preliquefaction	AD 1811-1812	Tuttle (1999)	
	Beta-102498	Charcoal collected 45 centimeters below sand blow; artifacts from B horizon more than 15 centimeters below sand blow	Preliquefaction	370 ± 50	AD 144 to 1650	AD 140 to 1670 Late Mississippian				
Bugg	Beta-108883	Charcoal	Postliquefaction	130 ± 40	AD 167 to 1950	AD 80 to 1000 Early Mississippian	AD 800 to 1000; sand blow deposited directly on cultural horizon; thickness of plow zone plus remnant A horizon below (50 centimeters) suggest sand blow formed ~1,000 years ago	Event X 900 ± 100 year	Tuttle (1999)	
	NA	Ceramics	Preliquefaction	NA	NA	AD 40 to 1000 Late Woodland-Early Mississippian				

TABLE 2.5.1-4. Summary of Age Constraints for New Madrid Seismic Zone Earthquakes

Name of Site	Lab Sample Number <sup>a</sup>	Material	Time Relationship of Sample to Liquefaction	14C Age, years BP ± 1-sigma	Calibrated Age 2-sigma (95% Probability) <sup>b</sup>	Age Estimate Based on Ceramics and Points	Maximum Age Range (published correlation, comments)	Estimated Event Correlation	Reference
Burkett	Beta-142708 (TR6-C100)	Charcoal	Preliquefaction (event 4)	110 ± 40	AD 167 to 1780 AD 180 to 1955	NA	Event 4	1811-1812 or 1895 Charleston	Tuttle (2001b)
	TR-6	Artifacts—Burkett phase	Preliquefaction (event 3)	NA	NA	~400 BC to AD 330 Early-Middle Woodland (radiocarbon dating of horizon by Prentice Thomas)	Event 3 probably occurred at end of Burkett phase (AD 300 ± 200 year)	Event W AD 300 ± 200 year  May be same event as older Towosaghy S1 event	Tuttle (M. Tuttle and Associates, electronic communication to Kathryn Hanson, February 27, 2003).
	TU-56	Artifacts—Mississippian and Burkett phase artifacts?	Postliquefaction (event 3)	NA	NA	Woodland-Mississippian	Event 3 probably occurred toward end of Burkett phase (AD 300 ± 200 year)	Event W AD 300 ± 200 year  May be same event as older Towosaghy S1 event	
	TU-56	Artifacts—Burkett phase	Preliquefaction (event 3) and postliquefaction (events 1 and 2)	NA	NA	~400 BC to AD 330 Early-Middle Woodland (radiocarbon dating of horizon by Prentice Thomas)	TU56-events 1 and 2 occurred after deposition of O'Bryan Ridge-phase artifacts and before deposition of Burkett-phase artifacts	Event U? 2350 BC ± 200 year  Perhaps same as event 1 at Eaker 2	
	TU-56	Artifacts—O'Bryan Ridge phase	Preliquefaction (events 1 and 2)	NA	NA	Late Archaic (3000 to 400 BC)	TR5—events 1 and 2 occurred during Late Archaic shortly after BC 2580; event 3 occurred during or soon after Burkett phase	TR-5: event U? 2350 BC ± 200 year	
	Beta-142448 (TR5-C9)	Charcoal	Postliquefaction (event 3)	70 ± 40	AD 1680 to 1740 AD 1810 to 1930 AD 1950 to 1955	NA	BL7—event 1 occurred after 2340 to 2190 BC; event 2 occurred after 2570 to 2990 BC	Perhaps same as event 1 at Eaker 2	
	TR5	Artifacts—Burkett phase	Preliquefaction (event 3)	NA	NA	~400 BC to AD 330 Early-Middle Woodland (radiocarbon dating of horizon by Prentice Thomas)		BL7—event U? included two earthquakes large enough to induce liquefaction; 2350 BC ± 200 year	
	Beta-142447 (TR5-C5)	Charcoal and artifacts—O'Bryan Ridge phase	Preliquefaction (events 1 and 2)	3980 ± 40	BC 2580 to 2430; close maximum (event 1)	Late Archaic (3000 to 400 BC)		Perhaps same as event 1 at Eaker 2	
	Beta-142445 (BW1-C2)	Charcoal from midden adjacent to mound	Reworked by natives; probably preliquefaction (events 1 and 2)	4090 ± 40	BC 2870 to 2800 BC 2760 to 2560 BC 2540 to 2490	NA			
	Beta-153985 (BW1-C4)	Charcoal from midden adjacent to mound	Reworked by aboriginals; probably preliquefaction (events 1 and 2)	4090 ± 40	BC 2870 to 2800 BC 2760 to 2560 BC 2540 to 2490	NA			
	Beta-153985 (BW1-C3)	Charcoal from contact between clay of mound and soil horizon below	Postliquefaction (event 1); preliquefaction (event 2)	3940 ± 50	BC 2570 to 2290; Contemporaneous	NA			

TABLE 2.5.1-4. Summary of Age Constraints for New Madrid Seismic Zone Earthquakes

Name of Site	Lab Sample Number <sup>a</sup>	Material	Time Relationship of Sample to Liquefaction	14C Age, years BP ± 1-sigma	Calibrated Age 2-sigma (95% Probability) <sup>b</sup>	Age Estimate Based on Ceramics and Points	Maximum Age Range (published correlation, comments)	Estimated Event Correlation	Reference
	Beta-142706 (BW1-C6)	Charcoal from soil horizon below sand blows of events 1 and 2 and within graben structure	Preliquefaction (events 1 and 2)	3970 ± 40	BC 2580 to 2400 BC 2380 to 2360	NA			
	Beta-142446 (BW2-C7)	Charcoal from soil horizon below lower sand blow	Preliquefaction (events 1 and 2)	3820 ± 30	BC 2340 to 2190 BC 2170 to 2150; Close maximum	NA			
	Beta-142707 (BW2-C8)	Charcoal from clay used to construct base of mound	Probably reworked by aboriginals; preliquefaction (event 1)	4300 ± 40	BC 3010 to 2980 BC 2940 to 2880	NA			
Cagle Lake	Beta-160377 (F101)	Wood from aboriginal post mold in top of sand blow	Postliquefaction	240 ± 60	AD 1500 to 1690 AD 1730 to 1810 AD 1920 to 1950; Close minimum	Site occupied by aboriginals following formation of sand blow	AD 1420 to 1690—prehistoric compound sand blow; exclude minimum constraining dates post-AD 1700	Event Y 1450 ± 150 year	Tuttle and Wolf (2003)
	Beta-166251 (C106)	Charcoal from aboriginal post mold in top of sand blow	Postliquefaction	170 ± 40	AD 1650 to 1890 AD 1910 to 1950	Site occupied by aboriginals following formation of sand blow			
	Beta-171217 (FSN116)	Hickory nutshell collected 0 to 5 centimeters below sand blow	Preliquefaction	440 ± 40	AD 1420 to 1500; Close maximum	NA			
	Beta-166250 (C104)	Charcoal collected 5 to 15 centimeters below sand blow	Preliquefaction	580 ± 40	AD 1300 to 1420	NA			
	Beta-166249 (C100)	Charcoal collected 47 centimeters below sand blow	Preliquefaction	460 ± 40	AD 1410 to 1480	NA			
			Preliquefaction	NA	NA	~AD 1400 to 1500 Late Mississippian; occupied at time of sand blow			
Central Ditch 1	Beta-108869	Charcoal	Postliquefaction	70 ± 40	AD 1690 to 1740 AD 1810 to 1930	NA	AD 800 to 1000 Radiocarbon dating—sand blow formed from AD 790 to 1240; Early Mississippian and Late Woodland artifacts in horizon immediately below—sand blow formed from AD 800 to 1000; A horizon developed in sand blow suggests it formed > 600 years ago	Event X 900 ± 100 year	Tuttle (1999)
	Beta-81308	Soil (30 centimeters thick, with few small artifacts possibly reworked)	Postliquefaction	940 ± 60	AD 1000 to 1240	AD 400 to 1000 Late Woodland			
	Beta-81309	Soil; artifacts	Preliquefaction	1120 ± 60	AD 790 to 1020	AD 400 to 1000 Late Woodland-Early Mississippian			

TABLE 2.5.1-4. Summary of Age Constraints for New Madrid Seismic Zone Earthquakes

Name of Site	Lab Sample Number <sup>a</sup>	Material	Time Relationship of Sample to Liquefaction	14C Age, years BP $\pm$ 1-sigma	Calibrated Age 2-sigma (95% Probability) <sup>b</sup>	Age Estimate Based on Ceramics and Points	Maximum Age Range (published correlation, comments)	Estimated Event Correlation	Reference
C1-Cooter	Beta-74678	Organic material	Postliquefaction	110 $\pm$ 60	AD 1660 to 1950	NA	AD 1410-1811; Event pre-dates 1811 based on soil development above sand blow, weathering characteristics of sand blow, and liquefaction of sand blow by subsequent event, probably 1811-1812	Probably correlates with event Y 1450 $\pm$ 150 year	Craven (1995)
	Beta-74099	Thatch from aboriginal dwelling	Preliquefaction	440 $\pm$ 50	AD 1410 to 1520 AD 1570 to 1630	NA	AD 1400 to 1650; sand blow deposited directly on occupation horizon; dating of thatch and artifacts provides close maximum		
Current River 2	Beta-110225	Charcoal	Postliquefaction	570 $\pm$ 60	AD 1300 to 1450	NA	AD 1310 to 1450	Event Y 1450 $\pm$ 150 year	Tuttle (1999)
	Beta-110223	Cypress knees	Preliquefaction	510 $\pm$ 60	AD 1310 to 1360 AD 1390 to 1480	NA			
	Beta-110224	Charcoal	Preliquefaction	640 $\pm$ 90	AD 1240 to 1440	NA			
Current River 8	Beta-110227	Root	Postliquefaction	Modern		NA	2 to 4 earthquakes, 3490 BC to AD 1670; weathering characteristics of upper 30 to 50 centimeters of dikes suggest that they are prehistoric		Tuttle (1999)
	Beta-110226	Plant material	Preliquefaction (2 to 4 subsequent events)	4560 $\pm$ 50	3490 to 3470 BC 3380 to 3090 BC	NA			
Dillahunt	Beta-166247 (C4)	Charcoal	Postliquefaction	70 $\pm$ 70	Modern	NA	AD 910 to 1490	Event Y (1450 $\pm$ 150 year)	Tuttle and Wolf (2003)
	Beta-166248 (C5)	Charcoal from base of soil developed in sand-blow crater	Postliquefaction	470 $\pm$ 50	AD 1400 to 1490; close minimum	NA	Compound sand blow (3 major units); events closely spaced in time; prehistoric based on soil development; C5 provides close minimum, whereas FSN4 and artifacts only provide maximum		
	Beta-171218 (FSN4)	Maize kernel fragment from 0 to 10 centimeters below sand blow	Preliquefaction	980 $\pm$ 70	AD 910 to 920 AD 960 to 1210	NA			
		Ceramics 10 to 20 centimeters below sand blow	Preliquefaction	NA	NA	Middle Woodland $\sim$ (200 BC to AD 400); soil development suggests at least 200 years between occupation and deposition of sand blow			
Dodd	Beta-102503	Charcoal	Postliquefaction	110 $\pm$ 50	AD 1670 to 1950	1400 to 1670 Late Mississippian—during this period	AD 1290 to 1460 from dating; AD 1400 to 1670 from archeology; AD 1400 to 1460 combining the two	Event Y (1450 $\pm$ 150 year)	Tuttle (1999) Tuttle et al. (1999b)
	Beta-119103	Charcoal; artifacts	Postliquefaction	120 $\pm$ 50	AD 167 to 1950	1400 to 1670 Late Mississippian			Tuttle and Schweig (2000)
	Beta-142449	Charred corn kernel from aboriginal wall trench dug into sand blow	Postliquefaction	490 $\pm$ 40	AD 1410 to 1460; close minimum				
	Beta-119102	Charcoal	Preliquefaction	630 $\pm$ 40	AD 1290 to 1410; close maximum	1000 to 1670 Middle-Late Mississippian			
	Beta-102502	Charcoal	Preliquefaction	770 $\pm$ 40	AD 1220 to 1300	1000 to 1670 Middle-Late Mississippian			



TABLE 2.5.1-4. Summary of Age Constraints for New Madrid Seismic Zone Earthquakes

Name of Site	Lab Sample Number <sup>a</sup>	Material	Time Relationship of Sample to Liquefaction	14C Age, years BP ± 1-sigma	Calibrated Age 2-sigma (95% Probability) <sup>b</sup>	Age Estimate Based on Ceramics and Points	Maximum Age Range (published correlation, comments)	Estimated Event Correlation	Reference
Eaker 1	Beta-91511	Charcoal (vertical root)	Postliquefaction	50 ± 50	AD 1690 to 1740 AD 1810 to 1930	NA	Either AD 1180 to 1630 or AD 1410 to 1650; soil development (including lamellae) above sand blow suggests it is prehistoric; liquefaction of sand blow suggests subsequent event, probably 1811-1812	Event Y (1450 ± 150 year)	Tuttle (1999)
	Beta-75326	Charcoal	Postliquefaction	170 ± 60	AD 1650 to 1950	NA			
	Beta-75325	Plant material (lateral root)	If preliquefaction, close maximum; if postliquefaction, close minimum	450 ± 60	AD 1410 to 1530 AD 1560 to 1630	NA			
	Beta-81313	Soil; ceramics	Preliquefaction	740 ± 70	AD 1180 to 1400	400 to 1000 Middle-Late Woodland			
Eaker 2	NA	Ceramics	Postliquefaction (event IV)	NA	NA	800 to 1000 Late Woodland-Early Mississippian	AD 470 to 1310—event IV; site occupied before and after event	Event X (900 ± 100 year)	Tuttle (1999)
	Beta-86810	Charcoal	Postliquefaction (event IV)	460 ± 60	AD 1400 to 1520 AD 157 to 1630	NA			
	Beta-86811	Charcoal	Postliquefaction (event IV)	510 ± 60	AD 1310 to 1360 AD 1390 to 1480	NA			
	Beta-77450	Charcoal	Postliquefaction (event IV)	660 ± 60	AD 1270 to 1420	NA			
	Beta-86190	Soil	Postliquefaction (event IV)	770 ± 60	AD 1180 to 1310	NA			
	Beta-86816	Soil and ceramics	Preliquefaction (event IV)	1420 ± 80	AD 470 to 480 AD 520 to 780	AD 400 to 1000 Late Woodland			
	Beta-86816	Soil and ceramics	Postliquefaction (event III)	1420 ± 80	AD 470 to 480 AD 520 to 780	AD 400 to 1000 Late Woodland	800 BC to AD 780 Event III	Event W ? AD 300 ± 200 year	Tuttle (1999)
	Beta-86814	Soil	Preliquefaction (event III)	2410 ± 90	800 to 360 BC 290 to 230 BC	NA			
	Beta-86814	Soil	Postliquefaction (event II)	2410 ± 90	800 to 360 BC 290 to 230 BC	NA	1430 to 800 BC Event II	Event V?	Tuttle (1999)
	Beta-81311	Soil	Preliquefaction (event II)	2970 ± 100	1430 to 910 BC	NA			
	Beta-86815	Soil	Preliquefaction (event II)	3020 ± 80	1430 to 910 BC	NA			
	Beta-86812	Soil	Preliquefaction (event II)	3200 ± 100	1690 to 1250 BC	NA			
	Beta-86812	Soil	Postliquefaction (event I)	3200 ± 100	1690 to 1250 BC	NA	3340 to 1250 BC Event I	Event U ? May correlate with events 1 and 2 at Burkett site	Tuttle (1999)
	Beta-86813	Soil	Preliquefaction (event I)	4180 ± 190	3340 to 2210 BC	NA			
Eaker 3	Beta-69618	Charcoal and artifacts	Postliquefaction	300 ± 60	AD 1460 to 1680 AD 1770 to 1800 AD 1940 to 1960	AD 1000 to 1400 Middle Mississippian	AD 800 to 1400 (Evidence for two events probably during same earthquake sequence)	Event X 900 ± 100 year	Tuttle (1999)
	NA	Ceramics	Preliquefaction	NA	NA	800 to 1000 Late Woodland-Early Mississippian			
Haynes	G-19080	Charcoal	Postliquefaction	455 ± 110	AD 1300 to 1660	AD 1000 to 1400 Middle Mississippian	AD 800 to 1400	Event X 900 ± 100 year	Tuttle (1999)
	NA	Ceramics	Preliquefaction	NA	NA	AD 800 to 1000 Early Mississippian			Tuttle et al. (2000)

TABLE 2.5.1-4. Summary of Age Constraints for New Madrid Seismic Zone Earthquakes

Name of Site	Lab Sample Number <sup>a</sup>	Material	Time Relationship of Sample to Liquefaction	14C Age, years BP $\pm$ 1-sigma	Calibrated Age 2-sigma (95% Probability) <sup>b</sup>	Age Estimate Based on Ceramics and Points	Maximum Age Range (published correlation, comments)	Estimated Event Correlation	Reference
Hillhouse	Beta-102500	Charcoal and ceramics	Postliquefaction	1150 $\pm$ 50	AD 780 to 1000	AD 400 to 1000 Late Woodland	AD 790 to 1000	Event X 900 $\pm$ 100 year	Tuttle (1999)
	Beta-102499	Charcoal	Preliquefaction	1140 $\pm$ 50	AD 790 to 1010	NA			
	Beta-102501	Soil	Preliquefaction	4880 $\pm$ 60	3780 to 3620 BC 3580 to 3530 BC	AD 400 to 1000 Late Woodland			
Hueys	Beta-91642	Charcoal (hearth) and ceramics	Postliquefaction	280 $\pm$ 60	AD 1470 to 1680 AD 1750 to 1810 AD 1940 to 1950	AD 800 to 1000 Late Woodland-Early Mississippian	AD 880 to 1000	Event X 900 $\pm$ 100 year	Tuttle (1999)
	Beta-108939	Charcoal (maize)	Postliquefaction	630 $\pm$ 50	AD 1290 to 1420	AD 800 to 1000 Late Woodland-Early Mississippian			
	Beta-91641	Charcoal and artifacts	Preliquefaction	1090 $\pm$ 50	AD 880 to 1030	AD 800 to 1000 Late Woodland-Early Mississippian			
	Beta-91643	Charcoal	Preliquefaction	1280 $\pm$ 60	AD 650 to 890	NA			
Johnson 5	Beta-102504	Charcoal	Postliquefaction	220 $\pm$ 50	AD 1540 to 1550 AD 1640 to 1700 AD 1720 to 1820 AD 1855 to 1860 AD 1920 to 1950		AD 770 to 1670 Minimum age not well constrained; probably formed during Late Woodland-Early Mississippian. Soil development suggests sand blow formed prior to 1811 and was exposed at the surface for at least 670 years	Event X 900 $\pm$ 100 year	Tuttle (1999)
	Beta-102505	Soil	Preliquefaction	1110 $\pm$ 80	AD 770 to 1040	AD 800 to 1000 Late Woodland-Early Mississippian			
K1 Champey Pocket							Event Z—AD 1812 Unweathered liquefaction features	AD 1812	Kelson et al. (1992 and 1996)
	Beta-49608	Charcoal	Post-monoclinial folding; colluvium	-	AD 1430 to 1650	NA	Event Y AD 1220 to 1650; ~AD 1400	Event Y (1450 $\pm$ 150 year)	
	Beta-49609	Charcoal	Pre-monoclinial folding	-	AD 1220 to 1390	NA			
	Beta-48553	Charcoal; artifacts	Postliquefaction	-	AD 430 to 890	AD 800 to 1000 Close minimum (third most recent event)	Event X AD 780 to 1000	Event X 900 $\pm$ 100 year	
K2 Proctor City							Event Z—AD 1812: Sand dikes and sand blow with no soil development	1812	Kelson et al. (1996)
			Post-scarp formation and re-development of graben (event Y)				Event Y—AD 1260 to 1650 Poorly constrained; couple hundred years prior to 1812 to erode scarp	Event Y (1450 $\pm$ 150 year)	
	CAMS-13559	Charcoal	Pre-scarp formation and re-development of graben (event Y)	660 $\pm$ 60	AD 1260 to 1410	NA	Event post-dates AD 1260		
	CAMS-13540	Charcoal	Post-graben formation (event X)	960 $\pm$ 60	AD 980 to 1220	NA	Event X AD 780 to 1000; close minimum	Event X 900 $\pm$ 100 year	
	CAMS-13538	Charcoal	Pre-graben formation (? younger) (event X)	990 $\pm$ 60	AD 900 to 1210	NA			
	CAMS-13537	Charcoal	Pre-graben formation (event X)	1110 $\pm$ 60	AD 780 to 1030	NA	Close maximum		

TABLE 2.5.1-4. Summary of Age Constraints for New Madrid Seismic Zone Earthquakes

Name of Site	Lab Sample Number <sup>a</sup>	Material	Time Relationship of Sample to Liquefaction	14C Age, years BP ± 1-sigma	Calibrated Age 2-sigma (95% Probability) <sup>b</sup>	Age Estimate Based on Ceramics and Points	Maximum Age Range (published correlation, comments)	Estimated Event Correlation	Reference
Kochtitzky Ditch 1	Beta-97573	Charcoal	Postliquefaction	2020 ± 60	BC 180 to AD 110 (reworked?)	AD 800 to 1670 Mississippian	AD 990 to 1660 Event occurred during occupation of site, probably during Late Mississippian	Event Y (1450 ± 150 year)	Tuttle (1999)
	Beta-102512	Charcoal	Postliquefaction	360 ± 50	AD 1440 to 1660	AD 800 to 1670 Mississippian			
	Beta-97574 Artifacts	Charcoal	Preliquefaction	960 ± 60	AD 990 to 1220	AD 800 to 1000 Mississippian; elsewhere at site this horizon contains Middle-Mississippian (AD 1000 to 1400) artifacts and Late-Mississippian house floor (AD 1400 to 1670)			
Lowrance	Beta-133011	Charcoal 43 centimeters below sand blow	Preliquefaction	330 ± 50	AD 1450 to 1660	NA	Probably 1811-1812	1811-1812	Tuttle et al. (2000)
L1 (Site WY)	Beta-74810	Charcoal	Postliquefaction	480 ± 60	AD 1400 to 1620	NA	AD 55 to 1620	Could correlate to event W (AD 300 ± 200 year), event X (900 ± 100 year), or event Y (1450 ± 150 year)	Li et al. (1998)
	Beta-92884 (S)	Dispersed carbon	Preliquefaction	2060 ± 60	195 BC to AD 75	NA			
	Beta-92883 (C2)	Charcoal	Preliquefaction	1850 ± 60	AD 55 to 340	NA			
L2 (Site WD)	Beta-71233 (S)	Twig	Preliquefactions (event 2) Postliquefaction (event 1)	240 ± 60	AD 1510 to 1950	NA	Two sand blows, 1811-1812 and 900 ± 100 year Lower sand blow exposed at surface ~800 ± 100 year prior to burial by younger sand blow	1811-1812 (event 2)	Li et al. (1998)
	Beta-71234	Soil (dispersed carbon)	Postliquefaction (event 1)	1140 ± 60	AD 770 to 1040	NA	Event X 900 ± 100 year (event 1)		
Main 8	GX-17728	Wood	Preliquefaction	4930 ± 160	BC 4035 to 3360	NA	Three generations of liquefaction features formed since BC 4040		Tuttle (1993)
New Franklin 3	Beta-84975	Charcoal	Postliquefaction	210 ± 60	AD 1530 to 1560 AD 1630 to 1950	NA	180 BC to AD 990	Event X 900 ± 100 year	Tuttle (1999)
	Beta-97577	Soil	Postliquefaction	1030 ± 60	AD 890 to 1170	NA			
	Beta-97578	Soil	Postliquefaction	1110 ± 50	AD 860 to 1020	NA			
	Beta-86191	Soil	Postliquefaction	1200 ± 60	AD 690 to 990	NA			
	Beta-97579	Soil	Preliquefaction	2000 ± 70	180 BC to AD 150	NA			
	Beta-84976	Soil	Preliquefaction	2050 ± 60	190 BC to AD 90	NA			
Nodena	Beta-133012 (T1-C1)	Charcoal	Preliquefaction (<1 centimeters below)	290 ± 50	AD 1470 to 1670 AD 1780 to 1800	NA	Two events in the same earthquake sequence AD 1450-1670	Event Y (1450 ± 150 year)	Tuttle et al. (2000)
	Beta-133013 (T1-C4)	Charcoal	Preliquefaction (45 centimeters below)	280 ± 50	AD 1480 to 1680 AD 1780 to 1800 AD 1940 to 1950	NA			
	Beta-133014 (T2-C1)	Charcoal (root cast into sand blow)	Postliquefaction	230 ± 50	AD 1520 to 1580 AD 1630 to 1690 AD 1730 to 1810 AD 1930 to 1950	NA			

TABLE 2.5.1-4. Summary of Age Constraints for New Madrid Seismic Zone Earthquakes

Name of Site	Lab Sample Number <sup>a</sup>	Material	Time Relationship of Sample to Liquefaction	14C Age, years BP $\pm$ 1-sigma	Calibrated Age 2-sigma (95% Probability) <sup>b</sup>	Age Estimate Based on Ceramics and Points	Maximum Age Range (published correlation, comments)	Estimated Event Correlation	Reference
	Beta-133015 (T2-C20)	Charcoal	Preliquefaction (9 centimeters below)	350 $\pm$ 40	AD 1450 to 1650	NA			
	Beta-133016 (T2-C101)	Charcoal	Preliquefaction (3 centimeters below)	340 $\pm$ 30	AD 1460 to 1650	NA			
		Ceramics	Postliquefaction	NA	NA	AD 1000 to 1700			
		Artifacts	Preliquefaction	NA	NA	AD 1400 to 1700			
Obion 200	Beta-146738	Wood W2 collected from silt deposit above sand blow	Postliquefaction	230 $\pm$ 40	AD 1530 to 1550 AD 1640 to 1680 AD 1740 to 1810 AD 1930 to 1950	NA	Before AD 1810 and After AD 1300 (based on probability distribution)	Event Y (1450 $\pm$ 150 year)	Tuttle (2001b)
	Beta-146737	Wood W1 collected within 1 centimeter of base of sand blow	Preliquefaction	590 $\pm$ 40	Close maximum AD 1300 to 1420	NA			
Obion 216	Beta-152008	Wood (W2 from outer 1 centimeter of horizontally bedded log buried by sand blow)	Preliquefaction	800 $\pm$ 60	AD 1060 to 1080 AD 1150 to 1290	NA	Event soon after AD 1300 (based on probability distribution)	Event Y (1450 $\pm$ 150 year)	Tuttle (2001b); Tuttle and Wolf (2003)
	Beta-152009	Wood (W4 from outer 1 centimeter of tree trunk in growth position in clay deposit beneath sand blow.	Preliquefaction	730 $\pm$ 60	AD 1160 to 1300	NA			
RP Haynes	Beta-133009 (C2)	Charcoal	Preliquefaction	160 $\pm$ 40	AD 1660 to 1950	NA	Event after AD 1000; possibly after AD 1660	Possibly 1811-1812	Tuttle et al. (2000); Barnes (2000)
	Beta-133010 (C5)	Charcoal	Preliquefaction	260 $\pm$ 80	AD 1450 to 1710 AD 1720 to 1890 AD 1910 to 1950	NA			
	Beta-142450 (C100) collected 40 centimeters below sand blow	Charcoal	Preliquefaction	970 $\pm$ 40	AD 1000 to 1170				
		Ceramics from horizon below sand blow	Preliquefaction	NA	NA	AD 800 to 1000 Mostly Late Woodland; few Early Mississippian shards			
Towosaghy (S1)	Beta-36669	Charcoal	Postliquefaction (event 2)	520 $\pm$ 60	AD 1414		Event 2 probably occurred in the early part of the period AD 539 to 991	Event X (?) 900 $\pm$ 100 year (event 2)	Saucier (1991)
	Beta-36670	Charcoal	Post- liquefaction (event 2)	1050 $\pm$ 120	AD 991 (intercept)		Event 1 estimated to have occurred <100 year prior to AD 539	Event 1 AD 440 to 540	
	Beta-36671	Charcoal	Preliquefaction (event 2) Postliquefaction (event 1)	1540 $\pm$ 110	AD 539 (intercept)				

TABLE 2.5.1-4. Summary of Age Constraints for New Madrid Seismic Zone Earthquakes

Name of Site	Lab Sample Number <sup>a</sup>	Material	Time Relationship of Sample to Liquefaction	14C Age, years BP ± 1-sigma	Calibrated Age 2-sigma (95% Probability) <sup>b</sup>	Age Estimate Based on Ceramics and Points	Maximum Age Range (published correlation, comments)	Estimated Event Correlation	Reference
Towosaghy (re-excavate S1 site)	Dating underway	Artifacts	Preliquefaction (event 3)	NA	NA	Sand dike crosscuts horizon containing artifacts	Event 3; not yet determined	Event 3; Not yet determined	Tuttle and Wolf (2003)
	Dating underway	Artifacts	Postliquefaction (event 1)	NA	NA	Late Woodland to Early Mississippian (AD 400 to 1000) above sand blow; few artifacts below sand blow	Evidence for event 1 but not event 2 of Saucier	May correlate to event W AD 300 ± 200 year (event 1)	
Walker	Artifacts on surface and within plow zone					Presence of Mississippian archeological site			Tuttle et al. (2000); Barnes (2000)
	Beta-133017 (T2-C1)	Charcoal	Postliquefaction	43210 ± 720 (probably reworked)	NA	NA	Trench T2—AD 1420 to 1670 during Late Mississippian Trench T3—Also during the Mississippian, probably during same event as seen in trench T2. Soil lamellae developed in upper 40 centimeters of sand dikes indicate that they are prehistoric	Event Y (1450 ± 150 year) Root cast may have been intruded by sand during subsequent event, 1811-1812	Tuttle et al. (2000)
	Beta-133018 (T2-C2)	Charcoal from cultural horizon < 1 centimeters below sand blow; artifacts	Preliquefaction	440 ± 40	AD 1420 to 1500 Close maximum	AD 1400 to 1670—Late Mississippian AD 1000 to 1400—Middle Mississippian (strap handle)			
	Beta-133019 (T3-C2)	Charcoal from root cast	Preliquefaction (same or later event)	230 ± 40	AD 1530 to 1550 AD 1640 to 1680 AD 1740 to 1810 AD 1930 to 1950	NA			
	Beta-133020 (T3-C3)	Organic material from deposit below cultural horizon	Artifacts in cultural horizon below sand blow Preliquefaction			Mississippian			
Yarbro 1	ISGS-2968	Tree root (large sample from outer ring sent to three labs)	Postliquefaction	640 ± 70	NA	NA	AD 1420 to 1670	Event Y (1450 ± 150 year)	Tuttle (1999)
	QL-4787		Postliquefaction	181 ± 16	AD 1668 to 1686 AD 1737 to 1788 AD 1791 to 1810 AD 1928 to 1954	NA			
	Beta-80749		Postliquefaction	130 ± 60	AD 1660 to 1950	NA			
	Beta-79237	Twig	Preliquefaction (close maximum)	370 ± 80	AD 1420 to 1670	NA			
	Beta-81310	Soil	Preliquefaction	-	AD 1420 to 1540 AD 1550 to 1640	NA			
Yarbro 2	Beta-79350	Pond nut	Postliquefaction	160 ± 60	AD 1650 to 1950	NA		1811-1812	Tuttle (1999)
	Beta-79354	Wood from top of A horizon	Postliquefaction	180 ± 70	AD 1540 to 1550 AD 1640 to 1950	NA			
	Beta-79355	Wood from base of A horizon	Postliquefaction	320 ± 60	AD 1450 to 1670 AD 1780 to 1800 AD 1945 to 1950	NA			

TABLE 2.5.1-4. Summary of Age Constraints for New Madrid Seismic Zone Earthquakes

Name of Site	Lab Sample Number <sup>a</sup>	Material	Time Relationship of Sample to Liquefaction	<sup>14</sup> C Age, years BP ± 1-sigma	Calibrated Age 2-sigma (95% Probability) <sup>b</sup>	Age Estimate Based on Ceramics and Points	Maximum Age Range (published correlation, comments)	Estimated Event Correlation	Reference
	Beta-79352	Large twig collected at the contact of the sand blow and pre-event paleosol	Preliquefaction	90 ± 60	AD 1670 to 1950	NA			
	Beta-79353	Wood	Preliquefaction	80 ± 60	AD 1670 to 1780 AD 1800 to 1950	NA			
Yarbro 3	Beta-84977	Tree	Preliquefactions	90 ± 40	AD 1680 to 1760 AD 1810 to 1940	NA		1811-1812	Tuttle (1999)
	Beta-84977	Tree	Postliquefaction	90 ± 40	AD 1680 to 1760 AD 1810 to 1940	NA	Two sand blows are interpreted to have formed during the same event, circa AD 1530 ± 130 year.	Event Y (1450 ± 150 year)	
	Beta-108882	Tree center	Preliquefaction	330 ± 40	AD 1445 to 1670 Plus 68 rings (AD 1513 to 1738)	NA			

Notes:

<sup>a</sup> Beta—Beta Analytic, Inc. (Miami, FL); CAMS—Center for Accelerator Mass Spectrometry (Livermore, CA); G—Krueger Enterprises' Geochron Laboratory; ISGS—Illinois State Geological Survey; QL—Quaternary Isotope Laboratory, University of Washington (Seattle, WA)

<sup>b</sup> Intervals that can be eliminated based on stratigraphic or historical evidence are shown in italics.

TABLE 2.5.1-5. Timing and Source of Liquefaction Events in Southern Atlantic Coastal Plain

Liquefaction Episode	Age, Years B.P.	Scenario 1		Scenario 2	
		Source	Magnitude <sup>a</sup>	Source	Magnitude <sup>a</sup>
1886 AD	113	Charleston	7.3	Charleston	7.3
A	546±17	Charleston	7+	Charleston	7+
B	1021±30	Charleston	7+	Charleston	7+
C	1648±74	northern part	~6.0	--	--
C'	1683±70	--	--	Charleston	7+
D	1966 ±212	southern part	~6.0	--	--
E	3548±66	Charleston	7+	Charleston	7+
F	5038± 166	Northern part	~6.0	Charleston	7+
G	5800±500	Charleston	7+	Charleston	7+

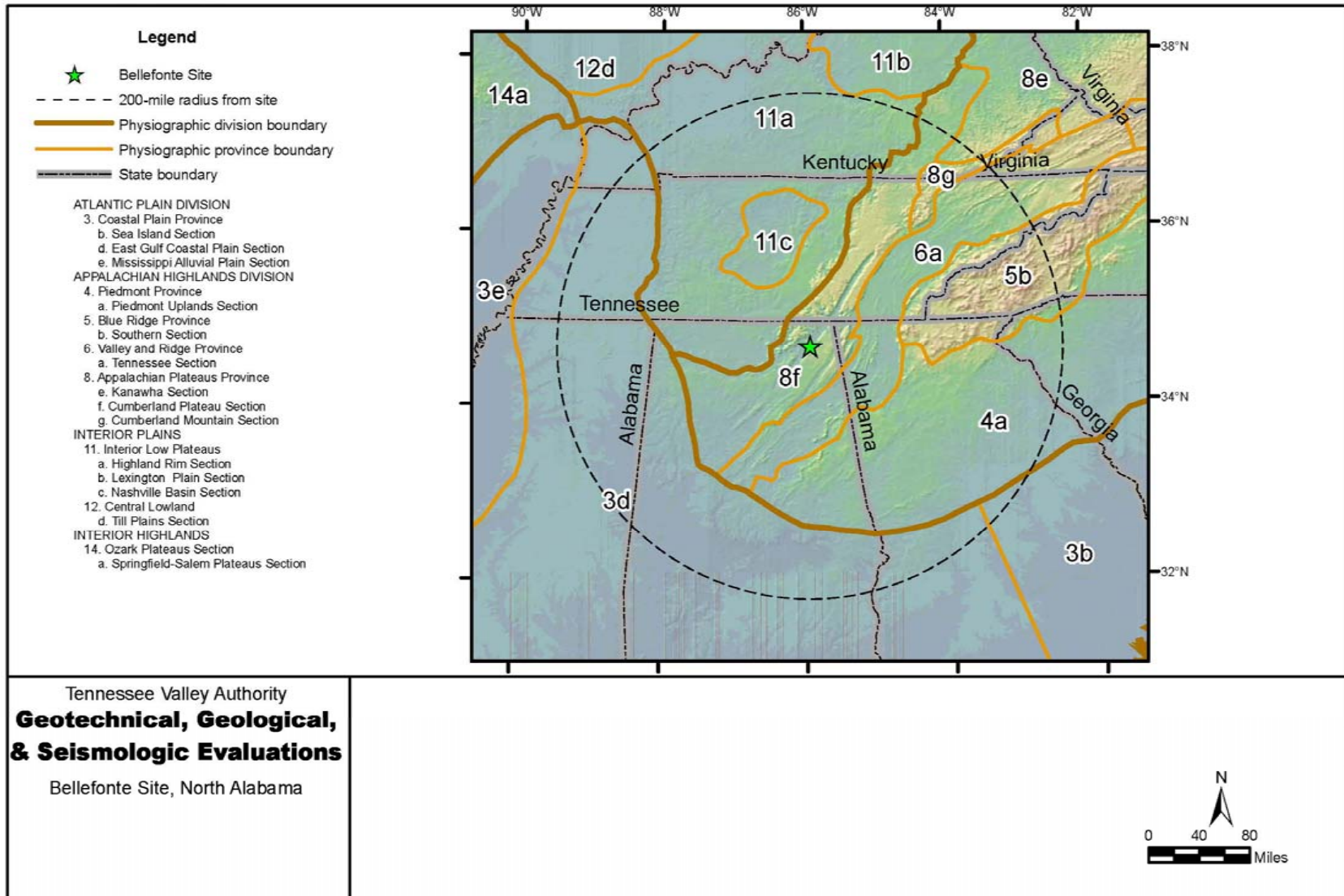
<sup>a</sup> Magnitude is  $M_w$ ; 1886 magnitude is from Johnston (1996b)  
Source: Talwani and Schaeffer (2001)

TABLE 2.5.1-6. Estimated Magnitudes and Peak Ground Accelerations of Prehistoric Earthquake Episodes in South Carolina Coastal Plain

Episode	Estimated Magnitudes			Estimated Peak Ground Accelerations (g)		
	Talwani & Schaeffer (2001)		Hu <i>et al.</i> (2002b)	This Study	Hu <i>et al.</i> (2002b)	This Study
	Empirical	Magnitude Bound				
A	7+	7.0	7.4 to 7.6	6.2 to 7.0	0.16 to 0.18	0.14
B	7+	7.0	7.4 to 7.6	6.2 to 6.8	0.16 to 0.18	0.14 to 0.15
C	~6	6.3 to 6.8	6.3 to 7.0	5.1 to 6.4	0.21 to 0.28	0.20 to 0.29
C'	7+	7.2	7.6 to 7.8	6.4 to 7.2	.016 to 0.17	0.14 to 0.15
D	~6	5.7			0.23 to 0.24	0.21 to 0.26
E	7+	7.0	6.8 to 7.0	5.6 to 6.4	0.31 to 0.42	0.30 to 0.53
F	~6		5.5 to 6.2	4.3 to 5.6	0.23 to 0.24	0.22 to 0.24
F'	7+		6.8 to 7.0	5.5 to 6.2		
G	7+	7.2				

Source: Leon *et al.* (August 2005).

S:\19800\19877\05\_0222\_r\fig\_02.5.1-01.mxd



**Figure 2.5.1-1. Regional Physiographic Map (200-Mile Radius)**  
(Source: physiographic province boundaries based on Fenneman and Johnson 1946 as shown on <http://water.usgs.gov/GIS/dsdl/physio.e00.gz>; base map ESRI, 2004)



	Ma.	Orogeny	Plate Tectonic Process
Jurassic	144		Symmetrical Rifting and Opening of Atlantic
Triassic	208		
Permian	245 286		
Carb.	Pa 320	ALLEGHANIAN	Subduction Collision with Africa
	Miss 360	ACADIAN	Subduction Terrane Accretion
Devonian	408		
Silurian	438		
Ordovician	505	TACONIC //////////////////// PENOBSCOT	A-Subduction Obduction Arc Collision/ Accretion
Cambrian	570		Trailing Margin Development
Late Proterozoic	1000	AVALONIAN	Subduction Volcanic Arc Generation
Middle Proterozoic		GRENVILLE	Rifting and Opening of Iapetus

<p>Tennessee Valley Authority <b>Geotechnical, Geological, &amp; Seismologic Evaluations</b> Bellefonte Site, North Alabama</p>	
---	--

S:\8600\877\05\_0222\_r1\_fig\_02.5.1-02.ai (2005-08-18, 12:50)

**Figure 2.5.1-2. Deformation-thermal Events Affecting the U.S. Appalachians and Possibly Related Plate Tectonic Processes (From Hatcher, 1989a)**

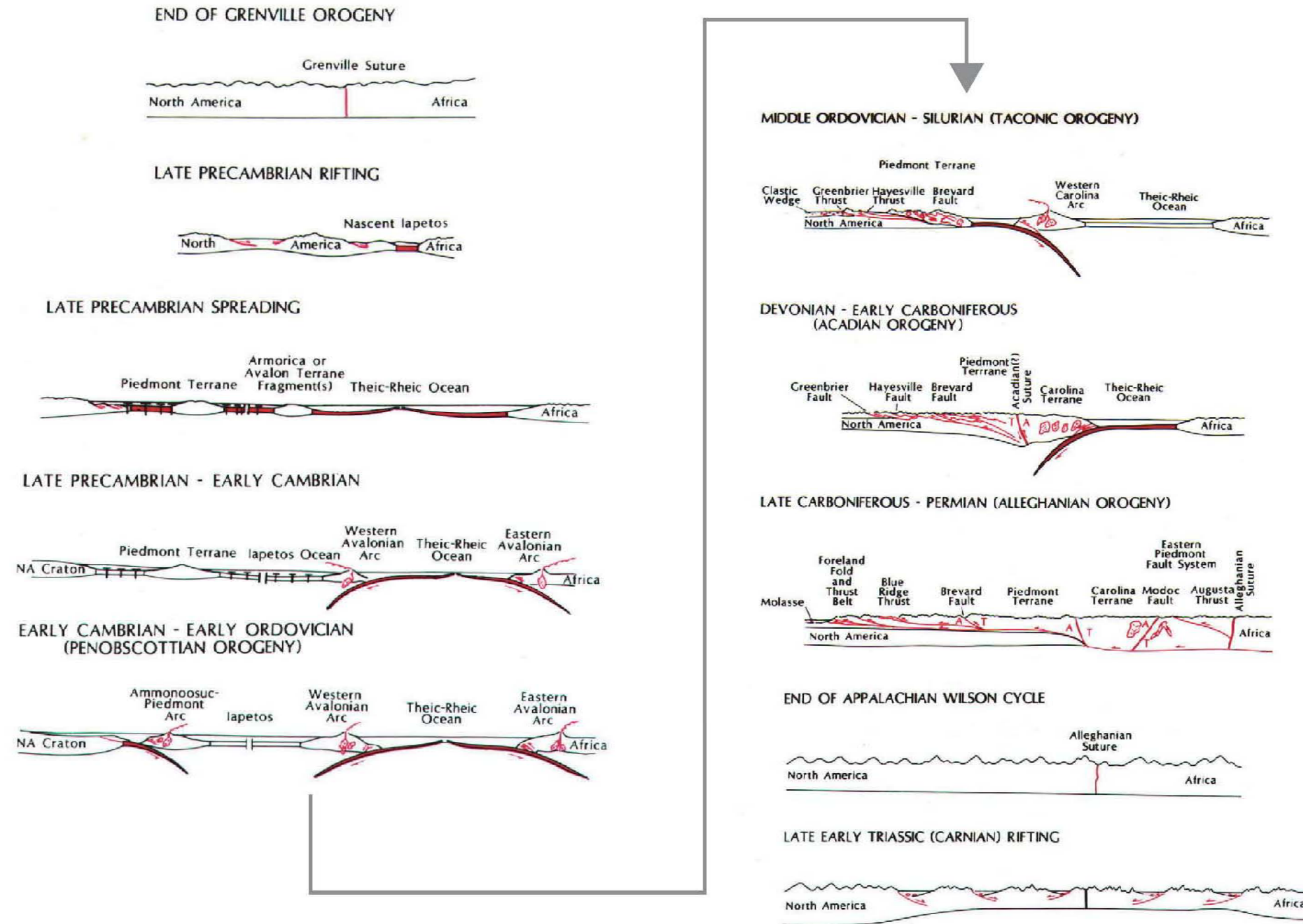


Figure 2.5.1-3. Tectonic Evolution of the Southern and Central Appalachian Orogen  
(From Hatcher, 1989b)

S:\1980019877\05\_0222\_r\_fig\_02.5.1-03.ai (2005-08-15, 11:37)

Tennessee Valley Authority  
**Geotechnical, Geological,  
& Seismologic Evaluations**  
Bellefonte Site, North Alabama

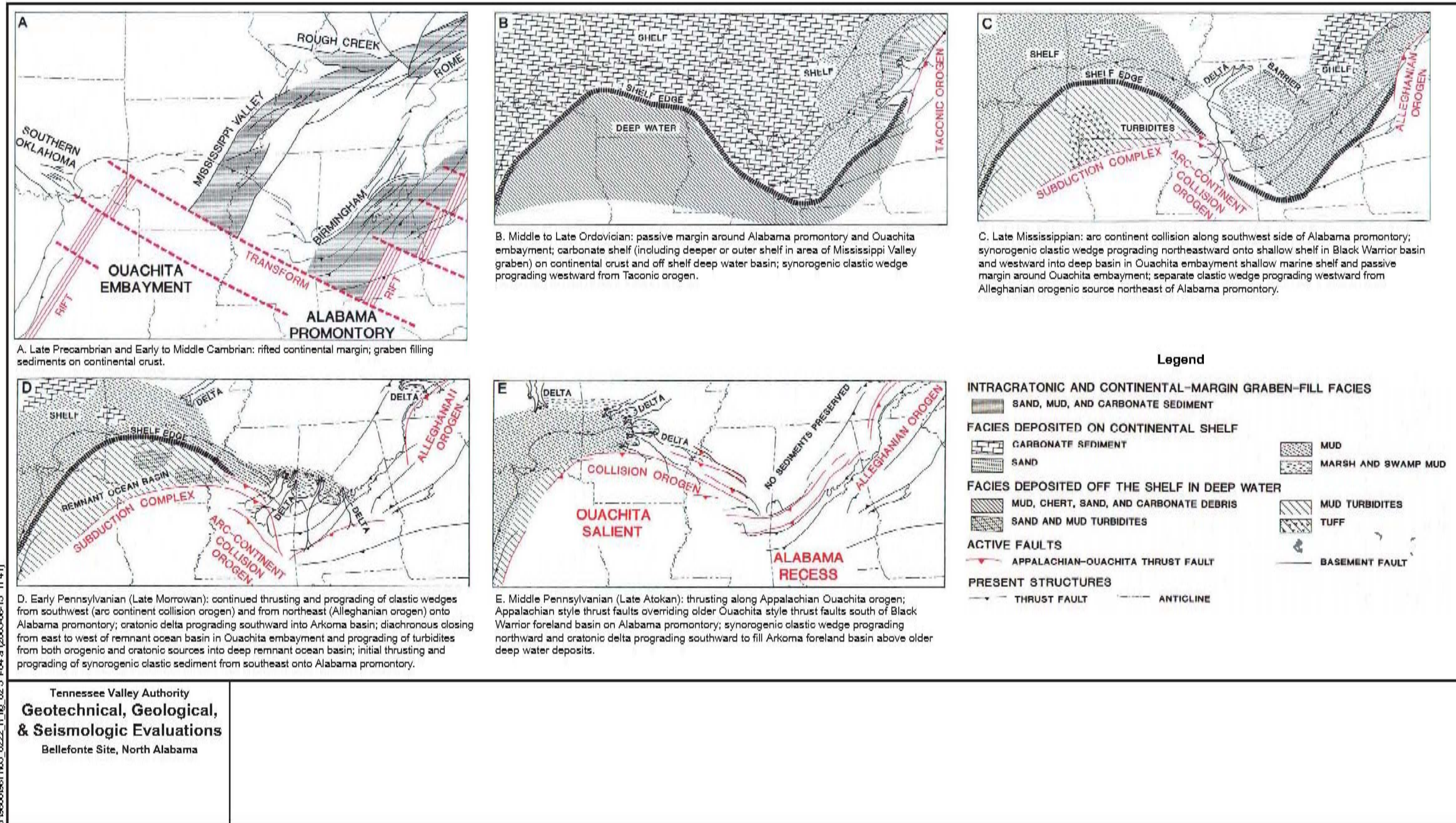
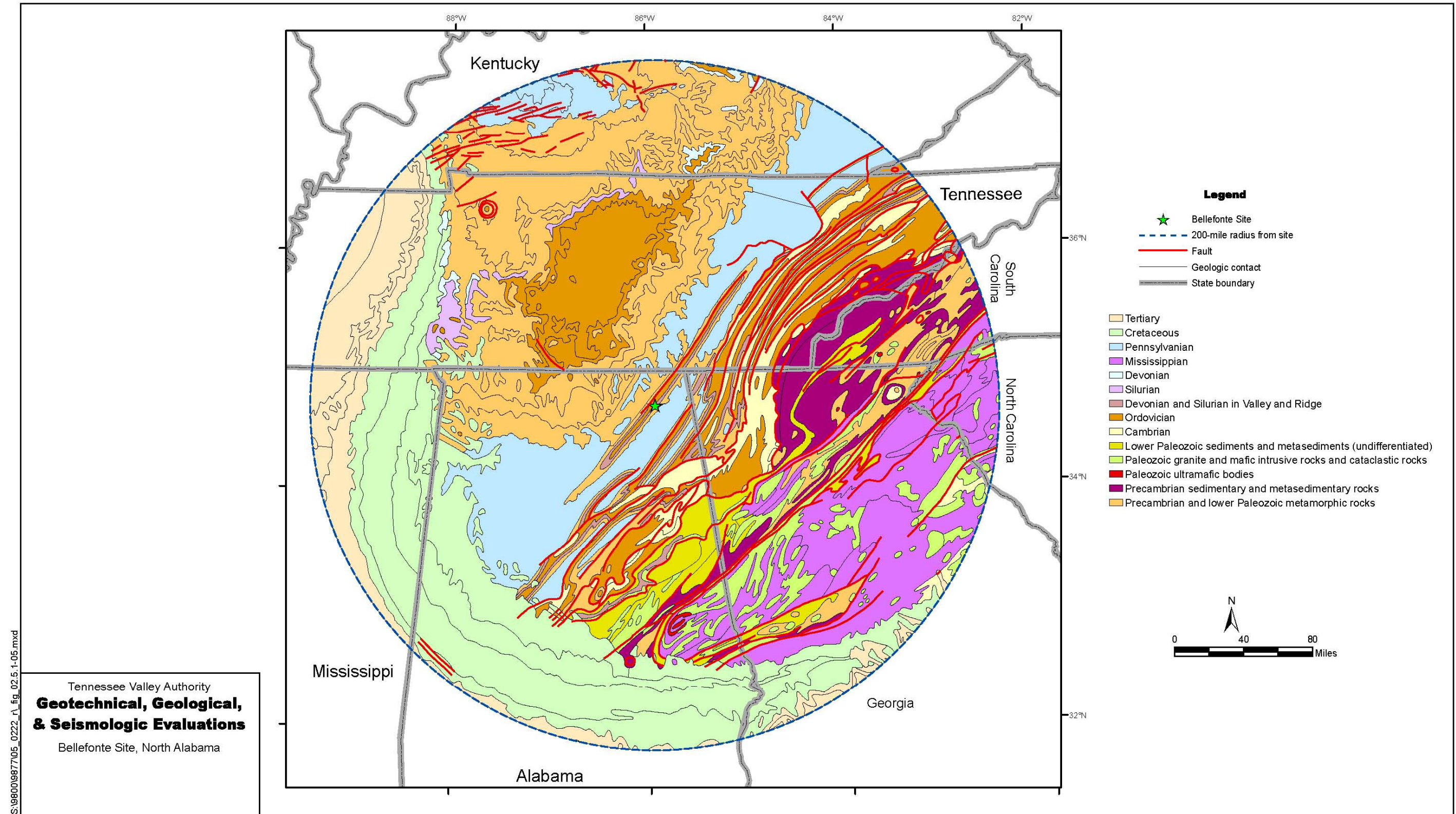


Figure 2.5.1-4. Paleogeographic Reconstructions of Phases in the Tectonic Evolution of the Appalachian-Ouachita Orogen (From Thomas, 1989a)

S:\986009\98677405\_00222\_r1\_fig\_02.5-1-04 at (2005-08-15 11:41)



S:\980019877\05\_0222\_r1\_fig\_02.5.1-05.mxd

Tennessee Valley Authority  
**Geotechnical, Geological,  
& Seismologic Evaluations**  
Bellefonte Site, North Alabama

**Figure 2.5.1-5. Regional Geologic Map (200-mile radius)**  
(Source: Schruben et al., 2005, <http://pubs.usgs.gov/dds/dds11>; base map ESRI, 2004)

LITHOTECTONIC UNIT	LITHOSTRATIGRAPHY	THICKNESS	
		AVERAGE SEISMIC VELOCITY	MECHANICAL ROLE
4	<u>Ouachita-Alleghanian synorogenic clastic wedge and equivalent foreland facies</u> PENNSYLVANIAN Pottsville Fm. (sandstone-mudstone-coal)	as much as 3605 m [11,820 ft] preserved below present erosion level	passive translation above stiff layer; local upper level detachments
	MISSISSIPPIAN <u>clastic-wedge facies on southwest</u> Parkwood Fm. (sandstone-mudstone) Floyd Shale <u>foreland facies on northeast</u> Bangor Limestone Hartselle Sandstone Pride Mountain Fm. (mudstone-sandstone)	3810 m/sec [12,500 ft/sec]	
3	<u>discontinuous variable shallow-marine facies, internal unconformities</u> MISSISSIPPIAN Tuscumbia Limestone Fort Payne Chert	122-490 (locally <8) m [400-1610 (locally <25) ft]	passive translation above stiff layer; local upper-level detachment (e.g., Coosa deformed belt)
	DEVONIAN Chattanooga Shale Frog Mountain Sandstone SILURIAN Red Mountain Fm. (sandstone-mudstone-hematite) MIDDLE AND UPPER ORDOVICIAN <u>distal facies of Taconic clastic wedge on east</u> Sequatchie Fm. (mudstone) Colvin Mountain Sandstone Greensport Fm. (mudstone) Athens Shale Lenoir--Little Oak Limestone <u>foreland facies on west</u> Chickamauga Limestone	5490 m/sec [18,000 ft/sec]	
2	<u>passive-margin carbonate shelf</u> UPPER CAMBRIAN--LOWER ORDOVICIAN Knox Group (dolostone-limestone-chert)	600-1250 m [1970-4105 ft] 6710 m/sec [22,000 ft/sec]	regional stiff layer
	1	<u>synrift facies, Birmingham graben (Ouachita rift)</u> LOWER AND MIDDLE CAMBRIAN Conasauga Fm. (shale-limestone-dolostone) Rome Fm. (shale-sandstone-limestone)  <u>early postrift facies, Blue Ridge rift</u> LOWER CAMBRIAN Shady Dolomite Chilhowee Group (sandstone)	
<u>crystalline basement rocks</u> PRECAMBRIAN			
Tennessee Valley Authority <b>Geotechnical, Geological, &amp; Seismologic Evaluations</b> Bellefonte Site, North Alabama			

S:\9800\9877\05\_0222\_1\fig\_02.5.1-06.ai (2005-08-15, 11:53)

**Figure 2.5.1-6. Stratigraphic Column in the Appalachian Thrust Belt in Alabama (Modified from Thomas, 2001)**

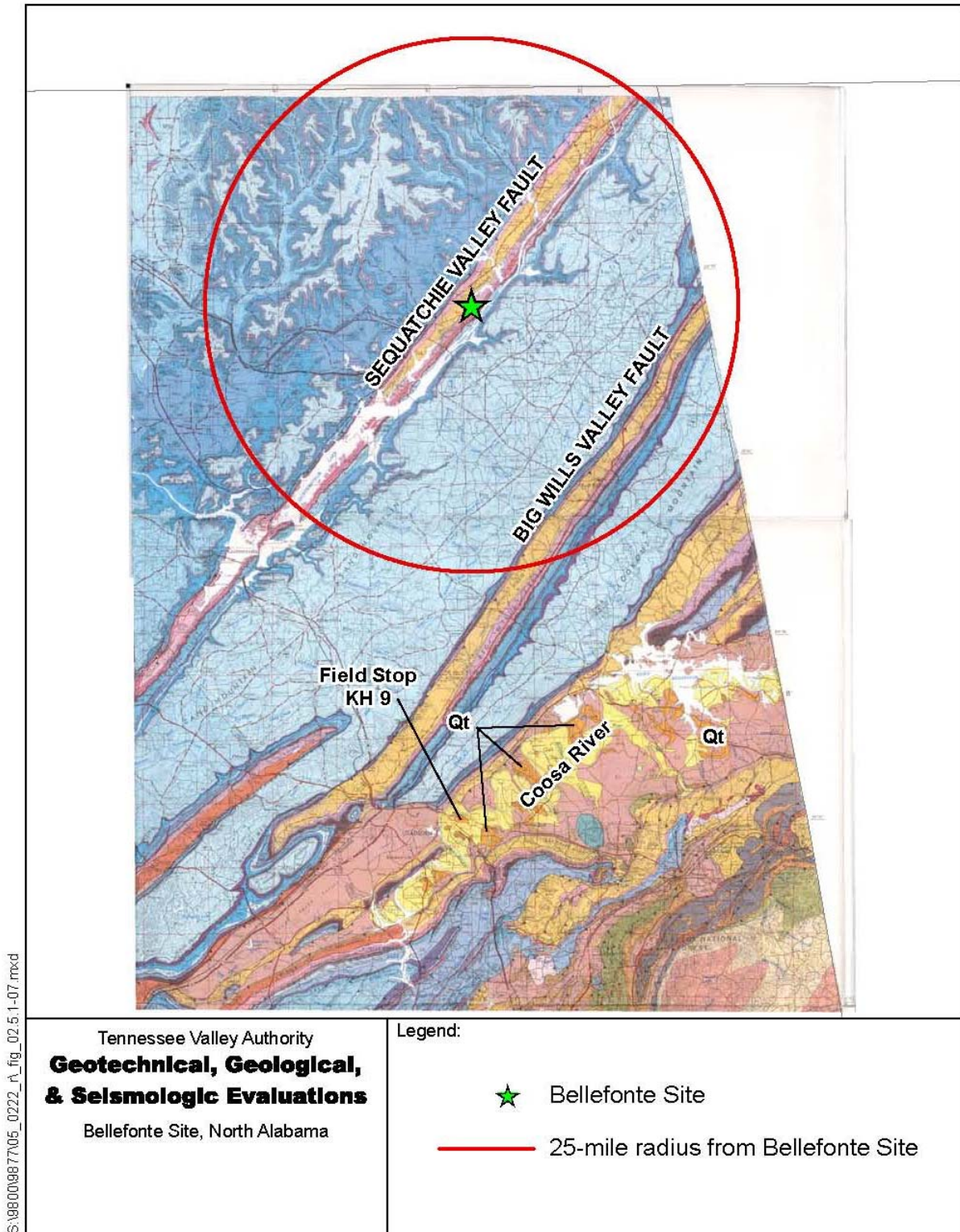


Figure 2.5.1-7. Geologic Map of Northeastern Alabama

(Source: modified from Osborne et al., 1988;

<http://www.gsa.state.al.us/gsa/GIS/geologydetails.html>)

(Note: see Figure 2.5.1-8 for explanation of geologic map units and symbols)

S:\40000\077\05\_0222\_r1.g\_02.5.1-08.a\_2005-08-15\_13:18

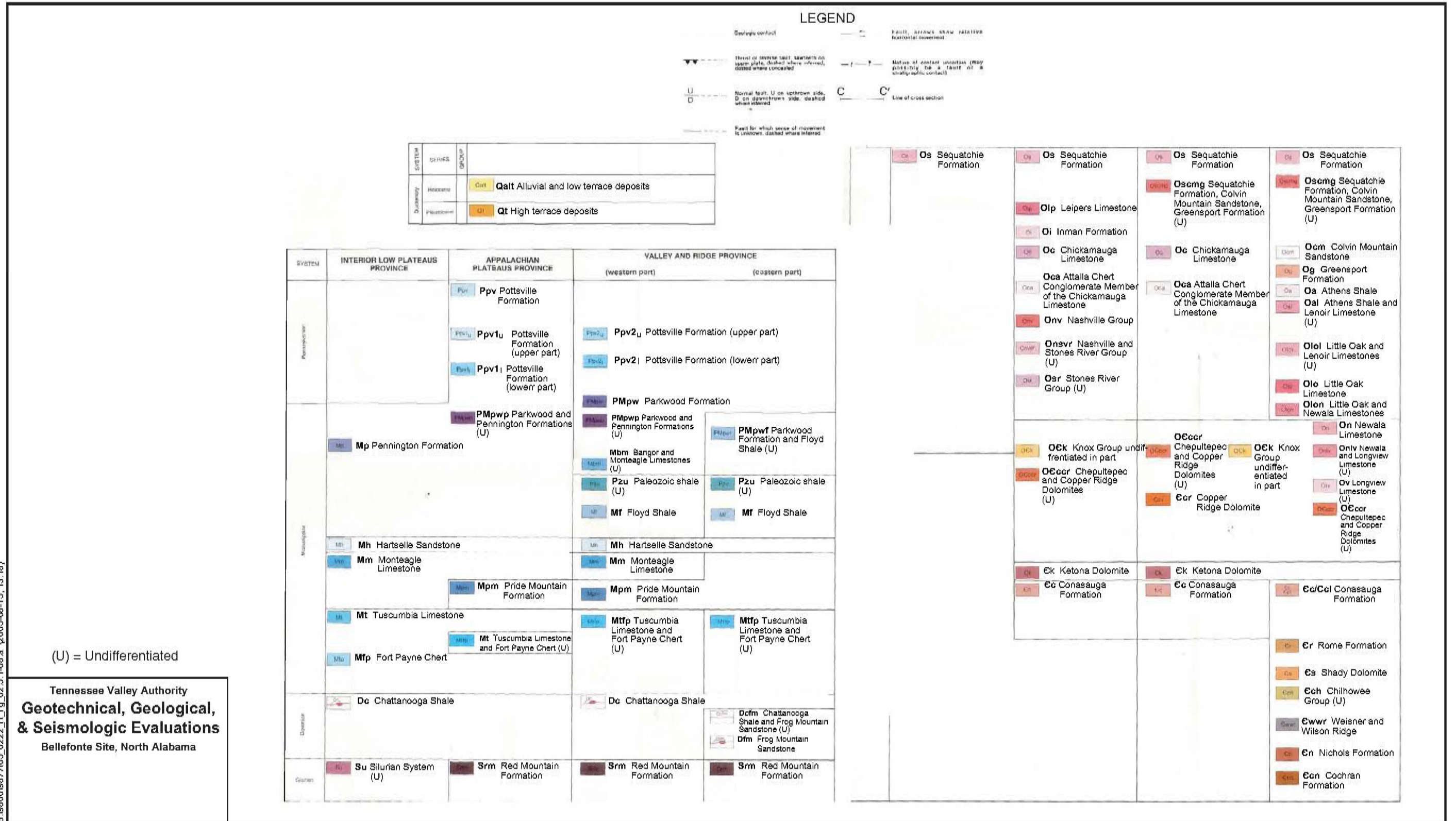


Figure 2.5.1-8. Explanation of Geologic Map Units and Symbols  
(Source: Osborne et al., 1988; <http://www.gsa.state.al.us/gsa/GIS/geologydetails.html>)

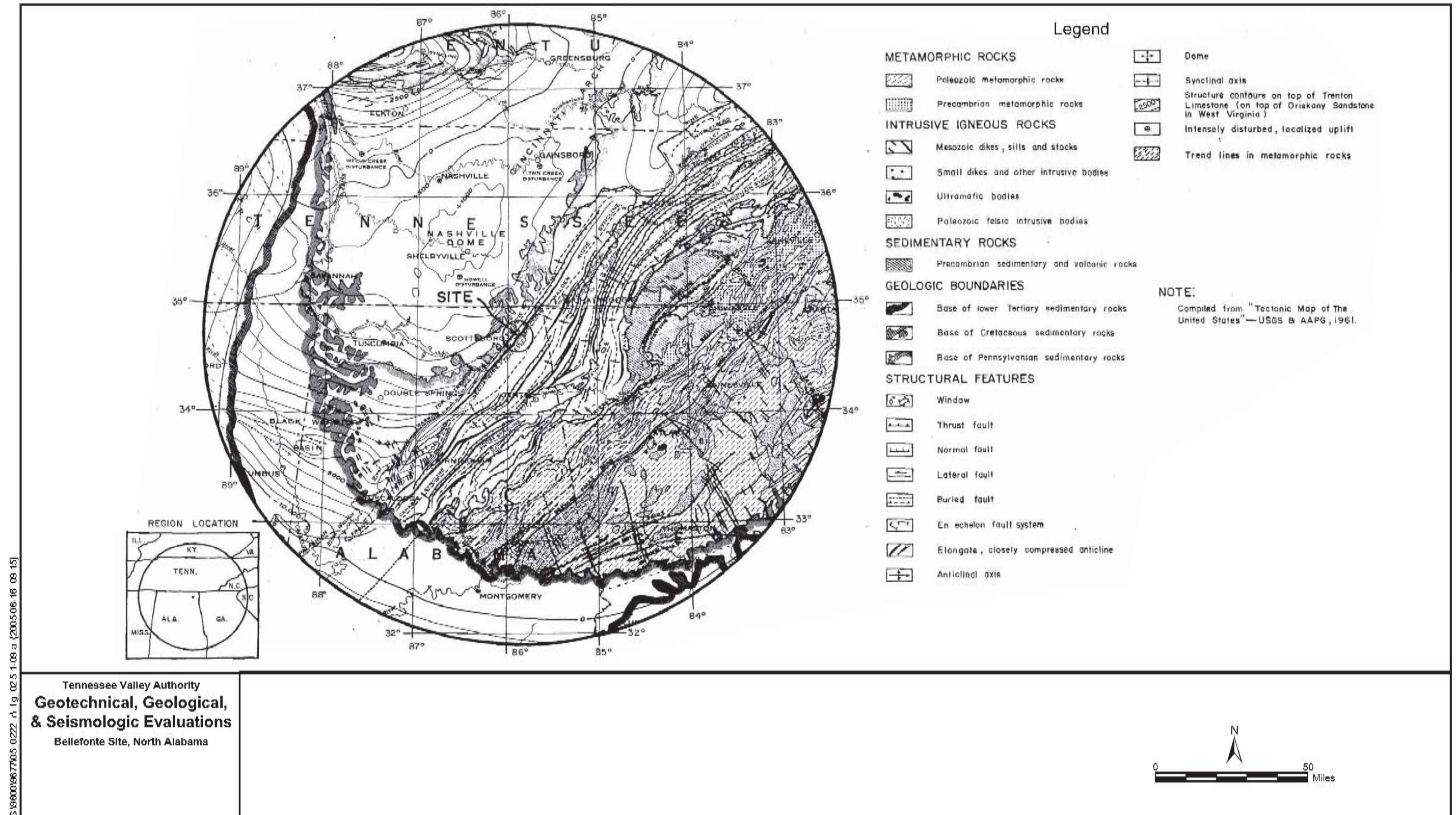


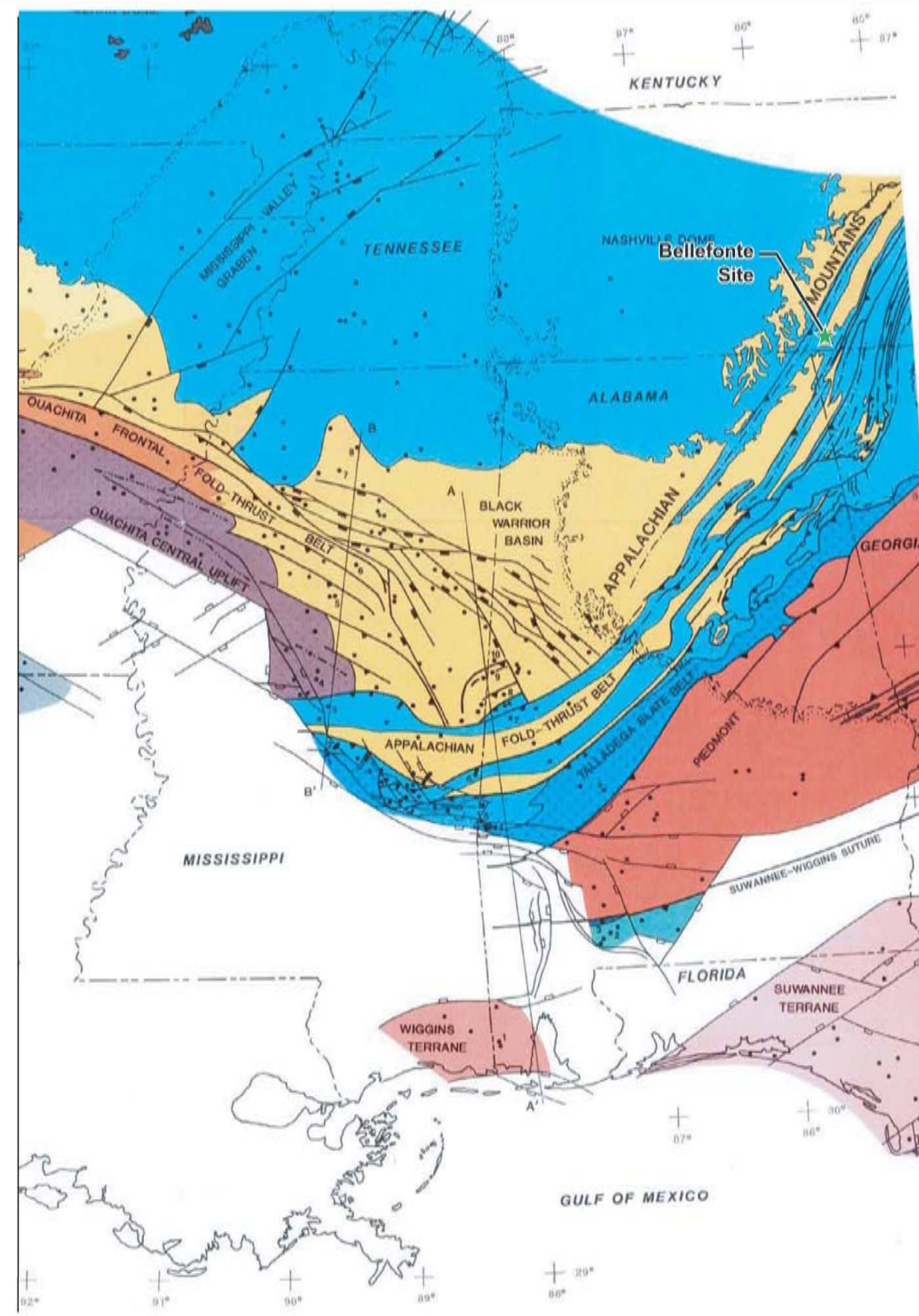
Figure 2.5.1-9. Regional Tectonic Map (200-mile radius)  
(From Figure 2.5-4, TVA, 1986)

S:\98001668.77905.0\222\_r1.g\_02.5.1-09 a (2005-06-16 09:15)



S:\9800\9877\05\_0222\_r\fig\_02.5.1-10.ai (2005-08-15, 13:25)

Tennessee Valley Authority  
**Geotechnical, Geological,  
& Seismologic Evaluations**  
Bellefonte Site, North Alabama



### Legend

**POST-OROGENIC MESOZOIC-CENOZOIC ROCKS OF GULF COASTAL PLAIN**

- CRATONWARD LIMIT OF COASTAL PLAIN STRATA (MAP)
- COASTAL PLAIN STRATA (CROSS SECTIONS A-A' AND B-B')

**POST-OROGENIC PALEOZOIC ROCKS**

- CRATONIC SHELF (MIDDLE WOLFCAMPIAN-UPPER PERMIAN)  
PART DERIVED FROM OROGENIC HIGHLANDS
- SUCCESSOR BASIN (DESMOINESIAN-GUADALUPIAN)

**SYNOROGENIC ROCKS (MERAMECIAN-DESMOINESIAN IN EASTERN OUACHITA FORELAND, MERAMECIAN-LOWER WOLFCAMPIAN IN MARATHON FORELAND)**

- DEEP-WATER TURBIDITE CLASTIC WEDGE
- SHALLOW-MARINE AND DELTAIC CLASTIC WEDGE  
LOWER PART GRADES CRATONWARD TO CARBONATE FACIES
- UNDIFFERENTIATED PRE-OROGENIC OFF-SHELF FACIES AND SYNOROGENIC DEEP-WATER CLASTIC WEDGE
- VOLCANIC ROCKS
- CLASTIC FACIES DERIVED FROM CRATONIC AND/OR DISTANT SOURCES

**PRE-OROGENIC ROCKS (CAMBRIAN-MISSISSIPPIAN)**

- CARBONATE-SHELF FACIES  
MAPPED AREA INCLUDES BASAL TRANSGRESSIVE CLASTIC UNIT, SEDIMENTARY FILL OF MISSISSIPPI VALLEY GRABEN, CLASTIC INTERBEDS DERIVED FROM CRATONIC SOURCES, AND DISTAL TONGUES OF SYNOROGENIC CLASTIC-WEDGE ROCKS  
MAPPED BOUNDARY BETWEEN CARBONATE-SHELF FACIES AND PROGADING SYNOROGENIC CLASTIC WEDGES IS DIACHRONOUS. TONGUES OF CLASTIC-WEDGE ROCKS PINCH OUT CRATONWARD INTO THE CARBONATE FACIES, AND THE LOWER PARTS OF CLASTIC WEDGES GRADE CRATONWARD INTO THE UPPER PARTS OF THE CARBONATE FACIES.  
ROCKS OF CONTRASTING TECTONIC SETTING NOT DIFFERENTIATED ON MAP:  
THIN DISTAL SOUTHWESTERN FRINGE OF ORDOVICIAN-SILURIAN SYNOROGENIC (TACONIC) CLASTIC WEDGE IN ALABAMA AND GEORGIA
- OFF-SHELF FACIES (MUDSTONE, CHERT, SANDSTONE, CARBONATE ROCKS)  
ROCKS OF CONTRASTING TECTONIC SETTING NOT DIFFERENTIATED ON MAP:  
DEVONIAN SYNOROGENIC (ACADIAN) DEEP-WATER TO SHALLOW-MARINE SEDIMENTARY AND VOLCANIC ROCKS IN TALLADEGA SLATE BELT IN ALABAMA AND GEORGIA  
MISSISSIPPIAN-PENNSYLVANIAN(?) POSSIBLY SYNOROGENIC DEEP-WATER CLASTIC SEDIMENTARY ROCKS IN TALLADEGA SLATE BELT IN CENTRAL MISSISSIPPI
- RIFT-RELATED IGNEOUS ROCKS

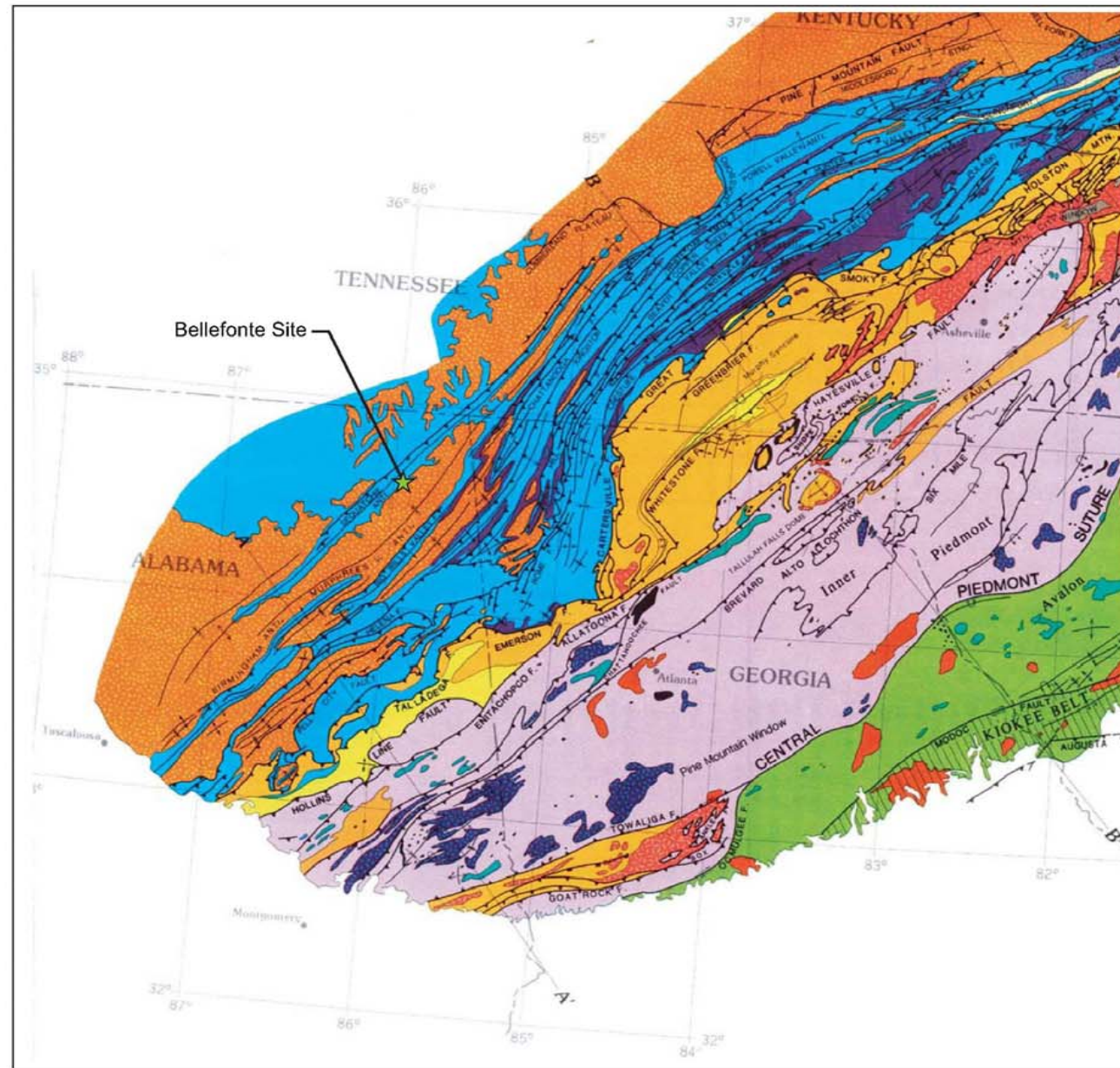
**PRECAMBRIAN CONTINENTAL CRYSTALLINE BASEMENT ROCKS**

- HIGHLY ALLOCHTHONOUS ROCKS AND/OR ACCRETED TERRANES
  - OUACHITA INTERIOR METAMORPHIC BELT (PHYLLITE, SLATE, QUARTZITE, MARBLE, SCHIST)
  - APPALACHIAN PIEDMONT (METAMORPHIC AND PLUTONIC ROCKS)
  - WIGGINS TERRANE (METAMORPHIC AND PLUTONIC ROCKS)
  - SUWANNEE TERRANE (UPPER PROTEROZOIC-CAMBRIAN FELSIC VOLCANIC BASEMENT ROCKS AND ORDOVICIAN-DEVONIAN CLASTIC SEDIMENTARY ROCKS)
  - ARC COMPLEX (VOLCANIC AND PLUTONIC ROCKS)
  - ULTRAMAFIC ROCKS

### MAP SYMBOLS

- WELL
- THRUST FAULT (BARB ON HANGING WALL)  
DOTTED WHERE COVERED BY POST-OROGENIC PALEOZOIC ROCKS
- ANTICLINE
- BROAD ANTICLINE (IDENTIFIED ON SEISMIC PROFILES)
- NORMAL FAULT, PALEOZOIC (BAR ON DOWNTHROWN BLOCK)
- VERY LOW-GRADE METAMORPHIC OVERPRINT
- NORMAL FAULT, POST-PALEOZOIC
- REVERSE FAULT, POST-PALEOZOIC
- LINE OF CROSS SECTION

Figure 2.5.1-10. Tectonic Map of the Appalachian-Ouachita Orogen  
(From Thomas, 1989b)



### Legend

- Triassic-Jurassic rift basins / Mesozoic intrusions and associated rocks (New England).
- Late Mississippian-Permian molasse and Middle Devonian-Permian molasse (New England) Carboniferous-Permian intrusions.
- North American Paleozoic platform / Taconian clastic wedge (Upper Ordovician-Silurian Martinsburg-Shawangunk patterned) / Acadian clastic wedge.
- Late Proterozoic and Cambrian clastic deposits of the North American continental margin / Late Proterozoic-Ordovician outer margin deposits of the Taconic allochthons and Hamburg klippe.
- North American basement massifs / Late Proterozoic alkalic plutons, Southern Appalachians / Chain Lakes massif / Chain Lakes pre-Arenigian cover.
- Alleghenian metamorphic overprint (approx; extent).
- Ultramafic rocks (includes mafic-Ultramafic complexes).
- North American outer margin cover sequence including late Proterozoic-Ordovician accretionary prisms / Cambrian-Middle Ordovician intrusions.
- Cambrian-Ordovician cover (including Ordovician arc volcanic rocks of medial New England) Late Proterozoic-Ordovician tonalitic gneisses amphibolites and granitoid intrusions. Includes Penobscottian (?) intrusions in entire orogen / basement of medial New England.
- Silurian-Early Devonian cover of the medial New England / Ordovician-Silurian-Devonian deep-water facies of the Talladega and Murphy belts / Acadian (Late Ordovician through Devonian) intrusions.
- Late Proterozoic-Cambrian sedimentary and volcanic rocks of Avalon / Late Proterozoic sedimentary and volcanic rocks of Avalon (basement?) / sequences belonging either to avalon or medial New England / Late Proterozoic-Cambrian intrusions

### MAP SYMBOLS

- A-A'** Cross-section line
- Geologic Boundary
- Steeply-dipping fault, sense of motion poorly known
- Thrust fault
- Normal fault
- Anticline (antiform), arrow indicates plunge
- Syncline (synform)
- Overturned anticline (antiform)
- Overturned syncline (synform)
- Strike-slip fault, arrows indicate dominant dextral sense of motion.
- Thrust fault with major dextral strike-slip component.
- Strike slip motion, both dextral and sinistral at different times

Tennessee Valley Authority  
**Geotechnical, Geological,  
& Seismologic Evaluations**  
Bellefonte Site, North Alabama

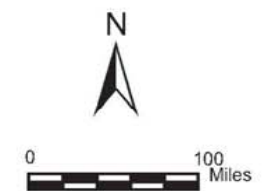


Figure 2.5.1-11. Tectonic Map of the Southern Appalachians Showing Locations of Regional Cross-sections A-A' and B-B' (From Hatcher et al., 1989d) (Note: see Figure 2.5.1-12 for cross-sections AA' and BB'')

S:\980019877\05\_0222\_1\_fig\_02.5.1-11.ai (2005-08-15, 13:27)

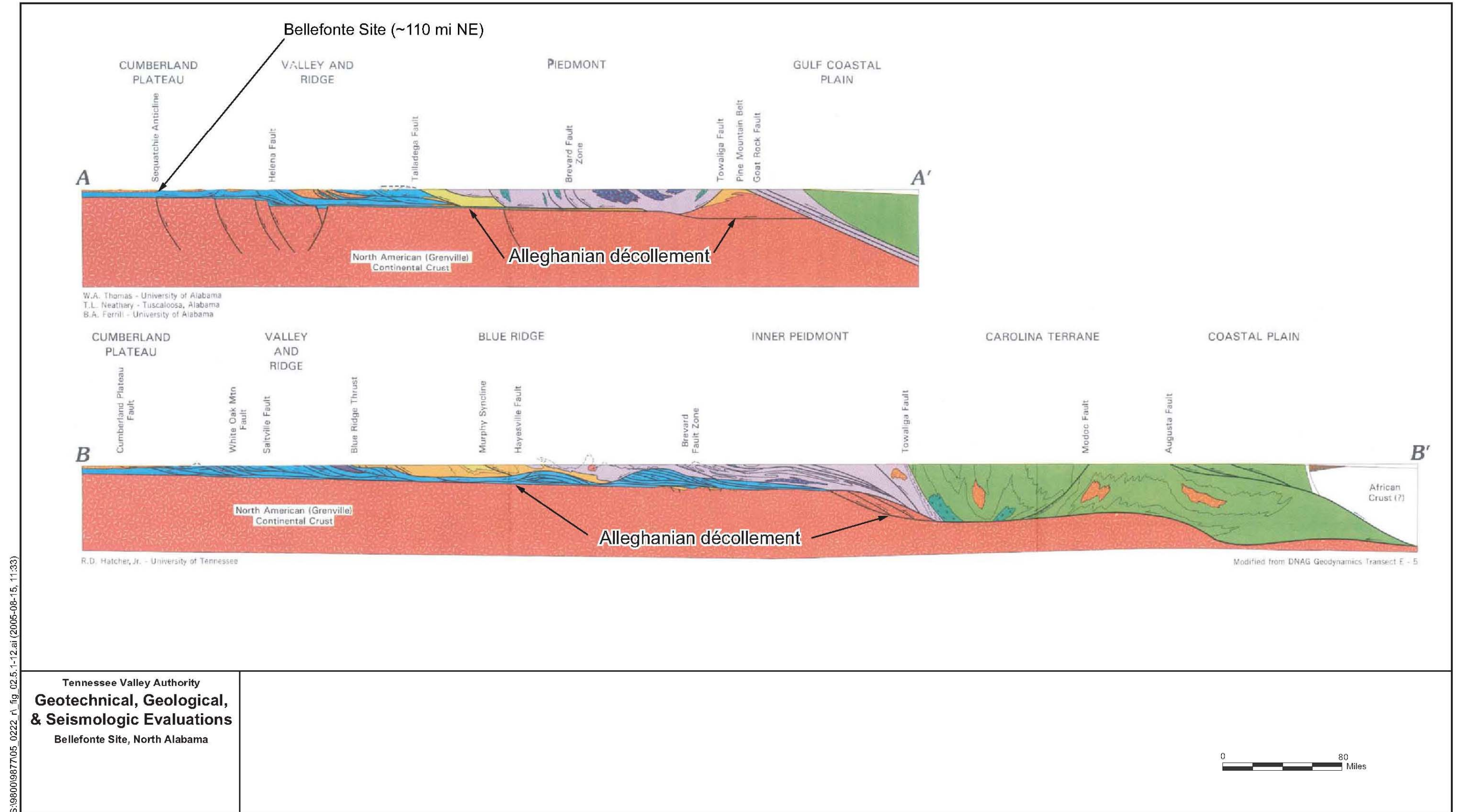
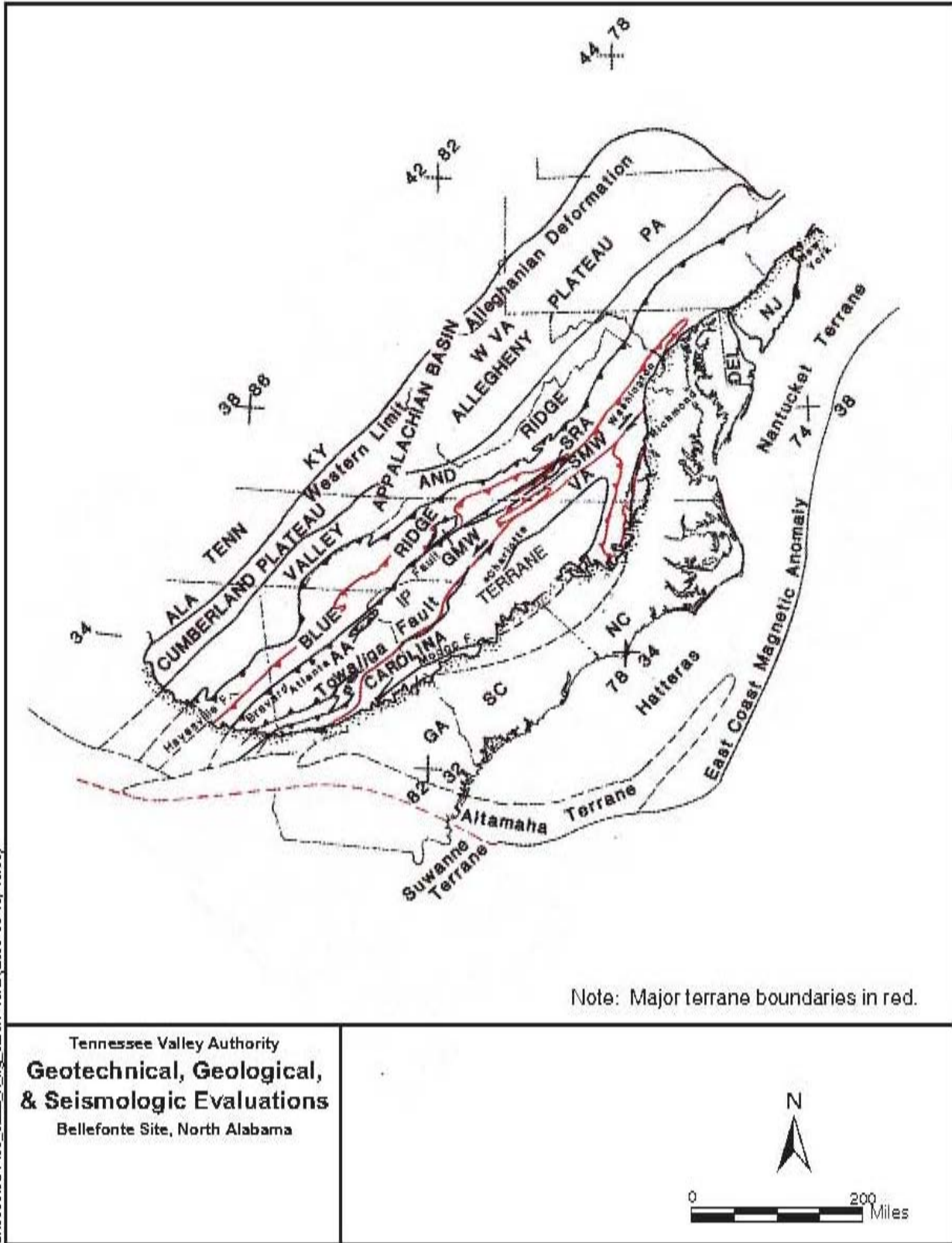


Figure 2.5.1-12. Regional Structural Cross-sections A-A' and B-B'  
(From Hatcher et al., 1989d) (Note: see Figure 2.5.1-11 for legend and location of cross-sections)

S:\980019877\05\_0222\_r1\_fig\_02.5.1-12.ai (2005-08-15, 11:33)



S:\69006987\06\_0222\_r\_fig\_02.5.1-13a1 (2006-09-15, 13:30)

**Figure 2.5.1-13. Major Geologic and Tectonic Features and Terrane Boundaries of the Southern Appalachians (From Hatcher et al., 1989b)**

S:\9800\9877\05\_0222\_r\_fig\_02.5.1-14.ai (2005-08-15, 13:32)

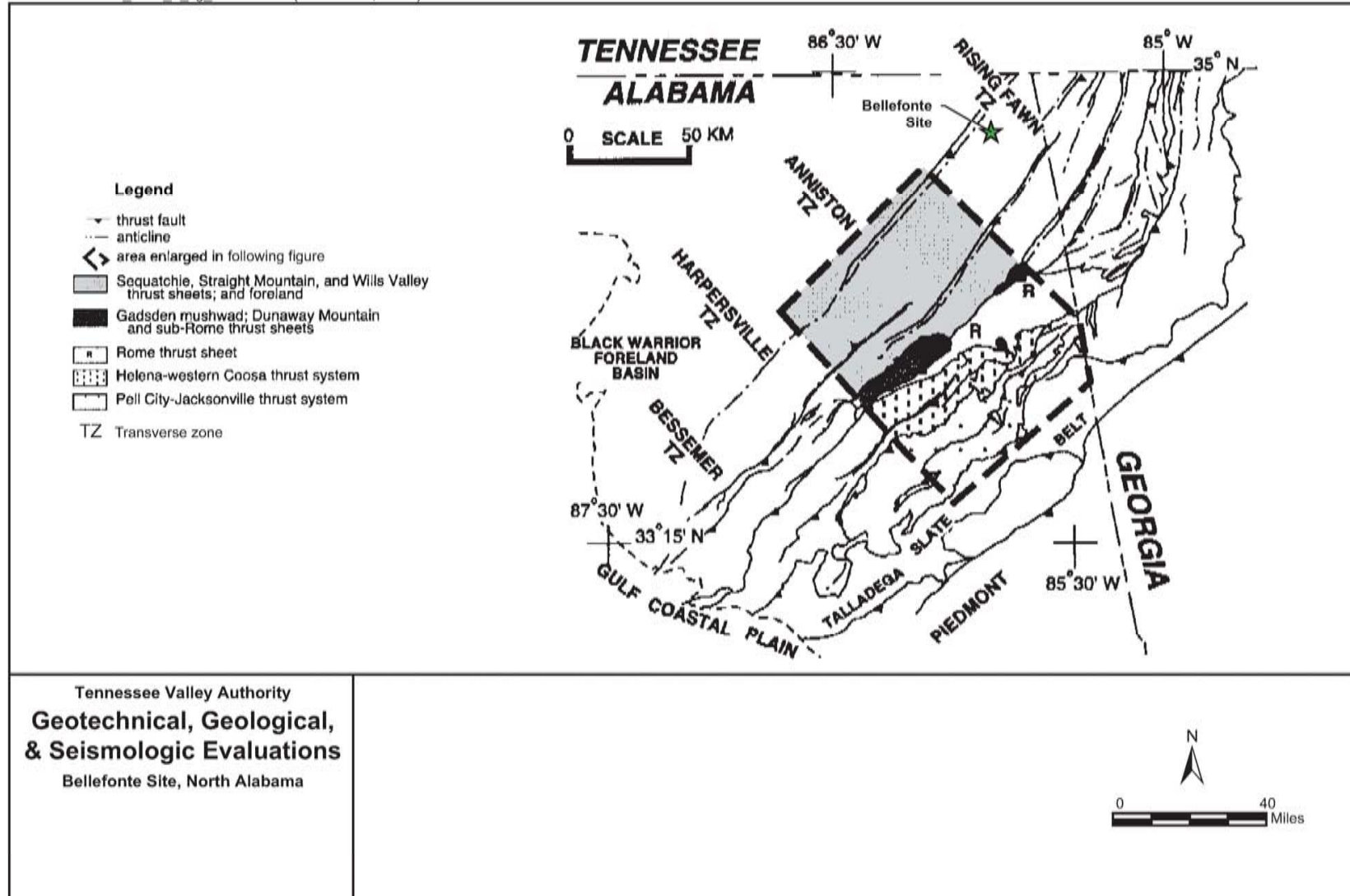


Figure 2.5.1-14. Structural Geology Map of Appalachian Orogen in Alabama and Georgia  
(From Thomas and Bayona, 2002)

S:\9800\9877\05\_0222\_\8\_fig\_02.5.1-15.ai (2005-08-15, 13:34)

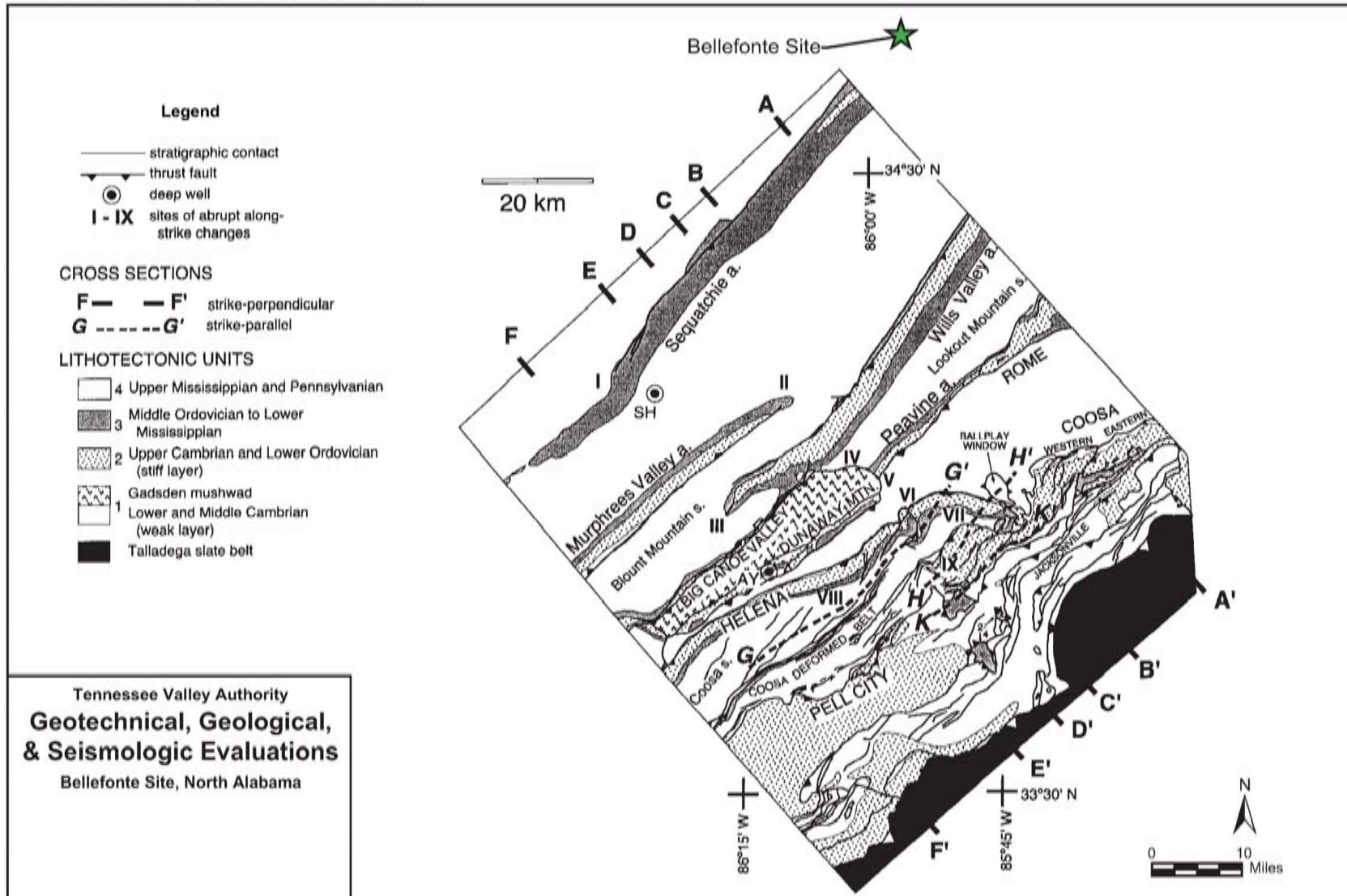


Figure 2.5.1-15. Geologic Map of the Anniston Transverse Zone in the Appalachian Thrust Belt in Alabama (From Thomas and Bayona, 2002)

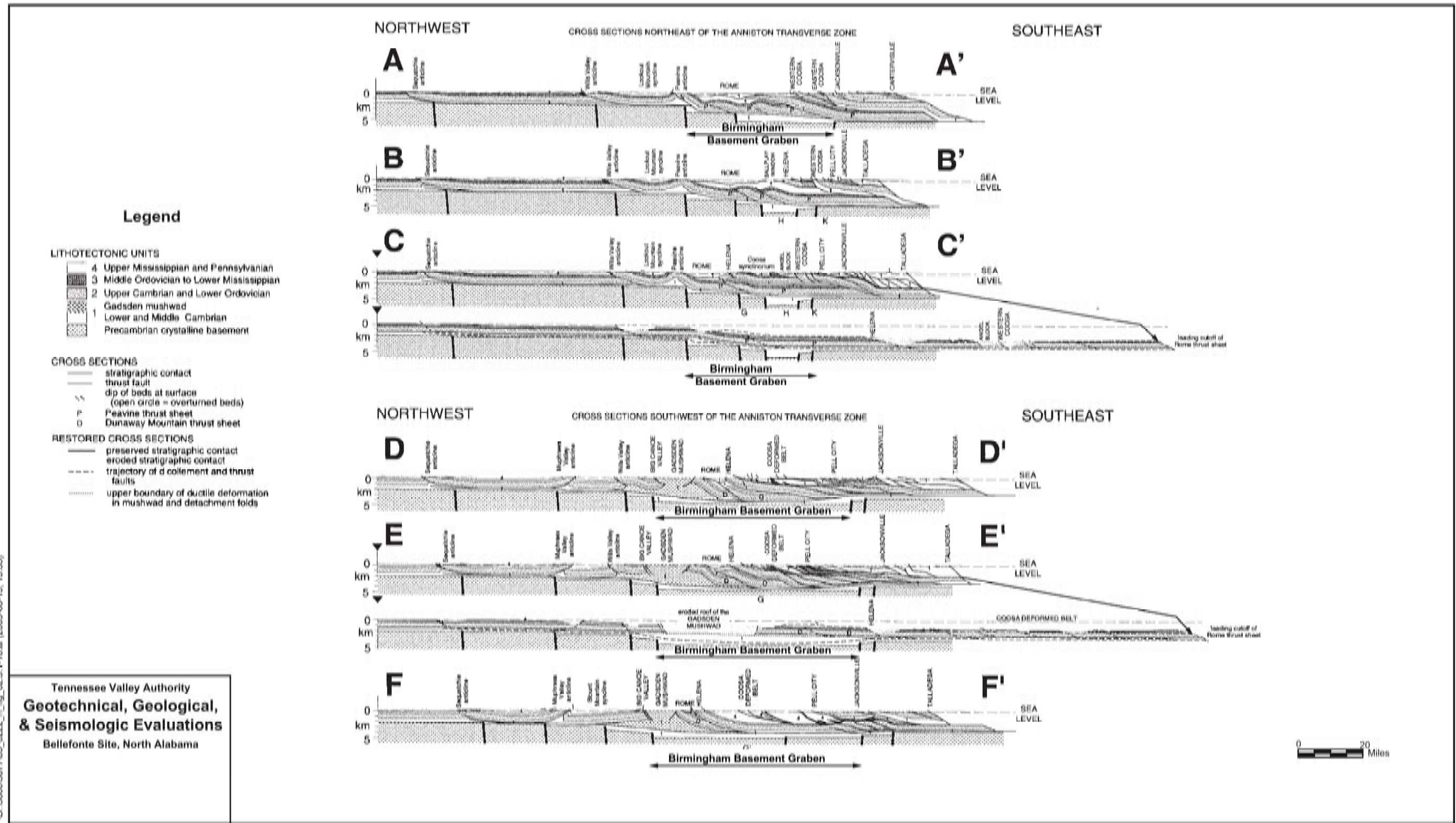


Figure 2.5.1-16. Structural Cross-sections, Appalachian Thrust Belt, Alabama  
(From Thomas and Bayona, 2002) (Note: Locations of cross-sections are shown in Figure 2.5.1-15)

S:\980009877\05\_0222\_4\_fig\_02.5.1-16.ai (2005-08-15, 13:35)

Tennessee Valley Authority  
**Geotechnical, Geological,  
& Seismologic Evaluations**  
Bellefonte Site, North Alabama

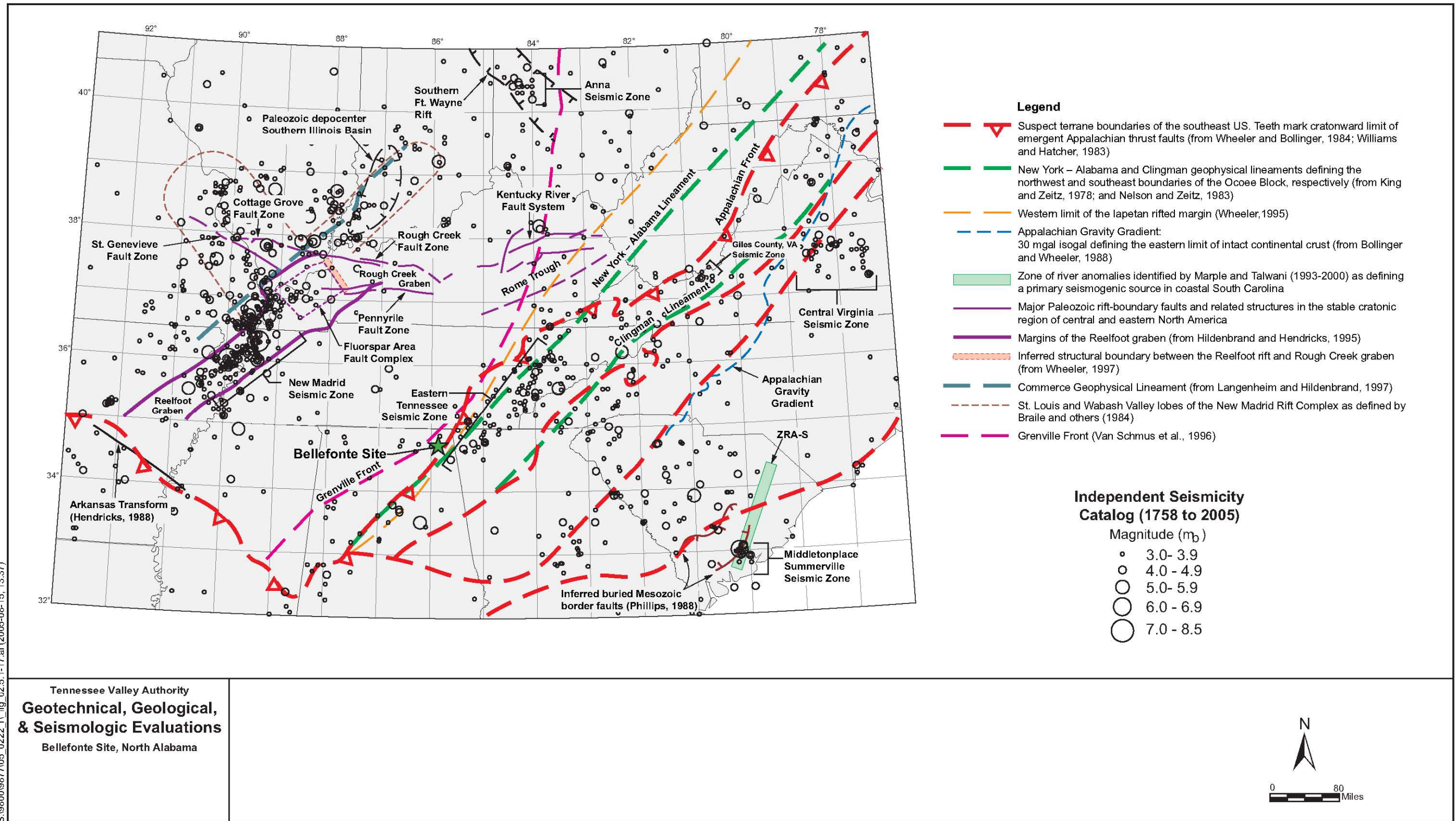


Figure 2.5.1-17. Map Showing Tectonic and Geophysical Elements of Central and Eastern North America with Independent Seismicity Catalog (References: Wheeler and Bolinger, 1984; Williams and Hatcher, 1983; King and Zeitz, 1978; Nelson and Zeitz, 1983; Wheeler, 1995; Bollinger and Wheeler, 1988; Marple and Talwani, 1993, 2000); Hildenbrand and Hendricks, 1995; Wheeler, 1997; Langenheim and Hildenbrand, 1997; Braile et al., 1984; Van Schmus et al., 1996)



S:\9800\9877\05\_0222\_r\fig\_02.5.1-18.ai (2005-08-15, 13:40)

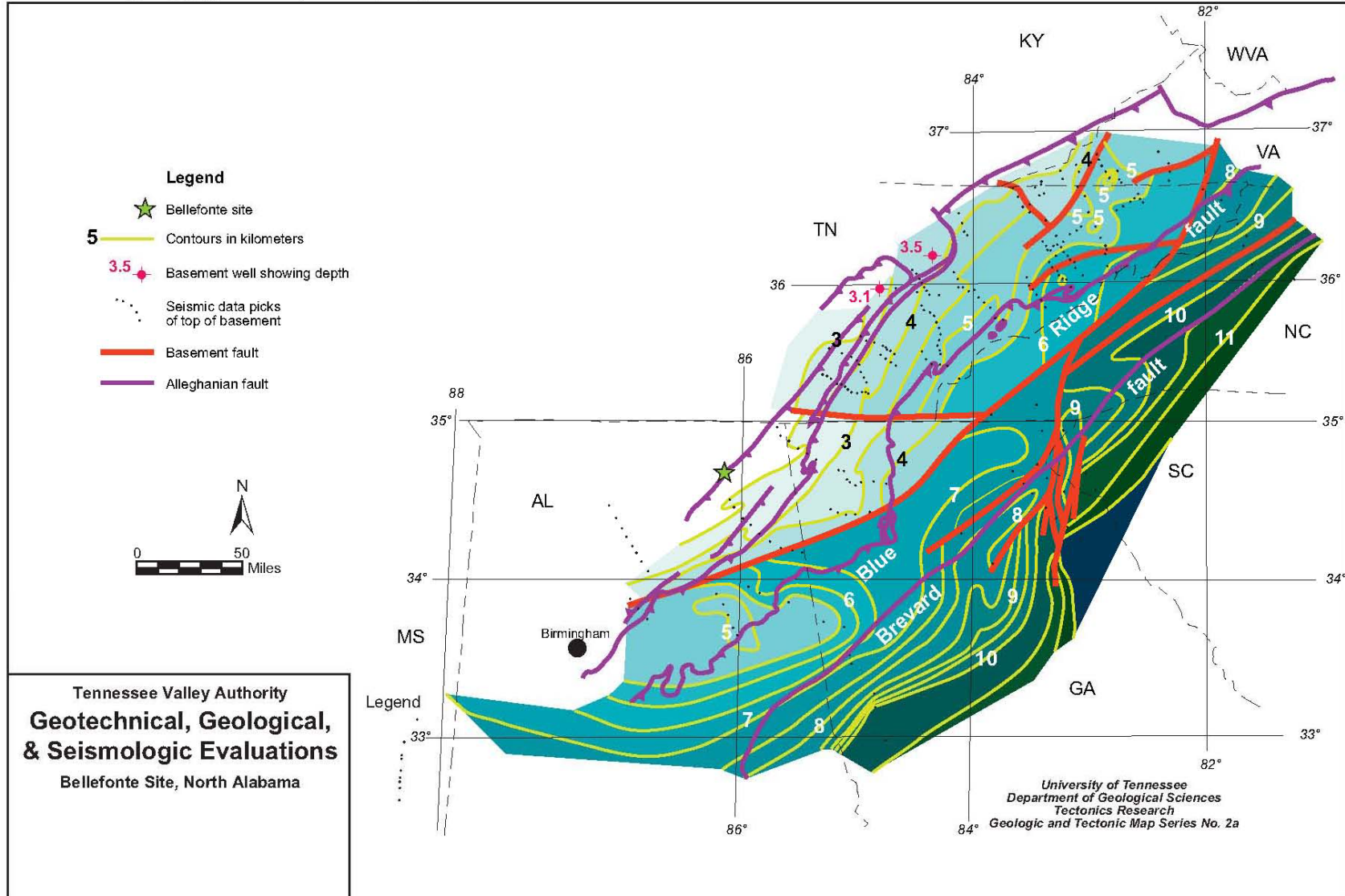


Figure 2.5.1-18. Structure Contour Map of the Top of Basement in the Southern Appalachian Orogen  
(From Hatcher and Lemiszki, 1998)

S:\9800\9877\05\_0222\_r\fig\_02.5.1-19.mxd

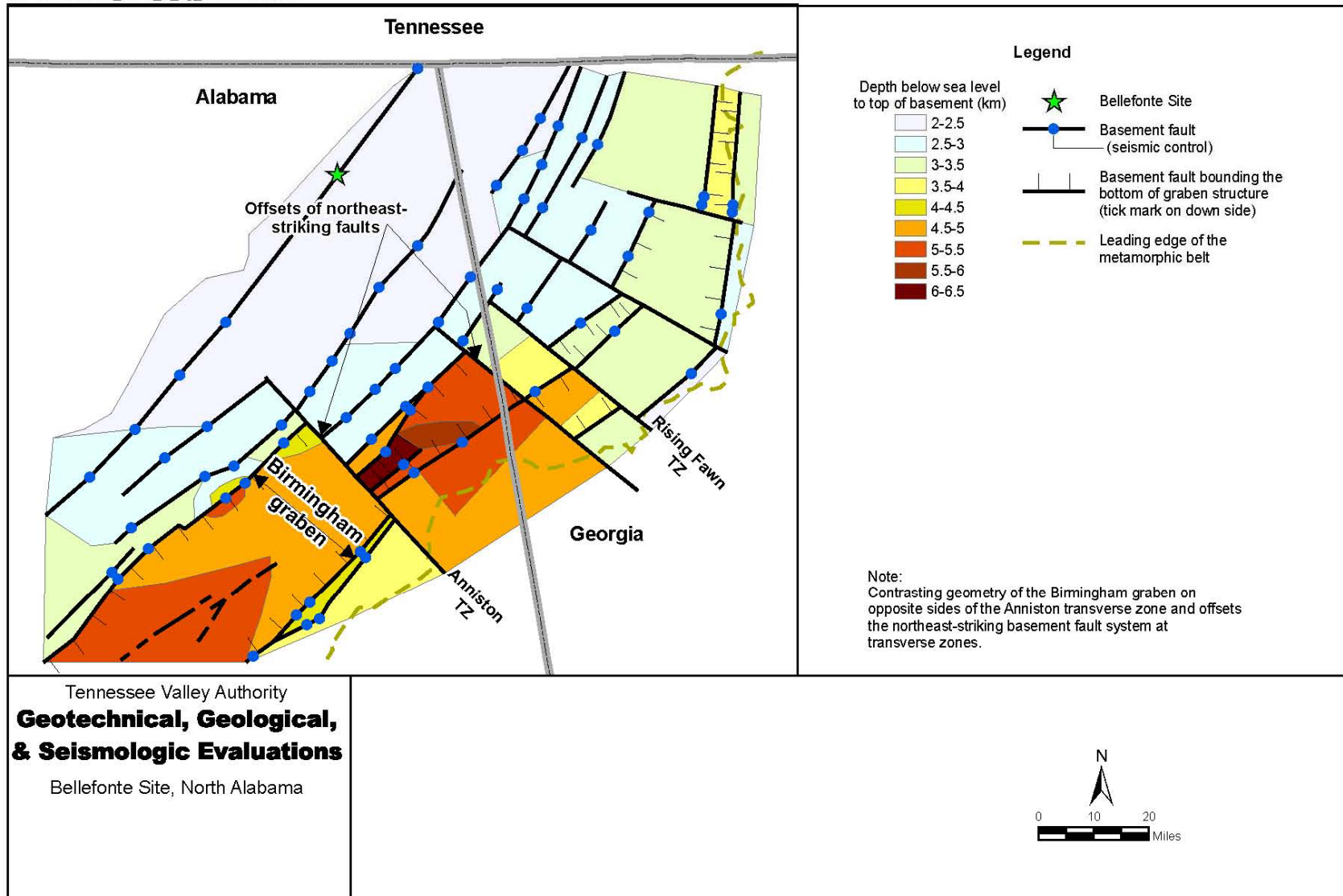
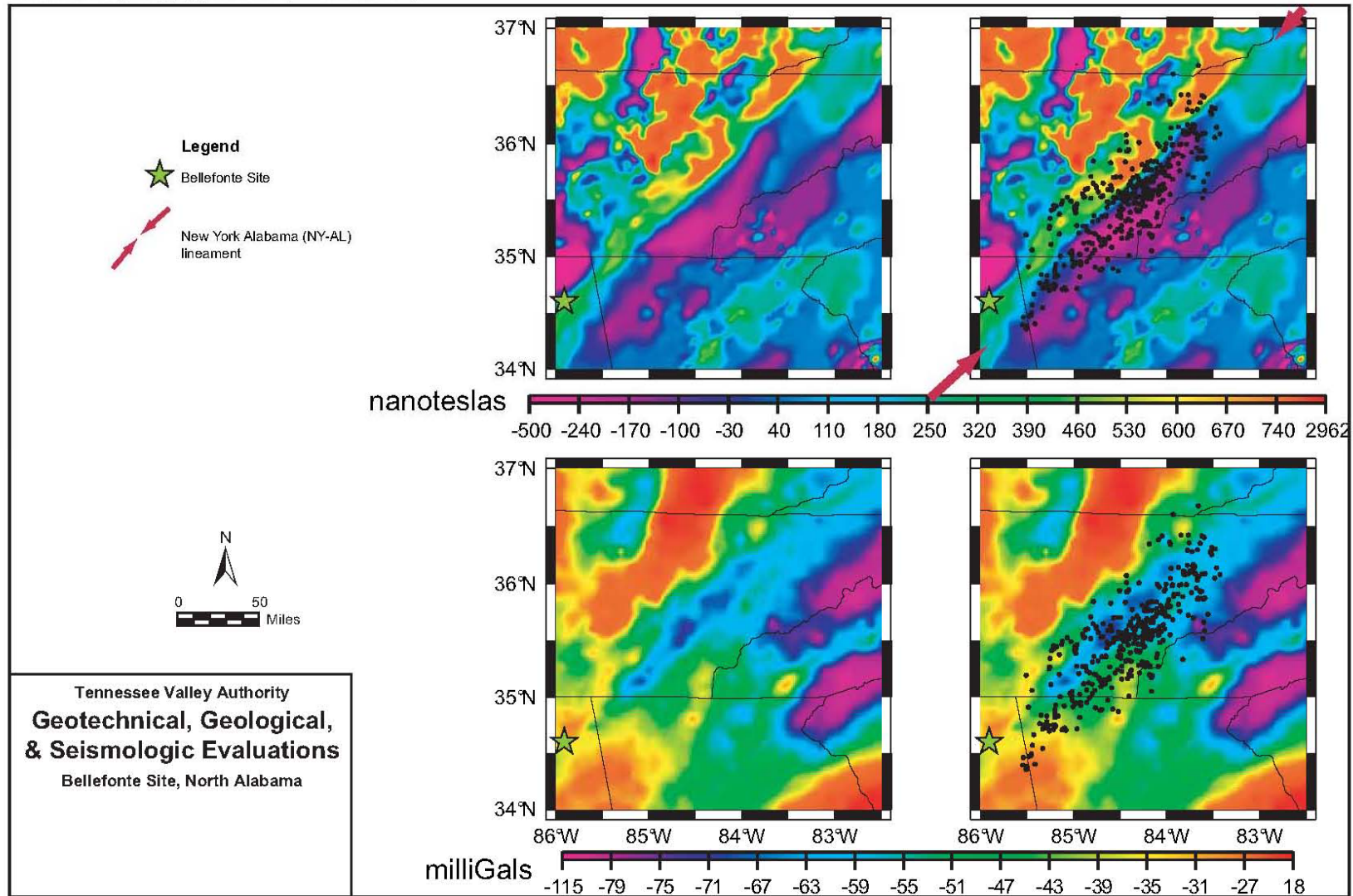


Figure 2.5.1-19. Map of Depth to Basement, Subdetachment Basement Faults, and Transverse Zones in the Foreland Thrust Belt, Alabama and Georgia (From Bayona et al., 2003)

S:\19800\19877\05\_0222\_n\_fig\_02.5.1-20.ai (2005-08-15, 13:44)



**Figure 2.5.1-20. Map of Magnetic Anomalies (top) and Bouger Gravity Anomalies (bottom) With and Without Relocated Earthquakes (1983-1994) (Modified from Vlahovic et al., 1998)**

S:\1980019877\05\_0222\_r\fig\_02.5.1-21.ai (2005-08-15, 13:47)

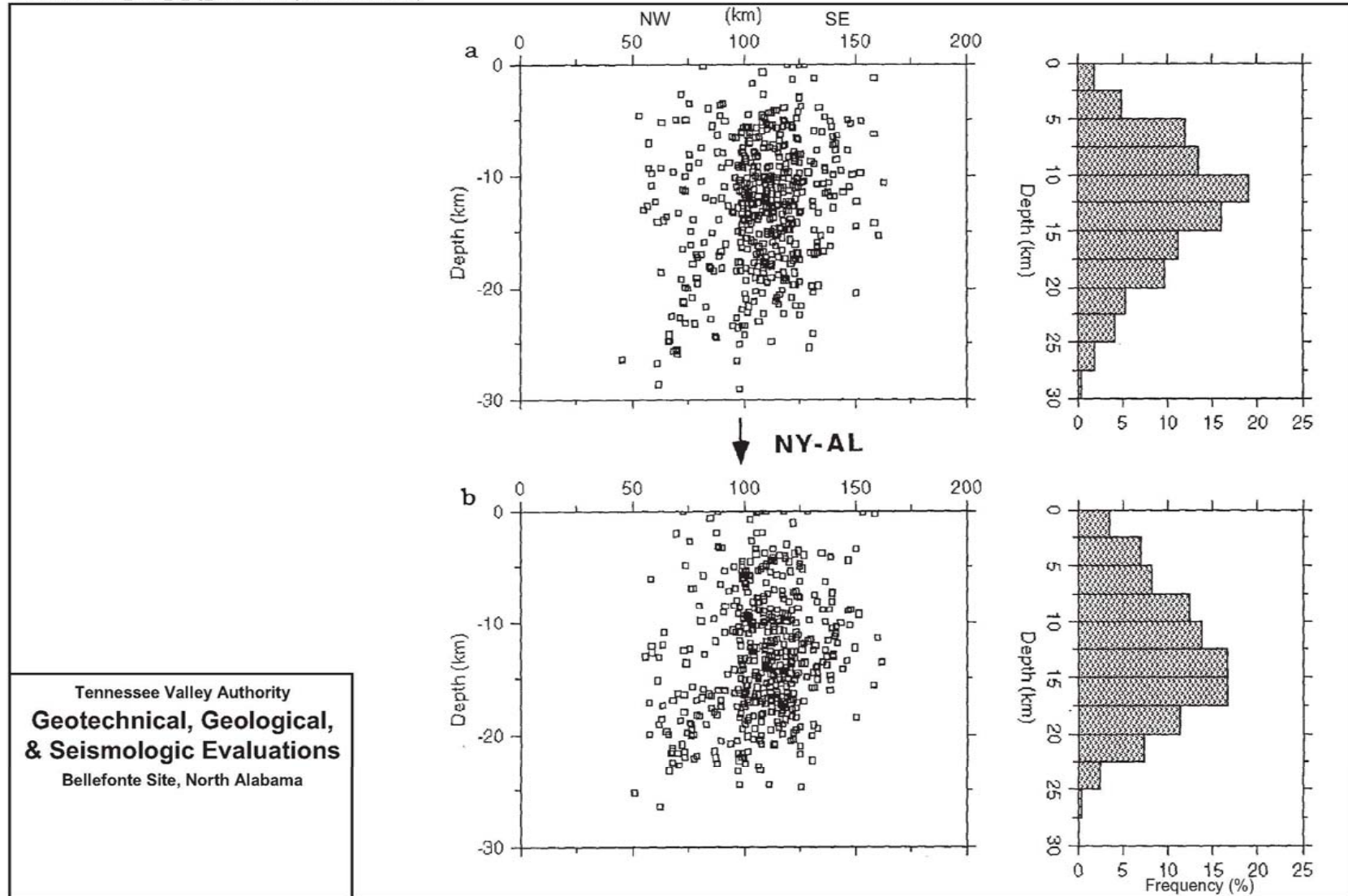


**Figure 2.5.1-21. Cross-section of East Tennessee Seismic Zone  
(From Vlahovic et al., 1998)**

S:\19800\9877\05\_0222\_r\fig\_02.5.1-22.ai (2005-06-16, 10:58)

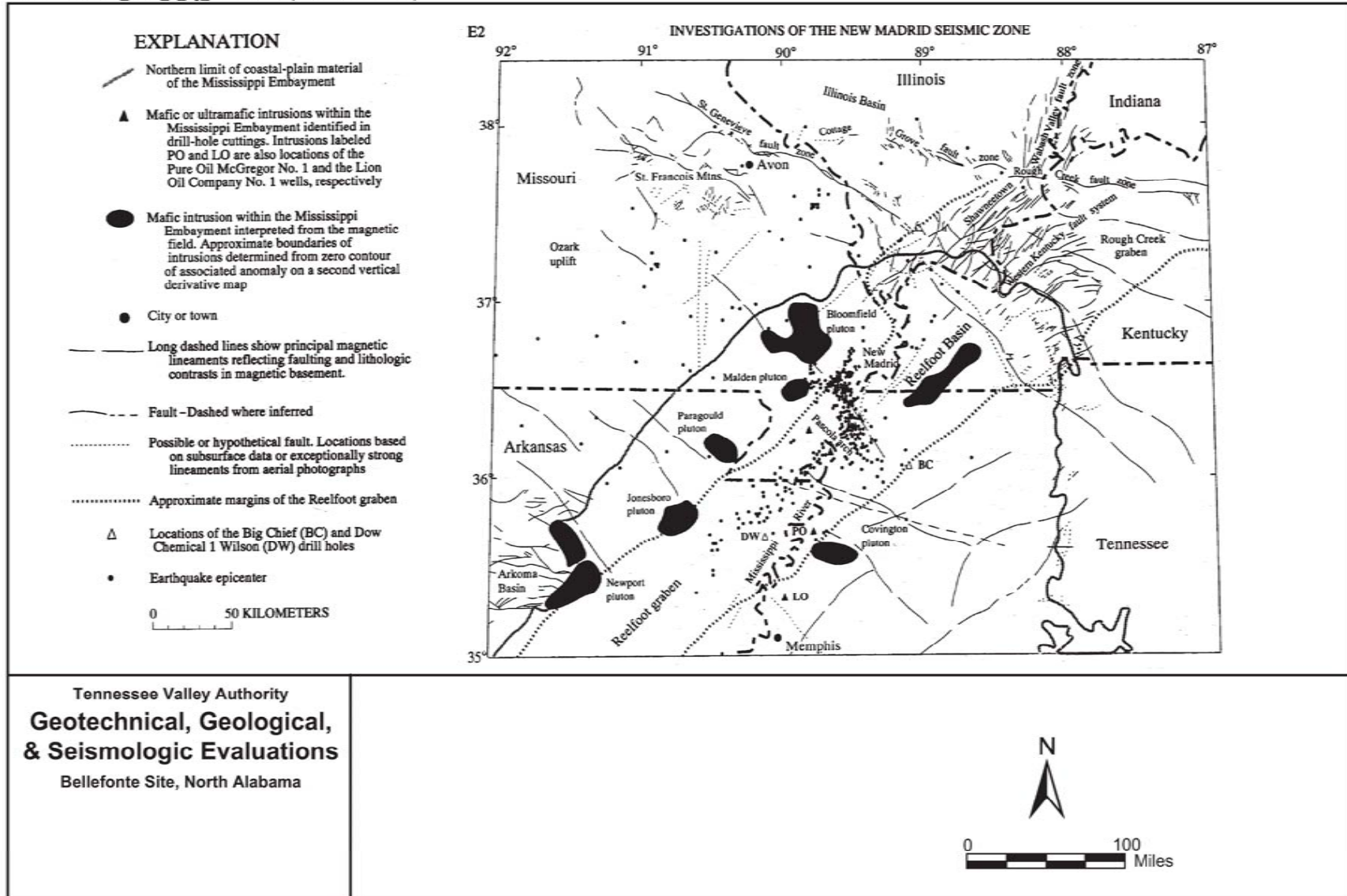


Figure 2.5.1-22. Map of New Madrid Seismic Zone and Northern Mississippian Embayment Region  
(From Hildenbrand and Hendricks, 1995)

S:\9800\9877\05\_0222\_r\fig\_02.5.1-23.ai (2005-08-15, 13:56)

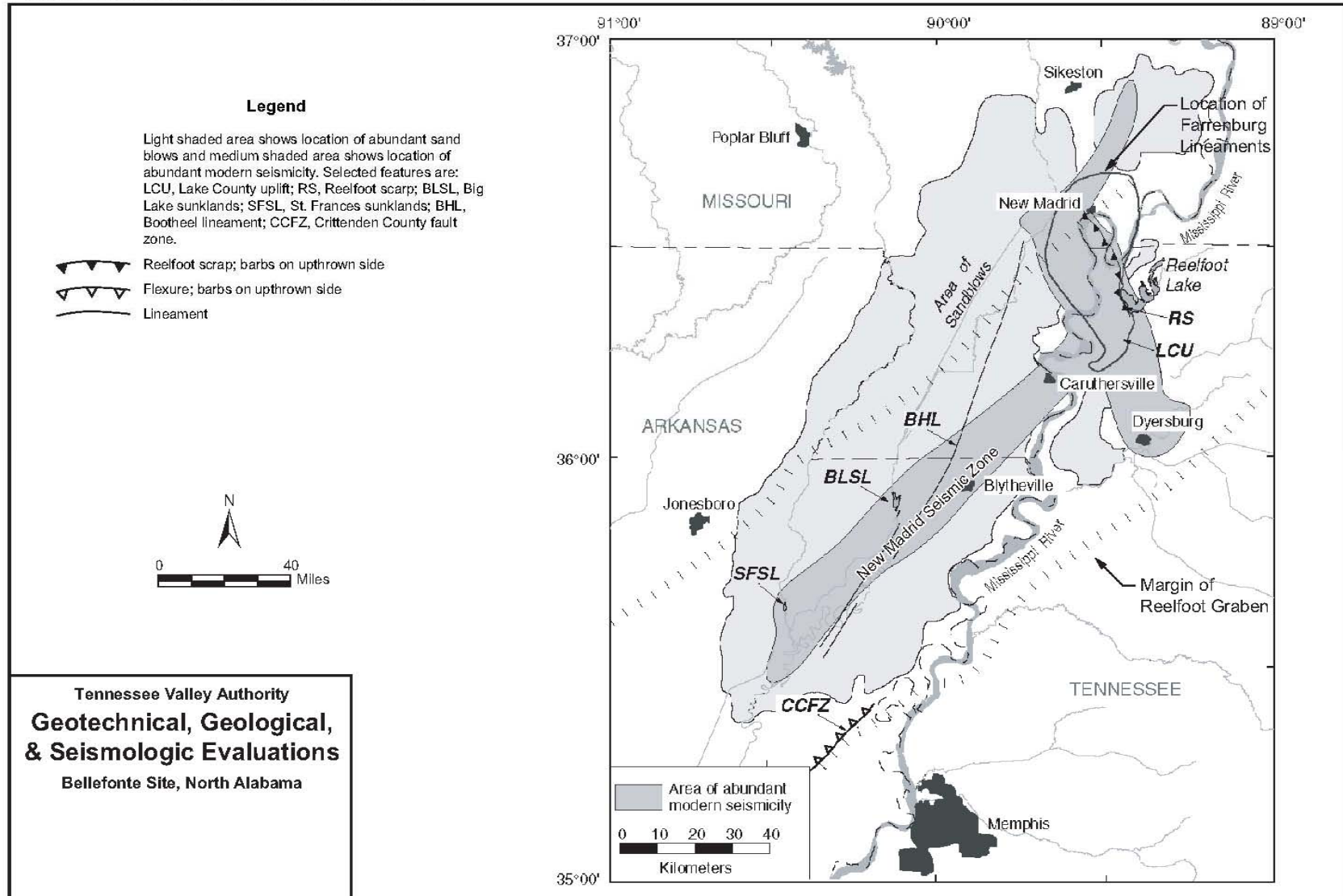


Figure 2.5.1-23. Schematic Map of the Reelfoot Scarp and Selected Features in the Area of the New Madrid Seismic Zone (Modified from Crone and Wheeler, 2000; location of Farrenburg lineaments from Baldwin et al., 2002)

S:\9800\9877\05\_0222\_r\fig\_02.5.1-24.ai (2005-08-15, 13:58)

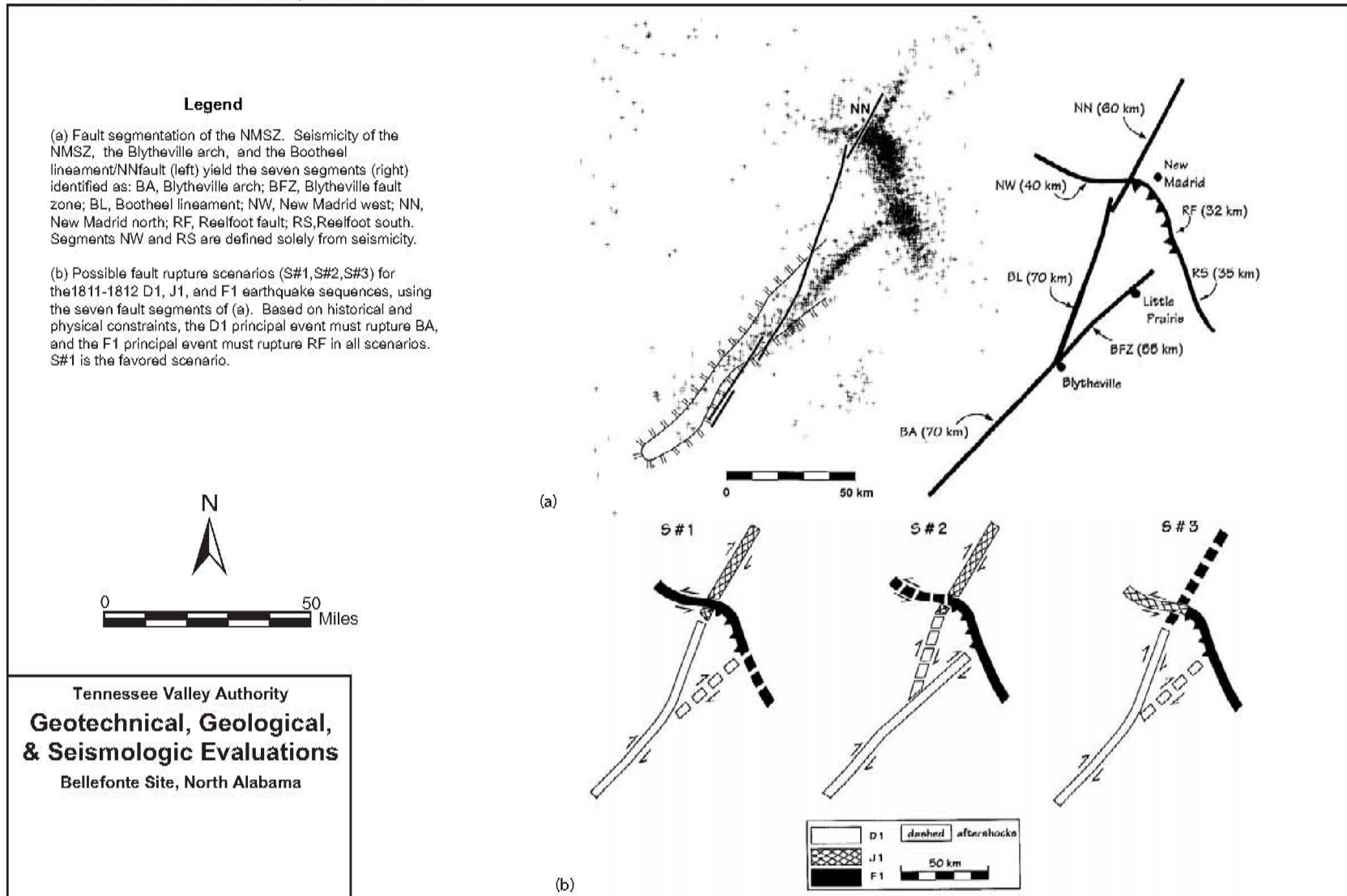
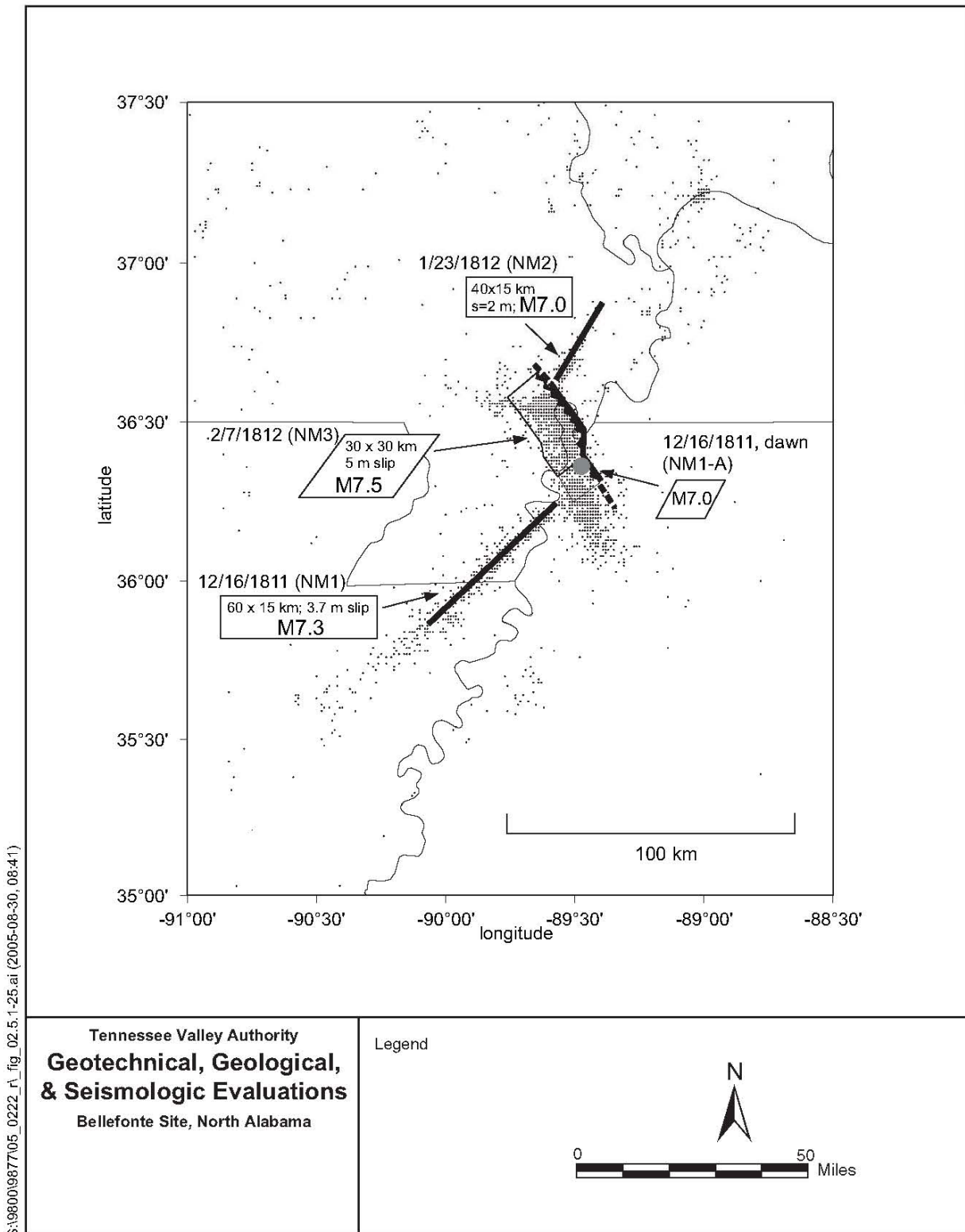
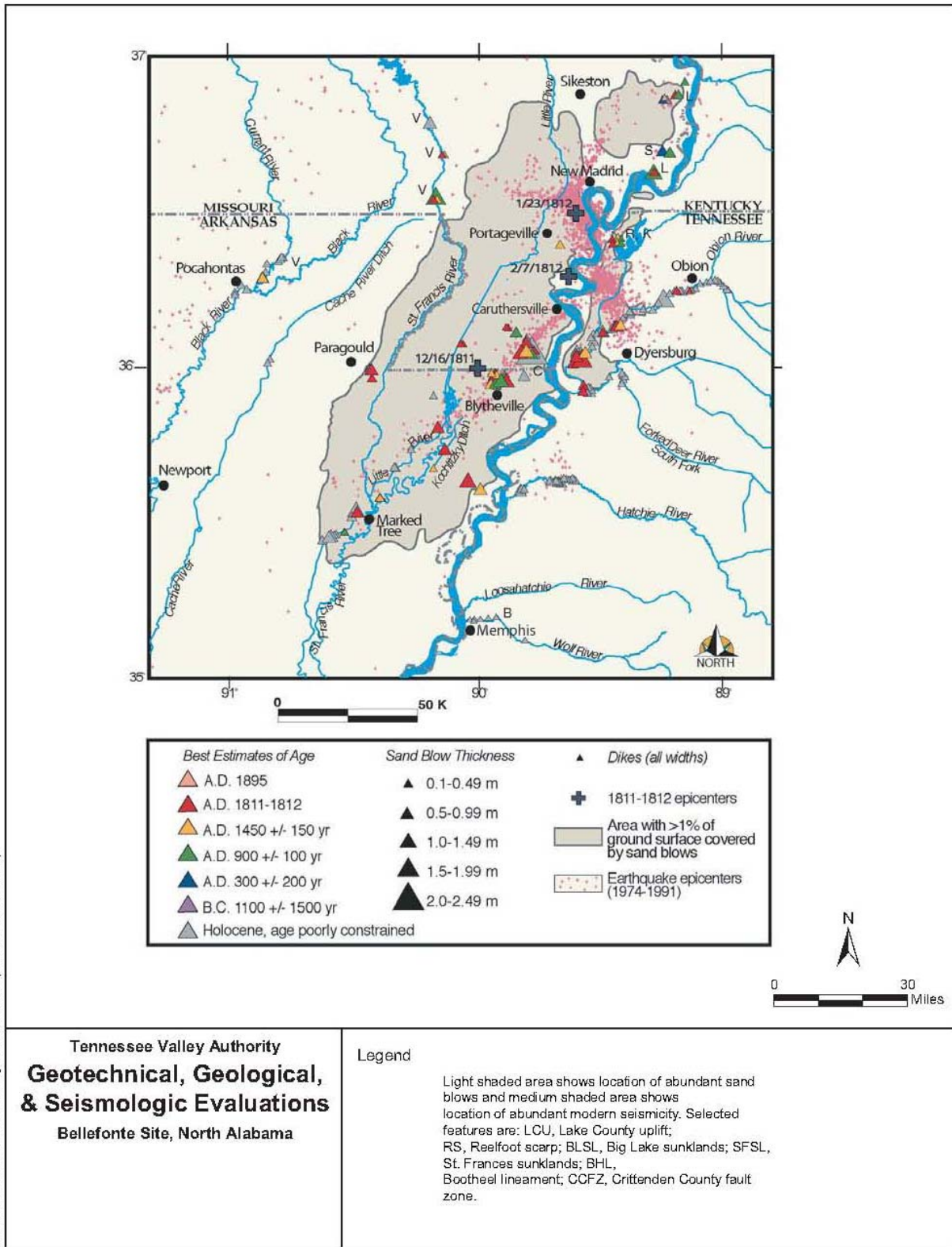


Figure 2.5.1-24. Central Fault System of New Madrid Seismic Zone  
(From Johnston and Schweig, 1996)



**Figure 2.5.1-25. Map Showing Location of New Madrid Seismic Zone as Illuminated by Seismicity Between 1974 and 1996 (From Hough and Martin, 2002)**





S:\9800\9877\05\_0222\_1\_fig\_02.5.1-26.ai (2005-08-30, 09:03)

**Figure 2.5.1-26. Map of New Madrid Seismic Zone Showing Estimated Ages and Measured Sizes of Liquefaction Features (From Tuttle et al., 2002)**

S:\9800\9877\05\_0222\_r\fig\_02.5.1-27.ai (2005-08-15, 14:10)

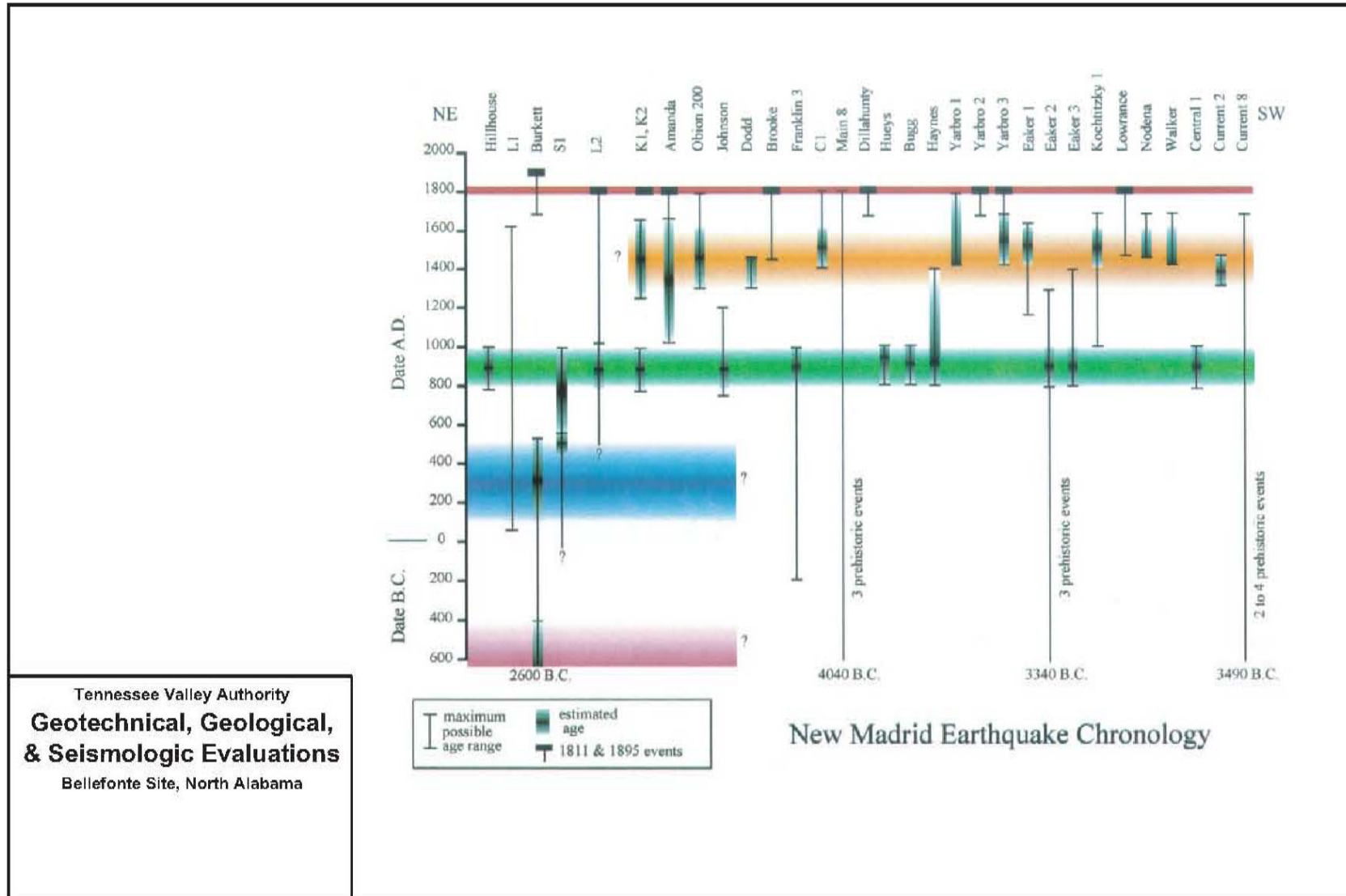


Figure 2.5.1-27. Earthquake Chronology for NMSZ from Dating and Correlation of Liquefaction Features at Sites Along NE-SW Transect Across Region (From Tuttle et al., 2002)

S:\19800\9877\05\_0222\_r\fig\_02.5.1 28.ai (2005 08 15, 14:11)

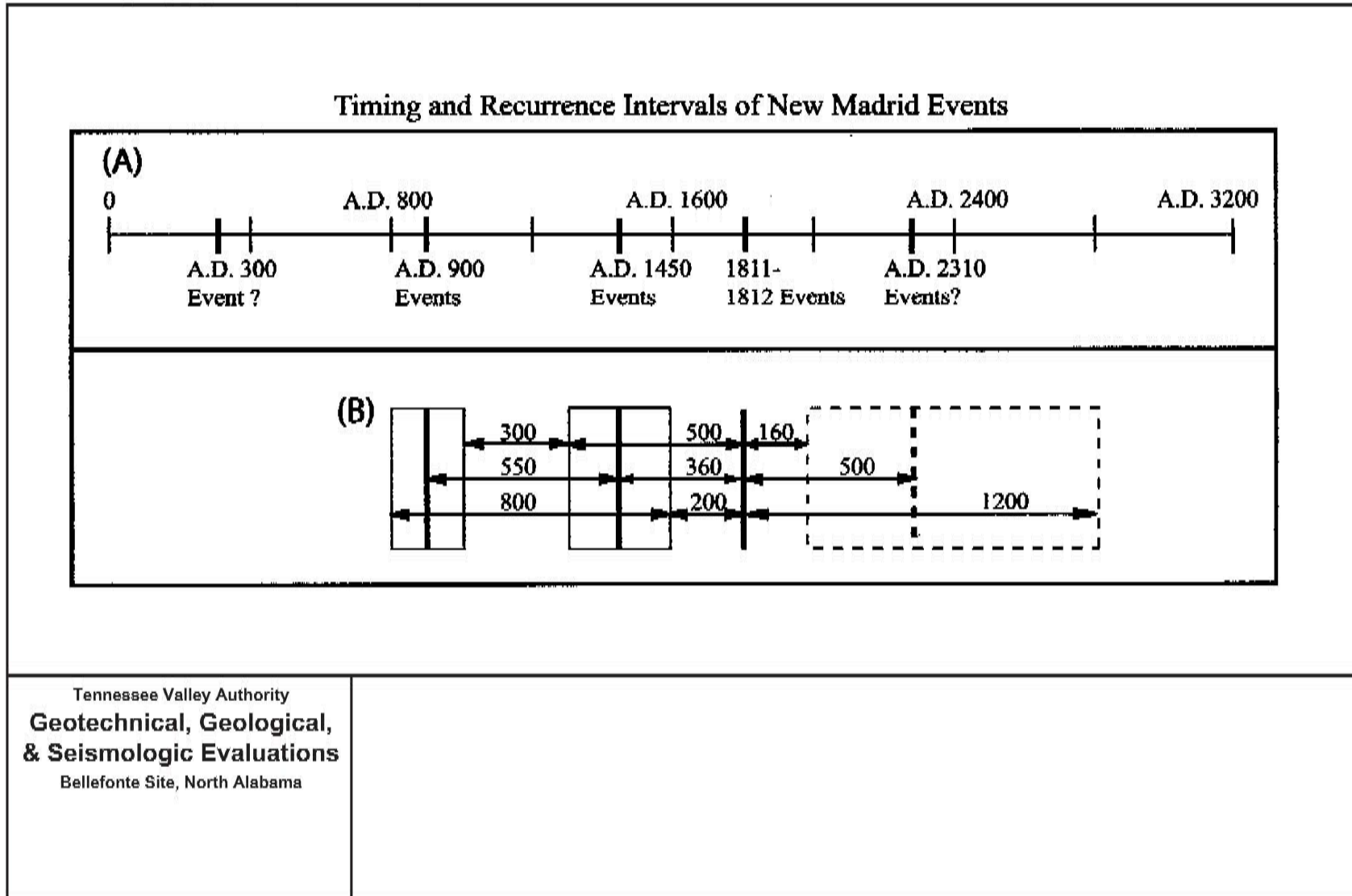
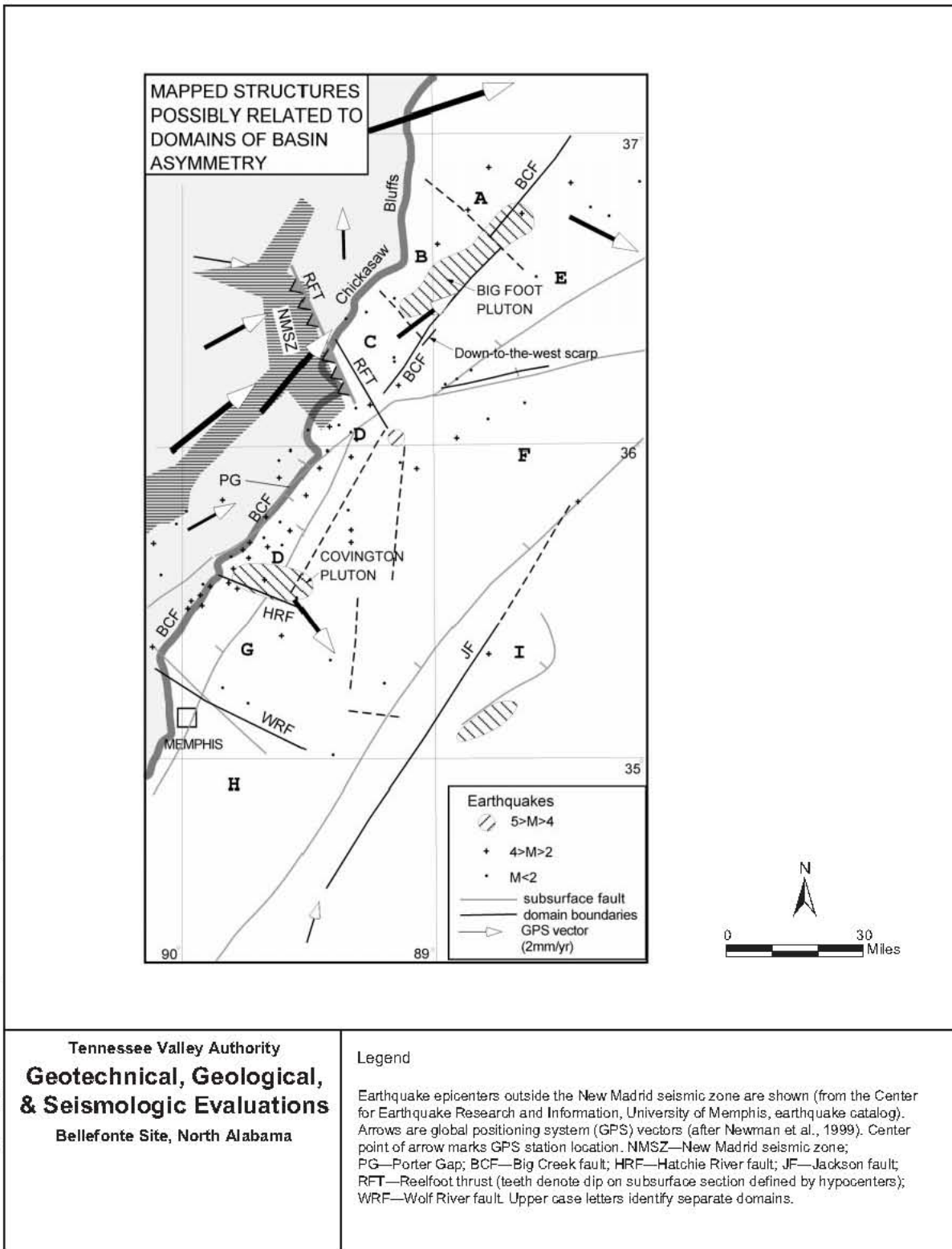


Figure 2.5.1-28. Timing and Recurrence Intervals of New Madrid Events  
(From Tuttle et al., 2002)



S:\9800\9877\05\_0222\_r1\_fig\_02.5.1-29.ai (2006-08-30, 09:06)

**Figure 2.5.1-29. Subsurface Structures Mapped in Paleozoic and Basement Rocks in Northeastern Mississippi Embayment (From Cox et al., 2001b) (Note: Based on Hildenbrand et al., 1982; Johnson et al., 1994)**

S:\9800\9877\05\_0222\_r\_fig\_02.5.1-30.ai (2005-08-30, 09:10)

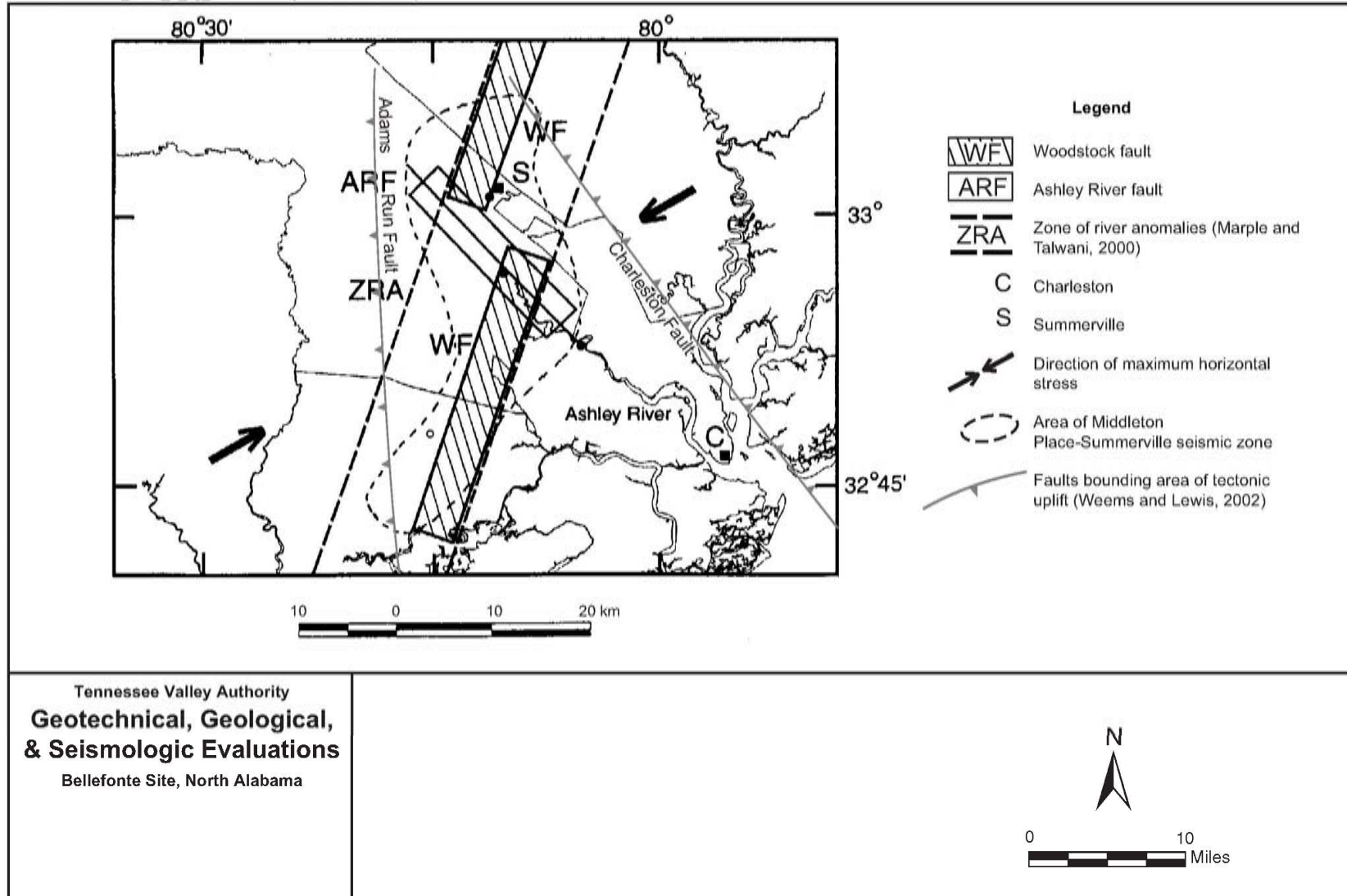


**Figure 2.5.1-30. Schematic Figure Showing Seismotectonic Elements in the Epicentral Region of the 1886 Earthquake (Talwani, 2000) (References: Marple and Talwani, 2000; Weems and Lewis, 2002)**

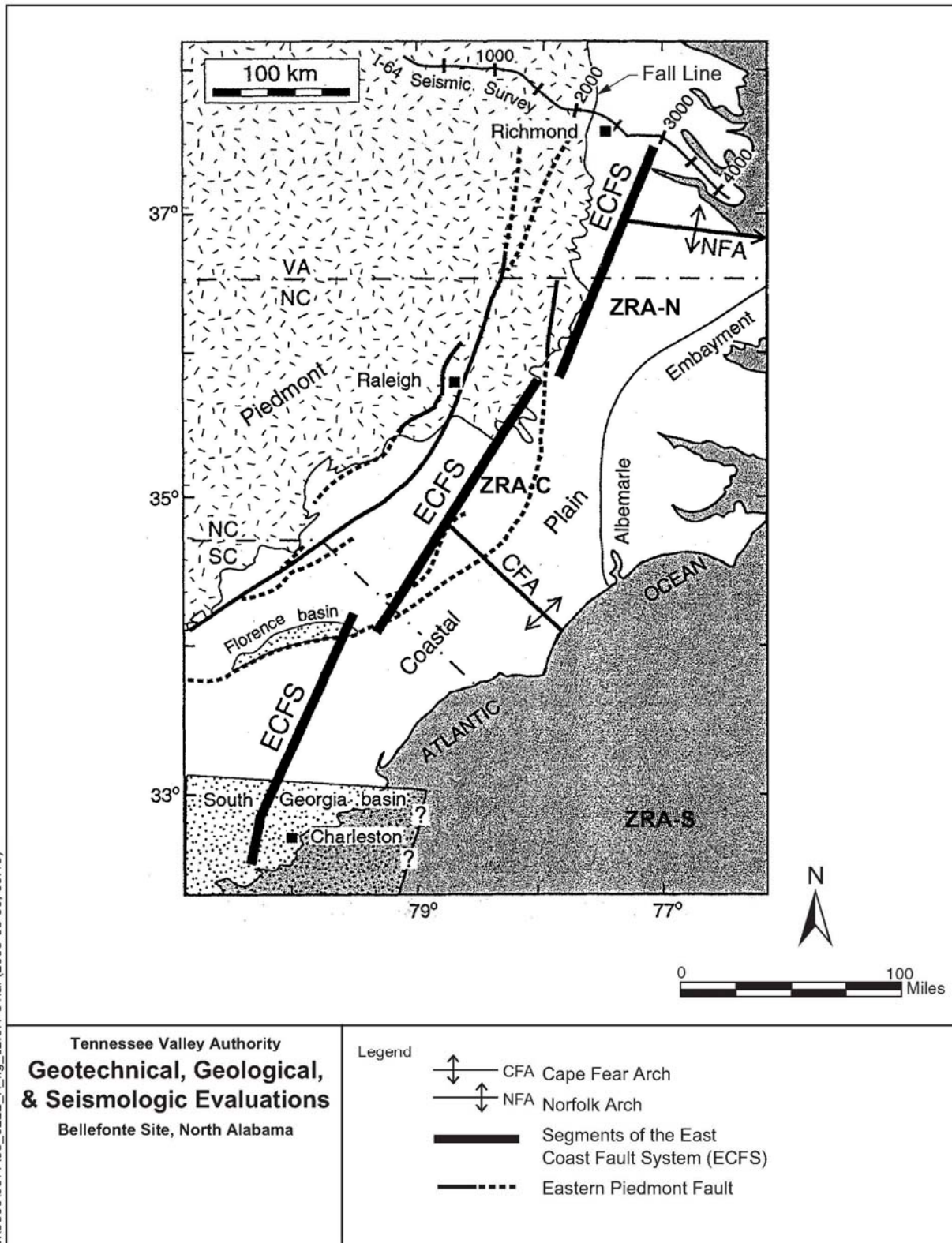
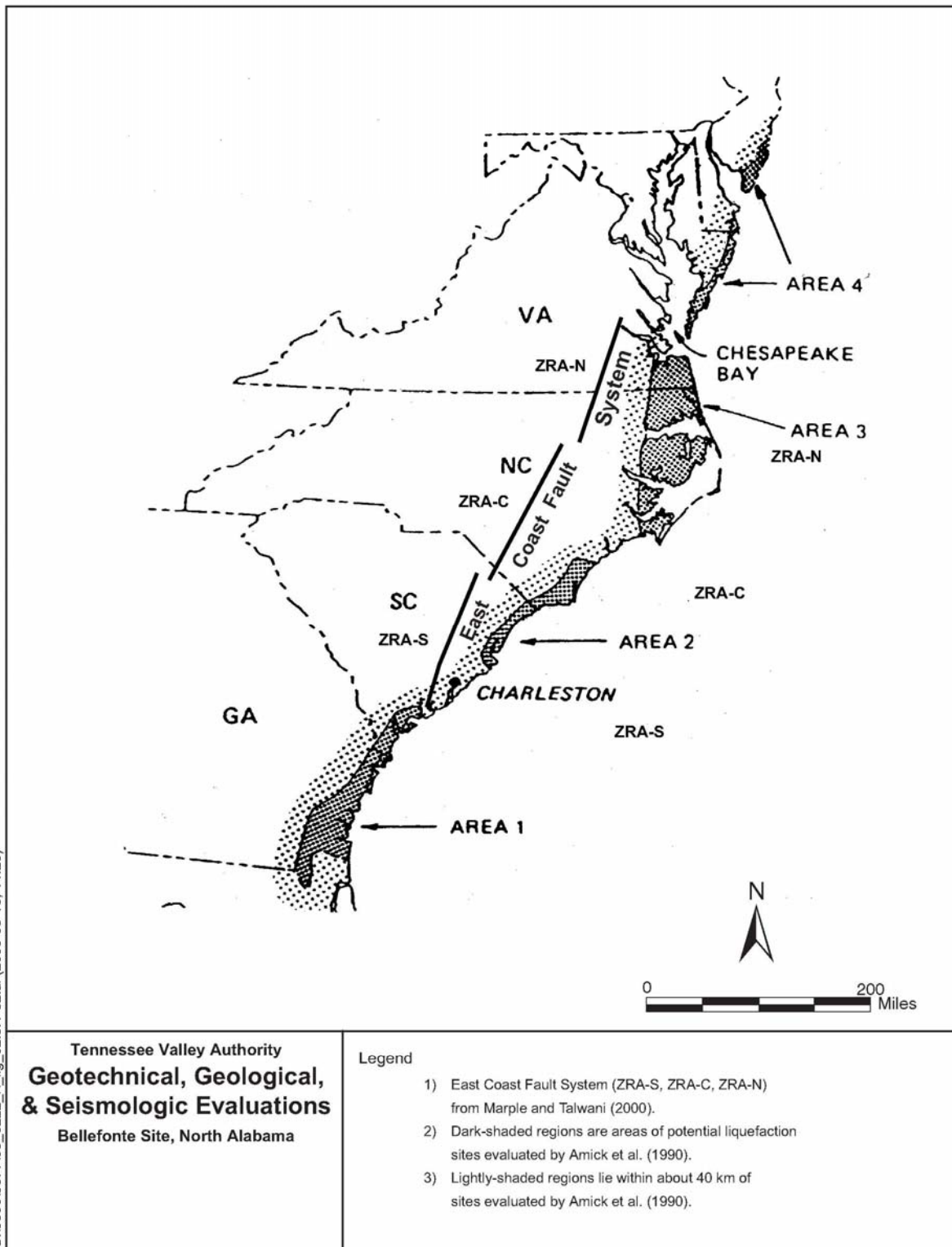
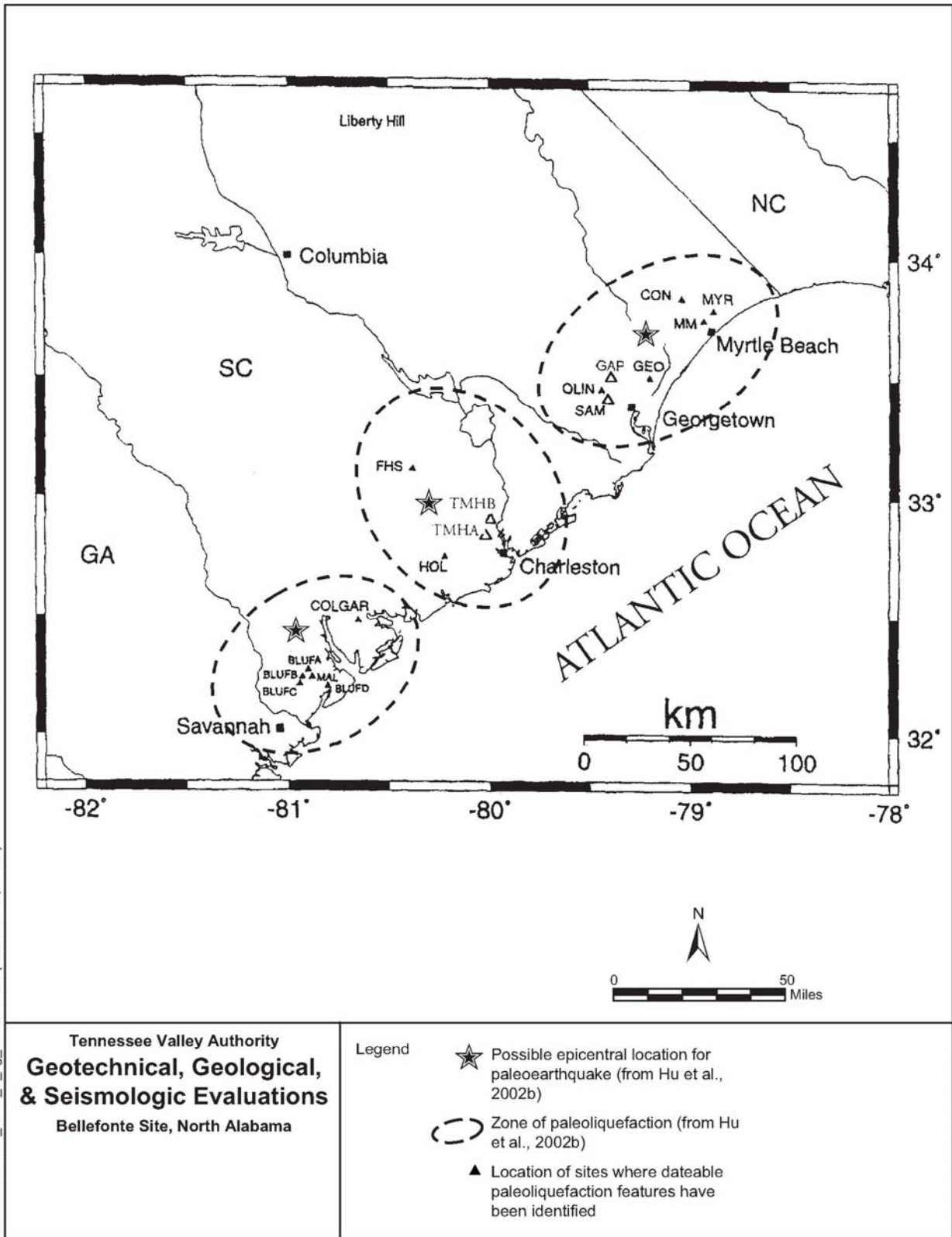


Figure 2.5.1-31. Location of the East Coast Fault System (ECFS)  
(Modified from Marple and Talwani, 2000)

S:\98000\9877105\_0222\_r\_fig\_02.5.1-31.ai (2005-08-30, 09:15)



**Figure 2.5.1-32. Distribution of Potential Liquefaction Sites Evaluated Along the Atlantic Coast Plain  
(Modified from Amick et al., 1990)  
(References: Marple and Talwani, 2000; Amick et al., 1990)**



S:\9800\9877\05\_0222\_1\_fig\_02.5.1-33.ai (2005-08-15, 14:35)

**Figure 2.5.1-33. Distribution of Paleoliquefaction Sites in South Carolina and North Carolina (Source: Hu et al., 2002b)**



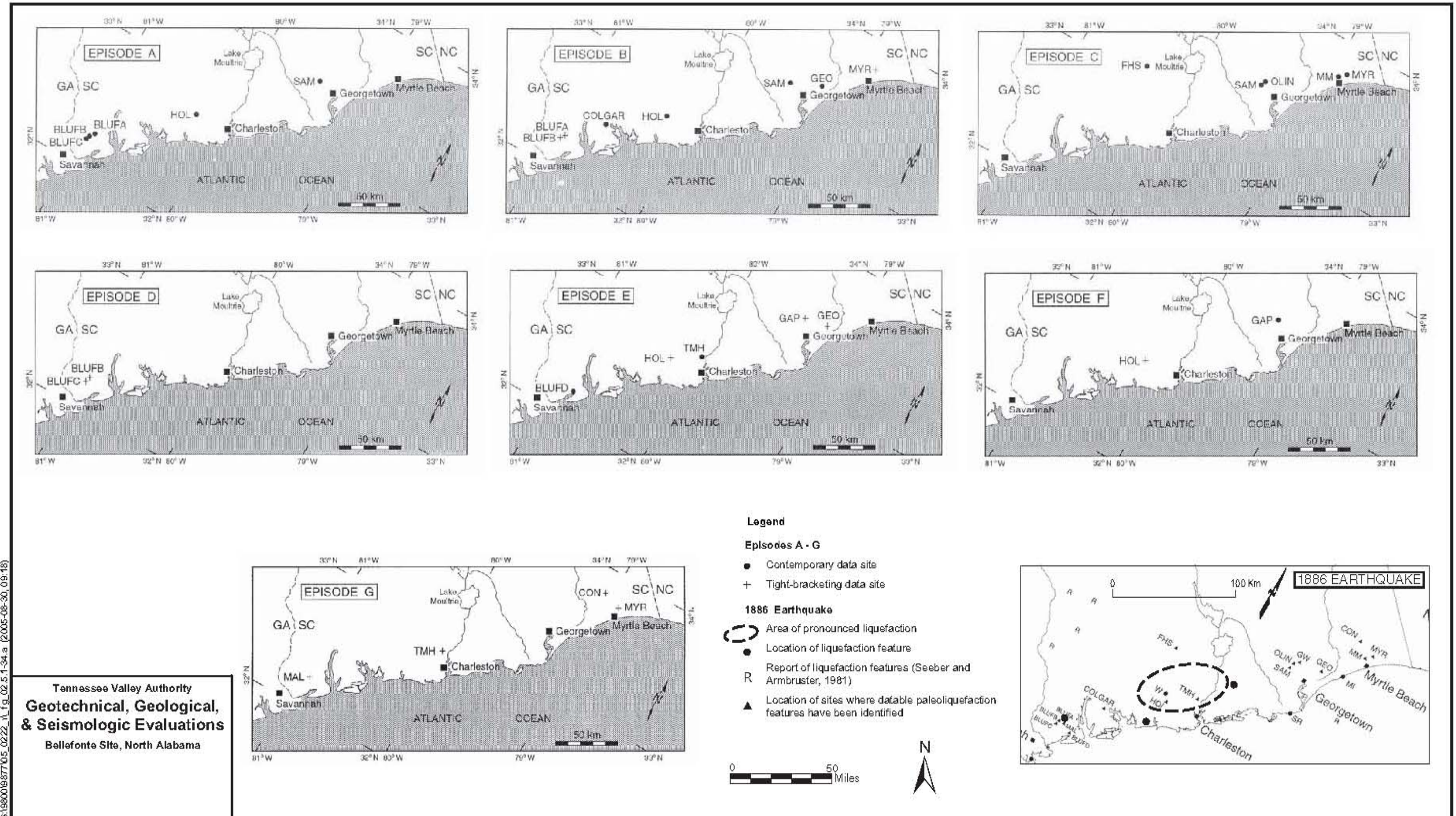


Figure 2.5.1-34. Maps Showing the Distribution of Liquefaction Sites for the 1886 Earthquake and the Distribution of Paleoliquefaction Sites Associated with Paleoearthquake Episodes A to G (From Talwani and Schaefer, 2001)

S:\1886018577\05\_0222\_1\fig\_02.5.1-34.a (2005-08-30, 09:18)

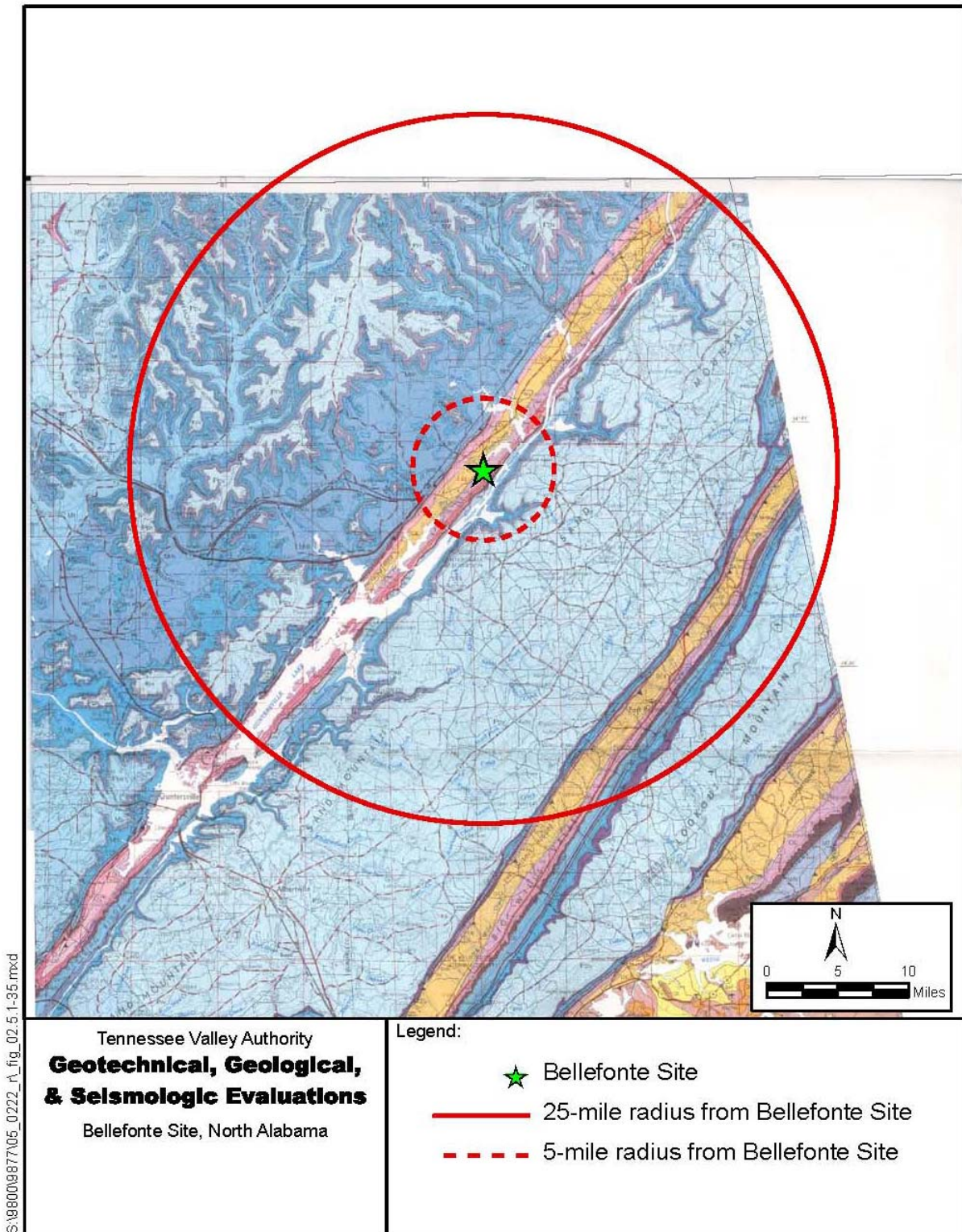


Figure 2.5.1-35. Geologic Map of the Site Vicinity (25-Mile Radius) and Site Area (5-Mile Radius)

(Source: modified from Osborne et al., 1988;

<http://www.gsa.state.al.us/gsa/GIS/geologydetails.html>)

(Note: see Figure 2.5.1-8 for explanation of the geologic map units and symbols)

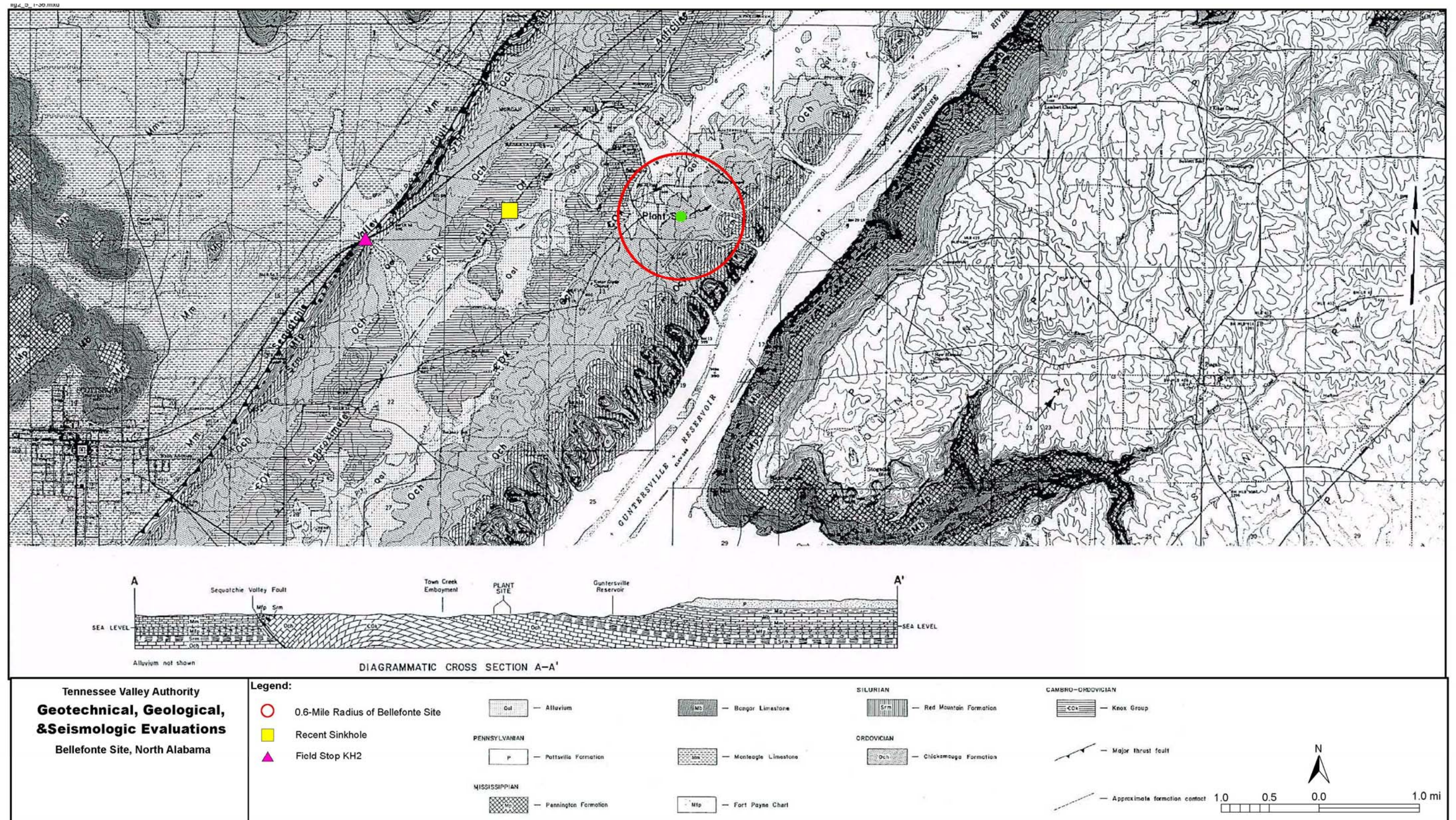


Figure 2.5.1-36. Geologic Map of the Site (0.6-Mile Radius) and Surrounding Area  
(Source: Modified from Figure 2.5-7, TVA, 1986)

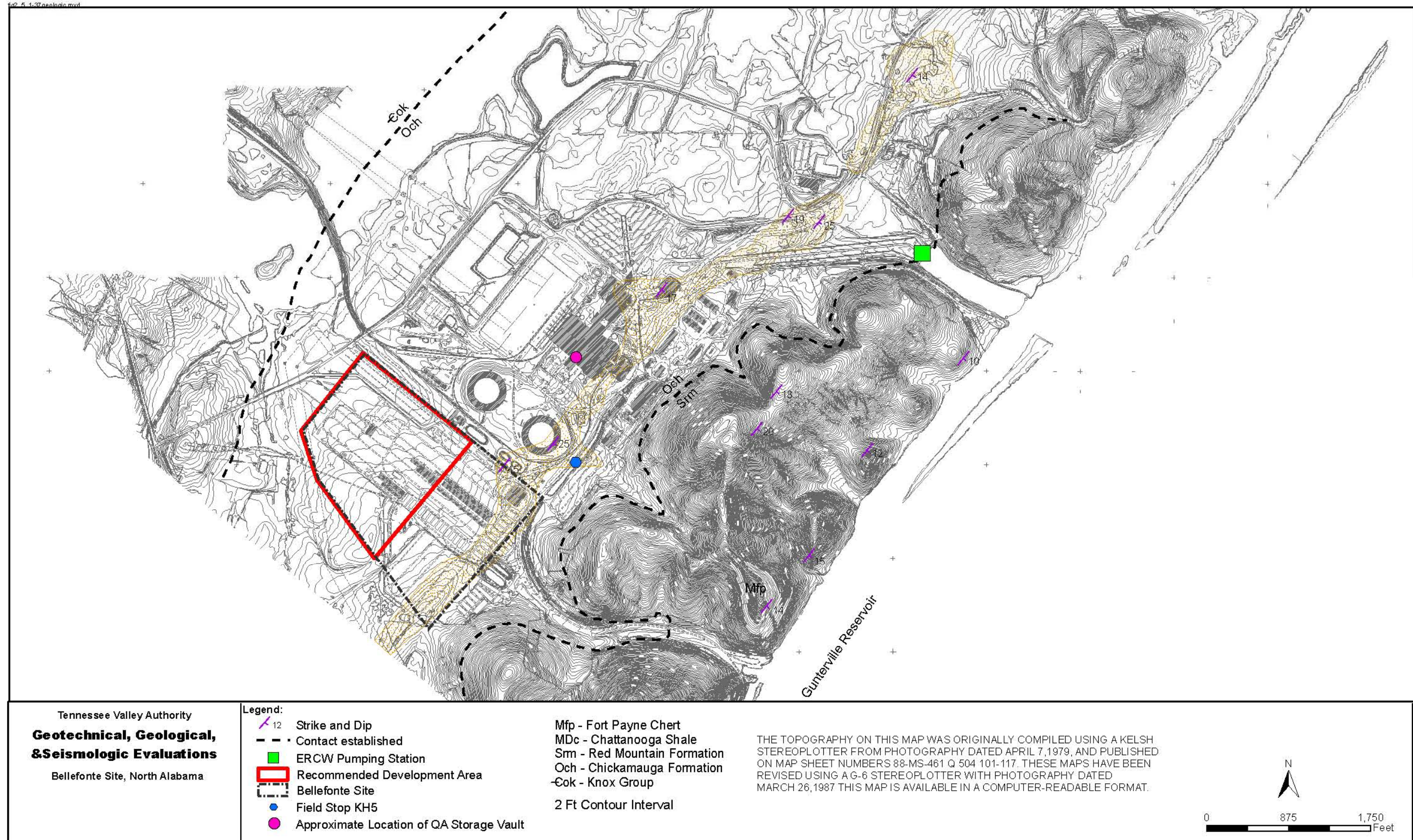
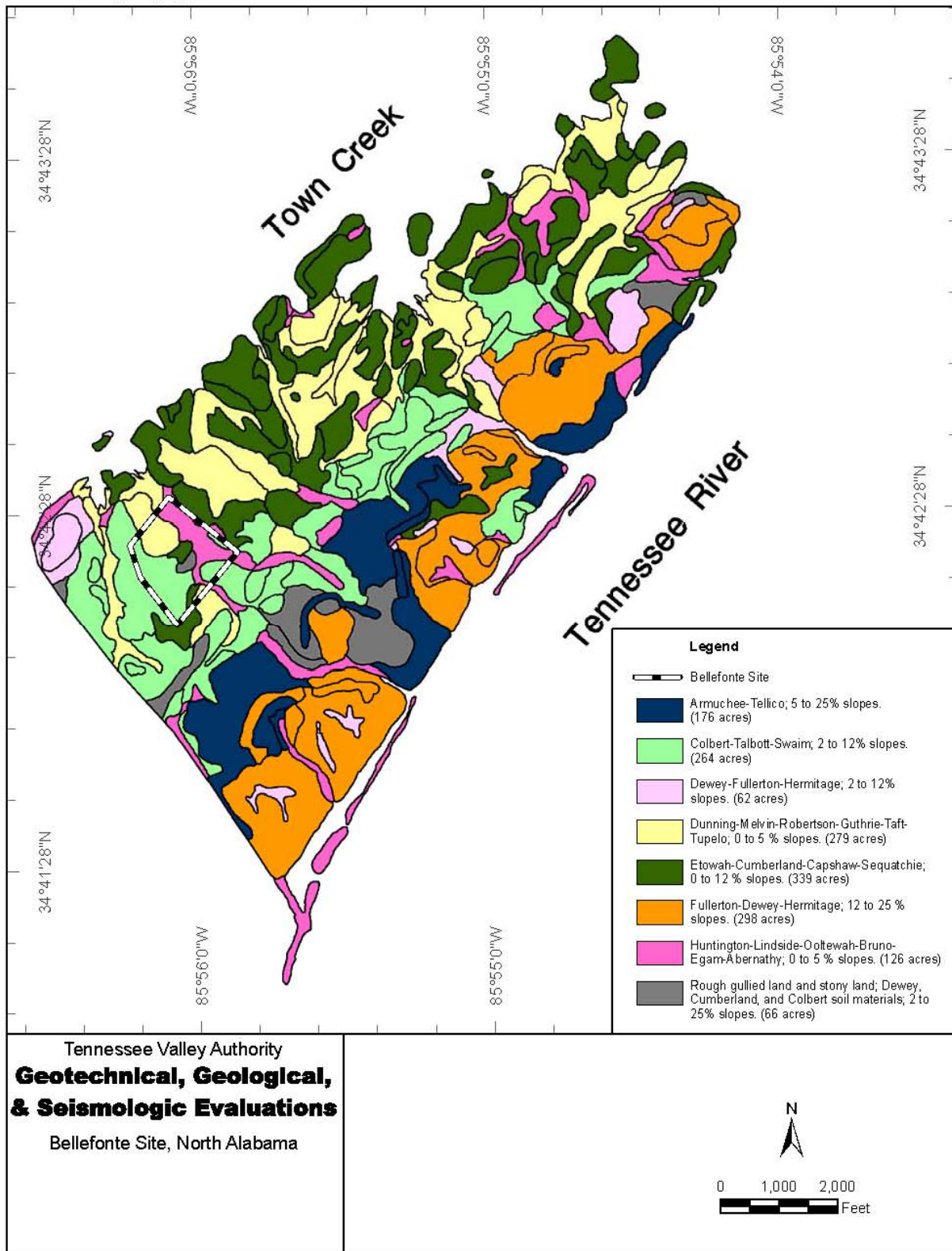


Figure 2.5.1-37. Geologic Map of the Footprint and Surrounding Area  
(Note: Geologic data from Figure 2.5.9 (TVA, 1986))

S:\19800\19877\05\_0222\_A\_fig\_02.5.1-38.mxd



**Figure 2.5.1-38. Soil Map of the Site Area  
(Source: Modified from Figure 3.1.3-1, TVA, 1997)**

S:\9800\9877\05\_0222\_r\fig\_02.5.1-39.ai (2005-08-30, 09:27)



Tennessee Valley Authority  
**Geotechnical, Geological,  
& Seismologic Evaluations**  
Bellefonte Site, North Alabama

Dissolution cavity observed in Chickamauga limestone outcrop approximately 500 feet northeast of the northeast corner of the Bellefonte site (Field Stop KH5). Knife at right of cavity is 5" long.

**Figure 2.5.1-39. Photograph of Small-Scale Dissolution Cavity in Chickamauga (Limestone at the Bellefonte Site)**

## 2.5.2 Vibratory Ground Motion

This section provides a detailed description of vibratory ground motion assessments that were carried out for the TVA Bellefonte Site. The section begins with a review of the existing approach in Regulatory Guide 1.165 (USNRC, 1997) for conducting the vibratory ground motion studies, and is followed by a summary of the performance-based approach that was used for the TVA Bellefonte Site to extend the requirements in Regulatory Guide 1.165 to achieve a uniform seismic safety performance within structures, systems, and components consistent with USNRC's safety goal policy. Following this review of the regulatory framework used for the project, results of the seismic hazard evaluation are documented and the SSE ground motion spectrum for horizontal and vertical motions are developed.

### Existing Guidance in Regulatory Guide 1.165

Regulatory Guide 1.165 (USNRC, 1997) provides guidance on methods acceptable to the NRC to satisfy the requirements of the seismic and geologic regulation, 10 CFR Part 100.23, for assessing the appropriate SSE ground motion levels for new nuclear power plants. Regulatory Guide 1.165 states that an acceptable starting point for this assessment at sites in the CEUS is the PSHA conducted by the EPRI-SOG in the 1980s (EPRI-SOG, 1988; EPRI, 1989). The EPRI-SOG evaluation involved a comprehensive compilation of geological, geophysical, and seismological data, evaluations of the scientific knowledge concerning earthquake sources, maximum earthquakes, and earthquake rates in the CEUS by six multi-disciplinary teams of experts in geology, seismology, geophysics, and, separately, development of state of knowledge earthquake ground motion modeling, including epistemic and aleatory uncertainties<sup>3</sup>. The uncertainty in characterizing the frequency and maximum magnitude of potential future earthquakes associated with these sources and the ground motion that they may produce was assessed and explicitly incorporated in the seismic hazard model.

Regulatory Guide 1.165 further specifies that the adequacy of the EPRI-SOG hazard results must be evaluated in light of more recent data and evolving knowledge pertaining to seismic hazard evaluation in the CEUS. Appendix E, Section E.3, of Regulatory Guide 1.165 outlines a three-step process for this evaluation, as follows.

**Step 1: Evaluate whether recent information suggests significant differences from the previous seismic hazard characterization.**

**Step 2: If potentially significant differences are identified, perform sensitivity analyses to assess whether those differences have a significant impact on site hazard.**

**Step 3: If Step 2 indicates that there are significant differences in site hazard, then the PSHA for the site is revised by either updating the previous calculations or, if**

<sup>3</sup> Epistemic uncertainty is attributable to incomplete knowledge about a phenomenon that affects our ability to model it. Epistemic uncertainty is reflected in a range of viable models, model parameters, multiple expert interpretations, and statistical confidence. In principle, epistemic uncertainty can be reduced by the accumulation of additional information. Aleatory uncertainty (often called aleatory variability) is uncertainty inherent in a non-deterministic (stochastic, random) phenomenon. Aleatory uncertainty is accounted for by modeling the phenomenon in terms of a probability model. In principle, aleatory uncertainty cannot be reduced by the accumulation of more data or additional information. Sometimes called randomness.

**necessary, performing a new PSHA. If not, the previous EPRI-SOG results may be used to assess the appropriate safe shutdown earthquake (SSE) ground motions.**

Regulatory Guide 1.165 calls for the SSE ground motions to be based on the site PSHA results for a reference probability of the median  $10^{-5}$  hazard level. The basis for the selected reference probability is described in Appendix B of Regulatory Guide 1.165. The reference probability was set equal to the median value of the annual frequency of exceeding the SSE ground motions (based on the median estimate of the hazard) computed for a specific set of licensed nuclear power plants. These probabilities were computed using ground motion models developed in the mid-to-late 1980s. As discussed in Regulatory Position 3 in Regulatory Guide 1.165, significant changes to the overall database for assessing seismic hazard in the CEUS may warrant a change in the reference probability. The availability of the recently developed EPRI ground motion characterization for the CEUS (EPRI, 2004) represents a significant advancement in the seismic hazard database for the CEUS, thereby requiring reconsideration of the reference probability approach. Appendix B of Regulatory Guide 1.165 also discusses that selection of another reference probability may be appropriate, such as one founded on risk-based considerations. The performance-based, risk-consistent approach as outlined below is the one taken in this application for developing the TVA Bellefonte SSE design ground motions.

### Regulatory Basis for the Performance-Based Approach

The SSE ground motion response spectra have been developed using the graded performance-based, risk-consistent method described in ASCE/SEI Standard 43-05, *Seismic Design Criteria for Structures, Systems, and Components in Nuclear Facilities* (ASCE/SEI, 2005). The method specifies the level of conservatism and rigor in the seismic design process such that the performance of structures, systems, and components of the plant achieve a uniform seismic safety performance consistent with the USNRC's safety goal policy statement (USNRC, 1986; USNRC, 2001). The ASCE/SEI Standard 43-05 approach is designed to achieve a quantitative safety performance goal, PF. The method is based on use of site-specific mean seismic hazard and assumes that the seismic design criteria (SDC) and procedures contained in NUREG-0800 are applied in SSC design.

The USNRC's safety goal policy statement recognizes that nuclear plant safety regulation is a societal risk management activity and provides the foundation for equitably managing the nuclear facility risk in the context of other societal risks. Subsequent to adopting the policy statement, the USNRC has continued to develop and evolve, supporting policies for a comprehensive risk management framework for nuclear regulation together with supporting implementation guidelines (USNRC, 1998; USNRC, 2002). The seismic design methodology provided in ASCE/SEI Standard 43-05 is a further step in the development of a risk-based standard for seismic design and regulation. The graded performance-based approach is compatible with the direction provided by the USNRC's Risk-informed, Performance-Based Regulation guidance (USNRC, 1998; USNRC, 1999) and with developing USNRC guidance for the determination of the design response spectrum (DRS) (McGuire et al., 2001; McGuire et al., 2002).

The ASCE/SEI Standard 43-05 seismic design method and criteria are intended to implement the USNRC's established qualitative safety goals and the companion



quantitative implementation objectives. The qualitative safety goals provide that the consequences of nuclear power plant operation should cause no significant additional risk to the life and health of individuals and that the societal risks to life and health from nuclear power plant operation should be comparable to or less than the risks posed by generating electricity by viable competing technologies and should not be a significant addition to other societal risks. The USNRC's quantitative objectives for implementation of the safety goals are stated in terms of risk to individuals and to society. For an average individual in the vicinity of a nuclear power plant, the risk that might result from a reactor accident should not exceed one-tenth of 1 percent (0.1 percent) of the sum of prompt fatality risks resulting from other accidents to which members of the population are generally exposed. The risk to the public of cancer due to nuclear power plant operation should not exceed one-tenth of 1 percent (0.1 percent) of the sum of cancer fatality risks resulting from all other causes (USNRC, 2001). A target  $10^{-4}$  mean annual risk of core damage due to all accident initiators can implement these quantitative safety goals.

The ASCE (2005) method assumes that seismic initiators should contribute no more than about 10 percent of the risk of core damage posed by all accident initiators. Thus, the Standard is intended to conservatively achieve a mean  $10^{-5}$  per year risk of core damage due to seismic initiators. The USNRC's SDC contained in NUREG-0800 conservatively assure a risk reduction factor of at least 10, as discussed in the next paragraph. Thus, a mean ground motion hazard of  $10^{-4}$  per year is appropriate for determining the site-specific DRS for the TVA Bellefonte Site (see discussion in Section 2.5.2.6.1).

The ASCE/SEI Standard 43-05 approach aims to conservatively assure a seismic safety target performance goal, PF, of mean  $10^{-5}$  per year for Seismic Design Criteria (SDC) SDC-5 SSCs. ANSI/ANS Standard 2.26-2004 Categorization of Nuclear Facility Structures, Systems, and Components for Seismic Design provides the criteria for selecting SDC and Limit State that establishes the Seismic Design Basis (SDB) for each SSC at a nuclear facility. The target mean annual performance goal for nuclear plants is achieved by coupling site-specific DRS with the deterministic SDC and procedures specified by NUREG-0800. The ASCE/SEI Standard 43-05 criteria for deriving a site-specific DRS are based on the conservative assumption that the SDC specified by NUREG-0800 achieve less than a 1 percent chance of failure for a given DRS. The conservatism of this assumption is demonstrated by analyses described in McGuire, et al. (2002), which show plant level risk reduction factors ranging from about 20 to about 40 are attained by the USNRC's SDC. The method is based on the use of mean hazard results consistent with the recommendation contained in McGuire, et al. (2002) and with the USNRC's general policy on the use of seismic hazard in risk-informed regulation.

### 2.5.2.1 Seismicity

The first step in the three-step process for evaluating seismic hazards at the Bellefonte Site involved an assessment of changes in seismicity for the site. The seismic history of the southeastern U.S. for the period from 1985 to present, as summarized in the existing earthquake catalogues, was evaluated to assess potential changes in the location, maximum magnitude, and frequency of earthquakes that could affect the Bellefonte Site. In addition, new information on historical earthquakes was identified and evaluated to update the existing information on the seismic setting of the Bellefonte Site. The development of an updated

earthquake catalog for the project region is described in Section 2.5.2.1.1. Information on significant recent earthquakes and significant newly identified historical earthquakes is provided in Section 2.5.2.1.2. Figure 2.5.2-1 shows the combined independent earthquake catalog developed for this study. The earthquake catalog listing is provided in Appendix I.

### 2.5.2.1.1 Earthquake Catalog

The data used to assess earthquake occurrence rates for the majority of seismic sources are the historical and instrumental earthquake record. An updated earthquake catalog of independent<sup>4</sup> earthquakes was developed for use in this study. This updated catalog was based on the independent earthquake catalog prepared for the 2004 TVA Dam Safety Seismic Hazard Assessment project (Geomatrix, 2004) that hereafter, is referred to as the TVA Dam Safety catalog. The TVA Dam Safety catalog is a composite of the catalogs listed in Table 2.5.2-1, and covers the region from 31°N to 41°N and 75°W to 93°W. Additional catalogs that have become available after development of the TVA Dam Safety catalog have been evaluated and new information and new earthquakes have been incorporated to update the TVA Dam Safety catalog for the present study. The development of the TVA Dam Safety catalog is described in Section 2.5.2.1.1.1, and specific modifications to update that catalog for use in the Bellefonte GG&S study are described in Section 2.5.2.1.1.2.

#### 2.5.2.1.1.1 Development of the TVA Dam Safety Catalog

The TVA Dam Safety catalog was developed through comparisons of available earthquake catalogs covering the southeastern and central U.S. The initial catalog used in development of the seismic hazard mapping project was the updated independent earthquake catalog prepared by the USGS as part of their National Ground Motion Hazard Mapping project (hereafter referred to as the 2002 USGS catalog). The primary source for the 2002 USGS catalog is the NCEER-91 catalog (Seeber and Armbruster, 1991) covering the period from 1627 to 1985. The NCEER-91 catalog was in turn based on the EPRI-SOG (1988) catalog. In developing the 2002 USGS Catalog, the NCEER-91 catalog was supplemented with the catalogs from the Advanced National Seismograph System (ANSS), Southeast U.S. Seismic Network (SEUSSN), Center for Earthquake Research and Information (CERI), Stover, Reagor, and Algermissen (Stover et al., 1984), Preliminary Determination of Epicenters (PDE), and Decade of North American Geology (DNAG), (Mueller et al., 1997; Dr. Charles Mueller, USGS, Denver, personal communication, 2003). The primary magnitude measure reported in these catalogs is body-wave magnitude  $m_b$ , which is considered to be equivalent to Nuttli magnitude,  $m_N$ , and to Lg-wave magnitude,  $m_{bLg}$ . The  $m_b$  values given in the NCEER-91 and the 2002 USGS catalogs were either converted from MMI (maximum Modified Mercalli Intensity) or MMI/FA (Felt Area), or based on reliable instrumental magnitudes, in the order of increasing preference. Dependent earthquakes (i.e., foreshocks and aftershocks) were identified and removed from the catalog following the criteria of Gardner and Knopoff (1974) (Dr. C. Mueller, personal communication, 2004). Additional information on the development of the 2002 USGS catalog (and its earlier 1996 version), including catalog, location, and magnitude authorities, conversion equations, treatment of significant earthquakes, is found in Mueller et al. (1997).

---

<sup>4</sup> The PSHA formulation used in this study assumes that the temporal occurrence of earthquakes conforms to a Poisson process, implying independence between the times of occurrence of earthquakes. Thus, it is necessary to remove dependent events (such as foreshocks and aftershocks) from the earthquake catalog before estimating earthquake frequency rates.

The TVA Dam Safety catalog was developed from the 2002 USGS catalog as follows. All significant earthquake catalogs that covered parts or all of the area from 31°N to 41°N and 75°W to 93°W were obtained for comparison to the USGS 2002 catalog. These include catalogs from the EPRI (EPRI-SOG, 1988), Multi-disciplinary Center for Earthquake Engineering Research (NCEER-91; Seeber and Armbruster, 1991), ANSS, SEUSSN, CERI, and National Earthquake Information Center (NEIC). The catalogs that were evaluated, area and time period of coverage, minimum magnitude considered, and source, are listed in Table 2.5.2-1. Each of these catalogs either excludes known non-tectonic events, such as mine blasts, collapses, reservoir-induced events, etc., or identifies them in the catalog listing. Additional listings of non-tectonic events (ANSS Web site), known reservoir-induced events (Dr. Martin Chapman, personal communication, December 4, 2003), and mine-related events (Street et al., 2002) also were obtained for use in developing the TVA Dam Safety catalog.

Each of the additional catalogs was compared to the 2002 USGS catalog, and earthquakes that were not in the 2002 USGS independent catalog were identified. These events were evaluated for dependency with earthquakes in the 2002 USGS catalog. Essentially, all events listed in other catalogs, including NCEER-91, ANSS, SEUSSN, CERI, PDE, and DNAG, that were not in the 2002 USGS catalog, were judged to be dependent events (aftershocks or foreshocks), duplicate events, non-tectonic events, or were excluded because the magnitude was less than  $m_b$  3.0 (the minimum magnitude of interest for developing earthquake occurrence parameters). Mr. Jeff Munsey of TVA and Dr. Martin Chapman (Virginia Tech) then reviewed the preliminary catalog, providing review comments regarding additional earthquakes, magnitudes for specific earthquakes, and criteria for identification of dependent events (i.e., time and distance windows). The parameters for many earthquakes were discussed in various telephone and email communications between the project team to assess appropriate modifications, additions, and deletions to the preliminary catalog. Specific changes to the 2002 USGS catalog that were made are as follows:

- Added earthquakes of  $m_b$  ~3.0 and larger occurring during 2002 to 2003 from CERI, ANSS, PDE, and PDE-W (preliminary data for most recent earthquakes) catalogs;
- Removed reservoir-induced events identified from a listing of reservoir events provided by Dr. M. Chapman (personal communication, December 4, 2003);
- Added 62 earthquakes selected from the list of newly identified historical earthquakes prepared as an addendum to the NCEER-91 catalog (“NCEER-91 revisions” by J. Armbruster);
- Removed mine blasts identified from a listing of known mine blasts published by Street et al. (2002);
- Removed additional mine blasts, bumps, and reservoir-induced events identified in the preliminary catalog during review by the project team;
- Added additional earthquakes from Reinbold and Johnston (1987) Southern Appalachian catalog that were not included in the 2002 USGS catalog; and
- Added published estimated of moment magnitude  $M$  for historical and instrumental earthquakes from Bakun and Hopper (2004a); Bakun et al. (2003); Woods (2003); Saikia et al. (1998); Johnston (1996a); Johnston et al. (EPRI) (1994); Street (1984); Hermann (1979); and Street et al. (1975).

The 2002 USGS catalog provided estimates of magnitude in terms of  $m_b$ . For earthquakes added to the 2002 USGS catalog, the available magnitude estimates were compiled and reviewed, and  $m_b$  was assigned consistent with the approach for selection of the magnitudes listed in the USGS and NCEER-91 catalogs (Mueller et al., 1997). As noted previously, available estimates of moment magnitude  $M$  also were compiled in the TVA Dam Safety catalog.

The TVA Dam Safety catalog was then reviewed for consistency in identification of dependencies among earthquakes as follows:

- Updated the identification of mainshocks versus dependent earthquakes for several historical earthquakes where the 2002 USGS Catalog apparently identified a smaller earthquake as the mainshock<sup>5</sup>; and
- Evaluated entire catalog for dependent events, and identified additional dependent earthquakes based on slight modification of Gardner and Knopoff (1974) distance windows to allow for larger uncertainties in location of historical events.

For the last item listed previously, comparison of the NCEER-91 and 2002 USGS catalogs showed that the 2002 USGS catalog included 138 earthquakes that are characterized as dependent events in NCEER-91. Review of the location and timing of these earthquakes indicates that most of these earthquakes did not satisfy the Gardner and Knopoff (1974) criteria for dependency based on distance. However, in review of the timing and location of events possibly associated with the 1811-1812 New Madrid, and 1886 Charleston mainshocks, it appears that the distance windows identified in Gardner and Knopoff, which are based on instrumentally located earthquake sequences, may be slightly small in consideration of the large uncertainty in the location of pre-instrumental earthquakes. Applying slightly expanded aftershock distance windows indicates that a majority of the earthquakes (approximately 80 of the 138) identified as dependent events in NCEER-91 can be characterized as dependent earthquakes. These 80 earthquakes were excluded from the final TVA Dam Safety catalog.

#### 2.5.2.1.1.2 Modifications to the TVA Dam Safety Catalog for the Bellefonte GG&S Catalog

The final Bellefonte GG&S catalog covers a region (31° to 41°N and 75° to 93°W) extending more than 200 miles in radius from the Bellefonte Site. This catalog was updated from the TVA Dam Safety catalog to include information on recent earthquakes, and to incorporate new information on location and magnitude of historical earthquakes and newly identified historical earthquakes. The specific sources of information that were used to update the TVA Dam Safety catalog are listed in Table 2.5.2-2. The new information includes data for 174 new historical earthquakes that are not included in the TVA Dam Safety catalog. A listing of the earthquakes in the Bellefonte GG&S catalog is provided in Appendix I. Newly discovered historic earthquakes added to the earthquake catalog come primarily from two

---

<sup>5</sup> In some cases, it appears that the criteria used by the USGS to identify mainshocks versus dependent events may have identified the first event in a sequence as the mainshock, even when a later event had a slightly larger magnitude ( $m_b$  or  $M$ ). In addition, updates to the magnitudes ( $M$ ) in the catalog resulted in several changes in the characterization of mainshock versus dependent events for some earthquake sequences. In both situations, the larger earthquake (identified as the mainshock) was added to the catalog, and the smaller earthquake (characterized as a dependent event) was deleted from the catalog (based on comparison of  $M$ ).

sources: (1) a report on “new” historical earthquakes in the central U.S. by Metzger et al. (2000), and (2) an unpublished listing of “new” historical earthquakes from locations throughout the study area compiled by the TVA in 2005 (TVA, 2005). The Metzger et al. (2000) report was supplemented by electronic files made available by Kent Moran (CERI, personal communication, 2005). Both of these listings are based on analysis of earthquake intensities as described in primary sources, primarily contemporary newspaper accounts.

Metzger et al. (2000) provided information for 103 newly identified earthquakes and 22 previously reported earthquakes occurring in the central U.S. during the time period from 1826 to 1899. Their information was obtained primarily through extensive review of microfilm records of historical newspapers. Metzger et al. (2000) assessed moment magnitudes from MMI assessments following the approach of Johnston (1996b). The authors usually assigned epicenters near the center of highest intensity, although for some earthquakes, the epicenters were placed equidistant from lower intensity reports, or slightly closer to a town that reported aftershocks than another community with similar mainshock intensities but no reports of aftershocks.

Following the review of the historical earthquake catalog used for the TVA Dam Safety study and the preliminary updates to the catalog developed for the Bellefonte study, the TVA (TVA, 2005) conducted research and developed information for additional new earthquakes occurring in the central and southeastern U.S. The TVA (2005) study gathered new information on historic earthquakes primarily by performing keyword searches of online versions of historical newspapers. Keyword searches of online newspapers were used from the following sources:

- Ancestry.com (historic newspapers and Family and Local History sections (<http://www.ancestry.com/search/>);
- Brooklyn Daily Eagle (<http://www.brooklynpubliclibrary.org/eagle/index.htm>);
- Historic Missouri Newspaper Project (<http://newspapers.umsystem.edu/Archive/skins/missouri/navigator.asp?BP=OK&GZ=T&AW=1081184405843>); and
- Colorado historical newspapers project (<http://www.cdpheritage.org/newspapers/about.html>).

Other online listings of historical earthquakes consulted include:

- Pennsylvania earthquakes list (<http://muweb.millersville.edu/~esci/geo/quake.html>);
- OhioSeis list (<http://www.dnr.state.oh.us/OhioSeis/html/eqcatlog.htm>); and
- Maryland Geological Survey (<http://www.mgs.md.gov/esic/brochures/earthquake.html>).

The TVA review of historical online records resulted in identification of 152 “new” historic earthquakes during the time period from 1758 to 1923, as well as additional intensity reports and other information for several previously reported earthquakes.

The additional information for previously reported earthquakes from Bakun and Hopper (2004b) and TVA (2005) was evaluated and was used to update the corresponding

earthquake data. The data from Bakun and Hopper (2004b) includes estimates of moment magnitude and new assessments of the epicentral location of historical earthquakes based on a reassessment of the felt intensity data. The approach for estimating **M** from the intensity data appears robust and the estimates of **M** were judged to be appropriate for use in the project catalog.

Bakun and Hopper (2004b) use three approaches to select a new preferred epicentral location. The preferred epicentral locations that are based on the intensity data alone, either the isoseismal area or maximum intensity, also were judged to be more reliable than previous locations (which typically were based on fewer intensity reports), and were accepted for use in the Bellefonte GG&S catalog. In the third approach, Bakun and Hopper (2004b) moved the preferred epicentral location to a known fault that is proximal to the intensity locations. This approach implies that a particular fault has ruptured, and in several cases, resulted in a significant relocation of the epicenter compared to the intensity data location (greater than 50 kilometers). Because this method for assigning the preferred epicentral location is based on a tectonic interpretation rather than based on the earthquake shaking data, it is not consistent with the methodology used to assign epicentral locations to other earthquakes in the catalog. Therefore, the initial location identified in Bakun and Hopper (2004b), which was based on intensity reports, was judged to be more appropriate and was adopted for use in updating the existing earthquake location. For several of these earthquakes, the preferred magnitude was adjusted to be consistent with the intensity-based epicentral location rather than the fault-based location.

With few exceptions, locations for the new earthquakes identified in TVA (2005) were assigned to the town or city with the highest MMI or a point between two localities interpreted to have the same intensity. With the exception of a few earthquakes with multiple intensity reports, there is insufficient data at present to define felt areas for these newly identified earthquakes. Therefore, the primary information regarding the magnitude for the TVA (2005) new earthquakes is the assumed maximum intensity.

For those earthquakes where a felt area could be identified, the intensity-area relationships of Johnston (1996b) were used to assign moment magnitude. For other earthquakes, maximum intensity data were used to develop estimates of  $m_b$  as follows. For new earthquakes from the TVA (2005) study,  $m_b$  was determined from the average of the following two relationships between maximum MMI and  $m_b$  magnitude and that used by Metzger et al. (2000):

$$m_b = 0.61 \times \text{MMI}_{\max} + 0.78 \text{ (Veneziano and Van Dyck, 1985)} \quad (2.5.2-1)$$

$$m_b = 2.37 + 0.0466 \times (\text{MMI}_{\max})^2 \text{ (Sibol et al., 1987)} \quad (2.5.2-2)$$

Metzger et al.'s (2000) maximum intensity-based magnitudes were expressed as moment magnitudes. Because these moment magnitudes (developed from the Johnston, 1996b relationship between MMI and **M**) appear to be systematically higher than the moment magnitudes resulting from conversion of  $m_b$  (developed from the Veneziano and Van Dyck (1985), and Sibol et al. (1987) equations) to **M** (based on Woods [2003]), the magnitudes for the Metzger et al. (2000) maximum MMI-based earthquakes were re-calculated as follows. The Metzger et al. (2000) MMI-based moment magnitudes were converted to  $m_b$  by adding

0.36 units based on Woods (2003) relationship between moment magnitude and  $m_b$ . In addition, new estimates of  $m_b$  were developed for each of these earthquakes using the two MMI -  $m_b$  equations listed previously. The average of the three  $m_b$  estimates is assigned as the best estimate of  $m_b$  for these earthquakes.

The resulting combined list of new earthquakes was reviewed for inclusion in the GG&S project catalog as follows. Earthquakes that had an  $m_b$  of less than 3.0 or that were located outside of the area of the original TVA Dam Safety (31° to 41°N and 75° to 93°W) were excluded. The remaining new historical earthquakes were then reviewed to assess possible dependencies with other earthquakes in the existing catalog, and those that were confidently identified as dependent events were excluded. After removal of the dependent events, a total of 174 new historical earthquakes are included in the Bellefonte GG&S catalog (all occurring between 1758 and 1923). In addition, 10 earthquakes occurring in 2004 and early 2005 were included in the Bellefonte GG&S catalog.

### 2.5.2.1.2 Recent Earthquakes and Historical Seismicity

The locations of newly identified historical earthquakes (pre-March 1985), and earthquakes occurring since March 1985 (post-EPRI-SOG, 1988) are compared to the spatial distribution of earthquakes included in EPRI-SOG evaluation in Figures 2.5.2-2 and 2.5.2-3, respectively. These figures show that there are no major differences in the spatial pattern of earthquakes for these three data sets. As noted in EPRI-SOG (1988), the Charleston, South Carolina, New Madrid, and ETSZ are identified as the most seismically active zones in the central and southeastern U.S.

#### 2.5.2.1.2.1 Recent Earthquakes

Three earthquakes of note (magnitude greater than  $m_{bLG}$  4.0) have occurred within 200 miles of the Bellefonte Site in the period post-1985. These are the March 27, 1987, Vonore, Tennessee, earthquake, the April 29, 2003, Fort Payne earthquake, and the 2004 earthquake near Braggville in west-central Alabama (Figure 2.5.2-3). Information on these earthquakes is summarized as follows. Additional, previously identified significant historical earthquakes are described in the BLNP FSAR.

##### **March 27, 1987            $m_{bLG}$ 4.2 ( $m_b$ 4.3) Vonore, Tennessee**

The Vonore, Tennessee, earthquake occurred in eastern Tennessee approximately 50 kilometers south of Knoxville. The USGS (Earthquake Hazards Program, U.S. Geological Survey Earthquake Search – Rectangular Area, [http://www.neic.cr.usgs.gov/neis/epic/epic\\_rect.html](http://www.neic.cr.usgs.gov/neis/epic/epic_rect.html)) lists the magnitude as  $m_{bLG}$  4.2 and  $m_b$  4.3. Minor damage, including cracked cinderblock walls, foundations, and chimneys, was reported over an 800-square-kilometer area, and the maximum MMI was VI (Nava et al., 1989). These authors also noted that the earthquake may have caused ground fissures along a ridge near Wellsville, but that the nature and time of origin of these features could not be conclusively determined. Focal mechanism solutions and the locations of aftershocks indicate that the earthquake occurred by right-lateral strike-slip on a north-south trending subvertical fault (Nava et al., 1989).

**April 29, 2003       $m_{bLg}$  4.9 (M 4.6) Fort Payne, Alabama**

The Fort Payne earthquake occurred in Dekalb County, in north-easternmost Alabama, near the Georgia border. The earthquake has a measured Lg wave magnitude ( $m_{bLg}$ ) of 4.9 and a moment magnitude (M) of 4.6. The Fort Payne earthquake occurred at the southern end of the ETSZ, and is one of the strongest earthquakes to have occurred in Alabama and in the ETSZ in historic time. The earthquake, and the October 24, 1997,  $m_{bLg}$  4.9 Escambia earthquake<sup>6</sup>, are the two largest earthquakes to have occurred in the southeastern U.S. since 1985.

The Fort Payne earthquake caused minor damage, including damage to chimneys, cracked walls and foundations, broken windows, and collapse of a 29-foot-wide sinkhole. These examples of damage, and other reports of shaking correspond to a maximum MMI of VI (U.S. Geological Survey, url: [http://pasadena.wr.usgs.gov/shake/cus/STORE/Xteak/ciim\\_display.html](http://pasadena.wr.usgs.gov/shake/cus/STORE/Xteak/ciim_display.html), Geological Survey of Alabama; url: <http://www.gsa.state.al.us/gsa/geologichazards/earthquakes/ftpayne.html>, and J. Munsey, TVA, personal communication, 2003). Based on reconnaissance in the epicentral area (J. Munsey, TVA, personal communication, 2003), no landslides were reported, and damage to chimneys was observed only for chimneys with masonry in poor/weakened condition. Other masonry, including chimneys in good condition, and several old masonry buildings did not appear to be damaged.

Studies of the earthquake focal mechanism indicate that the focal planes are subvertical and strike approximately north-south and east-west (Earthquake Center, St. Louis University, url: [http://www.eas.slu.edu/Earthquake\\_Center/NEW/20030429085937/index.html](http://www.eas.slu.edu/Earthquake_Center/NEW/20030429085937/index.html)). The earthquake occurred at a depth of about 9.5 to 13 kilometers based on studies of the compression (P) waves (Jemberie and Langston, 2003).

Strong motion instruments located on the crests of Buford and Carters Dams in western Georgia, at distances of about 85 and 145 kilometers, respectively, from the epicenter were triggered, possibly due to amplification in the earth embankment dams. The free-field (ground surface) and abutment instruments at both dams were not triggered (Yule and Grau, 2003). There are no strong motion instruments at the TVA Guntersville Dam near the Bellefonte Site. Strong ground shaking at the Sequoyah Nuclear Plant in eastern Tennessee apparently was slightly below the triggering threshold for the instrument (J. Munsey, TVA, personal communication, 2005).

**November 7, 2004       $m_b$  4.4 (M 4.3) Braggville, Greene County, Alabama**

An  $m_b$  4.4 earthquake occurred near Braggville, in Greene County, central-western Alabama on November 7, 2004. The maximum MMI was V (U.S. Geological Survey, [http://pasadena.wr.usgs.gov/shake/cus/STORE/Xqnax\\_04/ciim\\_display.html](http://pasadena.wr.usgs.gov/shake/cus/STORE/Xqnax_04/ciim_display.html)). No other information on this earthquake was identified.

---

<sup>6</sup> The Escambia earthquake occurred in southernmost Alabama at a distance greater than 200 miles from the Bellefonte Site. Therefore, this earthquake is not considered in this analysis.



### 2.5.2.1.2.2 Historical Earthquakes

Several newly identified moderate magnitude ( $m_b > 4$ ) historical earthquakes that occurred within 200 miles of the Bellefonte Site are included in the updated catalog (Figure 2.5.2-2). The available information about these earthquakes is summarized as follows.

#### **January 3, 1861      $m_b$ 4.3 (M 3.9)      North Carolina/Georgia Border Region**

An earthquake of MMI V and  $m_b$  4.3 (based on felt area) occurring on January 3, 1861, along the North Carolina/Georgia border region is identified as a new earthquake listing in NCEER-91. This earthquake may correspond to an EPRI-SOG (1988) listing for 1861 (no date) of  $m_b$  2.5 and located about 130 kilometers north of the NCEER-91 location.

#### **November 30, 1862      $m_b$ 4.8 (M 4.7)      Western Tennessee**

An earthquake that was felt throughout the northern Mississippi Valley occurred on the morning of November 30, 1862. Metzger et al. (2000) compiled newspaper reports and noted that MMI III effects were reported from Louisville, Kentucky, and St. Louis, Missouri; MMI IV effects were reported for Evansville, Illinois, and Cairo, Illinois; and MMI V effects were reported for Memphis, Tennessee. They locate the epicenter in western Tennessee between Memphis and Cairo, and assign a moment magnitude (M) of 4.7 to this earthquake.

#### **March/April, 1874      $m_b$ 4.4 (M 4.0)      Williamson, Tennessee**

An earthquake that was felt in Williamson County, Tennessee, was reported in the Franklin, Tennessee, Brooklyn Eagle newspaper on April 9, 1874 (TVA, 2005). The earthquake produced a large landslide, but the exact date of the earthquake was not reported. The maximum intensity was estimated as MMI VI to VII, however, because no additional reports of shaking were identified, the magnitude is assigned as  $m_b$  4.4 (TVA, 2005).

#### **September 18, 1881      $m_b$ 4.5 (M 4.2)      Newnan, Georgia**

An earthquake that was felt in Newnan, Georgia, late in the evening on September 17, 1881, (local time) was reported in the Atlanta Journal Constitution on September 20, 1881 (TVA, 2005). The shaking lasted for about 10 seconds, rattling houses and causing people to run outside. The maximum intensity was estimated as MMI VI, corresponding to  $m_b$  4.5 (TVA, 2005).

#### **October 5, 1899      $m_b$ 4.4 (M 4.0)      Smoky Mountains (Tennessee/North Carolina border)**

A "severe shock" was felt in the Smoky Mountains along the Tennessee/North Carolina border early in the morning on October 5, 1899. As reported in the Fort Wayne News on October 6, 1899, the earthquake lasted for more than 10 seconds and caused an opening for several hundred feet along Abrams Creek (TVA, 2005). Although the local effects indicate a strong earthquake, no reports of this earthquake from surrounding regions (such as Knoxville, Tennessee) were identified. The maximum intensity is uncertain, and is estimated as MMI V to VIII. Because no reports of shaking were identified outside of the local area, the magnitude is assigned as  $m_b$  4.4 (TVA, 2005).

**June 9, 1910**                      **m<sub>b</sub> 4.2 (M 3.9)**                      **Dalton, Georgia**

An earthquake that was felt in Dalton, Georgia, early in the evening on June 9, 1910 (local time) was reported in the Atlanta Journal Constitution on June 10, 1910 (TVA, 2005). The shaking lasted for a few seconds, shaking houses and causing people to run outside. The maximum intensity was estimated as MMI V to VI, corresponding to m<sub>b</sub> 4.2 (TVA, 2005).

### **2.5.2.2 Geologic Structures and Seismic Source Models**

As outlined previously, Appendix E, Section E.3, of Regulatory Guide 1.165, Step 1 specifies that recent information should be reviewed to evaluate if this information would indicate significant differences from the previous seismic hazard. Section 2.5.1 presents a summary of available geological, seismological, and geophysical data for the site region (200-mile radius), site vicinity (25-mile radius), and site area (5-mile radius) that provide the basis for evaluating seismic sources that contribute to the seismic hazard to the Bellefonte Site. This section presents a description of the seismic source characterizations from the EPRI-SOG (1988) evaluation followed by a summary of general approaches and interpretations of seismic sources used in more recent seismic hazard studies. Sections 2.5.2.4.1 and 2.5.2.4.3 present an evaluation of the new information relative to the EPRI-SOG (1988) seismic source evaluations.

#### **2.5.2.2.1 EPRI-SOG Source Evaluations**

The EPRI-SOG evaluation completed in the late 1980s (EPRI-SOG, 1988) involved assessments of the uncertainty in seismic source characterization in the CEUS by formal elicitation of six independent Earth Science Teams. The six teams were the Bechtel Group, Dames & Moore, Law Engineering, Rondout Associates, Weston Geophysical Corporation, and Woodward-Clyde Consultants. Each team evaluated geologic, geophysical, and seismological data to evaluate seismic sources in the CEUS and provided detailed documentation of their assessments in separate volumes of the EPRI-SOG (1988) evaluation. In the EPRI-SOG (1988) evaluation, tectonic features that might be seismogenic were identified, and their probability of activity was assessed. The study first identified and defined criteria for assessing the activity of a feature. These criteria include attributes such as spatial association with large- or small-magnitude earthquakes, evidence of geologically recent slip, orientation relative to the regional stress regime, and others. The study also assigned a relative weight or relative value of each criterion in assessing the probability of activity. The seismic sources interpreted from the tectonic features (i.e., “feature-specific source zones”) were assigned a probability of activity equivalent to that of the features.

The seismic source evaluations were one element of the seismic hazard model inputs for a PSHA for nuclear plant sites in the CEUS (EPRI, 1989). For the computation of hazard in the 1989 study, some of the seismic source parameters were modified or simplified from the original parameters defined by the EPRI-SOG (1988) evaluation. The parameters used in final PSHA calculations are summarized in EPRI (1989), which is the primary source for the EPRI-SOG seismic hazard model used in this GG&S study.

The seismic sources defined by each of the teams relative to the updated seismicity are shown in Figures 2.5.2-4 through 2.5.2-9. A screening criterion was implemented in the EPRI (1989) seismic hazard calculations in that all sources with combined hazard was less than

1 percent of the total hazard were excluded from the analysis. The sources that contributed 99 percent of the hazard at the Bellefonte Site are shown and labeled in these figures. The smaller inset figures show the complete set of seismic sources identified in the Bellefonte Site region by each of the EPRI-SOG teams.

Tables 2.5.2-3a through 2.5.2.3f summarize the significant sources that were included in the EPRI (1989) seismic hazard analysis for the Bellefonte Site and list additional sources within the 200-mile-radius region that do not significantly contribute to the hazard at the site. The EPRI (1989) evaluation indicated that the most significant contributors to hazard at the Bellefonte Site are the ETSZ, subdivisions of the crust around the ETSZ, and the New Madrid, Missouri, region (location of the 1811-1812 earthquakes). In addition, there is a minimal contribution from the Charleston, South Carolina, region sources (location of the 1886 earthquake).

### 2.5.2.2.2 LLNL-TIP Source Evaluations

A decade after the completion of the EPRI-SOG (1988) evaluation, LLNL (Savy et al., 2002) conducted a TIP of the SSHAC (1997) guidance for a Level IV analysis. SSHAC (1997) provides general guidance for conducting PSHA for important facilities and describes four levels of effort for quantifying epistemic uncertainty ranging from assessments by a single individual (Level I) to formalized elicitation of a panel of experts (Level IV). The EPRI-SOG (1988) evaluation can be considered the prototype of a SSHAC Level IV study. The LLNL-TIP project focused on issues related to the development of seismic zonation and earthquake recurrence models. Participants in the project included a Technical/Facilitator/Integrator (TFI) team, a panel of five expert evaluators, and expert proponents and presenters. Preliminary implementations for two sites in the southeastern U.S., the Vogtle site in Georgia, which is affected by the issue of the Charleston earthquake, and the Watts Bar site in Tennessee, which is close to the ETSZ, were completed as part of the TIP study. Although focused primarily on process, the LLNL TIP study provided assessments for some of the seismic sources significant to the Bellefonte Site region.

Seismic source models were developed for each of the five experts and through discussions at workshops, one-on-one interviews, and white papers, a set of common sources was identified as the basic building blocks for all the sources and alternative sources. The general boundaries of these common sources are shown in Figure 2.5.2-10. This minimum set of zones was then used to create the composite model of seismic sources that represented the range of feasible sources. These sources included five basic alternative zones for both the East Tennessee and Charleston sources, three for the South Carolina-Georgia seismic zone, and alternative zones for background earthquakes for both the East Tennessee and Charleston regions. The probability of activity was defined as the probability of “existence” of a particular source zone.

A description of the minimum set zones is provided in Table 2.5.2-4. A complete description of the logic tree representation of the experts’ interpretations for the Charleston and ETSZ and maximum magnitude distributions for alternative source zones is presented in Savy et al. (2002).

### 2.5.2.2.3 2002 USGS Earthquake Hazard Mapping Source Characterization Model

As part of the 2002 USGS National Seismic Hazard Mapping program, updated seismic hazard maps for the conterminous U.S. were produced in 2002 (Frankel et al., 2002). Input for revising the source characterization used in the 1996 hazard maps (Frankel et al., 1996) was provided by researchers through a series of regional workshops. Key issues that were addressed in the updated source characterization included new information regarding the location, size, and recurrence of repeating large magnitude earthquakes in the Charleston and New Madrid source regions. Although the USGS program does not use formal expert elicitation and full uncertainty quantification, the resulting seismic hazard model provides information on the current understanding of the seismic potential of the study region and the catalog of recorded earthquakes.

The USGS source model and earthquake catalog (in body wave magnitude,  $m_b$ ) developed by the USGS (Mueller et al., 1997) are shown in Figure 2.5.2-11. The general approach used by the USGS for modeling distributed seismicity in the CEUS is to use a Gaussian kernel smoother to define the spatial distribution of future earthquakes based on the recorded locations of past earthquakes throughout the CEUS. No boundaries are placed on the locations of ruptures associated with the spatially smoother earthquake locations.

Two broad regions are defined with different maximum magnitudes in the USGS model: an extended margin zone ( $M_{\max} = M 7.5$ ) and a craton zone ( $M_{\max} = M 7.0$ ). In addition, the USGS source model includes an East Tennessee regional source zone, alternative fault line sources for repeating large magnitude earthquakes in the NMSZ, and alternative zones for a Charleston seismic source zone. The maximum magnitude probability distribution assigned to the New Madrid fault sources is  $M 7.3$  (0.2),  $M 7.5$  (0.2),  $M 7.7$  (0.5),  $M 8.0$  (0.15). For the Charleston source, the maximum magnitude probability distribution used was:  $M 6.8$  (0.2),  $M 7.1$  (0.2),  $M 7.3$  (0.45),  $M 7.5$  (0.15). The USGS model uses a mean recurrence time of 500 years and 550 years for repeating large magnitude earthquakes in the New Madrid and Charleston regions, respectively, and assumes a time-independent model.

### 2.5.2.2.4 2004 TVA Dam Safety Seismic Hazard Analysis Seismic Source Model

In 2004, Geomatrix Consultants completed regional and site-specific dam safety seismic hazard assessments for all of the TVA's major dams (Geomatrix, 2004). As part of this study, Geomatrix developed a probabilistic seismic hazard model for the Tennessee Valley using a SSHAC Level II process. The project team was assisted by participatory review by an external peer review panel.

The study emphasized explicit incorporation of epistemic uncertainty through the use of logic trees in the PSHA. The source characterization effort was based on a review of published literature and discussion with active researchers. The study built upon previous studies including the EPRI-SOG (1988) evaluation, the LLNL-TIP study (Savy et al., 2002), the USGS National Seismic Hazard Project (Frankel et al., 2002), an EPRI-sponsored study to assess maximum magnitudes of earthquakes in stable continental regions (Johnston et al., 1994), and the EPRI (2004) CEUS ground motion project.

The seismic source model developed for the TVA Dam Safety study includes two types of sources, distributed seismicity sources and “fault-specific” sources of repeating large magnitude earthquakes. Two approaches were used to model the distributed seismicity sources: a zoneless approach similar to that used by the USGS to develop the 2002 hazard maps, and a seismotectonic zonation approach. Spatial smoothing of seismicity was employed in both approaches. Figures 2.5.2-12a through 2.5.2-12d show the alternative seismotectonic source zones defined by Geomatrix (2004) in the vicinity of the Bellefonte Site.

“Fault-specific” sources were used to model repeating large earthquakes that have been identified in two specific regions, near Charleston, South Carolina, and the New Madrid region at the junction of Missouri, Kentucky, and Tennessee.

### 2.5.2.3 Correlation of Earthquake Activity with Seismic Sources

Regulatory Guide 1.165 requires that the earthquake activity be correlated to seismic sources. The principal database for assessing earthquake recurrence is the historical and instrumental earthquake record. An updated catalog of independent historical and instrumental earthquakes covering the Bellefonte Site region was developed for use in the Bellefonte GG&S study (see discussion in Section 2.5.2.1.1).

The distribution of earthquake epicenters from the EPRI (pre-1985), the more recent (post-1985) instrumental events, and updated historical earthquakes for the site region are shown in Figures 2.5.2-1 through 2.5.2-3. Comparison of the updated earthquake catalog to the EPRI earthquake catalog yields the following conclusions:

- The updated catalog does not show any earthquakes within the site region that can be associated with a known geologic structure. As described in Section 2.5.1, the majority of seismicity in the Bellefonte Site region appears to be occurring at depth within the basement beneath the Appalachian décollement. The largest earthquake within the site vicinity, the 2003 M 4.6 Fort Payne earthquake likely reactivated a structure within the basement rock, but cannot be clearly associated with any of the major identified basement structures (Section 2.5.1.1.4.2(d)2; Figure 2.5.3-4).
- The updated earthquake catalog shows similar spatial distribution of earthquakes to that shown by the EPRI-SOG catalog, suggesting that no significant revisions to the geometry of seismic sources defined in the EPRI-SOG characterization is required.
- The updated GG&S earthquake catalog does not show a pattern of seismicity different from that exhibited by earthquakes in the EPRI-SOG catalog that would suggest a new seismic source in addition to those included in the EPRI-SOG characterizations.
- The updated GG&S earthquake catalog adds several magnitude  $m_b$  3 to 5 earthquakes in the time period covered by the EPRI-SOG catalog (principally prior to 1910). The effect of these additional events on estimated seismicity rates is assessed in Section 2.5.2.4.1.2.

### 2.5.2.4 Probabilistic Seismic Hazard Analysis and Controlling Earthquakes

This section describes the PSHA conducted for the Bellefonte Site. Following the procedures outlined in Appendix E, Section E.3 of Regulatory Guide 1.165, Sections 2.5.2.4.1 and

2.5.2.4.2 discuss the significance of new information on seismic source characterization and ground motion characterization, respectively, that are potentially significant relative to the EPRI-SOG (1988) seismic hazard model. Section 2.5.2.4.3 presents the results of PSHA sensitivity analyses used to test the impact of the new information on the seismic hazard. Using these results, an updated PSHA analysis was performed, as described in Section 2.5.2.4.4. The results of that analysis are used to develop uniform hazard spectra (UHS) and the identification of the controlling earthquakes (Section 2.5.2.4.5).

#### **2.5.2.4.1 New Information Relative to Seismic Source Evaluations (RG 1.165, E.3 Step 1 Evaluation)**

Several factors may produce changes in the level of seismic hazard at the Bellefonte Site compared to what would be estimated based on the EPRI-SOG evaluation. Seismic source characterization data and information that could affect the predicted level of seismic hazard include:

- Identification of a possible new seismic source in the site vicinity
- Changes in the characterization of the rate of earthquake occurrence for one or more seismic sources
- Changes in the characterization of the maximum magnitude for seismic sources.

##### **2.5.2.4.1.1 Identification of Seismic Sources**

Based on the review of new geological, geophysical, and seismological information that is summarized in Section 2.5.1, review of seismic source characterization models developed for post-EPRI-SOG seismic hazard analyses (Section 2.5.2.2), and comparison of the updated earthquake catalog to the EPRI-SOG evaluation (Section 2.5.2.3), no additional specific seismic sources have been identified.

As described in Section 2.5.1.1.4.2, additional information and analysis of subsurface data (e.g., industry seismic reflection profiles, deep wells) and seismicity data provides an improved understanding of structures within the Bellefonte Site region (200-mile radius), particularly with regard to the foreland Appalachian fold-thrust belt and possible relationships to subdetachment basement faults and zones of concentrated seismicity (e.g., ETSZ). However, the overall pattern of seismicity occurring on structures within the basement below the detachment was recognized at the time of the EPRI-SOG evaluation and the EPRI-SOG expert teams specified a variety of source geometries to represent the uncertainty in defining the source zone configurations.

Figures 2.5.2-13a and 2.5.2-13b compare the range of source zone geometries defined in the vicinity of the site by the EPRI-SOG expert teams (Figure 2.5.2-13a) and in subsequent studies (Figure 2.5.2-13b). The recent April 2003 **M** 4.6 Fort Payne earthquake is located at the southern extent of the concentrated seismicity that defines the ETSZ and is typical in both depth and focal mechanism to other earthquakes in the zone. The 2003 Fort Payne earthquake occurred just outside of the boundary of the East Tennessee seismic source zones defined by three of the EPRI-SOG expert teams and lies within the East Tennessee source zones (ETSZ) defined by the other three teams. This is also the case for more recent interpretations. The LLNL TIP (Savy et al., 2002) ETSZ does not include the 2003 Fort Payne

earthquake, but the USGS East Tennessee regional source zone (Frankel et al., 2002) and alternative source zones included in the Geomatrix (2004) hazard analysis do include the 2003 event. Therefore, the EPRI-SOG source zone interpretations are judged to adequately represent more recent interpretations of the ETSZ.

The EPRI-SOG expert teams confined the location of events similar to the 1811-1812 earthquakes to the region of concentrated seismicity in the NMSZ. More recent seismic hazard analyses (e.g., Frankel et al., 1996, 2002; Toro and Silva, 2001; Geomatrix, 2004) also restrict the occurrence of similar size events to this region, often placing the events on fault-specific sources within the NMSZ. Thus, no modification of the EPRI-SOG New Madrid source configurations is needed. The more recent data have suggested more frequent occurrences for these events, as discussed in Section 2.5.2.4.1.2.

Seismic sources defined by the EPRI-SOG expert teams to represent possible locations for repeats of the 1886 Charleston earthquake were typically not included in the EPRI (1989) hazard calculation for the Bellefonte Site because their contribution to the hazard was very small (< 1 percent). More recent data regarding the location and timing of repeating large magnitude earthquakes in the vicinity of Charleston, South Carolina, suggest alternative source configurations that fall within the range of EPRI-SOG source zone interpretations and (similar to New Madrid), more frequent occurrence of these events. These new interpretations are considered in this GG&S study (see Sections 2.5.2.4.3 and 2.5.2.4.4).

### 2.5.2.4.1.2 Earthquake Recurrence Rates

Section 2.5.2.1.1 describes the development of an updated earthquake catalog for the GG&S project region. This updated catalog includes modifications to the EPRI-SOG evaluation by subsequent researchers, the addition of earthquakes that have occurred after completion of the EPRI-SOG evaluation development (post March 1985), and identification of additional earthquakes in the time period covered by the EPRI-SOG evaluation for the project region (1758 to March 1985). The impact of the new catalog information was assessed by evaluating the effect of the new data on earthquake magnitude estimates and on earthquake recurrence estimates within the 200-mile region around the Bellefonte Site.

The earthquake recurrence rates computed in the EPRI-SOG (1988) evaluation included a correction to remove bias introduced by uncertainty in the magnitude estimates for individual earthquakes. The bias adjustment was implemented by defining an adjusted magnitude estimate for each earthquake,  $m_b^*$ , (Veneziano and Van Dyck, 1985) and then computing the earthquake recurrence parameters by maximum likelihood using earthquake counts in terms of  $m_b^*$ . The adjusted magnitude is defined by the relationship

$$m_b^* = m_b - \beta \sigma_{m_b | m_b \text{ instrumental}}^2 / 2 \quad (2.5.2-3)$$

when  $m_b$  is based on instrumentally recorded  $m_b$  magnitudes and by the relationship

$$m_b^* = m_b + \beta \sigma_{m_b | X}^2 / 2 \quad (2.5.2-4)$$

when  $m_b$  is based on other size measures  $X$ , such as maximum intensity,  $I_0$ , or felt area. The change in sign in the correction term from negative in Equation (2.5.2-3) to positive in

Equation (2.5.2-4) reflects the effects of the uncertainty in the conversion from size measure  $X$  to  $m_b$ . Parameter  $\beta$  is the Gutenberg-Richter  $b$ -value in natural log units. Values of the adjusted magnitude  $m_b^*$  were computed for the earthquakes in the updated catalog using the assessed uncertainties in the magnitude estimates and a value of  $\beta$  equal to  $0.95 \times \ln(10)$  based on the global  $b$ -value of 0.95 assigned to the CEUS by Frankel et al. (1996, 2002).

Values of  $\sigma_{m_b|X}$  range from 0.56 for  $m_b$  estimated from maximum intensity, to 0.2 to 0.3 for  $m_b$  estimated from various measures of felt area,  $\sigma_{m_b|m_b, instrumental}$  is typically set at 0.1.

Figure 2.5.2-14 shows a histogram of the difference between the values of  $m_b^*$  for the updated catalog and those given in the EPRI-SOG (1988) evaluation for earthquakes within 200 miles of the Bellefonte Site. The mean difference is essentially zero and the distribution of differences is relatively symmetric.

The EPRI-SOG (1988) procedure for computing earthquake recurrence rates was based on a methodology that incorporated data from both the period of complete catalog reporting and the period of incomplete catalog reporting. For the period of incomplete reporting, a probability of detection,  $P^D$ , was defined that represented the probability that the occurrence of an earthquake would ultimately be recorded in the earthquake catalog for the region (Veneziano and Van Dyck, 1985). The CEUS was subdivided into 13 "Completeness" regions that represented different histories of earthquake recording. Figure 2.5.2-15 shows the two completeness regions (3 and 4) that cover the area with 200 miles of the Bellefonte Site. The total time span of the EPRI-SOG catalog was then divided into six time intervals. Then using the observed seismicity and information on population density and the history of earthquake reporting across the CEUS, the probability of detection was estimated for each time interval within each completeness region for six magnitude intervals. Earthquake recurrence estimates were then made using the "equivalent period of completeness,"  $T^E$ , for each completeness region and all of the recorded earthquakes within the usable portion of the catalog. The equivalent period of completeness is computed by the expression

$$T_{ij}^E = \sum_k T_k \times P_{ijk}^D \quad (2.5.2-5)$$

where  $P_{ijk}^D$  is the probability of detection for completeness region  $i$ , magnitude interval  $j$ , and time period  $k$  of length  $T_k$ .

The updated earthquake catalog includes a number of newly identified earthquakes for the time period covered by the EPRI-SOG catalog, reassessment of the sizes of previously identified events, and earthquakes that have occurred after completion of the EPRI-SOG evaluation. The event counts for the EPRI-SOG and updated GG&S catalogs are given in Table 2.5.2-5.

Most of the newly identified earthquakes within 200 miles of the Bellefonte Site occurred in time periods identified in the EPRI-SOG evaluation as periods of incomplete catalog reporting ( $P^D < 1.0$ ). Comparisons of the earthquake counts for these time periods suggest that inclusion of the newly identified earthquakes in the estimation of catalog completeness would likely yield values of  $P^D$  near unity for the period post 1860 within completeness regions 3 and 4 for the two lowest magnitude intervals:  $3.3 \geq m_b^* > 3.9$  and  $3.9 \geq m_b^* > 4.5$ . This effect is illustrated by constructing so-called Stepp plots (Stepp, 1972) that show the



variation of earthquake rate with time for specific magnitude intervals for the region within 200 miles of the Bellefonte Site. The computation of rate starts at the end of the catalog and moves backward in time. At any point in time, the earthquake rate is defined as the number of earthquakes in the catalog from that point forward to the end of the catalog divided by the length of time from that point to the end of the catalog.

Figure 2.5.2-16 shows “Stepp” plots for the portions of EPRI-SOG completeness regions 3 and 4 that lie within 200 miles of the Bellefonte Site. The plot on the left shows the time variation of earthquake occurrence rates based on the EPRI-SOG catalog, and the plot on the right shows the occurrence rates based on the updated catalog. The observed rate of magnitude  $m_b$  3.3 to 3.9 earthquakes begins to steadily decrease for times greater than 15 years before the end of the EPRI-SOG catalog (times before 1970) and the rate for  $m_b$  3.9 to 4.5 earthquakes begins to decrease approximately for times greater than 75 years before the end of the EPRI-SOG catalog (times before 1910). In contrast, the occurrence rates remain relatively constant back to approximately 1860 for these two magnitude intervals using the updated catalog. The time variation of the rate for earthquakes larger than  $m_b$  4.5 shows somewhat erratic behavior due to the limited number of events.

The effect of the updated earthquake catalog on earthquake occurrence rates was assessed by computing earthquake recurrence parameters for the portions of EPRI-SOG completeness regions 3 and 4 that lie within 200 miles of the site. The truncated exponential recurrence model was fit to the seismicity data using maximum likelihood. Earthquake recurrence parameters were computed using the EPRI-SOG catalog and equivalent periods of completeness and using the updated catalog and the updated equivalent periods of completeness. It was assumed that the probability of detection for all magnitudes is unity for the time period of March 1985 to March 2005. The resulting earthquake recurrence rates are compared in Figure 2.5.2-17. For completeness region 3, essentially the same earthquake recurrence parameters are obtained using the EPRI-SOG and updated catalog and equivalent periods of completeness. For completeness region 4, use of the updated earthquake catalog and equivalent periods of completeness result in lower earthquake occurrence rates.

On the basis of the comparisons shown in Figures 2.5.2-14 and 2.5.2-17, it is concluded that the earthquake occurrence rate parameters developed in the EPRI-SOG evaluation adequately represent the seismicity rates within 200 miles of the Bellefonte Site based on more recent information.

The earthquake recurrence rate for the New Madrid and Charleston regions was also evaluated using results of paleoliquefaction studies. The results of studies of paleoliquefaction in the NMSZ (summarized in Section 2.5.1.1.4.3) have indicated that large earthquakes are more frequent than suggested by extrapolating the observed seismicity rates for small-to-moderate earthquakes up to large magnitudes ( $m_b \geq 7$ ). Figure 2.5.2-18 compares the seismicity rates estimated from the updated earthquake catalog to the rate for large magnitude events estimated from paleoliquefaction data. The error bars attached to the updated catalog rates represent 90 percent confidence intervals estimated by relative likelihood from the observed earthquake counts within the Bechtel team source zone 30 (Figure 2.5.2-4), a typical EPRI-SOG New Madrid source. The hatched box represents the 90 percent confidence interval for the paleoliquefaction rate based on three earthquake

sequences post 300 AD (e.g., Tuttle et al., 2005) and the solid circle indicates the rate used by Frankel et al. (2002) in the USGS National Hazard Mapping project (500-year repeat time). The recurrence relationships shown in the figure indicate the mean and 15<sup>th</sup> to 85<sup>th</sup> percentile recurrence rates for New Madrid sources computed from the EPRI-SOG seismic source models. As shown in the figure, the EPRI-SOG recurrence rates are very consistent with the seismicity rates estimated from the updated earthquake catalog but underestimate the rate for large earthquakes based on paleoliquefaction data by approximately an order of magnitude. Based on a similar comparison, Exelon (2003) concluded that the EPRI-SOG recurrence rates for large earthquakes in the NMSZ should be revised for PSHA calculations.

As discussed in Section 2.5.1.1.4.3, paleoliquefaction studies also have been conducted in the region of the 1886 Charleston, South Carolina, earthquake. The results of these studies have led to estimated repeat times for large earthquakes in the Charleston region of approximately 550 years (Frankel et al., 2002; Dominion, 2003; Geomatrix, 2004). This repeat time represents higher occurrence rates than obtained from the EPRI-SOG seismic hazard model (Dominion, 2003).

### 2.5.2.4.1.3 Assessment of Maximum Magnitude

The four types of seismic sources that contribute to the hazard at the Bellefonte Site are (1) representations of the ETSZ, (2) the local host/background zone, (3) representations of the NMSZ, and (4) to a very minor extent, sources representative of the 1886 Charleston earthquake. Figures 2.5.2-19 through 2.5.2-22 show the maximum magnitude distributions for these sources. The top plot in each figure shows the composite of the distribution developed by the EPRI-SOG (1988) expert teams in terms of the  $m_b$  magnitude scale, the magnitude scale used in the EPRI-SOG seismic hazard model. The bottom plot in each figure compares the composite EPRI-SOG maximum magnitude distribution to more recent assessments. These latter comparisons are made in terms of the moment magnitude scale,  $M$ . The composite  $m_b$  distributions were converted to moment magnitude using three equally weighted  $m_b - M$  relationships: by EPRI (1993),

$$m_b = -10.23 + 6.105M - 0.7632M^2 + 0.03436M^3 \quad (2.5.2-6)$$

by Atkinson and Boore (1995)

$$M = -0.39 + 0.98m_b \quad \text{for } m_b \leq 5.5 \quad (2.5.2-7)$$

$$M = 2.715 - 0.277m_b + 0.127m_b^2 \quad \text{for } m_b > 5.5$$

and by Johnston (1996a).

$$M = 1.14 + 0.24m_b + 0.0933m_b^2 \quad (2.5.2-8)$$

The transformed composite EPRI-SOG maximum magnitude distributions are compared to distributions developed by Savy et al. (2002), Frankel et al. (2002), and Geomatrix (2004).

Figure 2.5.2-19 summarizes the maximum magnitude assessments for sources representative of the ETSZ. The EPRI-SOG expert teams developed a broad uncertainty distribution for

maximum magnitude for these sources. When transformed into moment magnitude, this distribution spans nearly the same range as more recent assessments of the distribution for maximum magnitude, and the distributions have modes at similar magnitudes. Frankel et al. (2002) assigns a single value of  $M$  7.5 to all of the extended crust region shown in Figure 2.5.2-11, including the ETSZ. The magnitude of the largest earthquake in the updated catalog that lies within these sources is  $m_b$  5.2 (corresponding to events in August 31, 1861, and February 21, 1916).

Figure 2.5.2-20 summarizes the maximum magnitude assessments for sources that contain the Bellefonte Site (host zone) or represent local background sources that contribute to the hazard. The EPRI-SOG expert teams also developed a broad uncertainty distribution for maximum magnitude for these sources. When transformed into moment magnitude, the composite EPRI-SOG distribution again spans nearly the same range as more recent assessments, although it has a somewhat lower mode. Frankel et al. (2002) assigns a single value of  $M$  7.0 to all of the nonextended crust region shown in Figure 2.5.2-11, including the region around the Bellefonte Site. The largest historical earthquake in the updated catalog that lies within these sources is also  $m_b$  5.2.

The comparisons in Figures 2.5.2-19 and 2.5.2-20 show that for both the ETSZ and host zone/local background sources, more recent assessments have tended to place more weight on higher magnitudes than the EPRI-SOG expert teams. However, no large historical or prehistorical earthquakes have been identified in these sources that would provide evidence for larger maximum magnitudes, and the EPRI-SOG maximum magnitude distributions for these sources do span the range of more recent assessments. Therefore, the EPRI-SOG maximum magnitude assessments for these sources are judged to be appropriate for use in PSHA calculations for the Bellefonte Site. The minimum values for a few of these distributions (local sources defined by Law and Woodward-Clyde) were adjusted to be consistent with the largest observed earthquake in these sources (e.g., changing the low-weighted lower value of  $m_b$  4.2 to  $m_b$  5.2).

The maximum magnitude assessments for New Madrid seismic sources are shown in Figure 2.5.2-21. The distributions defined by Frankel et al. (2002) and Exelon (2004) represent distributions for the “characteristic” earthquake. The distribution developed by Exelon (2004) includes the  $\pm 1/4$  magnitude variation in the characteristic magnitude defined in the characteristic magnitude distribution developed by Youngs and Coppersmith (1985). More recent assessments of the size of characteristic New Madrid earthquakes are consistent with the EPRI-SOG evaluations of maximum magnitude for these sources.

The maximum magnitude assessments for Charleston, South Carolina, seismic sources are shown in Figure 2.5.2-22. The distributions defined by Frankel et al. (2002), Geomatrix (2004), and Savy et al. (2002) essentially represent distributions for the “characteristic” earthquake. The distribution developed by Geomatrix (2004) also includes the  $\pm 1/4$  magnitude variation in the characteristic magnitude defined in the characteristic magnitude distribution developed by Youngs and Coppersmith (1985). As was the case for New Madrid sources, more recent assessments of the maximum size of Charleston earthquakes are consistent with the EPRI-SOG evaluations.

#### 2.5.2.4.1.4 Summary of Seismic Source Assessments

The following conclusions are obtained from the review of seismic source characterization data.

- No new seismic sources have been identified.
- The EPRI-SOG evaluation seismicity rates for sources within 200 miles of the Bellefonte Site are consistent with seismicity rates defined using the updated earthquake catalog.
- The results of paleoliquefaction studies indicate that the frequency of large earthquakes in the New Madrid and Charleston source regions is more frequent than defined by the EPRI-SOG seismic hazard model.
- New data do not indicate a need to modify the EPRI-SOG evaluation maximum magnitude distributions for sources within 200 miles of the Bellefonte Site, with the exception of adjusting the lower tails of the distributions for a few sources to reflect the largest earthquake known to have occurred in each source.

#### 2.5.2.4.2 New Information Regarding CEUS Ground Motion Characteristics (RG 1.165, E.3 Step 1 Evaluation)

The EPRI-SOG evaluation characterized epistemic uncertainty in earthquake ground motions by using three strong-motion attenuation relationships. These were the relationships developed by McGuire et al. (1988), Boore and Atkinson (1987), and Nuttli (1986) combined with the response spectral relationships of Newmark and Hall (1982). These relationships were based, to a large extent, on modeling earthquake ground motions using simplified physical models of earthquake sources and wave propagation. The McGuire et al. (1988) and Boore and Atkinson (1987) models use random vibration theory to produce estimates of peak motion based on the predicted Fourier spectrum of motions. The weights assigned to the three sets of attenuation relationships in the EPRI-SOG study are a weight of 0.5 for the McGuire et al. (1988) relationships, a weight of 0.25 for the Boore and Atkinson (1987) relationships, and a weight of 0.25 for the Nuttli (1986)-Newmark and Hall (1982) relationships. The random (aleatory) variability about the three sets of median attenuation relationships was modeled as a lognormal distribution with a standard deviation of 0.5 in units of the natural log of peak motion amplitude.

Estimating earthquake ground motions in the CEUS has been the focus of considerable research since completion of the EPRI-SOG evaluation. The research has produced a number of ground motion attenuation relationships, many of which are based on the approach used by McGuire et al. (1988) and Boore and Atkinson (1987), but incorporating more recent information on the characteristics of the propagation of earthquake source and waves in the CEUS. EPRI (2004) has completed a study to characterize the estimation of strong ground motion in the CEUS for application in PSHA for nuclear facilities. This study was conducted following the SSHAC (1997) guidelines for a Level III analysis. SSHAC (1997) provided guidance on the appropriate methods to use for quantifying uncertainty in evaluations of seismic hazard. In a SSHAC Level III analysis, the responsibility for developing the quantitative description of the uncertainty distribution for the quantity of interest lies with an individual or team designated the Technical Integrator. The Technical Integrator is guided by a panel of experts (referred to as the Experts), whose role is to provide information, advice, and review. In the EPRI (2004) study, a panel of six ground motion Experts was assembled.

During a series of workshops, the Experts provided advice on the available CEUS ground motion attenuation relationships that they considered appropriate for estimating strong ground motion in the CEUS. The Experts also provided information on the appropriate criteria for evaluating the available ground motion models. The Technical Integrator then used this information to develop a composite representation of the current scientific understanding of ground motion attenuation in the CEUS.

The product of the EPRI (2004) study is a suite of ground motion relationships and associated relative weights that represent the uncertainty in estimating the median level of ground motion and its aleatory variability. The EPRI (2004) relationships are defined in terms of moment magnitude, **M**, while the EPRI-SOG attenuation relationships were defined in terms of body wave magnitude,  $m_b$ . Thus, direct comparison of the two sets requires a relationship between  $m_b$  and **M**. The relationship between  $m_b$  and **M** magnitudes was discussed in Section 2.5.2.4.1.3 and is evaluated using relationships published by EPRI (1993), Atkinson and Boore (1995), and Johnston (1996a). For purposes of comparing the EPRI-SOG and the EPRI (2004) median ground motion models, the three  $m_b$  - **M** relationships were used to estimate values of **M** for  $m_b$  values of 5, 6, and 7, and the results averaged, as indicated in the following table.

Body Wave Magnitude, $m_b$	Moment Magnitude, <b>M</b>			Average
	EPRI (1993)	Atkinson and Boore (1995)	Johnston (1996a)	
5	4.6	4.5	4.7	4.6
6	5.5	5.6	5.9	5.7
7	7.2	7.0	7.4	7.2

Figure 2.5.2-23 compares the EPRI (2004) median attenuation relationships to those used in the EPRI-SOG evaluation. EPRI (2004) defined the uncertainty in the median ground motions in terms of four ground motion “cluster” models. Each cluster represented a group of models based on a similar approach for ground motion modeling. The relationships shown in Figure 2.5.2-23 represent the median estimates of ground motions produced by the models within each cluster. The EPRI (2004) models also use either the Joyner-Boore distance measure or the closest distance to rupture distance measure while the EPRI-SOG (1988) ground motion models use hypocentral distance. In the comparisons shown in Figure 2.5.2-23, a hypocentral depth of 10 kilometers was used in conjunction with the EPRI-SOG ground motion models, consistent with their use in the EPRI (1989) PSHA calculation. Depths to the top of the rupture of 5, 3, and 1 kilometers were used for magnitudes  $m_b$  5, 6, and 7, respectively, in computing the equivalent surface distance from EPRI (2004) Cluster 3 models. The EPRI (2004) median models are generally consistent with the two spectral models used in the EPRI-SOG evaluation (McGuire et al., 1988; Boore and Atkinson, 1987). All of the EPRI (2004) median models predict lower levels of motion than obtained using the Nuttli (1986)-Newmark and Hall (1982) model.

EPRI (2004) provided guidance on the use of the models for various types of seismic sources. In particular, the Cluster 4 model, which is based on the Somerville et al. (2001) ground motion relationships, is not considered applicable to seismic sources where a significant portion of the hazard is due to earthquakes below magnitude **M** 6.0. This is

because Somerville et al. (2001) did not include earthquake magnitudes below  $M$  6.0 in their numerical simulations when developing their model. In general, the types of seismic source for which the Cluster 4 model would not be used are general area sources in the vicinity of the site (such as the ETSZ sources and the host/background sources in the EPRI-SOG model). The Cluster 4 model is applicable for computing hazard from large magnitude earthquakes, such as those contributing to the site hazard from the New Madrid and Charleston seismic sources.

In the EPRI (2004) representation of ground motion, the uncertainty in the median model for each ground motion cluster is defined by two additional models, one representing the 5<sup>th</sup> percentile of the uncertainty distribution for the median and one representing the 95<sup>th</sup> percentile. The range in these models defines the uncertainty range in the median ground motions. Figure 2.5.2-24 compares the composite range in median ground motions across all clusters for the EPRI (2004) ground motions models with the EPRI-SOG attenuation relationships. For  $m_b$  5 and 6, only models for Clusters 1, 2, and 3 are included in defining the range; Cluster 4 models are included in the range for  $m_b$  7. The uncertainty range for the EPRI (2004) peak acceleration relationships generally encompasses the three EPRI-SOG median relationships. However, for 1-Hz spectral acceleration (SA), the Nuttli (1986)-Newmark and Hall (1982) model lies outside of the uncertainty band for the EPRI (2004) ground motion models.

The EPRI (2004) study also developed an assessment of the aleatory variability about the median attenuation relationships. Figure 2.5.2-25 compares the EPRI (2004) assessments of aleatory variability (defined in terms of the standard deviation of  $\ln [SA]$ ) to the value used in the EPRI-SOG evaluation. The EPRI (2004) assessments are significantly larger than those used in the EPRI-SOG evaluation.

The purpose of the EPRI (2004) study was to develop a current representation of the state of knowledge of ground motion estimation for regional hard rock site conditions in the CEUS for use in PSHA applications. Therefore, it is considered appropriate for use in conducting the seismic hazard assessment for the Bellefonte Site.

#### 2.5.2.4.3 PSHA Sensitivity Analysis (RG 1.165, E.3 Step 2 Evaluation)

This section describes the sensitivity studies that were carried out to address changes in the EPRI-SOG PSHA model used in EPRI (1989). Based on the assessments in Section 2.5.2.4.1 and 2.5.2.4.2, and consistent with the requirements of Regulatory Guide 1.165, Position E.3, the following PSHA model adjustments are studied as part of PSHA sensitivity tests for the Bellefonte Site:

- Sensitivity to adjustment of the minimum value of maximum magnitude for a few EPRI-SOG sources upward to equal the largest known earthquake within the source zone, based on the updated GG&S earthquake catalog
- Sensitivity to new data relative to the occurrence of large earthquakes in the NMSZ
- Sensitivity to new data relative to the occurrence of large earthquakes in the Charleston, South Carolina, region
- Sensitivity to new ground motion models

The first step in the analysis was to demonstrate that the EPRI (1989) PSHA results could be reproduced. The original EPRI-SOG input files were obtained from EPRI and transformed into a format usable by Geomatrix PSHA software. PSHA calculations were then performed for 10-Hz and 1-Hz spectral velocities. Table 2.5.2-6 compares the frequency of exceeding a range of ground motion levels computed using the Geomatrix PSHA software with the EPRI (1989) results. For frequencies of exceedance greater than about  $10^{-6}$ , the differences are generally less than 5 percent in terms of frequency of exceedance, which translates into approximately 2.5 percent in terms of ground motion level.

The next step was identifying the controlling sources in the EPRI-SOG seismic hazard model. Table 2.5.2-7 lists the percent contribution by source to each expert team's total frequency of exceeding ground motion levels that correspond to the total mean annual exceedance frequencies (averaged across all six teams) of  $10^{-4}$  and  $10^{-5}$ . The hazard from each source is weighted by its probability of inclusion in the model (probability of activity). Sources that correspond to the ETSZ, the host/local background, New Madrid, and Charleston are identified. Most of the hazard for 10-Hz motions is contributed by the host source/local background and the ETSZ source, with the host source typically having the larger contribution of the two. For 1-Hz motions, the New Madrid sources typically have the largest contribution to the hazard. Charleston sources have some contribution to 99 percent of the total hazard only for the Woodward-Clyde team, and that contribution is only a few percent to the 1-Hz motion hazard.

During the assessment of source contributions, it was discovered that the original EPRI-SOG input files did not include sources 4 and 4a for the Bechtel team and source 217 for the Law team. The effect of adding these sources to the analysis is shown in Figure 2.5.2-26. The result is approximately a 3 to 5 percent increase in ground motion levels corresponding to mean hazard in the range of  $10^{-4}$  to  $10^{-5}$  and a 7 to 10 percent increase in ground motion levels corresponding to median hazard in the range of  $10^{-4}$  to  $10^{-5}$ . The values listed in Table 2.5.2-7 and in all subsequent analyses were computed using this corrected source list.

The first sensitivity analysis tests the effect of adjusting the EPRI-SOG maximum magnitude distributions to limit the lowest magnitude to be equal to the largest earthquake known to have occurred within each source. This represents a very small change in the inputs and the resulting effect on the hazard is negligible (<0.5 percent).

The next set of sensitivity analyses test the effect of incorporating sources of repeating large magnitude earthquakes at New Madrid and Charleston with return intervals of approximately 500 and 550 years, respectively, into the seismic hazard model. Ideally, the EPRI-SOG characterization of these sources should be updated to reflect the recent data. However, because of the large distance between these sources and the Bellefonte Site (> 200 miles), what is of primary importance is the characterization of the size and frequency of the largest earthquakes. This is illustrated by the magnitude-distance disaggregation of the mean hazard from the EPRI-SOG model. Figure 2.5.2-27 shows the contributions to the mean hazard at ground motion exceedance levels of  $10^{-4}$  and  $10^{-5}$  disaggregated into 0.1 unit magnitude intervals and three distance intervals. The hazard from distances greater than 300 kilometers (186 miles) is primarily from the ERPI-SOG New Madrid sources and is from earthquakes larger than  $m_b$  6.5.

The simplest form of an updated source characterization is to just add sources of repeating earthquakes at New Madrid and Charleston to the existing EPRI-SOG characterization for those regions. This approach results in a small degree of “double counting” of the occurrence of large earthquakes as the EPRI-SOG source characterization includes large magnitude earthquakes in these areas, although with lower frequencies of occurrence. As indicated in Figure 2.5.2-18, the existing EPRI-SOG seismic source model for New Madrid adequately characterizes the frequency of earthquakes smaller than the estimated size of the 1811-1812 earthquakes (magnitudes less than approximately  $m_b$  6.75). Therefore, a more appropriate update for use in calculating the hazard at the Bellefonte Site is to use the EPRI-SOG seismic source characterization to model the occurrence of these smaller earthquakes and to use more recent data to model the occurrence of large repeating earthquakes. This is accomplished by limiting the maximum magnitude for the EPRI-SOG seismic sources to  $m_b$  6.75.

Sensitivity analyses were performed to examine both of these alternative approaches to updating the EPRI-SOG models for New Madrid and Charleston and the potential impact of double counting the occurrence rate of large earthquakes. First, seismic sources for repeating large earthquakes at Charleston and New Madrid were simply added to the EPRI-SOG seismic source model. The seismic source characterization developed by Exelon (2004) for repeating earthquakes at New Madrid and by Geomatrix (2004) for Charleston was used to characterize these sources. The magnitude of the repeating earthquakes at New Madrid and Charleston are shown in Figures 2.5.2-21 and 2.5.2-22, respectively (the Exelon, 2004, characterization is similar to the Geomatrix, 2004, characterization). Figure 2.5.2-28 shows the resulting mean hazard curves for the EPRI-SOG sources, the repeating large earthquakes at New Madrid and at Charleston, and the combined mean hazard. The repeating large earthquakes at New Madrid contribute to the 10-Hz motion hazard for exceedance frequencies between  $10^{-2}$  and  $10^{-4}$  and are the dominant contributor to the 1-Hz motion hazard for exceedance frequencies less than about  $10^{-3}$ . Compared to the New Madrid source, the Charleston repeating earthquakes have only a very minor contribution to the hazard due to their smaller size and greater distance from the site. The inclusion of the updated source characterization for repeating large earthquakes at New Madrid results in a 1 to 10 percent increase in 10-Hz motions and a 100 to 150 percent increase in 1-Hz motions for mean frequencies of exceedance in the range of  $10^{-4}$  to  $10^{-5}$ . The effect on median hazard is somewhat smaller.

As discussed previously, a more appropriate simplified update of the EPRI-SOG characterization of New Madrid and Charleston that accounts for potential double counting of the occurrence of large earthquakes is to limit the maximum magnitude in the EPRI-SOG models for these sources to magnitudes smaller than the size of the repeating earthquakes and then add updated source characterization for the repeating earthquakes to the revised model. The revised update for New Madrid consists of setting the maximum magnitude for the EPRI-SOG New Madrid sources to  $m_b$  6.75 and adding the seismic source model for larger New Madrid earthquakes developed by Exelon (2003, 2004). A similar process was used to develop a simplified update of the seismic source characterization for Charleston sources, with the maximum magnitude for the EPRI-SOG sources limited to  $m_b$  6.5 and the Geomatrix (2004) characterization for large repeating earthquakes used to model reoccurrence of large earthquakes.



Figure 2.5.2-29 compares the hazard computed using the revised updated seismic source model for the New Madrid and Charleston sources to the hazard obtained by simply adding sources of repeating large earthquakes to the EPRI-SOG model. These results indicate that there is negligible effect (< 2 percent change in ground motion level) of “double counting” of large earthquakes in the range of  $10^{-4}$  to  $10^{-5}$  annual frequency of exceedance. The negligible impact of double counting is due to the large difference between the rate predicted by the EPRI-SOG models and the rate based on the results of recent paleoliquefaction studies (Figure 2.5.2-18).

The third PSHA sensitivity analysis evaluates the effect of replacing the three  $m_b$ -based ground motion attenuation models used in the EPRI-SOG (1988) model with the new  $M$ -based ground motion attenuation models developed by EPRI (2004). Figure 2.5.2-30 compares these hazard results for the EPRI-SOG (1988) seismic source characterization. The three  $m_b$ - $M$  relationships described in Section 2.5.2.4.1.3 were used to convert  $m_b$  magnitudes into moment magnitude for calculation of the hazard using the EPRI (2004) ground motion models. The effect of using the updated ground motion models on the 10-Hz motion hazard is to produce a small increase in ground motion for an exceedance frequency of  $10^{-4}$  (5 percent increase for mean hazard, 17 percent increase for median hazard) and larger increases in ground motions for lower exceedance frequencies (50 to 60 percent increase at  $10^{-5}$  exceedance frequency). The larger ground motions at lower exceedance frequencies is due in part to the increased level of aleatory variability (greater standard deviation) in the EPRI (2004) ground motion characterization compared to the value used in the EPRI-SOG (1988) hazard model (see Figure 2.5.2-25). For 1-Hz motion hazard, use of the EPRI (2004) ground motion model results in higher ground motions based on median hazard (24 to 40 percent increase in the range of  $10^{-4}$  to  $10^{-5}$  exceedance frequency) and lower ground motions based on mean hazard (33 to 44 percent decrease in the range of  $10^{-4}$  to  $10^{-5}$  exceedance frequency). The higher ground motions for median hazard is likely again due to larger aleatory variability in the EPRI (2004) ground motion characterization. The lower ground motions for mean hazard is due to replacement of the Nuttli-Newmark Hall model with models that all produce lower median ground motions (see Figures 2.5.2-23 and 2.5.2-24).

In summary, the PSHA sensitivity analyses indicate that both the updated characterization of repeating large magnitude earthquakes in the New Madrid region (and, to a minor extent, in the Charleston region) and the updated EPRI (2004) ground motion characterization lead to increases in the hazard at the Bellefonte Site at frequencies of exceedance of  $10^{-4}$  to  $10^{-5}$  that are important to defining the SSE ground motions.

#### 2.5.2.4.4 Updated PSHA (RG 1.165, E.3 Step 3 Evaluation)

The sensitivity evaluations described in Section 2.5.2.4.3 identified three specific elements of the EPRI-SOG evaluations that are impacted by the new information and data. The areas that require updating are: (1) the characterization of the size and rate of the more frequently occurring large magnitude New Madrid events originating on the fault system that generated the 1811-1812 earthquake sequence; (2) the characterization of the source geometry, recurrence, and magnitude of repeating large magnitude earthquakes in the Charleston region (which has only a very minor impact on the site hazard); and (3) new ground motion models for the CEUS. The modifications to the EPRI-SOG seismic hazard

model to incorporate these updates are discussed in the following sections. Note that, with the exception of the repeating large magnitude New Madrid and Charleston earthquakes, the seismicity parameters defined for the EPRI-SOG seismic sources are unchanged by new data and are found, consistent with Regulatory Guide 1.165 (USNRC, 1997), to be appropriate for use in the updated PSHA for the Bellefonte Site.

#### 2.5.2.4.4.1 New Madrid Repeated Large Magnitude Earthquake Source

The principal seismic activity within the upper Mississippi embayment is interior to the Reelfoot rift along the NMSZ. Recent seismologic, geologic, and geophysical studies have associated faults within the NMSZ with large magnitude historical earthquakes that occurred during 1811-1812 (see Section 2.5.1.1.4.3(a)1 for a discussion of new data). Paleoliquefaction studies provide evidence that large magnitude earthquakes have occurred on these faults more frequently than the seismicity rates specified in the EPRI-SOG source characterizations. Figure 2.5.2-31 shows the locations of these sources relative to the Bellefonte Site.

The EPRI-SOG source characterizations, as they stand, adequately address the uncertainty related to location, magnitude, and frequency of earthquakes that may occur on other potential seismic sources in the region of the NMSZ, such as recently identified active faults along the northern and southern rift margins (see discussion in Section 2.5.1.1.4.3(a)2, Table 2.5.1-1). Updating the EPRI-SOG seismic source evaluations for this study, therefore, focuses on the characterization of more frequent large magnitude events along the central fault system. The key source parameters are discussed in the following sections. The logic tree used to represent the uncertainty in the seismic source characterization model for the NMSZ central fault system is shown in Figure 2.5.2-32.

##### (a.) NMSZ Central Faults Source Geometry

Three fault sources are included in the updated characterization of the central fault system of the NMSZ: (1) the New Madrid South (NS) fault; (2) the NN; and (3) the RF (RF). The first three levels of the logic tree for these sources address the uncertainty in the research community regarding the location and extent of the causative faults that ruptured during the 1811-1812 earthquake sequence. This uncertainty is represented by alternative geometries for the NN, NS, and RF faults. These alternative geometries affect the distance from earthquake ruptures on these fault sources to the Bellefonte Site.

The locations of the faults that make up the New Madrid central fault system sources are shown in Figure 2.5.2-31 (inset A). For the New Madrid South fault (NS) source, two alternatives are considered, as described by Johnston and Schweig (1996): (1) the BA/BL (BA/Bootheel lineament); and (2) the BA/BFZ (BA/Blytheville fault zone) (also see Figure 2.5.1-31). Although modern seismicity is occurring primarily along the BFZ, Johnston and Schweig (1996) present arguments suggesting that the BA/BL is the most likely location for the main NM1 (D1) event and that major NM1 (D1) aftershocks occurred on the BFZ (the northeast extension of the Cottonwood Grove fault) (see Section 2.5.1.1.4.3(a)1 for a description of the 1811-1812 earthquake sequence and its relationship to the identified faults). Therefore, slightly greater weight is given to BA/BL [0.6] (total length of 132 kilometers [80 miles]) versus BA/BFZ [0.4] (total length of 115 kilometers [69 miles]).

Two alternative total lengths are considered for the NN source. The first, which is given the highest weight [0.7], allows for rupture of the 60-kilometer (36-mile) fault segment (NN, Figure 2.5.2-31) as defined by Johnston and Schweig (1996). Cramer (2001) uses a similar value (59 kilometers) (35.4 mile) as the length of his northeast arm. Concentrated seismicity defines the segment as ~40 kilometers (24 miles) long. Johnston (1996b), in modeling the source fault for the NM2 (J1) earthquake, extends the fault to the epicentral region of the 1895 Charleston, Missouri, earthquake (M 6.0-6.6), for a total length of 65 kilometers (39 miles). An alternative total length of 97 kilometers (58 miles) allows for the fault to extend north to include less well-defined seismicity trends noted by Wheeler (1997). Wheeler et al. (1997) and other researchers argue for a structural northern boundary to the rift in this region (Table 2.5.1-1). The New Madrid northern extension (NNE, Figure 2.5.2-31) is not as well defined by seismicity as is the NN segment. Also, the recurrence interval of large magnitude earthquakes in the northern Mississippi embayment appears significantly longer than the recurrence interval for NMSZ earthquakes based on paleoliquefaction studies. Van Arsdale and Johnston (1999) cite as evidence of a long recurrence interval (on the order of tens of thousands of years) the sparse seismicity, the lack of Holocene fault offsets in the Fluorspar Area fault complex along trend to the north, the presence of only minor Quaternary faulting, and the lack of discernable offset of the margins of Sikeston Ridge where it meets the NN. Given these observations, the longer (97 kilometers [58 miles]) fault length that includes the NN and NNE is given less weight [0.3].

Johnston and Schweig (1996) conclude from historical accounts that the NM3 (F1) event occurred on the RF (Figure 2.5.1-24). Johnston and Schweig (1996) identify three possible segments of the RF, a central 32-kilometer-long reverse fault defined by the RF scarp between the two northeast-trending strike-slip faults, a 35-kilometer-long segment (RS) that extends to the southeast, and a 40-kilometer-long (24 miles) segment west of the NN (Figure 2.5.1-24). Seismicity and geomorphic data indicate that the southeast segment is slightly shorter (25 to 28 kilometers) than indicated by Johnston and Schweig (Van Arsdale et al., 1999; Mueller and Pujol, 2001). Cramer (2001) uses a total length of 60 kilometers for the RF. The alternative fault rupture scenarios of Johnston and Schweig (1996) include rupture of a 40-kilometer-long northwest fault segment (Figure 2.5.1-24). Cramer (2001) assigns a length of 33 kilometers to this segment, which he refers to as the west arm. Mueller and Pujol (2001) note that this westerly arm is imaged as a vertical fault that terminates the Reelfoot thrust. They interpret the westerly arm as a left-lateral strike-slip fault kinematically linked to the Reelfoot thrust. Bakun and Hopper (2004b) suggest a preferred epicenter location at the northern end of the RS segment. Hough and Martin (2002) show a slightly different geometry for the northwestern portion of the fault and do not interpret the historical 1811-1812 earthquake ruptures to have extended to the rift margin on the southeast (Figure 2.5.1-25). Two alternative fault geometries are included in this study: (1) the RF fault includes the NW, RF, and RS segments as defined in Cramer (2001) [0.7]; and (2) a shorter RF that extends from the intersection with the NN fault and extends to the southeastern end of the RF as shown by Hough and Martin (2002) (Figure 2.5.2-14). The longer length is judged to be more consistent with displacements and magnitudes inferred for the NM3 event, and thus is given higher weight in the model.

### (b.) NMSZ Central Faults Maximum Earthquake Magnitude

The next level of the logic tree addresses the maximum magnitude for earthquakes on the three New Madrid fault sources. As discussed previously in section (a), specific faults and seismicity lineaments have been proposed as the sources of the 1811-1812 and previous earthquakes. In addition, researchers have suggested that the sizes of prehistoric earthquakes associated with these sources are similar to the 1811-1812 earthquakes (e.g., Tuttle et al., 2002). The identification of fault sources and repeated large earthquakes of similar size is suggestive of the behavior of crustal faults in more active regions and many recent studies (e.g., Frankel et al., 1996, 2002; Toro and Silva, 2001; Geomatrix, 2004) have used the concept of “characteristic” earthquakes to characterize the behavior of the New Madrid seismic source. The characteristic earthquake concept is that a seismic source generates repeated large earthquakes of similar size at a frequency that is greater than obtained by extrapolating a Gutenberg-Richter recurrence relationship fit to the observed seismicity rate for smaller-magnitude earthquakes, as illustrated in Figure 2.5.2-18. These characteristic earthquakes represent the largest earthquakes produced by the source, and as such represent the maximum magnitude event. Using the concept of characteristic earthquakes, seismic source characterizations of the New Madrid seismic source zone typically consider the 1811-1812 earthquakes to represent the maximum earthquake for this source. Table 2.5.1-2 summarizes recent estimates of the magnitude of the New Madrid 1811-1812 mainshocks.

Bakun and Hopper (2004b) provide preferred estimates of the locations and moment magnitudes and their uncertainties for the three largest events in the 1811-1812 sequence near New Madrid. Their preferred intensity magnitude  $M_I$ , which is their preferred estimate of  $M$ , is 7.6 (6.8 to 7.9 at the 95 percent confidence interval) for the December 16, 1811, Event (NM1), 7.5 (6.8 to 7.8 at the 95 percent confidence interval) for the January 23, 1812, Event (NM2), and 7.8 (7.0 to 8.1 at the 95 percent confidence interval) for the February 7, 1812, Event (NM3). The intensity magnitude  $M_I$  is the mean of the intensity magnitudes estimated from individual MMI assignments. In their analysis, Bakun and Hopper (2004b) consider two alternative eastern North America (ENA) intensity attenuation models, which they refer to as models 1 and 3. As indicated in Table 2.5.1-2, these two models give significantly different results for larger magnitude earthquakes. Bakun and Hopper (2004b) state that because these models are empirical relations based almost exclusively on  $M < 6$  calibration events “There is no way to confidently predict which relation better represents the MMI-distance data for  $M 7$  earthquakes in ENA” (p. 66, Bakun and Hopper, 2004b). They present arguments supporting their preference for model 3, but do not discount the results based on model 1.

Dr. Susan Hough (written communication, August 23, 2004) believes that there are insufficient data regarding the calibration of ENA earthquakes larger than  $M > 7$  to rely strictly on ENA models as was done in Bakun and Hopper (2004b). She offers arguments to support  $M 7.6$  (the size of the 2003 Bhuj earthquake) as a reasonable upper bound for the largest of the earthquakes in the 1811-1812 New Madrid earthquake sequence, which is more consistent with the estimates cited in Hough et al. (2000) and Mueller et al. (2004).

Mueller et al. (2004) use instrumentally recorded locations of recent earthquakes (assumed by Mueller et al. to be aftershocks of the 1811-1812 sequence) and models of elastic stress

change to develop a kinematically consistent rupture scenario for the mainshock earthquakes of the 1811-1812 New Madrid sequence. In general, the estimated magnitudes for NM1 and NM3 used in their analysis ( $M = 7.3$  and  $M = 7.5$ , respectively) are consistent with those previously published by Hough et al. (2000). Their results suggest that the mainshock Events NM1 and NM3 occurred on two contiguous faults, the strike-slip Cottonwood Grove fault and the Reelfoot thrust fault, respectively. The locations of the NM1 and NM3 Events on the Cottonwood Grove and RFs, respectively, are relatively well constrained. In contrast to the earlier Hough et al. (2000) study that located the NM2 earthquake on the NN, they suggest a more northerly location for the NM2 Event, possibly as much as 200 kilometers to the north in the Wabash Valley of southern Indiana and Illinois. Hough et al. (2005) also infer a similar more northerly location. Using Bakun and Wentworth's (1997) method, Mueller et al. (2004) obtain an optimal location for the NM2 mainshock at  $88.43^{\circ}\text{W}$ ,  $36.95^{\circ}\text{N}$  and a magnitude of  $M 6.8$ . They note that the location is not well constrained and could be fit almost as well by locations up to 100 kilometers northwest or northeast of the optimal location. Mueller et al. (2004) conclude that the three events on the contiguous faults increased stress near fault intersections and end points, in areas where present-day microearthquakes have been interpreted as evidence of primary mainshock rupture. They note that their interpretation is consistent with established magnitude/fault area results, and do not require exceptionally large fault areas or stress drop values for the New Madrid mainshocks.

With respect to the location of the NM2 Event, Bakun and Hopper (2004b) also discuss the paucity of MMI assignments available for this earthquake to the west of the NMSZ and the resulting uncertainty in its location. They note that the two MMI sites closest to the NMSZ provide nearly all of the control on the location of this event and that, based on these two sites, a location northeast of their preferred site would be indicated. However, they conclude that the lack of 1811-1812 liquefaction observations in western Kentucky, southern Illinois, and southern Indiana preclude an NM2 location in those areas. Bakun and Hopper (2004b) follow Johnston and Schweig (1996) in selecting a preferred location on the NN. S. Obermeier confirmed that liquefaction features in the Wabash Valley region that would support the more northerly location preferred by Mueller et al. (2004) are absent (Dr. Steve Obermeier, personal communication, August 24, 2004). He noted that he had looked specifically in the area cited in the Yearby Land account that was cited by Mueller et al. (2004) and observed evidence for only small sand blows and dune sands, but did not see features of the size and origin described in that account.

Dr. Arch Johnston (written communication, August 31, 2004) indicates that the estimates of Johnston (1996b) are likely to be high by about 0.2 to 0.3 magnitude units. Dr. Johnston indicates that he is working on developing revised estimates for a forthcoming paper.

The review of these new publications indicates that there still remain uncertainty and differing views within the research community regarding the size and location of the 1811-1812 earthquakes. Based on this review of these articles and the communications with Drs. Bakun, Hough, and Johnston, the maximum magnitude for the New Madrid central fault system faults was defined for the GG&S study as follows.

- Equal weight (one-third) is to be given to estimates based on Bakun and Hopper (2004b) and Hough et al. (2000)/Mueller et al. (2004), and the Johnston (written communication, August 31, 2004) revisions to Johnston (1996b).
- Results from both intensity attenuation relations (models 1 and 3) in the Bakun and Hopper (2004b) estimate are used. Based on Bakun and Hopper's preference for model 3, weights are assigned of 0.75 to model 3 and 0.25 to model 1.
- In the case of the Hough et al. (2000)/Mueller et al. (2004) estimates and the written communication, August 31, 2004) estimates, equal weight is assigned to the range of preferred values given for each earthquake.

The resulting characteristic magnitude distribution for each of the three faults is given in Table 2.5.2-8. Rupture sets 1 and 2 correspond to the revised Johnston (1996b) estimates, rupture sets 3 and 4 correspond to the Bakun and Hopper (2004b) estimates, and rupture sets 5 and 6 correspond to the Hough et al. (2000) estimates.

As discussed in the following section, the present interpretation of the paleoearthquake data is that the two prehistoric earthquake ruptures that occurred before the 1811-1812 sequence also consisted of multiple, large magnitude earthquakes. Therefore, for this assessment, the event is considered to be rupture of multiple (two to three) of the fault sources shown in Figure 2.5.2-31. Furthermore, the arguments for the high versus low magnitude assessments for the individual faults are considered to be highly correlated. Therefore, six alternative sets of ruptures were produced from the distributions developed previously for each fault, as shown in the logic tree in Figure 2.5.2-32 and given in Table 2.5.2-8.

The magnitudes listed in Table 2.5.2-8 are considered to represent the size of the expected maximum earthquake rupture for each fault within the NMSZ. Following the development of the characteristic earthquake recurrence model by Youngs and Coppersmith (1985), as modified by Youngs et al. (1988), the size of the next characteristic earthquake is assumed to vary randomly about the expected value following a uniform distribution over the range of  $\pm 1/4$  magnitude units. This range represents the aleatory variability in the size of individual characteristic earthquakes. For example, given that the expected magnitude for the characteristic earthquake on the NS fault source is **M** 7.8, the magnitude for the next characteristic earthquake is uniformly distributed between **M** 7.55 and **M** 8.05.

### (c.) NMSZ Central Faults Earthquake Recurrence

The best constraints on recurrence of repeated large magnitude NMSZ events result from paleoliquefaction studies throughout the New Madrid region and paleoseismic investigations of the RF scarp and associated fold. Based on studies of hundreds of earthquake-induced paleoliquefaction features at more than 250 sites, Tuttle et al. (2002) conclude that: (1) the fault system responsible for the New Madrid seismicity generated temporally clustered, very large earthquakes in AD 900  $\pm$ 100 and AD 1450  $\pm$ 150 years as well as in 1811-1812; (2) given uncertainties in dating liquefaction features, the time between the past three events may be as short as 200 years or as long as 800 years, with an average of 500 years; and (3) prehistoric sand blows probably are compound structures, resulting from multiple earthquakes closely clustered in time (i.e., earthquake sequences).

Cramer (2001) obtained a 498-year mean (440-year median) recurrence interval for New Madrid characteristic earthquakes based on a Monte Carlo sampling of 1,000 recurrence intervals using the Tuttle and Schweig (2000) uncertainties as a range of permissible dates ( $\pm$  two standard deviations) for the two most recent prehistoric earthquakes (i.e., AD 900  $\pm$ 100 and AD 1450  $\pm$ 135). Assuming a lognormal distribution with a coefficient of variation of 0.5 for inter-arrival time, Cramer (2001) obtained a 68 percent confidence interval for the mean recurrence interval of 267 to 725 years, and a 95 percent confidence interval of 162 to 1,196 years (ranges for one and two standard deviations, respectively).

Exelon (2003, Attachment 2 to Appendix B) presents a detailed assessment of the timing constraints on prehistoric New Madrid earthquakes and the development of occurrence rates for repeats of 1811-1812 earthquake sequence. The uncertainties in the ages of individual samples were used to constrain the timing of individual events. A Monte Carlo sample of 10,000 sets of time intervals between events was generated using these data. Two recurrence models were used to represent the occurrence of earthquake sequences, the commonly used Poisson (memoryless) model and a renewal model (one-step memory). The uncertainty in fitting these models to a sample of limited size (two closed time intervals, between 900 AD and 1450 AD and between 1450 AD and 1811-1812, and one open interval post 1812) together with the simulated distributions of time intervals provided uncertainty distributions on the recurrence rates for New Madrid sequences. For the renewal model, Exelon (2003) used a lognormal distribution to represent the time between earthquakes. Exelon (2004) repeated the analysis of the simulated time intervals between earthquake sequences using the Brownian Passage Time (BPT) model developed by Ellsworth et al. (1999) and Matthews et al. (2002) to represent the distribution of the time between earthquake sequences in the renewal model. Ellsworth et al. (1999) and Matthews et al. (2002) propose that the BPT model is more representative of the physical process of strain buildup and release on a seismic source than the other distribution forms that have been used for renewal models (e.g., the lognormal). Based on these arguments, the BPT model was used by the Working Group (2003) to assess the probabilities of large earthquakes in the San Francisco Bay area.

Figure 2.5.2-33 shows the uncertainty distributions for the mean repeat time between New Madrid earthquake sequences obtained by Exelon (2004). Application of the BPT model requires estimation of the aperiodicity coefficient  $\alpha$  that defines the variability in the timing of individual events. Because of the very limited sample size, Exelon (2004) did not estimate  $\alpha$  from the simulated data. Instead, they utilized the distribution for  $\alpha$  developed by the Working Group (2003) of 0.3 (wt 0.2), 0.5 (wt 0.5), and 0.7 (wt 0.3). These alternative values were incorporated into the uncertainty model for the New Madrid repeating earthquake source (Figure 2.5.2-32).

Following the process used by Exelon (2003, 2004), the occurrence rates for New Madrid large magnitude earthquake sequences were estimated using the distributions for mean repeat time shown in Figure 2.5.2-33. For the Poisson model, the occurrence rate is just the inverse of the mean repeat time. For the BPT-renewal model, an equivalent Poisson rate is obtained, allowing the exceedance rate from the New Madrid earthquake sequence to be added to the exceedance rate from all other sources. The equivalent Poisson rate,  $\lambda_{renewal}$ , is given by the expression:

$$\lambda_{renewal} = -\ln[1 - P_{renewal}(\text{event in time } t_0 \text{ to } t_0 + \Delta t)] / \Delta t \quad (2.5.2-9)$$

where  $t_0$  is the present time measured from the date of the most recent event,  $\Delta t$  is the time period of interest, and  $P_{renewal}()$  is the probability of the event occurring in the time interval  $\Delta t$ . The time period of interest,  $\Delta t$ , was taken to be 50 years. This is a somewhat long for the typical life span of a nuclear power plant, but longer values of  $\Delta t$  produce larger values of the average rate. The renewal recurrence model,  $P_{renewal}()$  is given by the expression:

$$P_{renewal}(\text{event in time } t_0 \text{ to } t_0 + \Delta t) = \frac{F(t_0 + \Delta t) - F(t_0)}{1 - F(t_0)} \quad (2.5.2-10)$$

where  $F()$  is the cumulative distribution for time between events. Equation (2.5.2-10) gives the probability of a single event in time  $\Delta t$  while the equivalent Poisson rate (Equation 2.5.2-9) is based on the probability of one or more events. However, the probability of two or more in the renewal model case is negligible.

For the BPT model,  $F()$  is given by:

$$F(t) = \Phi[u_1(t)] + e^{2/\alpha^2} \Phi[-u_2(t)]$$

$$u_1(t) = (\sqrt{t/\mu} - \sqrt{\mu/t}) / \alpha$$

$$u_2(t) = (\sqrt{t/\mu} + \sqrt{\mu/t}) / \alpha \quad (2.5.2-11)$$

$$f(t) = \left( \frac{\mu}{2\pi\alpha^2 t^3} \right)^{1/2} \exp\left( -\frac{(t-\mu)^2}{2\mu\alpha^2 t} \right)$$

where  $\mu$  is the mean inter-arrival time (repeat time),  $\alpha$  is the aperiodicity coefficient, and  $\Phi()$  is the standard normal cumulative probability function.

The uncertainty distributions for mean repeat time shown in Figure 2.5.2-33 were represented in the seismic hazard model by a five-point discrete approximation to a continuous distribution developed by Miller and Rice (1983). Table 2.5.2-9 lists the discrete distributions for mean repeat time and the equivalent Poisson rates. The Poisson and renewal recurrence models are given equal weight (Figure 2.5.2-32). The renewal model is considered more appropriate on a physical basis for the behavior of characteristic earthquakes on active faults. The Working Group (2003) applied weights of 0.7 and 0.6 to non-Poissonian behavior for the San Andreas and Hayward faults, respectively. For other, less active sources, they assigned a weight of 0.5 or less to non-Poissonian behavior. While the New Madrid faults are not plate boundary faults, they exhibit behavior that is similar to that expected for an active plate boundary fault. Equal weights represent maximum uncertainty as to which is the more appropriate model.

The paleoliquefaction data gathered in the New Madrid region indicate that the prehistoric earthquakes have occurred in sequences closely spaced in time relative to the time period



between sequences, similar to the 1811-1812 sequence. Figure 2.5.2-34, taken from Tuttle et al. (2002), shows the estimated earthquake sizes and event locations for the 1811-1812 sequence and the two previous sequences. These data indicate that the RF has ruptured in all three sequences, but the NN and NS sources may have produced earthquakes on the order of one magnitude unit smaller than the 1811-1812 earthquakes in previous sequences. Recent discussions with Dr. Tuttle (personal communication, 24 August, 2004) indicate that she considers that the difference between the size of the 1811-1812 earthquakes and those of the 900 and 1450 sequences are likely to be smaller than what was portrayed in Figure 6 of Tuttle et al. (2002). As a result, Exelon (2004) revised the model of Exelon (2003) for New Madrid sequences to consist of two alternative models of rupture or earthquake sequences. In Model A, all ruptures are similar in size to the 1811-1812 earthquakes. In Model B one-third of the sequences are the same as Model A, one-third of sequences contain a smaller rupture of the NN, and one-third of sequences contain a smaller rupture of the NS. The difference in magnitude from the 1811-1812 ruptures was set to be no more than one-half magnitude unit, and no ruptures are allowed to be less than **M** 7. All three earthquakes were included in the hazard calculation in all rupture sequences. Model A (always full ruptures) is given a weight of two-thirds and Model B a weight of one-third, based on Dr. Tuttle's expression of the difficulties in estimating the size of the pre 1811-1812 ruptures and her judgment that the difference between the rupture sizes was likely smaller than proposed in Tuttle et al. (2002).

The computation of the hazard from the New Madrid earthquake sequence uses the formulation outlined in Toro and Silva (2001). The frequency of exceedance,  $v(z)$ , from the earthquake sequence is given by the expression:

$$v(z)_{characteristic} = \lambda_{sequence} \left[ 1 - \prod_i \{1 - P_i(Z > z)\} \right] \quad (2.5.2-12)$$

where  $\lambda_{sequence}$  is the equivalent annual frequency of event clusters and  $P_i(Z > z)$  is the probability that earthquake  $i$  in the sequence produces ground motions in excess of level  $z$ .

#### 2.5.2.4.4.2 Charleston Repeating Large Magnitude Earthquake Source

The 1886 Charleston, South Carolina, earthquake was the largest earthquake occurring in historical time in the eastern U.S., and is considered to have a moment magnitude in the range of 6.8 to 7.5 (Bakun and Hopper, 2004b; Johnston, 1996b; Martin and Clough, 1994; Nuttli et al., 1979). Based on the felt intensity reports defining the meizoseismal area (area of maximum damage) and the occurrence of continuing seismic activity (the MPSSZ), the epicentral region of the 1886 earthquake is considered to be centered northwest of Charleston. Recent published and unpublished studies were reviewed during the GG&S hazard evaluation for information on the potential location and extent of the Charleston source and the maximum characteristic earthquake expected to occur on it (see discussion in Section 2.5.1.1.4.3(b)). These studies provide evidence that large magnitude earthquakes have occurred in the vicinity of Charleston more frequently than the seismicity rates specified in the EPRI-SOG (1988) source characterizations. These studies also indicate that the source geometries specified in the EPRI-SOG evaluation do not adequately capture the full range of possible source geometries. An updated source characterization logic tree for

repeating large magnitude Charleston earthquakes based on these new data is presented in Figure 2.5.2-35, and the basis for the alternative characterizations is described as follows.

#### **(a.) Charleston Earthquake Source Geometry**

The Charleston earthquake sources proposed in the EPRI-SOG evaluation (1988; Figures 2.5.2-4 through 2.5.2-9) generally are centered on the meizoseismal area of the Charleston earthquake, with some zones extending northwest into central South Carolina and southeast, offshore of Charleston. Based on new information regarding the timing and distribution of paleoliquefaction in the South Carolina Coastal Plain (Figure 2.5.1-33), the LLNL TIP (Savy et al., 2002) interpretations limit the location of the Charleston source to the coastal plain area, or along the ZRA-S (Figure 2.5.2-10). The preferred alternative in the LLNL TIP study is for a localized source zone centered on the meizoseismal area and the Woodstock fault. The LLNL TIP model also includes an alternative rectangular zone that extends along the ZRA-S (Figures 2.5.2-10 and 2.5.2-14). The 2002 USGS source characterization considers both a regional source zone and a local source zone centered on the Woodstock fault and the southern part of the ZRA-S (Figure 2.5.2-11). Both alternatives are given equal weight (Frankel et al., 2002).

Given the various interpretations and models reported in the recent literature for the location/extent of the source for the Charleston earthquake and other paleoearthquakes in coastal South Carolina, and for the location of a buried, potentially active fault system in South Carolina, this GG&S study considers a range of models that encompass the likely extent of the Charleston-type source(s). Two approaches are used to locate the occurrence of Charleston-type earthquakes. The first approach (the fault source approach) considers the geologic features or structures identified within the meizoseismal zone of the 1886 earthquake (along with potential extensions of these features beyond the meizoseismal zone), to identify the location of the causative source of the 1886 earthquake and future repeating large magnitude earthquakes. The second approach does not specify a source fault or fault zone for the Charleston-type earthquakes. Instead, the source is constrained to a zone that is defined by the area of strong ground shaking associated with sites of paleoliquefaction.

Several types of data provide constraints on the location and extent of the source fault(s) for Charleston-type earthquakes in the Atlantic Coastal Plain (see discussion in Section 2.5.1.1.4.3(b)). Two general fault sources have been postulated: the Ashley River/Woodstock faults in the meizoseismal area, and the north-northeast-trending zone of river anomalies (and associated faults and linear magnetic anomalies) referred to as the ZRA-S (Figures 2.5.1-30 and 2.5.1-31). The Woodstock fault and a fault zone localized along the southern part of the ZRA-S are included in the GG&S source characterization. The Woodstock fault (and Woodstock lineament) is shown as a solid line in Figure 2.5.2-31. The alternative fault source used in the GG&S study is identical to the USGS local source model (Frankel et al., 2002) that includes the southern part of the ZRA-S in addition to the Woodstock/Ashley River faults. Two other postulated fault sources (the Adams Run and Charleston faults, Figure 2.5.1-30) are located within the general region of the Ashley River and Woodstock faults, but because these sources all are located at approximately the same distance from the Bellefonte Site, these faults were not evaluated as separate/specific sources for repeating Charleston large magnitude earthquakes in the GG&S study. Three

alternative areal source zones are included in the source characterization for the GG&S study. These include the USGS 1996/2002 regional source zone (Frankel et al. 1996, 2002); an areal source zone based on the locations of Mesozoic basins developed by Geomatrix (2004); and a coastal zone defined by the LLNL-TIP study (Savy et al., 2002). The USGS 1996/2002 regional source zone for the Charleston source apparently was defined to include the ZRA-S and most of the paleoliquefaction sites along the South Carolina Coastal Plain. This source zone also encompasses parts of the Mesozoic basins in the coastal plain of South Carolina. The northwest margin of this areal source zone was not associated with any particular structure (Frankel et al., 1996).

The alternative areal source zone that is based on the locations of Mesozoic Basins along the coastal plain region in South Carolina extends southwest to the Georgia border and eastward in the offshore region, compared to the USGS regional source zone. The Mesozoic Basin source zone does not extend as far north as the extent of the ZRA-S (and the USGS regional source zone), but is consistent with the extent of paleoliquefaction features along the South Carolina Coastal Plain.

The third alternative is identical to the LLNL-TIP coastal zone (Savy et al., 2002) (Figure 2.5.2-10), which encompasses the three major centers of paleoliquefaction features identified in the South Carolina Coastal Plain. The centers of paleoliquefaction include one located northeast of Charlestown at Georgetown, one centered at Middleton Place (northwest of Charleston), and one located southwest of Charlestown at Bluffton (Figures 2.5.1-33, 2.5.1.34a, and 2.5.1-34b).

The weights assigned to the alternative source geometries are summarized in the logic tree in Figure 2.5.2-35. The localized fault approach is strongly preferred to the areal source zone approach (weights of 0.67 and 0.33, respectively) based on the presence of potentially active faults in the Middleton Place-Summerville area and geomorphic evidence for Quaternary deformation along the ZRA-S. The Woodstock fault is preferred to the USGS Local Source Zone (ZRA-S) (weights of 0.67 and 0.33, respectively) because of the presence of a known fault in the epicentral region compared to the inferred fault along the ZRA-S. For the areal source zone approach, the USGS regional areal source and Mesozoic Basin areal source are preferred to the TIP coastal plain source (weights of 0.4, 0.4, and 0.2, respectively) because of the distribution of the paleoliquefaction features used to infer a source location is in part a function of the presence of susceptible deposits that are localized along the coast and, therefore, do not provide uniform coverage throughout the region.

#### **(b.) Charleston Source Maximum Magnitude**

Characterization of the source of repeating large earthquakes at Charleston was also performed by applying the concept of characteristic earthquakes. The interpretation of the sizes of prehistoric earthquakes is more uncertain here than at New Madrid, but the interpretations do not suggest that the prehistoric events were much, if any, larger than the 1886 earthquake. Therefore, the maximum (characteristic) earthquake magnitude for the Charleston source is taken as equal to the magnitude of the 1886 Charleston earthquake. Because there are uncertainties regarding the magnitude of this earthquake, published magnitude estimates were used in the GG&S study to develop a maximum earthquake magnitude for the Charleston source (Table 2.5.2-10). Published estimates of the magnitude of the 1886 Charleston earthquake include that of Johnston (1996b), who suggested a

preferred value of  $M 7.3 \pm 0.26$ . This best estimate of  $M 7.3$  is based on a weighted average of magnitude estimates from multiple regression relationships between the area encompassed by individual MMI levels and magnitude. These empirical relationships were developed using intensity and area data collected from eastern North America and SCRs worldwide. Specifically, the best estimate magnitude of  $M 7.3$  is based on multiple regression relationships that maximize use of eastern North American data for MMI levels  $A_{felt}$ ,  $A_{IV}$ ,  $A_V$ ,  $A_{VI}$ , supplemented by worldwide data for MMI levels  $A_{VII}$  and  $A_{VIII}$ . Further, the  $A_{felt}$  relationship was modified to lower the effect of distant outlying reports, and the  $A_{VII}$  and  $A_{VIII}$  relationships were corrected for wedge effects of the coastal plain sediments (Johnston, 1996b; Bollinger et al., 1993).

Earlier magnitude estimates (Bollinger, 1977; Nuttli et al., 1979) gave an  $m_b$  ranging from 6.6 to 6.9. Bollinger (1977) and Nuttli et al. (1979) used similar approaches that relate MMI data to  $m_b$  using intensity attenuation with distance. Bollinger estimated the magnitude as  $m_b 6.8$ , while Nuttli et al. estimated the magnitude as  $m_b 6.6$ . Nuttli (1983) also used a relationship between the area of MMI IV and body-wave magnitude to estimate an  $m_b$  of 6.9 for the Charleston earthquake, concluding that a best estimate of the magnitude based on both techniques was  $m_b 6.7$ . These earlier estimates are represented with a mean value of  $m_b 6.75 \pm 0.15$  (Table 2.5.2-10).

In a new approach to estimating magnitude from MMI, Bakun and Hopper (2004b) developed a method to directly invert intensity observations to moment magnitude  $M$ . They obtained an estimate of  $M 6.9$  (6.4 to 7.2 at the 95 percent confidence level) for the 1886 Charleston earthquake.

An alternative approach for estimating the magnitude of the 1886 earthquake relies on back-calculation of ground motions from paleoliquefaction evidence (Martin and Clough, 1994). In this approach, the threshold  $p_{ga}$  required to cause ground deformation is estimated based on the intersection of the "layer curve effect" and the cyclic stress method for relating the percentage of a source layer that liquefies to the  $p_{ga}$ . Martin and Clough (1994) concluded that the liquefaction evidence was consistent with an earthquake no larger than  $M 7.5$ , and possibly as small as  $M 7.0$ . Their estimate is represented in the GG&S study by a magnitude range of  $M 7.25 \pm 0.25$  (Table 2.5.2-10).

In recent studies of soils that liquefied during paleoearthquakes attributed to the Charleston source, Hu et al. (2002a, b) used the approach of Martin and Clough (1994) to estimate the  $p_{gas}$  due to paleoearthquakes, and estimated magnitudes in the range of  $M 6.8$  to 7.6 for these paleoearthquakes from the  $p_{gas}$ . More recent work by Leon et al. (in press, August 2005) to assess the liquefaction resistance of older soils indicates the preliminary magnitude estimates published by Hu et al. are too high, and that the best estimate magnitude for the largest paleoearthquakes (Events A and C') are in the range of  $M 6.2$  to 7.2 (Table 2.5.1-6).

The previous magnitude estimates were used to evaluate the maximum earthquake for the Charleston source. The estimate by Johnston (1996b) is deemed more reliable than the estimates of Bollinger (1977) and Nuttli et al. (1979), because the relationships used by Johnston were based on revised interpretations of the extent of MMI shaking levels ( $A_{felt}$ ,  $A_{VII}$ ,  $A_{VIII}$ ) for the 1886 earthquake and on larger eastern North American and worldwide data sets. The new estimates from Bakun and Hopper (2004b) also are considered more

reliable than the Nuttli and Bollinger estimates because they are based on larger data sets of MMI estimates. Furthermore, all three of these types of estimates are considered more reliable than the estimates based on liquefaction and paleoliquefaction data. Therefore, the Johnston (1996b) and Bakun and Hopper (2004b) estimates are assigned higher weight (0.25 and 0.35) than the Bollinger and Nuttli et al. estimates (0.2) and the Martin and Clough (1994) and Leon et al. (2005) estimates (0.1 each) (Table 2.5.2-10).

### (c.) Charleston Earthquake Source Recurrence

The spatial distribution of seismically induced liquefaction features along the Atlantic seaboard has been used to assess the location and timing of pre-1886 earthquakes (Talwani and Schaeffer, 2001 and references cited therein).

Talwani and Schaefer (2001) provide two scenarios for the recurrence of earthquakes in the South Carolina Coastal Plain, and Geomatrix (2004) identified an alternative interpretation of one of Talwani's scenarios (Table 2.5.2-11). Scenarios 1 and 2 are based on the existence of one source located in the vicinity of Charleston; Scenario 3 is based on the existence of three sources, including one at Charleston, and one source to the north and one source to the south of Charleston. The paleoliquefaction data show that at least five earthquakes have occurred on the Charleston source. At least two additional earthquakes may have occurred on the northern or southern sources (Talwani and Schaefer, 2001). Alternatively, all the paleoliquefaction features may result from earthquakes occurring on the Charleston source, for a total of six or seven earthquakes on the Charleston source (Table 2.5.2-11).

An important issue in estimating the recurrence interval for moderate to large magnitude earthquakes in South Carolina is the uncertainty in the timing of paleoliquefaction events. Eight or nine earthquakes (that resulted in liquefaction) are interpreted to have occurred in South Carolina based on the ages and one-sigma uncertainties shown in Table 2.5.2-11. Not all of these events necessarily represent different earthquakes at higher confidence levels; thus, the total number of earthquakes may be fewer. Specifically, one, two, or three events may have occurred during the period from 1600 to 2000 ybp. Similarly, one or two events may have occurred around 5000 to 6000 ybp.

Another issue with respect to estimating the recurrence of large magnitude earthquakes in South Carolina is the interval during which the record of paleoliquefaction is considered to be complete. The potential for liquefaction varies in response to the changes in groundwater levels along the coastal plain. Specifically, as groundwater levels are thought to have risen in response to the Holocene rise in sea level, the potential for liquefaction has increased during the Holocene (Amick and Gelinas, 1991; Talwani and Schaefer, 2001).

Data summarized in Talwani and Schaefer (2001) indicates that worldwide, sea level was 10 meters below present msl prior to about 6000 ybp, and was even lower prior to that time, such that liquefaction likely could not have occurred in sediments at the ground surface prior to 6000 ybp. Locally, along the South Carolina and Georgia coast, msl rose to a high stand of about -3 meters to -1 meters msl from ~5300 to 3500 ybp, falling to about -3 to -6 meters msl from ~3500 to 2000 ybp, and then rising to present msl. When groundwater levels were lower, liquefaction may not have occurred during large magnitude earthquakes. Thus, even if large magnitude earthquakes occurred, they may not be represented by paleoliquefaction features, and the paleoseismic record would be incomplete for periods of

lower groundwater levels (Amick and Gelinis, 1991; Talwani and Schaefer, 2001). Talwani and Shaefer conclude that the paleoseismic record may be considered complete only for the past 2,000 years.

Based on review of the dates of paleoliquefaction events (Talwani and Schaeffer, 2001; Crone and Wheeler, 2000), the paleoliquefaction record likely is complete only for the past 2,000 years. Because the paleoseismic record does not appear to be complete for the period between 5800 and 2000 ybp, the recurrence intervals between older paleoliquefaction events likely is not representative of the recurrence times between paleoseismic events at Charleston. Therefore, for the recurrence assessment, two estimates are used for the completeness period for repeating large magnitude Charleston earthquakes, 2,000 years (weight of 0.9) and 6,000 years (weight of 0.1).

The recurrence scenarios are based on the time intervals between earthquakes in each model. For Scenarios 1 and 2, all of the paleoliquefaction is assumed to result from earthquakes occurring on the Charleston source, and the Charleston source is constrained to lie within the Charleston source zone. No separate northern or southern earthquake sources for the observed paleoliquefaction exist in these scenarios. The following paragraphs describe the event intervals for the shorter completeness period of 2,000 years.

For Scenario 1 in Table 2.5.2-11, the paleoliquefaction events that occurred at 1648 ybp and 1966 ybp (Events C and D) are assumed to represent two earthquakes on the Charleston source. Thus, there are four recurrence intervals for Charleston earthquakes in this scenario. The mean recurrence interval for Scenario 1 is 493 years. Because this scenario is not completely consistent with the observed distribution of paleoliquefaction sites for these two events, a low weight of 0.2 is assigned to Scenario 1.

For Scenario 2 in Table 2.5.2-11, only one paleoliquefaction event is assumed to have occurred in the period from 1600 ybp to 2000 ybp; this event occurred at 1683 ybp. Thus, there are three recurrence intervals for Charleston earthquakes in this scenario. This scenario is consistent with Scenario 2 as proposed by Talwani and Schaefer (2001). The mean recurrence interval for Scenario 2 is 562 years. This scenario is assigned a weight of 0.3 because the combined distribution of paleoliquefaction sites for this Event (C<sup>1</sup>) is generally similar to the distribution of paleoliquefaction sites for Charleston Events A, B, and E.

For Scenario 3, the paleoliquefaction observed to the north at Georgetown and dated at about 1648 ybp is assumed to have resulted from an earthquake on a northern source. In addition, the paleoliquefaction observed to the south near Bluffton and dated at 1966 ybp is assumed to have resulted from an earthquake on a southern source. Thus, for this scenario, no earthquakes occur on the Charleston source at 1648 ybp and 1966 ybp. This scenario is consistent with Scenario 1 as proposed by Talwani and Schaefer (2001). The annual frequency of earthquakes is based on the number of earthquakes estimated to have occurred during the past 2,000 years.

In Scenario 3, three earthquakes are interpreted to have occurred on the Charleston source (1886, 546 ybp, and 1021 ybp) during the past 2,000 years. There are two complete recurrence intervals (433 years and 475 years) and one incomplete recurrence interval in this scenario. Because the earthquake record (for earthquakes large enough to have caused

liquefaction) is assumed to be complete for the past 2,000 years, the minimum time interval between the earthquake at 1021 ybp and the previous earthquake is about 1,000 years. It is necessary to develop an estimate of this time interval to account for the observation that no earthquake occurred at Charleston for a minimum time interval of 1,000 years.

The timing of the earthquake that occurred prior to the 1021 ybp earthquake is constrained to the period from 2000 ybp to 3548 ybp because the paleoliquefaction record is assumed to be complete for the past 2,000 years and because the next known (older) paleoearthquake occurred at approximately 3548 ybp (Table 2.5.2-11). A series of 10 possible dates at 180-year intervals between 2000 and 3600 ybp was selected to estimate the duration of the time interval between the 1021 ybp earthquake and the previous earthquake. The resulting distribution for the third time interval is combined with the two measured recurrence intervals (433 and 475 years) to estimate the annual frequency of occurrence of the characteristic earthquake. The mean recurrence interval for Scenario 3 is 513 years. Scenario 3 is favored by Talwani and Schaefer (2001, their Scenario 1); thus, this scenario is assigned a weight of 0.5 (Table 2.5.2-11).

For the alternative completeness period of 6,000 years, additional paleoearthquake recurrence intervals between events at 3548, 5038, and 5800 ybp are included in Scenarios 1 and 2, and intervals for events at 3548 and 5800 ybp are included in Scenario 3.

Only one paleoliquefaction event can be attributed to the potential northern earthquake source and to the potential southern earthquake source during the past 5,800 years; therefore, the frequency of earthquakes on these sources is much lower than for the Charleston source. Because the distribution of paleoliquefaction sites is much more limited for a potential northern and southern source, Talwani and Schaefer (2001) infer that the magnitude for these earthquakes is significantly smaller ( $\sim M 6$ ) than the magnitude for the Charleston source ( $\sim M 7$ ). Alternatively, the limited distribution of paleoliquefaction features could result from a more distant large magnitude earthquake. This alternative source location is included in the GG&S source model through the regional source zone approach (e.g., Mesozoic Basin source zone; Figure 2.5.2-31). Based on the inferred smaller magnitude and lack of multiple events, additional explicit northern and southern source areas for the second model are not included in the GG&S hazard model. For this interpretation, modeling of recurrence based on seismicity in the Atlantic Coastal Plain adequately represents the recurrence of earthquakes at Bluffton and Georgetown.

The distribution of mean repeat times for repeating large magnitude Charleston earthquakes was developed using the process described in Section 2.5.2.4.4.1 for the repeating large magnitude New Madrid earthquakes. The data for event dates are given in Table 2.5.2-11. Data for prehistoric Event G and later events were used to simulate 10,000 sets of inter-arrival times for Charleston earthquakes. Figure 2.5.2-36 shows the resulting distributions for mean repeat time developed for the six recurrence scenarios given in Table 2.5.2-11. The consideration of the alternative completeness period of  $\sim 6,000$  years leads to longer mean repeat times.

The distributions of mean repeat time for repeating Charleston large magnitude earthquakes were also represented in the hazard analysis by five-point discrete approximations. Table 2.5.2-9 lists the distributions for mean repeat time and the equivalent

Poisson rate obtained using Equation (2.5.2-9) for a time increment of 50 years from the present. The Poisson and renewal recurrence models are again given equal weight, and the three-point discrete distribution for  $\alpha$  developed by the Working Group (2003) was used (Figure 2.5.2-35).

#### 2.5.2.4.4.3 Ground Motion Models

The updated PSHA was conducted using the representation of CEUS ground motions developed by EPRI (2004). Figure 2.5.2-37 shows the logic tree structure defined by EPRI (2004) to represent the uncertainty in the median ground motion relationship and in the aleatory variability about the median (standard deviation in the log of ground motion amplitude). As described in Section 2.5.2.4.2, the EPRI (2004) ground motion model defines four alternative sets of median ground motion models (termed model clusters) to represent the alternative modeling approaches. Three of these ground motion clusters are appropriate for use in assessing the hazard from moderate-sized local earthquakes occurring randomly in source zones and all four are to be used for assessing the hazard from large magnitude earthquakes. The first level of the logic tree shown in Figure 2.5.2-37 shows the weights assigned to the three median cluster models appropriate for local sources. The second level addresses the appropriate ground motion cluster median model to use for large magnitude earthquake sources. For the Bellefonte Site, these sources are the New Madrid and Charleston sources (both those defined in the EPRI-SOG model and the repeating large magnitude earthquake sources added for this analysis). Two alternatives are given, either use of the cluster model used for the local sources or use of the Cluster 4 model. The effect of this logic structure on the PSHA is as follows. Following the branch for Cluster 1 at the first node, two options are available. The first is to also use the Cluster 1 model for the large magnitude sources. The second option is to use Cluster 1 for only the local sources and use Cluster 4 for the large magnitude sources. This same logic is repeated for the branches for Clusters 2 and 3. The rift version of the Cluster 4 model was used for the New Madrid and Charleston sources.

The third level of the logic tree addresses the uncertainty in the median attenuation relationship for each ground motion cluster. This uncertainty is modeled by a three-point discrete distribution with ground motion relationships for the 5<sup>th</sup>, 50<sup>th</sup>, and 95<sup>th</sup> percentiles of the epistemic uncertainty in the median attenuation relationship for each ground motion cluster, as illustrated in Figure 2.5.2-37.

The fourth level of the ground motion logic tree addresses the uncertainty in the model for the aleatory variability in ground motions about the median attenuation relationship. EPRI (2004) represented the uncertainty in the aleatory variability by four alternative models with the weights shown in Figure 2.5.2-37.

The last level of the ground motion logic tree addresses the relationship between body wave magnitude,  $m_b$ , and moment magnitude,  $M$ . This conversion is required because the ground motion models are defined in terms of  $M$ , whereas the EPRI-SOG recurrence rates are defined in terms of  $m_b$ . Conversion between  $m_b$  and  $M$  was handled in the following manner.



The PSHA formulation used in this study for computing the frequency of exceeding a specified ground motion level,  $\nu(z)$ , can be written as:

$$\nu(z) = \lambda(m_0) \int_{m_0}^{m^u} f(m) \left\{ \int_0^{\infty} f(r|m) \cdot P(Z > z|m, r) dr \right\} dm \quad (\text{Eq. 2.5.2-13})$$

where  $\lambda(m_0)$  is the frequency of earthquakes above a minimum magnitude of interest,  $m_0$ ;  $f(m)$  is the probability density for earthquake magnitude between  $m_0$  and the maximum magnitude that can occur,  $m^u$ ;  $f(m|r)$  is the probability density function for distance between the site and the earthquake, which may depend on the earthquake magnitude; and  $P(Z > z|m, r)$  is the conditional probability of exceeding ground motion level  $z$  given the occurrence of an earthquake of magnitude  $m$ , at a distance  $r$  from the site. Equation 2.5.2-13 is applied source by source and the results summed over all sources to produce the total hazard.

The frequency of earthquakes,  $\lambda(m_0)$  and the probability density function  $f(m)$  are obtained from the EPRI-SOG source parameters defined in terms of  $m_b$ . The conditional probability of exceedance,  $P(Z > z|m, r)$ , for a specified value of  $m_b$  is obtained by first converting the  $m_b$  into moment magnitude,  $\mathbf{M}$ , then using one of the EPRI (2004) ground motion models to obtain the median and standard deviation of the ground motion measure  $Z$ . In order to incorporate the uncertainty in the  $m_b$ - $\mathbf{M}$  conversion, three alternative relationships between  $m_b$  and  $\mathbf{M}$  were used in the PSHA. The three relationships are those developed by Atkinson and Boore (1995), Johnston (1996a), and EPRI (1993) (see discussion in Section 2.5.2.4.4.3). These three relationships are commonly used in converting between  $m_b$  and  $\mathbf{M}$  for ground motion estimation. The three relationships were given equal weight in the PSHA. In addition, the characteristic-magnitudes for the repeating earthquakes at New Madrid and Charleston defined previously in terms of  $\mathbf{M}$  were converted to  $m_b$  for use in Equation 2.5.2-13. This conversion was performed using the same three relationships. The two conversions were assumed to be perfectly correlated – that is, when the Atkinson and Boore (1995) relationship is used to convert  $m_b$  to  $\mathbf{M}$  for obtaining the median and standard deviation of the ground motion measure, its inverse is used to convert characteristic magnitudes defined in terms of  $\mathbf{M}$  into  $m_b$ .

The ground motion attenuation relationships presented in EPRI (2004) define distance to the earthquake source in terms of either closest distance to the rupture plane or closest distance to the surface projection of the rupture plane (Joyner-Boore distance). In contrast, the EPRI-SOG seismic source models treat the earthquake ruptures as points in the integration over distance in Equation 2.5.2-13. However, EPRI (2004) provides a set of relationships to convert point-source distance to equivalent Joyner-Boore or rupture distance under the assumption that the orientation of the earthquake rupture (the strike of the fault) is uniformly distributed in azimuth between 0 and 360 degrees. These distance adjustments were used in the updated PSHA for the EPRI-SOG sources. The EPRI (2004) adjustment factors for the random placement of the rupture on the point source location were used because this model imposes the minimum additional information on the EPRI-SOG source interpretations. The EPRI (2004) point-source adjustments include both an adjustment from point-source distance to expected closest or Joyner-Boore distance and an additional

component of aleatory variability to account for the variability in rupture (or Joyner-Boore) distance for a given point-source distance.

#### 2.5.2.4.4.4 PSHA Results

The PSHA update was conducted by combining the hazard from EPRI-SOG seismic sources with updated maximum magnitude distributions as described previously with the hazard from the repeating large magnitude earthquake sources at New Madrid and Charleston. As discussed in Section 2.5.2.4.4.3, the hazard calculations were performed in terms of  $m_b$  magnitudes for earthquake occurrence rates (with conversion to  $M$  for ground motion estimation). Earthquakes occurring within the EPRI-SOG sources were treated as point sources, consistent with the EPRI-SOG evaluation, and the distance adjustment and additional aleatory variability factors discussed in Section 2.5.2.4.4.3 were applied. Repeating large magnitude earthquakes on the central New Madrid faults and in two Charleston fault-specific sources were assumed to rupture the entire fault, and the closest approach of the fault to the site was used as the distance to rupture. The distance adjustment factors of the EPRI (2004) models were not applied in calculating the hazard from these sources because the fault ruptures were specifically defined. As discussed in Section 2.5.2.4.4.1, the large magnitude earthquakes occurring on the central New Madrid faults were treated as clustered events using Equation 2.5.2-12, with rates given by Poisson or renewal models.

Figure 2.5.2-38 shows the hazard results for peak acceleration and 10-Hz and 1-Hz SA. Figure 2.5.2-38 shows the mean hazard curves and the 5<sup>th</sup>, 15<sup>th</sup>, 50<sup>th</sup> (median), 85<sup>th</sup>, and 95<sup>th</sup> fractile hazard curves. For  $p_{ga}$ , the width of the uncertainty distribution for the high frequency hazard is comparable to that obtained in the EPRI-SOG evaluation. For 1-Hz SA, the uncertainty distribution from the updated PSHA is narrower than that obtained in the EPRI-SOG evaluation, primarily because of the change in the characterization of ground motion modeling uncertainty.

Figure 2.5.2-39 shows the relative contributions of the main sources to the mean hazard, respectively. At low peak acceleration and 10-Hz SA levels, the distant repeating New Madrid earthquake source produces hazard comparable to the EPRI-SOG sources. As ground motion level increases, the EPRI-SOG sources become the dominant contributor to hazard for high-frequency ground motions. For 1-Hz SAs, the repeating New Madrid earthquake source is the principal contributor to hazard at nearly all ground motion levels. The source of repeating Charleston earthquakes has a negligible contribution to the hazard for all ground motion measures and levels because these earthquakes are smaller and occur at greater distances compared to the New Madrid earthquakes.

#### 2.5.2.4.4.5 Uniform Hazard Spectra for Rock and Identification of Controlling Earthquakes

PSHA calculations were performed for  $p_{ga}$  and SA at frequencies of 25, 10, 5, 2.5, 1, and 0.5 Hz (spectral periods of 0.04, 0.1, 0.2, 0.4, 1.0, and 2.0 seconds, respectively).

Figure 2.5.2-40 shows the UHS for rock site conditions developed from these results using the ground motion levels for each spectral frequency corresponding to the mean  $10^{-4}$ ,  $5 \times 10^{-5}$ ,

and  $10^{-5}$  annual frequencies of exceedance<sup>7</sup>.  $p_g$  is plotted at a frequency of 100 Hz (a period of 0.01 second).

The magnitude and distance for earthquakes controlling the hazard were identified following the procedure outlined in Appendix C of Regulatory Guide 1.165 (USNRC, 1997). Figure 2.5.2-41 shows the deaggregation of the mean hazard at the four controlling spectral frequencies (1, 2.5, 5, and 10 Hz) for mean exceedance frequencies of  $10^{-4}$  and  $10^{-5}$ .

Table 2.5.2-12 lists the magnitudes and distances for the controlling earthquakes computed for the mean  $10^{-4}$  and mean  $10^{-5}$  hazard. The values for the low-frequency hazard are listed considering only those earthquakes occurring at distances greater than 100 kilometers, consistent with the procedure outlined in Appendix C of Regulatory Guide 1.165 (USNRC, 1997) and with the fact that these earthquakes are the principal contributor to the low-frequency ground motion hazard.

### 2.5.2.5 Seismic Wave Transmission Characteristics of the Site

The conditions at the Bellefonte Site are described in Section 2.5.4.1. The description in this section indicates that the Bellefonte Site is underlain by approximately 5 to 20 feet of residual soils overlying weathered and unweathered limestone bedrock of the Chickamauga Formation. Field investigations indicate that weathered, fractured bedrock is limited to the upper few feet below the residuum at most of the Bellefonte Site, but can be up to 50 feet in thickness in two areas. Below the weathered bedrock, the limestone is generally fresh, hard, and has high shear wave velocity (greater than 9,000 ft/sec). Based on the potential facility design foundation depths and observed site conditions, major safety-related structures can be founded on fresh, hard bedrock. Therefore, the SSE ground motions are developed for a surface outcrop of the unweathered bedrock. Given that the shear wave velocity of this material is consistent with the hard rock site classification used for the EPRI (2004) ground motion model, the PSHA results and UHS developed in Section 2.5.2.4 are considered representative of surface motions on this outcropping material without modification. Under this condition, the rock motions shown in Figure 2.5.2-40 do not have to be modified to account for the effects of local soft rock or soil profiles on seismic wave propagation.

### 2.5.2.6 Safe Shutdown Earthquake Ground Motions

This section presents the development of ground motions for the SSE applicable to the Bellefonte Site. The horizontal SSE spectrum was developed using the approach described in ASCE/SEI Standard 43-05 (ASCE/SEI 2005). The vertical SSE spectrum was developed using vertical/horizontal spectral ratios recommended in McGuire et al. (2001).

#### 2.5.2.6.1 Technical Basis for the Performance-Based Approach to Define the SSE

The starting point for defining the SSE spectrum using the ASCE/SEI Standard 43-05 (ASCE/SEI, 2005) performance-based approach is the mean  $10^{-4}$  uniform hazard response spectrum (UHRS). As outlined in the response to Requests for Additional Information (RAI

<sup>7</sup>  $1.0e-4 = 10^{-4}$ ;  $5.0e-5 = 5 \times 10^{-5}$ ;  $1.0e-5 = 1 \times 10^{-5}$

ID: R7-6) submitted on October 11, 2004, to the USNRC by Exelon Generation Company (Exelon, 2004, p. 14-17), the technical basis for use of the mean  $10^{-4}$  spectrum is as follows.

- The ASCE/SEI Standard follows technical requirements in RG 1.165 except that a performance-based method is used to define the SSE rather than a hazard reference probability of median  $10^{-5}$  per year. For the ASCE/SEI Standard 43-05 approach, the starting ground motion level when scaled by the appropriate design factor results in a site-specific SSE such that the annual probability of unacceptable seismic effects on the plant, measured in terms of seismically induced core damage, is consistent with the risk calculated at nuclear plants in the U.S. designed to current requirements. The SSE spectrum derived using the ASCE/SEI Standard 43-05 is characterized by horizontal and vertical free-field ground motion response spectra at the ground surface.
- The quantitative safety goal of the ASCE/SEI Standard 43-05 is to achieve an annual frequency of seismically induced core damage that is mean  $10^{-5}$  or lower, when conservatively estimated by taking the onset of significant inelastic deformation of SSCs as the measure of unacceptable performance. The quantitative goal is achieved by determining the SSE spectrum amplitude at each structural period, such that SSCs designed to this spectrum using the NRC's SDC and procedures are assured of having a mean annual frequency against loss of function of less than  $10^{-5}$ . This performance goal determination of the SSE is consistent with the overall design objective identified in 10 CFR Part 50, Appendix S, section IV.a.1.ii, which reads:

*The nuclear power plant must be designed so that, if the Safe Shutdown Earthquake Ground Motion occurs, certain structures, systems, and components will remain functional and within applicable stress, strain, and deformation limits.*

- The design amplitude required to achieve this performance goal at each structural period can be calculated starting from the mean  $10^{-4}$  annual probability level of the seismic hazard spectrum in the free field at the ground surface, or from the  $10^{-5}$  annual probability level, or from any intermediate annual probability level. The design factor on the spectrum associated with each of these probability levels would be different, but they all would lead to the same SSE.
- For the ASCE/SEI Standard 43-05 approach, the basis for using the mean  $10^{-5}$  annual frequency of unacceptable performance as an appropriate performance goal for generic models of SSCs is seismic probabilistic risk assessments (PRAs) of existing nuclear power generation plants. A mean  $10^{-5}$  annual frequency of core damage from seismic events corresponds to the safest 50 percent of U.S. nuclear plants where a full seismic PRA has been performed. Table 2.5.2-13 provides these statistics.
- Using the mean  $10^{-5}$  annual frequency of core damage ensures that SSEs for future nuclear plant sites are risk-consistent with the safety performance of existing plants, which the Commission has determined to be adequately safe. The safety performance objective of developing the SSE spectrum is to ensure compliance with the public health and safety standard stated in the first paragraph in 10 CFR 100.23, as given below:

*This section sets forth the principal geologic and seismic considerations that guide the Commission in its evaluations of the suitability of a proposed site and adequacy*

*of the design bases established in consideration of the geologic and seismic characteristics of the proposed site, such that there is a reasonable assurance that a nuclear power plant can be constructed and operated at the proposed site without undue risk to the health and safety of the public ...*

The standard of no undue risk is met by deriving an SSE spectrum that results in a plant that is as safe as the plants currently operating. The results of the seismic PRA analyses summarized previously demonstrate that this objective is satisfied for a mean  $10^{-5}$  annual frequency of core damage.

- The design factor (also referred to as a scaling factor) used within ASCE/SEI Standard 43-05 to scale the mean  $10^{-4}$  spectrum to ensure the  $10^{-5}$  core damage frequency depends only on the hazard curve slope. The recommended design factor is given in Section 4.3 of Appendix B to the EGC ESP SSAR, as well as Section 2.2 of ASCE/SEI Standard 43-05. A similar design factor can also be derived from Equations 7.16 and 7.17 in NUREG/CR-6728 (McGuire et al., 2001). The design factor includes the assumptions that the risk reduction ratio (i.e., the ratio between the frequency of exceedance of the starting amplitude ( $10^{-4}$ ) and the desired mean core damage frequency is 10); that the logarithmic standard deviation of fragility is between 0.3 and 0.6, and that a conservatively assumed High-Confidence of Low Probability of Failure (HCLPF) seismic margin for design of at least 1.0 exists.
- By starting at a specified mean annual hazard probability of  $10^{-4}$  per year and assuming a risk reduction ratio of 10, the derived SSE is risk-equivalent to the average mean seismic CDF value of  $10^{-5}$  given in the table identified previously. The design factor together for the risk reduction ratio of 10 adjusts the SAs at a hazard probability of mean  $10^{-4}$  to achieve a probability ratio consistent with the CDF value of  $10^{-5}$ .

The design response spectrum calculated using ASCE/SEI Standard 43-05 is technically justified, appropriately conservative, and allowed within NRC's existing seismic regulations. Moreover, ASCE/SEI Standard 43-05 provides an SSE with a margin that is explicitly quantified.

### 2.5.2.6.2 Horizontal SSE Spectrum

The first step in developing the SSE horizontal motions is to construct a smooth response spectrum using the approach described in Appendix F of Regulatory Guide 1.165. Mean horizontal response spectra were computed for the controlling earthquakes defined in Table 2.5.2-12 using the extension of the EPRI (2004) ground motion model developed by Geomatrix (2004). These smooth mean response spectra are shown in Figures 2.5.2-42 and 2.5.2-43 for the mean  $10^{-4}$  and  $10^{-5}$  hazard levels, respectively. The smooth spectra for the controlling earthquakes were then scaled up to match the UHS and an envelop spectrum was constructed for each hazard level. These envelop spectra are listed in Table 2.5.2-14.

The ASCE/SEI Standard 43-05 (ASCE/SEI, 2005) approach defines a risk-consistent DRS in terms of the site-specific UHRS as:

$$\text{DRS} = \text{DF} * \text{UHRS}, \quad (\text{Eq. 2.5.2-14})$$

where UHRS is the site-specific UHRS, defined for Seismic SDC-5 at the mean  $10^{-4}$  annual frequency of exceedance, and DF is the Design Factor [called a scale factor (SF) in the terminology of NUREG/CR-6728 (McGuire et al., 2001)] defined based on the slope of the mean hazard curve between  $10^{-4}$  and  $10^{-5}$  mean annual frequency of exceedance. The derived DRS is a uniform risk spectrum that provides a consistent risk against failure across the facility SSCs. The procedure for computing the DRS is as follows.

For each spectral frequency at which the UHRS is defined, a slope factor  $A_R$  is determined from:

$$A_R = \frac{SA_{0.1H_D}}{SA_{H_D}} \quad (\text{Eq. 2.5.2-15})$$

where  $SA_{H_D}$  is the SA at the target mean UHRS exceedance frequency  $H_D$  (i.e.,  $10^{-4}/\text{yr}$ ) and  $SA_{0.1H_D}$  is the SA at  $0.1H_D$  (i.e.,  $10^{-5}/\text{yr}$ ). Then the DF at this spectral frequency is given by:

$$DF = \text{Maximum}(DF_1, DF_2) \quad (\text{Eq. 2.5.2-16})$$

For Seismic Design Category SDC-5, ASCE/SEI Standard 43-05 gives:

$$DF_1 = 1.0 \quad (\text{Eq. 2.5.2-17})$$

and

$$DF_2 = 0.6(A_R)^{0.80} \quad (\text{Eq. 2.5.2-18})$$

The derivation of DF is described in detail in Commentary to ASCE/SEI Standard 43-05.

The starting point for this calculation at a rock site is the smoothed surface rock spectra for  $10^{-4}$  and  $10^{-5}$  mean hazard. These are shown in Figures 2.5.2-42 and 2.5.2-43 and are listed in Table 2.5.2-14. The computation of the horizontal DRS is summarized in the table. The resulting horizontal DRS spectrum for the SSE motions is defined at the 10 spectral frequencies at which the smoothed hazard spectra were defined.

A smooth horizontal SSE spectrum was created using the response spectral shapes for CEUS rock ground motions given in McGuire et al. (2001). In this procedure, a spectral shape was created for the within-100-kilometer controlling earthquake for 5 and 10 Hz motions listed in Table 2.5.2-12. This spectral shape was scaled to the level of the DRS and used to interpolate between the defined DRS values over the frequency range of 5 to 100 Hz. Then a second shape was created for the greater-than-100 kilometer controlling earthquake for 1 and 2.5 Hz motions listed in Table 2.5.2-12. This spectral shape was scaled to the level of the DRS and used to interpolate between the defined DRS values over the frequency range of 0.25 to 2.5 Hz. The resulting smooth horizontal SSE spectrum is listed in Table 2.5.2-15 and is shown in Figure 2.5.2-44.

Dominion (2003) used an alternative approach to develop the SSE spectrum for the North Anna ESP site. Dominion (2003) estimated the effect of recent information on the hazard at the 29 sites used in Appendix B of Regulatory Guide 1.165 (USNRC, 1997) to define the

reference probability of median  $10^{-5}$ . Based on its analysis, Dominion concluded that an appropriate reference probability level for defining SSE ground motions is mean  $5 \times 10^{-5}$ . The USNRC, based on a review of the information provided in Dominion (2003) and their own assessments, accepted the mean  $5 \times 10^{-5}$  hazard level as appropriate for defining SSE ground motions (USNRC, 2005). The SAs corresponding to the mean  $5 \times 10^{-5}$  hazard level at the Bellefonte Site are shown in Figure 2.5.2-40 and are compared to the SSE spectrum developed from the ASCE/SEI 43-05 approach in Figure 2.5.2-44. The two approaches for defining the SSE produce similar ground motion levels.

### 2.5.2.6.3 Vertical SSE Spectrum

The vertical SSE spectrum was developed by using vertical to horizontal (V/H) response spectral ratios. Table 4.5 of McGuire et al. (2001) provides recommended V/H spectral ratios for CEUS rock site conditions. The ratios are given as a function of frequency and horizontal peak acceleration level. The V/H ratios for a peak acceleration range of 0.2 to 0.5g were interpolated to the spectral frequencies used to define the horizontal SSE. The resulting V/H ratios are listed in Table 2.5.2-14, along with the computed vertical motions. The resulting vertical SSE spectrum is listed in Table 2.5.2-15 and is shown in Figure 2.5.2-44.

### 2.5.2.6.4 Comparison with Standard Plant Spectrum

The horizontal SSE spectrum is compared in Figure 2.5.2-42 to the Regulatory Guide 1.60 spectrum scaled to a peak acceleration of 0.3g, which has been used as a standard plant design spectrum. The SSE spectrum exceeds the Regulatory Guide 1.60 shape spectrum for frequencies greater than about 13 Hz and lies well below the Regulatory Guide 1.60 shape spectrum at lower frequencies. The exceedance of the standard spectrum at high frequencies is consistent with exceedances observed at other rock sites (e.g., Dominion, 2003). A previous study by JR Benjamin and Associates and RPK Structural Mechanics Consulting (1993) has addressed the significance of these exceedances. The JR Benjamin and Associates and RPK Structural Mechanics Consulting (1993) study indicates that there are two factors that lead to reduced effectiveness of high frequency motions to adversely affect performance at high frequencies: (1) the increased incoherence of ground motions at frequencies greater than 10 Hz compared to those at lower frequencies; and (2) the capacity of structures and equipment in nuclear power plants to in-elastically absorb small displacements associated with high frequency ground motions without significant effect.

Additional studies are currently (fall 2005) underway at EPRI to further quantify the effects of high frequency spectral values on plant performance. These studies involve development of high-frequency reduction factors, modification to the lower bound earthquake magnitude used in the hazard analysis, resolution of variability of median ground motion model, and quantification of the thresholds of inelastic response at high frequency. Results of this ongoing work will be reviewed and integrated into the development of effective design spectra if TVA proceeds with additional work at the Bellefonte Site.

Table 2.5.2-1. Earthquake Catalogs for the Central and Southeastern U.S. Used in Development of the TVA Dam Safety Earthquake Catalog

Catalog	Reporting Period	Minimum Magnitude ( $m_b$ or $M$ ) <sup>a</sup>	Comments
USGS (National Ground Motion Hazard Mapping Project)	1702 – 2001	3.0	Final independent catalog for CEUS (covers intermountain region and CEUS), from Chuck Mueller at USGS Denver. Documentation is Mueller et al. (1997)
ANSS (USGS/NEIC)	1962 – present (March 1, 2005)	2.5	Entire U.S.; Includes all events from CERI (up through 2005) and SEUSSN (up through 2003)  <a href="http://quake.geo.berkeley.edu/anss/">http://quake.geo.berkeley.edu/anss/</a>
SEUSSN	1698 – 2003	0.0	Southeastern U.S.  <a href="http://www.geol.vt.edu/outreach/vtso/">http://www.geol.vt.edu/outreach/vtso/</a>
CERI	1974 – 2004 (January 1)	0.0	New Madrid Catalog; Central U.S.  <a href="http://folkworm.ceri.memphis.edu/">http://folkworm.ceri.memphis.edu/</a>
EPRI-SOG, 1988	~1627 – 1985		Superseded by NCEER-91.
NCEER-91	1627 – 1985	3.0	Update of EPRI to eliminate non-tectonic events, prepare new magnitude estimates, etc.
NCEER-91 Update	1830 – 1906	3.0	Revisions to NCEER-91 from John Armbruster at Lamont Doherty.  <a href="http://www.ldeo.columbia.edu/~armb/">http://www.ldeo.columbia.edu/~armb/</a>
EPRI 1994 (Johnston et al., 1994)	~1700 – 1992	~4.0	Worldwide catalog. Used moment magnitude estimates for some events of $M \sim 4$ to 5. No additional earthquakes.
Reinbold and Johnston (1987)		~2.0	Appalachian region catalog. Additional earthquakes provided from this catalog by Jeff Munsey.

a. The minimum magnitude indicates the minimum magnitude cut-off used when selecting data for each catalog (e.g., catalog search criteria), or the minimum magnitude of earthquakes in the catalog.



Table 2.5.2-2. New Seismicity Data for the Central and Southeastern U.S. Used in Development of Bellefonte GG&S Earthquake Catalog

<b>Catalog</b>	<b>Reporting Period</b>	<b>Minimum Magnitude (M)</b>	<b>Comments</b>
Metzger et al. (2000)	1826 – 1899	~3.3 (revised to 2.75)	New earthquakes and revisions to magnitudes ( <b>M</b> ) and locations of some earthquakes in the central U.S. (Reelfoot rift region). Some magnitudes and locations modified based on research by J. Munsey.
Bakun et al. (2003), Bakun and Hopper (2004a,b)	1827 – 1938	3.7	Revised locations and magnitudes ( <b>M</b> ) for selected CEUS earthquakes. Some magnitudes and locations modified based on additional data reviewed for this project.
TVA (2005)	1758 – 1923	2.6	New earthquakes identified for southeastern U.S. from available online newspaper and other sources. Data prepared by Jeff Munsey of TVA.
ANSS (USGS/NEIC)	January 1, 2004 – March 1, 2005	2.5	Entire U.S.; Includes data from CERI and SEUSSN (?)  <a href="http://quake.geo.berkeley.edu/anss/">http://quake.geo.berkeley.edu/anss/</a>
CERI	January 1, 2004 – March 1, 2005	0.0	New Madrid Catalog; Central U.S.  <a href="http://folkworm.ceri.memphis.edu/">http://folkworm.ceri.memphis.edu/</a>

Table 2.5.2-3a. Bechtel Seismic Sources

Source	Description	Probability of Activity ( $P_a$ )	Contributed to 99% of EPRI Hazard
<b>Sources Within 200-Mile Radius</b>			
25	New York-Alabama Geopotential Lineament-Tennessee Segment	0.30	Yes
25A	New York-Alabama Geopotential Lineament	0.43	Yes
BZ0	New Madrid Region	1.00	Yes
BZ3	Northern Great Plains Region	1.00	Yes
BZ5	Southern Appalachians Region	1.00	Yes
BZ6	Southern Eastern Craton Region	1.00	Yes
27	Frankfort-Bucyrus Rift Zone	0.2	No
F	SE Appalachians	0.35	No
15	Rosman Fault	0.05	No
24	Bristol block Geopotential Trends	0.25	No
G	NW S. Carolina	0.35	No
32	Kentucky River Fault System	0.35	No
33	Rough Creek-Shawneetown Fault Zone	0.2	No
31	Reelfoot Rift	0.6	No
K	Southern Illinois	0.35	No
BZ4	Atlantic Coastal Region	1.00	No
<b>Sources Beyond 200-Mile Radius</b>			
30	New Madrid	1.00	Yes
H	Charleston Area	0.5	No
N3	Charleston Faults	0.53	No

Source: EPRI-SOG (1988).

Table 2.5.2-3b. Dames and Moore Seismic Sources

Source	Description	Probability of Activity ( $P_a$ )	Contributed to 99% of EPRI Hazard
<b>Sources Within 200-Mile Radius</b>			
4	Appalachian Fold Belt (mutually exclusive with 4A-4D)	0.35	No <sup>a</sup>
4A	Kink in zone that includes seismicity in Eastern Tennessee	0.65	No <sup>a</sup>
8	Eastern Marginal Basin (Default Source Zone for Zones 5, 6, and 7)	0.08	Yes
41	Southern Cratonic Margin (Default Source Zone for Zones 42, 43, and 46)	0.12	Yes
71	Indiana Illinois Block	0.05	Yes
10B	Default Zone (Default for Zones 10 and 11)	0.39	No
10	Nashville Dome	0.30	No
5	East Continent Gravity High	0.3	No
53	Southern Appalachian Mobile Belt	0.26	No
52	Charleston Mesozoic Rift	0.46	No
<b>Sources Beyond 200-Mile Radius</b>			
21	New Madrid Compression Zone	0.75	Yes
54	Charleston Seismic Zone	0.70	Yes

a. This zone was not included in the EPRI (1989) analysis. This source zone was a significant contributor in the Sequoyah and Watts Bar nuclear plant hazard results. The sensitivity of the results at the Bellefonte Site to inclusion of zones 4 and 4A in the analysis are discussed in Section 2.5.2.4.3.

Source: EPRI-SOG (1988).

Table 2.5.2-3c. Law Engineering Seismic Sources

Source	Description	Probability of Activity ( $P_a$ )	Contributed to 99% of EPRI Hazard
<b>Sources Within 200-Mile Radius</b>			
17	Eastern Basement	0.62	Yes
115	Indiana Block	1.00	Yes
217	Eastern Basement (Background)	0.38	No <sup>a</sup>
117	Mississippi Embayment (Background Zone)	1.00	
1	East Continent Gravity High	0.32	No
8	Buried East Coast Mesozoic Basins	0.27	No
38 44	Mafic Plutons	0.43	No
38 45			
107	Eastern Piedmont (Background Zone)	1.00	No
108	Brunswick (Background Zone)	1.00	No
<b>Sources Beyond 200-Mile Radius</b>			
18	Postulated Faults in Reelfoot Rift	1.00	Yes
35	Charleston Seismic Zone	0.45	No

a. This zone was not included in the EPRI (1989) analysis. The sensitivity of the results at the Bellefonte Site to inclusion of zone 217 in the analysis is discussed in Section 2.5.2.4.3.

Source: EPRI-SOG (1988).

Table 2.5-3d. Rondout Associates Seismic Sources

Source	Description	Probability of Activity ( $P_a$ )	Contributed to 99% of EPRI Hazard
<b>Sources Within 200-Mile Radius</b>			
13	Southern NY-AL Lineament	1.0	Yes
25	Southern Appalachians	0.935	Yes
9	Eastern Tennessee	0.988	Yes
26	South Carolina Zone	1.0	Yes
50(C02)	Grenville Crust Background Source	1.0	Yes
5	East Continent Geophysical Anomaly	1.0	No
6	Central Tennessee	0.83	No
48	Tennessee/Illinois/Kentucky Lineament (TIKL) /Central Tennessee	0.874	No
52	Pre-Grenville Precambrian Craton (background)	1.0	No
49	Appalachian Crust (background)	1.0	No
27	Tennessee/Virginia Border	0.989	No
<b>Sources Beyond 200-Mile Radius</b>			
1	New Madrid	1.0	Yes
24	Charleston, SC	1.0	No

Source: EPRI-SOG (1988).

Table 2.5.2-3e. Weston Geophysical Seismic Sources

Source	Description	Probability of Activity ( $P_a$ )	Contributed to 99% of EPRI Hazard
<b>Sources Within 200-Mile Radius</b>			
24	NY-AL Clingman Block	0.9	Yes
103	Southern Appalachian (background source)	1.0	Yes
106	South Central (background source)	1.0	No
104	Southern Coastal Plain (background source)	1.0	No
101	S. Ontario-Ohio-Indiana (background source)	1.0	No
26	South Carolina Seismic Zone (Part of 104)	0.86	No
<b>Sources Beyond 200-Mile Radius</b>			
31	New Madrid	0.95	Yes
32	Reelfoot Rift Zone	1.0	Yes
25	Charleston South Carolina Seismic Zone	0.99	No

Source: EPRI-SOG (1988).

Table 2.5.2-3f. Woodward-Clyde Consultants Seismic Sources

Source	Description	Probability of Activity ( $P_a$ )	Contributed to 99% of EPRI Hazard
<b>Sources Within 200-Mile Radius</b>			
B39	Bellefonte Background Zone	1.0	Yes
31A	Blue Ridge (Combo 4,3 parts)	0.2	Yes
29	Central South Carolina Isostatic Gravity Saddle (Extended)	0.482	Yes
29A	Central South Carolina Isostatic Gravity Saddle (configuration #2)	0.482	
29B	Central South Carolina Isostatic Gravity Saddle (configuration #3)	0.436	
31	Blue Ridge (continuous)	0.2	No
44	New Madrid Loading Volume	0.7	No
<b>Sources Beyond 200-Mile Radius</b>			
40	Central Disturbed Zone of the Reelfoot Rift	0.921	Yes
30	Ashley River and Woodstock Faults	0.438	No

Source: EPRI-SOG (1988).

Table 2.5.2-4. Description of the Minimum Set Zones for the LLNL TIP Study

### Earthquake Source Zone

---

#### 1. General

Savy et al. (2002) present six maps showing the source zones significant to Vogtle and eight showing the source zones for Watts Bar. The maps show the individual zone geometries and the spatial relationships among the zones. The maps are not intended to represent any particular source model scenarios (i.e., particular combinations of the zones); the scenarios are summarized in the logic trees presented in Savy et al. (2002). A summary map showing the major source zone alternative boundaries is presented in Figure 2.5.2.-10.

#### 2. Charleston

- Zone IE is not shown. It coexists with IA and comprises two areas, which are coincident with the NE and SW areas of 1B

#### 3. SC-GA Piedmont /Coastal Plain

- 3A and 3C are exclusive alternatives

3A-2 and 3A-3 represent fuzzy boundary of 3A. Possible combinations are:

(3A-1)

(3A-1) + (3A-2)

(3A-1) + (3A-2) + (3A-3)

- 3B can exist without 3A or 3C
- 3B forms the background to 3A and 3C so the following combinations are possible:

3B

3A, (3B-3A)

3C, (3B-3C)

- Zone 7 forms the background to all Zone 3 alternatives and to Zone 6

#### 4. ETSZ

There are five basic alternative zone definitions for the ETSZ, 4A, 4B, 4C, 4D, and 4E, all of which have the same overall bounding geometry as Zone 4A.

- 4A-2 and 4A-3 represent a fuzzy boundary. Possible combinations are:

(4A-1) + (4A-2) + (4A-3)

(4A-1) + (4A-2)

(4A-1)

- Zone 4B is made up of two areas:

the geometry of 4B-1 is identical to 4A-1

the geometry of 4B-2 is identical to (4A-2) + (4A-3)



- possible combinations are:

(4B-1)

(4B-1 + (4B-2)

- The geometry of Zone 4C is identical to (4A-1) + (4A-2) + (4A-3), within which the sources are defined as eight discrete faults
- The geometry of Zone 4D is identical to (4A-1) + (4A-2) + (4A-3), within which the recurrence rate is inhomogeneous (rate spatial distribution determined by smoothing the seismicity map), rather than homogeneous as in each part of 4A, 4B, and 4E.
- The bounding geometry of Zone 4E is identical to (4A-1) + (4A-2) + (4A-3), but has a graded boundary defined by three cylindrical sources (Bender).

#### 5. Appalachian/Central US

- Zone 5 forms the background to the ETSZ, and comprises three areas. The alternative combinations are:

(5-1), (5-2), (5-3)

(5.1) + (5-2), (5-3)

(5-1), (5-2) + (5-3)

(5-1) - (5-2) + (5-3)

- For all 4A alternative definitions for the ETSZ other than (4A-1) + (4A-2) + (4A-3) and for definition (4B-1), seismicity in the remaining Zone 4 areas [(4A-2) or (4A-2) + (4A-3), (4B-2)] is included in Zone 5.
- The Zone 5 alternatives can exist with or without a small, separate Giles County zone (not shown).

---

Source: Savy et al. (2002).

Table 2.5.2-5. Earthquake Counts for Region within 200 Miles of the Bellefonte Site

		Event Counts within 200 miles of GG&S Site for Time Period:						
Magnitude Interval	Catalog	1625 – 780	1780 - 1860	1860 - 1910	1910 - 1950	1950 – 1975	1975 - March 1985	March 1985 - March 2005
<b>Completeness Region 3</b>								
3.3 ≤ m <sub>b</sub> * < 3.9	<i>P<sup>D</sup>*</i>	N/A**	N/A	0.182	0.489	0.76	1	
	EPRI-SOG	2	0	1	17	13	13	
	GG&S	2	3	27	32	23	17	14
3.9 ≤ m <sub>b</sub> * < 4.5	<i>P<sup>D</sup></i>	N/A	N/A	0.524	1	1	1	
	EPRI-SOG	0	1	5	14	11	2	
	GG&S	0	4	10	7	9	2	3
4.5 ≤ m <sub>b</sub> * < 5.1	<i>P<sup>D</sup></i>	N/A	0.233	0.721	1	1	1	
	EPRI-SOG	0	1	1	2	3	0	
	GG&S	0	0	6	4	2	0	0
5.1 ≤ m <sub>b</sub> * < 5.7	<i>P<sup>D</sup></i>	N/A	0.233	0.964	1	1	1	
	EPRI-SOG	0	0	0	2	0	0	
	GG&S	0	0	1	2	0	0	0
<b>Completeness Region 4</b>								
3.3 ≤ m <sub>b</sub> * < 3.9	<i>P<sup>D</sup></i>	N/A	N/A	0.324	0.749	0.749	1	
	EPRI-SOG	0	0	0	3	0	1	
	GG&S	0	0	4	5	1	0	0
3.9 ≤ m <sub>b</sub> * < 4.5	<i>P<sup>D</sup></i>	N/A	N/A	0.846	1	1	1	
	EPRI-SOG	0	1	1	2	0	0	
	GG&S	0	2	2	0	0	0	0
4.5 ≤ m <sub>b</sub> * < 5.1	<i>P<sup>D</sup></i>	N/A	0.432	1	1	1	1	
	EPRI-SOG	0	1	1	0	0	0	
	GG&S	0	0	1	0	0	0	0
5.1 ≤ m <sub>b</sub> * < 5.7	<i>P<sup>D</sup></i>	N/A	0.723	1	1	1	1	
	EPRI-SOG	0	0	0	0	0	0	
	GG&S	0	0	0	0	0	0	0

\* *P<sup>D</sup>* is probability of detection estimated in EPRI-SOG (1988).

\*\* N/A catalog considered unusable for this time period in EPRI-SOG (1988).

Table 2.5.2-6. Verification of Repeatability of EPRI-(1989) PSHA Results

10 Hz Spectra Velocity (cm/sec)	Mean Exceedance Frequency			15th% Exceedance Frequency			50th% Exceedance Frequency			85th% Exceedance Frequency		
	EPRI-SOG	This Study	% Difference	EPRI-SOG	This Study	% Difference	EPRI-SOG	This Study	% Difference	EPRI-SOG	This Study	% Difference
0.1	2.35E-02	2.39E-02	1.7%	3.84E-03	3.89E-03	1.3%	1.48E-02	1.48E-02	-0.1%	4.56E-02	4.37E-02	-4.3%
1	1.32E-03	1.33E-03	0.5%	1.28E-04	1.32E-04	3.0%	7.66E-04	7.76E-04	1.3%	2.83E-03	2.88E-03	1.9%
2	3.94E-04	4.03E-04	2.3%	3.00E-05	3.16E-05	5.4%	2.24E-04	2.24E-04	0.0%	8.32E-04	8.32E-04	0.0%
5	5.63E-05	5.82E-05	3.4%	6.25E-07	6.17E-07	-1.3%	2.65E-05	2.82E-05	6.3%	1.06E-04	1.10E-04	3.4%
10	8.54E-06	9.09E-06	6.5%	5.55E-09	5.75E-09	3.7%	2.73E-06	2.82E-06	3.2%	1.31E-05	1.45E-05	10.3%
20	8.11E-07	8.61E-07	6.2%	4.00E-10	5.13E-10	28.2%	1.13E-07	1.12E-07	-0.7%	1.06E-06	1.07E-06	1.1%
30	1.56E-07	1.72E-07	10.2%	3.01E-10	0.00E+00	-100.0%	1.10E-08	1.07E-08	-2.5%	1.77E-07	1.74E-07	-1.8%
1 Hz Spectral Velocity (cm/sec)	Mean Exceedance Frequency			15th% Exceedance Frequency			50th% Exceedance Frequency			85th% Exceedance Frequency		
	EPRI-SOG	This Study	% Difference	EPRI-SOG	This Study	% Difference	EPRI-SOG	This Study	% Difference	EPRI-SOG	This Study	% Difference
0.1	3.31E-02	3.43E-02	3.8%	8.45E-03	8.51E-03	0.7%	2.36E-02	2.40E-02	1.7%	5.41E-02	5.62E-02	3.9%
1	3.64E-03	3.68E-03	1.1%	5.23E-04	5.25E-04	0.3%	1.42E-03	1.41E-03	-0.5%	9.52E-03	9.55E-03	0.3%
5	3.77E-04	3.81E-04	1.1%	1.21E-05	1.29E-05	6.4%	4.77E-05	4.79E-05	0.3%	1.07E-03	1.10E-03	2.4%
10	1.16E-04	1.18E-04	1.8%	6.07E-07	7.08E-07	16.6%	7.30E-06	7.59E-06	3.9%	3.49E-04	3.47E-04	-0.7%
20	2.29E-05	2.32E-05	1.1%	7.08E-09	9.12E-09	28.8%	5.66E-07	6.46E-07	14.1%	6.14E-05	6.17E-05	0.4%
40	2.51E-06	2.62E-06	4.3%	3.01E-10	5.13E-10	70.4%	1.26E-08	1.66E-08	31.7%	4.12E-06	4.37E-06	5.9%
70	3.74E-07	3.97E-07	6.0%	3.01E-10	0.00E+00	-100.0%	6.01E-10	1.10E-09	82.4%	2.29E-07	2.75E-07	20.3%

Table 2.5.2-7. Source Contributions to Mean Hazard in EPRI-SOG Seismic Hazard Model

		10 Hz Spectral Velocity				1 Hz Spectral Velocity			
<b>Bechtel</b>									
Source	Mean 10 <sup>-4</sup>	%	Mean 10 <sup>-5</sup>	%	Mean 10 <sup>-4</sup>	%	Mean 10 <sup>-5</sup>	%	
25A <sup>a</sup>	4.23E-06	5.1	1.63E-07	2.7	1.05E-06	1.2	8.97E-08	1.3	
25 <sup>a</sup>	4.77E-06	5.8	1.81E-07	3.1	1.17E-06	1.3	9.90E-08	1.4	
BZ6	3.04E-06	3.7	1.25E-07	2.1	1.14E-06	1.3	9.58E-08	1.3	
BZ5	2.39E-05	28.9	1.19E-06	20.1	1.15E-05	12.8	7.64E-07	10.7	
BZ3 <sup>b</sup>	3.49E-05	42.1	4.04E-06	68.1	5.78E-06	6.4	7.24E-07	10.2	
BZ0	9.23E-06	11.1	2.27E-07	3.8	9.11E-06	10.2	3.73E-07	5.2	
30 <sup>c</sup>	5.36E-07	0.6	1.83E-09	0	5.95E-05	66.4	4.89E-06	68.8	
Total	8.28E-05	100	5.93E-06	100	8.96E-05	100	7.12E-06	100	
<b>Dames and Moore</b>									
Source	Mean 10 <sup>-4</sup>	%	Mean 10 <sup>-5</sup>	%	Mean 10 <sup>-4</sup>	%	Mean 10 <sup>-5</sup>	%	
71	7.95E-08	0.1	1.24E-09	0	1.37E-06	1.5	1.69E-07	1.4	
54	2.07E-11	0	3.56E-15	0	1.65E-07	0.2	9.75E-10	0	
41	4.25E-08	0.1	8.45E-10	0	6.40E-07	0.7	7.17E-08	0.6	
21 <sup>c</sup>	3.45E-07	0.6	1.05E-09	0	4.48E-05	49.5	3.30E-06	27.1	
8	3.80E-07	0.6	3.47E-08	0.6	1.62E-07	0.2	3.65E-08	0.3	
4A <sup>a</sup>	2.76E-05	46.1	1.89E-06	33.9	3.20E-05	35.3	5.89E-06	48.4	
4 <sup>b</sup>	3.08E-05	51.5	3.64E-06	65.4	1.12E-05	12.3	2.23E-06	18.3	
Total	5.98E-05	100	5.57E-06	100	9.06E-05	100	1.22E-05	100	
<b>Law</b>									
Source	Mean 10 <sup>-4</sup>	%	Mean 10 <sup>-5</sup>	%	Mean 10 <sup>-4</sup>	%	Mean 10 <sup>-5</sup>	%	
217	7.76E-07	2.1	9.52E-09	0.5	3.19E-08	0	8.43E-11	0	
18 <sup>c</sup>	3.97E-07	1.1	9.35E-10	0	6.30E-05	76.6	4.25E-06	67.1	
17 <sup>a</sup>	9.90E-06	27.3	5.63E-07	28.1	1.84E-05	22.4	1.96E-06	30.9	
115 <sup>b</sup>	2.51E-05	69.1	1.44E-06	71.6	7.07E-07	0.9	8.73E-09	0.1	
Total	3.63E-05	100	2.01E-06	100	8.23E-05	100	6.34E-06	100	
<b>Rondout</b>									
Source	Mean 10 <sup>-4</sup>	%	Mean 10 <sup>-5</sup>	%	Mean 10 <sup>-4</sup>	%	Mean 10 <sup>-5</sup>	%	
26	4.28E-08	0	1.28E-10	0	1.20E-06	0.8	2.34E-08	0.2	
25 <sup>a</sup>	7.21E-05	57	7.82E-06	52.1	3.77E-05	25.9	6.64E-06	45.8	
13 <sup>b</sup>	5.06E-05	40.1	7.15E-06	47.6	1.47E-05	10.1	2.08E-06	14.3	
9	1.08E-06	0.9	1.20E-08	0.1	4.18E-06	2.9	2.39E-07	1.7	
1 <sup>c</sup>	3.89E-07	0.3	6.73E-10	0	8.70E-05	59.7	4.66E-06	32.1	
50	8.38E-07	0.7	3.81E-08	0.3	4.28E-08	0	8.27E-10	0	
Total	1.26E-04	100	1.50E-05	100	1.46E-04	100	1.45E-05	100	
<b>Woodward-Clyde</b>									
Source	Mean 10 <sup>-4</sup>	%	Mean 10 <sup>-5</sup>	%	Mean 10 <sup>-4</sup>	%	Mean 10 <sup>-5</sup>	%	
40 <sup>c</sup>	7.58E-07	0.8	6.89E-09	0.1	5.21E-05	54.6	5.08E-06	47	
31A <sup>a</sup>	1.82E-05	19.9	1.31E-06	14.2	1.75E-05	18.3	2.84E-06	26.3	
29A <sup>d</sup>	2.50E-08	0	1.78E-10	0	1.74E-06	1.8	1.24E-07	1.1	
29 <sup>d</sup>	5.05E-08	0.1	5.16E-10	0	1.89E-06	2.0	1.78E-07	1.6	
B39 <sup>b</sup>	7.63E-05	83.3	8.26E-06	89	2.62E-05	27.4	3.10E-06	28.7	
Total	9.16E-05	100	9.28E-06	100	9.55E-05	100	1.08E-05	100	
<b>Weston</b>									
Source	Mean 10 <sup>-4</sup>	%	Mean 10 <sup>-5</sup>	%	Mean 10 <sup>-4</sup>	%	Mean 10 <sup>-5</sup>	%	
32 <sup>c</sup>	1.55E-08	0	2.05E-11	0	4.46E-06	4.6	2.00E-07	2.3	
31 <sup>c</sup>	1.22E-07	0.1	1.41E-10	0	3.77E-05	39.2	1.66E-06	19.3	
32/C11	1.62E-08	0	1.83E-11	0	5.21E-06	5.4	1.78E-07	2.1	
24 <sup>a,b</sup>	1.86E-04	92.3	2.11E-05	95.2	4.34E-05	45.2	5.71E-06	66.2	
103/C19	7.63E-06	3.8	3.81E-07	1.7	3.18E-06	3.3	2.59E-07	3	
103/C17	6.95E-06	3.5	6.83E-07	3.1	1.76E-06	1.8	1.95E-07	2.3	
Total	2.01E-04	100	2.22E-05	100	9.61E-05	100	8.63E-06	100	

a. East Tennessee seismic zone sources; b. Host/background sources; c. New Madrid sources; d. Charleston sources

Table 2.5.2-8. Magnitude Distributions for Repeating Large Magnitude New Madrid Earthquakes

Earthquake Rupture Set	Magnitude for Individual Faults (moment magnitude [M])			Weight
	New Madrid South	Reelfoot Thrust	New Madrid North	
1	7.8	7.7	7.5	0.1667
2	7.9	7.8	7.6	0.1667
3	7.6	7.8	7.5	0.25
4	7.2	7.4	7.2	0.0833
5	7.2	7.4	7.0	0.1667
6	7.3	7.5	7.0	0.1667

Table 2.5.2-9 (1 of 7) Earthquake Frequencies for Repeating Large Magnitude Earthquakes

Recurrence Model	Weight	Mean Repeat Time (years)	Equivalent Annual Frequency
New Madrid	0.10108	160	6.26E-03
Poisson	0.24429	259	3.86E-03
	0.30926	407	2.46E-03
	0.24429	685	1.46E-03
	0.10108	1,515	6.60E-04
New Madrid Renewal, $\alpha = 0.3$	0.10108	325	3.32E-03
	0.24429	401	9.96E-04
	0.30926	475	2.67E-04
	0.24429	562	4.98E-05
	0.10108	695	3.22E-06
New Madrid Renewal, $\alpha = 0.5$	0.10108	310	4.87E-03
	0.24429	430	2.19E-03
	0.30926	559	8.81E-04
	0.24429	728	2.49E-04
	0.10108	1,008	2.72E-05
New Madrid Renewal, $\alpha = 0.7$	0.10108	318	4.53E-03
	0.24429	494	2.28E-03
	0.30926	701	1.03E-03
	0.24429	986	3.35E-04
	0.10108	1,484	4.30E-05

Table 2.5.2-9 (2 of 7) Earthquake Frequencies for Repeating Large Magnitude Earthquakes

Recurrence Model	Weight	Mean Repeat Time (years)	Equivalent Annual Frequency
Charleston	0.10108	202	4.96E-03
Scenario 1 Poisson	0.24429	298	3.36E-03
	0.30926	420	2.38E-03
	0.24429	625	1.60E-03
	0.10108	1,111	9.00E-04
	0.10108	353	1.66E-04
Charleston Scenario 1 Renewal, $\alpha = 0.3$	0.24429	418	2.59E-05
	0.30926	476	4.62E-06
	0.24429	541	6.35E-07
	0.10108	635	3.38E-08
	0.10108	337	1.94E-03
Charleston Scenario 1 Renewal, $\alpha = 0.5$	0.24429	435	6.73E-04
	0.30926	532	2.26E-04
	0.24429	650	5.79E-05
	0.10108	833	6.66E-06
	0.10108	341	3.18E-03
Charleston Scenario 1 Renewal, $\alpha = 0.7$	0.24429	479	1.44E-03
	0.30926	627	6.05E-04
	0.24429	817	1.93E-04
	0.10108	1,128	2.86E-05

**Table 2.5.2-9 (3 of 7) Earthquake Frequencies for Repeating Large Magnitude Earthquakes**

<b>Recurrence Model</b>	<b>Weight</b>	<b>Mean Repeat Time (years)</b>	<b>Equivalent Annual Frequency</b>
Charleston	0.10108	202	4.94E-03
Scenario 2 Poisson	0.24429	311	3.22E-03
	0.30926	459	2.18E-03
	0.24429	714	1.40E-03
	0.10108	1,389	7.20E-04
	Charleston Scenario 2 Renewal, $\alpha = 0.3$	0.10108	403
Charleston Scenario 2 Renewal, $\alpha = 0.3$	0.24429	480	4.09E-06
	0.30926	552	4.52E-07
	0.24429	634	3.49E-08
	0.10108	754	7.72E-10
	Charleston Scenario 2 Renewal, $\alpha = 0.5$	0.10108	375
Charleston Scenario 2 Renewal, $\alpha = 0.5$	0.24429	499	3.29E-04
	0.30926	626	7.65E-05
	0.24429	783	1.21E-05
	0.10108	1,031	6.26E-07
	Charleston Scenario 2 Renewal, $\alpha = 0.7$	0.10108	375
Charleston Scenario 2 Renewal, $\alpha = 0.7$	0.24429	553	9.36E-04
	0.30926	750	2.90E-04
	0.24429	1,010	5.92E-05
	0.10108	1,442	4.06E-06



Table 2.5.2-9 (4 of 7) Earthquake Frequencies for Repeating Large Magnitude Earthquakes

Recurrence Model	Weight	Mean Repeat Time (years)	Equivalent Annual Frequency
Charleston	0.10108	151	6.62E-03
Scenario 3 Poisson	0.24429	245	4.08E-03
	0.30926	385	2.60E-03
	0.24429	649	1.54E-03
	0.10108	1,471	6.80E-04
	0.10108	337	2.58E-04
Charleston Scenario 3 Renewal, $\alpha = 0.3$	0.24429	418	2.59E-05
	0.30926	495	2.60E-06
	0.24429	586	1.57E-07
	0.10108	725	1.95E-09
	0.10108	310	2.57E-03
Charleston Scenario 3 Renewal, $\alpha = 0.5$	0.24429	437	6.59E-04
	0.30926	576	1.37E-04
	0.24429	756	1.66E-05
	0.10108	1,052	4.87E-07
	0.10108	312	3.76E-03
Charleston Scenario 3 Renewal, $\alpha = 0.7$	0.24429	495	1.31E-03
	0.30926	714	3.60E-04
	0.24429	1,018	5.63E-05
	0.10108	1,545	2.14E-06

**Table 2.5.2-9 (5 of 7) Earthquake Frequencies for Repeating Large Magnitude Earthquakes**

<b>Recurrence Model</b>	<b>Weight</b>	<b>Mean Repeat Time (years)</b>	<b>Equivalent Annual Frequency</b>
Charleston	0.10108	420	2.38E-03
Scenario 4 Poisson	0.24429	575	1.74E-03
	0.30926	758	1.32E-03
	0.24429	1,020	9.80E-04
	0.10108	1,563	6.40E-04
	Charleston Scenario 4 Renewal, $\alpha = 0.3$	0.10108	583
	0.24429	658	1.64E-08
	0.30926	722	2.14E-09
	0.24429	791	2.36E-10
	0.10108	885	1.14E-11
	Charleston Scenario 4 Renewal, $\alpha = 0.5$	0.10108	565
	0.24429	680	4.07E-05
	0.30926	786	1.17E-05
	0.24429	907	2.76E-06
	0.10108	1,085	3.28E-07
	Charleston Scenario 4 Renewal, $\alpha = 0.7$	0.10108	569
	0.24429	731	3.25E-04
	0.30926	890	1.24E-04
	0.24429	1,080	3.84E-05
	0.10108	1,373	6.24E-06

**Table 2.5.2-9 (6 of 7) Earthquake Frequencies for Repeating Large Magnitude Earthquakes**

<b>Recurrence Model</b>	<b>Weight</b>	<b>Mean Repeat Time (years)</b>	<b>Equivalent Annual Frequency</b>
Charleston	0.10108	463	2.16E-03
Scenario 5 Poisson	0.24429	649	1.54E-03
	0.30926	877	1.14E-03
	0.24429	1,191	8.40E-04
	0.10108	1,923	5.20E-04
	0.10108	696	4.90E-09
Charleston Scenario 5 Renewal, $\alpha = 0.3$	0.24429	783	3.05E-10
	0.30926	859	2.65E-11
	0.24429	942	1.81E-12
	0.10108	1,059	4.05E-14
	0.10108	666	4.80E-05
Charleston Scenario 5 Renewal, $\alpha = 0.5$	0.24429	807	9.08E-06
	0.30926	940	1.86E-06
	0.24429	1,093	2.98E-07
	0.10108	1,320	1.95E-08
	0.10108	666	4.79E-04
Charleston Scenario 5 Renewal, $\alpha = 0.7$	0.24429	869	1.41E-04
	0.30926	1,071	4.06E-05
	0.24429	1,316	8.89E-06
	0.10108	1,694	8.45E-07

**Table 2.5.2-9 (7 of 7) Earthquake Frequencies for Repeating Large Magnitude Earthquakes**

<b>Recurrence Model</b>	<b>Weight</b>	<b>Mean Repeat Time (years)</b>	<b>Equivalent Annual Frequency</b>
Charleston	0.10108	463	2.16E-03
Scenario 6 Poisson	0.24429	649	1.54E-03
	0.30926	877	1.14E-03
	0.24429	1,220	8.20E-04
	0.10108	1,923	5.20E-04
Charleston Scenario 6	0.10108	712	2.95E-09
Renewal, $\alpha = 0.3$	0.24429	801	1.71E-10
	0.30926	880	1.34E-11
	0.24429	967	8.05E-13
	0.10108	1,088	1.58E-14
Charleston Scenario 6	0.10108	682	3.98E-05
Renewal, $\alpha = 0.5$	0.24429	828	7.07E-06
	0.30926	965	1.38E-06
	0.24429	1,124	2.05E-07
	0.10108	1,360	1.21E-08
Charleston Scenario 6	0.10108	682	4.36E-04
Renewal, $\alpha = 0.7$	0.24429	893	1.21E-04
	0.30926	1,103	3.33E-05
	0.24429	1,358	6.85E-06
	0.10108	1,752	5.89E-07

Table 2.5.2-10. Magnitude Comparisons for 1886 Charleston Earthquake in Charleston Region

Reference Source	Approach for Magnitude Estimation	Weight for Approach	Magnitude	Assigned Weighting	Mean Magnitude (M)
Johnston, 1996b	Felt Area for 1886 eq.; based on worldwide database	0.25	<b>M</b> 7.3 ± 0.26	0.185, 0.63, 0.185	7.3
Bollinger, 1977; Nuttli et al., 1979	Intensity distribution for 1886 eq.; based on U.S. data	0.2	$m_b$ 6.75 ± 0.15 (~ <b>M</b> 6.82 ± 0.22) <sup>a</sup>	0.185, 0.63, 0.185	6.8
Martin and Clough, 1994	Liquefaction data from 1886 eq.	0.1	<b>M</b> 7.25 ± 0.25	0.185, 0.63, 0.185	7.25
Bakun and Hopper, 2004a	Intensity data for 1886 eq.; based on U.S. data	0.35	$M_I$ 6.9 <sup>b</sup>		6.9
Leon et al. (August 2005)	Paleoliquefaction data from previous eqs. at/near Charleston <sup>c</sup>	0.1	<b>M</b> 7.0 ± 0.2 <sup>d</sup>	0.185, 0.63, 0.185	7.0
				<b>Weighted Mean</b>	7.06
2002 USGS National Seismic Hazard Mapping Project (Frankel et al., 2002)	Consideration of available magnitude estimates	--	<b>M</b> 6.9, 7.1, 7.3, 7.5	0.2, 0.2, 0.45, 0.15	7.2

a.  $m_b$  to **M** conversion based on Johnston (1996a) and Atkinson and Boore (1995) (equal weight).

b.  $M_I$  – Intensity magnitude is considered equivalent to **M** (Bakun and Hopper, 2004a).

c. **M** – Magnitude based on magnitude bound method and Energy Stress method; assumed equal to **M**.

d. Magnitude based on magnitude estimates for largest paleoearthquakes at Charleston (1886 and Events A and C' in Leon et al., 2005).

Table 2.5.2-11. Recurrence Scenarios for Charleston Repeating Large Magnitude Earthquakes

Paleo-Liquefaction Event <sup>a</sup>	Age (years before 1999 AD) <sup>a</sup>	Year of Event AD (BC)	Recurrence Scenario 1 (0.2) <sup>b</sup>			Recurrence Scenario 2 (0.3) <sup>a</sup>			Recurrence Scenario 3 (0.5) <sup>a</sup>		
			Source	Magnitude (M)	Interval (years) <sup>c</sup>	Source	Magnitude (M)	Interval (years) <sup>c</sup>	Source	Magnitude (M)	Interval (years) <sup>c</sup>
1886 EQ	113	1886	Charleston	7.3 <sup>d</sup>	>119	Charleston	7.3 <sup>d</sup>	>119	Charleston	7.3 <sup>d</sup>	>119
A	546 ± 17	1453	Charleston	7+	433	Charleston	7+	433	Charleston	7+	433
B	1021 ± 30	978	Charleston	7+	475	Charleston	7+	475	Charleston	7+	475
C	1648 ± 74	351	Charleston	7+	627	--	--	--	Northern	6+	?
C <sup>1</sup>	1683 ± 70	316	--	--	--	Charleston	7+	662	--	--	--
D	1966 ± 212	33	Charleston	7+	318	--	--	--	Southern	6+	?
E	3548 ± 66	(1549)	Charleston	7+	1582	Charleston	7+	1865	Charleston	7+	2527
F	5038 ± 166	(3039)	Charleston	7+	1490	Charleston	7+	1490	Northern	6+	?
G	5800 ± 500	(3801)	Charleston	7+	762	Charleston	7+	762	Charleston	7+	2252

a. Data and recurrence scenarios 2 and 3 are from Talwani and Schaeffer (2001).

b. Recurrence Scenario 1 developed by Geomatrix (2004).

c. Recurrence interval is for large magnitude earthquakes on Charleston earthquake source.

d. 1886 magnitude from Johnston (1996b).

Table 2.5.2-12. Controlling Earthquakes

Spectral Frequency	Mean Exceedance Frequency	Distances $\leq$ 100 km			Distances $>$ 100 km		
		% Total	Mean Magnitude ( $m_b$ )	Mean Distance (km)	% Total	Mean Magnitude ( $m_b$ )	Mean Distance (km)
10 Hz	$10^{-4}$	67	5.5	22	33	7.3	350*
	$10^{-5}$	93	5.6	12	7	7.4	350*
5 Hz	$10^{-4}$	47	5.6	22	53	7.3	350*
	$10^{-5}$	79	5.7	14	21	7.4	350*
2.5 Hz	$10^{-4}$	21	5.8	23	79	7.3	350*
	$10^{-5}$	39	5.9	17	61	7.4	350*
1 Hz	$10^{-4}$	6	6.1	30	94	7.3	350*
	$10^{-5}$	11	6.3	25	89	7.4	350*

\* Distance to central New Madrid faults.

Table 2.5.2-13. Mean Seismic CDF for Plants Performing Seismic PRA  
**Table 2.2 from NUREG 1742 (EPRI Results)**

<b>Plant</b>	<b>Mean Seismic CDF</b>
South Texas Project 1 & 2	1.90E-07
Nine Mile Point 2	2.50E-07
La Salle 1 & 2	7.60E-07
Hope Creek	1.06E-06
D.C. Cook 1 & 2	3.20E-06
Salem 1 & 2	4.70E-06
Oyster Creek	4.74E-06
Surry 1 & 2	8.20E-06
Millstone 3	9.10E-06
Beaver Valley 2	1.03E-05
Kewaunee	1.10E-05
McGuire 1 & 2	1.10E-05
Seabrook	1.20E-05
Beaver Valley 1	1.29E-05
Indian Point 2	1.30E-05
Point Beach 1 & 2	1.40E-05
Catawba 1 & 2	1.60E-05
San Onofre 2 & 3	1.70E-05
Columbia (WNP No. 2)	2.10E-05
TMI 1	3.21E-05
Oconee 1, 2, and 3	3.47E-05
Diablo Canyon 1 & 2	4.20E-05
Pilgrim 1	5.80E-05
Indian Point 3	5.90E-05
Haddam Neck	2.30E-04
<b>Median of Mean Seismic CDF Value</b>	<b>1.20E-05</b>
<b>Mean of Mean Seismic CDF Value</b>	<b>2.50E-05</b>



Table 2.5.2-14. Computation of SSE Spectra

Frequency (Hz)	Mean 10 <sup>-4</sup> UHRS (g)	Mean 10 <sup>-5</sup> UHRS (g)	DF2	Horizontal DRS	Horizontal SSE	V/H Ratios	Vertical SSE
100.00	0.1920	0.6408	1.574	0.302	0.302	1.00	0.302
75.00					0.421	1.12	0.471
62.50					0.556	1.14	0.634
50.00	0.4851	1.6658	1.610	0.781	0.781	1.12	0.875
40.00					0.836	1.07	0.894
33.33	0.5251	1.7567	1.577	0.828	0.828	0.97	0.803
25.00	0.5026	1.7020	1.592	0.800	0.800	0.88	0.704
20.00					0.759	0.83	0.630
16.67					0.707	0.80	0.566
13.33					0.627	0.78	0.489
11.11					0.556	0.76	0.422
10.00	0.3455	1.0741	1.487	0.514	0.514	0.75	0.385
9.01					0.486	0.75	0.364
6.67					0.404	0.75	0.303
5.00	0.2603	0.6679	1.275	0.332	0.332	0.75	0.249
4.00					0.293	0.75	0.220
3.33					0.265	0.75	0.199
2.50	0.1956	0.4436	1.155	0.226	0.226	0.75	0.169
2.00					0.205	0.75	0.154
1.67					0.185	0.75	0.139
1.33					0.159	0.75	0.119
1.18					0.144	0.75	0.108
1.00	0.1067	0.2454	1.168	0.125	0.125	0.75	0.093
0.67					0.122	0.75	0.092
0.50	0.0850	0.2440	1.395	0.119	0.119	0.75	0.089
0.33					0.082	0.75	0.062
0.25	0.0437	0.1291	1.428	0.062	0.062	0.75	0.047

Table 2.5.2-15. SSE Spectra (5 percent damping) for the Bellefonte Site

<b>Frequency (Hz)</b>	<b>Horizontal SSE</b>	<b>Vertical SSE</b>
100.00	0.302	0.302
75.00	0.421	0.471
62.50	0.556	0.634
50.00	0.781	0.875
40.00	0.836	0.894
33.33	0.828	0.803
25.00	0.800	0.704
20.00	0.759	0.630
16.67	0.707	0.566
13.33	0.627	0.489
11.11	0.556	0.422
10.00	0.514	0.385
9.01	0.486	0.364
6.67	0.404	0.303
5.00	0.332	0.249
4.00	0.293	0.220
3.33	0.265	0.199
2.50	0.226	0.169
2.00	0.205	0.154
1.67	0.185	0.139
1.33	0.159	0.119
1.18	0.144	0.108
1.00	0.125	0.093
0.67	0.122	0.092
0.50	0.119	0.089
0.33	0.082	0.062
0.25	0.062	0.047

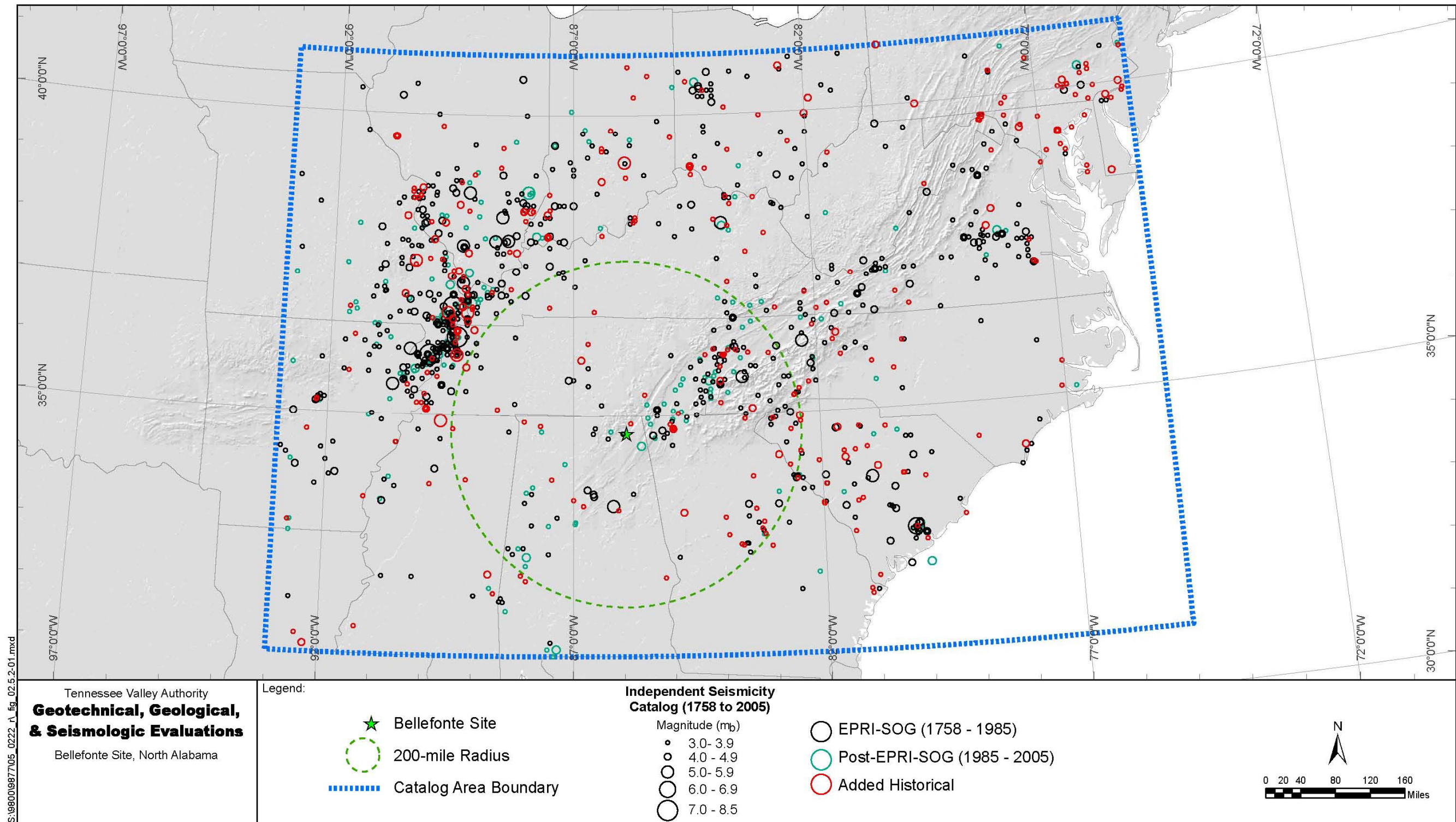


Figure 2.5.2-1. Independent Earthquake Catalog for Study Region (1758-2005)

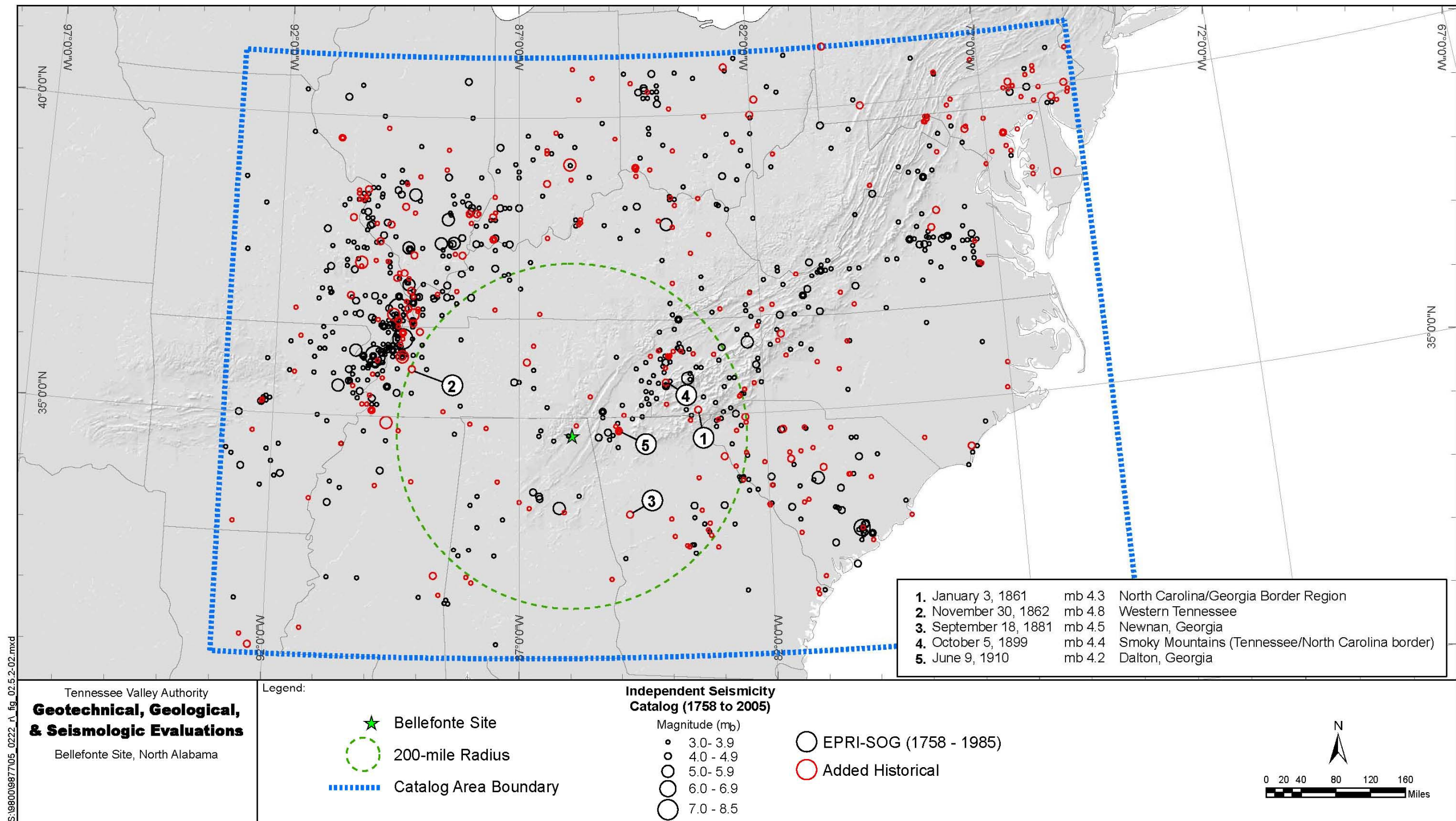


Figure 2.5.2-2. Independent Earthquake Catalog for Study Region Showing EPRI-SOG (1758-1985) and Added Historical Events

S:\9800\987705\_0222\_A\_fig\_02.5.2-02.mxd

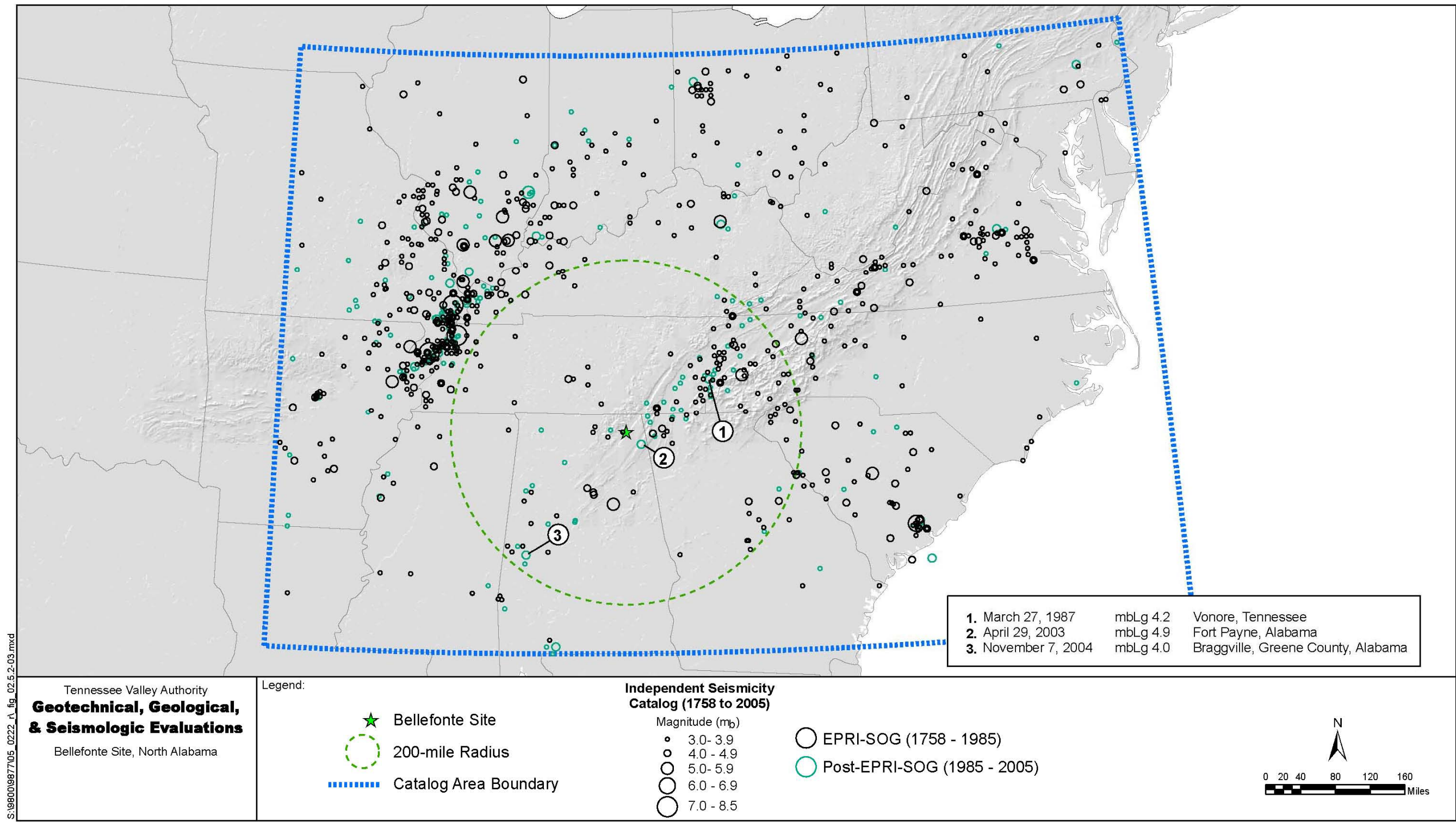


Figure 2.5.2-3. Independent Earthquake Catalog for Study Region Showing EPRI-SOG (1758-1985) and post-EPRI-SOG (1985-2005) Events

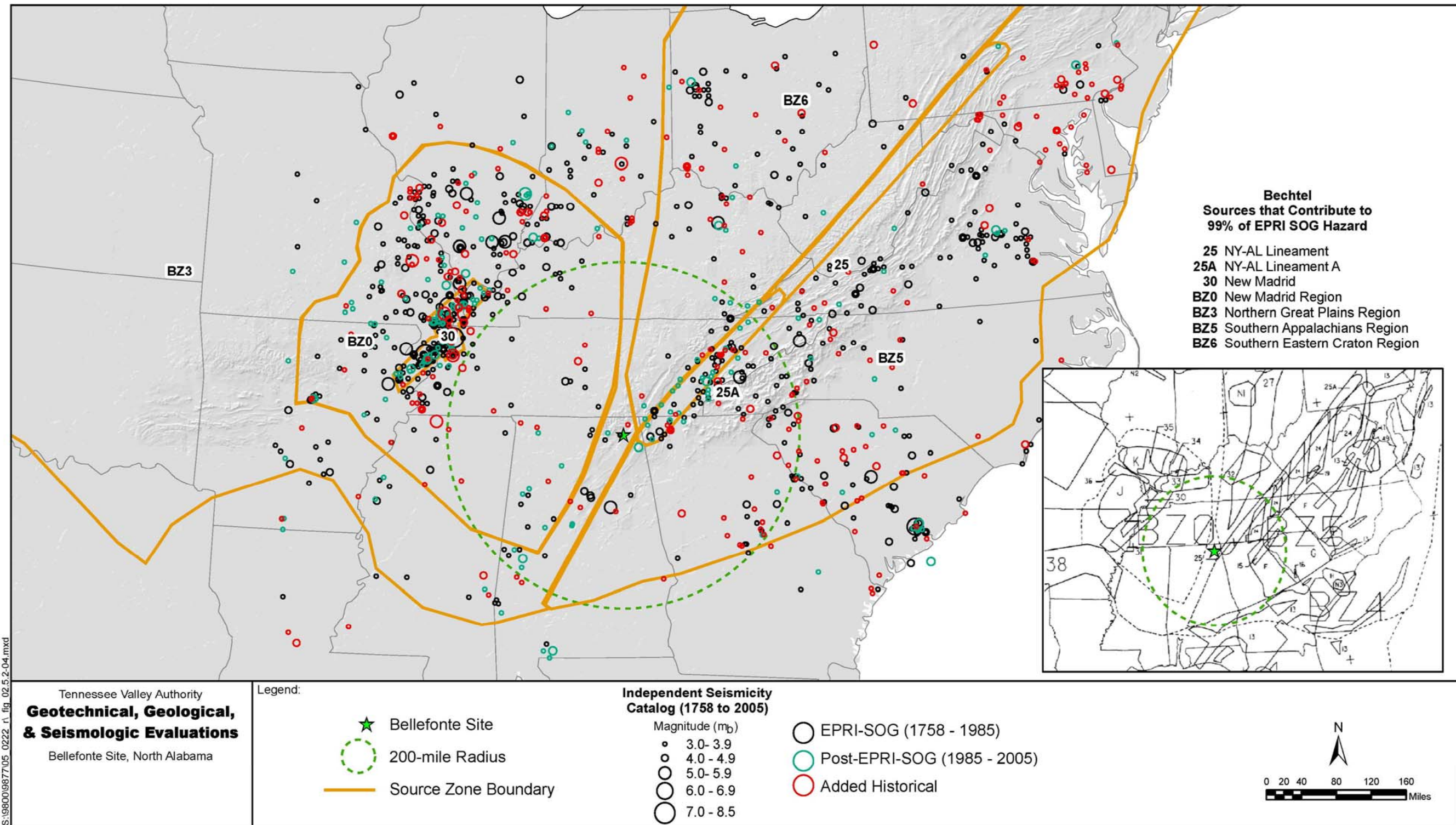


Figure 2.5.2-4. Bechtel EPRI-SOG Source Map

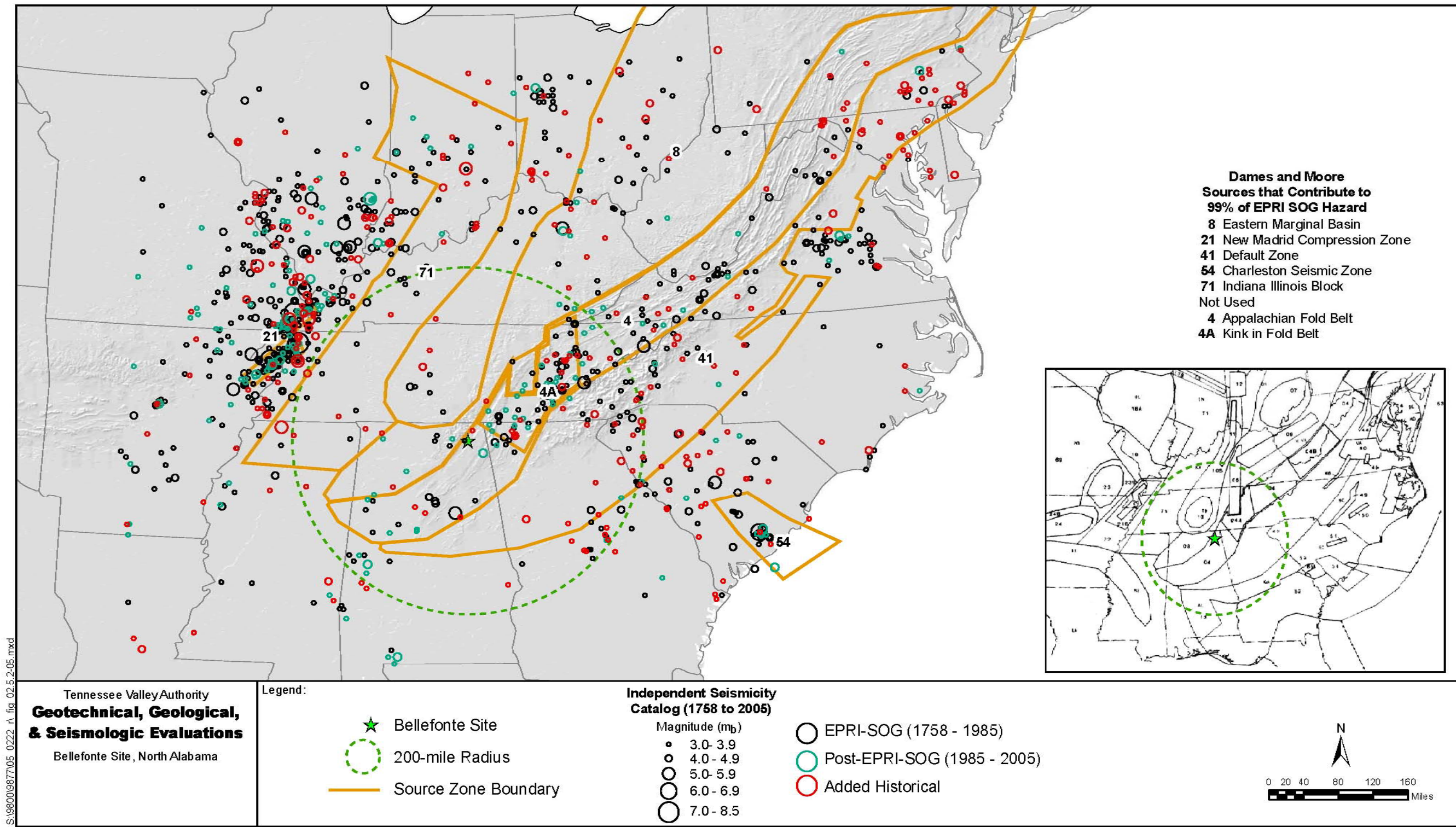


Figure 2.5.2-5. Dames and Moore EPRI-SOG Source Map

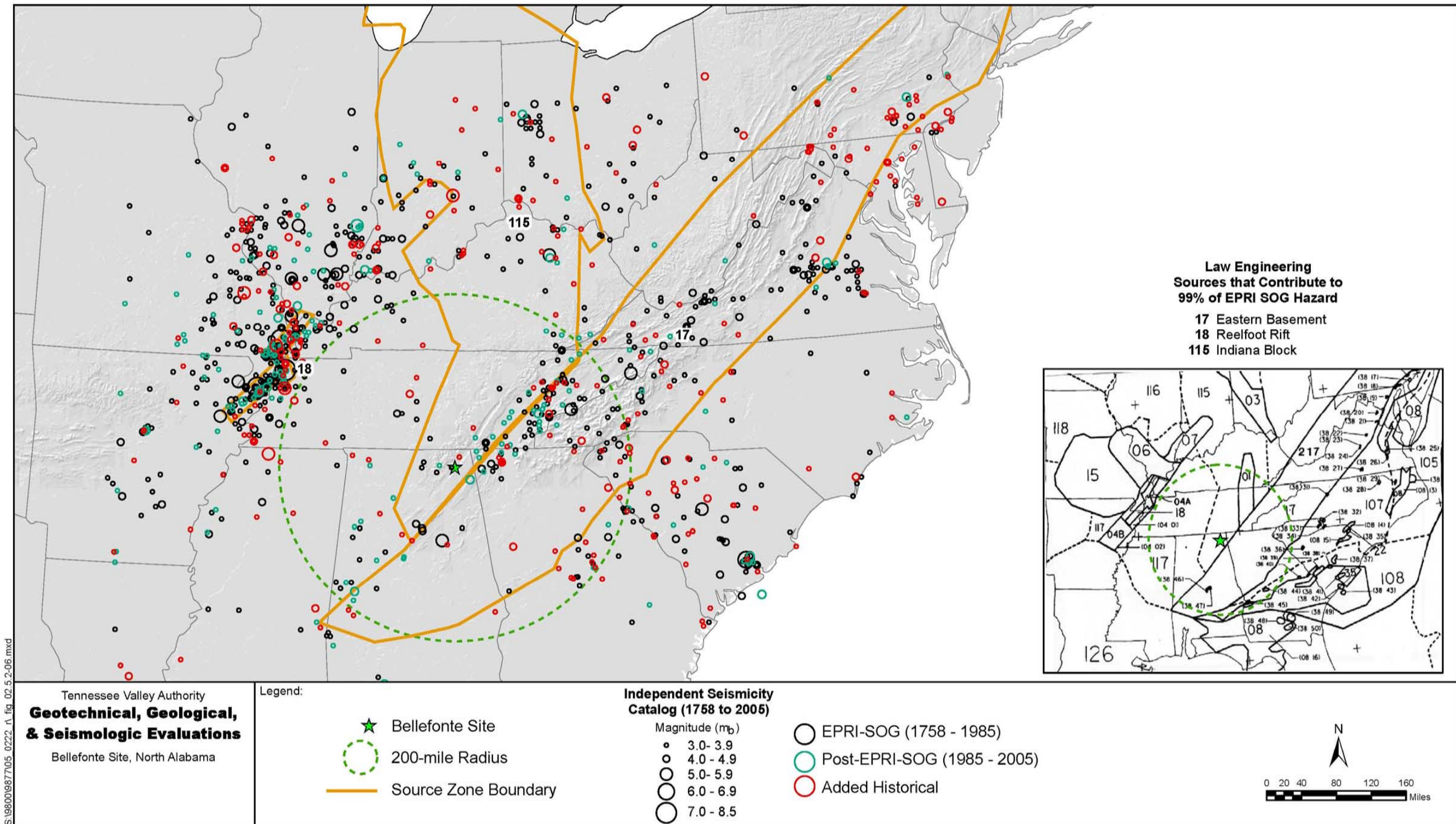


Figure 2.5.2-6. Law Engineering EPRI-SOG Source Map



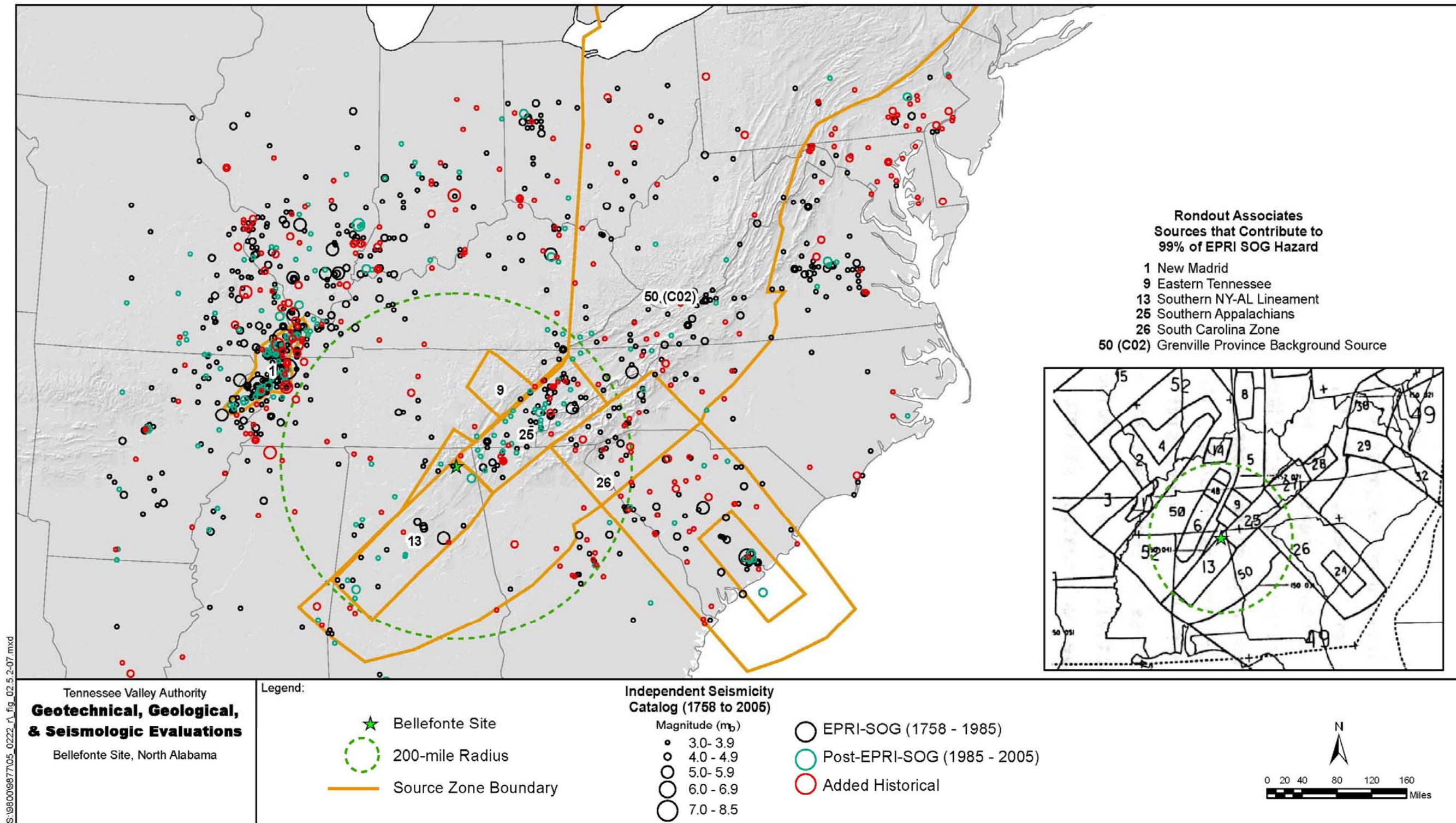


Figure 2.5.2-7. Rondout Associates EPRI-SOG Source Map

S:\98009677\05\_0222\_1\_fig\_02.5.2-07.mxd

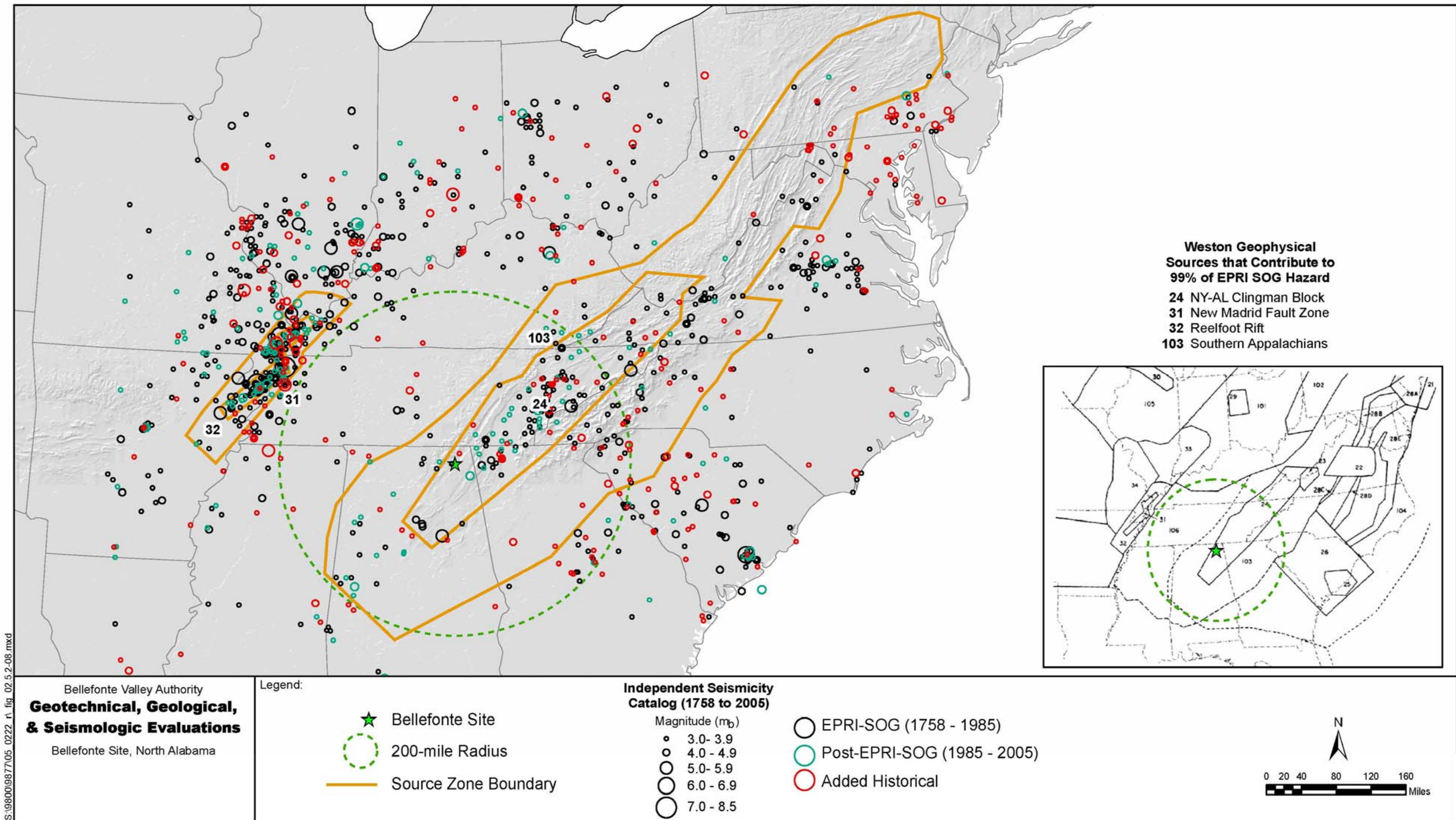


Figure 2.5.2-8. Weston Geophysical EPRI-SOG Source Map

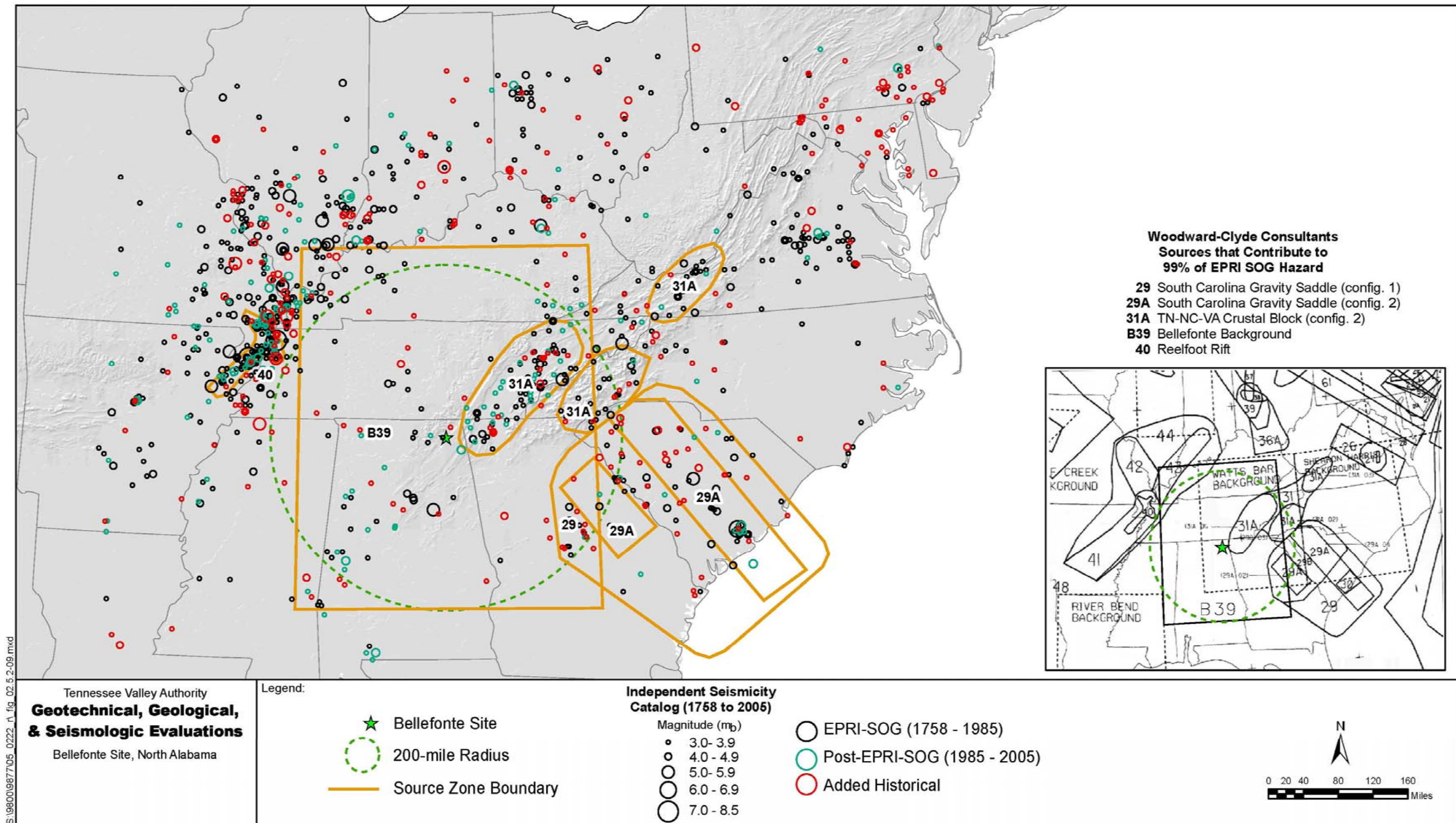
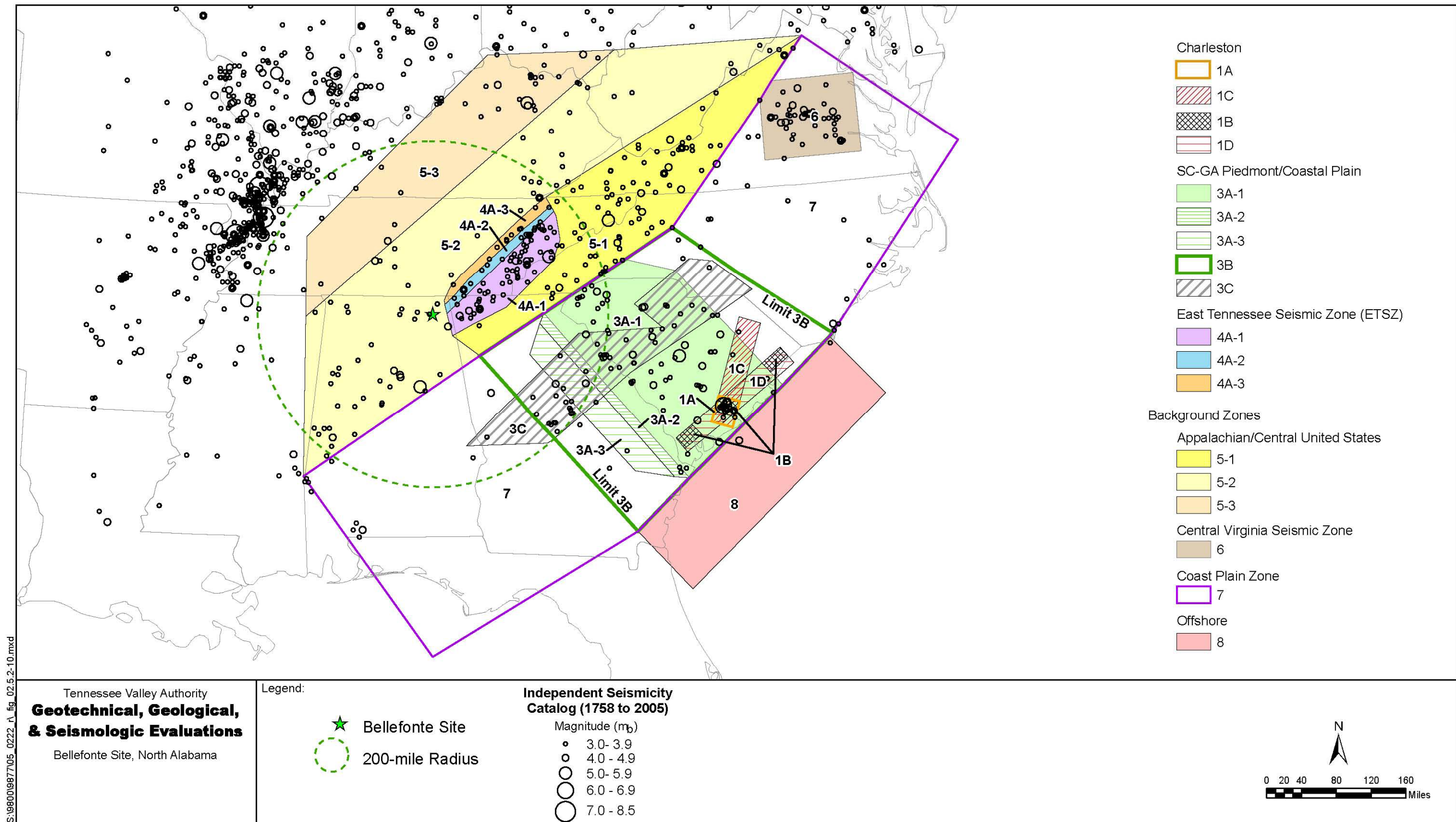


Figure 2.5.2-9. Woodward-Clyde Consultants EPRI-SOG Source Map

S:\1980019877\05\_0222\_r1\_fig\_02.5.2-09.mxd



S:\9800\9877\05\_0222\_r1\_fig\_02.5.2-10.mxd

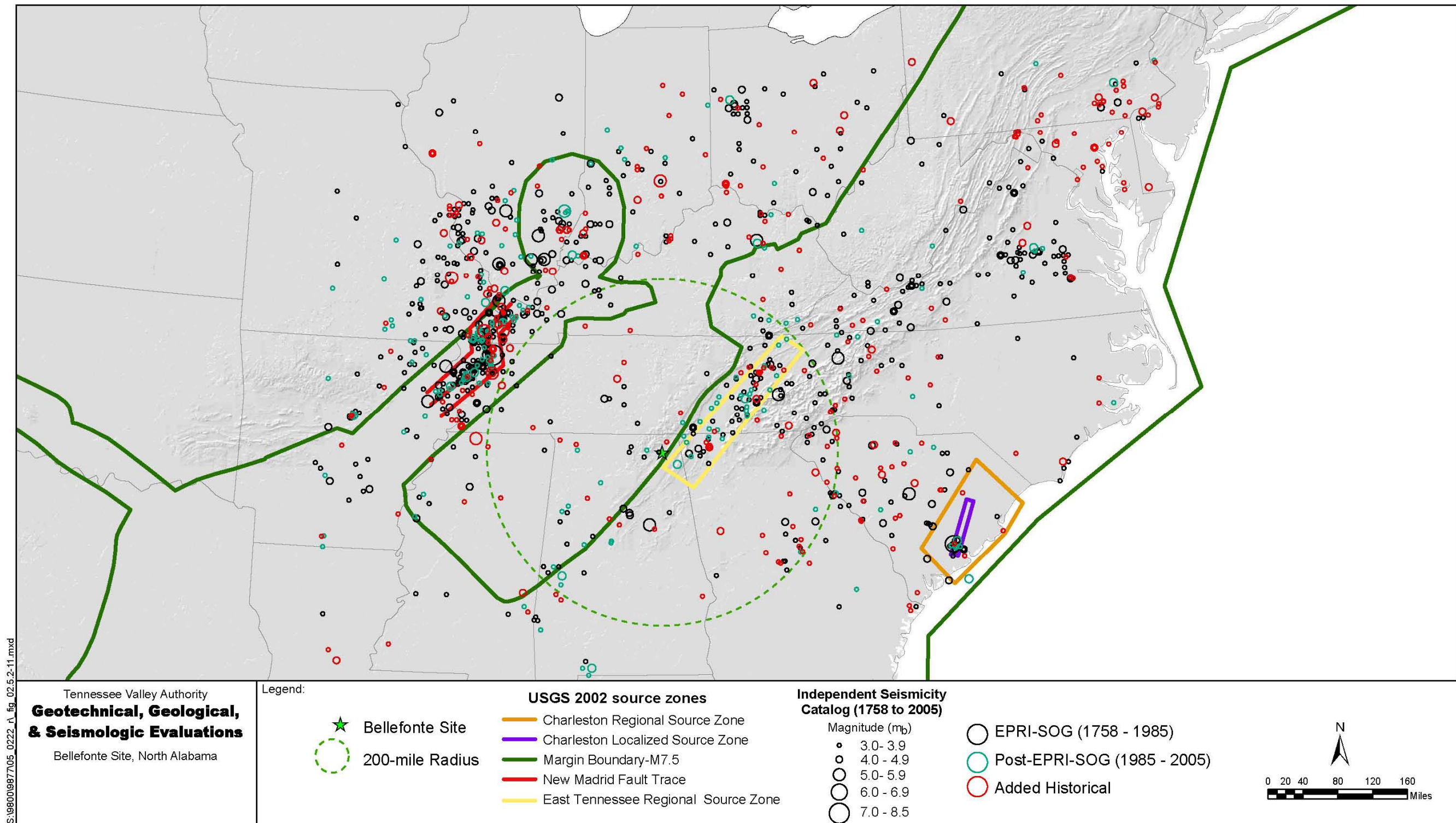


Figure 2.5.2-11. USGS National Seismic Hazard Mapping Project Source Model  
(Frankel et al., 2002)

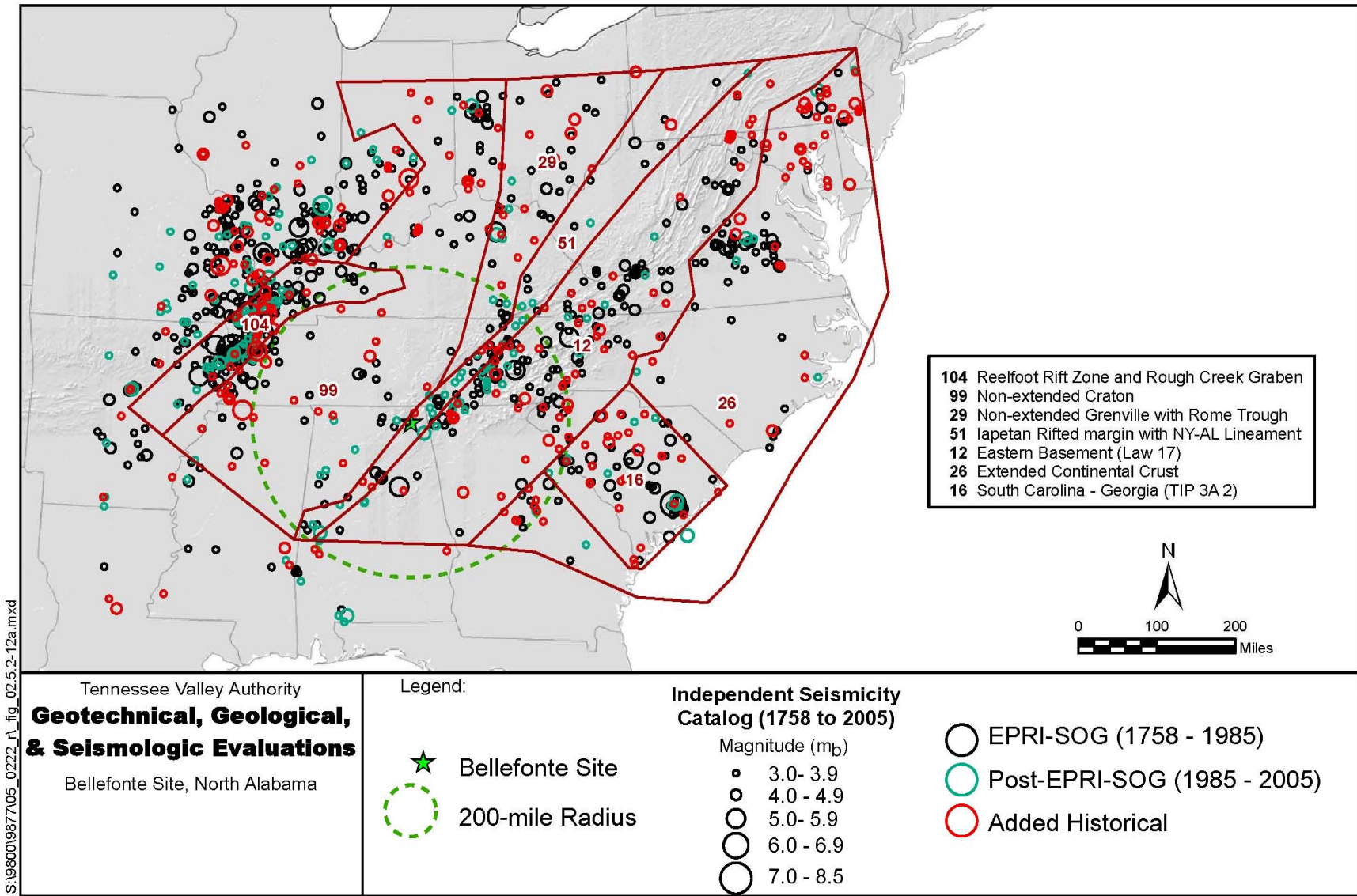


Figure 2.5.2-12(a). TVA Dam Safety Seismic Hazard Analysis Seismotectonic Source Zones (Geomatrix, 2004)

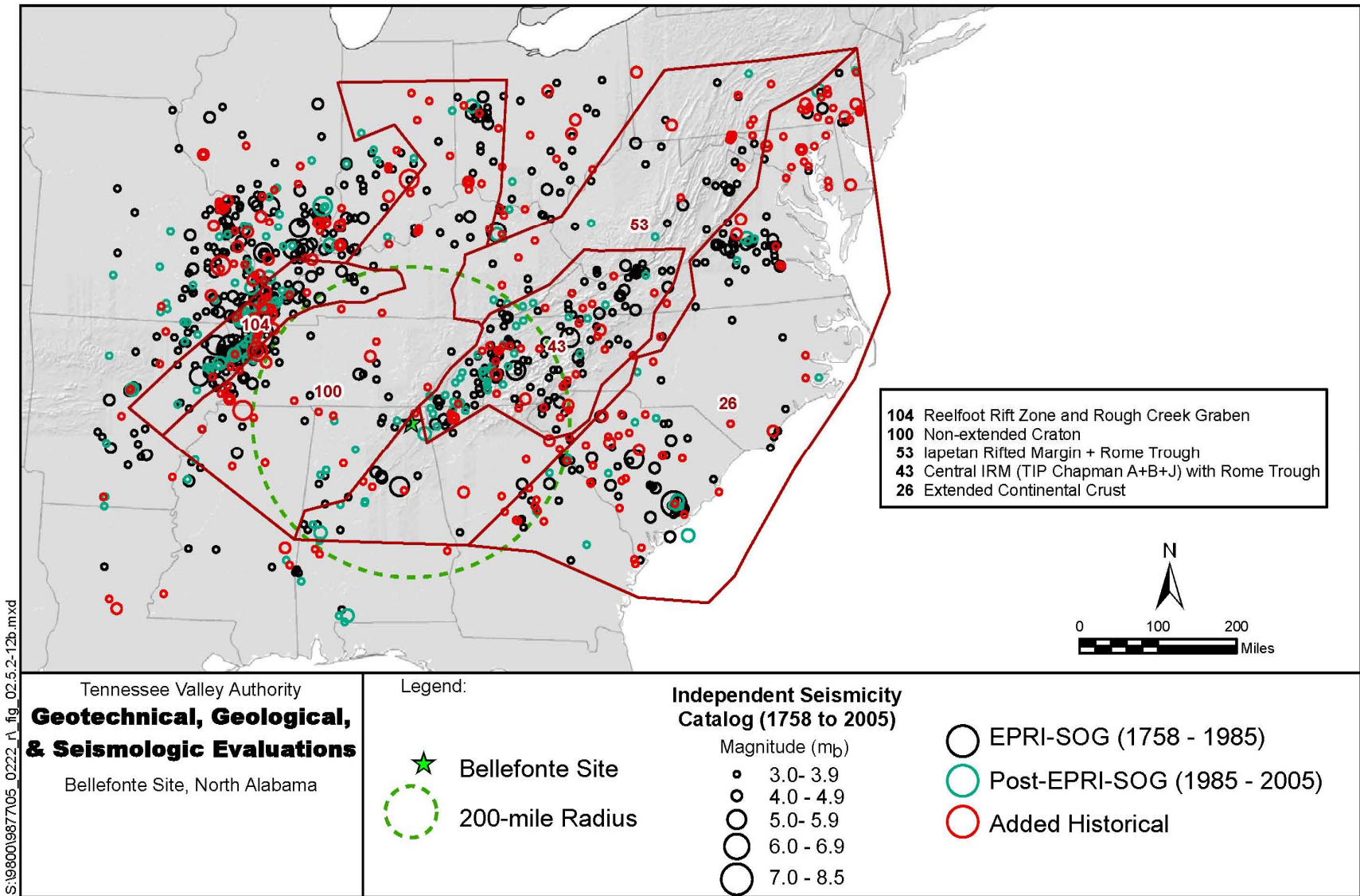


Figure 2.5.2-12(b). TVA Dam Safety Seismic Hazard Analysis Seismotectonic Source Zones (Geomatrix, 2004)

S:\19800\9877\05\_0222\_r1\_fig\_02.5.2-12b.mxd

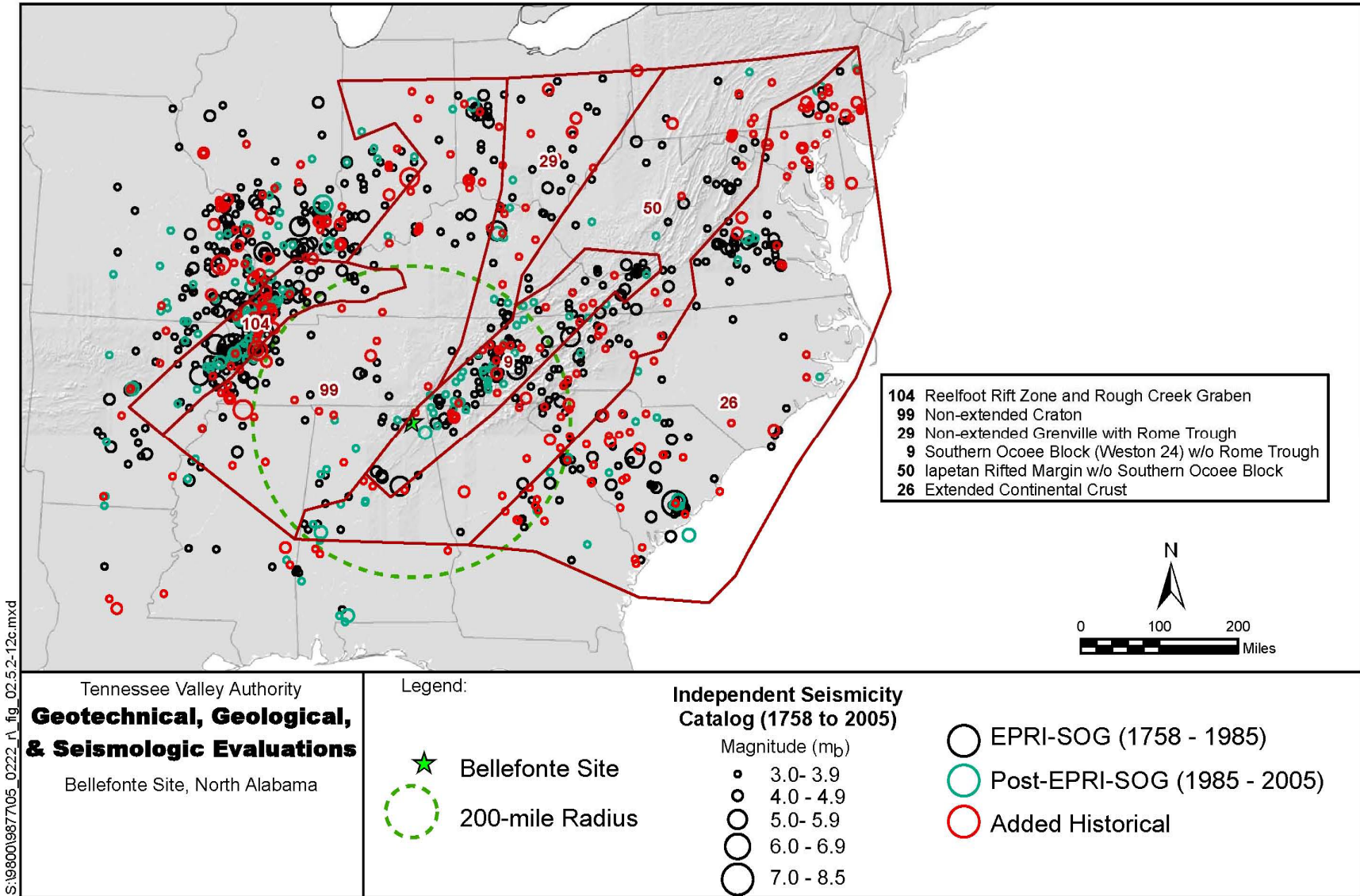


Figure 2.5.2-12(c). TVA Dam Safety Seismic Hazard Analysis Seismotectonic Source Zones (Geomatrix, 2004)



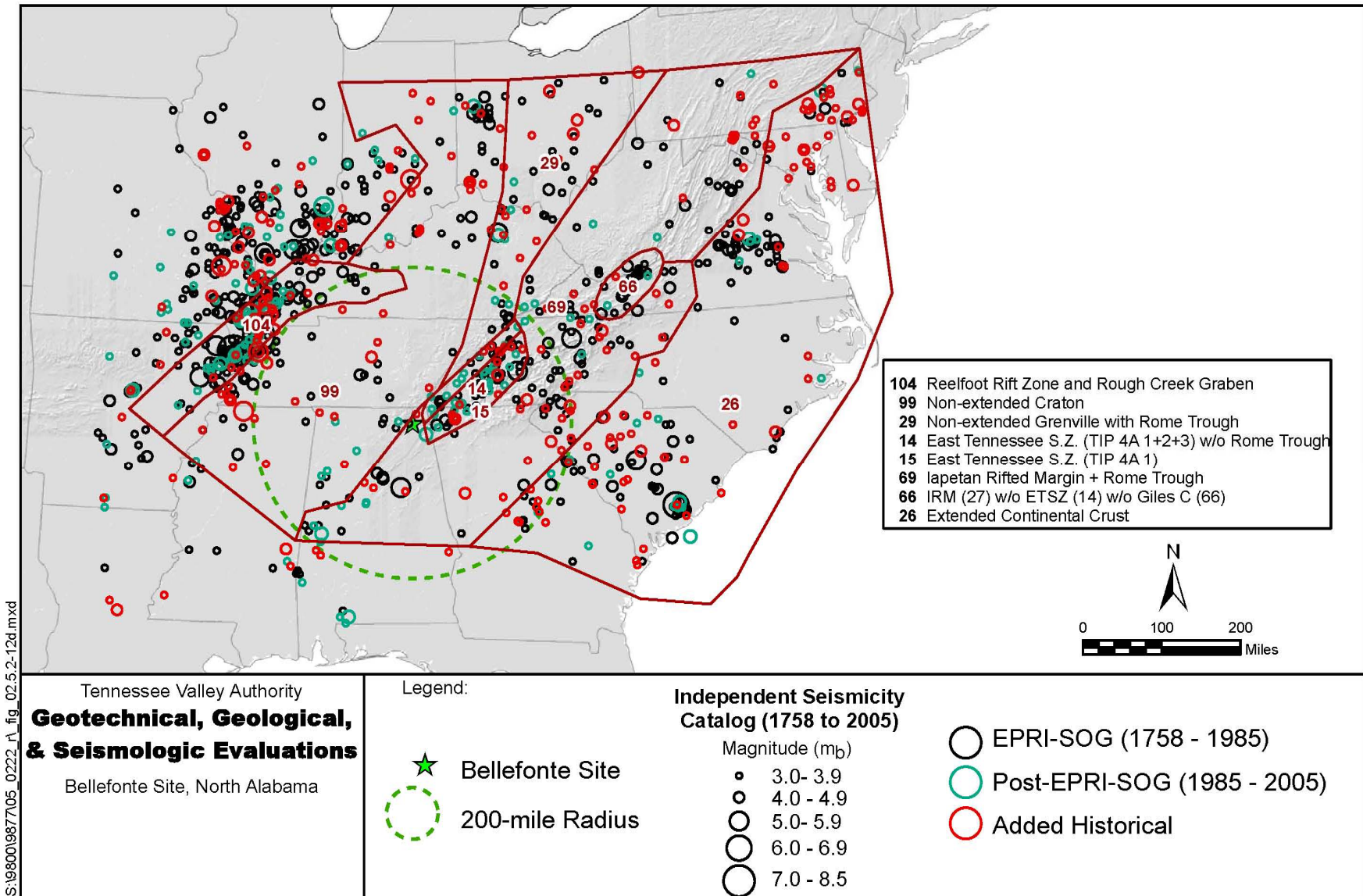


Figure 2.5.2-12(d). TVA Dam Safety Seismic Hazard Analysis Seismotectonic Source Zones (Geomatrix, 2004)

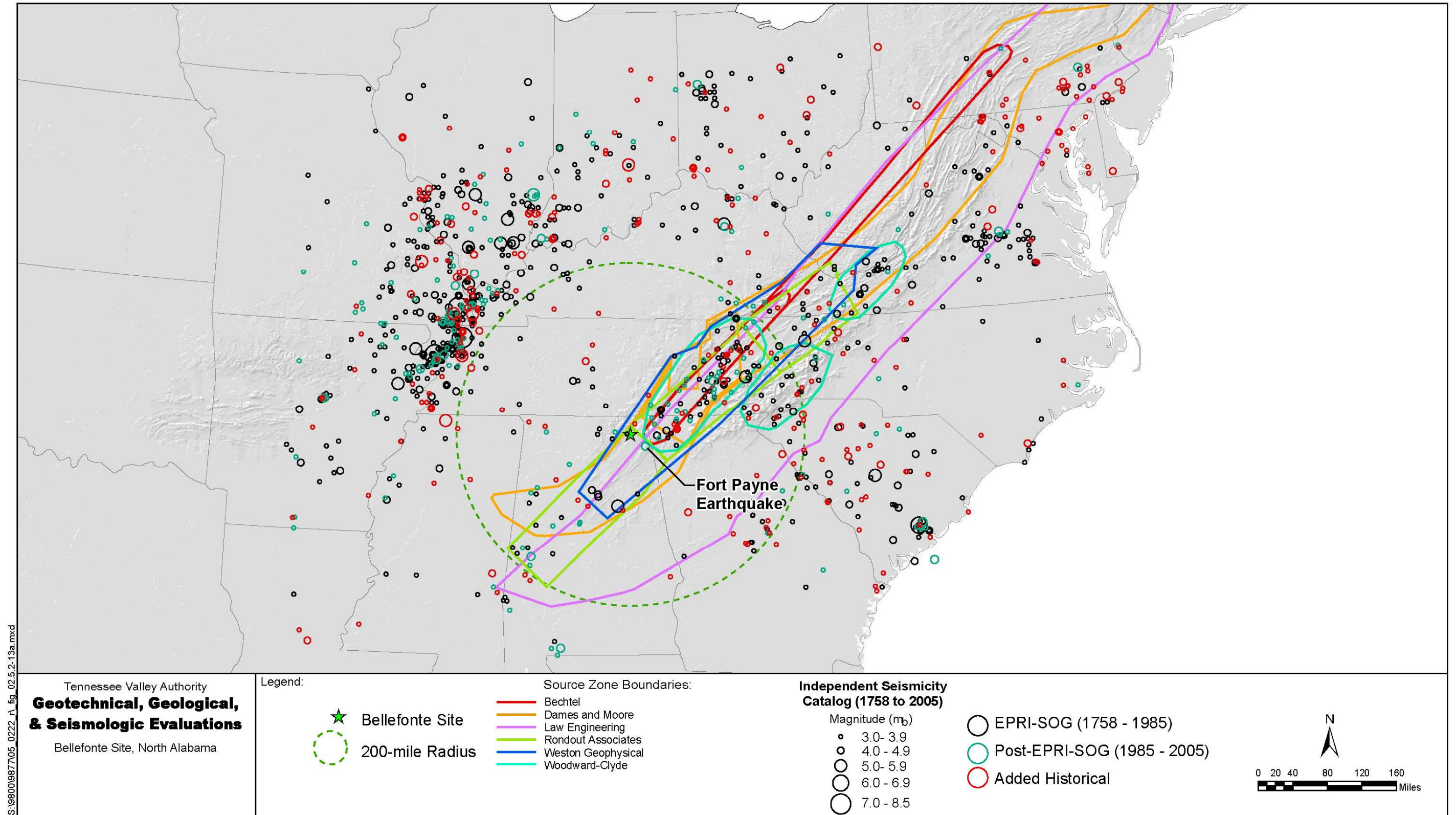
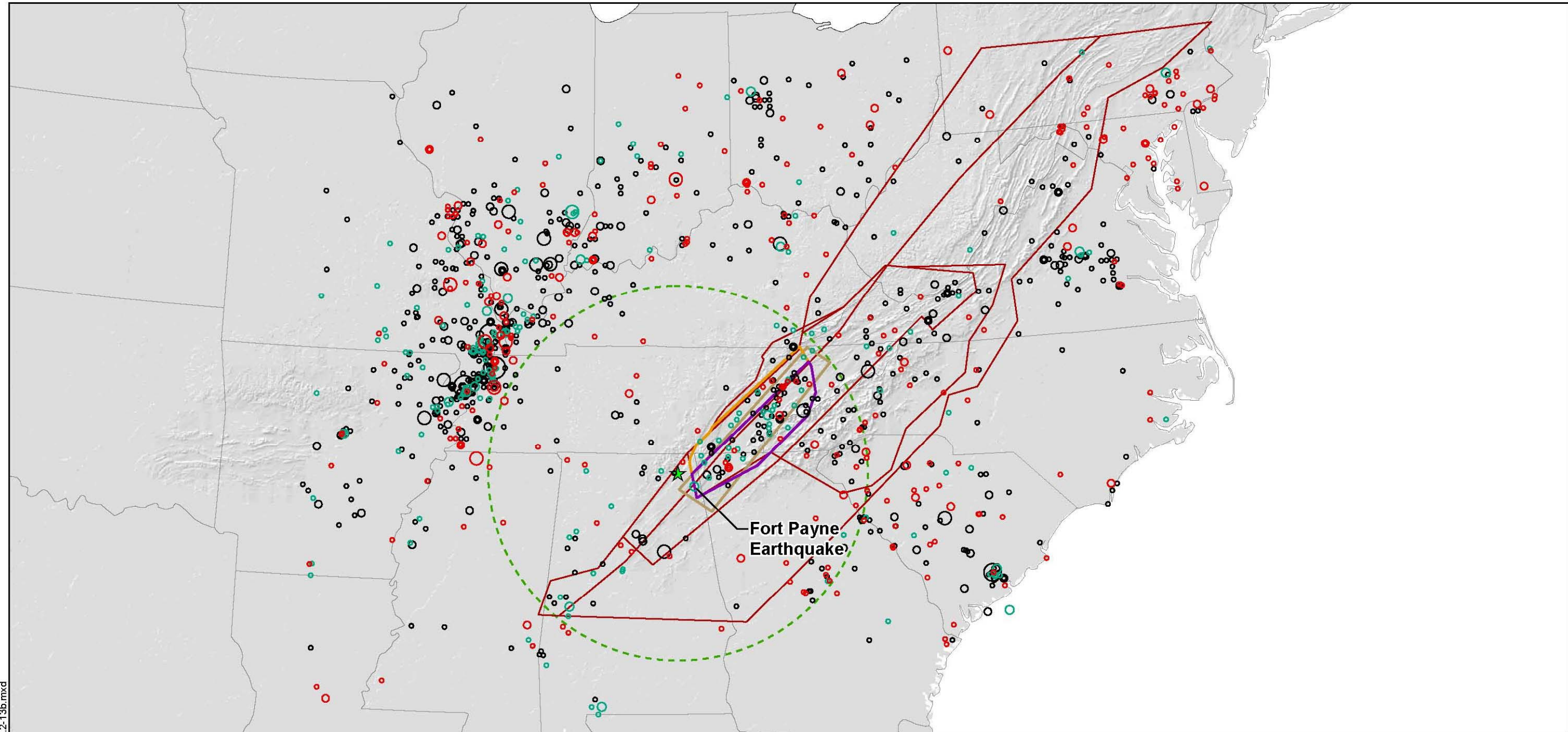


Figure 2.5.2-13(a). Composite of EPRI-SOG Seismic Sources Representing the East Tennessee Seismic Zone



S:\9800\987705\_0222\_1\_fig\_02.5.2-13b.mxd

Tennessee Valley Authority  
**Geotechnical, Geological,  
& Seismologic Evaluations**  
Bellefonte Site, North Alabama

Legend:

- Bellefonte Site
- 200-mile Radius

- Source Zone Boundaries:
- LLNL TIP 4A-1
  - LLNL TIP 4A-1+2+3
  - USGS - East Tennessee Regional Source Zone
  - Geomatrix (2004)

**Independent Seismicity  
Catalog (1758 to 2005)**

- Magnitude ( $m_b$ )
- 3.0 - 3.9
  - 4.0 - 4.9
  - 5.0 - 5.9
  - 6.0 - 6.9
  - 7.0 - 8.5

- EPRI-SOG (1758 - 1985)
- Post-EPRI-SOG (1985 - 2005)
- Added Historical

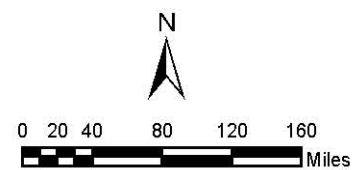


Figure 2.5.2-13(b). Composite of Post EPRI-SOG Seismic Sources Representing the East Tennessee Seismic Zone

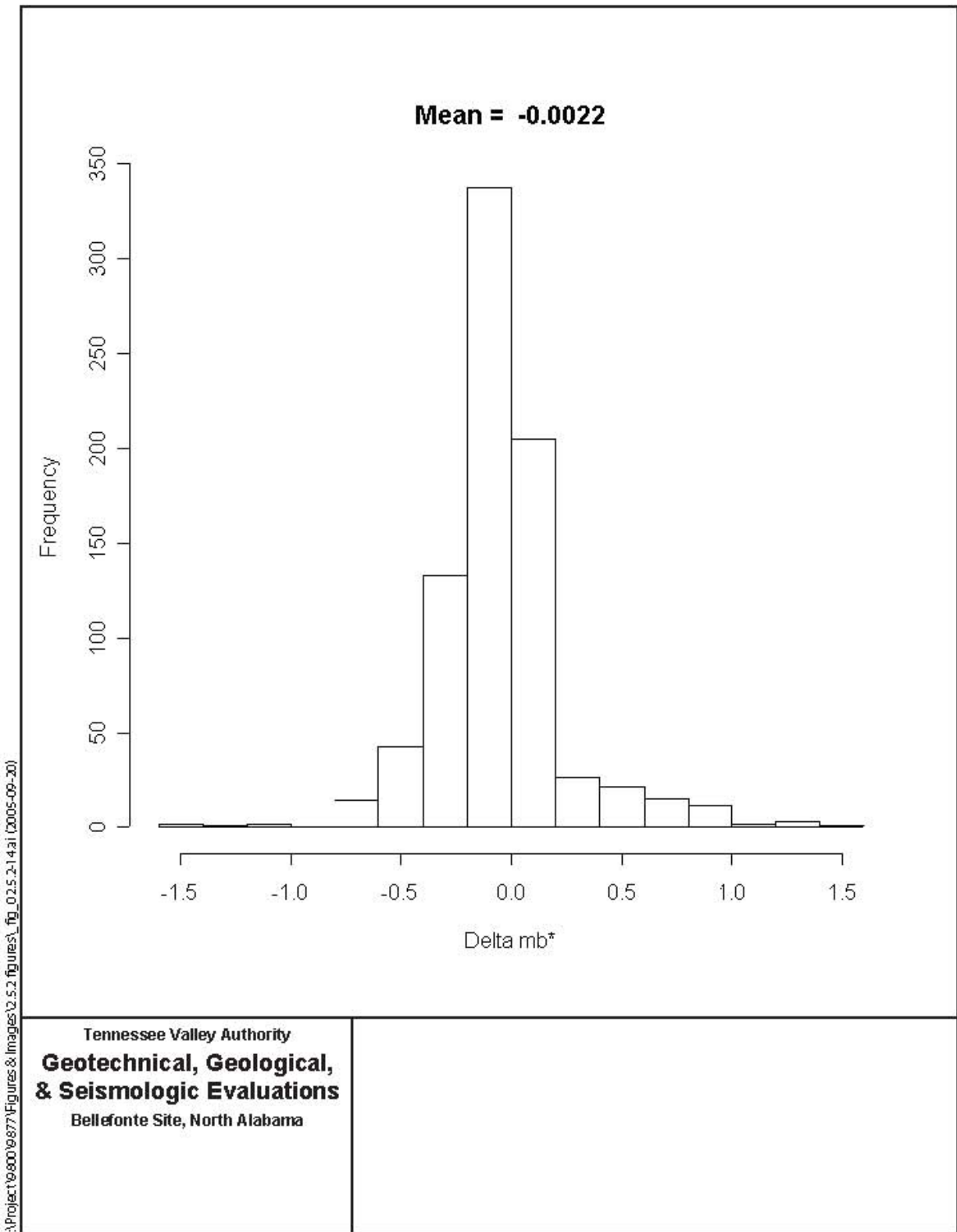


Figure 2.5.2-14. Histogram of the Difference between  $mb^*$  for the Updated Catalog and  $mb^*$  defined in the EPRI-SOG (1988) Catalog for Earthquakes within 200 Miles of Bellefonte site

I:\Project\9800\9877\Figures & Images\2.5.2 figures\\_fig\_02.5.2-15.ai (2005-09-20)

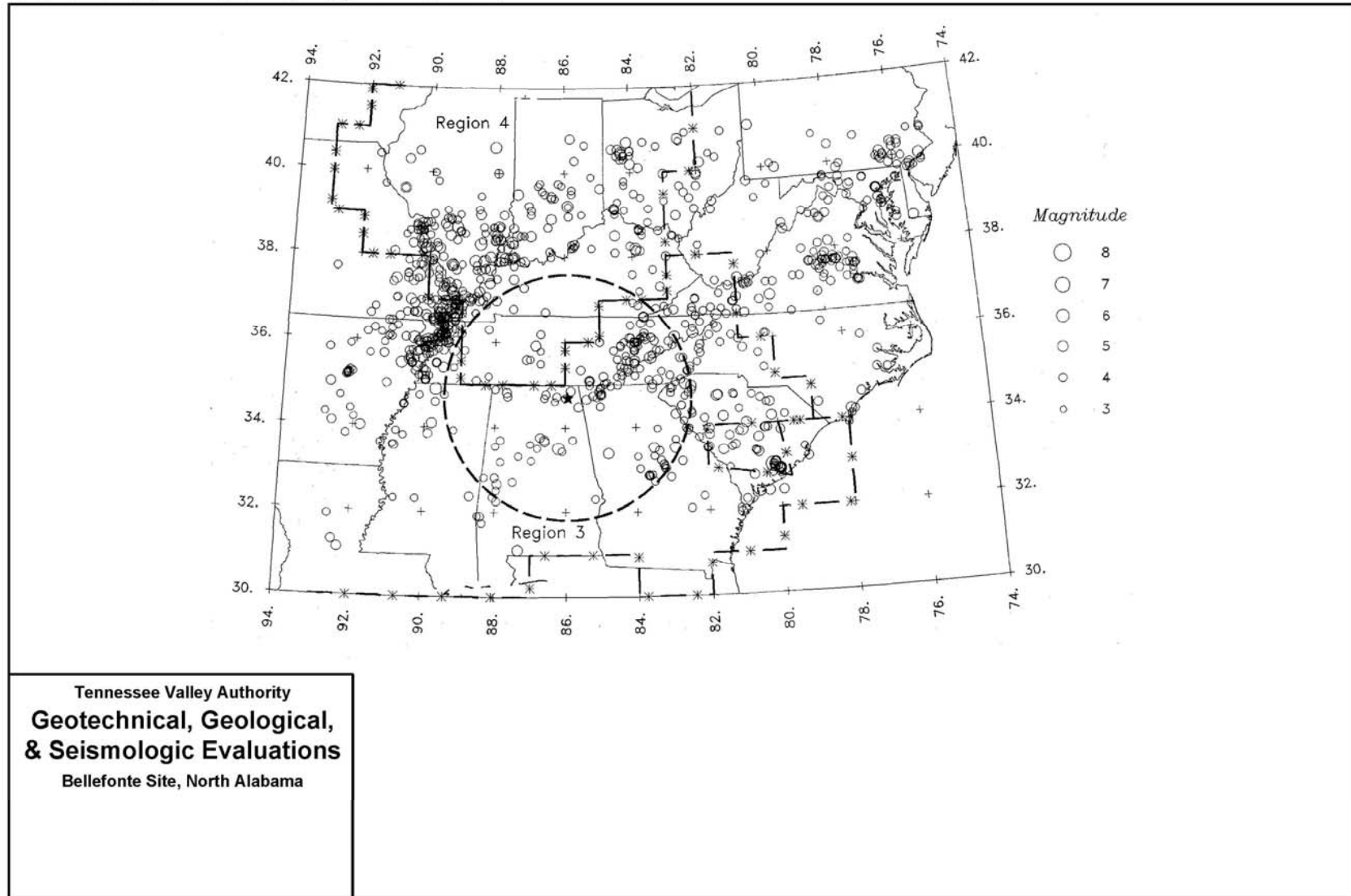


Figure 2.5.2-15. Earthquakes in the Updated Catalog ( $m_b^* \geq 3.3$ ) and EPRI-SOG (1988) Completeness Regions Covering the area within 200 miles of the Bellefonte Site

I:\Project\9800\9877\Figures & Images\2.5.2 figures\\_fig\_02.5.2-16.ai (2005-09-20)

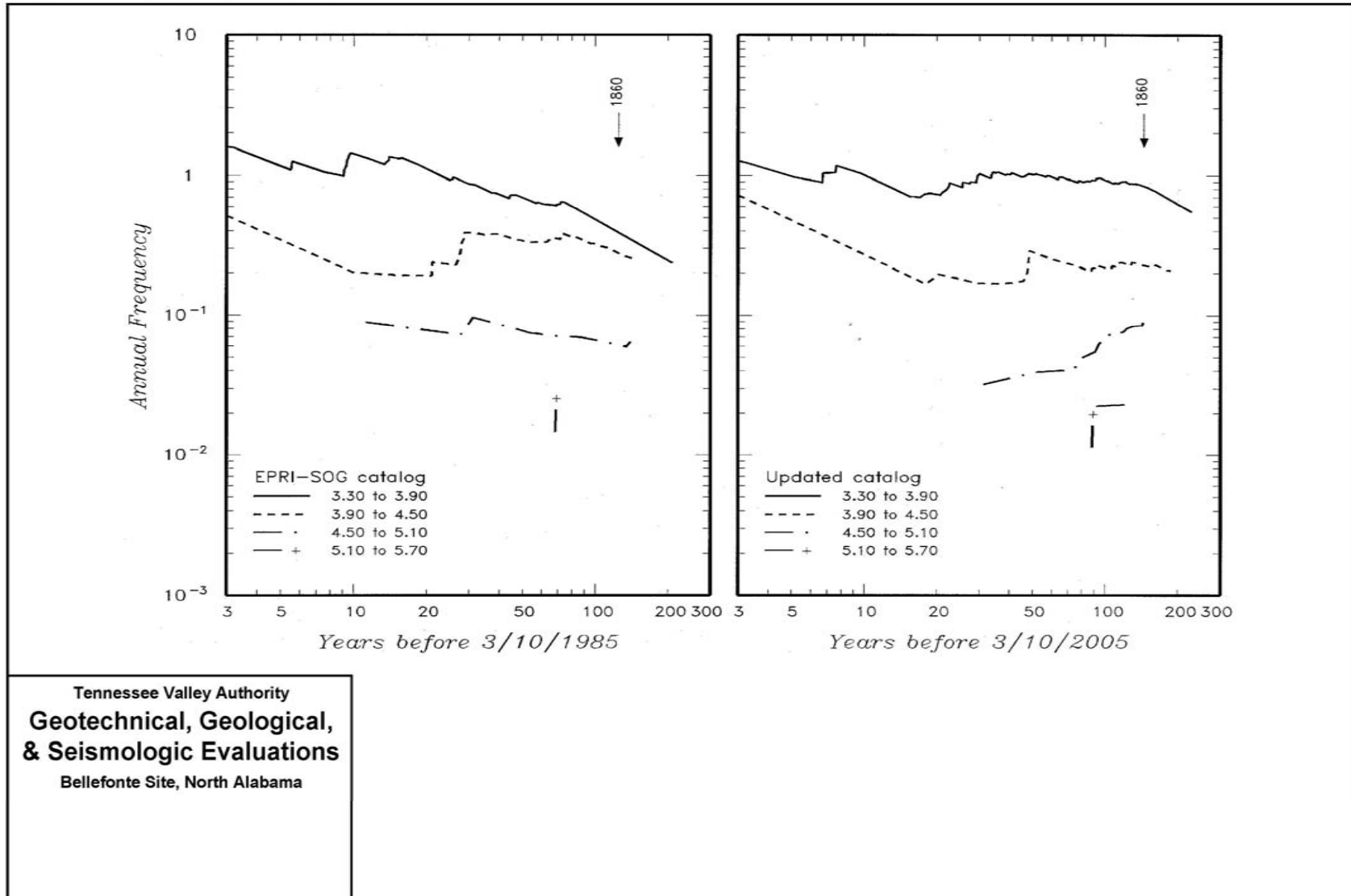


Figure 2.5.2-16. "Stepp" Plots for 200-mile Radius Region around the Bellefonte Site

I:\Project\9800\9877\Figures & Images\2.5.2 figures\\_fig\_02.5.2-17.ai (2005-09-20)

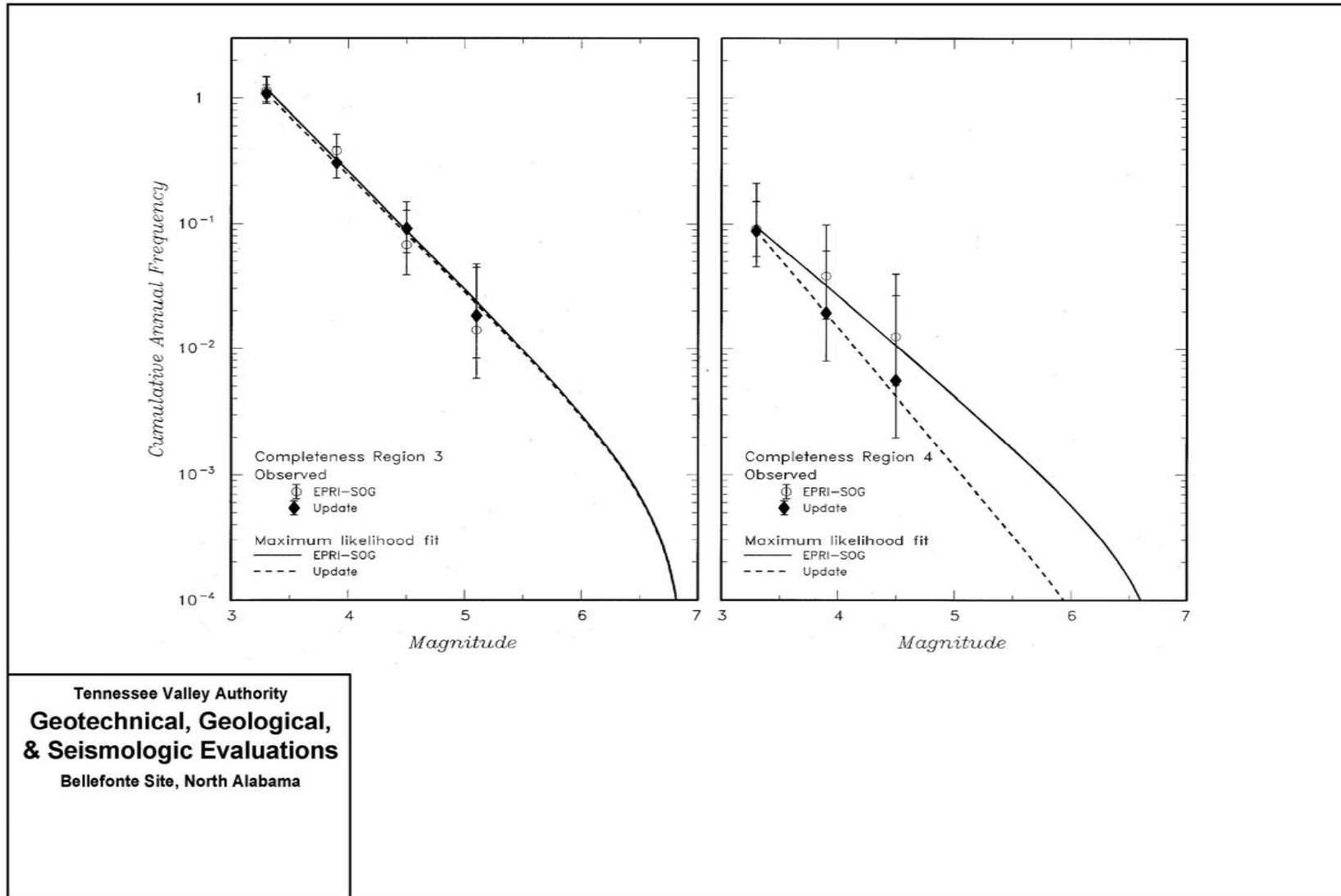
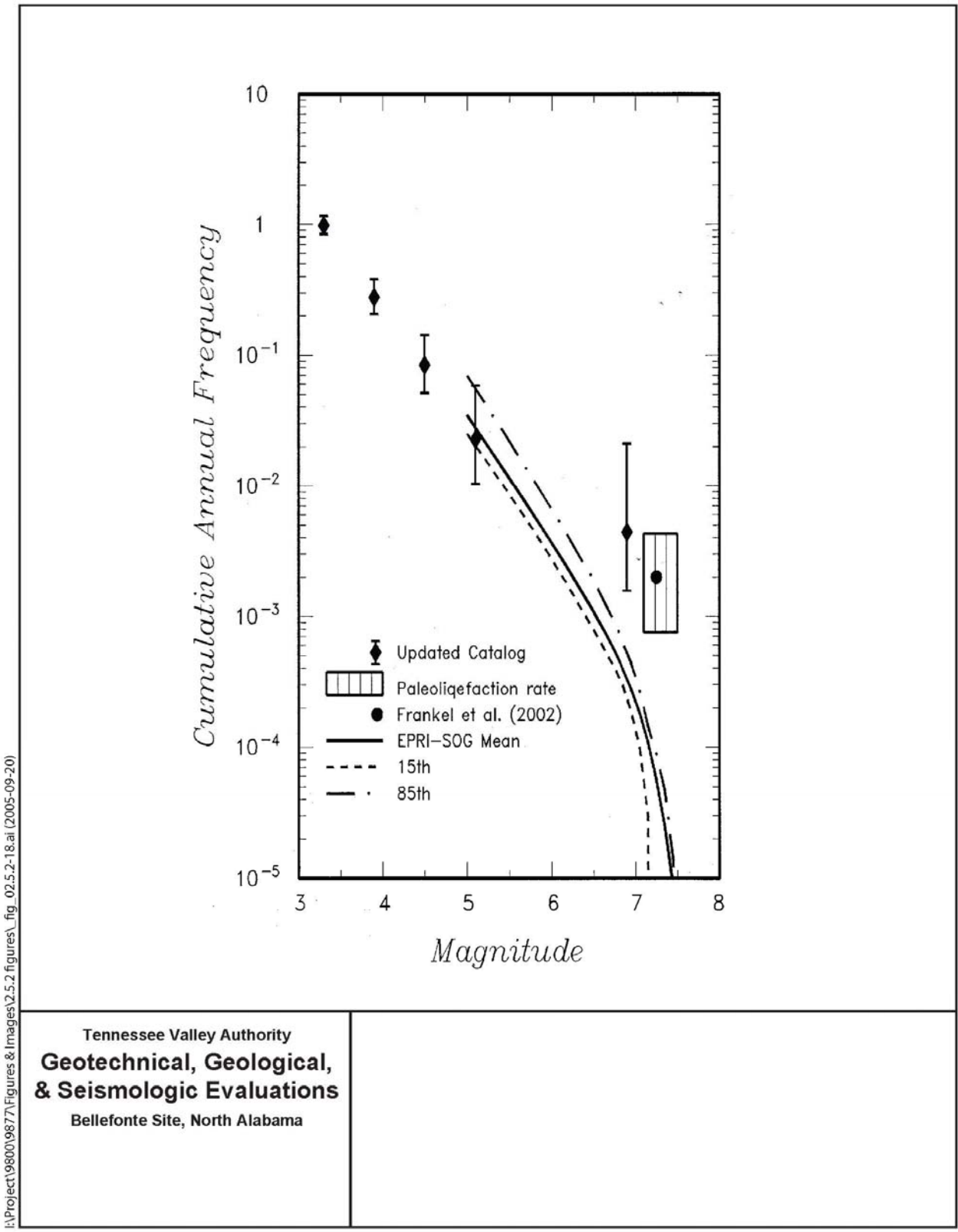


Figure 2.5.2-17. Earthquake Recurrence Rates Estimated for the “Equivalent Period of Completeness” for the Portions of EPRI-SOG Completeness Regions 3 and 4 within 200 Miles of the Bellefonte ESP Site

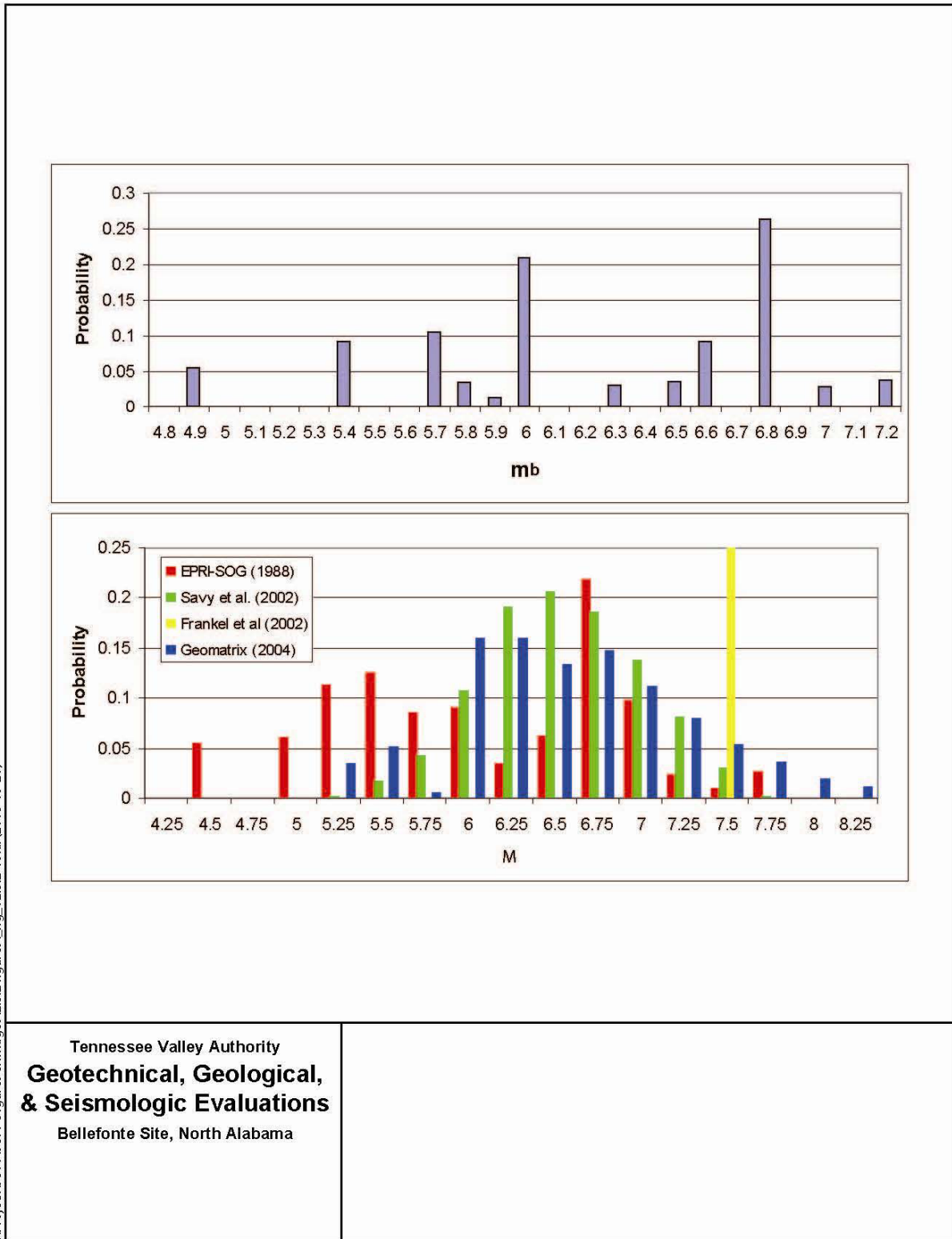


I:\Project\19800\19877\Figures & Images\2.5.2 figures\fig\_02.5.2-18.ai (2005-09-20)

Tennessee Valley Authority  
**Geotechnical, Geological,  
& Seismologic Evaluations**  
Bellefonte Site, North Alabama

Figure 2.5.2-18. Earthquake Recurrence Rates for New Madrid Seismic Sources





I:\Project\9800\9877\Figures & Images\2.5.2 figures\fig\_02.5.2-19.ai (2005-09-20)

Tennessee Valley Authority  
**Geotechnical, Geological,  
& Seismologic Evaluations**  
Bellefonte Site, North Alabama

**Figure 2.5.2-19. Maximum Magnitude Distributions for Sources Representing the East Tennessee Seismic Zone. (top) Composite EPRI-SOG Distribution in Terms of mb. (bottom) Composite EPRI-SOG Distribution in Terms of M Compared to More Recent Assessments**

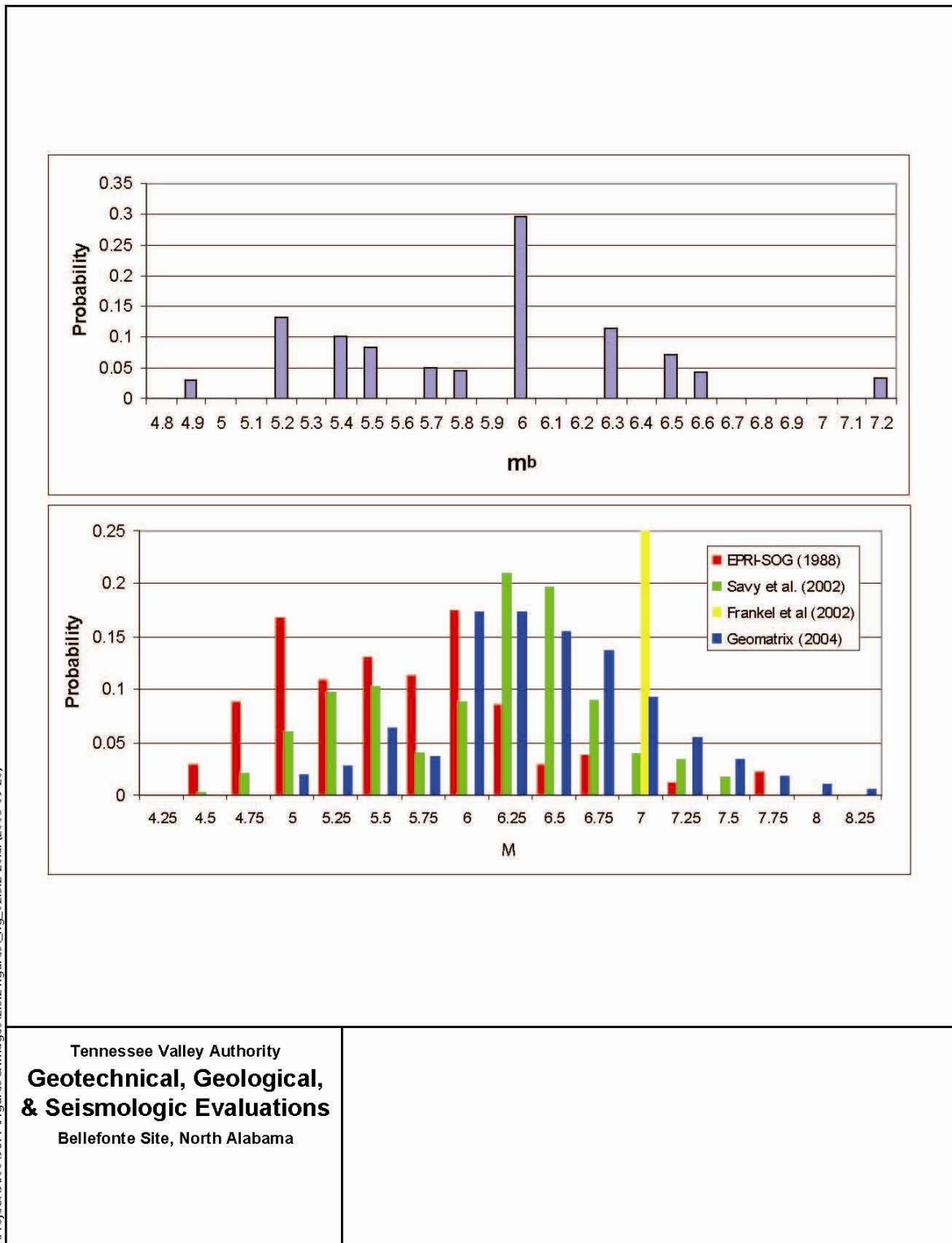
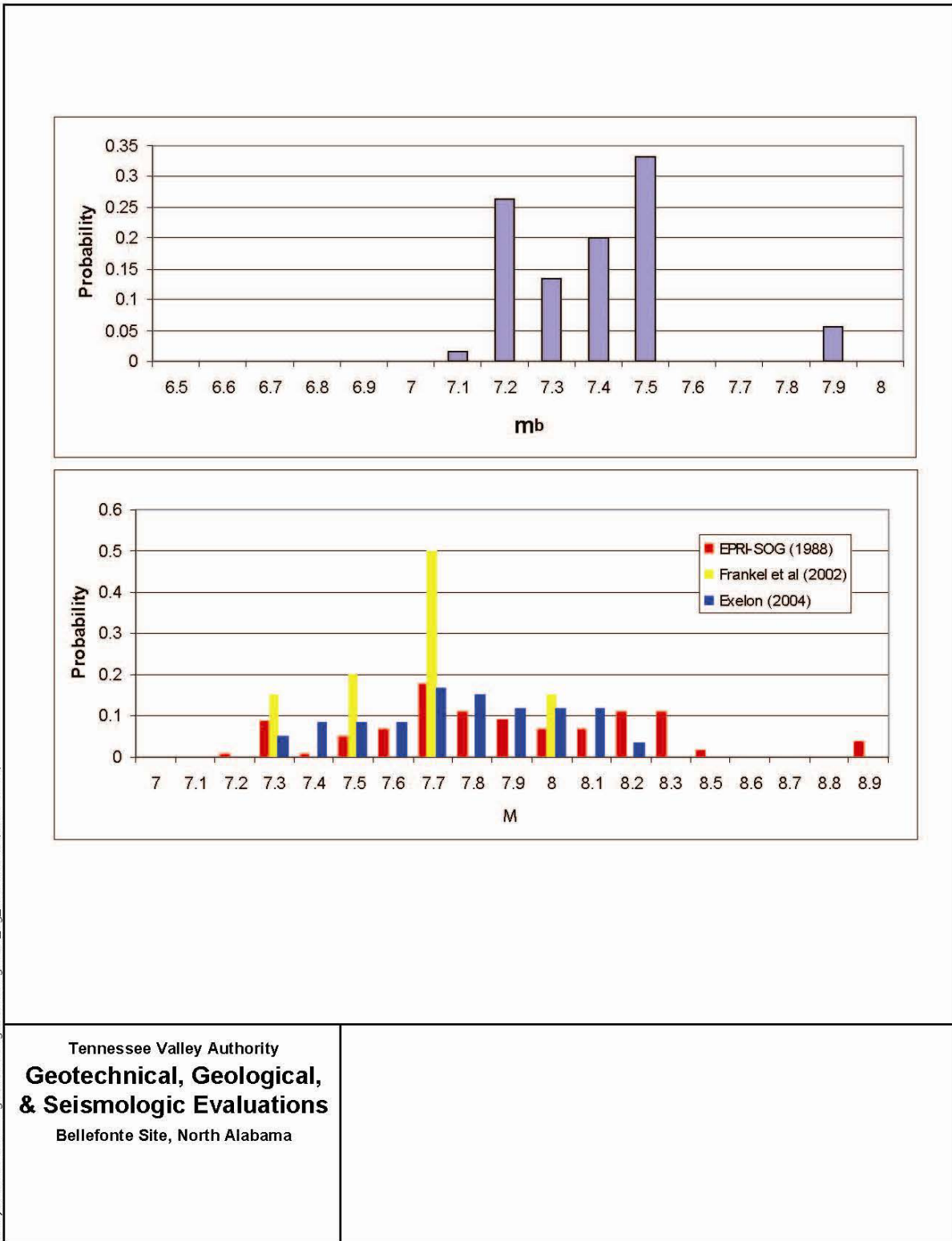


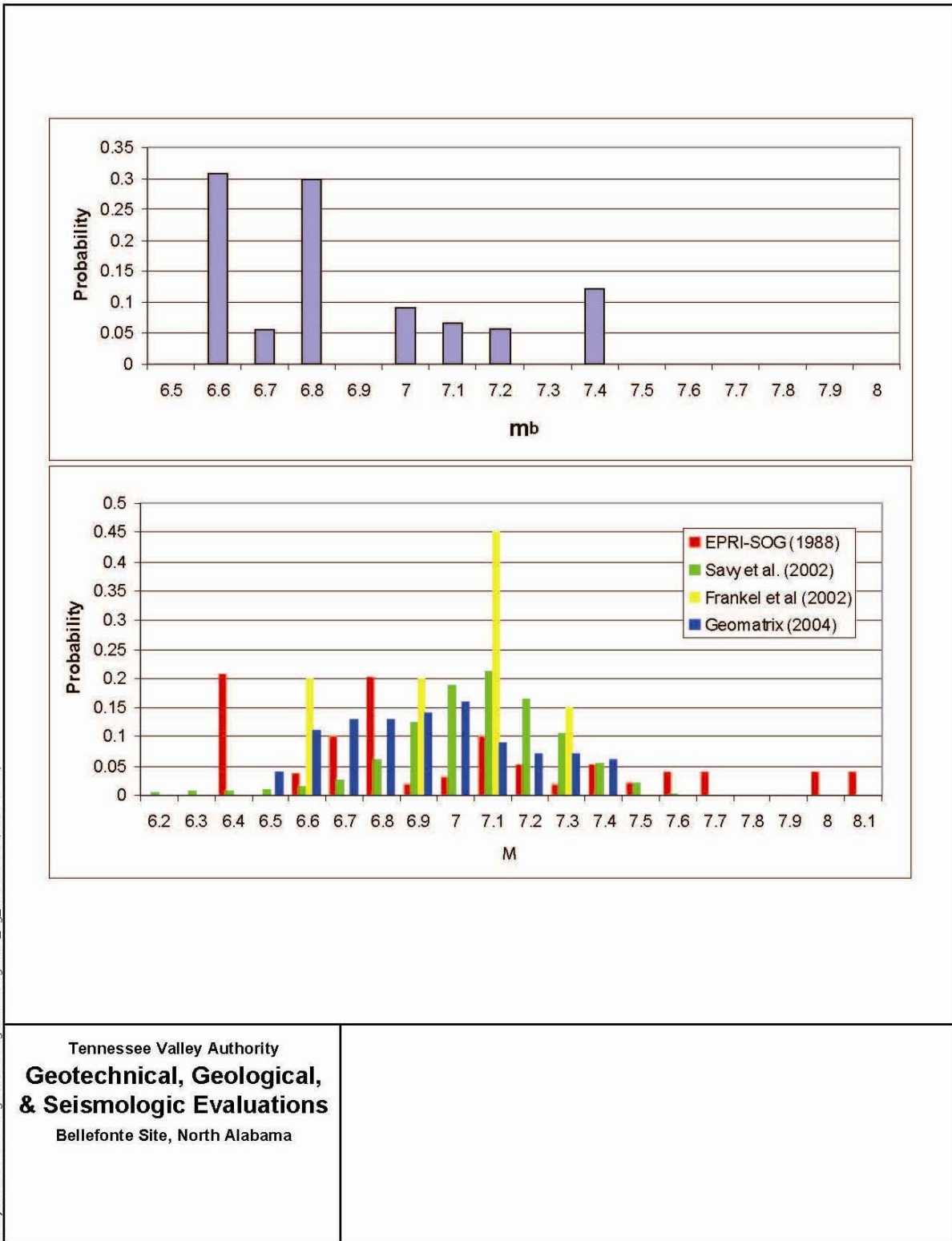
**Figure 2.5.2-20. Maximum Magnitude Distributions for Sources Representing the Host/Background Seismic Source for the Bellefonte Site. (top) Composite EPRI-SOG Distribution in Terms of mb. (bottom) Composite EPRI-SOG Distribution in Terms of M Compared to More Recent Assessments**



I:\Project\9800\9877\Figures & Images\2.5.2 figures\fig\_02.5.2-21.ai (2005-09-20)

Tennessee Valley Authority  
**Geotechnical, Geological,  
& Seismologic Evaluations**  
Bellefonte Site, North Alabama

**Figure 2.5.2-21. Maximum Magnitude Distributions for Sources Representing the New Madrid Seismic Zone. (top) Composite EPRI-SOG Distribution in Terms of mb. (bottom) Composite EPRI-SOG Distribution in Terms of M Compared to More Recent Assessments**



I:\Project\9800\9877\Figures & Images\2.5.2 figures\fig\_02.5.2-22.ai (2005-09-20)

Tennessee Valley Authority  
**Geotechnical, Geological,  
& Seismologic Evaluations**  
Bellefonte Site, North Alabama

**Figure 2.5.2-22. Maximum Magnitude Distributions for Sources Representing the Source of the 1886 Charleston Earthquake. (top) Composite EPRI-SOG Distribution in Terms of mb. (bottom) Composite EPRI-SOG Distribution in Terms of M Compared to More Recent Assessments**

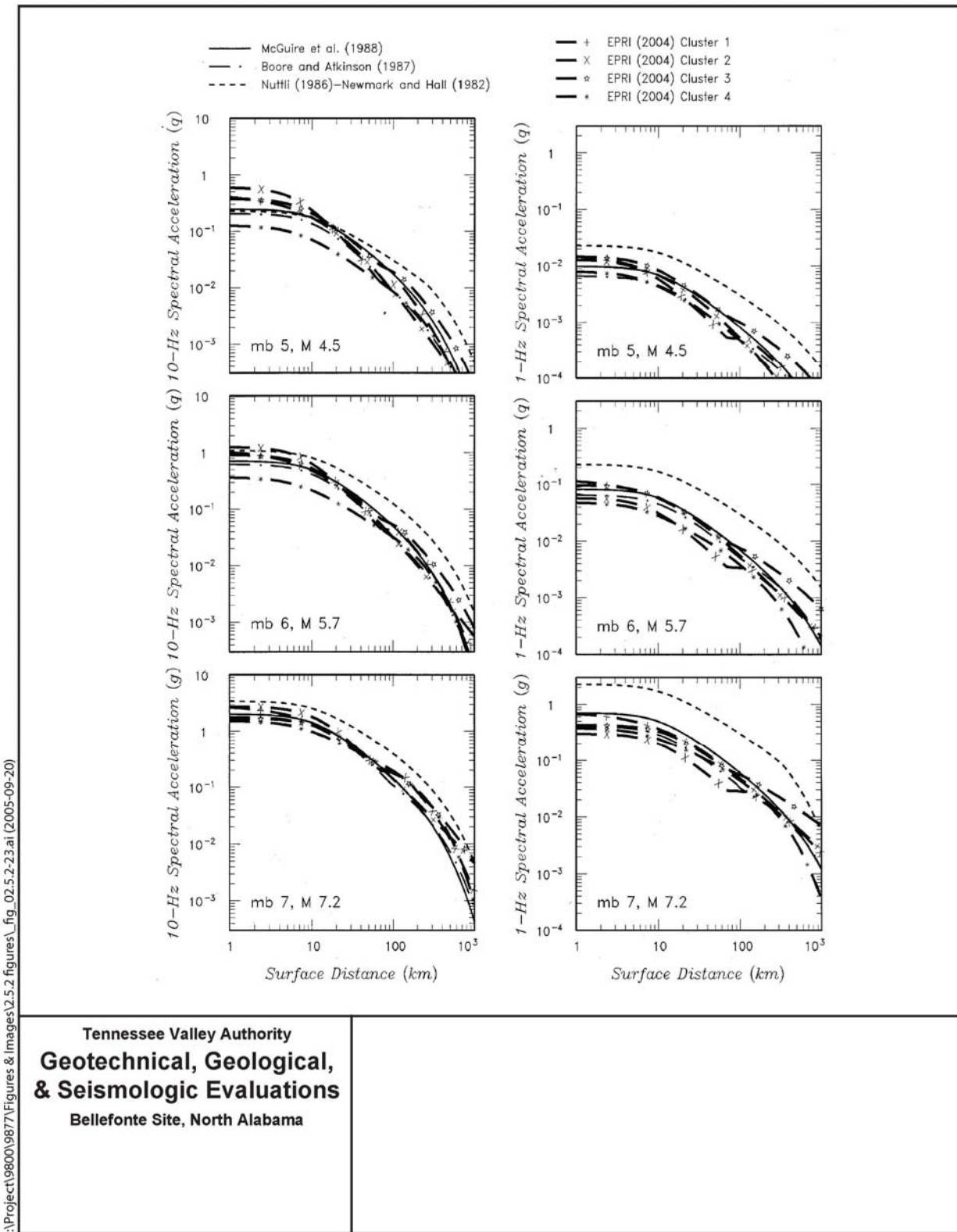
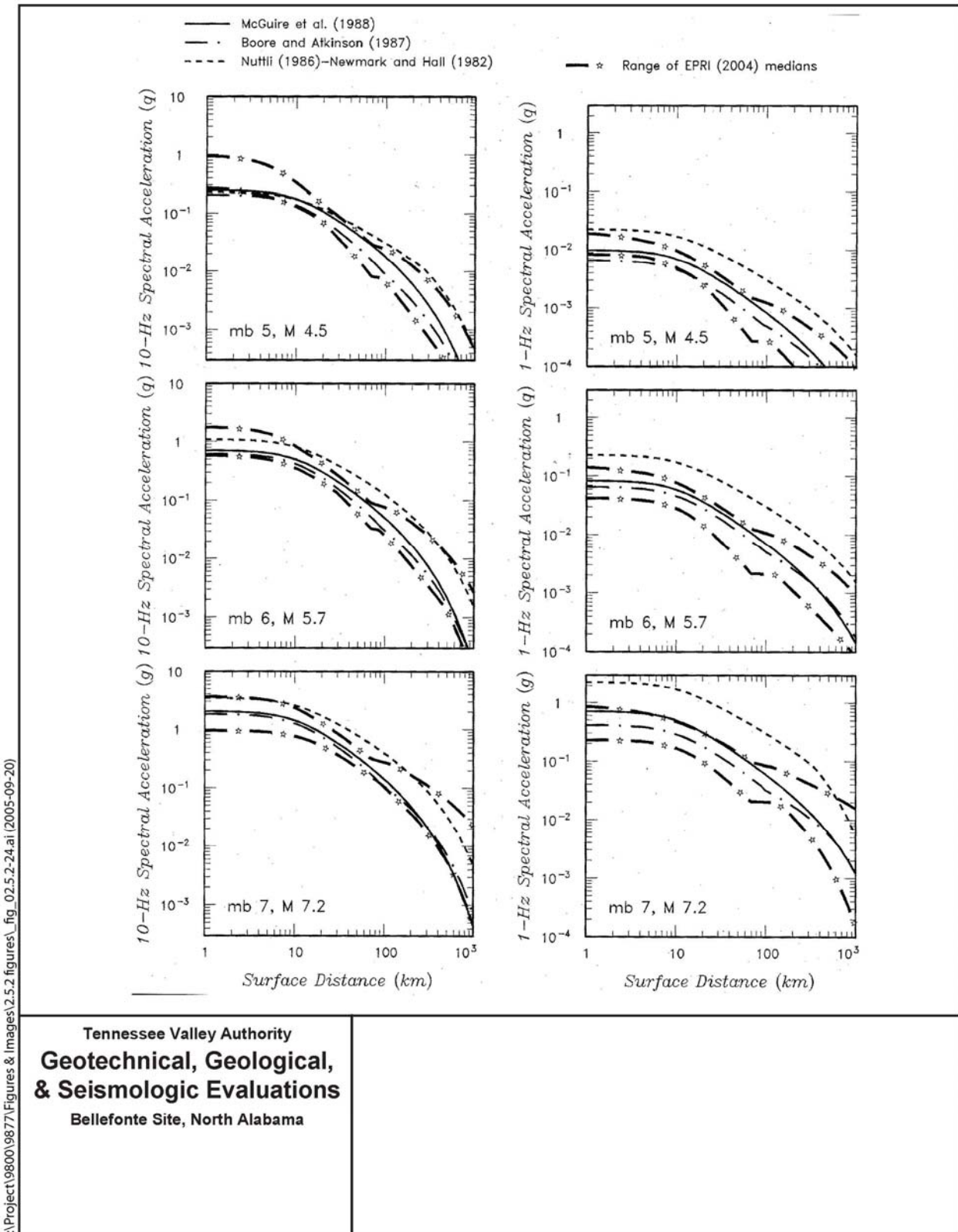


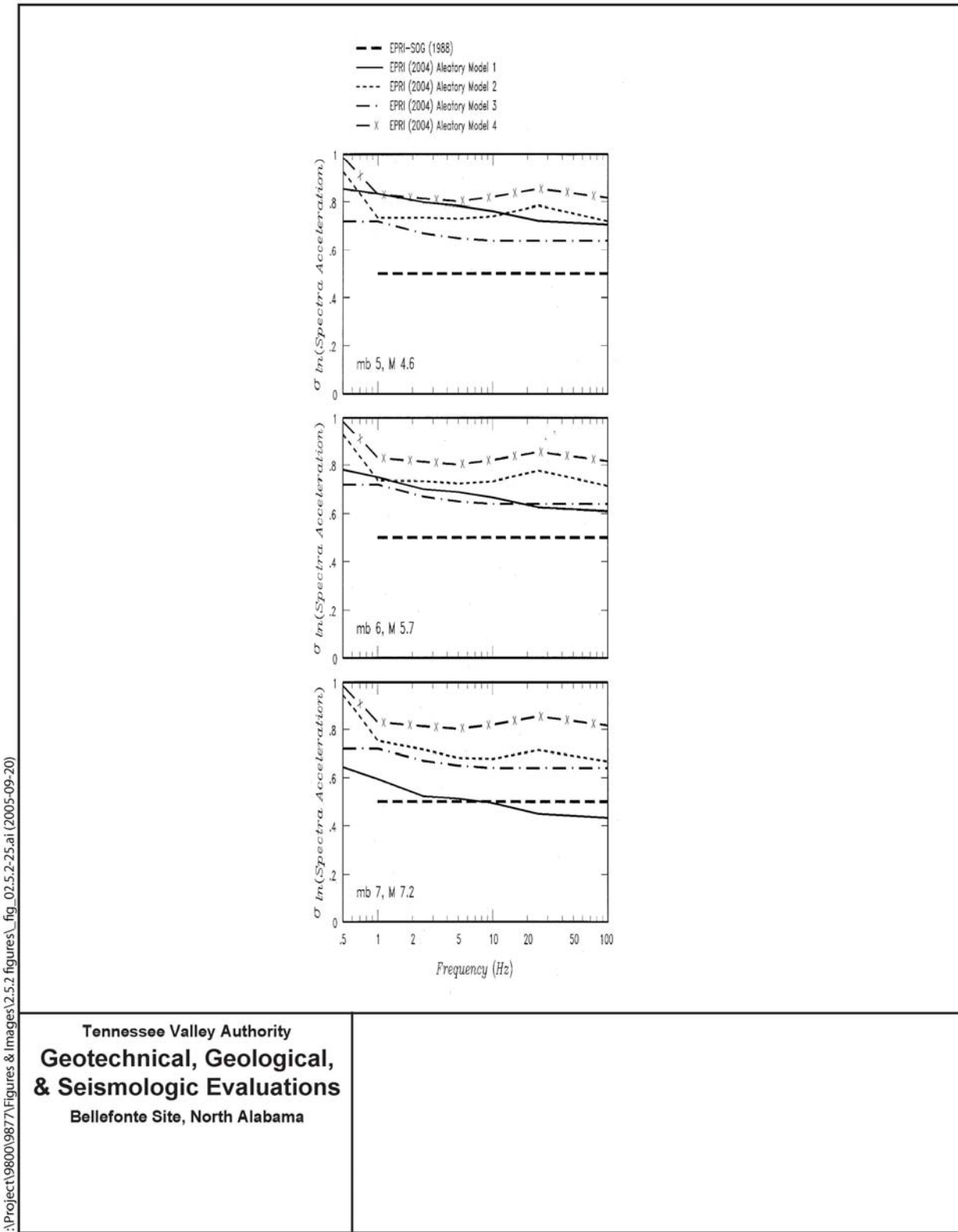
Figure 2.5.2-23. Comparison of the EPRI-SOG (1988) and EPRI (2004) Median Ground Motion Models



I:\Project\9800\9877\Figures & Images\2.5.2 figures\fig\_02.5.2-24.ai [2005-09-20]

Tennessee Valley Authority  
**Geotechnical, Geological,  
 & Seismologic Evaluations**  
 Bellefonte Site, North Alabama

**Figure 2.5.2-24. Uncertainty Range for the EPRI (2004) Ground Motion Models Compared to the EPRI-SOG (1988) Median Models**



\\Project\19800\9877\Figures & Images\2.5.2-figures\fig\_02.5.2-25.ai (2005-09-20)

Tennessee Valley Authority  
**Geotechnical, Geological,  
 & Seismologic Evaluations**  
 Bellefonte Site, North Alabama

**Figure 2.5.2-25. Comparison of the EPRI-SOG (1988) and EPRI (2004) Models for Aleatory Variability in Ground Motions**

I:\Project\9800\9877\Figures & Images\2.5.2 figures\\_fig\_02.5.2-26.ai (2005-09-20)

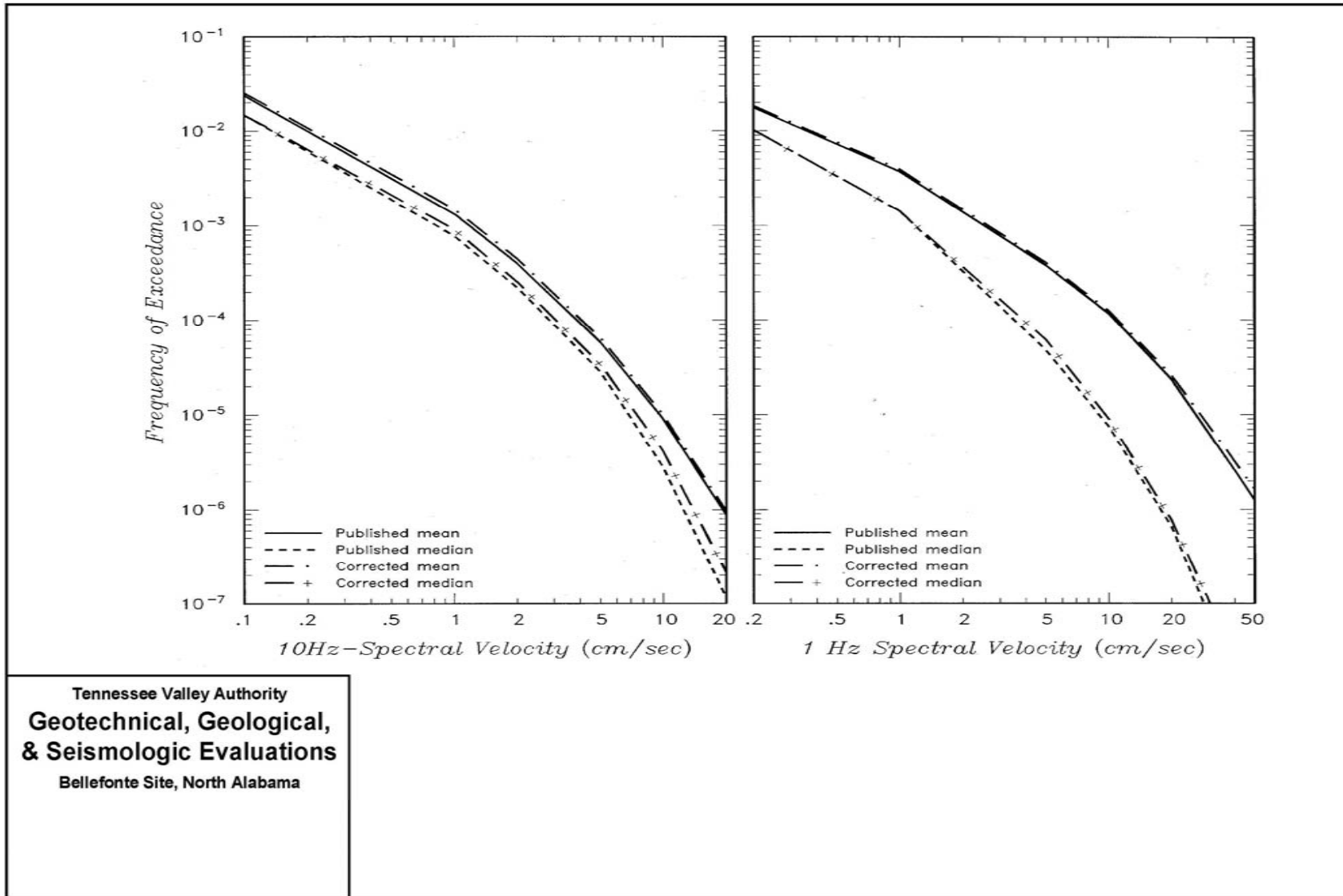


Figure 2.5.2-26. Effect on Hazard of the "Correction" to the 99 Percent Hazard Source List for the Bellefonte Site in the EPRI-SOG (1988) Seismic Hazard Model



I:\Project\9800\9877\Figures & Images\2.5.2 figures\fig\_02.5.2-27.ai (2005-09-20)

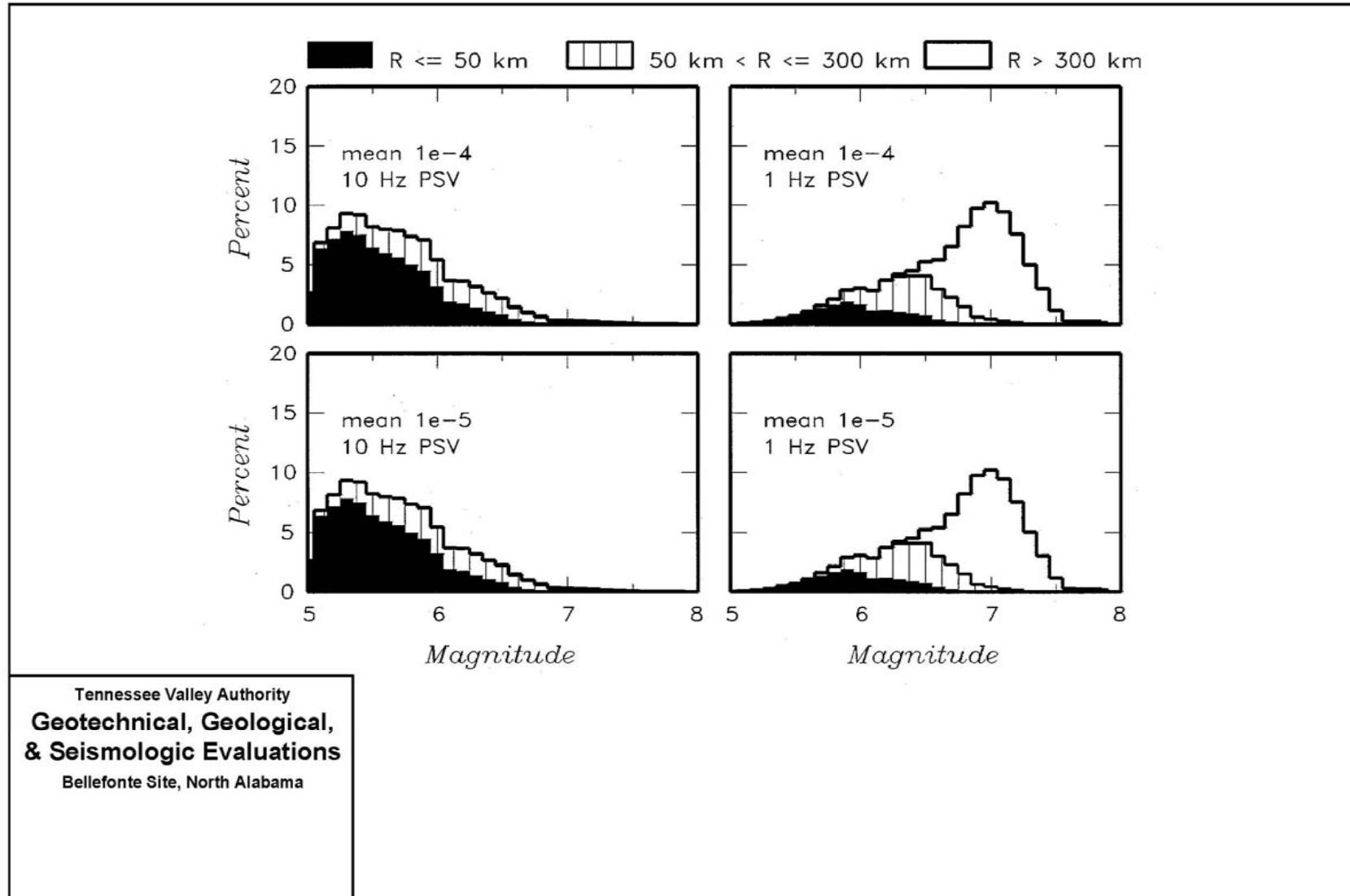


Figure 2.5.2-27. Disaggregation of Hazard from the EPRI-SOG (1998) Seismic Source Model.

I:\Project\9800\9877\Figures & Images\2.5.2 figures\\_fig\_02.5.2-28.ai (2005-09-20)

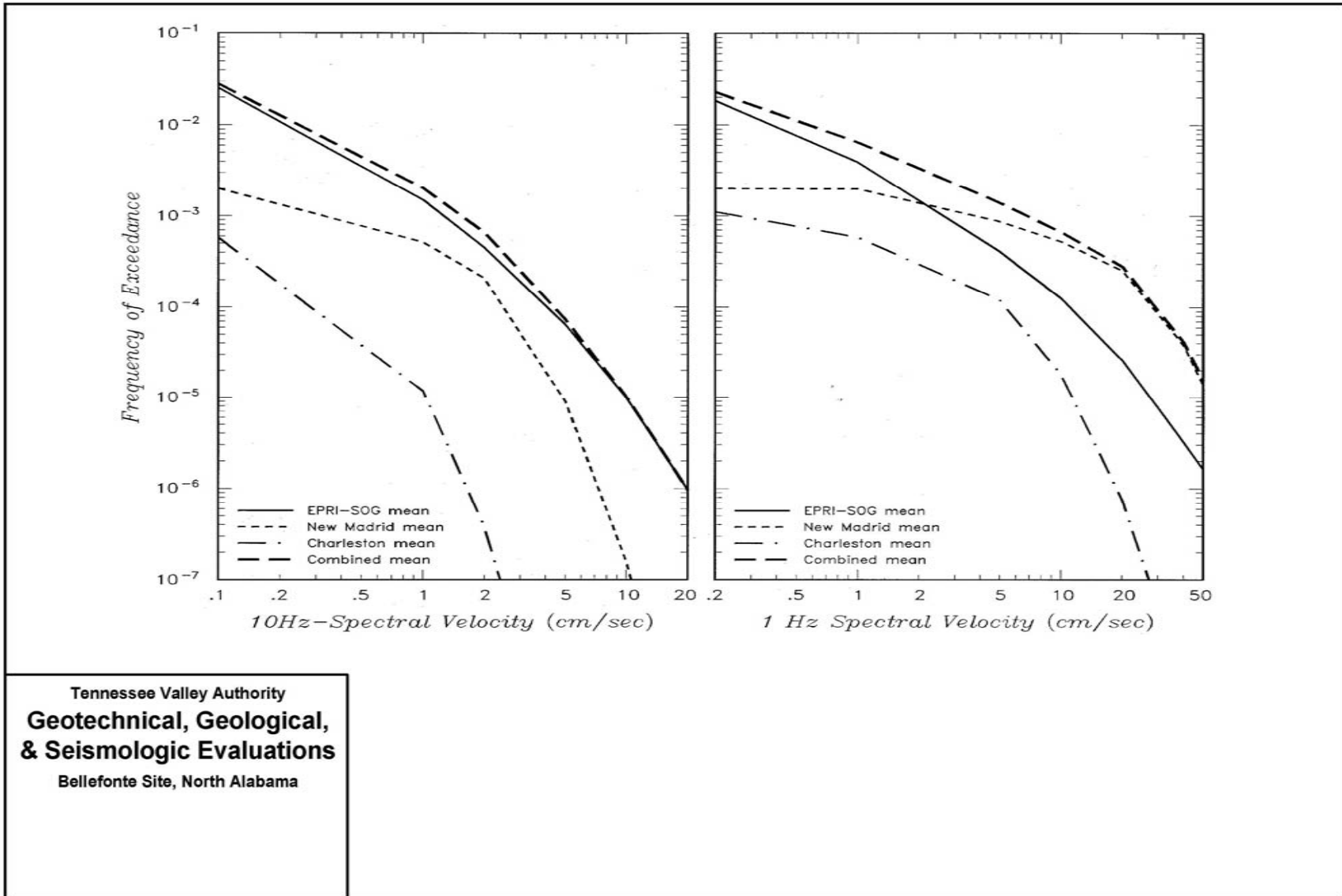


Figure 2.5.2-28. Effect of Adding Sources of Repeating Large Magnitude New Madrid and Charleston Earthquakes on the Site Hazard

I:\Project\9800\9877\Figures & Images\2.5.2 figures\\_fig\_02.5.2-29.ai (2005-09-20)

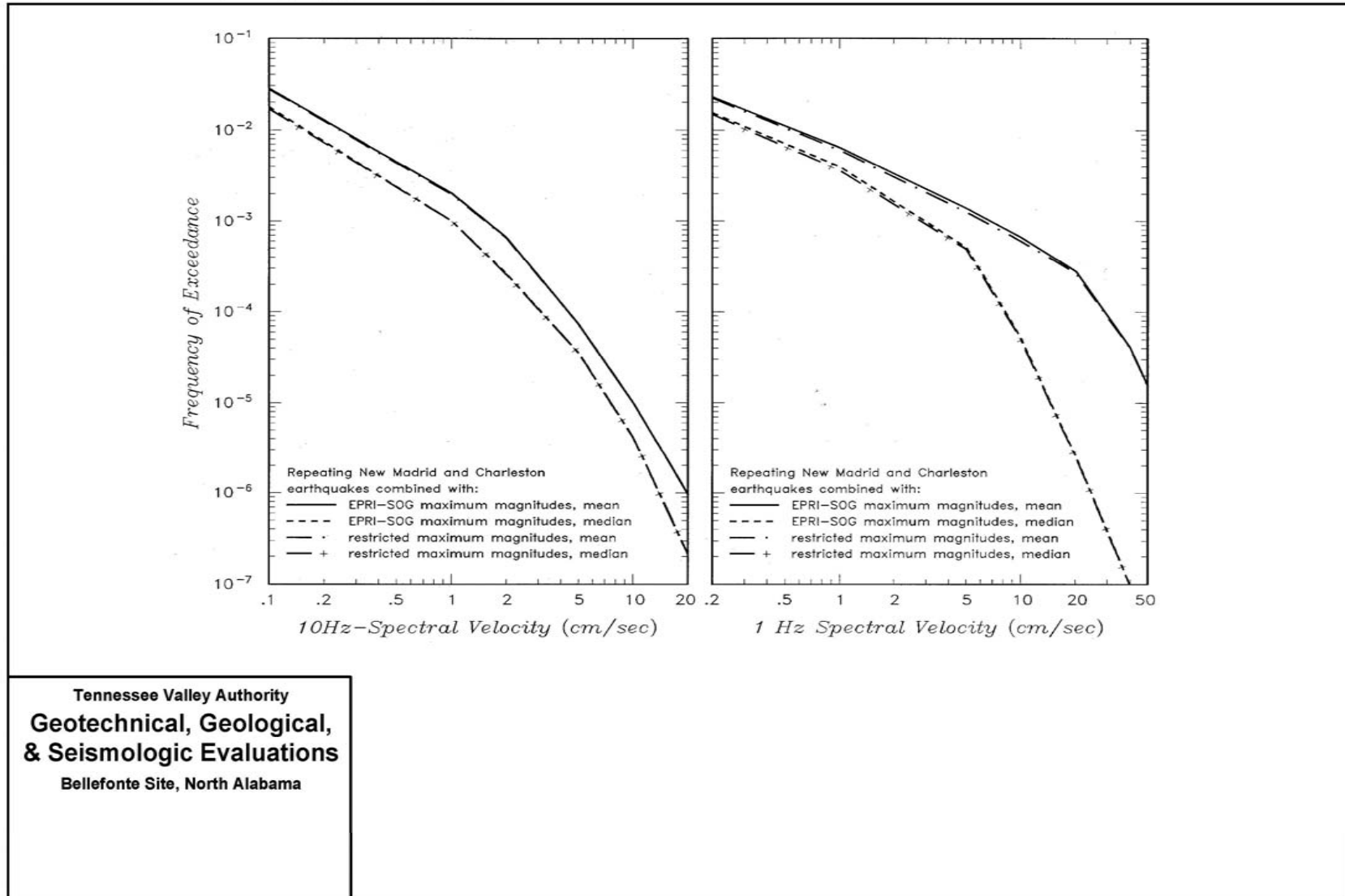


Figure 2.5.2-29. Effect of Including Sources of Repeating Large Magnitude New Madrid and Charleston Earthquakes with Adjustments for Double-Counting on the Site Hazard

I:\Project\9800\9877\Figures & Images\2.5.2 figures\\_fig\_02.5.2-30.ai (2005-09-20)

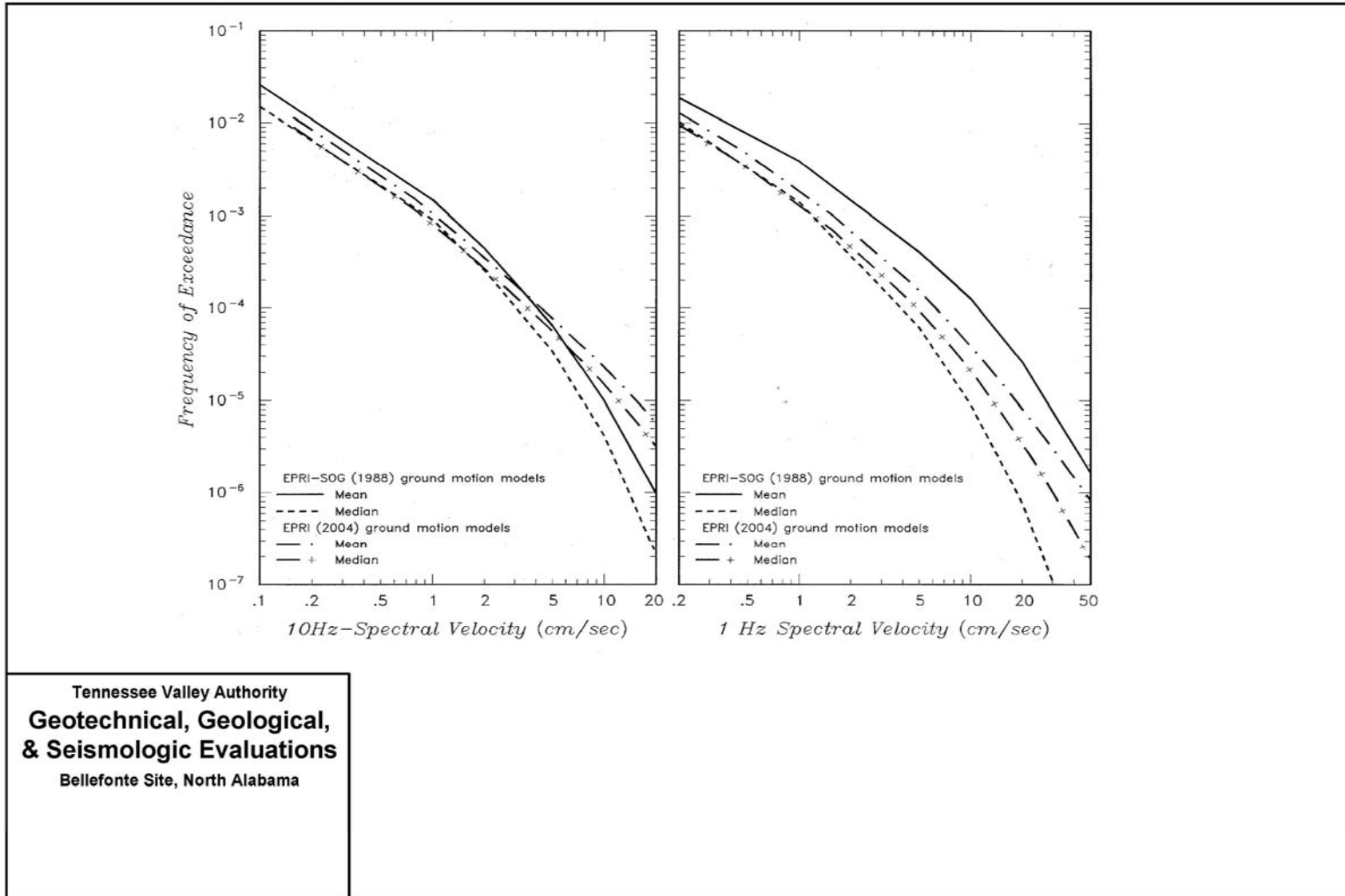


Figure 2.5.2-30. Effect of Use of the EPRI (2004) Ground Motion Model on Site Hazard

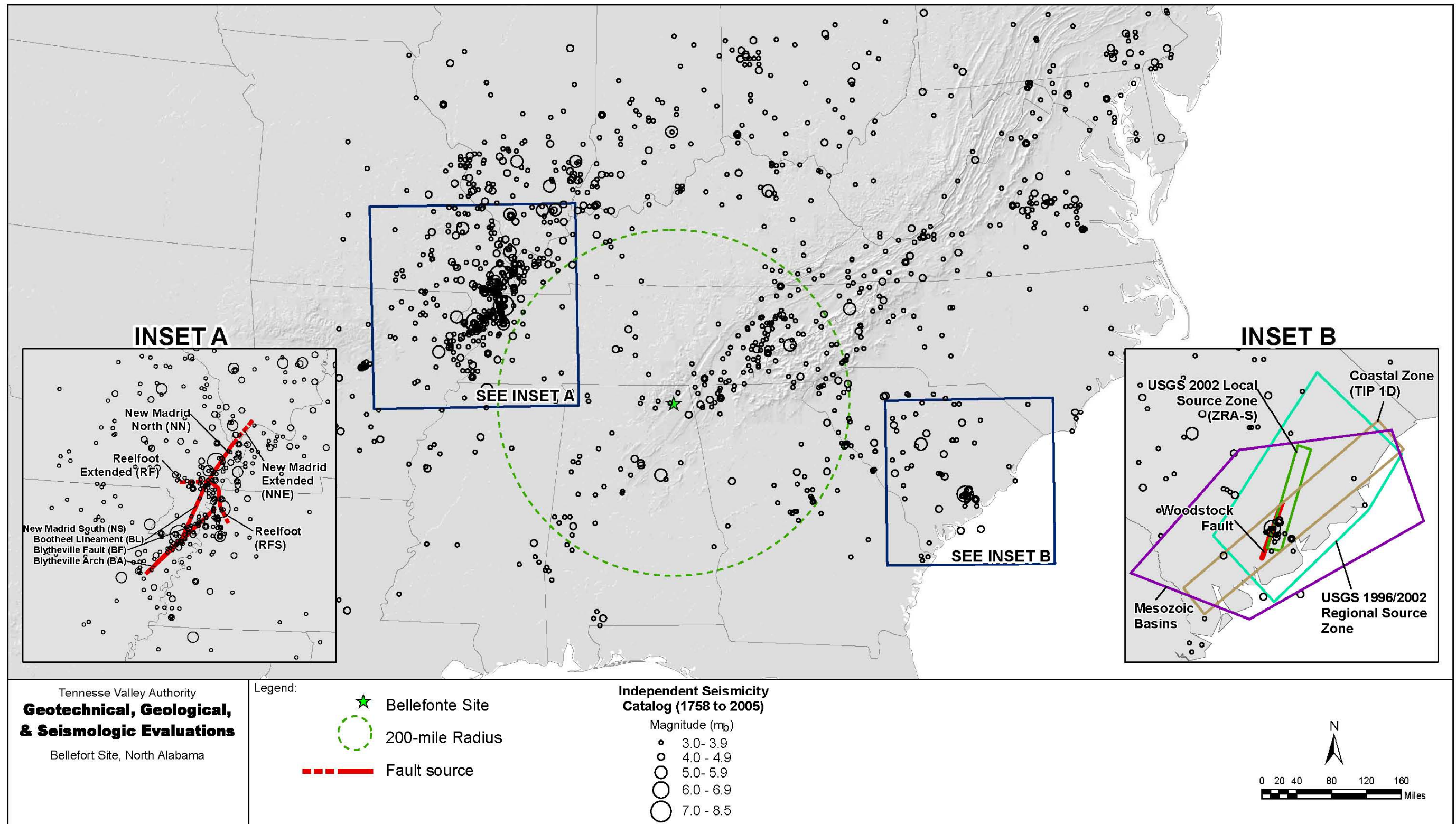
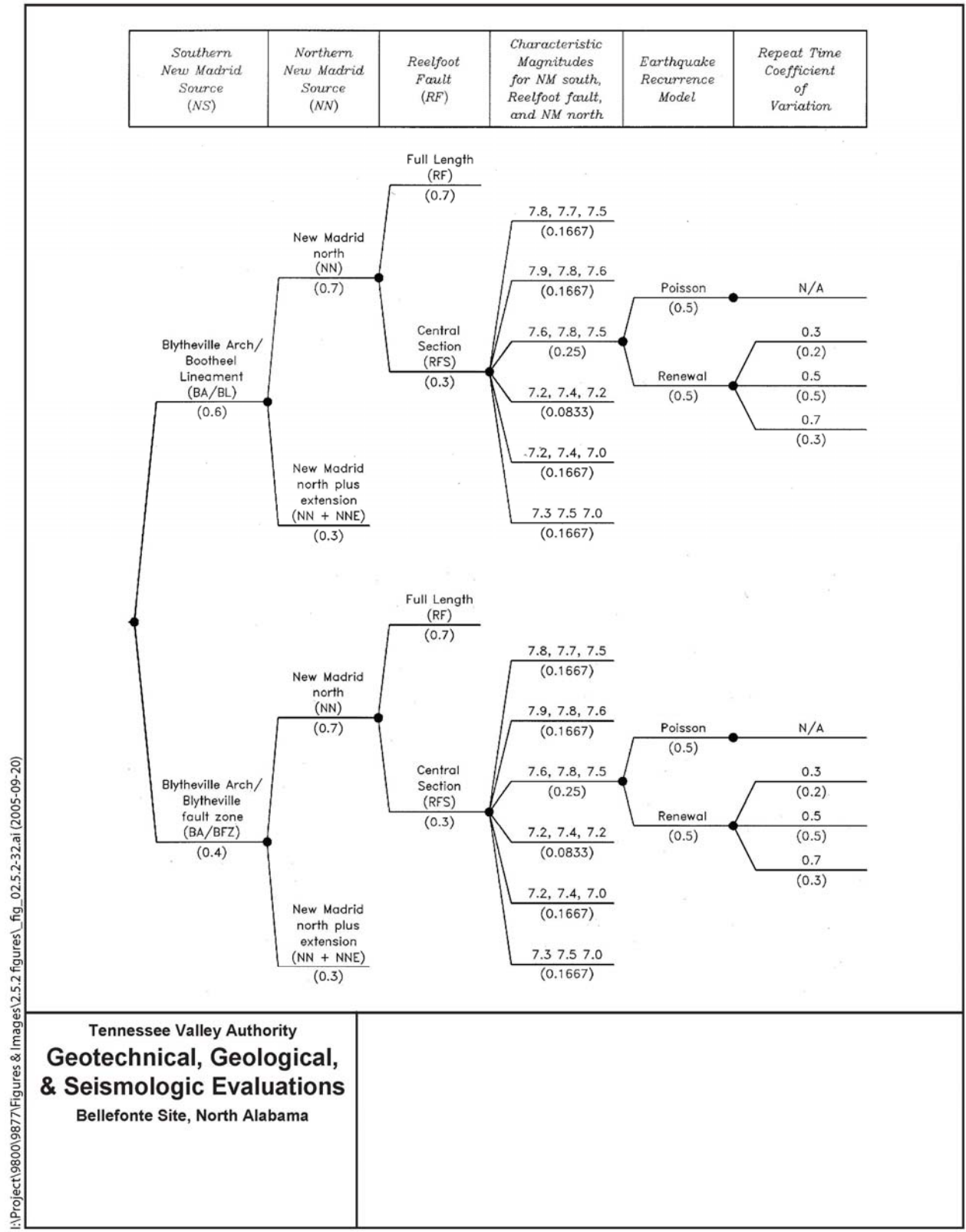


Figure 2.5.2-31. New Madrid (Inset A) and Charleston (Inset B) Repeating Large Magnitude Earthquake Sources



I:\Project\9800\9877\Figures & Images\2.5.2 Figures\fig\_02.5.2-32.a1 (2005-09-20)

**Tennessee Valley Authority**  
**Geotechnical, Geological,**  
**& Seismologic Evaluations**  
Bellefonte Site, North Alabama

**Figure 2.5.2-32. Source Characterization Logic Tree for Repeating Large Magnitude New Madrid Earthquakes**

I:\Project\9800\9877\Figures & Images\2.5.2 figures\fig\_02.5.2-33.ai (2005-09-20)

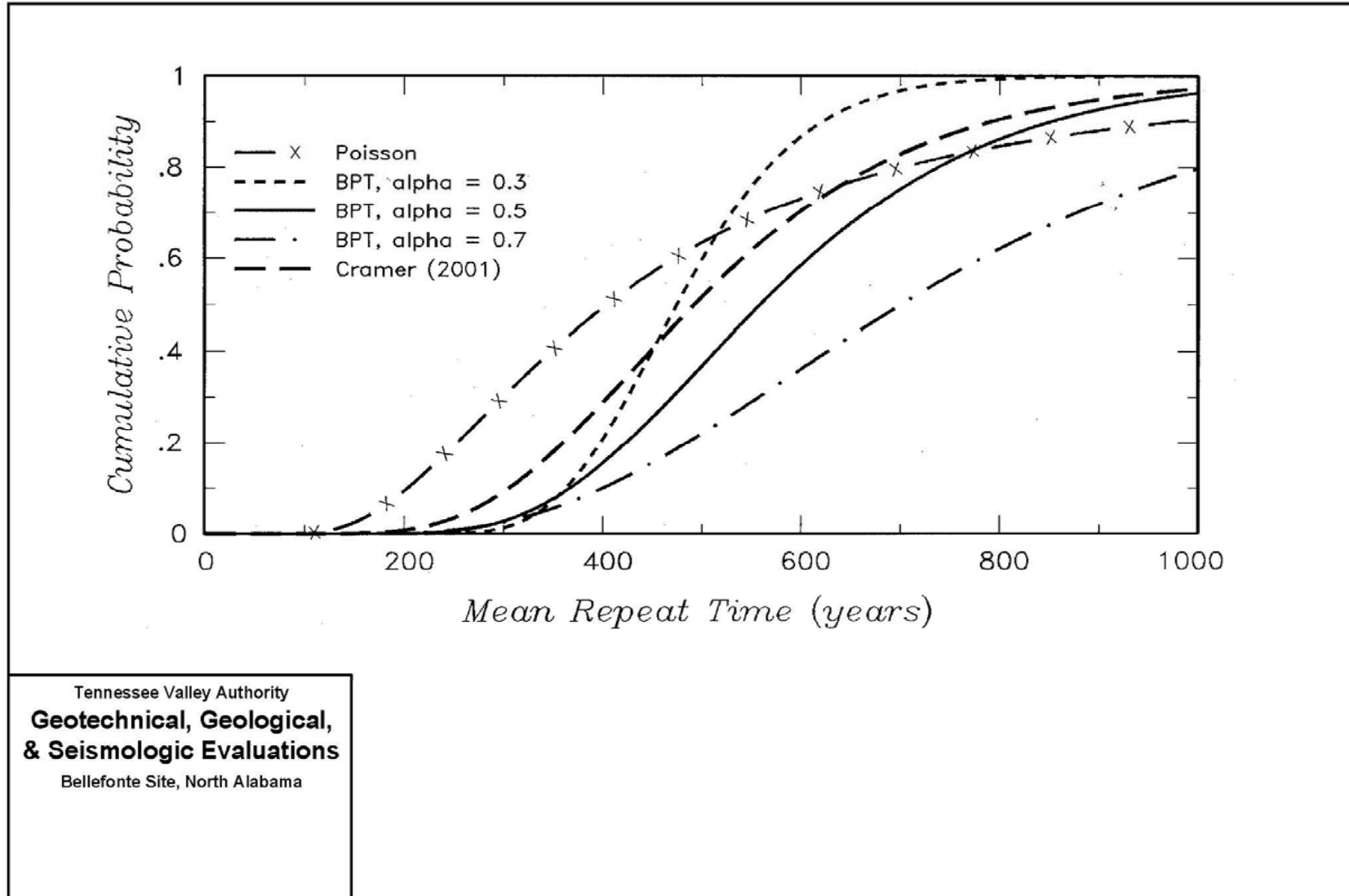


Figure 2.5.2-33. Distributions for Mean Repeat Time for New Madrid Repeating Large Magnitude Earthquakes

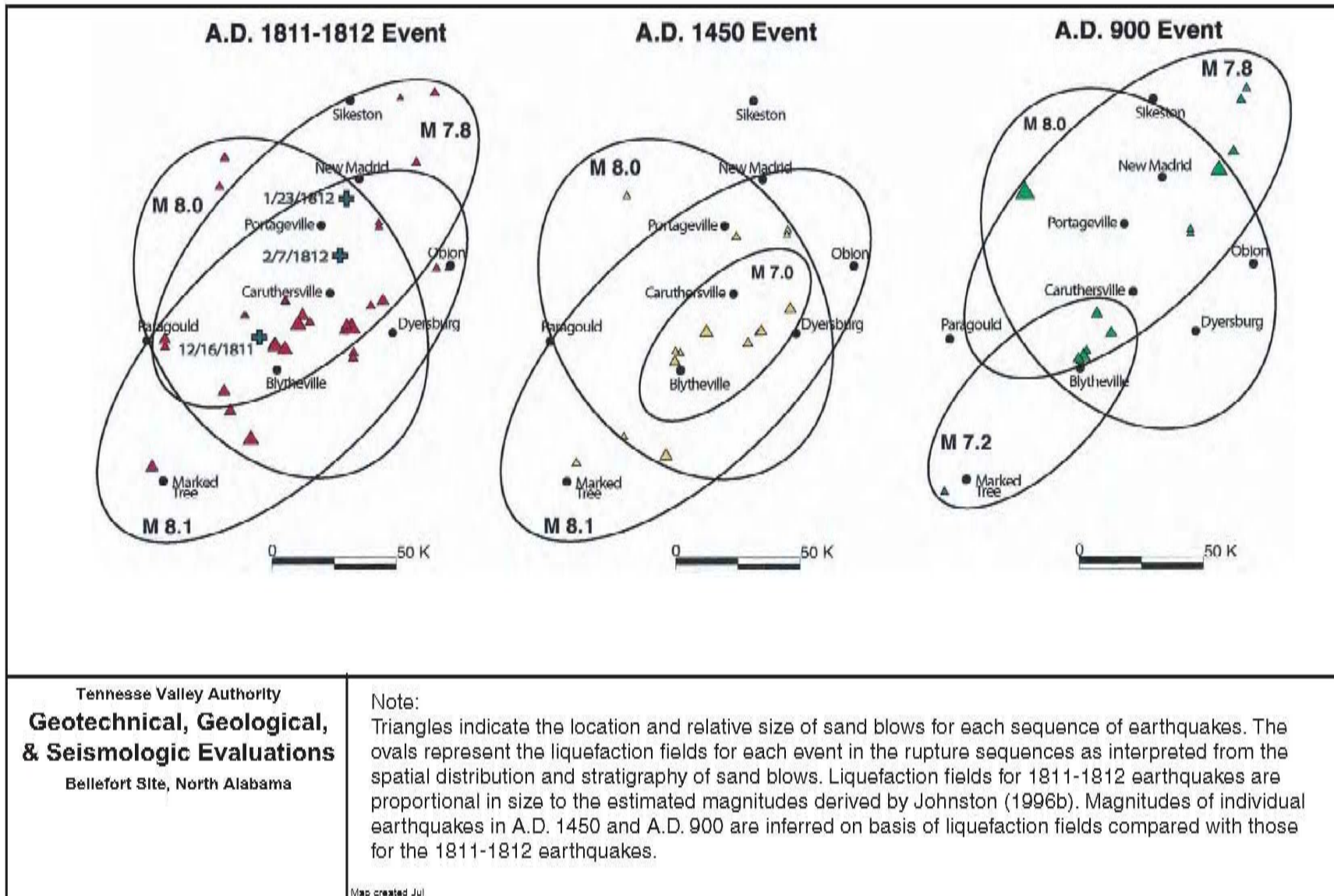
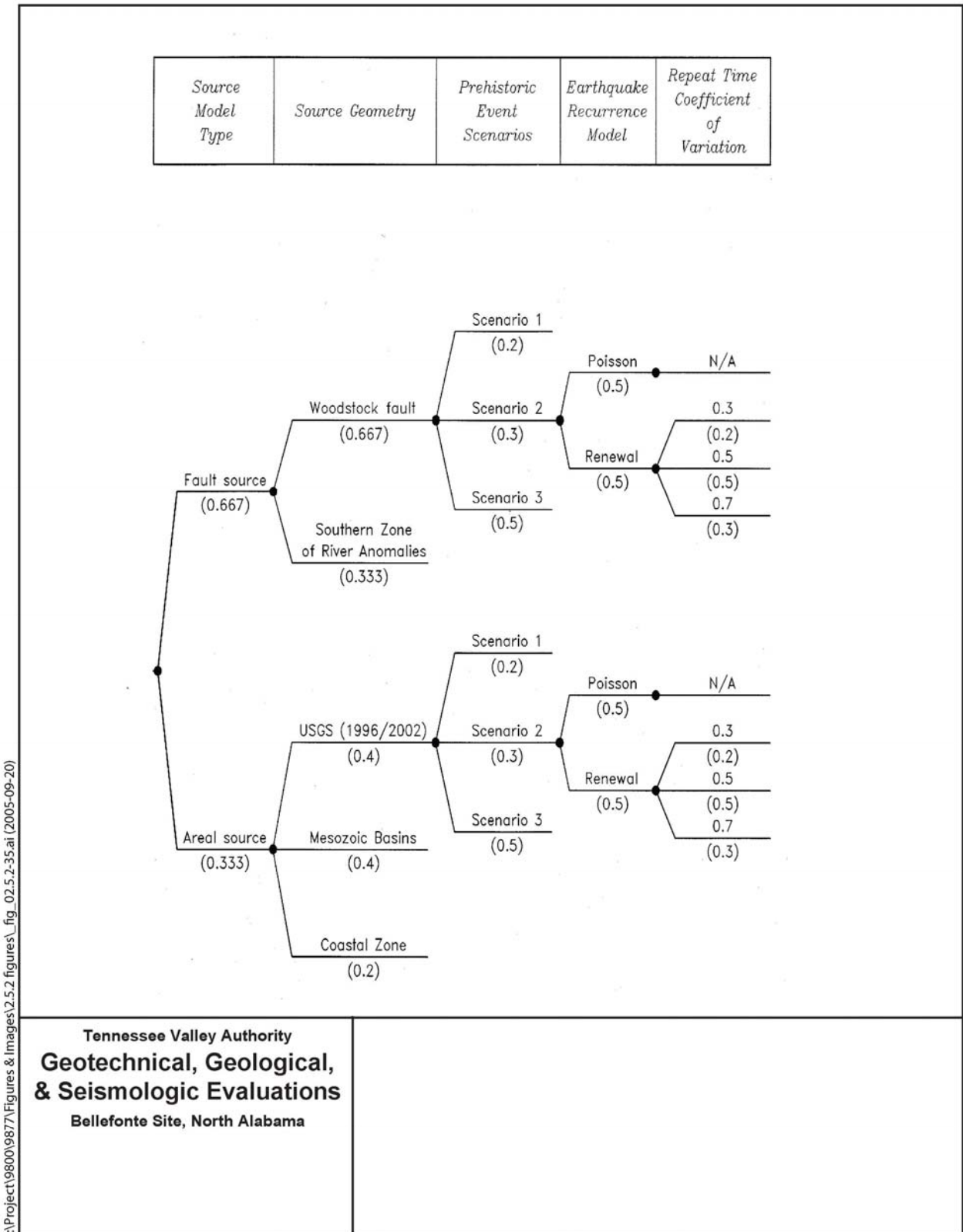


Figure 2.5.2-34. Earthquake Rupture Sequences for Repeating Large Magnitude New Madrid Earthquakes (From Tuttle et al., 2002)

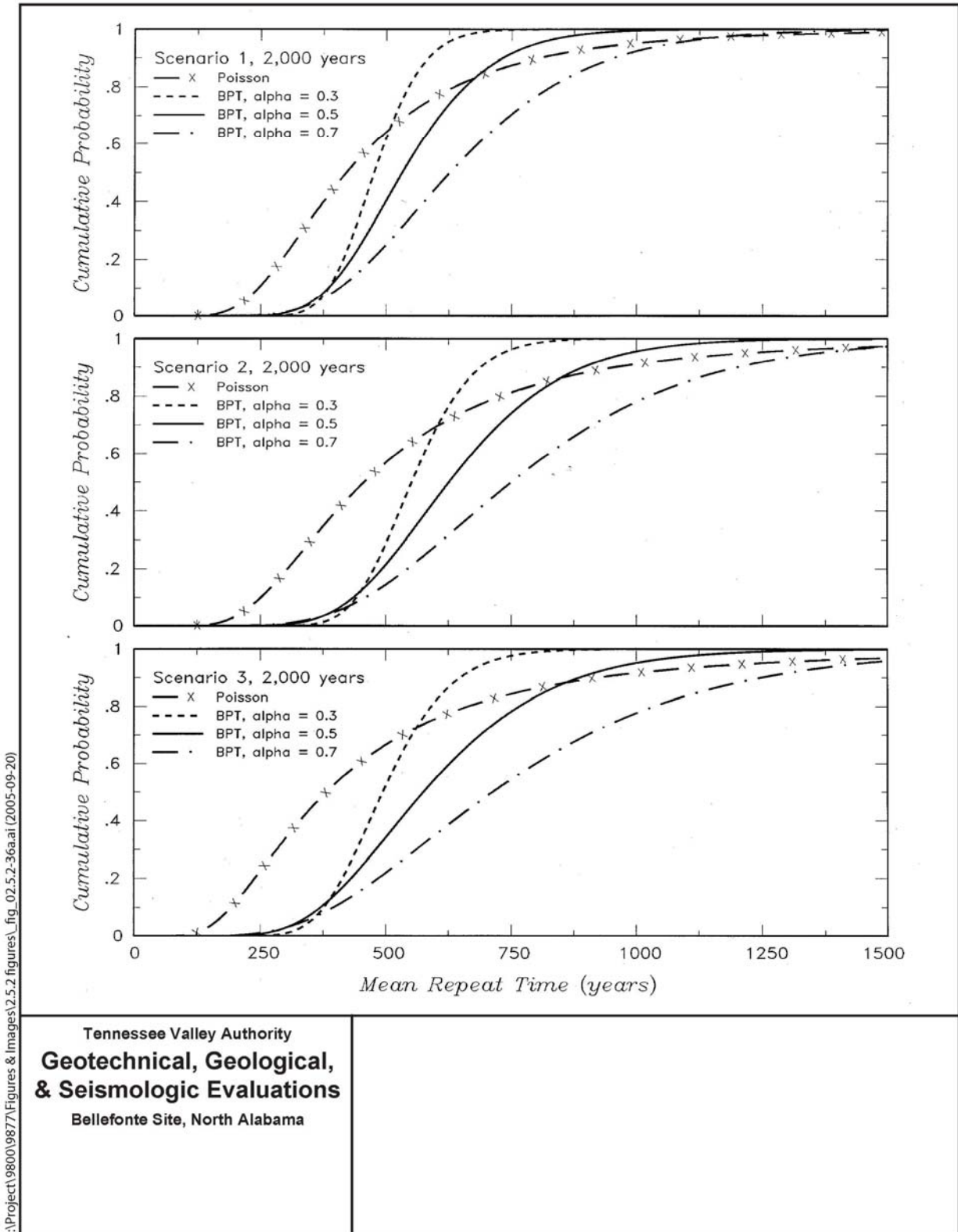




I:\Project\9800\9877\Figures & Images\2.5.2 figures\fig\_02.5.2-35.ai (2005-09-20)

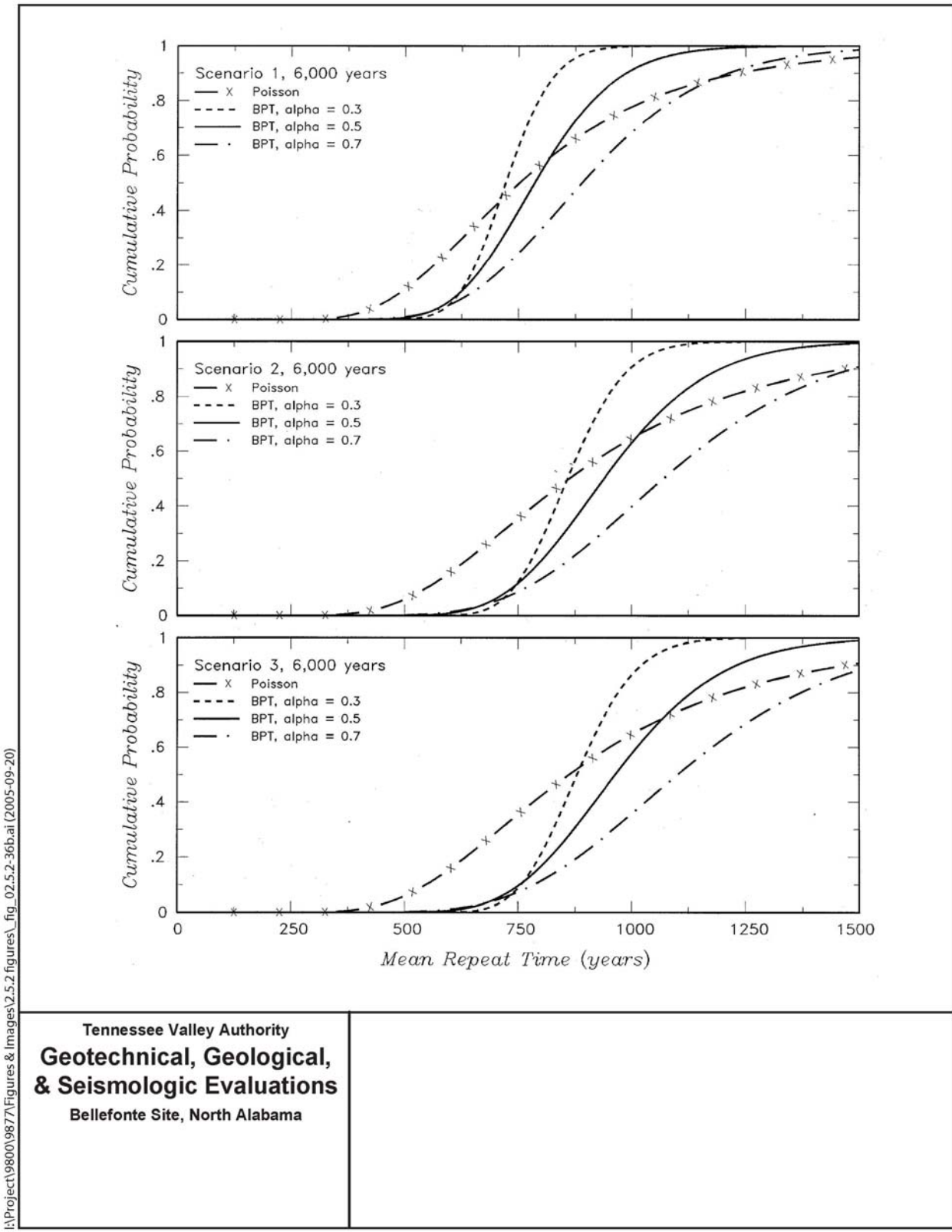
Tennessee Valley Authority  
**Geotechnical, Geological,  
& Seismologic Evaluations**  
Bellefonte Site, North Alabama

Figure 2.5.2-35. Source Characterization Logic Tree for Repeating Large Magnitude Charleston Earthquakes



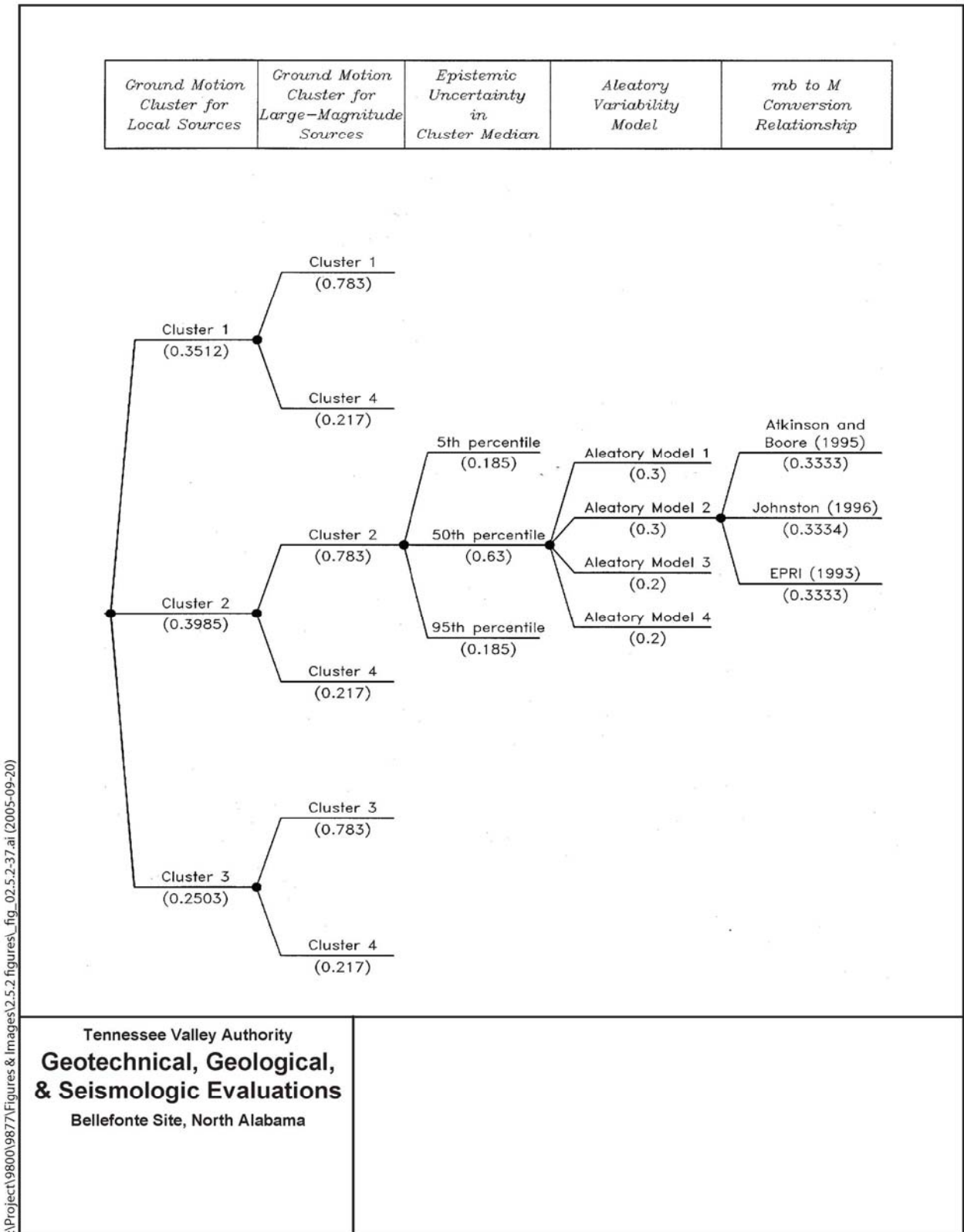
\\Project\9800\9877\Figures & Images\2.5.2 figures\_fig\_02.5.2-36a.at (2005-09-20)

Figure 2.5.2-36(a). Distributions for Mean Repeat Time for Charleston Repeating Large Magnitude Earthquakes



I:\Project\9800\9877\Figures & Images\2.5.2 figures\fig\_02.5.2-36b.ai (2005-09-20)

Figure 2.5.2-36(b). Distributions for Mean Repeat Time for Charleston Repeating Large Magnitude Earthquakes



I:\Project\9800\9877\Figures & Images\2.5.2 figures\_fig\_02.5.2-37.ai (2005-09-20)

Tennessee Valley Authority  
**Geotechnical, Geological,  
& Seismologic Evaluations**  
Bellefonte Site, North Alabama

Figure 2.5.2-37. Logic Tree for Ground Motion Models

E:\Project\9800\9877\Figures & Images\2.5.2 figures\\_fig\_02.5.2-38.ai (2005-09-20)

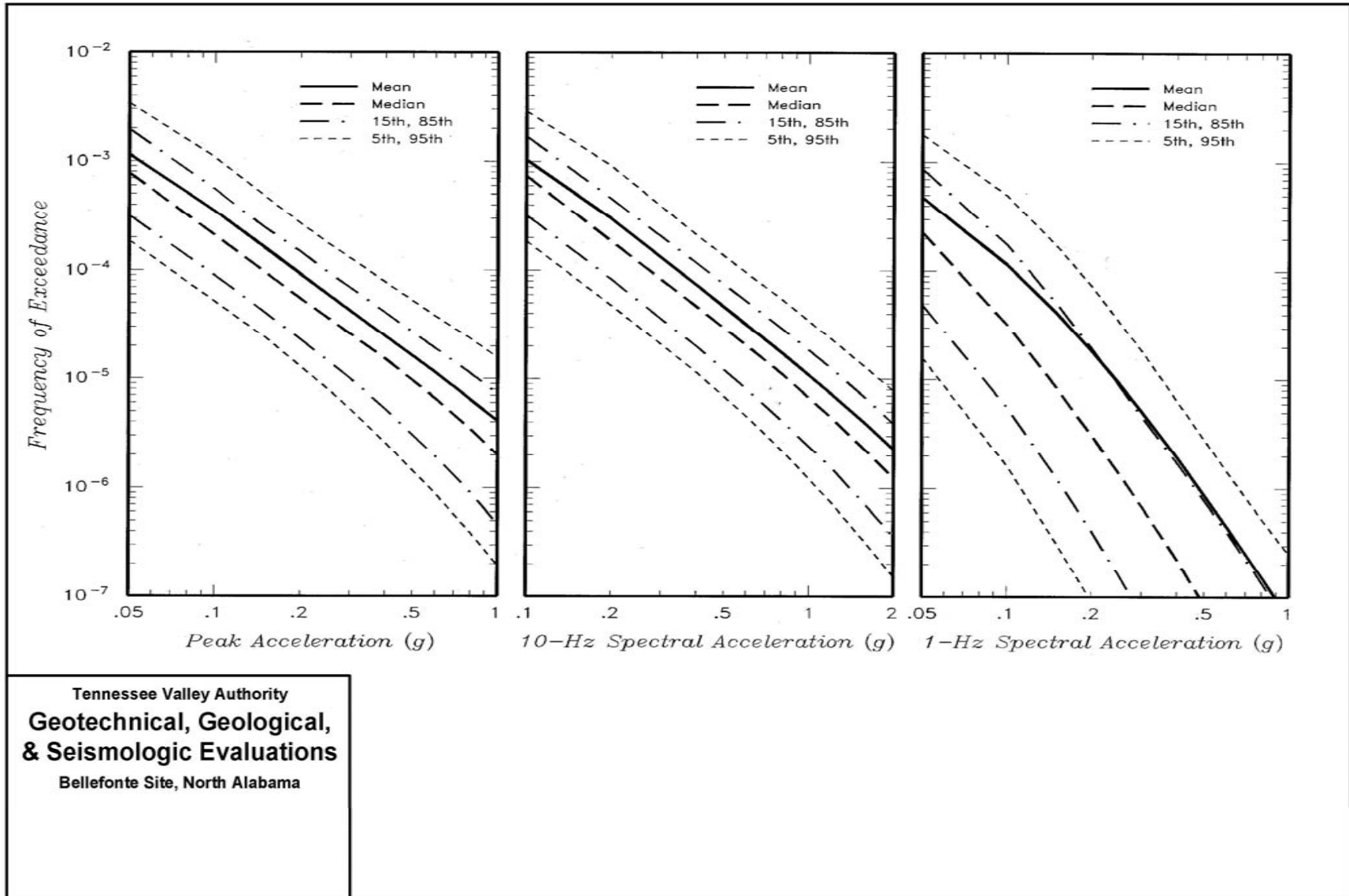


Figure 2.5.2-38. Mean and Fractile Hazard Curves from Updated PSHA

I:\Project\9800\9877\Figures & Images\2.5.2 figures\\_fig\_02.5.2-39.ai (2005-09-20)

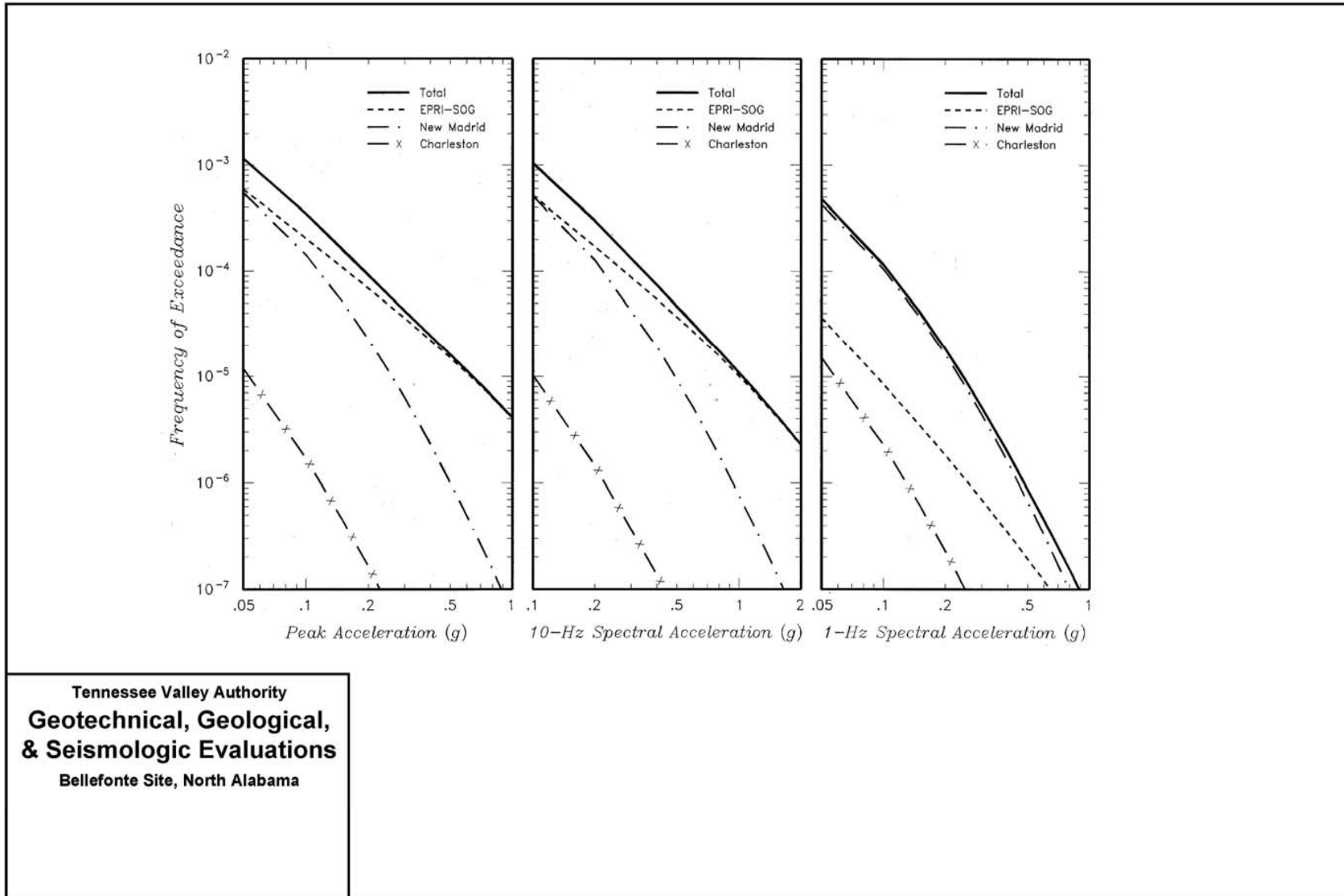
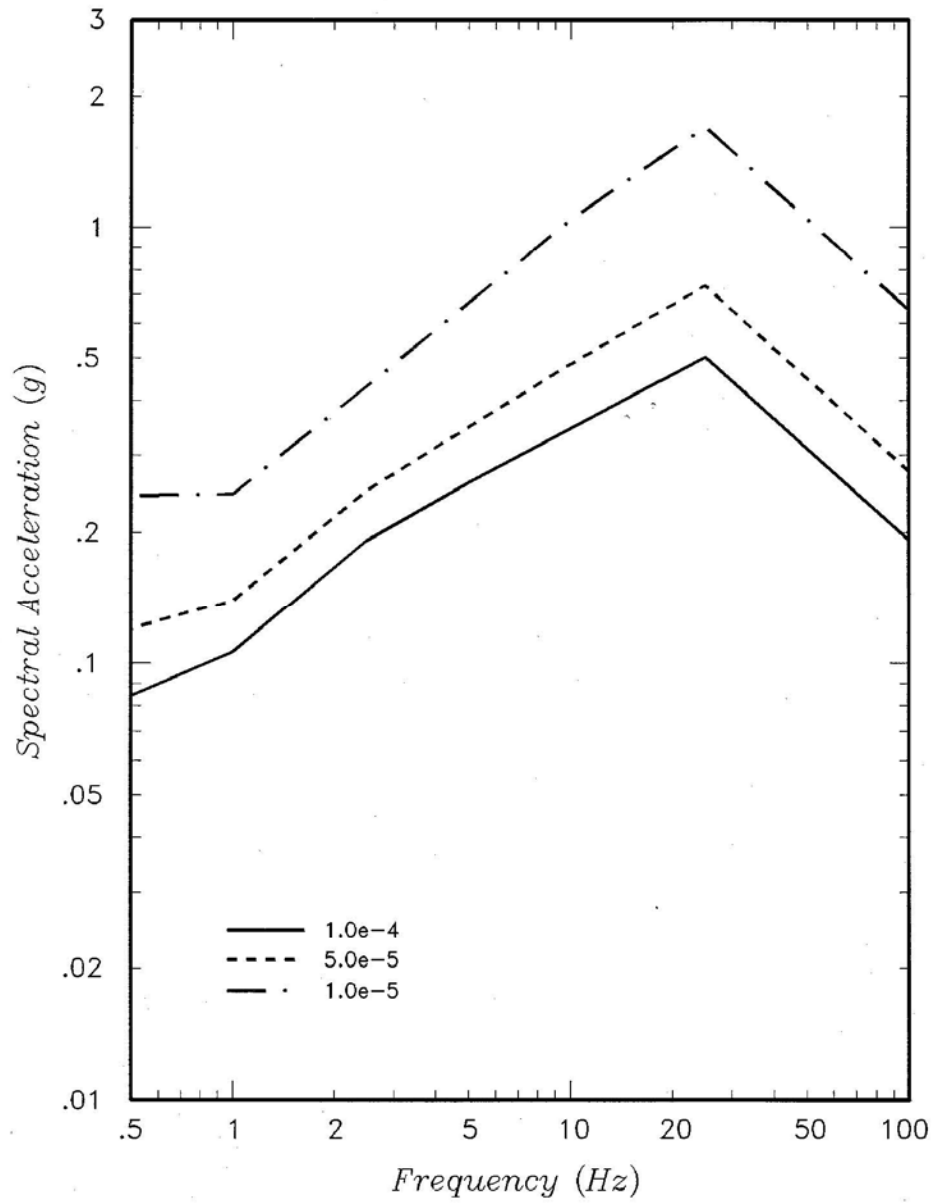


Figure 2.5.2-39. Seismic Source Contributions to Mean Hazard



I:\Project\9800\9877\Figures & Images\2.5.2 figures\fig\_02.5.2-40.ai (2005-09-20)

Tennessee Valley Authority  
**Geotechnical, Geological,  
& Seismologic Evaluations**  
Bellefonte Site, North Alabama

Figure 2.5.2-40. Uniform Hazard Spectra

I:\Project\9800\9877\Figures & Images\2.5.2 figures\\_fig\_02.5.2-41.ai (2005-09-20)

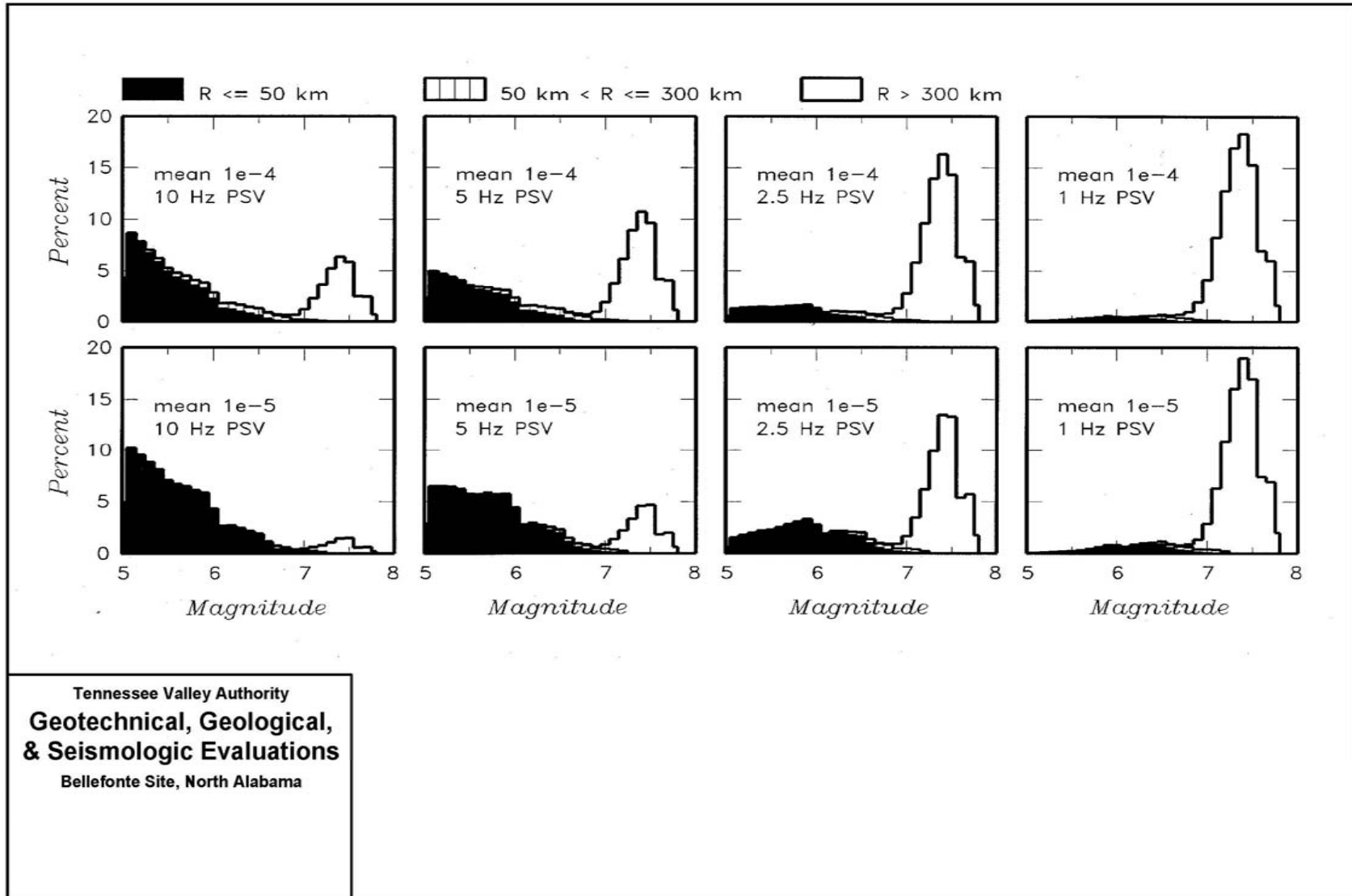
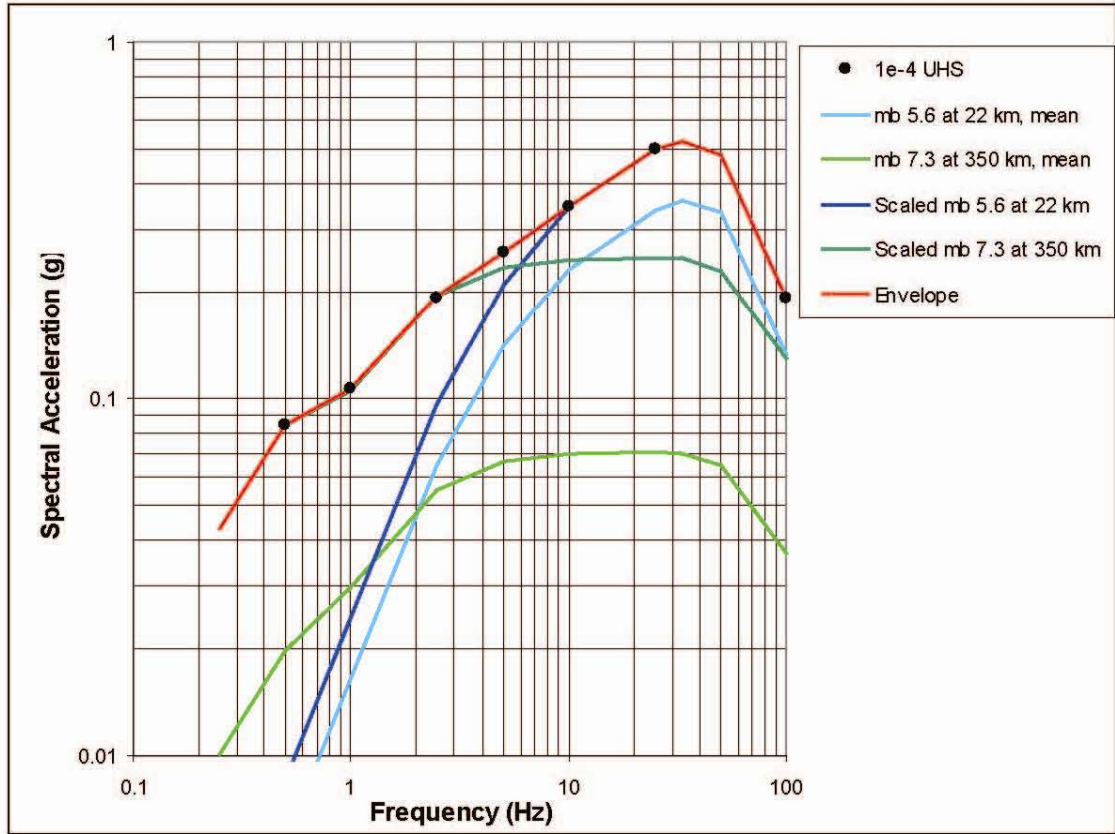


Figure 2.5.2-41. Disaggregation of Mean Hazard

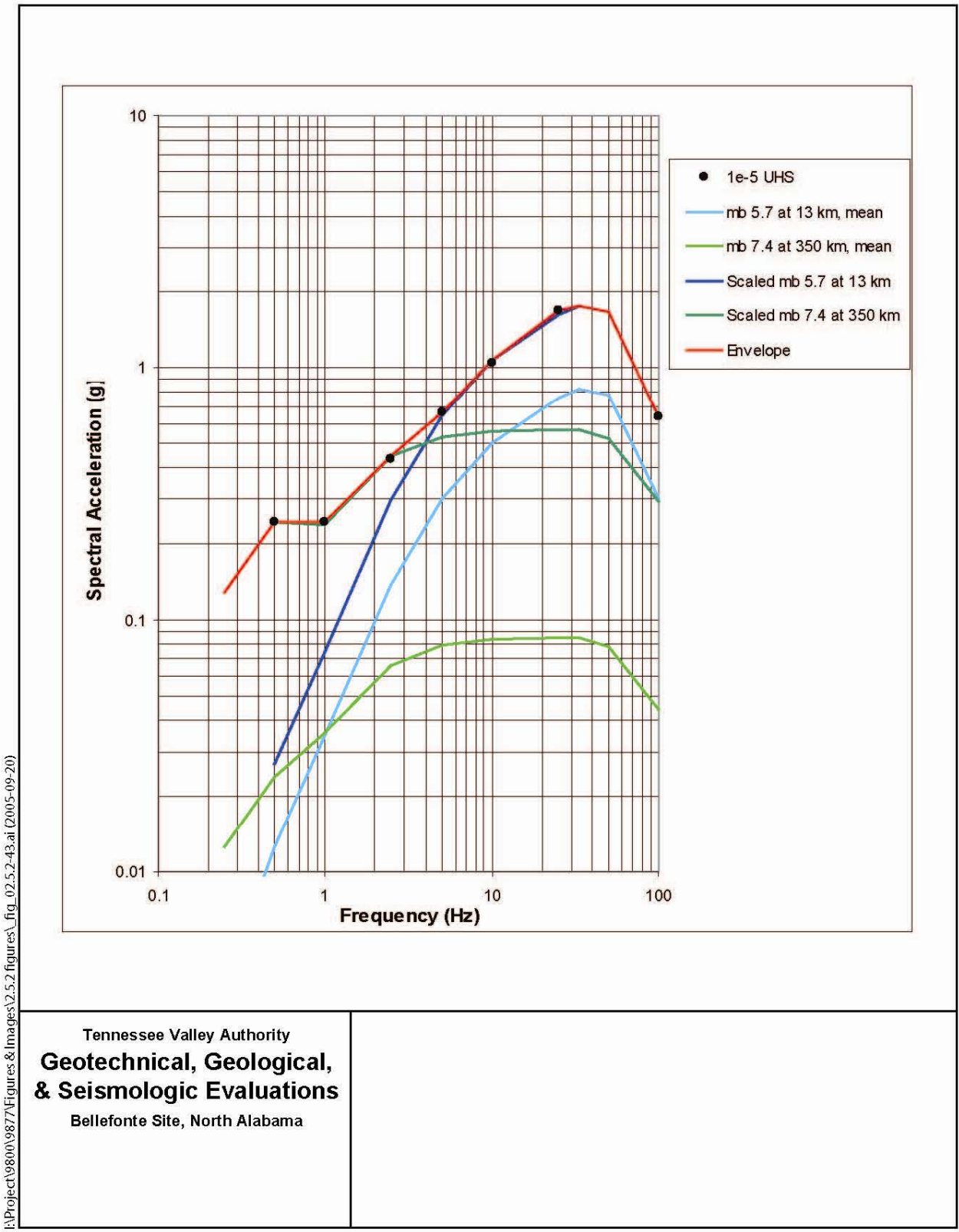




I:\Project\9800\9877\Figures & Images\2.5.2 figures\fig\_02.5.2-42.ai (2005-09-20)

Tennessee Valley Authority  
**Geotechnical, Geological,  
& Seismologic Evaluations**  
Bellefonte Site, North Alabama

Figure 2.5.2-42. Development of Smoothed Response Spectrum for Mean 10-4 Ground Motions



I:\Project\9800\9877\Figures & Images\2.5.2 figures\fig\_02.5.2-43.ai (2005-09-20)

Tennessee Valley Authority  
**Geotechnical, Geological,  
& Seismologic Evaluations**  
Bellefonte Site, North Alabama

Figure 2.5.2-43. Development of Smoothed Response Spectrum for Mean 10-5 Ground Motions

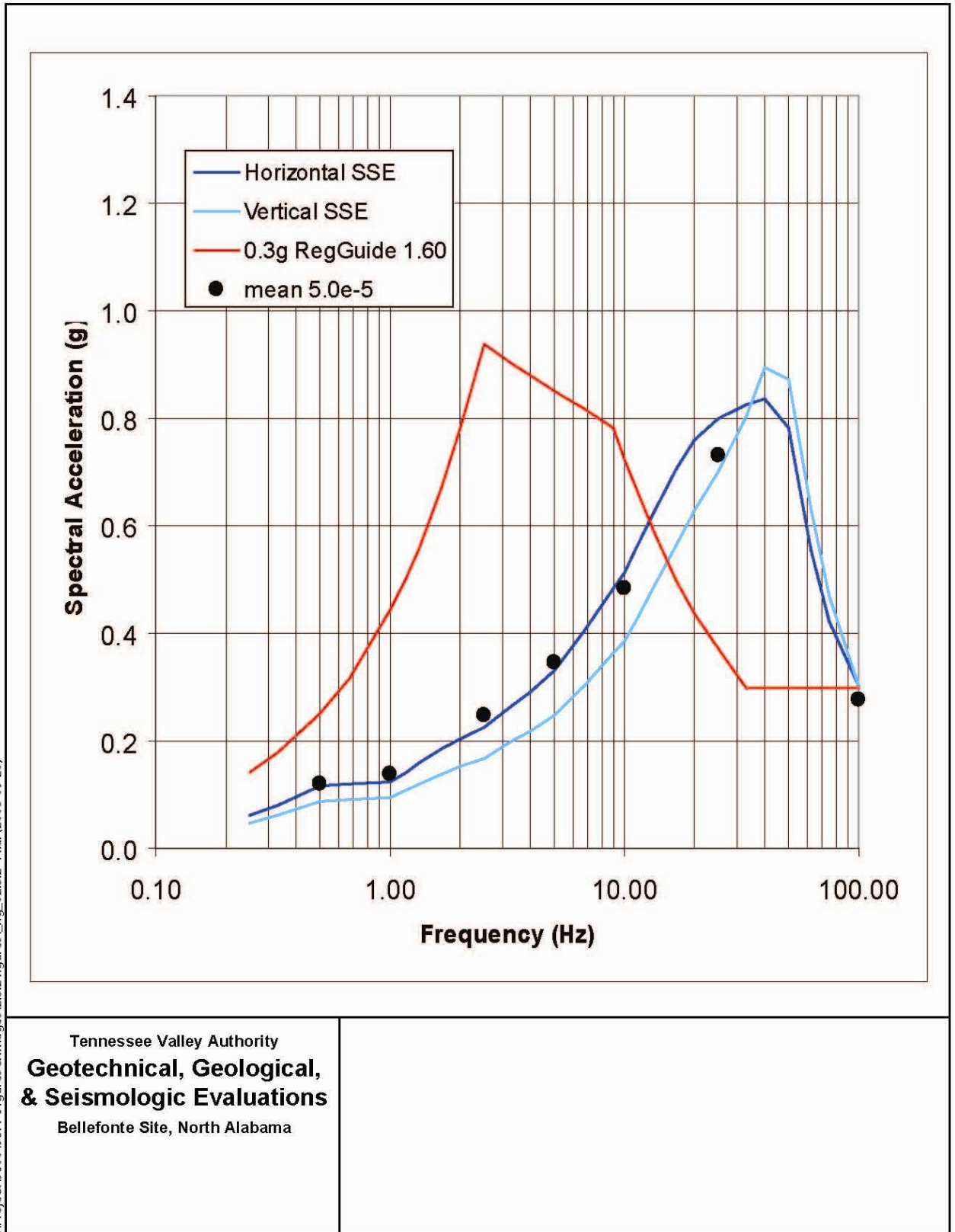


Figure 2.5.2-44. SSE Spectra (5 percent damping) for the Bellefonte Site



## 2.5.3 Surface Faulting

This section describes the evidence gathered to date for faulting or the absence of faulting at the Bellefonte Site and surrounding site area. The following aspects of the geology and seismicity of the site region are discussed:

- Geologic evidence, or lack thereof, for surface deformation (Section 2.5.1.1)
- Earthquakes associated with capable tectonic sources (Section 2.5.1.2)
- Ages of most recent deformation (Section 2.5.1.3)
- Relationship between tectonic structures in the site area and regional structures (Section 2.5.1.4)
- Characterization of identified capable tectonic sources (Section 2.5.1.5)
- Identified zones of Quaternary deformation (Section 2.5.1.6)
- Potential for surface tectonic deformation at the site (Section 2.5.1.7)

Results of the surface faulting study indicate that there is no evidence for Quaternary tectonic surface faulting or fold deformation at the Bellefonte Site, and no capable tectonic sources have been identified within 25 miles of the site. A capable tectonic source is a tectonic structure that can generate both vibratory ground motion and tectonic surface deformation, such as faulting or folding at or near the earth's surface in the present seismotectonic regime (Regulatory Guide 1.165, USNRC, 1997). Minor karst features related to dissolution preferentially occurring along joints are present at the site and in the site area, but these features do not pose a surface rupture or displacement hazard (additional description of these features is provided Section 2.5.4.2.1).

### 2.5.3.1 Geological, Seismological, and Geophysical Investigations

The following investigations have been performed as part of the Bellefonte Site characterization study:

- **Compilation and Review of Existing Data and Literature** – The BLNP FSAR (TVA, 1986) provides detailed geologic maps and descriptions of the stratigraphy and structure within a 3- to 5-mile radius of the Bellefonte Site. Detailed subsurface information from the construction reports for the BLNP that described geologic structures observed in the foundation excavations also was reviewed, and personnel involved in the BLNP site characterization studies were contacted. Soil surveys of Jackson County that include the Bellefonte Site were acquired and reviewed. Published maps and literature pertaining to the structure, tectonics, and stratigraphy of the site region also were reviewed.
- **Interpretation of Aerial Photography** – Pre-construction and post-construction aerial photographs were obtained from the TVA Map Store in Chattanooga, Tennessee.
- The photographs of the footprint and site were examined to look specifically for evidence of tectonic or non-tectonic (e.g., karst or dissolution features) surface deformation. The 1966 photos and selected 1935 pre-inundation photos provide coverage along the Sequatchie Valley thrust in the site area. These photos were reviewed to assess the presence or absence

of geomorphic features indicative of potential Quaternary activity along the only mapped fault within 5 miles of the site.

- **Lineament Analysis** – Previous investigations of the TVA Bellefonte Plant conducted in support of the FEIS (TVA, 1997, Appendix F) identified photolineaments across the site. As part of the GG&S investigation, existing aerial photographs and topographic maps were reviewed to confirm the presence of previously identified lineaments, to evaluate whether any previously unidentified lineaments may be present, and to evaluate whether there is any geomorphic evidence to indicate a surface rupture hazard associated with the lineaments that intersect the site. In addition to aerial photographs of the site and site area, the U.S. Geological Survey Hollywood, Alabama, 7.5-minute topographic map (dated 1947 and photo revised 1980) was reviewed to identify topographic lineaments.

The lineament evaluation focused on the Bellefonte footprint and the directly adjacent areas. After review of all the available materials, it was determined that the clearest and most comprehensive coverage of the Bellefonte Site and surrounding area was provided by the set of 1:4,800 scale black-and-white photographs taken in 1970. These high-resolution photographs provide excellent shading contrast that allows lineaments to be readily identified (Figure 2.5.3-1). Therefore, these photographs were the primary reference for the photolineament evaluation of the site.

Aerial photographs were studied both individually and as stereo pairs. Topographic lineaments were noted by observing apparent trends such as water and wind gaps in the adjacent ridge, linear drainage features, and embayments in Town Creek, which may indicate large-scale structural controls. Lineaments were also noted if a distinct shading contrast was apparent that did not correspond to an obvious cultural feature, such as a fence row or road. In cases where the contrasts were very subtle, attempts were made to observe the feature on adjacent or overlapping photographs. Features that were questionable and could not be traced across multiple images were not designated as lineaments. As lineaments were identified, they were traced onto a topographic map for future reference and digitizing.

Figure 2.5.3-2 shows lineaments identified during this investigation and during the previous study (TVA, 1997). Results of the two studies are generally similar in that most lineaments identified are oriented northwest-southeast or southwest-northeast. North- and east-trending lineaments, which are present, are not as common. A discussion of the origin and significance of the lineaments is presented in Section 2.5.3.2.

- **Field Reconnaissance** – Field reconnaissance was conducted as part of the Bellefonte Site characterization activities. The initial field reconnaissance focused on review of the geology of the site (within approximately 0.6 mile of the footprint) and site area (within a radius of about 5 miles). Photolineaments and karst features observed from the review of previous studies and aerial photographs were reviewed in the field. A reconnaissance along the Sequatchie Valley thrust fault and related fold within the site area also was conducted. The second field reconnaissance was conducted in conjunction with an aerial reconnaissance. The structures within the Appalachian fold and thrust belt in the site vicinity (25-mile radius) and in the epicentral region of the 2003 Fort Payne earthquake (approximately 25 to 30 miles from the site) were the primary focus of this reconnaissance. The reconnaissance included a review of the Quaternary deposits mapped along the Coosa River in the Gadsen

to Weiss Lake region, approximately 20 miles from the epicentral region of the Fort Payne earthquake, and a historical landslide also in the epicentral region of this earthquake. A map showing the extent of the aerial reconnaissance and ground reconnaissance is shown in Figure 2.5.3-3.

- **Discussions with Current Researchers in the Area** – Researchers familiar with the structural and tectonic framework of the region (Dr. R. D. Hatcher; University of Tennessee, personal communication, January 14 and February 1, 2005; Dr. C. A. Powell, CERL, University of Memphis (personal communication, March 2, 2005; and Dr. W. A. Thomas, University of Kentucky/Alabama Geological Survey, personal communication, February 8, 2005), Quaternary geology of the southern Appalachian region (Dr. H. H. Mills, Tennessee Technological University, personal communication, April 29, 2005; Ms. D. Raymond, Alabama Geological Survey, personal communication), geologic mapping of the Coosa River terraces (Mr. E. Osborne, Alabama Geological Survey, personal communication, February 8, 2005), and karst development (Dr. B. Beck, Bellefonte Review Panel, May 13, 2005) were contacted. These researchers provided recent published and in-press publications for our review.
- **Review of Seismicity Data** – A comprehensive review of both instrumental as well as historical earthquakes was completed for the GG&S study (see Section 2.5.2.1).

### 2.5.3.2 Geological Evidence, or Absence of Evidence, for Surface Deformation

As shown in Figure 2.5.1-35, two bedrock faults, the Sequatchie Valley and Big Wills Valley thrust faults, are mapped within Paleozoic rocks in the site vicinity (25-mile radius), and one of these, the Sequatchie Valley thrust fault, is within the site area (5-mile radius). Basement faults that may have influenced the development of these thrust faults are inferred from interpretation of seismic profile data. Descriptions of these faults are presented in Section 2.5.3.2.1, and a discussion of the evidence that indicates they are not capable tectonic sources is presented in Section 2.5.3.6.

As noted in the BLNP FSAR (TVA, 1986) and the FEIS (TVA, 1997), there is no intense folding or major faulting of the bedrock at the BLNP site and adjacent area. Small-scale fractures and one small fault were identified in the BLNP foundation excavation exposures. The minor displacement observed was investigated by core drilling and recorded by surface mapping (TVA, 1986 and Detailed Supplementary Information Reports cited therein). No additional faults or folds in exposed bedrock at the site were observed during reconnaissance investigations for this study.

Photolineaments identified in the TVA (1997) study from examination of 1972 (predisturbed) and 1990 aerial photographs were reviewed for this study. A summary of the results of the lineament analysis conducted for this study is presented in Section 2.5.3.2.2.

The most prominent lineaments that intersect the footprint of the Bellefonte Site trend approximately N50°W, orthogonal to bedrock strike. These lineaments are defined by linear drainage segments (observed in pre- and post-construction topographic maps and photos). Another set of lineaments parallel the bedrock strike. Less distinct lineaments (tonal changes) having north-south and east-west trends also were observed in the vicinity of the site. None of these north-south or east-west lineaments can be traced regionally and the continuity and expression of the lineaments appear to vary in different lithologic bedrock units. The trends of

the major lineaments appear to reflect the orientation of prominent joints that have been mapped in the site area (TVA, 1986; TVA, 1997).

The seismic refraction and microgravity surveys conducted in the Bellefonte project footprint were designed to provide additional subsurface information across the site, and over some of the major lineaments. The results of this survey showed localized depressions in the top of less-weathered bedrock (higher P-wave layer) that sometimes correlated with some of the more prominent lineaments at the site (Technos, Inc., Appendix C). The more prominent lineaments appear to represent either strike-oriented belts of dipping strata that may be prone to dissolution relative to surrounding strata, or cross-structural solutionally enlarged joints and/or fractures that have facilitated groundwater movement and weathering. There is no geomorphic or geologic mapping evidence to suggest that any of these lineaments is associated with a capable tectonic fault or pose a surface rupture hazard.

### **2.5.3.2.1 Geologic Structures in the Site Vicinity (25-Mile Radius)**

Key observations made from the literature review and field reconnaissance regarding the geologic structures in the site vicinity (25-mile radius) are summarized as follows.

#### **2.5.3.2.1.1 Sequatchie Valley Anticline and Thrust Fault**

The Sequatchie anticline is the most northwesterly structure of the southern Appalachians (Thomas and Bearce, 1969; Thomas, 1986). It is an elongated asymmetric anticline that extends 250 miles from Morgan County, Tennessee, to Jefferson County, Alabama. The northwest limb of the anticline is steep along its entire length; and, a northwest-verging thrust fault extends along the northwest flank of the anticline from near its northeastern end 150 miles southwestward. At its north end, the anticline is formed over a ramp linking the Cambrian Rome Formation with Pennsylvanian clastic rocks (Wiltschko in Hatcher et al., 1989c). The displacement on this fault decreases toward the south to a point about 70 miles southwest of the Alabama-Tennessee state line where the fault disappears completely (Thomas and Bayona, 2002). The gently dipping southeast limb in the site vicinity extends into the broad, flat-bottomed Coalburg syncline that underlies Sand Mountain.

Wells drilled to Precambrian rocks indicate that depth to basement rocks is approximately 8,400 feet beneath the Sequatchie anticline in northern Alabama, and stratigraphic observations in well and regional seismic data suggest that the structure soles into the regional detachment near the base of the Paleozoic cover sequence (Thomas, 1986; Thomas and Bayona, 2002).

The Sequatchie Valley thrust fault is mapped along the northwest margin of Backbone Ridge, within 2.1 miles of the Bellefonte Site at its closest distance (Figure 2.5.1-36). No exposures of the Sequatchie thrust fault were observed during the reconnaissance for the GG&S study and none are described in the mapping conducted as part of the BLNP site characterization activities (TVA, 1986). Excavations in a landfill operation located approximately 3.2 miles from the Bellefonte Site along Backbone Ridge (Field Stop KH2, Figure 2.5.1-36), provide good exposures of steeply dipping strata and deformation (possibly backthrusts) in the hanging wall of the Sequatchie thrust. Backbone Ridge is formed where Fort Payne chert is preserved in the hanging wall of the thrust fault (Osborne et al., 1988). Backbone Ridge terminates at the western margin of the Guntersville Reservoir along Mud Creek, approximately 4 miles northeast of the Bellefonte Site. Northeast of Mud Creek, this formation is absent and the strong geomorphic expression of the steeply dipping beds is less apparent.



No deformation or geomorphic features indicative of potential Quaternary activity have been reported in the literature for this fault, and none were identified during aerial and field reconnaissance and air photograph interpretation undertaken for this study of the Bellefonte Site.

### 2.5.3.2.1.2 Wills Valley Anticline and Thrust Fault

The Wills Valley anticline and associated thrust fault also lies within the northwestern (frontal) part of the Appalachian thrust belt, which is characterized by broad, flat-bottomed synclines and large-scale, northeast-trending, narrow asymmetric anticlines. The Wills Valley fault is located 17 miles southeast of the Bellefonte Site (Osborne et al., 1988).

The Wills Valley thrust fault, like the Sequatchie Valley thrust fault, is of regional extent and soles into the regional detachment at a depth of about 10,000 feet (Thomas and Bayona, 2002; Bayona et al., 2003). The thrust fault crops out at the western margin of the Wills Valley on the eastern flank of Sand Mountain. No deformation or geomorphic features indicative of potential Quaternary activity have been reported in the literature for this fault, and none were identified during aerial and field reconnaissance undertaken for this Bellefonte Site.

### 2.5.3.2.1.3 Sub-detachment Basement Faults

Based on interpretation of seismic reflection profile data, Bayona et al. (2003) identify faults within the basement below the detachment that appear to have controlled the location of the Sequatchie Valley and Wills Valley thrust faults and folds (Figure 2.5.1-16). The inferred subdetachment basement fault associated with the Sequatchie Valley thrust fault is inferred to lie beneath the site based on correlations between picks on seismic lines that are located approximately 23 miles and 30 miles to the northeast and southwest of the Bellefonte Site, respectively (Figure 2.5.1-19). Based on the inferred locations of this basement fault and detachment, the closest distance of this fault to the Bellefonte Site would be greater than or equal to approximately 8,400 feet (1.6 miles). The closest distance of the inferred basement fault in Wills Valley is approximately 19 miles. There are no seismicity alignments or surface geologic evidence to indicate that these faults have been reactivated in the current tectonic stress field. No deformation or geomorphic features indicative of potential Quaternary activity have been reported in the literature for these faults, and none were identified during aerial and field reconnaissance undertaken for this study.

### 2.5.3.2.2 Results of Lineament Analysis

As described in Section 2.5.3.1, a lineament analysis was undertaken as part of the Bellefonte study to identify and characterize lineaments that intersect the Bellefonte Site. The most prevalent lineament that intersects the site trends southeast-northwest and extends across most of the Bellefonte footprint (Figure 2.5.3-2). The lineament is identified primarily by a water gap through the ridge southeast of the footprint area. The lineament also aligns with a series of right-angle turns in Town Creek (northwest of the Bellefonte footprint) and with a small gully shown in pre-construction topographic maps of the BLNP site (Figure 2.5-9 in TVA, 1986) indicating that bedrock structure, probably jointing, likely is controlling the drainage pattern. This lineament is one of a series of subparallel lineaments that are apparent along the Tennessee River Valley in the vicinity of the Bellefonte plant, and is part of the overall topographic fabric of the area. The location of these lineaments likely is related to large-scale structural deformation that resulted in joint formation in the limestone bedrock. These joints cause the

bedrock to become weaker compared to surrounding rock, and also become areas of preferential groundwater flow. The result is that surface erosion and karst development occurs preferentially along these features, resulting in the topographic expressions.

A series of northeast-southwest lineaments also was noted in both the previous FEIS investigation (TVA, 1997) and this study. These parallel bedrock strike and likely reflect changes in lithology and possible strike-parallel jointing (possibly related to small flexures along the flank of the Sequatchie anticline) in the southeast-dipping limestone bedrock. The lineaments appear as shading differentials on the black-and-white photographs, and probably reflect different moisture contents in the various strata that comprise the Chickamauga Formation. Whereas both studies identified a series of such lineaments, the GG&S evaluation identified additional northeast-southwest lineaments in and near the Bellefonte Site footprint.

The previous investigation identified one north-south lineament that extends through the Bellefonte Site footprint. Whereas this lineament was not identified during the GG&S evaluation, a similar feature was observed 800 feet to the west. The lineament was identified through shading variations on the 1970 photographs; although it was quite subtle, it could be traced across two adjacent photographs.

One east-west lineament was identified in the current study. This feature is located on the topographic ridge northeast of the Bellefonte Site footprint, and was identified on aerial photographs as a small linear erosional feature near the top of the ridge. The feature did not extend into the Bellefonte Site footprint.

The overall pattern of lineaments identified during this investigation agrees with the results of the previous study (TVA, 1997). The overall orientations of the prominent lineaments in the site area are also consistent with the orientation of major joint sets observed in the Appalachian Plateau region (i.e., one across and one subparallel to the strike of major structures) (Wiltchko in Hatcher et al., 1989) and in the excavation exposures for the BLNP (TVA, 1986). North-south and east-west lineaments, which are minor joint sets seen regionally (Wiltchko in Hatcher et al., 1989a) are rare and do not result in prominent topographic or photographic features in the site area. Although north-south and east-west joint orientations agree with the trends for sub-detachment earthquakes in the region as evidenced by focal mechanism analysis, studies show that activity is occurring on the basement structures that are decoupled from the Valley and Ridge structures mapped at the surface above the detachment (Chapman et al., 1997, 2002).

The most significant lineament that may affect groundwater flow and resulting karst development at the Bellefonte Site extends southeast-northwest through the Bellefonte Site footprint and is one of a series of similarly oriented features that comprise a dominant strike-perpendicular trend in the larger topographic pattern of the site area. Strike-parallel lineaments probably reflect variations in the lithology and water content of the dipping limestone, and may have some local impact on karst development, particularly in the eastern and southeastern part of the study footprint (see discussion in Section 2.5.1.2.5).

The photogeologic interpretation identified no geomorphic evidence that would indicate differential uplift or surface deformation (e.g., warping, tilting) associated with the lineaments that intersect the site. This absence of differential uplift or surface deformation indicates that these lineaments are not related to capable tectonic faults.

### 2.5.3.3 Correlation of Earthquakes with Capable Tectonic Sources

There have been no historically reported earthquakes within 25 miles of the site that can be associated with a mapped bedrock fault. Historical earthquakes in the site vicinity, including the M 4.6 Fort Payne earthquake in 2003, have been postulated to be associated with reactivated faults in the basement below the Appalachian detachment. There is no apparent correlation between the location of historical seismicity within 25 miles of the site and mapped subdetachment basement faults (Figure 2.5.3-4).

Potential seismogenic sources inferred from seismicity that is occurring in basement rocks below the detachment are considered in the characterization of alternative seismic sources included in the PSHA (Section 2.5.2).

### 2.5.3.4 Ages of Most Recent Deformation

As discussed in Section 2.5.3.2, none of the faults within the site vicinity (25-mile radius) exhibit evidence for Quaternary activity. The mapped surface faults formed during the culmination of the Alleghanian orogeny at the end of the Paleozoic. Hatcher et al. (1989b) summarizes evidence for the timing of deformation of the foreland during the Alleghanian orogeny. Deformation of the foreland affected rocks as young as Pennsylvanian and early Permian, and may have continued later. Foreland deformation may have ended as early as 286 to 266 Ma, the age of the youngest deformed foreland unit, the Dunkard Group in Pennsylvania, Ohio, and West Virginia. The subdetachment basement faults are inferred to be Iapetan normal faults that likely formed initially during the late Proterozoic and early Paleozoic. These faults may have been reactivated during subsequent orogenies, but there is no evidence of surface deformation associated with reactivation of these faults in post-Alleghanian time.

### 2.5.3.5 Relationship of Tectonic Structures in the Site Area to Regional Tectonic Structures

As described in Section 2.5.1.1.4.2(a), mapped surface bedrock faults within the site vicinity (25-mile radius) are part of the Appalachian foreland fold-thrust belt that developed during the Alleghanian orogeny. The culmination of the Alleghanian orogeny occurred in the late Paleozoic. There is no new information to suggest that the thrust faults within the Appalachian foreland thrust belt are capable tectonic structures as defined by Regulatory Guide 1.165 (Appendix A) (USNRC, 1997). The subdetachment basement faults are inferred to represent the most cratonward of a zone of Iapetan normal faults.

### 2.5.3.6 Characterization of Capable Tectonic Structures

A 'capable tectonic source' as defined by the Nuclear Regulatory Commission (USNRC, 1997) (Regulatory Guide 1.165, Appendix A), is described by at least one of the following characteristics:

- (a) presence of surface or near-surface deformation of landforms or geologic deposits of a recurring nature within the last approximately 500,000 years or at least once in the last approximately 50,000 years
- (b) a reasonable association with one or more large earthquakes or sustained earthquake activity that usually is accompanied by significant surface deformation

- (c) structural association with a capable tectonic source having characteristics of section (a) above, such that movement on one could be reasonably expected to be accompanied by movement on the other

The two mapped bedrock faults within a 25-mile radius of the Bellefonte Site, the Sequatchie Valley thrust fault, and the Big Wills Valley thrust fault, are judged to not be capable tectonic sources. This conclusion is based on the following lines of evidence: (1) both faults sole into the regional detachment at depths of about 1.6 and 1.9 miles, respectively, and, thus, do not extend to the hypocentral depth at which moderate to large magnitude earthquakes typically nucleate; (2) northeast-trending thrust faults are not favorably oriented for reactivation in the contemporary stress field (northeast to east-northeast-directed maximum horizontal compression); (3) no evidence of Quaternary deformation is reported in the literature or was observed during field and aerial reconnaissance conducted for this study; and (4) instrumentally recorded seismicity, including the 2003 Fort Payne earthquake (the largest earthquake recorded in the ETSZ) occurs within basement rocks below the Paleozoic cover sequence overlying the regional Appalachian detachment (at depths of greater than 3 miles).

No historic earthquake in the site region has been known to cause faulting at or near the surface. Neither the Sequatchie Valley thrust fault nor the Big Wills Valley thrust fault are genetically or structurally related to any known capable tectonic source. The BLNP FSAR (TVA, 1986) concludes that structurally related major northeast-trending faults within the Valley and Ridge Province are inactive based on: (1) detailed geologic mapping investigations throughout the province in which no evidence of active faulting since the Paleozoic is described, implied, or inferred; (2) dating of a sample from the Copper Creek fault near the Clinch River breeder reactor site by potassium-argon methods that indicated last movement occurred 280-290 Ma  $\pm$  0 Ma; and (3) a core boring through the Missionary Ridge fault (at Chickamauga Dam) that indicated that material had recrystallized along the fault and core samples from the Tellico Project that showed the Knoxville fault as an unbroken sample at several locations.

The inferred sub-detachment basement faults in the site vicinity also are judged to not be capable tectonic sources. There is no apparent association of seismicity with these faults (Figure 2.5.2-4), and there is no evidence of surface or near-surface Quaternary deformation to suggest that these faults are capable tectonic sources.

### 2.5.3.7 Designation of Zones of Quaternary Deformation in Site Region

No significant zones of Quaternary deformation that would require additional investigation are identified within the site area. No evidence for surface deformation at the site was observed during the field or aerial reconnaissance. Based on review of existing BLNP documents, mapping, and subsurface investigations conducted for this study, the lineaments mapped in the vicinity of the site likely are related to lithologic differences, solutionally enlarged joints, and/or fractures that have facilitated groundwater movement and weathering in the upper part of the Chickamauga limestone (see discussion in Section 2.5.1.2.5). Small drainages and gullies appear to have localized along the zones of more weathered bedrock.

The results of the seismic refraction and microgravity surveys show that most of the site (including the proposed location of the reactor building) is underlain by competent rock with little indication of deep weathering. An exception is the southeastern part of the area, where deeper weathering zones and clay-filled voids were found. However, based on decrease in the

size and abundance of dissolution features at the revised Bellefonte Site and the expected depth of excavation that is planned for the proposed new structures, these features will not pose a surface rupture or displacement hazard.

### **2.5.3.8 Potential for Surface Tectonic Deformation at the Site**

The potential for tectonic deformation at the Bellefonte Site is judged to be negligible. This conclusion is based on mapping of bedrock in the region (BLNP FSAR, TVA, 1986; Osborne et al., 1988) that identified no evidence for surface faulting or deformation that would pose a hazard to the Bellefonte Site and the absence of geomorphic features indicative of Quaternary deformation as reported in the previous BLNP reports and literature and inferred from observations made during the field and aerial reconnaissance conducted for this study.



fig2\_5\_3-1\_1970aerial.mxd

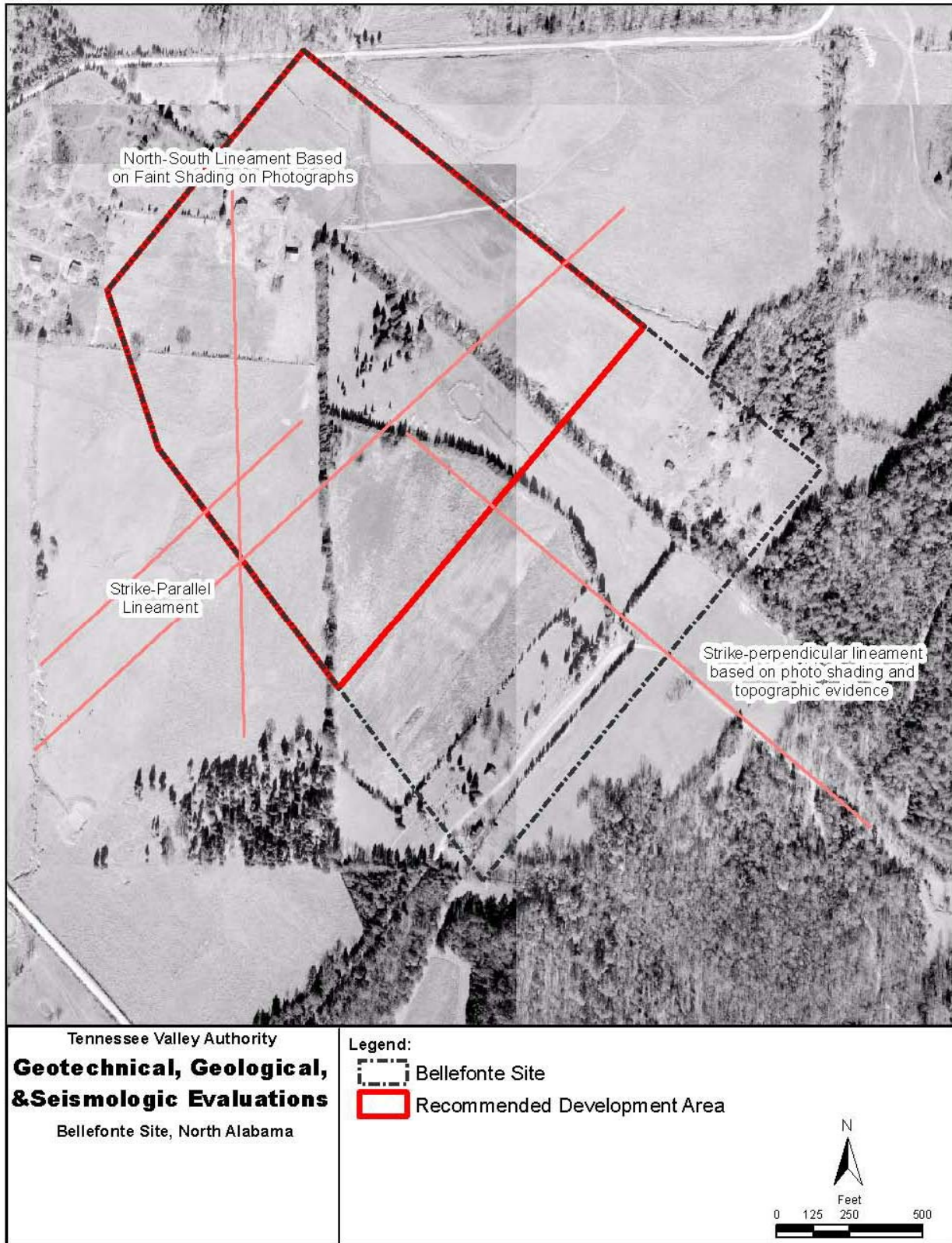


Figure 2.5.3.1. 1970 Aerial Photograph of the Bellefonte Site Showing Features Used to Define Lineaments

fig2\_5\_3-2\_aerial\_lineaments.mxd

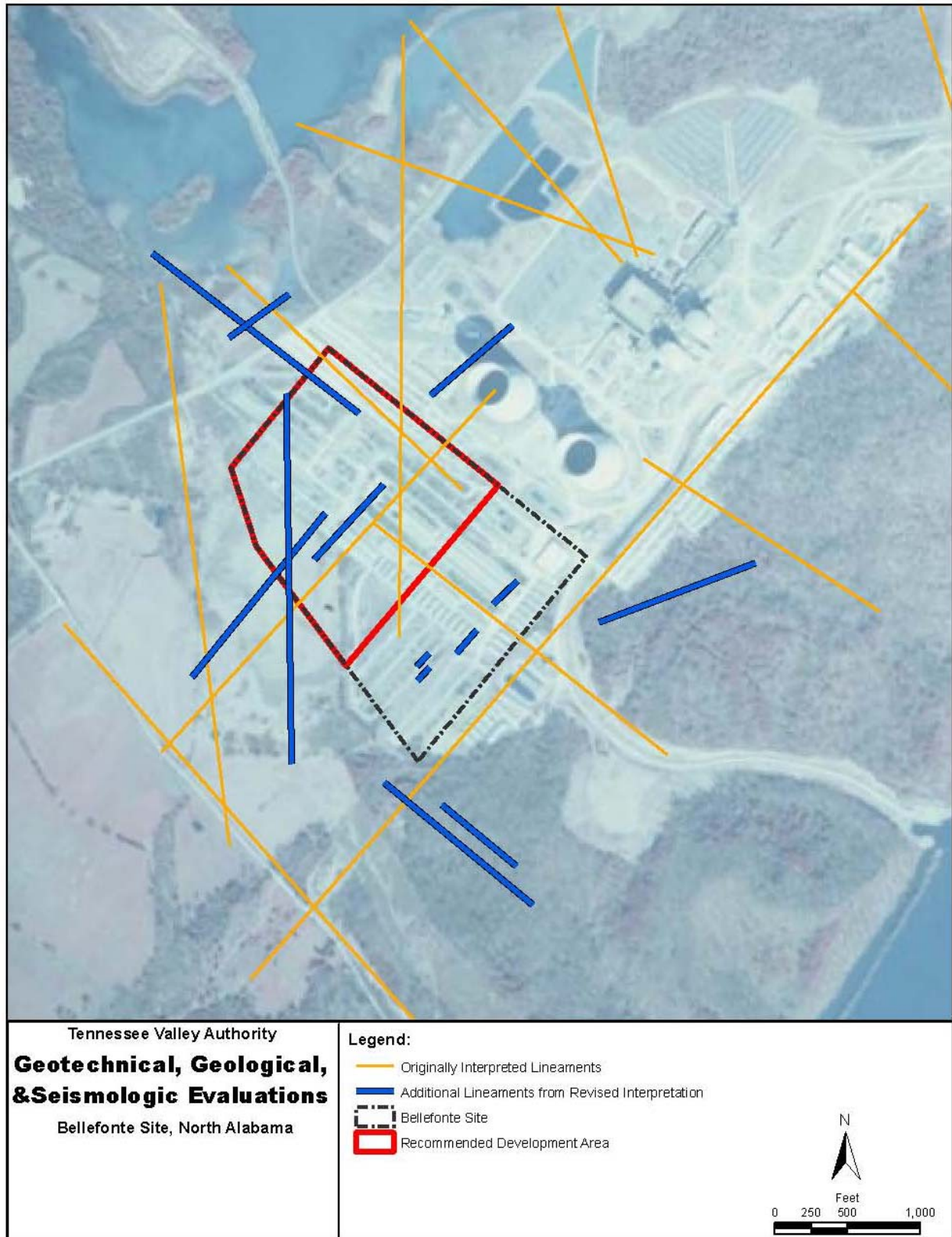
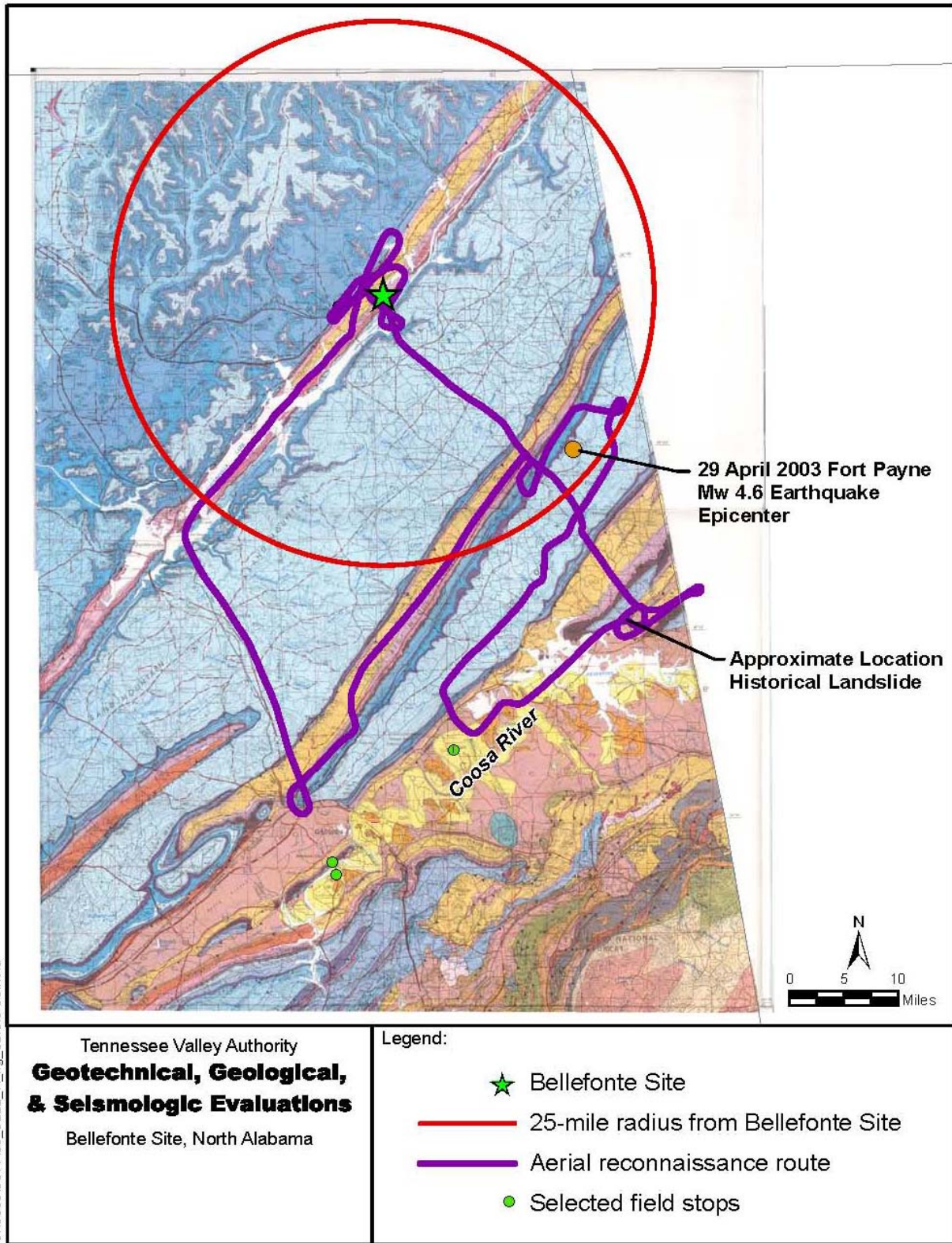


Figure 2.5.3-2. Interpreted Lineaments at the Bellefonte Site





**Figure 2.5.3-3. Aerial and Field Reconnaissance**  
(Base map: Osborne et al., 1988; <http://www.gsa.state.al.us/gsa/GIS/geologydetails.html>)  
(Note: see Figure 2.5.1-8 for explanation of units and symbols)



S:\9800\9877\05\_0222\_r\fig\_02.5.3-04.mxd

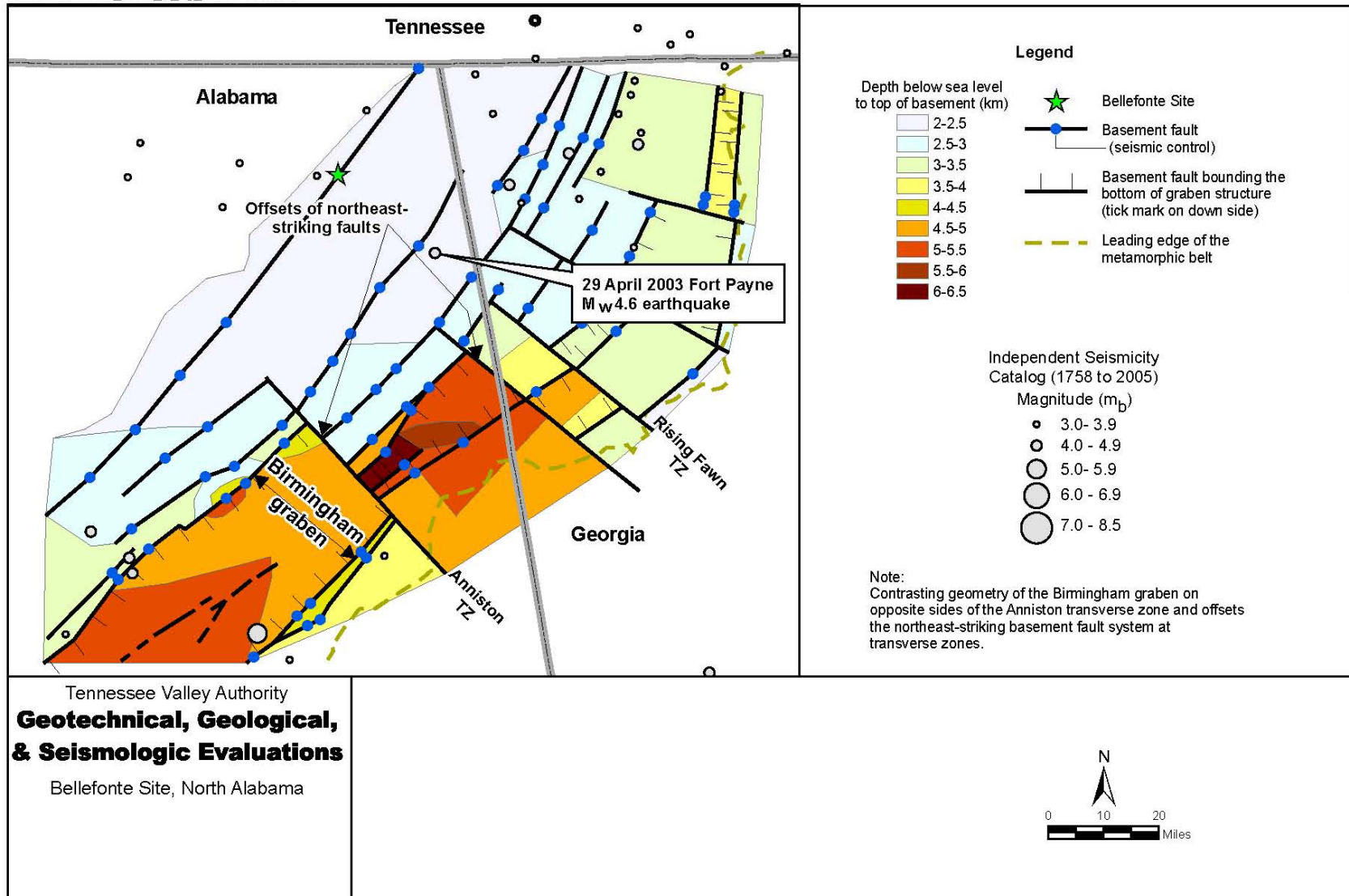


Figure 2.5.3-4. Seismicity Relative to Mapped Basement Faults  
(Modified from Bayona et al., 2003)



## 2.5.4 Stability of Subsurface Materials and Foundations

This section summarizes information about the stability of subsurface materials and foundations. The information was developed on the basis of field explorations performed at the Bellefonte Site and on laboratory tests performed on soil and rock samples obtained during the field exploration program. Results of field investigations and laboratory tests performed at the adjacent BLNP site in the 1970s and 1980s as summarized in the BLNP FSAR (TVA, 1986) were also considered in this assessment, based on the proximity of the BLNP and Bellefonte Sites and on the similarity in geology at the two sites. This information served as a basis for evaluating excavation and backfill issues, construction excavation and dewatering, earthfill and granular fill requirements, groundwater, response of soil and rock to dynamic loading, liquefaction potential, static stability, techniques to improve subsurface conditions, potential requirements for subsurface instrumentation, and issues related to construction. Results of these evaluations, along with the methods and results of field and laboratory testing programs, are summarized in the following subsections.

### 2.5.4.1 Geologic Features

The stability of subsurface materials and foundations for future structures will be evaluated based on the geologic conditions at the Bellefonte Site. An overview of these geologic conditions is described in this section. Detailed descriptions of regional and site geologic features are presented in Sections 2.5.1 and 2.5.2. A brief overview of the Bellefonte Site setting and surface conditions is presented in Section 1.3.1. Detailed descriptions of site geologic and geotechnical conditions encountered during the field investigations at the Bellefonte Site are presented in Sections 2.5.4.2, 2.5.4.3, and 2.5.4.4.

#### 2.5.4.1.1 Site Geologic Conditions

Safety-related results of explorations at the Bellefonte Site revealed that 3.8 to 20 feet of residual soils overlie weathered and unweathered limestone bedrock of the Chickamauga Formation. At most of the Bellefonte Site, the weathered, fractured bedrock is limited to the upper few feet below the residuum. Highly weathered, fractured bedrock with some clay-filled cavities extends to at least 95 feet bgs at a localized area within the southeastern portion of the Bellefonte Site. Below the weathered bedrock, the limestone is generally fresh, hard, and of high compressive strength (greater than 12,000 psi). Based on the range of potential facility design foundation depths (39.5 to 84.2 feet bgs, as described in Section 1) and observed site conditions throughout most of the project area, major safety-related structures can be founded on fresh, hard bedrock, or on engineered fill placed over fresh, hard bedrock.

As detailed in Section 2.5.4.4, the seismic refraction surveys identified three different subsurface layers at the Bellefonte Site; L1, with compressional wave (P-wave) velocity of less than 4,000 feet per second (fps), L2, with P-wave velocity of less than 16,000 fps, and L3, with P-wave velocity of 20,000 fps or greater. L1 is generally interpreted as residual soil and fill over bedrock, L2 is interpreted to comprise a range of materials from highly weathered bedrock with some clay-filled cavities to slightly weathered bedrock, and L3 is interpreted as high quality, fresh bedrock. Zones of deeper weathering (thicker L1 and L2 layers) are generally parallel to bedrock strike, as indicated by the two northeast-southwest trending bands where the depth and thickness of the L2 layer are greatest (Figures 2.5.4-6a, 2.5.4-6b, and 2.5.4-6c). The lateral

boundaries of these zones are confirmed by microgravity and borehole data, as described in Sections 2.5.4.3 and 2.5.4.4.

The seismic refraction data, microgravity data, and borehole observations indicate that geologic conditions are relatively uniform at most of the site. Except for the two areas (discussed below), the top of rock (L2 layer) is generally flat to slightly irregular and does not indicate areas of deep weathering of the limestone surface. The top of the L3 layer exhibits more variability than the top of the L2 layer, but is still relatively flat. The top of the L3 Layer is encountered at less than 30 feet bgs across most of the site.

Two zones of greater weathering were identified from the results of the seismic refraction, microgravity surveys, and borehole data: the eastern anomaly zone and western anomaly zone.

#### 2.5.4.1.1.1 Eastern Anomaly Zone

An area with highly weathered limestone is limited to a strike-oriented zone (the “eastern anomaly zone”) within the southeastern portion of the Bellefonte Site (southeast of boreholes B-8 and B-15, shown in Figure 2.5.4-1a). Areas of deepest weathering occur across the southeast-northwest trending lineament that aligns with the water gap that extends from the edge of the Bellefonte Site southeast to the Tennessee River, and with drainage patterns in Town Creek to the northwest (Figure 2.5.3-2). Boreholes indicate that this deeply weathered zone is characterized by interbedded, weathered limestone and clay (see Section 2.5.4.3.1.2). Boreholes B-2 and B-10 were drilled within this zone (Figure 2.5.4-1a). At borehole B-2, interbedded, highly weathered limestone and clay-filled voids are present to a depth of 58 feet bgs. At borehole B-10, competent bedrock is present to a depth of 49 feet bgs, but highly weathered bedrock and clay-filled voids are present below, from 49 to at least 95 feet bgs. The extensively weathered conditions and depth extent of the weathered bedrock at these boreholes in the eastern anomaly zone would result in excessive excavation and grouting to prepare a suitable subgrade, and therefore the eastern anomaly zone is not considered a desirable location for safety-related structures.

#### 2.5.4.1.1.2 Western Anomaly Zone

Conditions at a second strike-oriented zone of apparently deeper weathering as indicated by seismic refraction surveys (the “western anomaly zone,” located farther to the west than the eastern anomaly zone discussed previously) are characterized by slightly weathered, high quality bedrock, with presence of clay-filled cavities limited to the upper 10 feet of bedrock. Boreholes B-9A, B-12, and B-13 were advanced in this zone, and bedrock quality was high compared with the eastern anomaly zone (e.g., boreholes B-2 and B-10). Microgravity data collected across the western zone indicate only a slight decrease in gravity values, and values are much higher than those collected from the southeastern portion of the site. Marginally more fractures are present in the upper 40 feet of bedrock at boreholes B-9A, B-12, and B-13 than at nearby boreholes outside the strike-oriented weathering zones (e.g., boreholes B-1 and B-7). Bedrock quality is considered suitable for foundations of major safety-related structures within the western zone.

While conditions at the eastern anomaly zone may be less desirable for development of safety-related structures than other portions of the site, conditions at boreholes B-8 and B-15 indicate the presence of hard, fresh bedrock within 15 feet bgs, and these locations effectively delineate the eastern anomaly zone. For these reasons, a recommended development area that includes

large areas of relatively unweathered bedrock has been delineated, as shown in Figure 2.5.4-1a (and other figures).

### 2.5.4.1.1.3 Groundwater

Groundwater surface levels were measured in 26 monitoring wells and piezometers located on the TVA property during the GG&S Study. The depth to water has ranged from approximately 0.5 to 8 foot below grade at the Bellefonte Site. Between March 2, 2005, May 4, 2005, and September 21, 2005, water elevations in wells and piezometers at the Bellefonte Site fluctuated between approximately 1.56 and 9.79 feet, with the higher elevations observed in March and lowest in September. Fluctuations in all the monitored wells, including those outside the Bellefonte Site footprint, ranged from slightly more than 1 foot to more than 14 feet. Potentiometric gradients are toward the Town Creek embayment to the northwest, and average approximately 0.01 foot/foot across the Bellefonte Site. Groundwater conditions at the Bellefonte Site are considered suitable for future development.

Groundwater level measurements were made in 26 monitoring wells and piezometers located on the TVA property. Results are tabulated in Table 2.5.4-8, and shown graphically in Figures 2.5.4-9a, 2.5.4-9b, 2.5.4-9c, and 2.5.4-9d. A chart of water elevations at the four Bellefonte Site piezometers in each of the four monitoring events is included as Figure 2.5.4-10.

Results of groundwater measurements made on March 2, May 4, July 28, 2005, and September 21, 2005, indicate that at the Bellefonte Site, the depth to water has ranged from approximately 1.5 to 9.8 feet below grade. Water levels at the Bellefonte Site were highest in March and lowest in September. Potentiometric gradients are toward the Town Creek embayment to the northwest, and average approximately 0.01 foot/foot across the Bellefonte Site. Fluctuations in all the monitored wells, including those outside the study footprint, ranged from slightly more than 1 foot to more than 14 feet. Measured water levels likely represent a semi-confined piezometric surface, as samples of residuum recovered from borings have been described as dry to moist as deep as approximately 15 feet bgs.

Slug tests were performed in the four new piezometers (P-1 through P-4) completed during the investigation. Results are shown in Table 2.5.4-10, and slug test methods and results are described in Appendix H. Computed hydraulic conductivity values for three of the piezometers range from 2.6 by  $10^{-4}$  to 8.2 by  $10^{-4}$  centimeters per second (cm/s). These values are in good agreement with values computed from packer testing in the existing plant area, which ranged from 4.0 by  $10^{-4}$  to 5.3 by  $10^{-4}$  cm/s. The computed value for the remaining piezometer (P-1) is 5.0 by  $10^{-6}$  cm/s, which is two orders of magnitude lower than the values computed for the other three piezometers. Piezometer P-1 is located in the northwestern portion of the Bellefonte Site, in an area where the seismic refraction data indicate that conditions are relatively uniform with little weathering (see Section 2.5.4.4.1.2).

None of the groundwater observations are considered to affect the suitability of the Bellefonte Site for future development.

### 2.5.4.1.2 Geologic Hazards

As part of the evaluation of geologic features, the potential for geologic hazards at the Bellefonte Site was reviewed (see discussion in Section 2.5.1.2.5). As noted in Section 2.5.1.2.5, earthquake activity with its resulting ground motion effects is judged to be the primary geologic

hazard to the Bellefonte Site. The potential for tectonic surface deformation is judged to be negligible. A detailed discussion of vibratory ground motion and potential for surface faulting at the Bellefonte Site is provided in Sections 2.5.2 and 2.5.3, respectively.

The only other potential geologic hazard that was identified at the Bellefonte Site involved limestone rock that could, under certain conditions, be susceptible to dissolution and karst formation. Whereas most of the Bellefonte Site is underlain by competent bedrock within 20 feet bgs, weathered karst features were identified within the eastern anomaly zone. There is no indication of significant karst development elsewhere at the site. The karst feature in the eastern anomaly zone is considered a localized phenomenon that does not extend into the recommended development area for the following reasons:

- The strike-parallel trends in weathered bedrock indicate that lithologic or structural variations in the dipping limestone have resulted in preferential dissolution along certain strata, and areas outside those strata are underlain by competent bedrock that is less susceptible to development of karst features such as sinkholes or large voids.
- No surface expressions of sinkholes could be found anywhere within the outcrop belt of the Chickamauga Formation near the Bellefonte Site, based on reviews of aerial photographs dating from the 1970s through 2000, and on visual reconnaissance of areas most likely to contain karst formations.
- Downward hydraulic gradients required to remove dissolved material have not been observed at or near the Bellefonte Site. In fact, some wells and boreholes in the study footprint have been artesian, indicating upward gradients.

These factors suggest that sinkhole development is not currently active. While it is possible that vertical groundwater gradients were downward in some areas prior to impoundment of the Tennessee River, and some sinkhole development may have occurred near the eastern anomaly zone in the past, based on the available data, there is no indication of active sinkholes anywhere within the site, and no indication of any significant karst features northwest of the line including boreholes B-8 and B-15.

As discussed in Section 2.5.3, the eastern and western lineaments within the Bellefonte project footprint also do not pose a hazard from surface displacement or warping caused by faulting of either of these features. Results of field and aerial reconnaissance studies, as well as reviews of the site and regional geology, determined that neither of these features represent a fault displacement hazard.

## **2.5.4.2 Properties of Subsurface Materials**

Numerous field explorations and laboratory tests were performed to characterize the engineering properties of subsurface materials at the Bellefonte Site.

### **2.5.4.2.1 Properties from Field Explorations**

Data on the engineering properties of subsurface materials were obtained from study field explorations conducted at the Bellefonte Site as part of the GG&S study. Data from earlier studies is also available in the BLNP FSAR (TVA, 1986). Subsurface material properties obtained during the field investigations are presented in the following sections of this report, along with interpretations of the data:



- Soil and bedrock descriptions, soil standard penetration test (SPT) results, and rock quality designation (RQD) results: summary in Section 2.5.4.3.1, soil and rock core logs in Appendix A
- Soil data from CPT soundings, including interpreted soil types, strength properties, pore pressure dissipation test results, and seismic shear wave velocity: summary in Section 2.5.4.3.2, data in Appendix B
- Bedrock shear wave (S-wave) and compression wave (P-wave) velocity: summary in Section 2.5.4.4, data in Appendices C and D

Subsurface material property information in the BLNP FSAR (TVA, 1986) includes results of numerous field explorations at the BLNP site, adjacent and northeast of the Bellefonte Site. These field explorations included:

- More than 120 boreholes with rock coring, ranging to depths of more than 250 feet bgs,
- More than 100 additional boreholes were drilled primarily to the top of bedrock, for soil characterization at the plant site, intake channel, and conveyance systems north and east of the BLNP site, and
- Borehole geophysical results at dozens of locations.

In view of the proximity of the BLNP site to the Bellefonte Site, the field data included in the BLNP FSAR were used to augment the database of information developed at the Bellefonte Site. In general, subsurface conditions at the BLNP site are very similar to conditions at most of the Bellefonte Site, with the exception of the eastern anomaly zone. Comparisons of conditions between the two sites are presented in Sections 2.5.4.3.1.3, 2.5.4.4.2, and 2.5.4.4.3.

### 2.5.4.2.2 Properties from Laboratory Testing

Geotechnical laboratory tests were performed on soil and bedrock samples collected during the Bellefonte Site field activities. These tests were performed by S&ME, Inc., between March 1 and March 18, 2005, at their laboratory in Louisville, Tennessee, as described in Revision 1 of the Laboratory Workplan (CH2M HILL, 2005b). The laboratory tests were selected and performed in accordance with the applicable guidance in Regulatory Guide 1.138 (USNRC, 2003b), and applicable American Society for Testing and Materials (ASTM) and American Association of State Highway and Transportation Officials (AASHTO) standards. Samples for testing were assigned by CH2M HILL after review of borehole logs obtained in the field and in consideration of potential facility design requirements, as summarized below:

- Geotechnical tests on rock samples consisted of unconfined compression tests (ASTM D2938), both with and without axial and radial strain measurements (ASTM D3148).
- Geotechnical tests on soil samples consisted of Atterberg limits (ASTM D4318), gradation (ASTM D422), fines fraction (ASTM D1140), moisture content (ASTM D2216), bulk and dry density (ASTM D2937 and D1587), soil pH (ASTM D4972 and AASHTO T289), and unconsolidated-undrained triaxial shear tests (ASTM D2850).

The Bellefonte Site laboratory test results for rock samples are presented in Table 2.5.4-1, and results for soil are summarized in Table 2.5.4-2. The full laboratory data report is included in

Appendix F. Interpretations of the test results as they relate to site stability and response to loading are presented in Section 2.5.4.3 through Section 2.5.6.

### 2.5.4.3 Bellefonte Site Explorations

Field explorations at the Bellefonte Site were performed as described in Revision 2 of the Field Workplan (CH2M HILL, 2005a), and Addenda Nos. 1 and 2 of the Field Workplan. The field explorations were selected and performed in accordance with the applicable guidance in Regulatory Guide 1.132 (USNRC, 2003a), and in accordance with ASTM and other national standards. All field exploration activities were performed by CH2M HILL staff, or by subcontractors with oversight by CH2M HILL.

- S&ME, Inc. of Louisville, Tennessee, performed drilling and sampling of soil and bedrock, cone penetrometer soundings, and installation of groundwater piezometers between February 7 and February 25, 2005, and performed additional drilling and sampling between July 11 and 25, 2005.
- Technos, Inc. of Miami, Florida, performed surface seismic refraction surveys at the Bellefonte Site in late January 2005, and again in late June and early July 2005.
- Technos, Inc. also completed a limited microgravity survey in late July 2005.
- GeoVision of Corona, California, performed suspension logging tests on February 21, 2005, within rock core holes advanced by S&ME, Inc.
- Great Southern Engineering of Trinity, Alabama, surveyed coordinates and elevations of the investigation locations in February and July 2005.

Details of the field investigation activities, and descriptions of key findings, are presented in the following subsections and in Section 2.5.4.4 and appendices.

#### 2.5.4.3.1 Geotechnical Boreholes and Rock Cores

Soil boreholes and rock cores were advanced at 18 locations within the Bellefonte Site, as shown in Figure 2.5.4-1. Boreholes B-1 through B-6, B-6A, and a separate borehole drilled to install piezometer P-3, were drilled in February 2005. Based on results in these boreholes and seismic refraction testing, additional boreholes B-7, B-8, B-9, B-9A, and B-10 through B-15 were drilled in July 2005.

##### 2.5.4.3.1.1 Boring, Coring, and Sampling Methods

Soil boreholes were advanced through residual soils to refusal using hollow-stem augers. Top of bedrock was encountered at depths ranging from 5 to 20 feet bgs. HQ- or NQ-type rock cores were then advanced to between 94 and 116 feet bgs at boreholes B-1 through B-15, 25 feet bgs at borehole B-6A, and to 24.5 feet bgs at borehole P-3. Rock core casing was advanced through the overburden soils and significantly weathered bedrock to prevent borehole collapse during rock coring. A rubber-tire drill rig was used for drilling at most locations. Borehole B-5 in the southwest corner of the footprint was drilled with a track-mounted drill rig because ground conditions in this area precluded access with a rubber-tire drill rig.

Soil and rock samples were collected and managed as described in the Field Workplan (CH2M HILL, 2005a). Split-spoon soil samples were collected at numerous intervals from the

boreholes. Representative sections of split-spoon samples were stored in glass jars for shipment to the S&ME, Inc. geotechnical testing laboratory. Three Shelby tube samples were also collected for shipment to the S&ME, Inc. geotechnical testing laboratory. Rock core samples were collected from the entire depth of each rock core and stored in wooden core boxes. A selected number of rock samples were managed as special care rock core specimens by sealing with plastic, foil, and paraffin wax. The soil samples and special care rock core specimens were delivered under chain of custody to the S&ME, Inc. geotechnical laboratory for testing. Test results are summarized in Section 2.5.4.2.2.

Upon completion of boreholes and rock cores to their final depths, suspension logging tests were performed in the uncased portions of three rock cores (boreholes B-1, B-2, and B-6), as described in Section 2.5.4.4.3. Piezometers were installed in the upper bedrock at boreholes B-2 (P-2), B-3 (P-1), B-6A (P-4), and at P-3, as described in Section 2.5.4.3.3.

Bentonite-cement grout was used to abandon the remaining boreholes. Grout was placed via tremie through the entire depths of boreholes B-1 and B-4 through B-15. Bentonite-cement grout was also placed in the rock core holes below the piezometer screens at boreholes B-2 and B-3.

### 2.5.4.3.1.2 Drilling and Sampling Observations and Results

Soil boring and rock core logs for each investigation location are included in Appendix A. Figures 2.5.4-2a and 2.5.4-2b show cross-sections through the site, directed along the alignments shown in Figure 2.5.4-1a. Figure 2.5.4-3 shows the interpreted top of rock elevation contours for the Bellefonte Site, based on borehole data. Table 2.5.4-3 is a summary of soil and rock conditions observed in boreholes during the drilling and sampling program.

The following conditions were interpreted from the drilling and sampling program:

#### 2.5.4.3.1.2.1 Overburden Soil

Overburden soil was encountered over bedrock at each borehole location, ranging from 3.8 to 20 feet in thickness. At most locations, the soils consisted of clay residuum (CL or CH, according to the Unified Soil Classification System, or USCS), with a layer of roadway gravel in the upper few feet bgs. Deeper intervals of sand and gravel were encountered at a few locations (boreholes B-3, B-4, B-6, B-9, and B-14).

#### 2.5.4.3.1.2.2 Weathered Limestone

Weathered limestone bedrock was limited to the first 10 feet below the top of bedrock at most of the boreholes. Where encountered, the weathered bedrock typically included numerous fractures per foot length, with some clay lining of fractures or clay infilling of measurable thickness. At five locations (boreholes B-1, B-3, B-5, B-8, and B-15), the bedrock was of high quality and fresh immediately below the contact with unconsolidated soils. The RQD, a measure of the unfractured length of rock core specimens, was greater than 80 percent for the rock cores from these locations. At nine locations (boreholes P-3, B-4, B-7, B-9, B-9A, B-11, B-12, B13, and B-14), only a few to 10 feet of weathered bedrock was encountered over fresh, high quality bedrock.

Weathered bedrock was encountered at greater depths at boreholes B-2, B-6, and B-10. At borehole B-2, highly weathered and fractured bedrock with numerous clay-filled voids and iron oxide staining was encountered to a depth of 59 feet bgs. At borehole B-6, similar weathered bedrock conditions were observed to a depth of 19 feet bgs. At both boreholes B-2 and B-6, high

quality bedrock (with RQD greater than 80 percent) was present below the weathered bedrock to the bottom of the boreholes. However, conditions were different at borehole B-10. At this location, high quality bedrock (with RQD greater than 75 percent) was observed from approximately 4 feet below top of rock to a depth of 49 feet bgs; however, highly weathered bedrock with numerous clay-filled voids and iron oxide staining was present from 49 feet bgs to the bottom of the borehole (94 feet bgs). All three of these boreholes are located within the eastern anomaly zone, as described in Section 2.5.4.4.

#### 2.5.4.3.1.2.3 Unweathered Bedrock

At all locations except borehole B-10, fresh, high quality limestone bedrock is present from the bottom of the weathered zone to the bottom depth of the rock core. Below the weathered zone, limestone RQD of 90 to 100 percent is typical, though a few isolated zones have RQD as low as 60 percent. Throughout the cores (below the weathered zone), the limestone is typically described as light to dark grey, micritic to finely crystalline, with bedding planes inclined at approximately 20 degrees. Abundant stylolites were encountered throughout, typically aligned with the bedding planes. Where encountered, fractures were typically fresh and in direct contact.

Fossiliferous zones were encountered at boreholes B-4, B-6, B-6A, B-7, B-9A, B-10, B-12, and B-13; and calcite-filled vugs were identified in several of the rock cores.

#### 2.5.4.3.1.3 Comparison of Bedrock Conditions at the Bellefonte and BLNP Sites

Bedrock conditions observed at the Bellefonte Site are similar to conditions at the BLNP site, with some notable differences. As discussed in Section 2, the Sequatchie Valley anticline strikes at approximately north 40 degrees east, such that the Bellefonte Site is generally along-strike with the BLNP site. Therefore, bedrock at common elevations between the sites generally represents similar lithology.

Bedrock conditions at the BLNP site are described in detail in the BLNP FSAR (TVA, 1986). Several boreholes and rock core holes were advanced near the existing BLNP buildings during the BLNP site investigation, which are approximately along-strike to the northeast of the Bellefonte Site:

- Three of these BLNP site rock cores were advanced to similar or greater depth than the Bellefonte Site boreholes: “R+22-50+78” (identification notation used in the FSAR) was advanced to approximately 140 foot depth, “T-50+00” to 150 feet, and “R-52+00” to over 200 foot depth.
- Downhole geophysics were performed at the first two of these BLNP boreholes, and resulting dynamic rock properties from these locations are summarized in Section 2.5.4.4.3.2.
- BLNP site borehole “Z-50+00” is the westernmost of the boreholes with rock coring advanced near the BLNP site, which is approximately along-strike with Bellefonte Site borehole B-12.

The approximate locations of these BLNP boreholes are indicated in Figure 2.5.4-1a. Other boreholes were advanced at the BLNP site and reported in the FSAR. However, only the BLNP site boreholes shown are discussed herein, because these boreholes have appropriate depth of

penetration, orientation along-strike, and availability of downhole geophysics results for comparison with the Bellefonte Site boreholes. Top of rock elevation at these BLNP boreholes ranged from 601 to 625 feet above mean sea level (amsl), which is consistent with the range in top of rock elevation at the Bellefonte Site boreholes. At the BLNP boreholes, a few zones of weathering, including clay-filled cavities of up to a few feet thickness, were observed in the upper 5 to 10 feet of bedrock. Below this upper weathered zone, high quality bedrock with minimal evidence of voids was encountered in each of these BLNP site boreholes. Fractures or partings, where encountered, were in direct contact with no measurable thickness or voids.

Conditions at these BLNP site boreholes were consistent with conditions within the recommended development area of the Bellefonte Site. However, within the eastern anomaly zone at the Bellefonte Site, greater depths of weathered bedrock were encountered, and more frequent and thicker clay-filled cavities were encountered at the Bellefonte Site than at the BLNP site. A plot of observed clay-filled cavity thickness versus depth below top of bedrock at the Bellefonte Site and BLNP site boreholes is included as Figure 2.5.4-4. The distribution of clay-filled cavities in the Bellefonte Site boreholes is divided into two groups: boreholes at the eastern anomaly zone (B-2, B-6, and B-10), and boreholes from the recommended development area (other boreholes). Table 2.5.4-4 presents observations of the voids identified at the Bellefonte Site boreholes. As shown in Figure 2.5.4-4, the vast majority of voids were encountered in the upper 10 to 20 feet of bedrock at the BLNP site boreholes. A few clay-filled seams were encountered below this depth in the more than 50 borings advanced at the BLNP site, but these were typically less than a few tenths of 1 foot in thickness, and only a few were observed. Similar conditions were observed at the Bellefonte Site boreholes within the recommended development area. However, measurable clay-filled cavities up to several feet thick were observed at Bellefonte Site boreholes B-2 and B-10 within the eastern anomaly zone, at depths of up to 95 feet bgs.

A series of “metabentonite” beds were noted on some of the BLNP site rock core logs in the FSAR. Several of these were present at elevations that were sampled for the Bellefonte Site boreholes. Possible metabentonite beds were observed in rock cores at two of the Bellefonte Site boreholes: at 82.5 feet bgs at borehole B-10, and at 22.7 to 22.8 feet bgs at borehole B-12. The observed possible metabentonite beds were approximately 0.1 foot thick at each location. The presence of these thin metabentonite beds in the bedrock is not considered to have any negative effect on site suitability.

### 2.5.4.3.2 GG&S Cone Penetrometer Test Soundings

CPT soundings were advanced at 22 locations across the Bellefonte Site, as shown in Figure 2.5.4-1b (soundings C-1 through C-22). The primary objectives of the CPT soundings were to obtain information that could be used to estimate the engineering properties of the residual soils, to identify the top of bedrock, and to conduct downhole shear wave velocity tests, as discussed further in Section 2.5.4.4.2. CPT soundings were not conducted at the BLNP site during preparation of the FSAR.

#### 2.5.4.3.2.1 CPT Methods

The CPT soundings were advanced through overburden soils using a 20-ton truck-mounted rig. Tip stress, sleeve stress, and pore pressures were monitored continuously throughout the depth of each CPT sounding. Refusal of each CPT sounding was identified by the S&ME, Inc. rig

operator, based on the tip pressure. At locations where refusal was reached at depth less than 5 feet, a second sounding was attempted to verify the depth of refusal.

Results of the CPT soundings are provided in Appendix B. These results include tip resistance, sleeve friction, and pore pressure measurements as a function of depth for each of the soundings. Appendix B includes additional information about the S&ME, Inc. CPT equipment.

Seismic shear wave velocity measurements were also obtained from the overburden at seven CPT sounding locations (C-1A, C-7, C-10, C-10A, C-16, C-18, and C-21). To generate the seismic shear-wave source, a wooden beam was placed on steel plates, held in close contact with the ground by the weight of the CPT rig. The beam was then struck by a horizontal blow from a sledge hammer, creating the shear wave. The shear wave velocity was calculated by measuring the arrival times of the shear wave to geophones embedded in the CPT probe. True-interval and pseudo-interval measurements of shear wave velocity were obtained among the CPT soundings.

Pore pressure dissipation tests were performed at two locations (C-16, 10 foot depth and C-4A, 2 foot depth). The dissipation test involved stopping the cone as it was being pushed into the soil and then measuring excess porewater pressure dissipation as a function of time. Typically, these tests were carried out until at least 50 percent dissipation of excess pore pressure was observed. Procedures followed for saturation of the transducer and monitoring pore pressures were in accordance with ASTM requirements.

#### 2.5.4.3.2.2 CPT Observations and Results

Detailed logs and tabulated CPT data with depth are included in Appendix B. Table 2.5.4-5 lists the elevation of refusal of the 22 CPT soundings, and brief descriptions of soil types interpreted from the tip and sleeve stresses (Robertson and Campanella, 1988). Table 2.5.4-6 lists the results of CPT seismic shear wave velocity tests.

Six of the CPT soundings were located within approximately 10 feet of boreholes B-1 through B-6 (CPT soundings C-7, C-10, C-1, C-4, C-18, and C-21, respectively). At five of these six locations, the CPT refusal elevation was within 2 feet above or below the top of weathered bedrock identified by the boreholes and rock cores. The only major variation was near B-2, where the CPT refusal elevation was 9.3 feet higher than the top of rock identified at the borehole. At four locations, refusal was encountered less than 2 feet bgs (CPT soundings C-8, C-9, C-13, and C-20). These four CPTs are in the central portion of the Bellefonte Site, at locations where blast rock boulders from BLNP site construction may have been used as fill to create the relatively flat existing ground surface. If so, it is possible that the refusal elevation indicates the presence of boulders from past fill operations, and not the top of bedrock. The extent of blast rock fill at the site may be further investigated as necessary once a future facility design has been selected, but does not affect the suitability of the site for development.

As shown in Table 2.5.4-5, the interpreted CPT soil types generally consist of fine-grained soils (silts or clays), with some interbedded sands and gravels. A layer of sand or gravel was interpreted over clay at a number of CPT locations, consistent with observations made in the boreholes. At CPT soundings C-18 and C-19, located southwest of areas of past site grading activities, the interpreted soil types were fine-grained soils and clays without a surface layer of gravel, consistent with observations at borehole B-5.

The CPT seismic test results summarized in Table 2.5.4-6 indicate that the S-wave velocity of the overburden soils at the Bellefonte Site range from 354 to 1,527 fps. The higher velocities are correlated with locations in the central portion of the Bellefonte Site, whereas some of the lower velocities (at CPT soundings C-1 and C-18) are located near the perimeter of the site, where fewer past grading activities were performed.

### 2.5.4.3.3 GG&S Piezometer Installation and Groundwater Monitoring

Four new piezometers were installed to monitor groundwater elevations near the Bellefonte Site. Table 2.5.4-7 lists the construction data for these piezometers. They were installed approximately 15 feet into bedrock using the same rock coring method described in Section 2.5.4.3.2. Each piezometer was constructed of 2-inch schedule 40 PVC material, with 15 feet of well screen. The piezometers were completed at the surface using flush-mount type completions and concrete pads. Each new piezometer was slug tested using a solid slug (slug removal method) and electronic data logger as described in Appendix H, and summarized in Section 2.5.4.6.

The four new piezometers, along with 28 existing wells and piezometers located across the TVA Bellefonte property, were used for monitoring groundwater levels during the GG&S study. Water levels were measured three times (one more event is planned) using a Solonist™ electronic water level indicator. All measurements were made to a marked location on the top of the inner well casing, or if a mark was not present, to the northern lip of the casing.

Table 2.5.4-8 lists the water level data and well depths for the monitoring locations. Results are described in Section 2.5.4.6.

### 2.5.4.3.4 Survey of Investigation Locations

Coordinates and elevations of each borehole, CPT sounding, piezometer, and seismic refraction line location were surveyed by Great Southern Engineering, Inc. of Huntsville, Alabama. The survey report is included as Appendix E. The resulting coordinates and elevations are presented in various figures and tables in this report.

## 2.5.4.4 Geophysical Surveys

Four types of geophysical surveys were performed at the Bellefonte Site: (1) Seismic refraction surveys by Technos, Inc. of Miami, Florida; (2) Seismic cone shear wave velocity measurements in overburden soils by S&ME, Inc. at a number of CPT locations; (3) suspension logging tests by GeoVision of Corona, California, at boreholes B-1, B-2, and B-6, and (4) a microgravity survey was also completed by Technos, Inc. All geophysical survey activities were performed in accordance with the Field Workplan (CH2M HILL, 2005a) and Addenda, and were overseen by CH2M HILL personnel. This information for the Bellefonte Site was supplemented with geophysical results documented in the BLNP FSAR. The geophysical methods performed at the BLNP site, as summarized in the BLNP FSAR, include downhole and cross-hole geophysical surveys.

### 2.5.4.4.1 Seismic Refraction Surveys

A total of 35 seismic refraction geophysical survey lines were advanced at the site, for a total length of approximately 19,700 linear feet. Locations of the survey lines are shown in

Figure 2.5.4-1c. The locations were selected to provide coverage over identified lineaments at the site, as well as provide representative coverage of the Bellefonte Site.

#### 2.5.4.4.1.1 Seismic Refraction Survey Methods

Seismic refraction procedures were used to determine the seismic P-wave velocity structure of the subsurface. This survey method involved generating seismic P-waves at the ground surface, which propagated through the soil and rock and were recorded by geophones at known distances from the source. Details on the seismic refraction methods and results are included in Appendix C1.

The seismic refraction surveys were performed by Technos, Inc., the Geophysics Subcontractor. A 24-channel Geometrics StrataVisor NZ seismograph was used to record the data. A total of 24, 4.5-Hz geophones were used, with a maximum geophone spread of 92 feet. Geophones were mounted on a landstreamer to couple them with the ground surface at most of the survey lines. At line L1000 the geophones were planted into the surface of the residual soils using 3-inch spikes. Seismic refraction surveys at eight lines were performed in January 2005 (L1000, L2000, L2001, and L3000 through L7000, with a total length of 3,200 linear feet). Based on the results of these lines and boreholes drilled in February 2005, another 27 seismic refraction lines were performed in late June and early July 2005 to collect more extensive data across the Bellefonte Site.

An elastic weight drop (EWD) was used as the seismic source. Five drops were made at each spread location, nominally spaced 100 feet from each end, 20 feet from each end, and at the middle of the spread. Two to eight stacks of energy were used at each drop location. The geophone spreads were moved down the survey lines in 80-foot increments, providing 12-foot overlap between spreads.

Data were processed using industry standard software to produce topographic models of P-wave velocity along each survey location, as detailed in Appendix C.

#### 2.5.4.4.1.2 Seismic Refraction Survey Results

The data at each survey line identified three separate P-wave velocity zones, based on the first arrival times. The three zones consist of the following:

- The upper layer ("L1") that corresponds to residual soil or fill material, with P-wave velocity ranging from 1,000 fps (at L1000) up to 4,600 fps.
- The middle layer ("L2") that corresponds to limestone bedrock with average P-wave velocities of 16,000 fps to 20,000 fps. In most of the study area, this layer consists of rock that is competent and appears unweathered in appearance. Exceptions occur in the eastern anomaly zone, where the L2 layer is deeply weathered in places.
- The bottom layer ("L3") that corresponds to unweathered (or less weathered) limestone. The top of this layer has an average P-wave velocity of 20,000 fps.

The interpreted depths of these layers were calculated assuming that velocity increases with depth in the subsurface. If a lower velocity layer is present beneath a higher velocity layer (i.e., such as soft residual soils below compacted fill), the actual depth to weathered bedrock may be less than indicated by the data. Therefore, the actual contact depths are expected to be either the



same or slightly less than modeled, i.e., the actual depth to 20,000 fps layer may be shallower than indicated.

The apparent depth of refracting layers can also differ depending on the orientation of the geophone spreads. This was evaluated by comparing the interpreted depths to tops of the L2 and L3 layers as estimated from two intersecting lines. For all intersections in the seismic grid, the average difference in the interpreted top of the L2 layer was approximately 4 feet, and the difference in the interpreted top of the L3 layer was approximately 13 feet. The differences are the result of heterogeneous subsurface conditions that result in different seismic wave travel times depending on the direction of travel. The differences were most pronounced in areas with the strongest refraction anomalies. However, the general trends indicating areas with deeper weathering profiles are consistent in all the refraction data.

The refraction data indicate that the interpreted top of the L2 layer ranges from less than 1 foot to approximately 54 feet bgs at the survey locations. However, the depth under most of the area is less than 12 feet, as indicated by the median value of 11.7 feet bgs. The interpreted depth to the L3 layer ranges from less than 1 foot to 85 feet bgs, with a median value of 28 feet bgs.

Figures 2.5.4-5a through 2.5.4-5d show selected representative cross-section models of subsurface conditions. Graphical results for all lines are included in Appendix C.

Figures 2.5.4-6a through 2.5.4-6c show contours of the top of the L2 layer, top of the L3 layer, and thickness of the L2 layer. The majority of the site is underlain by apparently hard, uniform limestone that exhibits little relief in the surface of layers L2 and L3. Two areas of deeper weathering (thicker L2 layer) are generally parallel to bedrock strike (southwest-northeast), as indicated by the two northeast-southwest trending bands where the depth and thickness of the L2 fps layer are greatest (the eastern and western anomaly zones). Weathering may reflect subtle changes in lithology within the southeasterly dipping limestone that cause those strata to be more easily dissolved than the adjoining layers. Weathering may also be affected by structural deformation in the bedrock, which may have resulted in strike-parallel fracturing along the flanks of the Sequatchie anticline.

In addition to the strike-parallel trends associated with the eastern and western anomaly zones, the eastern anomaly zone appears to be related to the southeast-northwest trending lineament that aligns with the water gap that extends from the edge of the Bellefonte Site southeast to the Tennessee River, and with drainage patterns in Town Creek to the northwest (see Section 2.5.3.2.2). This zone is near impoundments located southeast of the Bellefonte Site, where sinkholes have reportedly formed in the past, draining water from the ponds (TVA, "Engineering Report for Sump Collection Pond Modifications, Bellefonte Nuclear Plant, September, 1993"). The southeast-northwest trending lineament appears to be part of a large-scale structural deformation that resulted in strike-perpendicular fracturing along the flanks of the Sequatchie anticline, and is apparently a zone of preferential groundwater movement. The combination of structural weakening and groundwater movement has resulted in a relatively deep weathering profile in this area.

Boreholes indicate that this deeply weathered zone is characterized by interbedded highly weathered limestone and clay (see Section 2.5.4.3.1.1 for detailed discussion of borehole observations). Boreholes B-2 and B-10 were drilled within the eastern anomaly zone, as shown in Figures 2.5.4-6a through 2.5.4-6c. Both boreholes penetrated deeply weathered bedrock confirming the geophysical data for the eastern zone. However, bedrock quality at

boreholes B-8 and B-15 is high throughout the depth of each borehole (95 feet bgs), and these locations therefore delineate the northwestern extent of the eastern anomaly zone.

Borehole conditions at the western anomaly zone show that this zone is more desirable for future development. Boreholes B-9A, B-12, and B-13 were advanced in this zone, and bedrock quality was high in these boreholes. No evidence of clay-filled voids was observed below the upper 10 feet of weathered bedrock at these boreholes. Marginally more fractures are present in the upper 40 feet of bedrock at boreholes B-9A, B-12, and B-13 than at nearby boreholes outside the strike-oriented weathering zones (B-1 and B-7), but bedrock quality is considered suitable for foundations of safety-related structures.

Boreholes also confirm that bedrock quality is high between and northwest of the eastern and western anomaly zones, with little evidence of weathering, as indicated by the seismic refraction surveys. In these areas, the seismic refraction surveys indicate that the L3 layer (with P-wave velocity greater than 20,000 fps) is present at depths of 25 feet or less. Boreholes B-1, B-3, B-5, B-11, and B-14 each confirm that bedrock quality is high throughout the borehole depths (95 to 115 feet bgs) in the area northwest of the anomaly zones, consistent with the seismic refraction survey results. Further, boreholes B-7, B-8, and B-15 confirm similar conditions in the area between the two strike-oriented anomaly zones. The strike-parallel trends in the seismic refraction survey results indicate that lithologic or structural variations in the dipping limestone have resulted in increased fracturing and preferential dissolution along certain strata. The borehole data confirm that dissolution is most pronounced in the eastern anomaly zone, with little evidence of dissolution northwest of a line including boreholes B-8 and B-15.

#### 2.5.4.4.2 Seismic Cone

CPT seismic shear wave velocity tests were performed at eight CPT locations, as discussed in Section 2.5.4.3.2. Results are summarized in Table 2.5.4-6, and are included in Appendix B. Each of the CPT seismic shear wave velocity tests was performed in residuum or fill soils above bedrock. The CPT seismic test results summarized in Table 2.5.4-6 indicate that the S-wave velocity of the overburden soils at the Bellefonte Site range from 354 to 1,527 fps.

Although seismic cone tests were not conducted for the BLNP site, downhole velocity tests were conducted in residuum or fill at 23 locations, as reported in the BLNP FSAR (Figures 2.5.4-15 through 2.5.4-37 of TVA, 1986). The methods used for the BLNP site were similar to those used for the Bellefonte Site investigation, except that the procedures involved drilling a borehole and lowering the velocity transducer rather than pushing the geophone in with the CPT system. The BLNP downhole velocity tests were performed primarily at the intake channel and essential cooling water line locations located north and east of the BLNP units. Soils at these locations consisted primarily of residual clay and weathered bedrock (clayey or silty gravel). The average S-wave velocity results from the downhole tests in the residuum at the BLNP site ranged from 336 to 1,217 fps, consistent with the seismic cone results from the Bellefonte Site.

#### 2.5.4.4.3 Suspension Logging Tests

Suspension logging tests were performed within three rock core holes advanced at the Bellefonte Site (B-1, B-2, and B-6). GeoVision performed the suspension logging tests, with support from S&ME, Inc. The objective of the suspension logging tests was to obtain S-wave and P-wave velocity values as a function of depth. The S-wave velocity values were used to determine whether the unweathered rock met the hard rock requirements for the site response

analyses and SSE determination discussed in Section 2.5.2. The seismic hazard model defines hard rock as having an S-wave velocity of 9,000 fps or more. Results of the suspension logging tests were also used in comparisons to data measured in rock at the BLNP site. The BLNP data included P-wave velocity results from geophysical logging with a Birdwell tool, as well as crosshole results to depths of nearly 100 feet using explosive sources.

#### 2.5.4.4.3.1 Test Methods

Prior to performing the tests, each of the boreholes B-1, B-2, and B-6 was advanced to final depth using HQ coring equipment. Steel casing was installed through the residuum or fill and weathered bedrock at each borehole to ensure borehole integrity. Water was maintained to within a few feet of ground surface in each borehole.

The suspension logging tests were performed using an OYO Model 170 Suspension Logging Recorder and Probe. A detailed description of the procedure is provided in Appendix D. A seismic source is mounted near the base of the probe, and a pair of receivers are mounted approximately 3 feet apart from one another, centered approximately 12 feet above the source. The source generated a P-wave in the pore fluid near the base of the probe, which was converted to a S-wave and separate P-wave at the borehole wall. The shear wave traveled up along the wall, and the resulting compression wave was measured by the receiver pair. The S-wave and P-wave velocity for the interval between the receivers was then calculated based on the difference in wave arrival times.

Shear wave measurements were performed at 0.5-foot intervals in each borehole, starting from approximately 15 feet above the bottom of the boreholes. Tests were performed in bedrock below the depth of casing at each borehole (i.e., near the top of unweathered limestone). Tests could not be performed within the cased interval, due to interference effects from the steel casing. Casing depths at boreholes B-1, B-2, and B-6 were 8.5 feet, 51 feet, and 7 feet bgs, respectively.

#### 2.5.4.4.3.2 Test Results

The resulting suspension logging profiles of bedrock S-wave velocity with elevation at the Bellefonte Site are shown on the left side of Figure 2.5.4-7. As shown, bedrock S-wave velocity was greater than 9,000 fps throughout the depth of uncased boreholes B-1 and B-2, and greater than 8,500 fps within uncased borehole B-6. Lower velocities measured at the extreme upper portions of the profiles for boreholes B-1 and B-2 likely indicate interference with the surface casing at these locations, the low velocities are only seen at the extreme upper portions of these boreholes.

The right side of Figure 2.5.4-7 shows plots of shear wave velocity with depth from two borehole logging tests performed at the BLNP site (borehole R+22-50+78 and borehole T-50+00), as reported in the BLNP FSAR (Figures 2.5-160 and 2.5-188 of TVA, 1986). The BLNP tests involved use of a Birdwell logging tool. P-wave velocities were obtained during the test and then converted to S-wave velocities on the basis of an assumed Poisson's ratio. In contrast, the suspension logging tests performed at the Bellefonte Site directly measured both P-wave and S-wave velocity, and allowed calculation of Poisson's ratio. The depth of the Birdwell tests at the BLNP site ranged from 100 to 150 feet bgs. As shown, the profiles of S-wave velocity with elevation at these locations are greater than 9,000 fps.

Table 2.5.4-9 lists the average S-wave and P-wave velocities from downhole measurements at the three Bellefonte Site boreholes calculated over the depth of each profile and at the two BLNP site boreholes. Table 2.5.4-9 also includes the average P-wave and calculated S-wave velocities from two cross-hole dynamic surveys performed at the BLNP site (between BLNP boreholes Q+47-47+88 and R-49+00, and between BLNP boreholes R+22-50+78 and S-50+00).

As shown in Table 2.5.4-9, the average S-wave velocity ranges from 9,012 to 10,065 fps among the Bellefonte Site suspension logging test locations, which is generally consistent with the downhole survey results from the BLNP site. The calculated average S-wave velocity from the BLNP cross-hole surveys (9,227 fps) is slightly lower than the average S-wave velocity from the BLNP site downhole surveys, and on the low end of the range of S-wave velocity from the Bellefonte Site suspension logging tests.

The results for P-wave velocity and Poisson's ratio from the downhole surveys at the two sites are also similar, though slightly higher at the BLNP boreholes. The average P-wave velocities at the Bellefonte Site boreholes (16,853 to 19,166 fps) are similar to but slightly lower than the P-wave velocity for less-weathered bedrock interpreted from the seismic refraction surveys (20,000 fps), as reported in Section 2.5.4.4.1. The average Poisson's ratios from suspension logging tests at the Bellefonte Site boreholes (0.28 to 0.31) are consistent with results from unconfined compression tests on bedrock specimens, as listed in Table 2.5.4-1.

#### 2.5.4.4.4 Microgravity Surveys

Microgravity measurements were made at 127 locations along four transects at the Bellefonte Site (Figure 2.5.4-1c). Measurements were made to confirm the results of the refraction survey. Microgravity data were acquired using a Scintrex CG-5 gravimeter (see Appendix C2 for details of microgravity data collection). Data were aligned with portions of five seismic refraction survey lines. The stations were spaced 20 feet apart, except along line 12000, where a 10-foot spacing was used. Microgravity measurements were made to verify the locations and boundaries of the seismic refraction anomalies, and to provide further confirmation that the western portion of the study area is underlain by competent bedrock.

Figures 2.5.4-8a through 2.5.4-8e show the microgravity data, along with corresponding seismic refraction profiles. Gravity measurements show excellent agreement with the seismic refraction data. Gravity values decrease between 75 and 210 microgals ( $\mu\text{Gals}$ ) over the low p-wave velocity zone in the eastern anomaly zone. The largest gravity value decrease is along seismic line 9000, where a 210  $\mu\text{Gal}$  gravity variation was observed over a pronounced p-wave anomaly in the L1 and L2 layers, and where boring B-10 penetrated an apparent clay-filled solution feature (see Section 2.5.4.3.1.2). Similar gravity anomalies were observed along two other transects located over the eastern anomaly zone, although the decrease in gravity values was smaller in these areas. The locations and boundaries of these gravity anomalies are in excellent agreement with the boundaries shown in the seismic profiles and indicated by boring data.

Gravity values in the central and northwestern portion of the study area are generally more uniform than those in the eastern and southeastern portion of the site. Gravity values corresponding to seismic line L25000 did not show any significant anomalies, and are in good agreement with the seismic refraction data. A broad gravity anomaly of approximately 30  $\mu\text{Gals}$  was observed along seismic refraction line L2000 over an area where the L2 layer showed a pronounced valley (the western anomaly zone). The broad shape and low magnitude of this gravity low suggest that the subsurface material in this area is somewhat less dense than in

adjacent areas, but much denser and less weathered than material underlying the eastern anomaly zone. Boring data confirm this observation. Borings B-9, B-12, and B-13, which were drilled in the western anomaly zone, did not penetrate any voids similar to those found in borings B-2 or B-10, which were drilled through the eastern anomaly zone (see Section 2.5.4.3.1.2). RQD values for cores from borings B-9, B-12, and B-13 were somewhat lower than values for nearby cores, but did not indicate significant karst features or intense bedrock fracturing.

In summary, the gravity values confirm the boundaries of the seismic refraction anomalies, and, along with core data, indicate that the bedrock located west and northwest of the eastern anomaly zone is likely to be competent and relatively free of significant karst zones. No significant features were identified in the gravity profiles that had not been previously identified in seismic and borehole investigations.

### 2.5.4.5 Excavation and Backfill

Three potential facility designs are under consideration for development at the Bellefonte Site. The three facility types and associated foundation depths for safety-related structures consist of:

- The General Electric Economic Simplified Boiling Water Reactor (ESBWR) with a foundation depth of 69 feet,
- The Westinghouse AP-1000 Nuclear Steam Supply System Reactor (AP1000) with a foundation depth of 39.5 feet, and
- The Toshiba Advanced Boiling Water Reactor (ABWR) with a foundation depth of 84.2 feet.

Detailed design of any future facility will be initiated at a later phase, if the Bellefonte Site is determined to be suitable for development of a nuclear power facility, and after the facility type has been selected. Additional geotechnical investigations and engineering evaluations will be required to support the detailed design in accordance with RG 1.70 and other guidance (USNRC, 1978b). At the present phase, to assess site suitability, the general types and depths of foundations for the three potential designs have been evaluated with consideration of subsurface site conditions.

#### 2.5.4.5.1 Plans and Sections

Standard plans have been developed for each of the three potential facility types (ESBWR, AP1000, and ABWR). The standard plan includes the typical elevation drawings of safety-related structures (with standard foundation depths), and the standard configuration of these structures relative to one another. However, the potential siting of the major safety-related structures within the Bellefonte Site has not yet been developed. It is anticipated that the siting of structures may be selected based in part on the findings of this GG&S study.

#### 2.5.4.5.2 Construction Excavation and Dewatering

Excavation methods for facility foundations will likely vary based on soil and rock consistency at the structure locations. As presented in Sections 2.5.4.2 through 2.5.4.4, the depth from ground surface to high quality limestone bedrock is less than 20 feet over a majority of the Bellefonte Site. More extensively weathered limestone, resulting in depths of greater than 95 feet bgs to high quality limestone in a few areas, is present in the eastern anomaly zone. At

the BLNP facility, all safety-related structures were founded directly on high quality bedrock, with foundation depths ranging from a few feet to 40 feet below pre-existing grade.

Results of the drilling and sampling program indicate that the residuum is generally too soft and too fine-grained to serve as a suitable foundation layer for major safety-related structures, and the weathered rock is generally too variable in consistency to serve as a suitable foundation layer. Loads applied to these formations could cause unacceptable total and/or differential settlement as the soft residuum or the infilled material within the weathered rock compress with time. For these reasons, it is anticipated that major safety-related structures would be founded on high-quality bedrock or on engineered fill over bedrock, and not directly on soil or weathered bedrock.

At the Bellefonte Site, excavation through existing fill, residual soils, and weathered limestone bedrock could be performed with standard excavation equipment or by ripping. Excavation through high quality bedrock with S-wave velocity of approximately 9,000 fps or greater would likely require blasting, as was performed at the BLNP facility, or rock splitting methods. Rock splitting methods using hydraulic pressures, expansive agents, or mechanical wedging would produce significantly less noise and vibrations than blasting, but would be slower than blasting. The appropriate hard-rock excavation method will depend in part on the foundation depth of the selected facility, and quality of the associated rock mass.

In some areas of the site, weathered bedrock may extend deeper than the planned foundation depths for one or more of the three facility designs under consideration. In such areas, the extensively weathered bedrock would likely be removed down to high quality bedrock, and structural compacted fill would be placed at a thickness necessary to develop the subgrade for the foundations. Alternately, the structure locations could be shifted to areas of shallower depth to high quality bedrock, reducing the need for such over-excavation. Either method is consistent with a suitable site for development.

Upon completion of excavation to high quality bedrock, isolated locations of deeper weathering or clay-filled joints, fractures, or voids may be observed at the base of the excavation. As necessary, such zones would be grouted or otherwise improved to form a competent foundation subgrade. Subgrade improvement methods are further considered in Section 2.5.4.12.

Excavation dewatering methods will vary based on the subsurface conditions at the selection location and the excavation depth required for the specific power-generating system. Section 2.5.4.6 presents the groundwater conditions observed at and near the Bellefonte Site. During past construction activities at the BLNP facility, foundation excavations were generally constructed in high quality bedrock. Groundwater infiltration was efficiently managed using pumps placed in the low points of the excavation. For future development at the Bellefonte Site, foundations may be deeper than for the BLNP facility, depending on the choice of reactor type. Also, in isolated intervals within the Bellefonte Site, excavation sidewalls may contain greater depths of soil and weathered bedrock. This is especially applicable to the eastern anomaly zone (see Section 2.5.4.4), but may also be applicable to a lesser extent at other areas of the site, such as the western anomaly zone along boreholes B-9A, B-12, and B-13. These unconsolidated and weathered materials will have a greater effective porosity and hydraulic conductivity than high quality bedrock, and therefore could result in a greater rate of groundwater infiltration. For deep excavations in such materials, construction of pressure relief wells may be required. The

methods and extent of construction dewatering will be designed after selection of the facility design and building locations at the Bellefonte Site.

### 2.5.4.5.3 Earthfill and Granular Fill

Earthfill and granular fill will be required to backfill excavation sidewalls, and potentially to prepare a competent foundation subgrade in areas of deep weathered bedrock. In general, the residuum and the weathered backfill will be unsuitable for structural backfill without processing due to the high percentage of silt and clay size material that is prevalent in these materials. These materials could be used for landscaping and at other locations that will not support structural loads. The unweathered limestone could potentially serve as suitable backfill if crushed and screened prior to use.

As for the Bellefonte facility construction, offsite borrow sources of earthfill and granular fill are available within reasonable haul distance to the site and could be used for granular fill requirements. Required engineering properties and sources of earthfill and granular fill would be developed during the COL phase. Earthfill and granular fill requirements do not affect the determination of site suitability.

### 2.5.4.6 Groundwater

Groundwater level measurements were made in 32 monitoring wells and piezometers located on the TVA property. Results are tabulated in Table 2.5.4-8, and shown graphically in Figures 2.5.4-9a through 2.5.4-9c. A chart of water elevations at the four Bellefonte Site piezometers in each of the three monitoring events is included as Figure 2.5.4-10.

Results of groundwater measurements made on March 2, May 4, and July 28, 2005, indicate that at the Bellefonte Site, the depth to water has ranged from approximately 0.5 to 8 feet below grade. Water levels at the Bellefonte Site were highest in March and lowest in July. Potentiometric gradients are toward the Town Creek embayment to the northwest, and average approximately 0.01 foot/foot across the Bellefonte Site. Fluctuations in all the monitored wells, including those outside the study footprint, ranged from less than 1 foot to nearly 13 feet. Measured water levels likely represent a semi-confined piezometric surface, as samples of residuum recovered from borings have been described as dry to moist as deep as approximately 15 feet bgs.

Slug tests were performed in the four new piezometers (P-1 through P-4) completed during the investigation. Results are shown in Table 2.5.4-10, and slug test methods and results are described in Appendix H. Computed hydraulic conductivity values for three of the piezometers range from  $2.6 \times 10^{-4}$  to  $8.2 \times 10^{-4}$  cm/s. These values are in good agreement with values computed from packer testing in the existing plant area, which ranged from  $4.0 \times 10^{-4}$  to  $5.3 \times 10^{-4}$  cm/s. The computed value for the remaining piezometer (P-1) is  $5.0 \times 10^{-6}$  cm/s, which is two orders of magnitude lower than the values computed for the other three piezometers. Piezometer P-1 is located in the northwestern portion of the Bellefonte Site, in an area where the seismic refraction data indicate that conditions are relatively uniform with little weathering (see Section 2.5.4.4.1.2).

None of the groundwater observations are considered to affect the suitability of the Bellefonte Site for future development.

### 2.5.4.7 Response of Soil and Rock to Dynamic Loading

It is anticipated that the safety-related structures will be located on hard rock, having a low-strain shear wave velocity in excess of 9,000 fps. Little, if any, shearing strain effects would be expected for a rock with this S-wave velocity under seismic loading, and therefore, no cyclic laboratory tests were conducted on rock samples from the Bellefonte Site to establish the variation in shear modulus and material damping of the hard rock with shearing straining amplitude. Likewise, one-dimensional site response studies were not performed below the top of hard rock when determining the SSE for the site. As discussed in Section 2.5.2, the PSHA model for the site defines a ground shaking hazard for rock with a shear wave velocity of 9,000 fps or more, making the results of the PSHA directly useable rather than requiring modifications for local amplification or deamplification as the ground motion propagates through soil or soft rock.

Additional evaluations of the response of soil and rock to dynamic loading will need to be considered based on the location, placement, and requirements of the selected reactor system. These future evaluations could include soil-structure interaction, particularly for those non-safety-related structures that are located on weathered bedrock or soil. If structures are supported on soil or weathered rock, or if the safety-related structures are not supported on hard rock, cyclic testing of borrow material, weathered rock, or native soils may be required to establish the shear modulus and material damping ratio variation with shearing strain amplitude. This information would be used to conduct site response or soil-structure interaction analyses. Inasmuch as these requirements will change significantly for the three reactor systems currently being considered, further evaluation of the response of soil and rock to dynamic loading were not necessary at this time.

### 2.5.4.8 Liquefaction Potential

The potential for soils at the Bellefonte Site to liquefy under the SSE was evaluated. In this discussion, soil liquefaction refers to a change of soil state from a competent condition to a low-strength condition as a consequence of excess porewater pressure development and reduced effective stress. While the increase in porewater pressure can be the result of various types of static and transient loadings, cyclic loading as a result of the SSE would be the most likely potential cause of liquefaction at the Bellefonte Site. Earthquake-induced liquefaction occurs only under certain soil, groundwater, and cyclic loading conditions. For example, loose cohesionless soils located below the groundwater table are prone to liquefaction when levels of shaking result from a moderate-to-large earthquake.

In addition to liquefaction of sand-like cohesionless soils, cyclic strength loss of clay-like soils can occur under certain dynamic loading conditions. In such conditions, seismic shearing strains develop such that the undrained shear strength of the clay reduces from its peak strength possibly to its residual strength. While this will not usually result in the same magnitude of strength loss as may be observed in cohesionless soils, the phenomenon can result in reduction of foundation bearing capacity.

#### 2.5.4.8.1 Methodology for Assessing Liquefaction

Procedures in U.S. NRC Regulatory Guide 1.198 (NRC, 2003c) were followed when assessing the liquefaction potential at the Bellefonte Site. RG 1.198 references state-of-the-art practices to evaluate liquefaction potential, as presented at the National Center for Earthquake Engineering



Research (NCEER) workshops in 1996 and 1998 (Youd et al., 2001). More recent research on the potential for cyclic failure of clay-like soils was also considered Boulanger and Idriss, 2004) during this evaluation.

As summarized in RG 1.198, earthquake-induced liquefaction is most likely to develop in loose silts and fine sands. In some cases, gravels may be susceptible to liquefaction, if surrounded by finer-grained deposits or if the void spaces are filled with finer materials. As summarized in RG 1.198, cohesive soils are generally not considered liquefiable if they have fines content greater than 30 percent, and also have either: (1) a USCS classification of clay; or (2) plasticity index (PI) greater than 30. Further, if a clay deposit has a clay content greater than 15 percent by weight, a liquid limit greater than 35 percent, and natural water content lower than 90 percent, it is generally not considered liquefiable. Soils above the historic, current, or reasonably anticipated future water table are also not subject to liquefaction. However, recent research (e.g., Boulanger and Idriss, 2004) indicates that fine-grained soils with PI greater than 7 are considered “clay-like” soils, and are not subject to the same types of liquefaction behavior as sands (Boulanger and Idriss, 2004). These clay-like soils may, however, be subject to build-up in porewater pressures and a reduction in shear strength under cyclic loading, and the consequences of cyclic loading (and associated strain-softening) should be considered.

The potential for liquefaction in sand-like soils is determined by comparing the cyclic shearing stresses induced by the design earthquake to the liquefaction resistance of the soil. Either simplified or rigorous methods can be used for these analyses. For the Bellefonte site liquefaction assessment, simplified methods were used. In this approach the normalized induced cyclic shearing stress ratio (CSR) was defined by the  $p_{ga}$  at the ground surface, the total and effective overburden stresses at the depth of interest, and a soil deformability factor; the normalized liquefaction resistance ratio (CRR) was determined on the basis of the SPT blowcounts adjusted for hammer energy, overburden stress, and fines content. A magnitude scaling factor (MSF) was also introduced to account for the predominant magnitude of the design seismic event.

Following procedures in RG 1.198, the potential for liquefaction was determined on the basis of the ratio of the CRR to CSR with appropriate adjustments – which is also referred to as the factor of safety (FOS) against liquefaction. Interpretations of the FOS followed the RG 1.198 criteria as summarized below:

1. Soil elements with low FOS ( $\leq 1.1$ ) would achieve conditions wherein soil liquefaction should be considered to have been triggered.
2. Soil elements with a high FOS ( $\geq 1.4$ ) would suffer relatively minor cyclic porewater pressure generation.
3. Soil elements with intermediate FOS (FS  $\sim 1.1$  to 1.4) should be assigned strength values between the values appropriate for conditions 1 and 2 above.

#### 2.5.4.8.2 Results of Liquefaction Evaluation

Most of the soils above bedrock encountered in boreholes at the Bellefonte Site do not meet the criteria to be considered potentially liquefiable. The residual soils consist predominantly of fine-grained cohesive clay with fines content greater than 30 percent and PI greater than 30, as

indicated in the borehole logs and laboratory test results listed in Table 2.5.4-2. Following RG 1.198, these materials are not considered liquefiable.

A few exceptions to the general cohesive consistency of soils were noted, as follows.

- At several borehole locations, crushed surface stone or gravel was placed in the upper few feet below ground surface during previous operations at the site. Also, thin clayey gravel intervals (possibly weathered bedrock) were noted near the bedrock surface at several boreholes (B-2, B-6, B-9, B-9A, B-10, and B-14). However, these gravel materials are not considered to be of liquefaction concern, because it is likely that the surface gravel would be removed or regraded prior to construction of any safety-related structures. These surface gravel intervals are also above the high-water level observed at most locations of the site.
- The deeper gravel intervals located below the groundwater table were generally observed to have cohesive clay infilling or are in a dense condition, and are likely not subject to liquefaction.
- Potentially liquefiable sands were observed at two boreholes. At Borehole B-4, a soft silty sand deposit was encountered from 3.5 to 5 feet bgs, directly above bedrock. Test results for a sample from this interval indicate that fines content is greater than 30 (31 percent), but it was not cohesive, was loose (with an SPT blowcount of 3), and is therefore potentially liquefiable. A similar deposit was observed at borehole B-3 from 3.5 to 4 feet bgs.
- No liquefiable deposits were encountered below the top of competent bedrock in any of the boreholes.

For the liquefaction assessment, the sand intervals encountered at boreholes B-3 and B-4 are considered to be potentially liquefiable. Soil conditions at borehole B-4 were therefore used to evaluate the FOS against liquefaction using the simplified method presented in Section 2.5.4.8.1. SPT blowcounts were obtained with an automatic hammer having an energy ratio of approximately 60 percent. The groundwater table was assumed to be located at the ground surface for the liquefaction assessment. The pga from the SSE at the ground surface was defined as 0.3g, similar to the pga on hard rock. While the pga level in the hard rock could amplify slightly as it propagates through the soil to the ground surface, this amplification potential was not evaluated primarily because of the limited thickness of the soil layer. If amplification effects were considered, a slightly higher ground acceleration could occur. As will be discussed in the next paragraph, liquefaction was predicted at the pga of 0.3g, leading to the conclusion that the liquefiable material will have to be removed or improved. Higher ground accelerations would not change this conclusion. For the liquefaction evaluation, earthquake magnitudes ranging from 5 to 7.5 were considered.

Following the methodology described above, the sand intervals encountered above bedrock at boreholes B-3 and B-4 were determined to have a FOS of less than 1.0 during the SSE. This FOS does not meet the minimum FOS (less than 1.1) specified by RG 1.198 under the expected safe-shutdown earthquake magnitude and pga, and therefore would achieve conditions where soil liquefaction would be triggered.

The standard of engineering practice is to not locate structures above liquefiable soils because of the potential for loss in bearing support as the liquefied soil loses strength or because of settlement that results as excess porewater pressures in liquefied soil dissipate following the

earthquake. As a result, potentially liquefiable soils present above bedrock (such as the sand deposits encountered at boreholes B-3 and B-4) would need to be either removed or otherwise improved during future construction of safety-related structures. The extent of such removal or improvement would be evaluated once specific structure designs and locations are selected. Considering the shallow depth to bedrock across the Bellefonte Site (especially within the recommended development area shown in Figure 2.5.4-1a), liquefaction potential could be readily mitigated, and therefore liquefaction is not considered to pose any site suitability concerns.

In view of the shallow rock elevations and the potential for settlement of the clay-like soil, it is expected that most clay-like soils will be removed below safety-related structures, with the safety-related structure founded on either rock or engineered fill located on rock. However, some non-safety-related structures could be located on the residuum above the rock. In addition to confirming that the residuum will provide adequate bearing and settlement for gravity loading, the potential effects of cyclic shear strength reduction in these clay-like soils will need to be considered in detail. These evaluations would be appropriate during the COL phase of the development when the location, weight, and foundation elevation have been established. While not usually as catastrophic as complete liquefaction of cohesionless soils, the cyclic effects to the clay-like soil could reduce the bearing capacity of foundations, and the induced porewater pressures from cyclic shearing strains could lead to post-seismic settlements. As with the liquefaction of sand-like soils, the potential concerns with cyclic shear strength reduction of clays can be readily mitigated due to the shallow depth to bedrock, and therefore this phenomenon is not considered to pose any site suitability concerns.

#### **2.5.4.9 Earthquake Design Basis**

Evaluation of ground motions associated with earthquakes at the Bellefonte Site is presented in Sections 2.5.2.6 and 2.5.2.7.

#### **2.5.4.10 Static Stability**

##### **2.5.4.10.1 General**

With any of the three potential reactor types currently under consideration for the Bellefonte Site, the foundation for safety-related structures would likely be founded either directly on competent bedrock, or on controlled fill above competent bedrock. Because of the shallow depth of rock in most areas of the Bellefonte Site, it is not anticipated that safety-related structures would be founded directly on in situ soils.

##### **2.5.4.10.2 Rock Supported Foundations**

Geotechnical data (described in Sections 2.5.4.2 through 2.5.4.4) indicate that fresh limestone bedrock is present within 20 feet bgs across the Bellefonte Site, except in the eastern anomaly zone. Deeper and more extensive zones of bedrock weathering are present at boreholes B-2 and B-10 in the eastern anomaly zone. Following are recommendations regarding construction of foundations on bedrock within the recommended development area, and within the eastern anomaly zone, respectively.

### 2.5.4.10.2.1 Rock Foundations in the Recommended Development Area

The recommended development area, as shown in Figure 2.5.4-1a and other figures, includes the portion of the Bellefonte Site northwest of and including boreholes B-8 and B-15. Fresh bedrock was encountered within 15 feet of ground surface at boreholes B-8 and B-15, both within a few hundred feet northwest of the eastern anomaly zone. The recommended development area also includes the western anomaly zone, within which boreholes B-9A, B-12, and B-13 were completed. The upper 40 feet of bedrock at these boreholes typically has marginally more fractures than the surrounding areas, but the RQD of this rock is typically still greater than 80 percent (with a few exceptions) and there is no evidence of clay-filled voids below the upper 10 feet of weathered bedrock in this zone. Therefore, bedrock is of high quality and considered suitable for safety-related foundation development within the western anomaly zone, and throughout the recommended development area.

The unconfined compression strength of 10 fresh bedrock core samples collected at the Bellefonte Site ranged from 12,000 up to 34,700 psi (Table 2.5.4-1). The ultimate bearing capacity of foundations in unweathered bedrock can be calculated as a function of the rock unconfined compression strength, which would result in an ultimate bearing capacity on the order of  $10^6$  psf. However, the allowable bearing pressure would likely be specified on the order of  $10^5$  psf, in accordance with building codes for fresh limestone bedrock with high RQD. The average bearing capacity requirements are expected to be less than  $10^4$  psf for the three potential facility designs. The allowable bearing pressures of fresh rock foundations would be much higher than this value. Therefore, fresh bedrock is considered suitable for future foundation development at the Bellefonte Site, and such material is encountered within 20 feet bgs at each borehole within the recommended development area.

Potential rebound and settlement of foundations on fresh bedrock will be evaluated during COL based on the foundation depth, the foundation bearing pressure, the elasticity of the bedrock materials, and Poisson's ratio. The secant modulus of four rock unconfined compression (UC) samples with strain measurements ranged from 3.7 by  $10^6$  to 10.9 by  $10^6$  psi, as listed in Table 2.5.4-1. Comparison of expected rebound and settlement against tolerable values for the selected design will be performed during COL. Considering the high modulus of the bedrock (low compressibility) and high RQD of the fresh bedrock (typically greater than 90 percent), rebound and settlement of foundations on fresh bedrock are expected to be manageable, and suitable for future development at the Bellefonte Site.

### 2.5.4.10.2.2 Rock Foundations in the Eastern Anomaly Zone

The higher frequency and depth of weathered bedrock and clay-filled voids within the eastern anomaly zone, as indicated by seismic refraction surveys, microgravity surveys, and boreholes B-2 and B-10, may be the result of the lateral movement of groundwater across the site, and associated limestone dissolution. It is also possible that some features indicate past or recent sinkhole development in this area, where vertical movement of groundwater has dissolved the limestone and carried the material downward through solution conduits in the bedrock. However, as discussed in Section 2.5.4.1.2, no surface expressions of sinkholes could be found anywhere within the outcrop belt of the Chickamauga formation near the Bellefonte plant, and recent downward vertical groundwater gradients have not been observed in the area. These factors suggest that sinkhole development in the eastern anomaly zone is not currently active.

Regardless of the cause of the dissolution features in the eastern anomaly zone, the seismic refraction survey data and borehole results indicate that this area is not desirable for development of major safety-related structures. Clay-filled voids were present at borehole B-10 at a depth of at least 95 feet bgs, and it is possible that similar depths of extensive weathering and dissolution are present at other locations within the southeastern anomaly zone, as indicated by the seismic refraction data. For these reasons, high quality bedrock may be prohibitively deep to construct rock foundations within the eastern anomaly zone. It is recommended that major safety-related structures be located within the recommended development area shown in Figure 2.5.4-1a (and other figures).

### 2.5.4.10.3 Soil-Supported Foundations

Foundations of major safety-related structures may be constructed on engineered fill over fresh bedrock in some locations. This may be required where the designed facility foundation depth is above the unweathered bedrock surface. In such areas, significantly weathered bedrock (i.e., with numerous fractures, clay-filled voids, and soft intervals) as observed at the site would not be used as foundation subgrade, and would instead be excavated and replaced with engineered fill. The bearing capacity of the subgrade will, therefore, depend on the engineering properties of the fill. The engineered fill material and compaction specifications would be developed during COL to provide an appropriate bearing capacity safety factor.

Because of the shallow depth of in situ soil within the recommended development area at the Bellefonte Site (less than 20 feet bgs), it is not anticipated that major safety-related structures will be founded directly on in situ soils for any of the three potential facility designs – rather, they will either be constructed directly on bedrock or on engineered fill over bedrock.

### 2.5.4.10.4 Lateral Pressures

Lateral earth pressures on the sidewalls of belowgrade structures will include the active or at-rest pressure of compacted engineered backfill plus hydrostatic pressures. Most safety-related structures will be very rigid and therefore at-rest conditions are expected to develop for these structures; some non-safety-related structures, whose retaining walls are more flexible, or free-standing retaining walls could develop active pressures.

The distribution of static lateral pressures will depend on the selected facility foundation depths, post-construction water levels, backfill specifications, and compaction methods. Dynamic lateral pressures will depend on these parameters, as well as predicted ground motions.

Static and dynamic lateral pressures on subsurface structures would be evaluated during COL, once the facility design has been selected and specifications are prepared. Lateral earth pressures may result in modifications to backfill material and compaction specifications during COL, but are not considered to affect the suitability of the Bellefonte Site for future development.

## 2.5.4.11 Design Criteria

### 2.5.4.11.1 Bearing Capacity of Rock Supported Foundations

The minimum factor of safety for bearing pressures on rock supported foundations is commonly selected as between 2.0 for dead and transient live loads, and 3.0 for dead and

frequent or continuous live loads (NAVFAC, 1982). These factors of safety are recommended for future rock supported foundations at the Bellefonte Site (TVA, 1986). However, for such foundations, the actual FOS will likely be much higher than this, as described in Section 2.5.4.10.2, because the actual bearing pressure of facility foundations would likely be much lower than the ultimate bearing capacity of rock. Methods to evaluate bearing capacity during COL are also discussed in Section 2.5.4.10.2.

#### **2.5.4.11.2 Bearing Capacity of Soil Supported Foundations**

The minimum recommended FOS for bearing pressures on engineered fill is 3.0 for dead and continuous live loads. This minimum FOS would apply to foundations placed on engineered fill over fresh bedrock. It is not expected that major safety-related structures would be founded directly on native soil or weathered bedrock.

#### **2.5.4.11.3 Slope Stability Criteria**

No earthen slopes are present near the Bellefonte Site, and no earthen slopes would be required for operation or safe shutdown of any of the three potential facility designs. Stability of excavation sidewalls during construction will be considered during COL, but these will be backfilled prior to operation. Therefore, slope stability is not considered to affect site suitability for future development.

Minimum FOSs against excavation sidewall instability during construction will be considered during COL. A FOS of 1.3 is recommended for short-term static conditions during construction. Transient dynamic loads during construction would likely be evaluated by finite element modeling of potential displacements.

#### **2.5.4.12 Techniques to Improve Subsurface Conditions**

Fresh bedrock is expected to form an excellent subgrade material at the facility. Foundations for any of the three potential facility designs could be founded directly on fresh bedrock throughout the Bellefonte Site, with the exception of the eastern anomaly zone (southeast of boreholes B-8 and B-15).

Minor clay-filled cavities present at the bedrock surface would be cleaned out and filled with concrete or grout prior to foundation construction. Cavities that extend significantly below the foundation subgrade or rock excavation sidewalls could be intercepted by drill holes and filled by pumping a concrete slurry. Such voids could be filled to a minimum depth of twice the surface width of the void. Similar methods were used to prepare the foundation subgrades at the BLNP site (TVA, 1986).

In the eastern anomaly zone southeast of boreholes B-8 and B-15, a greater and more variable depth to fresh bedrock was indicated by the geophysics and boreholes than at the rest of the Bellefonte Site. In this area, pinnacles of fresh bedrock likely alternate with slots of deeper weathering, resulting in an uneven and relatively deep fresh bedrock surface. Clay-filled cavities alternating with highly weathered bedrock intervals extend below the practical foundation excavation depth for all three potential facility designs at borehole B-10, and such conditions are likely present in other locations southeast of boreholes B-8 and B-15.

If safety-related structures would be located southeast of boreholes B-8 and B-15, a significant amount of subgrade improvement may be necessary. This may require more extensive cleaning

and grouting of voids (as described previously for the fresh bedrock surface), and possibly the construction of structural bridges over deep filled slots in the bedrock surface. To minimize the scope, cost, and uncertainties associated with such subgrade improvement, it is recommended that the development of major safety-related structures be confined to the recommended development area bounded on the southeast by boreholes B-8 and B-15. The recommended development area is shown in Figure 2.5.4-1a (and other figures).

#### **2.5.4.13 Subsurface Instrumentation**

Instrumentation systems required to assure that the facility is performing in accordance with engineering design requirements will be identified during COL. The geotechnical instrumentation is expected to include multiple seismometers for monitoring levels of ground shaking during earthquakes, piezometers for monitoring groundwater conditions, and settlement gauges to check settlement during construction and under long-term gravity loads. Some of these instrumentation systems would be installed during construction to monitor the response of the bedrock to excavations and reloading from structures.

As part of any instrumentation effort, an installation and monitoring program would be developed. The installation and monitoring program would outline types and requirements for the instrumentation, methods of calibration and installation, long-term monitoring and maintenance requirements, and action plans to implement if instruments approach or exceed a predetermined trigger level.

#### **2.5.4.14 Construction Notes**

Construction notes are not applicable for this Bellefonte Site Study. Construction notes for the adjacent BLNP site are included in Section 2.5.4 of the BLNP FSAR (TVA, 1986). These construction notes indicate that, with the exception of some grouting requirements at the base of the BLNP site structures, facility construction was accomplished without significant difficulties.

TABLE 2.5.4-1  
Summary of Rock Unconfined Compression Strength Test Results  
*TVA Bellefonte GG&S Evaluations*

Core Section Tested			Conditions at Failure			
Borehole	Top Depth (ft)	Bottom Depth (ft)	Unit Weight (pcf)	UC <sup>1</sup> Strength (psi)	Secant Modulus (x10 <sup>6</sup> psi)	Poisson's Ratio
B-1	13.9	15.1	171	34,704	--- <sup>2</sup>	---
B-1 <sup>3</sup>	95.75	96.6	169	19,647	10.9	0.30
B-2	93	93.9	168	12,097	3.74	0.13
B-3	20.85	21.6	170	16,628	---	---
B-3 <sup>3</sup>	59	60.15	169	17,986	9.14	0.27
B-3	89.1	90.65	170	13,635	---	---
B-4 <sup>4</sup>	89.15	90.3	170	17,689	---	---
B-5 <sup>4</sup>	59.7	60.7	169	21,017	---	---
B-6	24.85	25.5	170	13,229	7.84	0.29
B-6	89.55	90.55	170	13,053	---	---

Notes:

<sup>1</sup> UC Strength = Unconfined Compression Strength.

<sup>2</sup> --- = Not applicable, strains were not monitored in this test.

<sup>3</sup> Secant modulus and Poisson's ratio were measured prior to cracking sounds in this sample.

<sup>4</sup> Test specimen size was approximately 1.85-inch diameter by 3.9-inch length. All other specimens were 2.47-inch diameter by 5.6-inch length.

Unconfined compression strength was tested in accordance with ASTM D2938.

Elastic moduli (secant modulus and Poisson's Ratio) were tested in accordance with ASTM D3148.



TABLE 2.5.4-2  
Summary of Soil Test Results  
TVA Bellefonte GG&S Evaluations

Sample Tested			Atterberg Limits				Gradation					USCS	Soil pH	Moisture Content (%)	Dry Unit Weight (pcf)	UU-Triaxial Su (psf)
Borehole	Top Depth (ft)	Bottom Depth (ft)	Samp. Type	LL	PL	PI	Gravel (%)	Sand (%)	P200 Fines (<0.075 mm) (%)	Clay (<0.005 mm) (%)						
B-1	3.5	5	Jar	82	22	60	---	---	87	---	CH	---	33.1	---	---	
B-2	3.5	5	Jar	47	16	31	---	---	80	---	CL	---	20.6	---	---	
B-2	16	17	Jar	73	20	53	---	---	54	---	CH	---	28.4	---	---	
B-3	4	6	ST	34	15	19	0	8	92	35	CL	4.5	19.8	106.3	1285	
B-4	3.5	4	Jar	---	---	---	---	---	31	---	---	---	23.6	---	---	
B-5	3.5	5.5	ST	78	22	56	10	15	75	53	CH	7.5	32	94.7	580	
B-5	6	7.6	ST	42	16	26	17		62	33	CL	7.7	19.3	106.1	1670	
B-6	6	7.5	Jar	60	16	44	---	---	41	---	CH	---	16.5	---	---	

Notes:

--- = Test not performed for this sample.

Dry Density = Reported result is the average for specimens tested for unconsolidated-undrained (UU) triaxial shear strength.

UU Triaxial Su = Undrained shear strength as tested by UU triaxial shear. Reported result is the average Su for the specimens tested.

Sample Type: "Jar" = Jar sample collected during SPT. "ST" = Shelby tube sample.

USCS = Unified Soil Classification System.

TABLE 2.5.4-3  
Summary of Borehole Observations  
*TVA Bellefonte GG&S Evaluations*

Observation	B-1	B-2	B-3	B-4	B-5	B-6	B-6A	B-7	B-8
Ground Elevation, ft amsl	612.6	621.3	607.1	631.0	618.8	629.2	629.3	617.5	618.1
Northing, ft	1530214.9	1529648.0	1530779.3	1529863.7	1529746.6	1528925.3	1528929.8	1529888.4	1530047.8
Easting, ft	625826.4	626589.4	625985.2	627062.5	625400.8	626162.8	626167.0	626234.2	626529.8
Overburden Soil Thickness, ft	7.5	20.0	8.5	5.0	8.0	7.5	7.0	4.0	10.7
Overburden Soil Description	CL	GP (0-1') CL (1-20')	GC & SP (0-4') CL (4-8.5')	GP (0-1.5') CL (1.5- 3.5') SC (3.5- 5.0')	CL	GP (0-1.5') CL with GP & GC intervals (1.5-7.5')	See Borehole B- 6	GP (0-1') CL (1-4')	CL
Elevation: Top of Bedrock, ft amsl	605.1	601.3	598.6	626.0	610.8	621.7	622.3	613.5	607.4
Weathered Bedrock Thickness, ft	0	59	0	2.5	0	11.5	10	6.5	0
Weathered Bedrock Description	None	Limestone, mostly gravel size, iron stained, clay coatings & interbeds	None	Limestone, weathered fractures	None	Limestone, interbedded clay seams, iron stained weathered fractures	Limestone, interbedded clay seams, iron stained weathered fractures	Limestone, mostly gravel size, no oxidation, relatively fresh.	None
Elevation: Top of Fresh Limestone, ft amsl	605.1	542.3	598.6	623.5	610.8	610.2	612.3		607.4
Fresh Bedrock Description	Limestone, RQD = 81- 100%	Limestone, RQD = 95- 100%	Limestone, RQD = 71- 100%	Limestone, RQD = 90- 100%	Limestone, RQD = 79- 100%	Limestone, RQD = 82- 100%	Limestone, RQD = 60- 90%	Limestone, RQD = 94- 100%	Limestone, RQD = 94- 100%
Total Depth of Rock Core, ft	116	115	99	95	95	95	25	95.7	95.6

TABLE 2.5.4-3  
Summary of Borehole Observations  
*TVA Bellefonte GG&S Evaluations*

<b>Observation</b>	<b>B-1</b>	<b>B-2</b>	<b>B-3</b>	<b>B-4</b>	<b>B-5</b>	<b>B-6</b>	<b>B-6A</b>	<b>B-7</b>	<b>B-8</b>
Elevation: Bottom of Rock Core, ft amsl	496.6	506.3	508.1	536.0	523.8	534.2	604.3	521.8	522.5
<b>Observation</b>	<b>B-9</b>	<b>B-9A</b>	<b>B-10</b>	<b>B-11</b>	<b>B-12</b>	<b>B-13</b>	<b>B-14</b>	<b>B-15</b>	<b>P-3</b>
Ground Elevation, ft amsl	618.9	619.6	623.9	609.0	612.2	616.0	601.5	621.2	605.8
Northing, ft	1529850.1	1529753.7	1529833.9	1530464.0	1530292.1	1530047.0	1530902.9	1529624.4	1530422.3
Easting, ft	625727.9	625846.5	626790.7	625490.0	626318.0	626029.0	625428.1	626214.3	625061.1
Overburden Soil Thickness	8.6	10.2	10.0	9.0	14.6	10.0	3.8	8.0	6.5
Overburden Soil Description	CL (0-6.5') GC (6.5-8.6')	CL	GP (0-2') CL (2-10')	CL	CL	CL	CL (0-2.5') GC (2.5-3.8')	CL	GP (0-3') CL (3-6.5')
Elevation: Top of Bedrock, ft amsl	610.3	609.4	613.9	600.0	597.6	606.0	597.7	613.2	599.3
Weathered Bedrock Thickness, ft	9.4	1.6	4	4	0	7	4.2	0	2
Weathered Bedrock Description	Limestone, slightly weathered fractures, RQD = 20-30%, no clay-filled voids	Limestone, mostly fractured fragments and clay.	Limestone, gravel size pieces with clay (10-12'), slightly weathered clay-lined partings (12-14') Becomes highly weathered with clay-filled voids below 49.5')	Limestone, slightly weathered, RQD = 23%, no clay-filled voids.	None	Limestone and Clay, limestone stringers 1-2" thick.	Limestone, numerous fresh fractures.	None	Limestone, weathered fractures

TABLE 2.5.4-3  
Summary of Borehole Observations  
*TVA Bellefonte GG&S Evaluations*

Observation	B-1	B-2	B-3	B-4	B-5	B-6	B-6A	B-7	B-8
Elevation: Top of Fresh Limestone, ft amsl	600.9	607.8	609.9	596.0	597.6	599.0	593.5	613.2	597.3
Fresh Bedrock Description	Limestone, RQD = 90-100%	Limestone, RQD = 84% (13-18') RQD = 94 - 100% below	Limestone, RQD = 76-100% (14-49.5') Becomes highly weathered with clay-filled voids below 49.5' to end of borehole.	Limestone, RQD = 82 - 100%	Limestone, RQD = 54% (14.6-22') RQD = 72-88% (22-47') RQD = 94-100% (47-95.1')	Limestone, RQD = 70-100% (17-47') RQD = 90-100% (47-95')	Limestone, RQD = 58% (8-13') RQD = 86-100% (13-95.6')	Limestone, RQD = 80-97% (8-32.7') RQD = 95-100% (32.7-96.2')	Limestone, RQD = 84-100%
Total Depth of Rock Core, ft	95.5	95.4	94.0	95.4	95.1	95.2	95.6	96.2	24.5
Elevation: Bottom of Rock Core, ft amsl	523.5	524.2	529.9	513.6	517.1	520.8	505.9	525.0	581.3

Notes:

amsl = above mean sea level.

Northing and easting are State Plane Coordinates.

Ground surface elevations listed for B-3, B-6A, and P-3 are based on the surveyed top of casing (TOC) elevations for piezometers P-1, P-4, and P-3, respectively, plus vertical measurements from TOC to adjacent ground surface.

Overburden Soil Description is based on the visual USCS soil classification.

TABLE 2.5.4-4  
Summary of Cavities Observed in GG&S Rock Cores  
*TVA Bellefonte GG&S Evaluations*

Borehole	Interval (bgs)		Average Depth Below TOR (ft)	Thickness (ft)	Conditions within Cavity
	Top	Bottom			
B-1	No cavities observed				No cavities encountered
B-2	25	29	7.0	up to 3.6	3.6' not recovered, clay- and gravel-filled, depth and thickness between limestone ledges unknown
	29	34	11.5	up to 4.1	4.1' not recovered, clay- and gravel-filled, depth and thickness between limestone ledges unknown
	34	38.3	16.2	up to 4.3	2.8' not recovered, clay- and gravel-filled, depth and thickness between limestone ledges unknown
	38.3	39	18.7	0.2	0.2' of possible limestone gravel missing, depth uncertain
	39	44	21.5	up to 4.6	4.6' not recovered, speculate soft clay-filled cavity
	44	49	26.5	up to 5	5' not recovered, speculate soft clay-filled cavity
	49	53	31.0	up to 4	5' not recovered, speculate soft clay-filled cavity
	53	58	35.5	up to 3.9	3.9' not recovered, gravel and possibly clay-filled, depth and thickness between limestone ledges unknown
B-3	8.5	13.5	2.5	0.4	0.4' not recovered -- perhaps a weathered, gravelly interval/no clay; depth uncertain
B-4	6.25	7.3	1.8	1.05	Clay filled -- recovered 0.7' of clay
B-5	10	14.7	4.4	0.5	0.5' not recovered -- perhaps a weathered, gravelly interval/no clay; depth uncertain
	14.7	19.7	9.2	0.2	0.2' not recovered -- perhaps a weathered, gravelly interval/no clay; depth uncertain

TABLE 2.5.4-4  
Summary of Cavities Observed in GG&S Rock Cores  
*TVA Bellefonte GG&S Evaluations*

Borehole	Interval (bgs)		Average Depth Below TOR (ft)	Thickness (ft)	Conditions within Cavity
	Top	Bottom			
B-6	8	9	1.0	1	Clay filled -- recovered 0.2' of clay
	9	9.65	1.8	0.65	Predominantly clay-filled with some limestone rock fragments; depth uncertain
	9.95	10.9	2.9	0.95	Predominantly clay-filled with some limestone rock fragments; depth uncertain
	11	11.4	3.7	0.4	Predominantly clay-filled with some limestone rock fragments; depth uncertain
	11.4	14	5.2	2.6	No recovery, perhaps a weathered, gravelly interval
	14	17.5	8.3	1.5	1.5' not recovered -- perhaps a weathered, gravelly interval/no clay; depth uncertain
	17.5	19	10.8	0.4	0.4' not recovered -- perhaps a weathered, gravelly interval/no clay; depth uncertain
B-7	6	8.5	3.25	2.5'	Possible clay-filled void
B-8	No cavities observed				No cavities encountered
B-9	No cavities observed				No cavities encountered
B-9A	No cavities observed				No cavities encountered

TABLE 2.5.4-4  
Summary of Cavities Observed in GG&S Rock Cores  
*TVA Bellefonte GG&S Evaluations*

Borehole	Interval (bgs)		Average Depth Below TOR (ft)	Thickness (ft)	Conditions within Cavity
	Top	Bottom			
B-10	49.45	53.55	41.5	4.1	Clay-filled cavity. May contain thin, weak limestone ledge at 51.5. Lost some circulation
	56	59	47.5	3	Clay-filled cavity. May contain thin, weak limestone ledge at 57'
	59	62.5	50.75	3.5	Clay-filled cavity. May contain thin, weak limestone ledge at 59
	64	76.8	60.4	12.8	Clay-filled cavity with weathered limestone
	79	80	69.5	1	Clay-filled cavity
	80.45	82.5	71.475	2.05	Clay-filled cavity
	86	94	80	8	Clay-filled cavity
B-11	No cavities observed				No cavities encountered
B-12	22.7	22.8	8.15	0.1	Thin clay-lined cavity
B-13	10	12	1	2	Interbedded limestone ledges with clay
B-14	No cavities observed				No cavities encountered
B-15	No cavities observed				No cavities encountered
P-3	No cavities observed				No cavities encountered

Notes:

bgs = below ground surface.

TOR = top of rock.

TABLE 2.5.4-5  
Summary of CPT Sounding Observations  
*TVA Bellefonte GG&S Evaluations*

Location	Northing (ft)	Easting (ft)	Ground Elevation (ft amsl)	Refusal Depth (ft bgs)	Refusal Elevation (ft amsl)	Soil Description
C-1	1530785.7	625985.8	606.8	8.8	598.0	(0-1.5' & 2.3-3') silt or fine sand, (1.5-2.3'): gravel or sand, (3-8.8'): silt or clay
C-2	1530476.9	626388.4	613.1	13.2	599.9	(0-2' & 6.5-13.2'): silt, sand or gravel, (2-6.5'): silt or clay
C-3	1530202.4	626709.9	617.6	5.6	612.0	(0-3'): silt or fine sand, (3-4'): silt or sand, (4-5.6'): sand or gravel
C-4	1529857.2	627062.9	631.1	6.1	625.0	(0-3.5'): sand or gravel, (5.8-6.1'): silt or fine sand, (3.5-5.8'): silty clay or clay
C-5	1530733.2	625277.1	603.3	5.5	597.8	(0-3'): silt or fine sand, (3-3.6'): sand or gravel, (3.6-5.5'): clay or silty clay
C-6	1530457.1	625693.2	609.3	10.6	598.7	(0-6.7'): sand or gravel, (6.7-10.6'): silt or clay
C-7	1530220.8	625818.8	612.4	5.3	607.1	(0-5'): clay, (5-5.3'): sand or gravel
C-8	1530041.3	626095.6	616.0	1.5	614.5	NA
C-9	1529852.2	626344.9	617.6	0.6	617.0	NA
C-10	1529633.2	626591.3	621.1	10.4	610.7	(0-2.7'): fine gravel, (2.7-10.4'): silty clay to clay
C-11	1529447.2	626852.4	628.1	9.4	618.7	(0-4'): silt or fine sand, (4-5.4'): silt or silty clay, (5.4-9.4'): clay
C-12	1530110.6	625474.2	613.9	2.4	611.5	(0-1.9'): silt or fine sand, (1.9-2.4'): sand or gravel
C-13	1529745.1	625884.9	619.6	1.2	618.4	NA
C-14	1529570.9	626060.6	620.5	9.5	611.0	(0-8'): sand or gravel, (8-9.5'): clay
C-15	1529300.0	626336.7	623.8	5.8	618.0	(0-3.6'): sand or gravel, (3.6-5.8'): clay
C-16	1529245.0	626722.4	626.5	13.3	613.2	(0-4.2'): fine gravel or sand, (4.2-7.4'): clay, (7.4-8'): silt or clay, (8-13.3'): clay



TABLE 2.5.4-5  
Summary of CPT Sounding Observations  
*TVA Bellefonte GG&S Evaluations*

Location	Northing (ft)	Easting (ft)	Ground Elevation (ft amsl)	Refusal Depth (ft bgs)	Refusal Elevation (ft amsl)	Soil Description
C-17	1529061.3	626555.7	631.0	3.3	627.7	(0-1.5'): silt or fine sand, (1.5-3.3'): fine gravel or sand
C-18	1529745.7	625395.4	618.7	6.8	611.9	(0-1.4'): silt or fine sand, (1.4-3.6'): fine gravel or sand, (3.6-6.8'): clay
C-19	1529554.5	625523.7	622.9	10.9	612.0	(0-1.8'): silt or fine sand, (1.8-4.5'): silt or clay, (4.5-10.9'): sand interbedded with clay overlying sands
C-20	1529202.4	625816.1	622.7	0.6	622.1	NA
C-21	1528921.3	626158.2	629.2	9.0	620.2	(0-5'): fine gravel or sand, (5-5.5'): silt or fine sand, (5.5-9'): fine gravel or sand
C-22	1528667.7	626279.4	641.9	5.3	636.6	(0-2'): silt or fine sand, (2-5.3'): fine gravel or sand

Notes:

NA = CPT visual log not available/not enough data collected for soil classification.

amsl = above mean sea level.

bgs = below ground surface.

Northing and easting are State Plane Coordinates.

TABLE 2.5.4-6  
CPT Soil Shear Wave Velocity Results  
*TVA Bellefonte GG&S Evaluations*

Location	Top Depth (ft bgs)	Bottom Depth (ft bgs)	Average Interval Depth (ft bgs)	Shear Wave Velocity, Vs (fps)
C-1A	1.1	4.4	2.7	354
C-1A	3.9	7.2	5.5	524
C-7	1.3	4.5	2.9	501
C-10 <sup>1</sup>	5.8	9.1	7.5	923
C-10 <sup>1</sup>	9.1	10.5	9.8	1527
C-10A <sup>1</sup>	5.5	8.7	7.1	817
C-10A	6.1	9.4	7.7	931
C-16 <sup>1</sup>	5.9	9.3	7.6	1247
C-16 <sup>1</sup>	9.3	10.9	10.1	870
C-18 <sup>1</sup>	5.8	6.9	6.3	532
C-21 <sup>1</sup>	5.9	9.2	7.5	1060

Notes:

<sup>1</sup> Shear wave velocity was tested by pseudo-interval tests. Others were true interval tests.

bgs = below ground surface.

fps = feet per second.

TABLE 2.5.4-7  
Piezometer Construction Data  
TVA Bellefonte GG&S Evaluations

Well	Reported Well Depth (2)	Top of Casing Elevation (ft. MSL)	Source of TOC (ft. MSL)	2-Mar-05		4-May-05		28-Jul-05		21-Sep-05	
				Depth to Water (ft. below TOC)	Groundwater Elevation (ft. MSL)	Depth to Water (ft. below TOC)	Groundwater Elevation (ft. MSL)	Depth to Water (ft. below TOC)	Groundwater Elevation (ft. MSL)	Depth to Water (ft. below TOC)	Groundwater Elevation (ft. MSL)
P1	27.0	606.70	Civil Survey	0.51	606.19	1.35	605.35	1.08	605.62	3.95	602.75
P2	40.3	620.91	Civil Survey	0.55	620.36	2.32	618.59	5.89	615.02	7.11	613.80
P3	24.3	604.41	Civil Survey	3.36	601.05	4.88	599.53	5.50	598.91	6.88	597.53
P4	24.9	628.95	Civil Survey	5.00	623.95	8.00	620.95	13.32	615.63	14.79	614.16
W10	11.6	603.20	Note 2	4.60	598.60	6.92	596.28	8.40	594.80	DRY	DRY
W12	34.3	622.95	Note 2	12.75	610.20	19.35	603.60	25.51	597.44	27.17	595.78
W14	40.9	659.05	Note 2	23.81	635.24	DRY	DRY	DRY	DRY	DRY	DRY
W15	20.4	648.68	Note 2	12.90	635.78	NM	NM	DRY	DRY	DRY	DRY
W16	28.4	638.39	Note 2	3.50	634.89	5.32	633.07	12.10	626.29	12.74	625.65
W17	15.0	626.60	Civil Survey	3.62	622.98	8.04	618.56	15.14	611.46	15.85	610.75
W18	23.0	652.02	Note 2	NM	NM	24.15	627.87	25.30	626.72	DRY	DRY
W19	24.6	615.81	Note 2	7.88	607.93	15.30	600.51	19.27	596.54	19.77	596.04
W20	37.3	635.12	Note 2	27.55	607.57	31.95	603.17	35.27	599.85	37.25	597.87
W22	43.4	631.80	Note 2	NM	NM	21.58	610.22	23.93	607.87	24.41	607.39
W29	75.5	625.00	Note 3	5.77	619.23	DRY	DRY	DRY	DRY	DRY	DRY
W30	43.6	605.86	Note 2	7.68	598.18	8.58	597.28	9.92	595.94	10.60	595.26
W31	18.2	616.81	Note 2	10.73	606.08	14.85	601.96	19.01	597.80	DRY	DRY
W32	33.0	625.95	Note 2	2.95	623.00	4.89	621.06	8.25	617.70	9.20	616.75

TABLE 2.5.4-7  
Piezometer Construction Data  
*TVA Bellefonte GG&S Evaluations*

Well	Reported Well Depth (2)	Top of Casing Elevation (ft. MSL)	Source of TOC (ft. MSL)	2-Mar-05		4-May-05		28-Jul-05		21-Sep-05	
				Depth to Water (ft. below TOC)	Groundwater Elevation (ft. MSL)	Depth to Water (ft. below TOC)	Groundwater Elevation (ft. MSL)	Depth to Water (ft. below TOC)	Groundwater Elevation (ft. MSL)	Depth to Water (ft. below TOC)	Groundwater Elevation (ft. MSL)
W33	37.3	625.95	Civil Survey	5.71	620.24	7.71	618.24	10.84	615.11	DRY	DRY
W9	13.7	605.80	Note 2	2.40	603.40	6.61	599.19	10.60	595.20	11.93	593.87
WT1	150.6	605.82	Note 2	0.61	605.21	1.10	604.72	1.35	604.47	2.17	603.65
WT2	150.4	625.74	Note 2	11.30	614.44	13.00	612.74	13.63	612.11	14.32	611.42
WT3	150.4	608.19	Note 2	5.80	602.39	6.76	601.43	8.20	599.99	9.85	598.34
WT4	150.2	598.99	Note 2	2.10	596.89	3.16	595.83	3.95	595.04	4.41	594.58
WT5	150.4	623.80	Note 4	NM	NM	17.40	606.40	17.15	606.65	18.74	605.06
WT6	150.4	611.76	Note 2	8.60	603.16	10.28	601.48	12.81	598.95	14.50	597.26

Notes:

1. Civil Survey Data Provided by Mr. Hank Juilian/TVA.
  2. For all wells other than P-1 through P-4 and W29, well construction data provided by Mr. Hank Julian/TVA.
  3. Elevation estimated from USGS topographic map.
  4. Well is below pavement - measurements are made relative to pavement surface.
- NM = Not measured because well could not be found or accessed during monitoring event.

TABLE 2.5.4-8  
Groundwater Elevation Measurements  
TVA Bellefonte GG&S

Well	Reported Well Depth (2)	Top of Casing Elevation (ft. MSL)	Source of TOC (ft. MSL)	2-Mar-05		4-May-05		28-Jul-05	
				Depth to Water (ft. below TOC)	Groundwater Elevation (ft. MSL)	Depth to Water (ft. below TOC)	Groundwater Elevation (ft. MSL)	Depth to Water (ft. below TOC)	Groundwater Elevation (ft. MSL)
P1		606.70	Civil Survey	0.51	606.19	1.35	605.35	1.08	605.62
P2		620.91	Civil Survey	0.55	620.36	2.32	618.59	5.89	615.02
P3		604.41	Civil Survey	3.36	601.05	4.88	599.53	5.50	598.91
P4		628.95	Civil Survey	5.00	623.95	8.00	620.95	13.32	615.63
W10	11.6	603.20	Note 2	4.60	598.60	6.92	596.28	8.40	594.80
W12	34.3	622.95	Note 2	12.75	610.20	19.35	603.60	25.51	597.44
W14	40.9	659.05	Note 2	23.81	635.24	DRY	<618.15	DRY	DRY
W15	20.4	648.68	Note 2	12.90	635.78	NM		DRY	DRY
W16	28.4	638.39	Note 2	3.50	634.89	5.32	633.07	12.10	626.29
W17	15.0	626.60	Civil Survey	3.62	622.98	8.04	618.56	15.14	611.46
W18	23.0	652.02	Note 2	NM	NM	24.15	627.87	25.30	626.72
W19	24.6	615.81	Note 2	7.88	607.93	15.30	600.51	19.27	596.54
W20	37.3	635.12	Note 2	27.55	607.57	31.95	603.17	35.27	599.85
W22	43.4	631.80	Note 2	NM	NM	21.58	610.22	23.93	607.87
W23	14.9	636.50	Note 2	9.38	627.12	9.96	626.54	10.25	626.25
W24	14.3	642.28	Note 2	1.76	640.52	2.77	639.51	3.78	638.50
W25	9.8	628.32	Note 2	NM	<618.52	DRY	<618.52	DRY	DRY
W26	13.8	628.13	Note 2	NM	<614.33	DRY	<614.33	DRY	DRY

TABLE 2.5.4-8  
Groundwater Elevation Measurements  
TVA Bellefonte GG&S

Well	Reported Well Depth (2)	Top of Casing Elevation (ft. MSL)	Source of TOC (ft. MSL)	2-Mar-05		4-May-05		28-Jul-05	
				Depth to Water (ft. below TOC)	Groundwater Elevation (ft. MSL)	Depth to Water (ft. below TOC)	Groundwater Elevation (ft. MSL)	Depth to Water (ft. below TOC)	Groundwater Elevation (ft. MSL)
W27	15.0	629.38	Note 2	6.80	622.58	7.01	622.37	7.75	621.63
W28	15.0	632.24	Note 2	6.72	625.52	9.72	622.52	11.15	621.09
W29	75.5	625.00	Note 2	5.77	619.23	DRY	<549.50	DRY	DRY
W30	43.6	605.86	Note 2	7.68	598.18	8.58	597.28	9.92	595.94
W31	18.2	616.81	Note 2	10.73	606.08	14.85	601.96	19.01	597.80
W32	33.0	625.95	Note 2	2.95	623.00	4.89	621.06	8.25	617.70
W33	37.3	625.95	Civil Survey	5.71	620.24	7.71	618.24	10.84	615.11
W9	13.7	605.80	Note 2	2.40	603.40	6.61	599.19	10.60	595.20
WT1	150.6	605.82	Note 2	0.61	605.21	1.10	604.72	1.35	604.47
WT2	150.4	625.74	Note 2	11.30	614.44	13.00	612.74	13.63	612.11
WT3	150.4	608.19	Note 2	5.80	602.39	6.76	601.43	8.20	599.99
WT4	150.2	598.99	Note 2	2.10	596.89	3.16	595.83	3.95	595.04
WT5	150.4	623.80	Note 2	NM	NM	17.40	606.40	17.15	606.65
WT6	150.4	611.76	Note 2	8.60	603.16	10.28	601.48	12.81	598.95

Notes:  
Civil Survey Data Provided by TVA.  
For all wells other than P-1 through P-4, well construction data provided by TVA.  
NM = Not measured because well could not be found or accessed during monitoring event.

TABLE 2.5.4-9  
Summary of Bedrock S-wave and P-wave Velocity from Field Tests – Bellefonte and BLNP Sites  
*TVA Bellefonte GG&S Evaluations*

Boring ID	Top Elevation (ft amsl) <sup>1</sup>	Bottom Elevation (ft amsl)	Average <sup>2</sup> S-wave Velocity (ft/sec)	Average <sup>2</sup> P-wave Velocity (ft/sec)	Poisson's Ratio
<b>Bellefonte Site Boreholes <sup>3</sup></b>					
B-1	604.4	510.9	10065	19166	0.31
B-2	564.0	519.7	9996	18078	0.28
B-6	607.9	547.2	9012	16853	0.30
<b>BNP Site Boreholes <sup>4</sup></b>					
R+22-50+78	610.6	476.6	10652	20675	0.32 <sup>5</sup>
T-50+00	611.4	511.9	10860	22376	0.32 <sup>5</sup>
<b>BNP Cross-Hole Tests <sup>6</sup></b>					
Average	600 to 615	525 to 535	9227	17584	N/A

Notes:

<sup>1</sup> amsl = above mean sea level.

<sup>2</sup> Average values listed are for fresh bedrock, starting below the zone of significant weathering near the top of bedrock.

<sup>3</sup> For the Bellefonte Site boreholes, data are from the suspension logging tests performed by GeoVision (see Appendix D).

<sup>4</sup> For the BLNP Site Boreholes, data are from borehole velocity tests performed by the Birdwell Division of Honeywell, as reported in Figures 2.5-161 and 2.5-189 of the BNP FSAR (TVA, 1986).

<sup>5</sup> Poisson's Ratio was assumed for these tests.

<sup>6</sup> Cross-hole surveys were performed in deep bedrock between two pairs of boreholes at the BNP Site, as summarized in Figure 2.5-196 of the BNP FSAR (TVA, 1986). The pairs consisted of Boreholes Q+47-47+88 to R-49+00, and R+22-50+78 to S-50+00. Results listed are the averages for both pairs over the listed depths.

**TABLE 2.5.4-10**  
Results of Hydraulic Conductivity from Slug Tests at GG&S Site Piezometers  
*TVA Bellefonte GG&S Evaluations*

Piezometer	Hydraulic Conductivity, $K_h$ (cm/second)				
	Test Number			Summary	
	Test 1	Test 2	Test 3	Minimum	Maximum
P-1	5.0E-06	---	---	5.0E-06	5.0E-06
P-2	7.4E-04	8.0E-04	8.2E-04	7.4E-04	8.2E-04
P-3	2.8E-04	3.3E-04	2.6E-04	2.6E-04	3.3E-04
P-4	7.0E-04	7.0E-04	6.2E-04	6.2E-04	7.0E-04
Overall				5.0E-06	8.2E-04

Average  $K_h$  of GG&S Site piezometer slug tests: 5.3E-04 cm/second.

Average  $K_h$  from previous drawdown tests in BNP area: 4.0E-04 cm/second.

Notes:

--- = only one test performed at this location.



fig2.5.4-1a Borehole Piezometer Locations.mxd

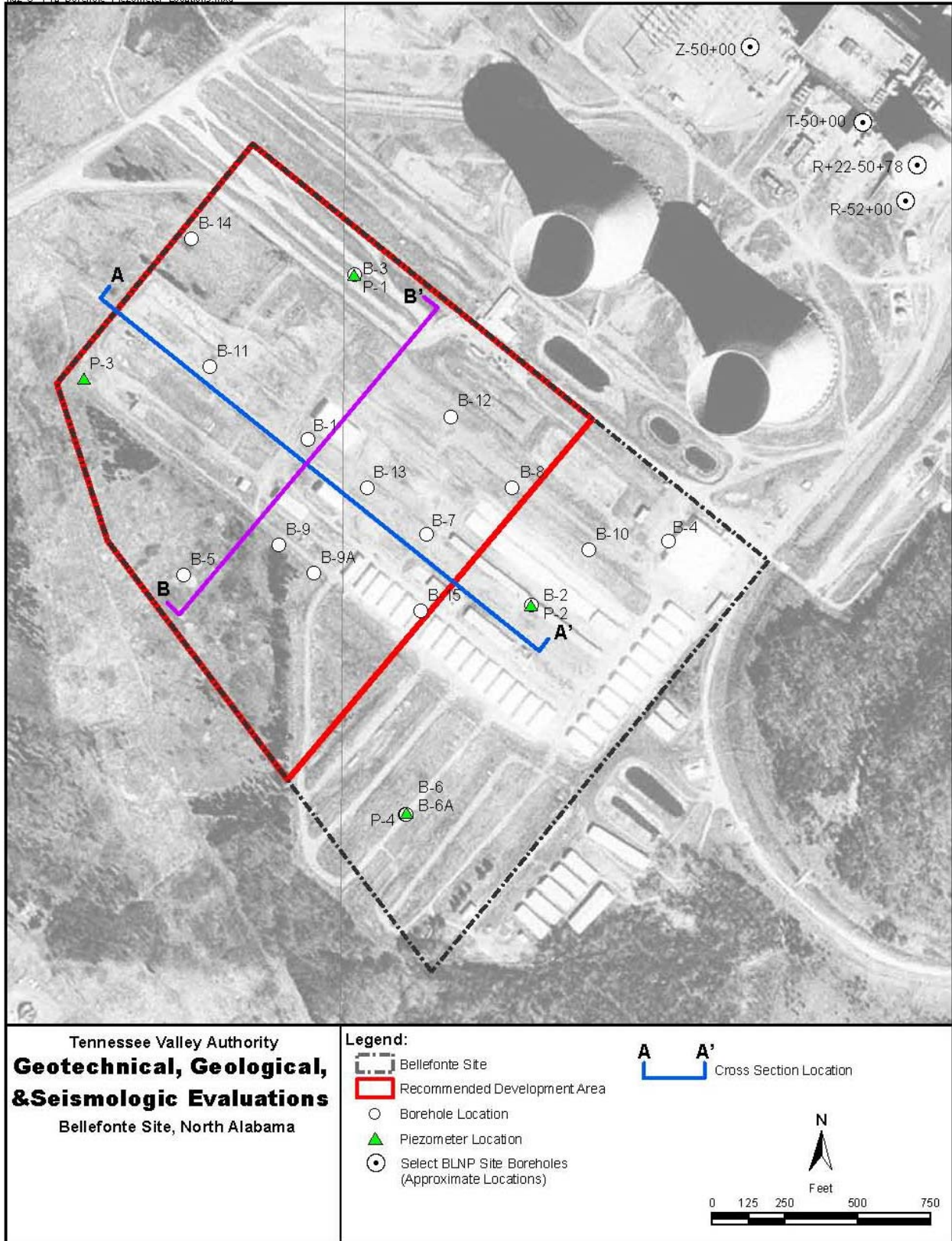


Figure 2.5.4-1(a). Borehole and Piezometer Locations

fig2\_5\_4-1b\_Borehole\_CPT\_Locations.mxd

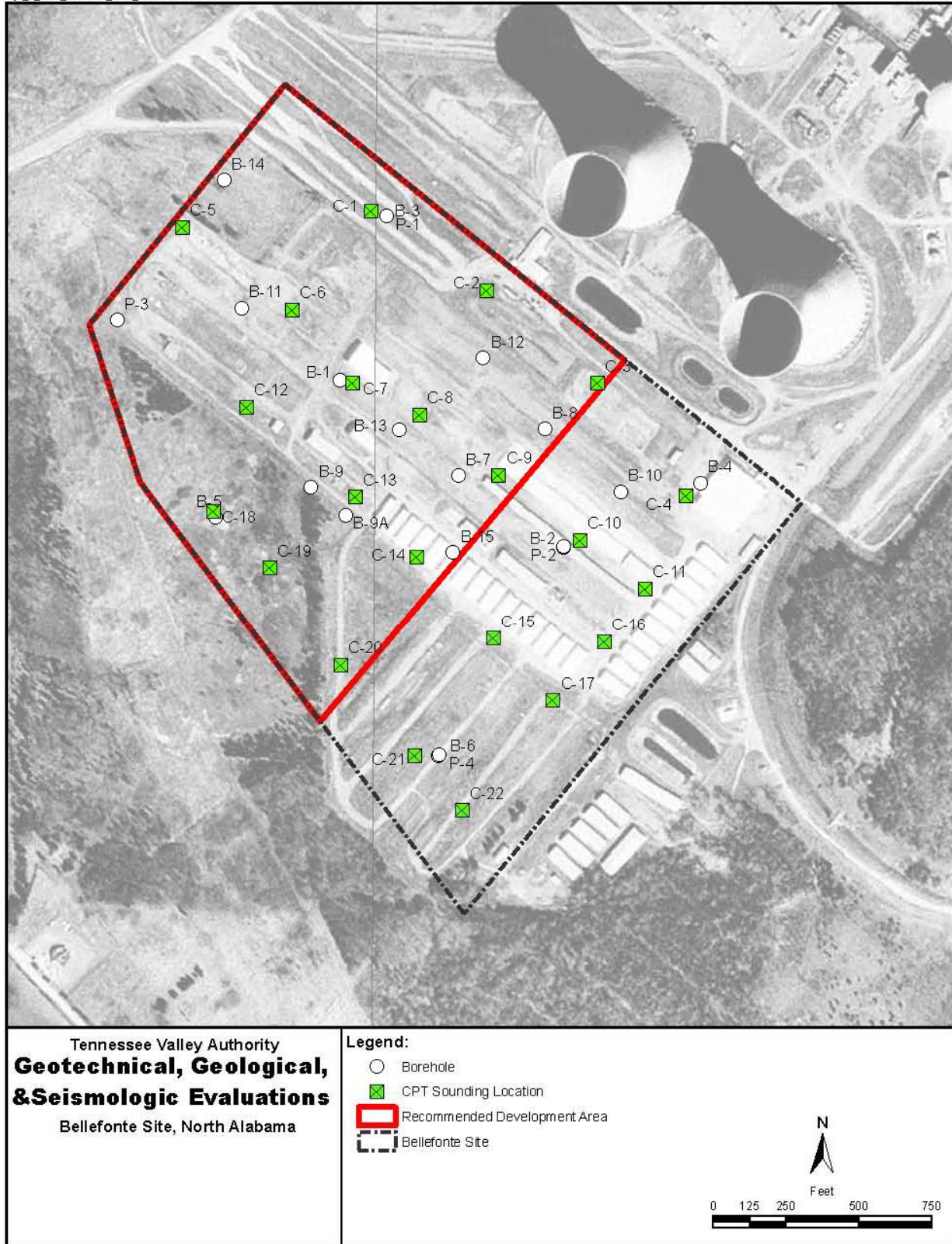


Figure 2.5.4-1(b). CPT Sounding Locations

fig2\_5\_4-1c\_seismic\_refraction\_lines.mxd

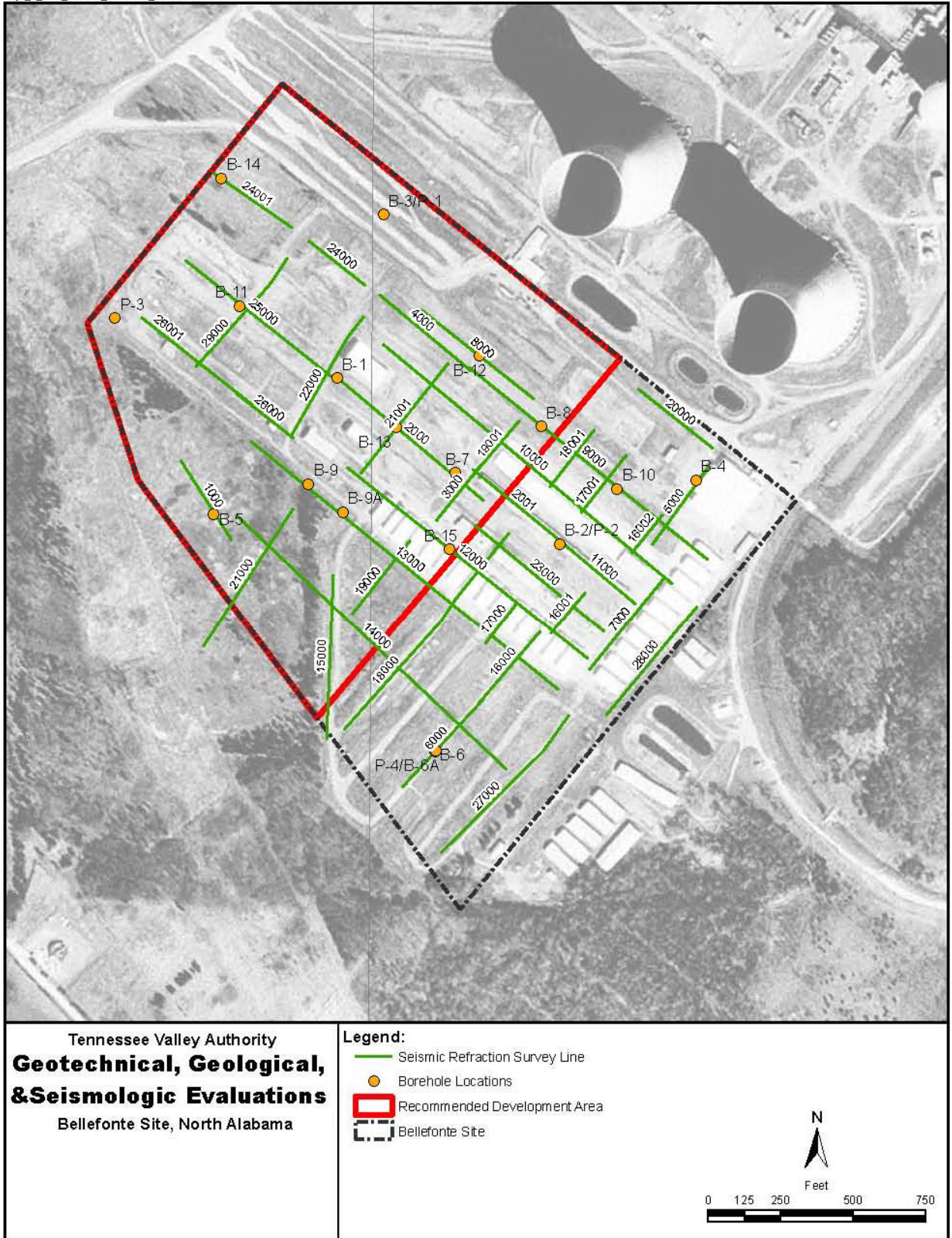
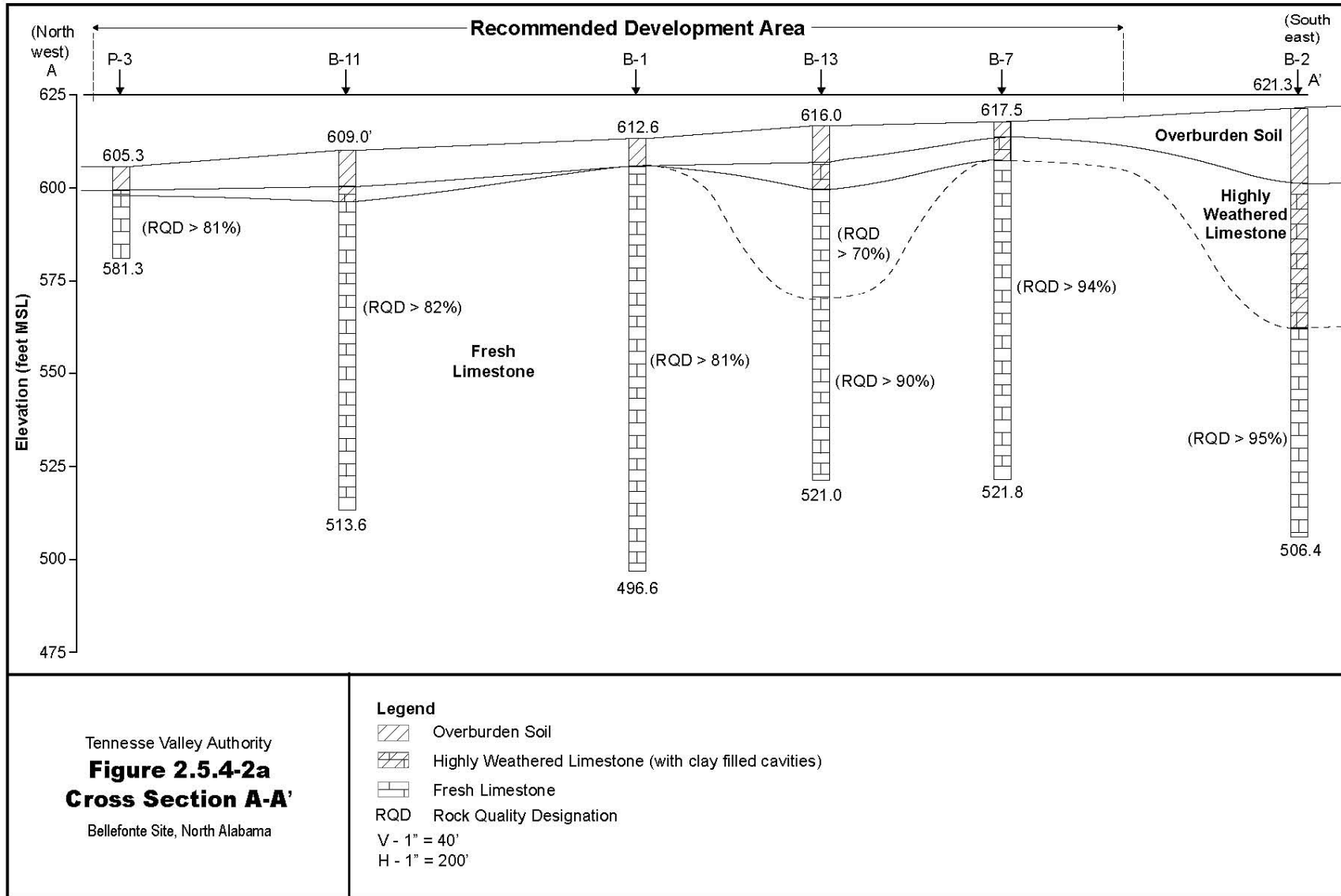
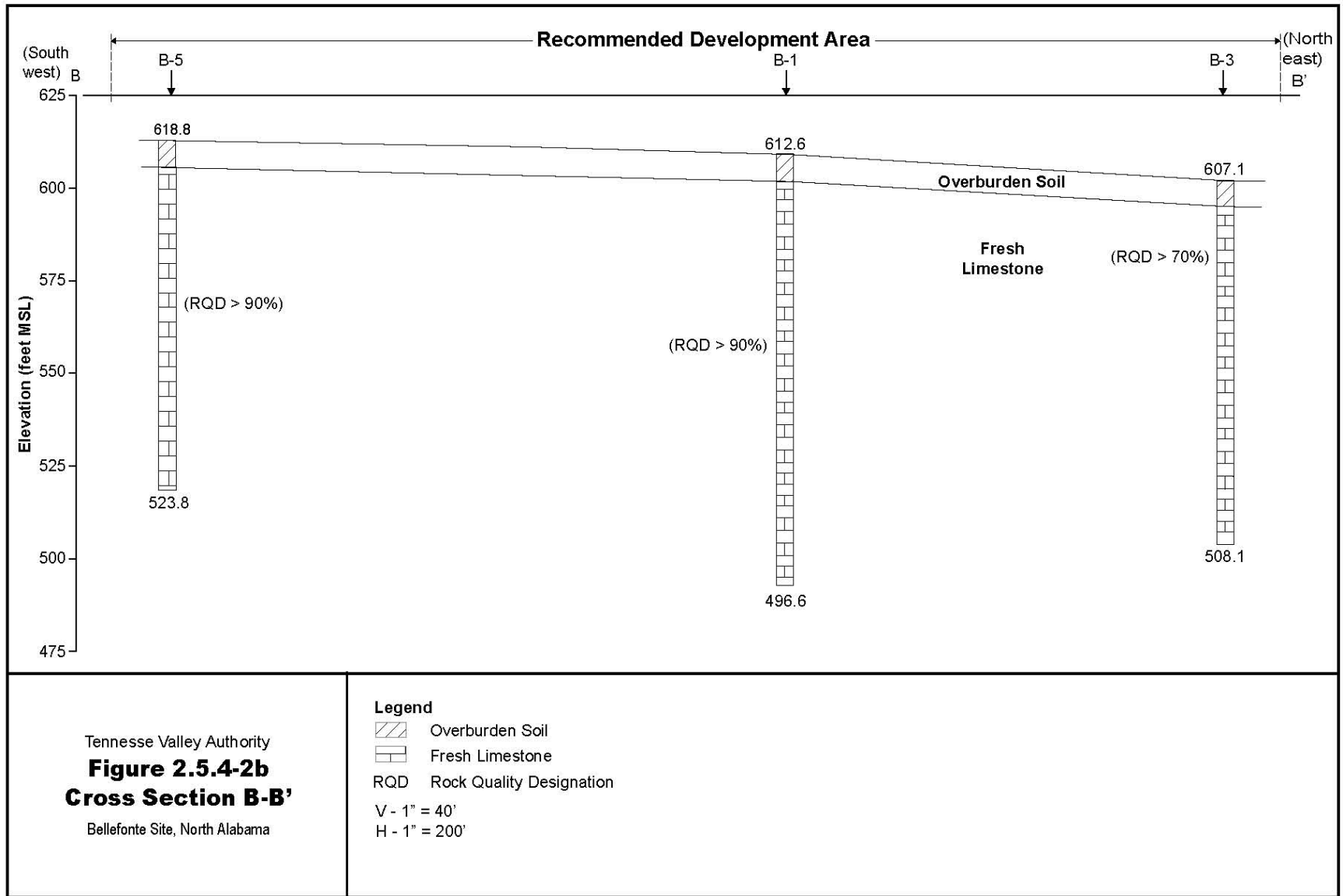


Figure 2.5.4-1(c). Seismic Refraction Survey Line Locations



E082005024MKE 32.403.01.0.G Cross Section A-A' 8-30-05 jsh/mke

**Figure 2.5.4-2(a). Cross-section A-A'**



E:\082005024MKE 32.403.01.0.G BS\_Figure 5.2b\_v4.ai 8-30-05 jls/mke

**Figure 2.5.4-2(b). Cross-section B-B'**

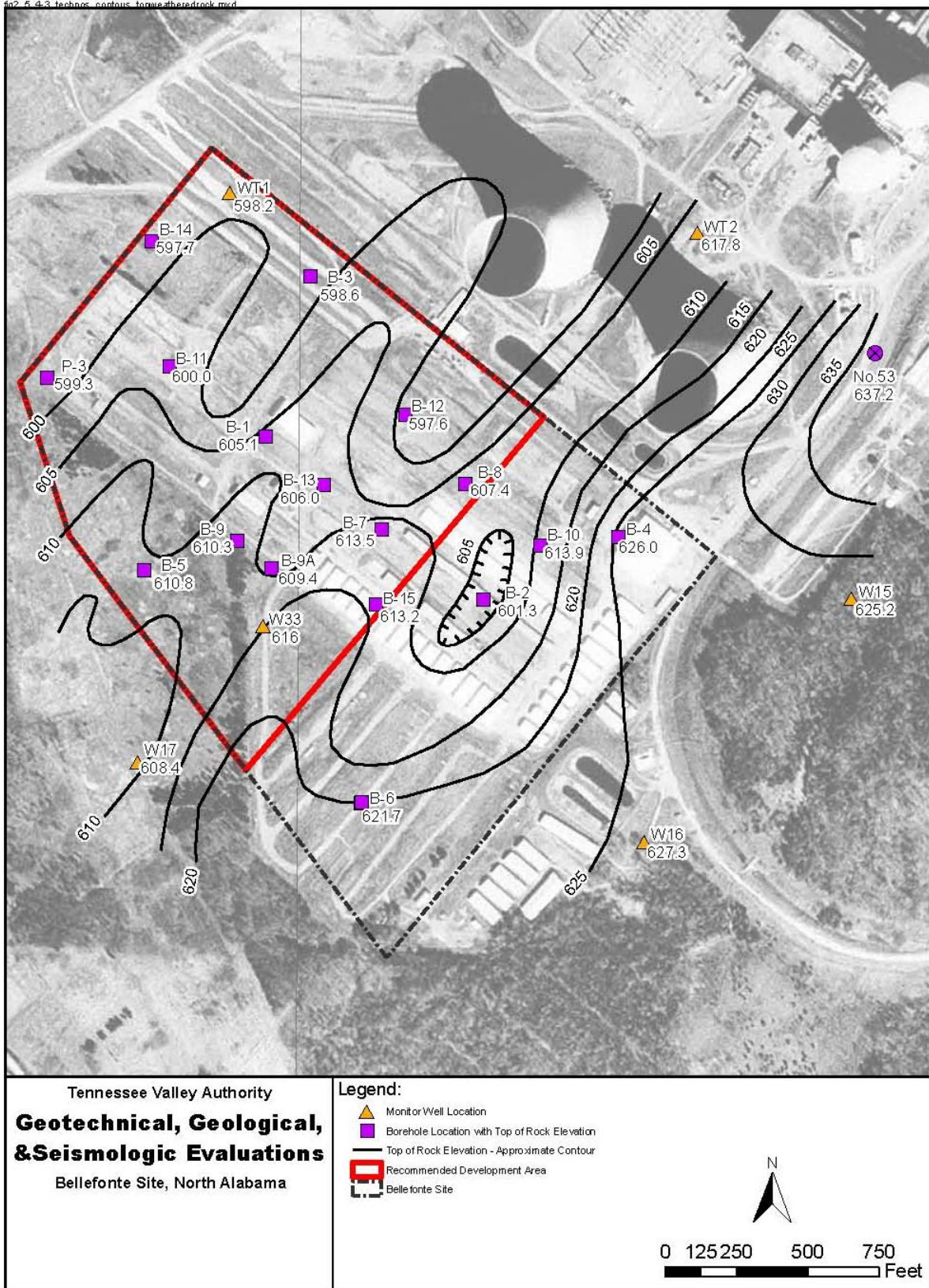


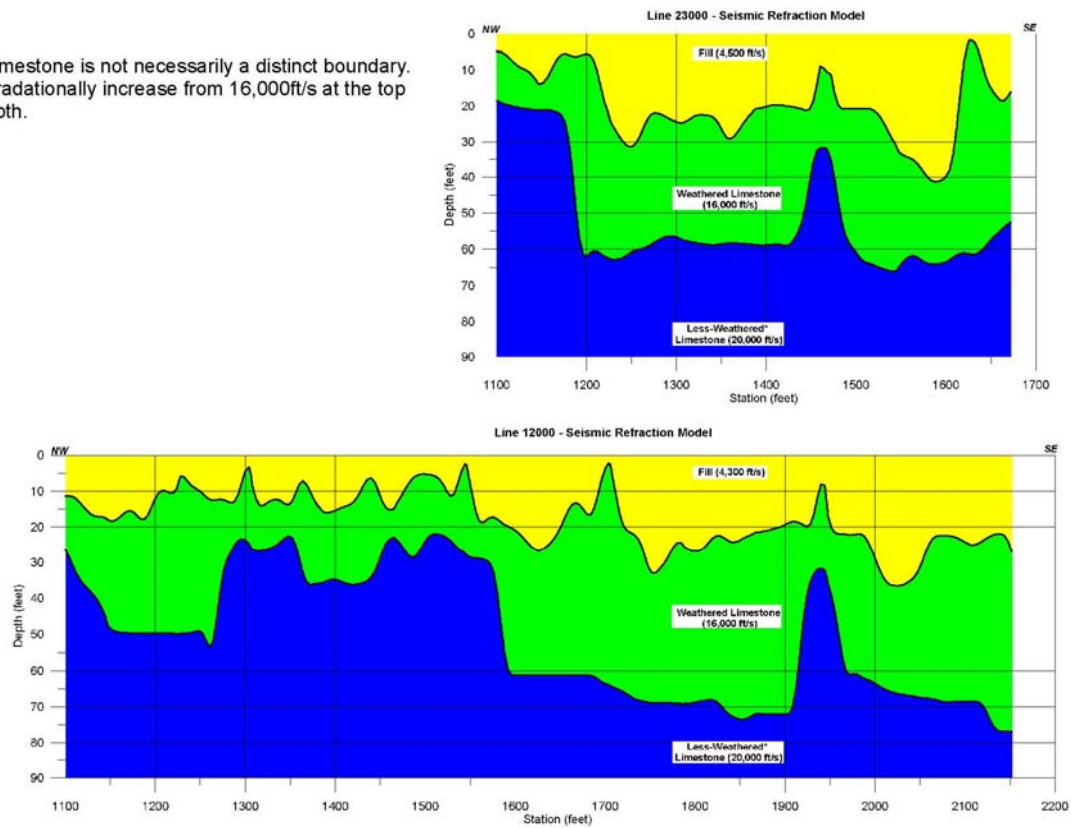
Figure 2.5.4-3. Top of Bedrock Elevations



fig2\_5\_4-5a\_line12000\_23000.mxd

4x vertical exaggeration

\* Interpreted less-weathered limestone is not necessarily a distinct boundary. P-wave velocity values may gradually increase from 16,000ft/s at the top of rock to 20,000ft/s at this depth.



Tennessee Valley Authority  
**Geotechnical, Geological,  
& Seismologic Evaluations**  
Bellefonte Site, North Alabama



Legend:  
 Recommended Development Area  
 Bellefonte Site



Figure 2.5.4-5(a). P-Wave Velocity Model Profiles - Lines 12000 and 23000



fg2\_5\_4-5b\_line2001.mxd

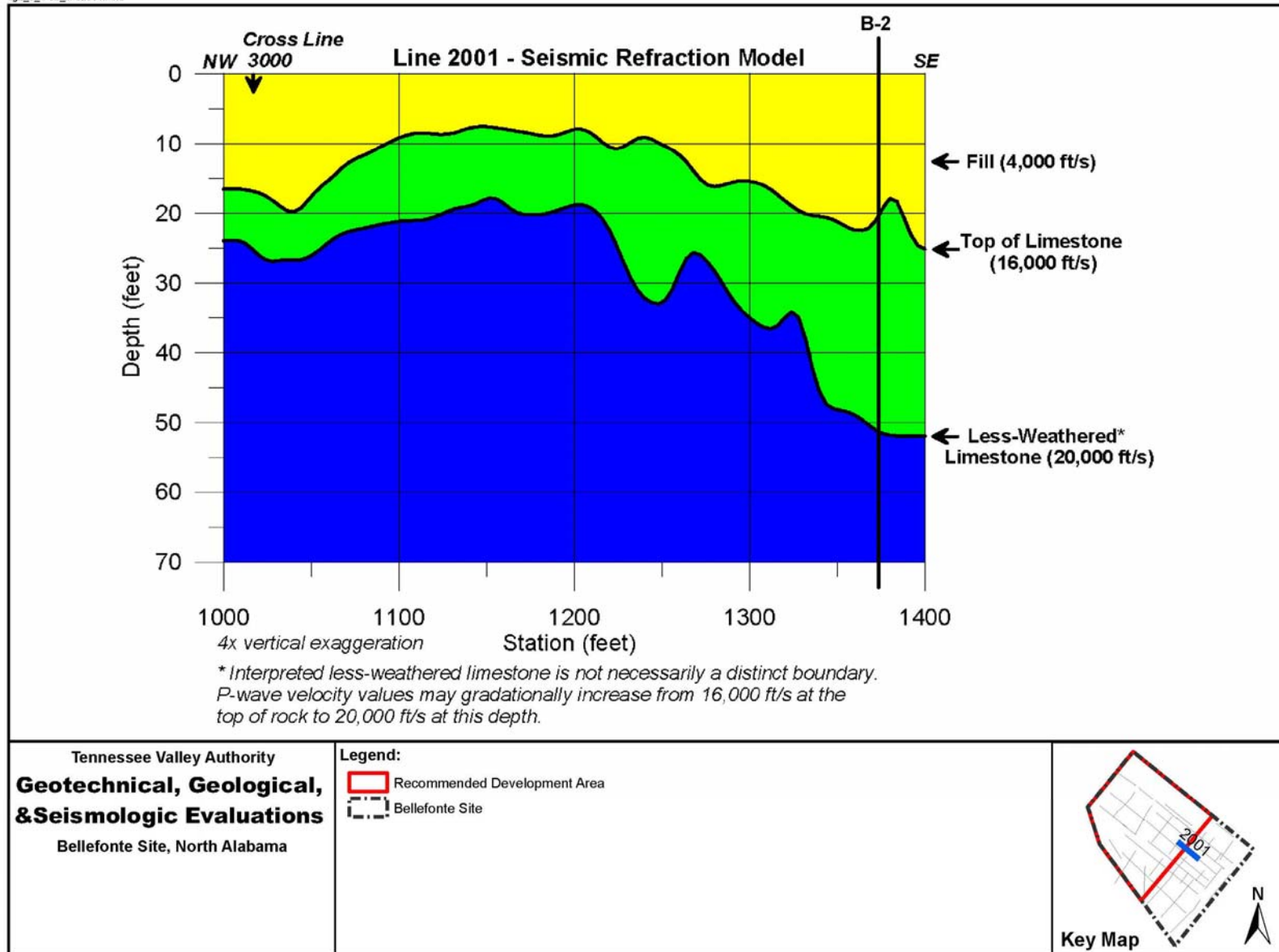


Figure 2.5.4-5(b). P-Wave Velocity Model Profile - Line 2001

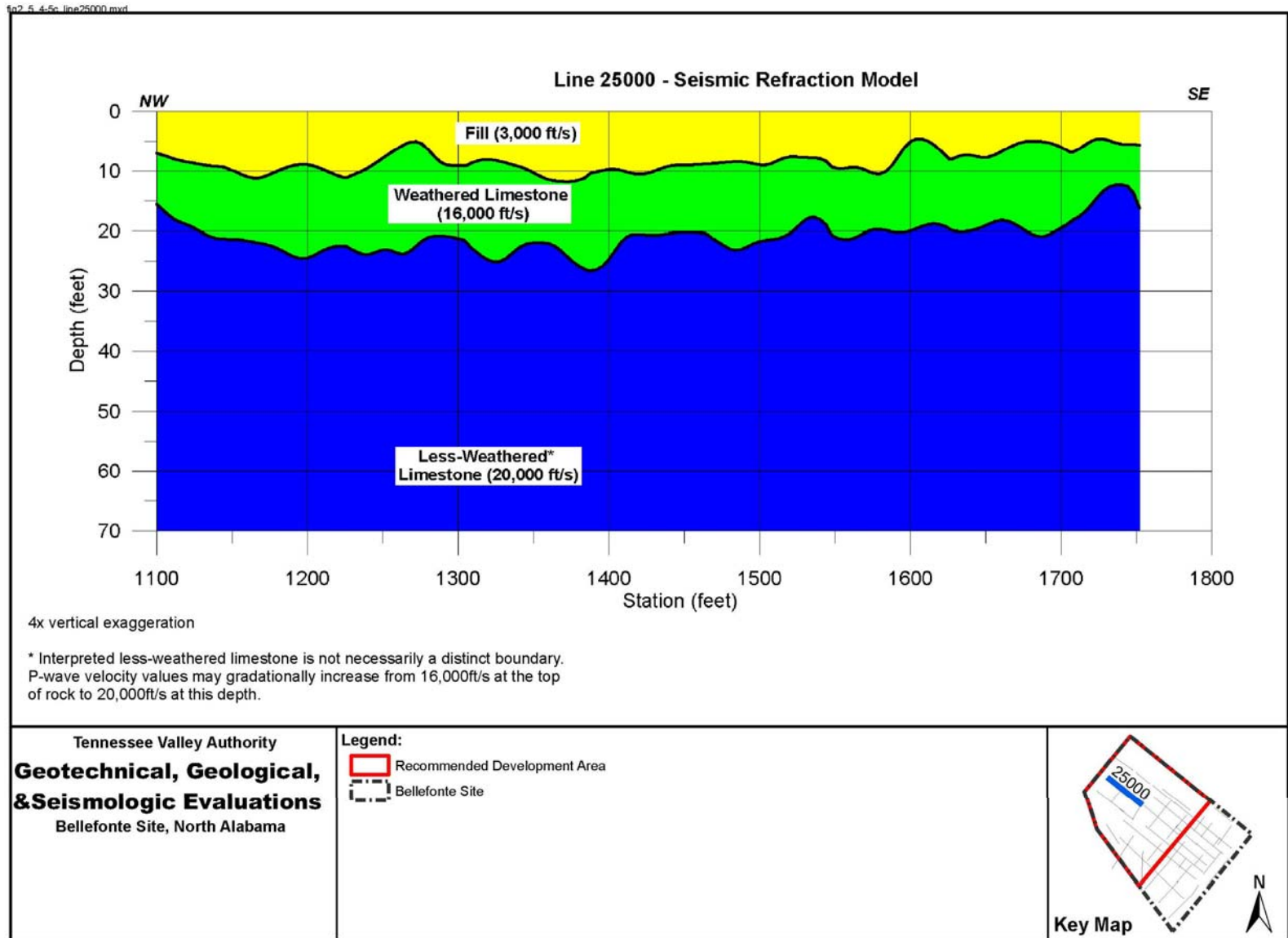


Figure 2.5.4-5(c). P-Wave Velocity Model Profile - Line 25000

fig2\_5\_4-5d\_line9000\_17001.mxd

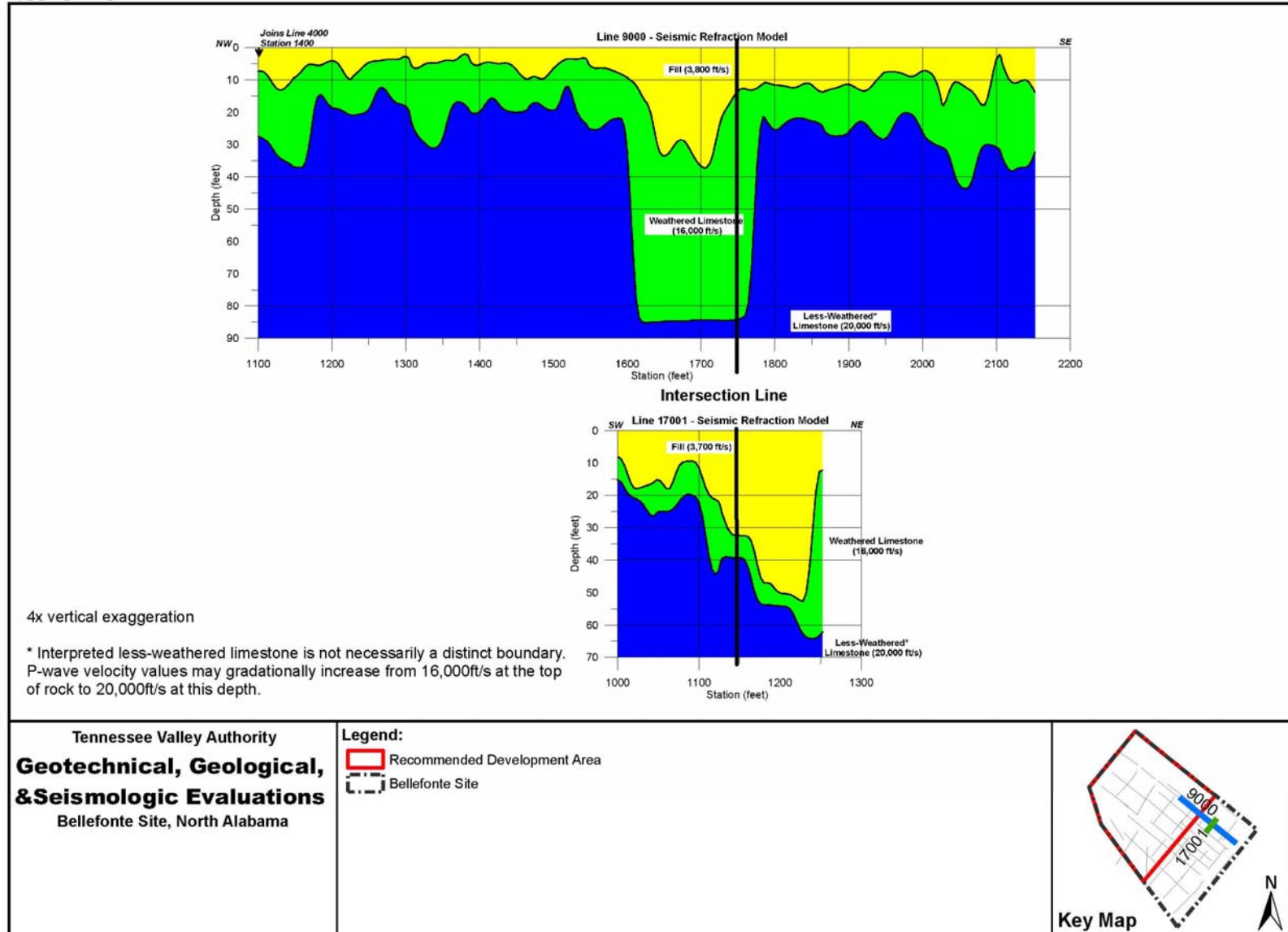


Figure 2.5.4-5(d). P-Wave Velocity Model Profiles - Lines 9000 and 17001

fig2.5.4-6a\_top\_weathered\_rock.mxd

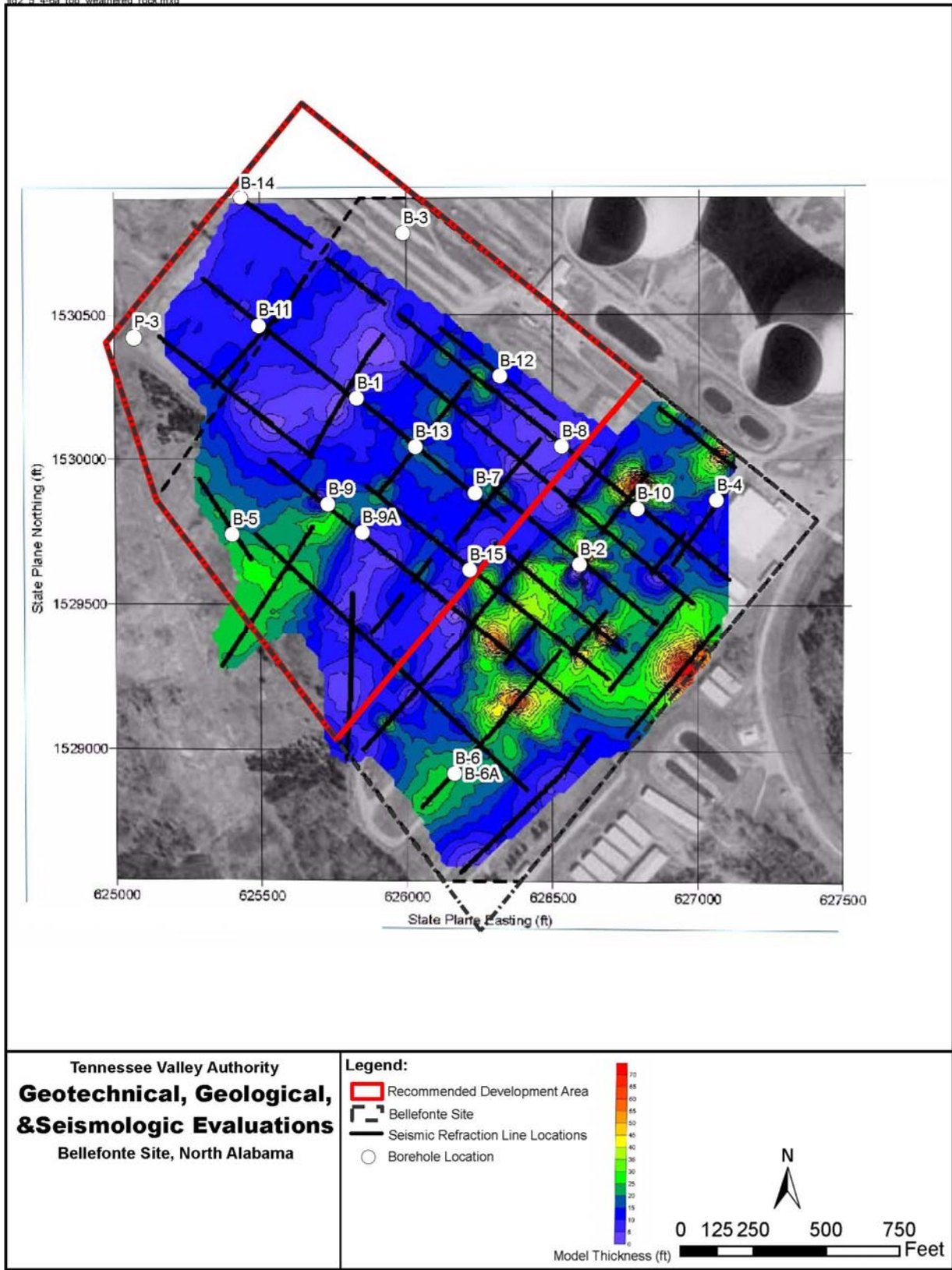


Figure 2.5.4-6(a). Top of L2 Layer - P-Wave Velocity Model

fig2.5.4-6b\_top\_less-weathered\_rock.mxd

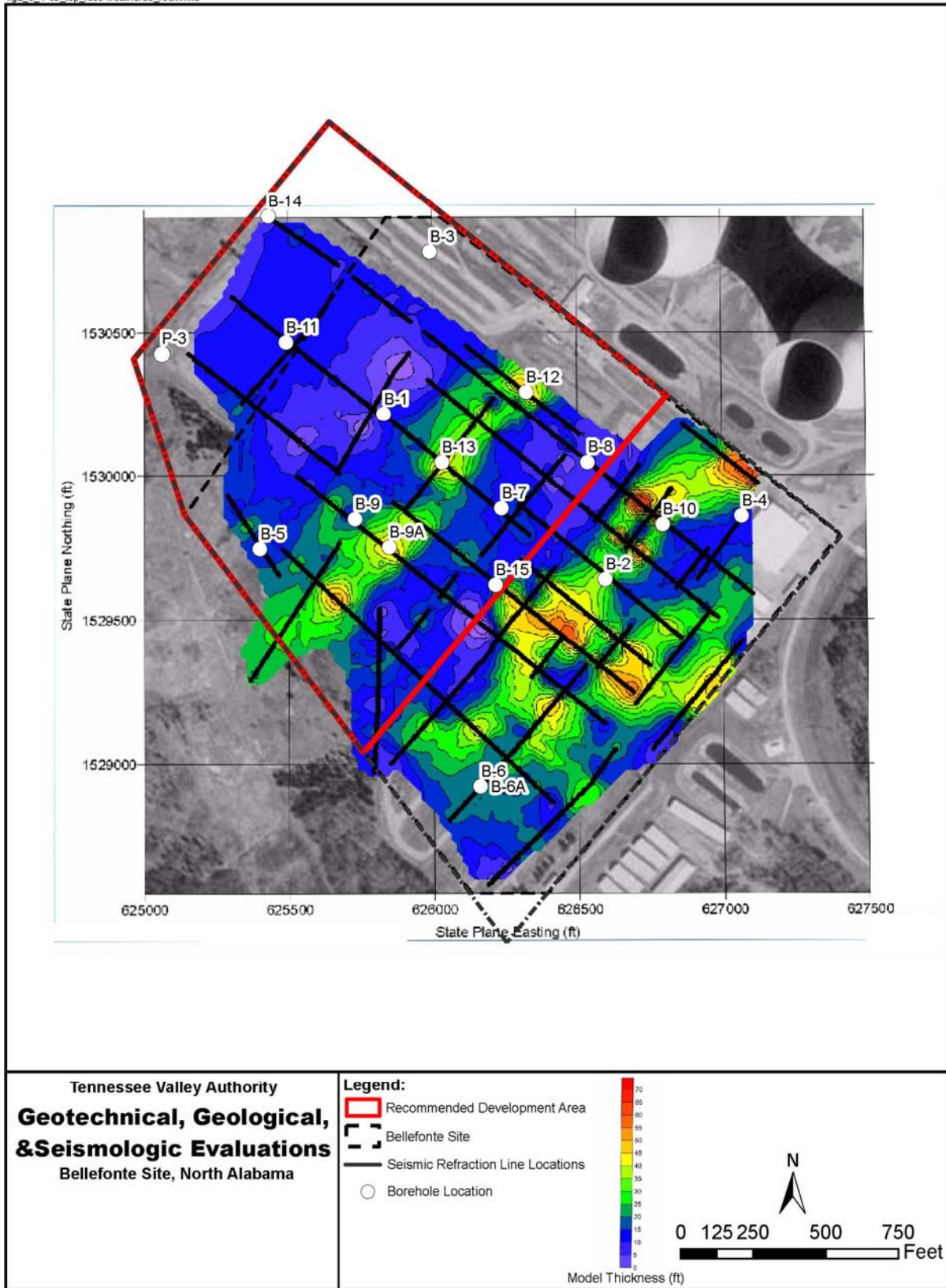


Figure 2.5.4-6(b). Top of L3 Layer - P-Wave Velocity Model

fig2\_5\_4-6c\_thickness\_weathered\_rock.mxd

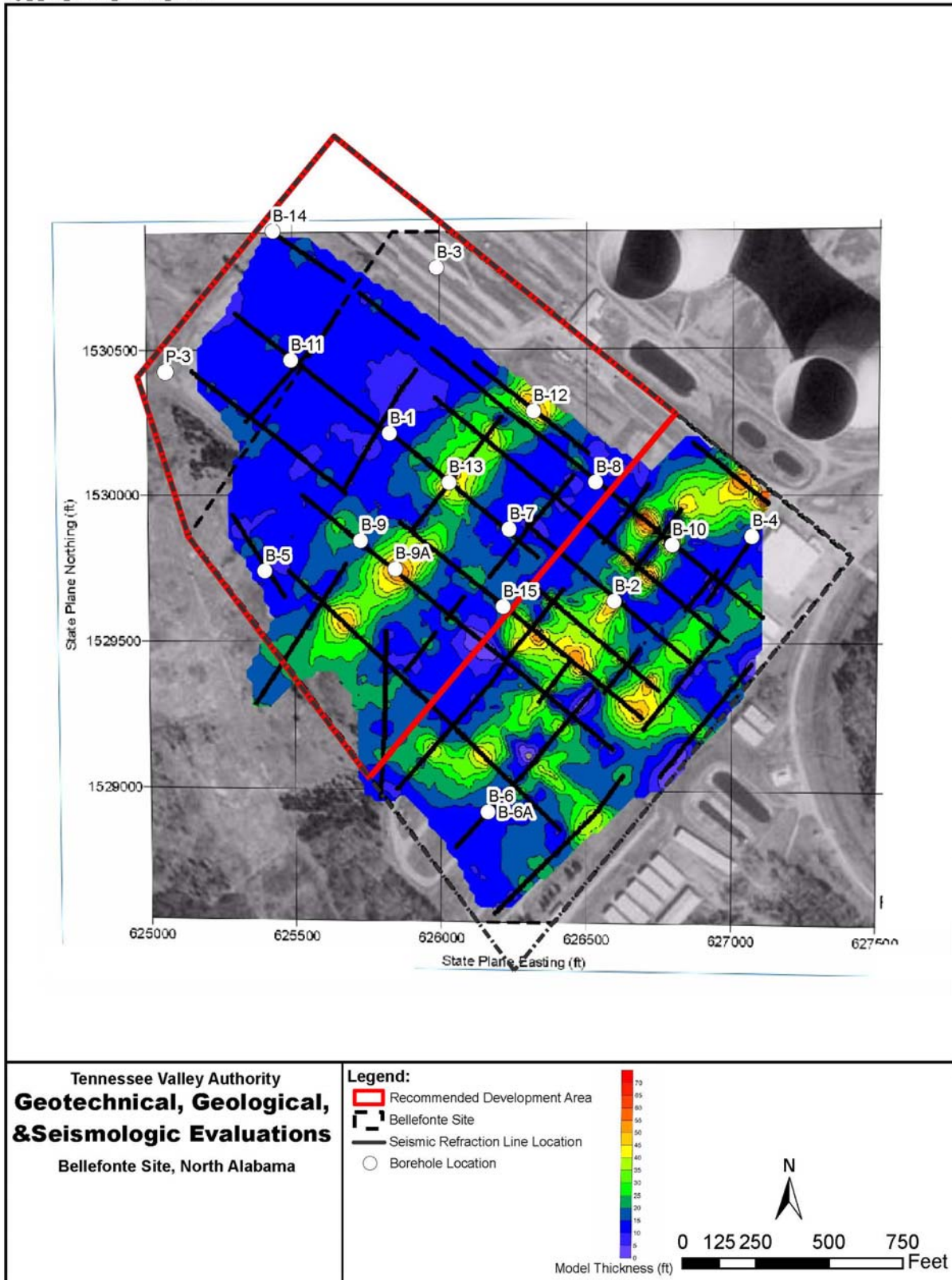


Figure 2.5.4-6(c). Thickness of L2 Layer - P-Wave Velocity Model

fig2\_5\_4-7\_Bedrock\_Swave\_velocity\_depth.mxd

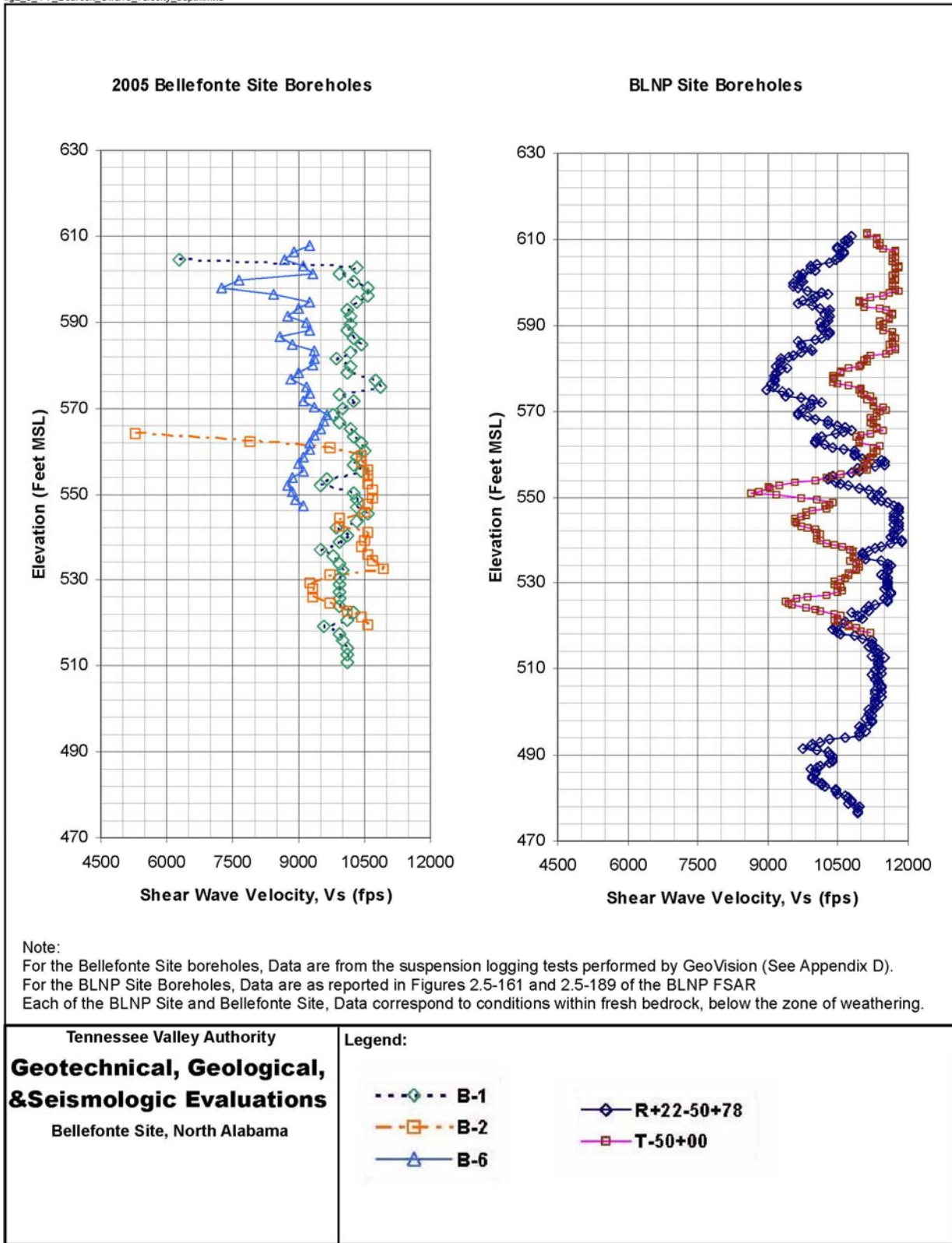


Figure 2.5.4-7. Bedrock S-Wave Velocity with Depth - Bellefonte and BLNP Site Boreholes

fig2\_5\_4-8a.mxd

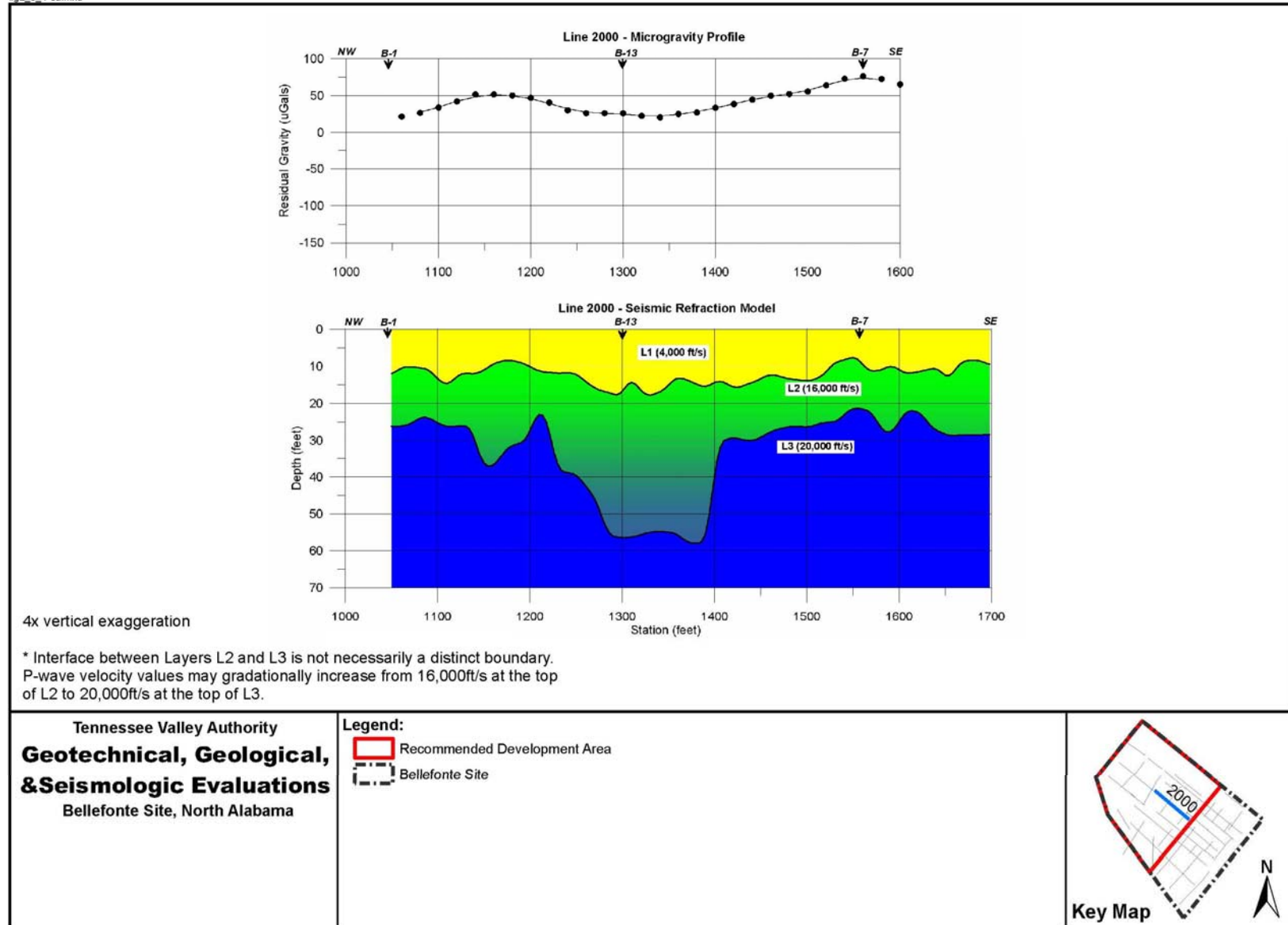


Figure 2.5.4-8(a). Microgravity and Seismic Refraction Model Profile - Line 2000



fig2\_5\_4-8b.mxd

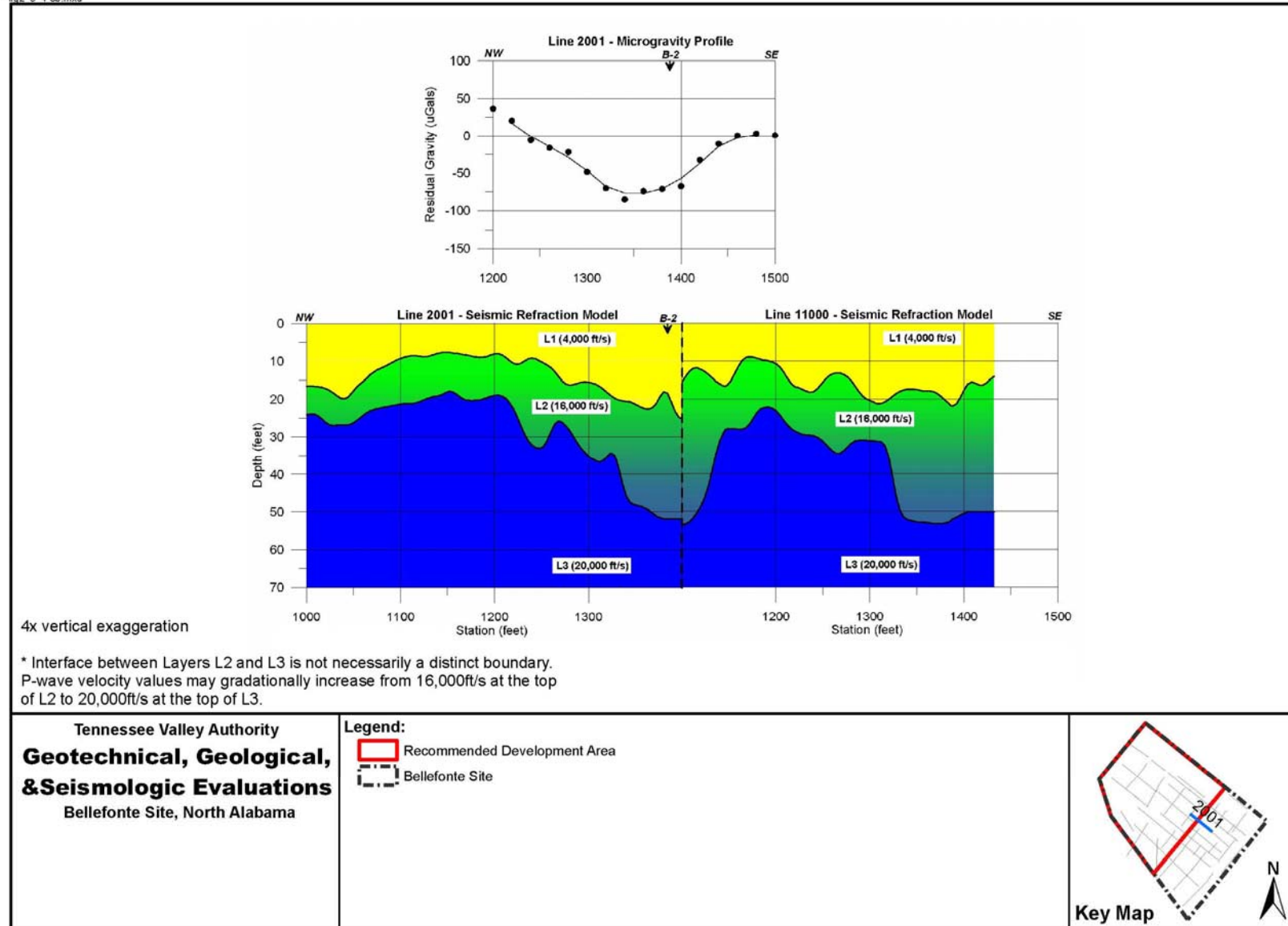


Figure 2.5.4-8(b). Microgravity and Seismic Refraction Model Profile - Line 2001

fig2\_5\_4-8c.mxd

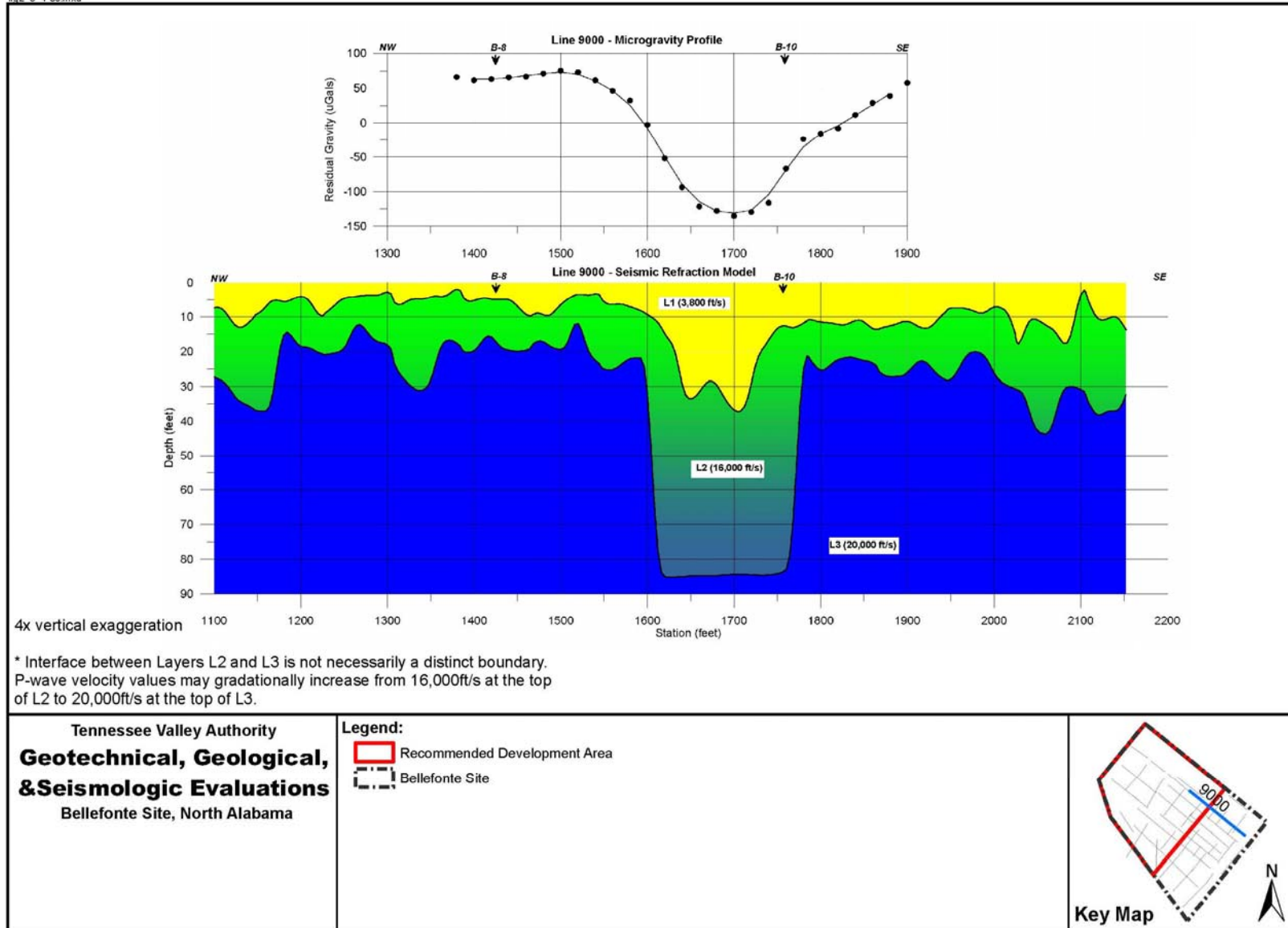


Figure 2.5.4-8(c). Microgravity and Seismic Refraction Model Profile - Line 9000

fig2\_5\_4-8d.mxd

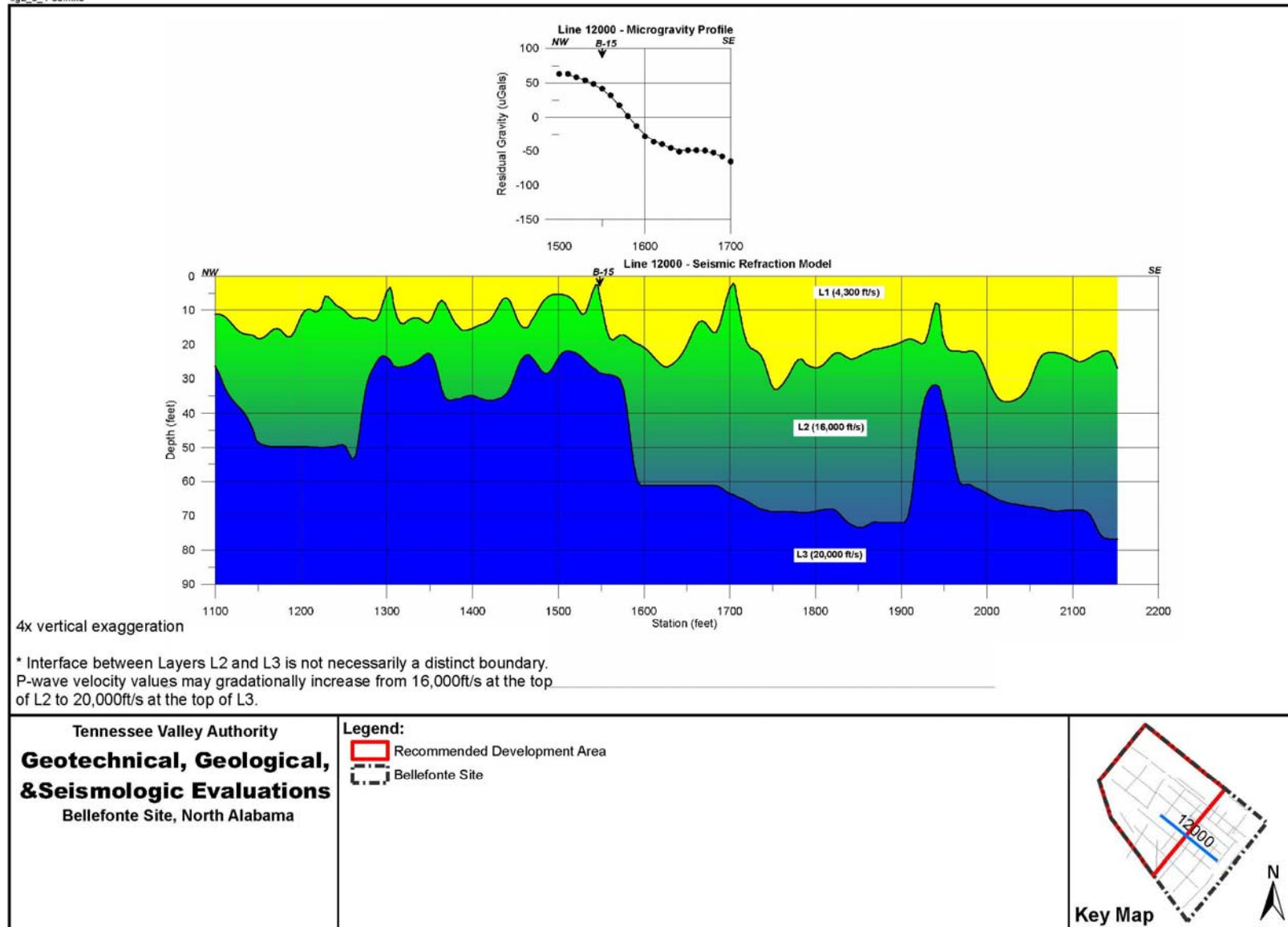


Figure 2.5.4-8(d). Microgravity and Seismic Refraction Model Profile - Line 12000

fig2\_5\_4-8e.mxd

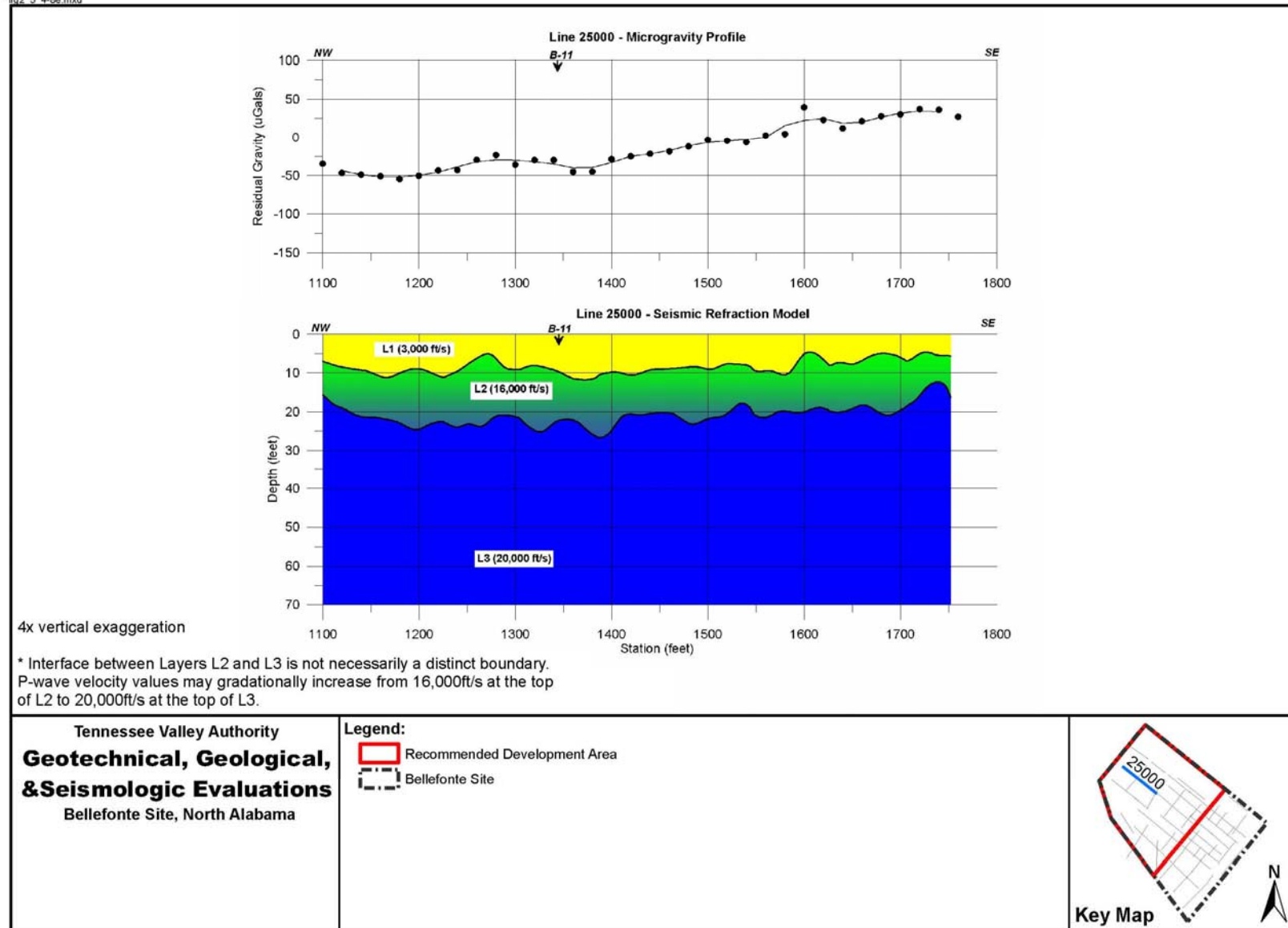


Figure 2.5.4-8(e). Microgravity and Seismic Refraction Model Profile - Line 25000

fig2.5\_4-9a\_March\_Potentiometric.mxd

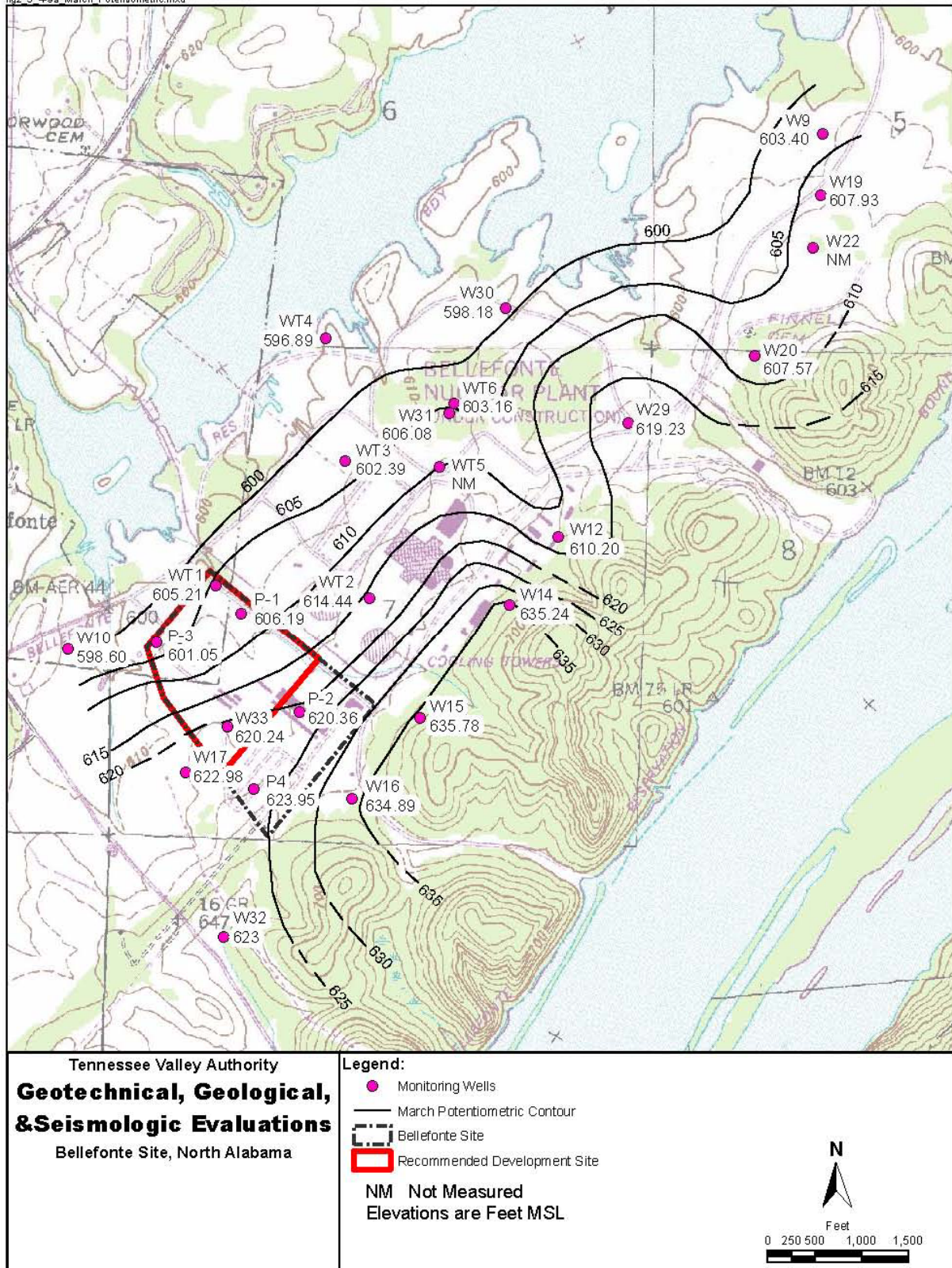


Figure 2.5.4-9(a). Potentiometric Surface Map - March 2, 2005

fig2\_5\_4-9b\_May\_Potentiometric.mxd

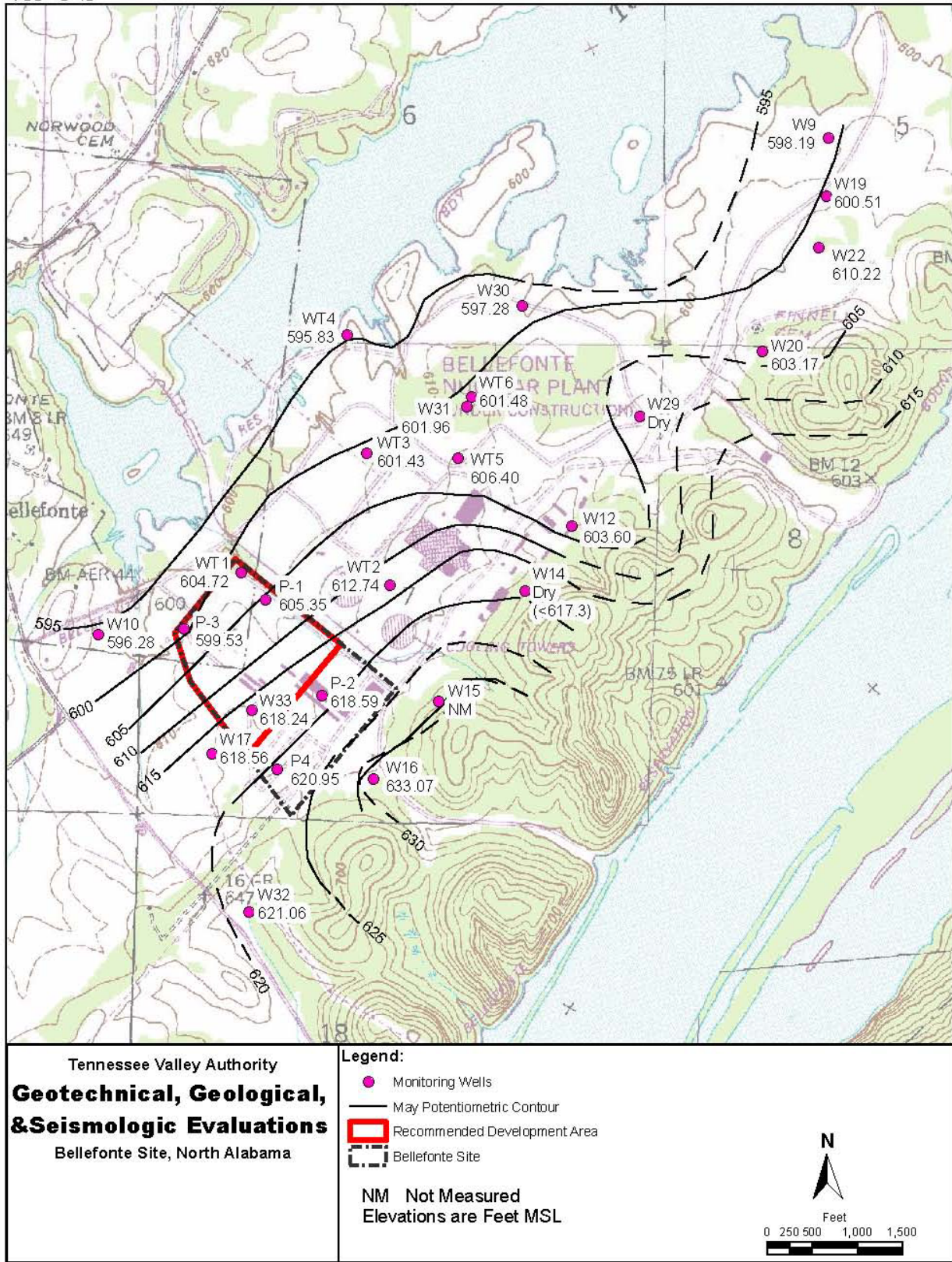


Figure 2.5.4-9(b). Potentiometric Surface Map - May 4, 2005

fig2\_5\_4-9c\_July\_Potentiometric.mxd

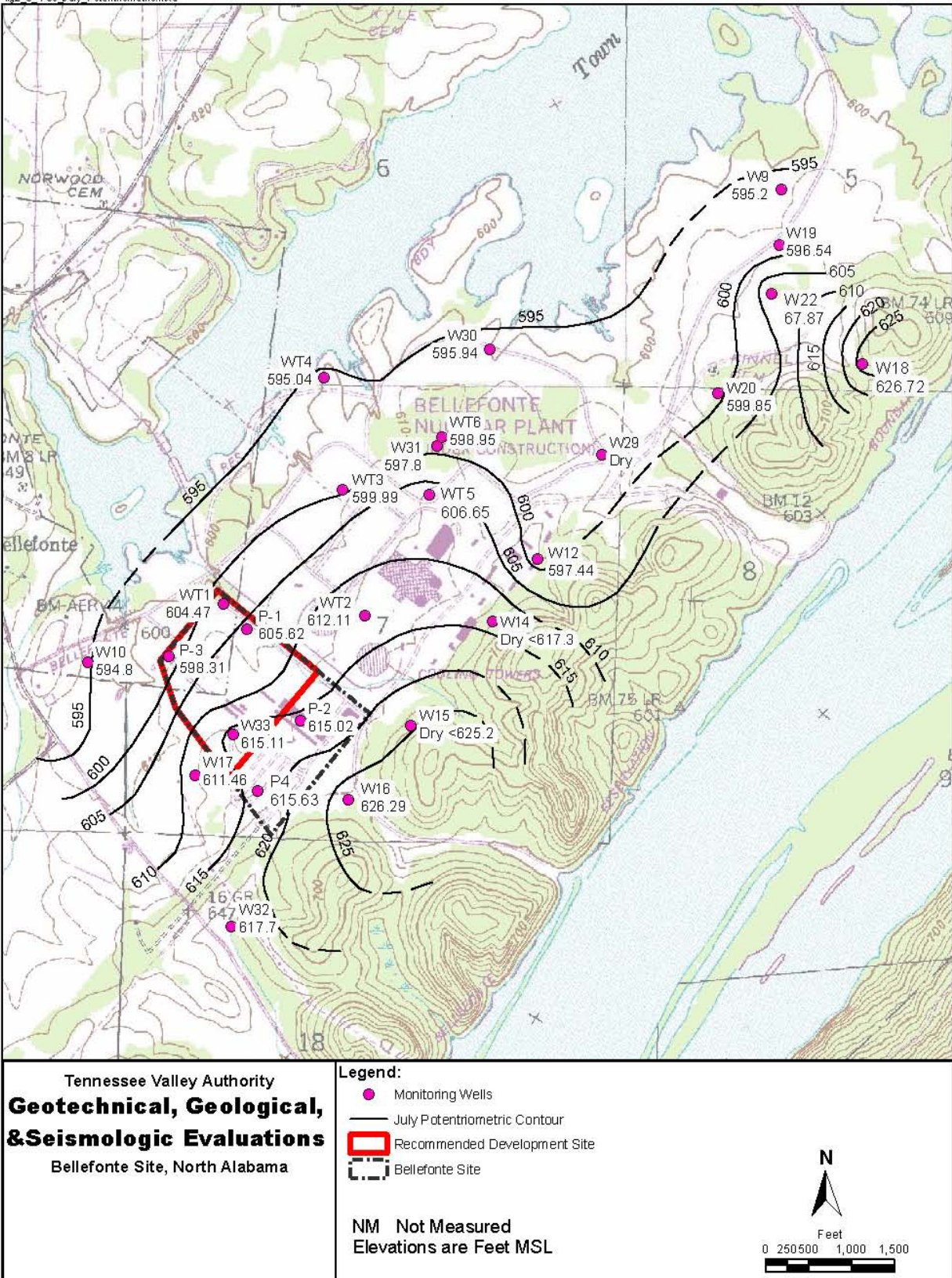


Figure 2.5.4-9(c). Potentiometric Surface Map - July 8, 2005

fig2.5.4-9d\_Sept\_Potentiometric.mxd

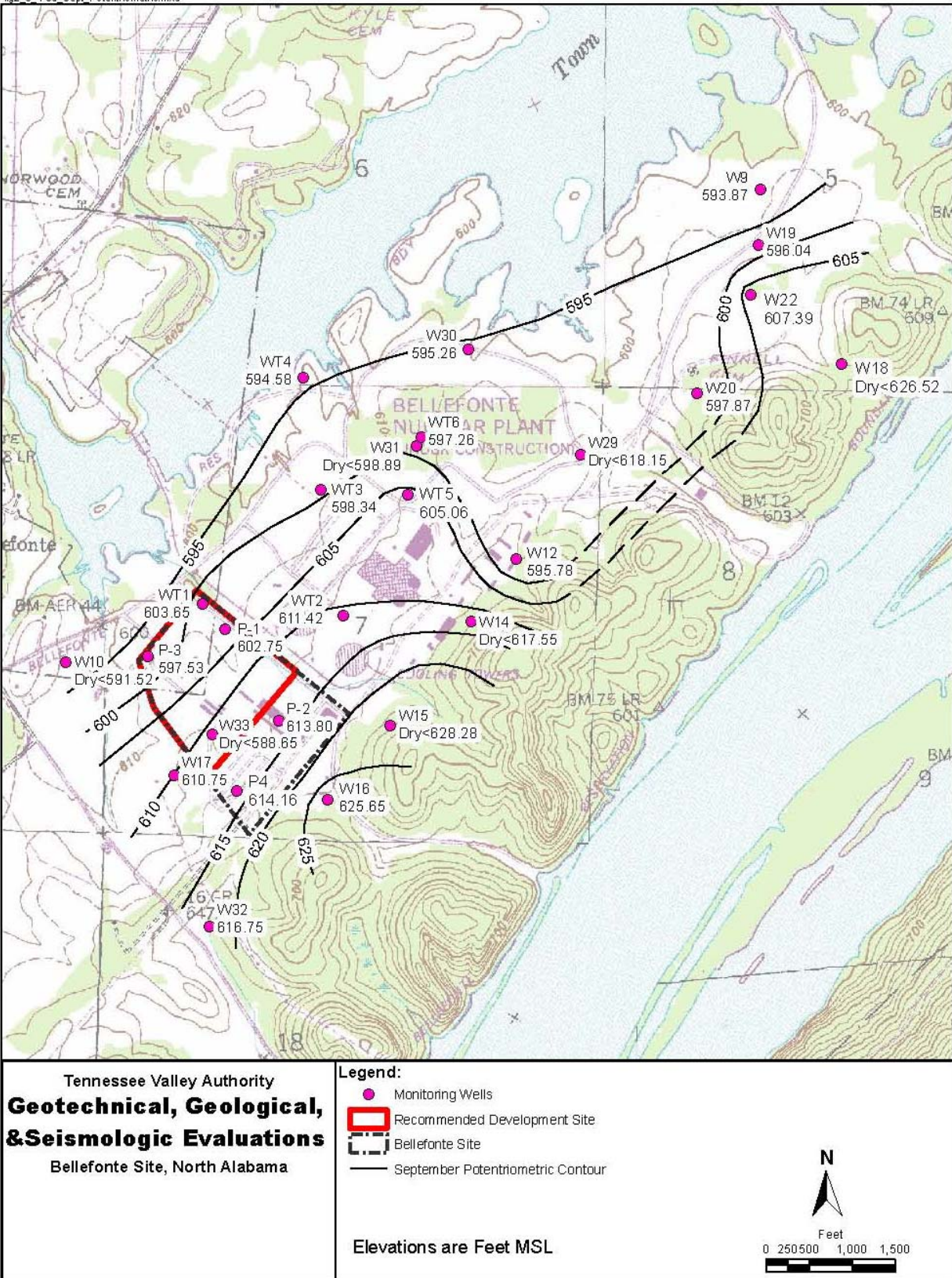


Figure 2.5.4-9(d). Potentiometric Surface Map – September 2005



fig2\_5\_4-10\_Graph of Groundwater Elevations in Vicinity of Bellefonte Study Area, 2005.mxd

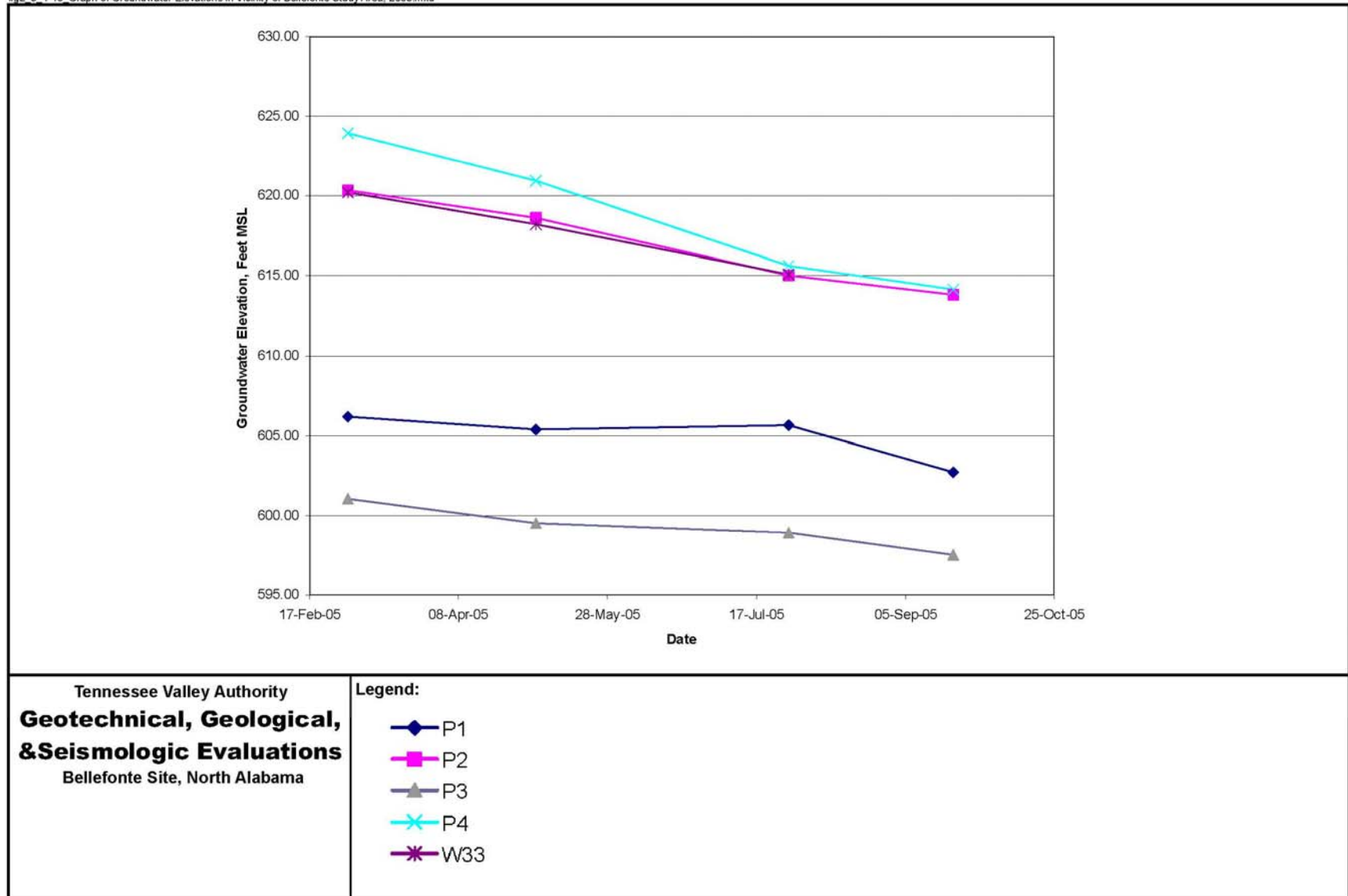


Figure 2.5.4-10. Graph of Bellefonte Site Groundwater Elevations - 2005



## 2.5.5 Stability of Slopes

No earthen slopes are present near the Bellefonte Site, and no earthen slopes would be required for operation or safe shutdown of any of the three potential facility designs. Stability of excavation sidewalls during construction will be considered during COL, but these will be backfilled prior to operation. Therefore, slope stability is not considered to affect site suitability for future development. Criteria that will be applied to slope stability during construction are discussed in Section 2.5.4.11.

### 2.5.5.1 Compaction Specifications

Compaction specifications will be developed during COL, and do not affect the suitability of the Bellefonte Site for future development.



## 2.5.6 Embankments and Dams

There are no anticipated embankments or dams at the Bellefonte Site that would be used for plant flood protection or for impounding cooling water. Therefore, neither embankments nor dams are considered to affect the suitability of the Bellefonte Site for future development. Specific consideration of the potential for upstream dams to cause an inundation of the Bellefonte Site will be considered during COL, in Section 2.4 of the SAR.



## 2.5.7 Section 2 References

10 CFR Part 100. 2002. "Reactor Site Criteria." *Code of Federal Regulations*. Office of the Federal Register. December 03, 2002.

Abbott, J., R. L. Gelinias, and D. C. Amick. 1999. "Investigation of Suspect Liquefaction Features at the Savannah River Site, South Carolina." In Hanson, K. L., K. I. Kelson, M. A. Angell, and W.R. Lettis, eds. *Techniques for Identifying Faults and Determining Their Origin*. Nuclear Regulatory Commission NUREG/CR-5503. pp. A-3 to A-26.

Amick, D., and R. Gelinias. 1991. "The Search for Evidence of Large Prehistoric Earthquakes Along the Atlantic Seaboard." *Science*. Vol. 251. pp. 655-658.

Amick, D., R. Gelinias, G. Maurath, R. Cannon, D. Moore, E. Billington, and H. Kemppinen. 1990. "Paleoliquefaction Features Along the Atlantic Seaboard." U.S. Nuclear Regulatory Commission, NUREG/CR-5613 RA. 146 pp.

Anderson, K., and J. Spotila. 2001. "The Relationship of Geologic Structure to the Giles County Seismic Zone in Southwest Virginia, Based on Fracture Mapping in Allochthonous Paleozoic Structure." *Geological Society of America Abstracts with Programs. Southeast Section Meeting* ([http://gsa.confex.com/gsa/2001SE/finalprogram/abstract\\_4795.htm](http://gsa.confex.com/gsa/2001SE/finalprogram/abstract_4795.htm)).

ASCE/SEI. 2005. "American Society of Civil Engineers, Seismic Design Criteria for Structures, Systems, and Components in Nuclear Facilities." ASCE Standard. ASCE/SEI 43-05.

Atkinson, G. M., and D. M. Boore. 1995. "Ground Motion Relations for Eastern North America." *Bulletin of the Seismological Society of America*. Vol. 85. No. 1. pp. 17-30.

Atkinson, G. M., and T. C. Hanks. 1995. "A High Frequency Magnitude Scale." *Bulletin of the Seismological Society of America*. Vol. 85. No. 3. pp. 825-833.

Bakun, W. H., A. C. Johnston, and M. G. Hopper. 2003. "Estimating Locations and Magnitudes of Earthquakes in Eastern North America from Modified Mercalli Intensities." *Bulletin of the Seismological Society of America*. Vol. 93. pp. 190-202.

Bakun, W. H., and A. McGarr. 2002. "Differences in Attenuation among the Stable Continental Regions." *Geophysical Research Letters*. Vol. 29. No. 23. 4 pp.

Bakun, W. H., and C. M. Wentworth. 1997. "Estimating Earthquake Location and Magnitude from Seismic Intensity Data." *Bulletin of the Seismological Society of America*. Vol. 87. pp. 1502-1521.

Bakun, W. H., and M. G. Hopper. 2004a. "Magnitudes and Locations of the 1811-1812 New Madrid, Missouri, and the 1886 Charleston, South Carolina, Earthquakes." *Bulletin of the Seismological Society of America*. Vol. 94. pp. 64-75.

Bakun, W. H., and M. G. Hopper. 2004b. *Catalog of Significant Historical Earthquakes in the Central United States*. U.S. Geological Survey Open-File Report 2004-1086. 142 pp.

- Baldwin, J. N., A. D. Barron, K. I. Kelson, J. B. Harris, and S. Cashman. 2002. "Preliminary Paleoseismic and Geophysical Investigation of the North Farrenburg Lineament: Primary Tectonic Deformation Associated with the New Madrid North Fault." *Seismological Research Letters*. Vol. 73. No. 3. pp. 393-413.
- Barnes, A. A. 2000. "An Interdisciplinary Study of Earthquake-Induced Liquefaction Features in the New Madrid Seismic Zone, Central United States." M.S. Thesis. Auburn University, Alabama, 266 pp.
- Bayona, G., W. A. Thomas, and R. Van der Voo. 2003. "Kinematics of Thrust Sheets Within Transverse Zones: a Structural and Paleomagnetic Investigation in the Appalachian Thrust Belt of Georgia and Alabama." *Journal of Structural Geology*. Vol. 25. pp. 1193-1212.
- Bear, G. W., J. A. Rupp, and A. J. Rudman. 1997. "Seismic Interpretation of the Deep Structure of the Wabash Valley Fault System." *Seismological Research Letters*. Vol. 68. No. 4. pp. 624-640.
- Behrendt, J. C., and A. Yuan. 1987. "The Helena Banks Strike-Slip (?) Fault Zone in the Charleston, South Carolina, Earthquake Area: Results From a Marine, High-Resolution, Multichannel, Seismic-Reflection Survey." *Geological Society of America Bulletin*. Vol. 98. No. 5. pp. 591-601.
- Behrendt, J. C., and A. Yuan. 1986. "Strike-slip on Reactivated Triassic (?) Basin Boundary Fault Zones as Sources of Earthquakes near Charleston, South Carolina." *Proceedings of the Third U.S. National Conference on Earthquake Engineering*. Vol. 1. pp. 33-54.
- Bollinger, G. A., A. C. Johnston, P. Talwani, L. T. Long, K. M. Shedlock, M. S. Sibol, and M. C. Chapman. 1991. "Seismicity of the Southeastern United States; 1698 To 1986." In Slemmons, D.B., E.R. Engdahl, M.D. Zoback, and D. Blackwell, eds. *Neotectonics of North America*. Boulder, Colorado: Geological Society of America. Decade Map. Vol. I. pp. 291-308.
- Bollinger, G. A., and M. G. Hopper. 1971. "Virginia's Two Largest Earthquakes – December 22, 1875, and May 31, 1897." *Bulletin of the Seismological Society of America*. Vol. 61. pp. 1033-1039.
- Bollinger, G. A., and R. L. Wheeler. 1988. *The Giles County, Virginia, Seismogenic Zone – Seismological Results and Geological Interpretations*. U.S. Geological Survey Professional Paper 1355. 85 pp.
- Bollinger, G. A., and R. L. Wheeler. 1983. "The Giles County Seismic Zone." *Science*. Vol. 219. pp. 1063-1065.
- Bollinger, G. A., M. C. Chapman, and M. S. Sibol. 1993. "A Comparison of Earthquake Damage Areas as a Function of Magnitude Across the United States." *Bulletin of the Seismological Society of America*. Vol. 83. pp. 1064-1080.
- Bollinger, G. A., R. D. Law, M. C. Pope, R. H. Wirgart, and R. S. Whitmarsh. 1992. "Geologically Recent Near-Surface Faulting In The Valley And Ridge Province: New Exposures of Extensional Faults In Alluvial Deposits, Giles County, SW Virginia." (Abs.) *Geological Society of America Abstracts with Programs*. Vol. 24. No. 7. p. 152.
- Boore, D. M., and G. M. Atkinson. 1987. "Stochastic Prediction of Ground Motion and Spectral Response Parameters at Hard-Rock Sites in Eastern North America." *Bulletin of the Seismological Society of America*. Vol. 77. No. 2. pp. 440-467.



- Boulanger, R. W., and I. M. Idriss. (2004). "Evaluating the Potential for Liquefaction or Cyclic Failure of Silts and Clays," Report UCD/CGM-04/01, Center for Geotechnical Modeling, University of California, Davis, CA, 130 pp.
- Braile, L. W., W. J. Hinze, and G. R. Keller. 1997. "New Madrid Seismicity, Gravity Anomalies, and Interpreted Ancient Rift Structures." *Seismological Research Letters*. Vol. 68. No. 4. pp. 599-610.
- Braile, L. W., W. J. Hinze, J. L. Sexton, G. R. Keller, and E. G. Lidiak. 1982. "The Northeastern Extension of the New Madrid Seismic Zone." In McKeown, F. A., and L. C. Pakiser, eds. *Investigations of the New Madrid, Missouri, Earthquake Region*. U.S. Geological Survey Professional Paper 1236. pp. 175-184.
- Braile, L., W. Hinze, J. Sexton, G. R. Keller, and E. Lidiak. 1984. "Tectonic Development of the New Madrid Seismic Zone." In Hays, W. W., and P. L. Gori, eds. *Proceedings of the Symposium on the New Madrid Seismic Zone*. U.S. Geological Survey Open-File Report 84-770. pp. 204-233.
- Champion, J., K. Mueller, A. Tate, and M. Guccione. 2001. "Geometry, Numerical Models, and Revised Slip Rate for the Reelfoot Fault and Trishear Fault-Propagation Fold, New Madrid Seismic Zone." *Engineering Geology*. Vol. 62. pp. 20-31.
- Chapman, J. 1977. *Archaic Period Research in the Lower Little Tennessee River Valley. Icehouse Bottom, Harrison Branch, Thirty Acre Island, Calloway Island*. Tennessee Valley Authority.
- Chapman, M. C. 1996. "Focal Mechanisms and the Geometry of Basement Faults in the Eastern Tennessee Seismic Zone." *Seismological Research Letters*. Vol. 67. No. 2. p. 35.
- Chapman, M. C., C. A. Powell, G. Vlahovic, and M. S. Sibol. 1997. "A Statistical Analysis of Earthquake Focal Mechanisms and Epicenter Locations in the Eastern Tennessee Seismic Zone." *Bulletin of the Seismological Society of America*. Vol. 87. pp. 1522-1536.
- Chapman, M. C., J. W. Munsey, C. A. Powell, S. C. Whisner, and J. Whisner. 2002. "The Eastern Tennessee Seismic Zone: Summary After 20 Years of Network Monitoring." *Seismological Research Letters*. Vol. 73. No. 2. p. 245.
- Chapman, M. C., Virginia Tech, personal communication, February 4, 2005.
- Chapman, M.C., Virginia Tech, personal communication, December 4, 2003.
- Chiu, S. C., J. M. Chiu, and A. C. Johnston. 1997. "Seismicity of the Southeastern Margin of Reelfoot Rift, Central United States." *Bulletin of the Seismological Survey*. Vol. 68. No. 5. pp. 785-796.
- Cook, F. A., D. S. Albaugh, L. D. Brown, S. Kaufman, J. E. Oliver, and R. D. Hatcher. 1979. "Thin-Skinned Tectonics in the Crystalline Southern Appalachians; COCORP Seismic-Reflection Profiling of the Blue Ridge and Piedmont." *Geology*. Vol. 7. pp. 563-567.
- Cook, F. A., L. D. Brown, S. Kaufman, and J. E. Oliver. 1983. "COCORP Seismic Reflection Traverse Across the Southern Appalachians." *AAPG Studies in Geology*. No. 14.
- Cox, R. T., R. B. Van Arsdale, and D. Larsen. 2002. *Paleoseismology of the Southeastern Margin of the Reelfoot Rift in the Vicinity of Memphis, Tennessee*. Final Technical Report submitted to the U.S. Geological Survey. NEHRP Contract Number 02HQGR0025. 15 pp.

- Cox, R. T., R. B. Van Arsdale, and J. B. Harris. 2001b. "Identification of Possible Quaternary Deformation in the Northeastern Mississippi Embayment Using Quantitative Geomorphic Analysis of Drainage-Basin Symmetry." *Geological Society of America Bulletin*. Vol. 113. pp. 615-624.
- Cox, R. T., R. B. Van Arsdale, J. B. Harris, and D. Larsen. 2001a. "Neotectonics of the Southeastern Reelfoot Rift Zone Margin, Central United States, and Implications for Regional Strain Accommodation." *Geology*. Vol. 29. No. 5. pp. 419-422.
- Cramer, C. H. 2001. "A Seismic Hazard Uncertainty Analysis for the New Madrid Seismic Zone." *Engineering Geology*. Vol. 62. pp. 251-266.
- Craven, J. A. 1995. "Paleoseismological Study in the New Madrid Seismic Zone Using Geological and Archeological Features to Constrain Ages of Liquefaction Deposits." Unpublished M. S. Thesis: University of Memphis. 51 pp.
- Crone, A. J. 1998. "Defining the Southwestern End of the BA, Northeastern Arkansas: Delimiting a Seismic Source Zone in the New Madrid Region." *Seismological Research Letters*. Vol. 69. No. 4. pp. 350-358.
- Crone, A. J. 1992. "Structural Relations and Earthquake Hazards of the Crittenden County Fault Zone, Northeastern Arkansas." *Seismological Research Letters*. Vol. 63. No. 3.
- Crone, A. J., and R. L. Wheeler. 2000. *Data for Quaternary Faults, Liquefaction Features, and Possible Tectonic Features in the Central and Eastern United States, East of the Rocky Mountain Front*. U.S. Geological Survey Open-File Report 00-0260. 342 pp.
- Crone, A. J., R. L. Baum, D. J. Lidke, D. N. D. Sather, L. A. Bradley, and A. C. Tarr. 2001. *Landslides Induced by Hurricanes Mitch in El Salvador--An Inventory and Descriptions of Selected Features*. U.S. Geological Survey Open-File Report 01-444.
- Dominion. 2003. North Anna Early Site Permit Application, Dominion Nuclear North Anna LLC, Docket No. 05200008. September 25.
- Drake, A. A., A. K. Sinha Jr., J. Laird, and R. E. Guy. 1989. "The Taconic Orogen." In Hatcher, R.D., Jr., W.A. Thomas, and G.W. Viele, eds. *The Appalachian-Ouachita Orogen in the United States. Boulder, Colorado: Geological Society of America, The Geology of North America*. Vol. F-2. pp. 101-177.
- Dutton, C. E. 1889. *The Charleston Earthquake of August 31, 1886*. U.S. Geological Survey Ninth Annual Report. 1887-88. pp. 203-528.
- Earthquake Center, Dr. Robert Herrmann, St. Louis University, St. Louis, MO. "Earthquake Summary Pages for 203, Fort Payne Earthquake Information Page." Available at: [http://www.eas.slu.edu/Earthquake\\_Center/NEW/20030429085937/index.html](http://www.eas.slu.edu/Earthquake_Center/NEW/20030429085937/index.html). Web page last modified 05/02/2003. Web page visited 11/14/2003.
- Ellsworth, W. L., M. V. Matthews, R. M. Nadeau, S. P. Nishenko, P. A. Reasenber, and R. W. Simpson. 1999. "A Physically-based Earthquake Recurrence Model for Estimation of Long-Term Earthquake Probabilities." *Proceedings of the Workshop on Earthquake Recurrence: State of the Art and Directions for the Future*. Istituto Nazionale de Geofisica. Rome, Italy. February 22-25.

- EPRI. 2004. *CEUS Ground Motion Project Final Report*. Technical Report 1009684. Electric Power Research Institute. Palo Alto, California.
- EPRI. 1993. *Guidelines for Determining Design Basis Ground Motions*. Technical Report 102293. Electric Power Research Institute. Palo Alto, California. Vol. 1.
- EPRI. 1989. *Probabilistic Seismic Hazard Evaluations at Nuclear Power Plant Sites in the Central and Eastern United States*. Technical Report NP-6395-D. Electric Power Research Institute. Palo Alto, California.
- EPRI-SOG. 1988. *Seismic Hazard Methodology for the Central and Eastern United States*. Technical Report NP-4726-A. Electric Power Research Institute. Palo Alto, California. Vols. 1-10.
- ESRI. 2004. ArcGIS 9 ESRI Data & Maps, Media Kit. Redlands, California: Environmental Systems Research Institute, Inc. 2004.
- Exelon. 2004. Response to Request for Additional Information Letter No. 7. Exelon Generation Company, LLC. ESP application for Clinton site. October 11.
- Exelon. 2003. Early Site Permit Application. Exelon Generation Company, LLC. ESP application for Clinton site. Docket No. 05200007. September 25.
- Fenneman, N. M. 1938. *Physiography of the Eastern United States*. New York: McGraw-Hill Book Co. 714 pp.
- Frankel, A. D., M. D. Petersen, C. S. Mueller, K. M. Haller, R. L. Wheeler, E. V. Leyendecker, R. L. Wesson, S. C. Harmsen, C. H. Cramer, D. M. Perkins, and K. S. Rukstales. 2002. *Documentation for the 2002 Update of the National Seismic Hazard Maps*. U.S. Geological Survey Open-File Report 02-420. 33 pp.
- Frankel, A., C. Mueller, T. Barnhard, D. Perkins, E.V. Leyendecker, N. Dickman, S. Hanson, and M. Hopper. 1996. *National Seismic-Hazard Maps; Documentation*. U.S. Geological Survey Open-File Report 96-532. 110 pp.
- Gardner, J. K., and L. Knopoff. 1974. "Is the Sequence of Earthquakes in Southern California, with Aftershocks Removed, Poissonian?" *Bulletin of the Seismological Society of America*. Vol. 64. No. 5. pp. 1363-1367.
- Geological Survey of Alabama. "Geographic Information Systems Geologic Map." Available at: <http://www.gsa.state.al.us/gsa/GIS/geologydetails.html>. Page updated March 02.
- Geological Survey of Alabama. "Geological Hazards Program, Geological Survey of Alabama Fort Payne Earthquake, April 29, 2003." Available at: <http://www.gsa.state.al.us/gsa/geologichazards/earthquakes/ftpayne.html>. Web page visited June 12, 2005.
- Geomatrix Consultants, Inc. 2004. *Dam Safety Seismic Hazard Assessment*. Report prepared for the Tennessee Valley Authority. Vols. 1 and 2. September.
- Granger, D. E., J. W. Kirchner, and R. C. Finkel. 1997. "Quaternary Dncutting Rate of the New River, Virginia, Measured from Differential Decay of Cosmogenic <sup>26</sup>Al and <sup>10</sup>Be in Cave-Deposited Alluvium." *Geology*. Vol. 25. No. 2. pp. 107-110.

- Gresko, M. J. 1985. "Analysis and Interpretation of Compressional (P Wave) and Shear (SH Wave) Reflection Seismic and Geologic Data over the Bane Dome, Giles County, Virginia." Unpublished Ph.D. thesis. Virginia Polytechnic Institute and State University. 74 pp.
- Grollmund, B., and M. D. Zoback. 2001. "Did Deglaciation Trigger Intraplate Seismicity in the New Madrid Seismic Zone?" *Geology*. Vol. 29. No. 2. pp. 175-178.
- Harris, L. D., and K. C. Bayer. 1979. "Sequential Development of the Appalachian Orogen Above a Master Decollement - A Hypothesis." *Geology*. Vol. 7. pp. 568-572.
- Harrison, R. W., and A. Schultz. 2002. "Tectonic Framework of the Southwestern Margin of the Illinois Basin and its Influence on Neotectonism and Seismicity." *Seismological Research Letters*. Vol. 73. No. 5. pp. 698-731.
- Harrison, R. W., and A. Schultz. 1994. "Strike-Slip Faulting at Thebes Gap, Missouri and Illinois, Implications for New Madrid Tectonism." *Tectonics*. Vol. 13. No. 2. pp. 246-257.
- Harrison, R. W., D. Hoffman, J. R. Palmer, J. D. Vaughn, C. L. Wiscombe, J. P. McGeekin, W. J. Stephenson, J. K. Odum, R. A. Williams, and S. L. Forman. 1999. "An Example of Neotectonism in a Continental Interior – Thebes Gap, Midcontinent, United States." *Tectonophysics*. Vol. 305. pp. 399-417.
- Hatcher, R. D., Jr., Department of Geological Sciences, University of Tennessee, personal communication, February 1, 2005.
- Hatcher, R. D., Jr., Department of Geological Sciences, University of Tennessee, personal communication, January 14, 2005.
- Hatcher, R. D., Jr. 1989a. "Appalachian Introduction." In Hatcher, R. D., Jr., W. A. Thomas, and G. W. Viele, eds. *The Appalachian-Ouachita Orogen in the United States*. Boulder, Colorado: Geological Society of America. Vol. F-2. Chapter 1. pp. 1-6.
- Hatcher, R. D., Jr. 1989b. "Tectonic Synthesis of the U.S. Appalachians." In Hatcher, R.D., Jr., W. A. Thomas, and G. W. Viele, eds. *The Appalachian-Ouachita Orogen in the United States*. Boulder, Colorado: Geological Society of America, *the Geology of North America*. Vol. F-2. Chapter 14. pp. 511-535.
- Hatcher, R. D., Jr. 1987. "Tectonics of the Southern and Central Appalachian Internides." *Annual Reviews, Earth Planet Science*. Vol. 15. pp. 337-362.
- Hatcher, R. D., Jr. 1978. "Tectonics of the Western Piedmont and Blue Ridge, Southern Appalachians: Review and Speculation." *American Journal of Science*. Vol. 278. pp. 276-304.
- Hatcher, R. D., and P. J. Lemiszki. 1998. "Contours on the Basement Surface Beneath the Valley and Ridge and Blue Ridge and Piedmont of Alabama, Georgia, Tennessee, the Carolinas, and SW Virginia." *Geologic and Tectonic Map Series*. University of Tennessee, Department of Geological Sciences, Tectonics Research. No. 2a.
- Hatcher, R. D., Jr., and I. Zietz. 1980. "Tectonic Implications of Regional Aeromagnetic and Gravity Data from the Southern Appalachians." In Wones, D. R., ed. *Proceedings, The Caledonides in the U.S.A.* IGCP Project 27. Blacksburg, Virginia Polytechnic Institute and State University Memoir 2. pp. 235-244.

Hatcher, R. D., Jr., P. J. Lemiszki, and C. Montes. 1998. "Boundary Conditions of Foreland Fold-thrust Belt Deformation from 3-D Reconstruction of a Curved Segment of the Southern Appalachian Basement Surface and Base of the Blue Ridge-Piedmont Thrust Sheet: Progress Report and Initial Results." *American Association of Petroleum Geologists Extended Abstracts*. Vol. 1. pp. A281-A284.

Hatcher, R. D., Jr., W. A. Thomas, P. A. Geiser, A. W. Snoke, S. Mosher, and D. V. Wiltschko. 1989a. "Alleghanian Orogen." In Hatcher, R. D., Jr., W. A. Thomas, and G. W. Viele, eds. *The Appalachian-Ouachita Orogen in the United States*. Geological Society of America, *The Geology of North America*. Vol. F-2.

Hatcher, R. D., Jr., W. A. Thomas, and G. W., Viele, eds. 1989b. *The Appalachian-Ouachita Orogen in the United States*. Boulder, Colorado: Geological Society of America, *The Geology of North America*. Vol. F-2.

Hatcher, R. D., Jr., W. A. Thomas, P. A. Geiser, A. W. Snoke, S. Mosher, and D. V. Wiltschko. 1989c. "Alleghanian Orogen." In Hatcher, R. D., Jr., W. A. Thomas, and G. W. Viele, eds. *The Appalachian-Ouachita Orogen in the United States*. Boulder, Colorado: Geological Society of America, *The Geology of North America*. Vol. F-2. Chapter 5. pp. 233-318.

Hatcher, R.D., Jr., P. H. Osberg, A. A. Drake, Jr., P. Robinson, and W. A. Thomas. 1989d. "Tectonic Map of the U.S. Appalachians." In Hatcher, R.D., Jr., W. A. Thomas, and G. W. Viele, eds. *The Appalachian-Ouachita Orogen in the United States*. Boulder, Colorado: Geological Society of America, *The Geology of North America*. Vol. F-2. Plate 1.

Heigold, P. C., and D. R. Kolata. 1993. "Proterozoic Crustal Boundary in the Southern Part of the Illinois Basin." *Tectonophysics*. Vol. 217. pp. 307-319.

Hermann, R. B. 1979. "Surface Wave Forcal Mechanisms for Eastern North American Earthquakes with Tectonic Implications." *Journal of Geophysical Research*. Vol. 84. pp. 3543-3552.

Hildenbrand, T. G., and D. Ravat. 1997. "Geophysical Setting of the Wabash Valley Fault System." *Seismological Research Letters*. Vol. 68. No. 4.

Hildenbrand, T. G., and J. D. Hendricks. 1995. "Geophysical Setting of the Reelfoot Rift and Relations Between Rift Structures and the New Madrid Seismic Zone." In Shedlock, K.M., and A.C. Johnston, eds. *Investigations of the New Madrid Seismic Zone*. U.S. Geological Survey Professional Paper 1538-E. pp. E1-E30.

Hildenbrand, T. G., M. F. Kane, and J. D. Hendricks. 1982. "Magnetic Basement in the Upper Mississippi Embayment Region--a Preliminary Report. In McKeown, F. A., and L. C. Pakiser, eds. *Investigations of the New Madrid, Missouri, Earthquake Region*. U.S. Geological Survey Professional Paper 1236. pp. 39-53.

Hildenbrand, T. G., W. D. Stuart, and P. Talwani. 2001. "Geologic Structures Related to New Madrid Earthquakes Near Memphis, Tennessee, Based on Gravity and Magnetic Interpretations." *Engineering Geology*. Vol. 62. pp. 105-121.

Horton, J. W., Jr., A. A. Drake, Jr., D. W. Rankin, and R. D. Dallmeyer. 1991. *Preliminary Tectonostratigraphic Terrane Map of the Central and Southern Appalachians*. U.S. Geological Survey Miscellaneous Investigation Series I-2163, scale 1:2,000,000.

- Hough, Dr. Susan. U. S. Geological Survey, personal (electronic) communication, August 23, 2004.
- Hough, S. E., R. Bilham, K. Mueller, W. Stephenson, R. Williams, and J. Odum. 2005. "Wagon Loads of Sand Blows in White County, Illinois." *Seismological Research Letters*. Vol. 76. No. 3. pp. 373-386.
- Hough, S. E., and S. Martin. 2002. "Magnitude Estimates of Two Large Aftershocks of the 16 December 1811 New Madrid Earthquake." *Bulletin of the Seismological Society of America*. Vol. 92. No. 8. pp. 3259-3268.
- Hough, S., J. G. Armbruster, L. Seeber, and J. F. Hough. 2000. "On the Modified Mercalli Intensities and Magnitudes of the 1811-1812 New Madrid, Central United States, Earthquakes." *Journal of Geophysical Research*. Vol. 105. No. B10. pp. 23,839-23,864.
- Hu, K., S. L. Gassman, and P. Talwani. 2002a. "In-situ Properties of Soils at Paleoliquefaction Sites in the South Carolina Coastal Plain." *Seismological Research Letters*. Vol. 73. No. 6. pp. 979-991.
- Hu, K., S. L. Gassman, and P. Talwani. 2002b. "Magnitudes of Prehistoric Earthquakes in the South Carolina Coastal Plain from Geotechnical Data." *Seismological Research Letters*. Vol. 73. No. 6. pp. 964-978.
- Hunt, C. B. 1967. *Physiography of the United States*. San Francisco: W. H. Freeman and Company. 480 pp.
- Hutchinson, D. R., J. A. Grow, and K. D. Klitgord. 1983. "Crustal Structure Beneath the Southern Appalachians; Nonuniqueness of Gravity Modeling." *Geology*. Vol. 11. pp. 611-615.
- Jack R. Benjamin and Associates, Inc. and RPK Structural Mechanics Consulting. 1993. "Analysis of High-Frequency Seismic Effects," Report EPRI TR-102470, prepared for EPRI, October 1993.
- Jemberie, A. L., and C. A. Langston. 2003. "Regional Wave Propagation in the Southeastern United States." (Abs.). *EOS Transactions, American Geophysical Union*. Vol. 84. No. 46. Fall Meeting Supplement.
- Johnston, A. C. 1996a. "Seismic Moment Assessment of Earthquakes in Stable Continental Regions-I. Instrumental Seismicity." *Geophysical Journal International*. Vol. 124. pp. 381-414.
- Johnston, A. C. 1996b. "Seismic Moment Assessment of Earthquakes in Stable Continental Regions-III. New Madrid 1811-1812, Charleston 1886, and Lisbon 1755." *Geophysical Journal International*. Vol. 126. No. 3. pp. 314-344.
- Johnston, A. C., and E. S. Schweig. 1996. "The Enigma of the New Madrid Earthquakes of 1811-1812." *Annual Review, Earth Planet. Science*. Vol. 24. pp. 339-384.
- Johnston, A. C., CERL, University of Memphis, personal communication, August 31, 2004.
- Johnston, A. C., D. J. Reinbold, and S. I. Brewer. 1985. "Seismotectonics of the Southern Appalachians." *Bulletin of the Seismological Society of America*. Vol. 75. pp. 291-312.

- Johnston, A. C., K. J. Coppersmith, L. R. Kanter, and C. A. Cornell. 1994. *The Earthquakes of Stable Continental Regions*. Final report submitted to Electric Power Research Institute (EPRI), TR-102261. Vol. 3.
- Julian, H. E. 1993. "Bellevue Nuclear Plant Subsurface Investigation of Diesel Fuel Release." *Tennessee Valley Authority Engineering Laboratory*. Report WR28-1-88-115. 24 pp. (plus Appendices A-H).
- Kaufmann, R. D., and L. T. Long. 1996. "Velocity Structure and Seismicity of Southeastern Tennessee." *Journal of Geophysical Research*. Vol. 101. No. B4. pp. 8531-8542.
- Kean, A. E., and L. T. Long. 1981. "A Seismic Refraction Line along the Axis of the Southern Piedmont and Crustal Thickness in the Southeastern United States." *Earthquake Notes*. Vol. 51. No. 4. pp. 3-13.
- Keller, G. R., A. E. Bland, and J. K. Greenberg. 1982. "Evidence for a Major Late Precambrian Tectonic Event (Rifting?) in the Eastern Mid-Continent Region, United States." *Tectonics*. Vol. 1. pp. 213-223.
- Kelson, K. I., G. D. Simpson, R. B. Van Arsdale, C. C. Haraden, and W. R. Lettis. 1996. "Multiple Late Holocene Earthquakes Along the Reelfoot Fault, Central New Madrid Seismic Zone." *Journal of Geophysical Research*. Vol. 101. No. B3. pp. 6151-6170.
- Kelson, K. I., R. B. Van Arsdale, G. D. Simpson, and W. R. Lettis. 1992. "Assessment of the Style and Timing of Surficial Deformation Along the Central Reelfoot Scarp, Lake County, Tennessee." *Seismological Research Letters*. Vol. 63. No. 3. pp. 349-356.
- Kenner, S., and P. Segall. 2000. "A Mechanical Model for Intraplate Earthquakes: Application to The New Madrid Seismic Zone." *Science*. Vol. 289. pp. 2329-2332.
- King, E. R., and I. Zietz. 1978. "The New York-Alabama Lineament; Geophysical Evidence for a Major Crustal Break in the Basement Beneath the Appalachian Basin." *Geology*. Vol. 6. pp. 312-318.
- Kolata, D. R., and T. G. Hildenbrand. 1997. "Structural Underpinnings and Neotectonics of the Southern Illinois Basin: An Overview." *Seismological Research Letters*. Vol. 68. No. 4. pp. 499-510.
- Kolata, D. R., and W. J. Nelson. 1991. "Tectonic History of the Illinois Basin." In Leighton, M. W., D. R. Kolata, D. F. Oltz, and J. J. Eidel, eds. *Interior Cratonic Basins*. American Association of Petroleum Geologists Memoir. Vol. 51. pp. 263-285.
- Langenheim, V. E., and T. G. Hildenbrand. 1997. "Commerce Geophysical Lineament--its Source Geometry, and Relation to the Reelfoot Rift and New Madrid Seismic Zone." *Geological Society of America Bulletin*. V. 109. No. 5. pp. 580-595.
- Law, R. D., E. S. Robinson, M. Pope, and R. T. Williams. 2000. "Folding and Faulting of Plio-Pleistocene Sediments in Giles County, SW Virginia: 1) Surface Data and Interpretation." *Geological Society of America Abstracts with Program*. Vol. 32. No. 2. p. A-57.

- Law, R. D., E. S. Robinson, J. S. Cynrak, S. Sayer, R. T. Williams, J. Callis, and M. Pope. 1997. "Geologically-Recent Faulting and Folding of Alluvial Sediments near Pearisburg, Giles County, Virginia-Tectonic Faulting or Karst Subsidence in Origin?" (Abs.) *Eos, Transactions of the American Geophysical Union*. Vol. 78. No. 17 (supplement). p. S316.
- Law, R. D., M. C. Pope, R. H. Wirgart, K. A. Eriksson, D. Carpenter, E. S. Robinson, and G. A. Bollinger. 1993. "Geologically Recent Near-Surface Folding and Faulting in the Valley and Ridge Province: New Exposures of Extensional Faults in Alluvial Sediments, Giles County, SW Virginia." (Abs.) *EOS Transactions, American Geophysical Union*. Vol. 74. No. 16. p. 282.
- Leon, E., S. L. Gassman, and P. Talwani. 2005. "Effect of Soil Aging on Assessing Magnitudes and Accelerations of Prehistoric Earthquakes." *Earthquake Spectra*. Vol. 21. No. 3. pp. 737-759. August.
- Li, Y., E. S. Schweig, M. P. Tuttle, and M. A. Ellis. 1998. "Evidence for Large Prehistoric Earthquakes in the Northern New Madrid Seismic Zone, Central United States." *Seismological Research Letters*. Vol. 69. pp. 270-276.
- Long, L. T., and R. D. Kaufmann. 1994. "The Velocity Structure and Seismotectonics of Southeastern Tennessee." *Seismological Research Letters*. Vol. 65. No. 3/4. p. 223.
- Luzietti, E. A., L. R. Kanter, E. S. Schweig, K. M. Shedlock, and R. B. Van Arsdale. 1992. "Shallow Deformation along Crittenden County Fault Zone near the Southeastern Boundary of the Reelfoot Rift, Northeast Arkansas." *Seismological Research Letters*. Vol. 63. No. 3. pp. 263-275.
- Manspeizer, W., J. DeBoer, J. K. Costain, A. J. Froelich, C. Coruh, P. E. Olsen, G. J. McHone, J. H. Puffer, and D. C. Powell. 1989. "Post-Paleozoic Activity." In Hatcher, R. D., Jr., W. A. Thomas, and G. W. Viele, eds. *The Appalachian-Ouachita Orogen in the United States*. Boulder, Colorado: Geological Society of America, *The Geology of North America*. Vol. F-2. Chapter 6. pp. 319-374.
- Marple, R. T., and P. Talwani. 2000. "Evidence for a Buried Fault System in the Coastal Plain of the Carolinas and Virginia – Implications for Neotectonics in the Southeastern United States." *Geological Society of America Bulletin*. Vol. 112. No. 2. pp. 200-220.
- Marple, R. T., and P. Talwani. 1993. "Evidence of Possible Tectonic Upwarping Along the South Carolina Coastal Plain from an Examination of River Morphology and Elevation Data." *Geology*. Vol. 21. pp. 651-654.
- Marple, R. T., and P. Talwani. 1992. "The Woodstock Lineament: A Possible Surface Expression of the Seismogenic Fault of the 1886 Charleston, South Carolina, Earthquake." *Seismological Research Letters*. Vol. 63. No. 2. pp. 153-160.
- Marple, R. T., P. Talwani, and N. K. Olson. 1994. "A Postulated North-Northeast Trending Fault System in the Coastal Plain of North and South Carolina." (Abs.) *Seismological Research Letters*. Vol. 65. No. 3/4. p. 224.
- Martin, J. R., and G. W. Clough. 1994. "Seismic Parameters from Liquefaction Evidence." *Journal of Geotechnical Engineering*. Vol. 120. No. 8. pp. 1345-1361.
- Matthews, M. V., W. L. Ellsworth, and P. A. Reasenber. 2002. "A Brownian Model for Recurrent Earthquakes." *Bulletin of the Seismological Society of America*. Vol. 92. pp. 2233-2250.



- McBride, J. H., A. M. Pugin, W. J. Nelson, T. H. Larsen, S. L. Sargent, J. A. Devera, F. B. Denny, E. W. Woolery. 2003. "Variable Post-Paleozoic Deformation Detected by Seismic Reflection Profiling Across the Northwestern "Prong" of New Madrid Seismic Zone." *Tectonophysics*. Vol. 368. pp. 171-191.
- McGuire, R. K., W. J. Silva, and C. J. Constantino. 2002. *Technical Basis for Revision of Regulatory Guidance on Design Ground Motions: Development of Hazard- and Risk-Consistent Seismic Spectra for Two Sites*. NUREG/CR-6769. U.S. Nuclear Regulatory Commission, Washington, D.C.
- McGuire, R. K., W. J. Silva, and C. J. Constantino. 2001. *Technical Basis for Revision of Regulatory Guidance on Design Ground Motions: Hazard- and Risk-Consistent Ground Motion Spectra Guidelines*. NUREG/CR-6728. U.S. Nuclear Regulatory Commission, Washington, D.C.
- McGuire, R. K., G. R. Toro, and W. J. Silva. 1988. *Engineering Model of Earthquake Ground Motion for Eastern North America*. Electric Power Research Institute Technical Report NP-6074. Electric Power Research Institute, Palo Alto, California.
- McKeown, F. A., R. M. Hamilton, S. F. Diehl, and E. E. Glick. 1990. "Diapiric Origin of the Blytheville and Pascola Arches in the Reelfoot Rift, East Central United States: Relation to the New Madrid Seismic Zone." *Geology*. Vol. 18. pp. 1158-1162.
- Metzger, A. G. 2000. *Documentation, Location and Size-Estimation of "New" Historical Earthquakes in the Central United States: Continuation*. U.S. Geological Survey Contract No. 1434-HQ-97-GR-03064. Final Technical Report. March.
- Metzger, A. G., J. G. Armbruster, and L. Seeber. 2000. *Documentation, Location and Size-Estimation of "New" Historical Earthquakes in the Central United States: Continuation*. U.S. Geological Survey Contract No. 1434-HQ-97-GR-03064. Final Technical Report. March.
- Mihills, R. K., and R. B. Van Arsdale. 1999. "Late Wisconsin to Holocene Deformation in the New Madrid Seismic Zone." *Bulletin of the Seismological Society of America*. Vol. 89. pp. 1019-1024.
- Miller, A. C., and T. R. Rice. 1983. "Discrete Approximations of Probability Distributions." *Management Science*. Vol. 29. pp. 352-362.
- Miller, R. A. 1974. "The Geologic History of Tennessee." *Tennessee Div. Geology Bull.* 74. 63 pp.
- Mills, H. H. 2005. "Relative-age Dating of Transported Regolith and Application to Study of Landform Evolution in the Appalachians." *Geomorphology*. Vol. 67. pp. 63-96.
- Mills, H. H., Tennessee Technological University, personal communication, April 29, 2005.
- Mills, H. H., and J. M. Kaye. 2001. "Drainage History of the Tennessee River: Review and New Metamorphic Quartz Locations." *Southeastern Geology*. Vol. 40. pp. 75-97.
- Mills, H. H. 1986. "Possible Differential Uplift of New River Terraces in Southwestern Virginia." *Neotectonics: An International Journal of Crustal Dynamics*. Vol. 1. pp. 75-86.
- Moran, Kent, CERL, personal (electronic) communication, January 31, 2005.
- Mueller, C., U. S. Geological Survey, personal (electronic) communication, February 18, 2003.
- Mueller, C., U. S. Geological Survey, personal (electronic) communication, October 6 and 14, 2003.

- Mueller, K., S. E. Hough, and R. Billham. 2004. "Analysing the 1811-1812 New Madrid Earthquakes with Recent Instrumentally Recorded Aftershocks." *Nature*. Vol. 429. pp. 284-288.
- Mueller, K. and J. Pujol. 2001. "Three-Dimensional Geometry of the Reelfoot Blind Thrust: Implications for Moment Release and Earthquake Magnitude in the New Madrid Seismic Zone." *Bulletin of the Seismological Society of America*. Vol. 91. pp. 1563-1573.
- Mueller, K., J. Champion, M. Guccione, and K. Kelson. 1999. "Fault Slip Rates in the Modern New Madrid Seismic Zone." *Science*. Vol. 286. pp. 1135-1138.
- Mueller, C., M. Hopper, and A. Frankel. 1997. *Preparation of Earthquake Catalogs for the National Seismic-Hazard Maps: Contiguous 48 States*. U.S. Geological Survey Open-File Report 97-464.
- Munsey, J. TVA, personal communication, January 9, 2004.
- Munsey, J. TVA, personal communication, May 25, 2004.
- Munsey, J. TVA, electronic and personal communication, September 10, 2003.
- Nava, S. J., J. W. Munsey, and A. C. Johnston. 1989. "First Fault Plane Identification in the Southern Appalachians: The  $m_{blg}$  Vonore, Tennessee, Earthquake of March 27, 1987." *Seismological Research Letters*. Vol. 60. No. 3. pp. 119-129.
- Nelson, A. E., and I. Zeitz. 1983. "The Clingman Lineament, Other Aeromagnetic Features, and Major Lithotectonic Units in Part of the Southern Appalachian Mountains." *Southeastern Geology*. Vol. 24. pp. 147-157.
- Nelson, K. D., and J. Zhang. 1991. "A COCORP Deep Reflection Profile across the Buried Reelfoot Rift, South-Central United States." *Tectonophysics*. Vol. 197. pp. 271-293.
- Newman, A. S., J. Stein, J. Weber, J. Engeln, A. Mao, and T. Dixon. 1999. "Slow Deformation and Lower Seismic Hazard at the New Madrid Seismic Zone." *Science*. Vol. 284. pp. 622.
- Newmark, N. M., and W. J. Hall. 1982. *Earthquake Spectra and Design*. Berkeley, California: Earthquake Engineering Research Institute.
- Nuttli, O. W. 1986. Letter to J. B. Savy. In Bernreuter, D., J. Savy, R. Mensing, J. Chen, and B. Davis. *Seismic Hazard Characterization of 69 Nuclear Plant Sites East of the Rocky Mountains: Questionnaires*. Prepared by Lawrence Livermore National Laboratory. NUREG/CR-5250, UCID-21517, Vol. 7.
- Nuttli, O. W. 1983. "Average Seismic Source-Parameter Relations for Mid-Plate Earthquakes." *Bulletin of the Seismological Society of America*. Vol. 73. pp. 519-535.
- Nuttli, O. W., G. A. Bollinger, and D. W. Griffiths. 1979. "On the Relations Between Modified Mercalli Intensity and Body-Wave Magnitude." *Bulletin of the Seismological Society of America*. Vol. 69. pp. 893-909.
- Obermeier, S. F. U.S. Geological Survey, Emeritus, Reston, Virginia; EqLiq Consulting, personal (electronic) communication, August 24, 2004.
- Obermeier, S. F., E. C. Pond, S. M. Olson, and R. A. Green. 2002. "Paleoliquefaction Studies in Continental Settings." In Ettensohn, F. R., N. Rast, and C. E. Brett, eds. *Ancient Seismites*. Boulder, Colorado: Geological Society of America Special Paper 359. pp. 13-27.

- Obermeier, S. F., E. C. Pond, and S. M. Olson, with contributions by R. A. Green, T. D. Stark, and J. D. Mitchell. 2001. *Paleoliquefaction Studies in Continental Settings: Geologic and Geotechnical Factors in Interpretations and Back-Analysis*. U.S. Geological Survey Open-File Report 01-29. 75 pp.
- Obermeier, S. F., R. B. Jacobson, J. P. Smoot, R. E. Weems, G. S. Gohn, J. E. Monroe, and D. S. Powars. 1990. *Earthquake-Induced Liquefaction Features in the Coastal Setting of South Carolina and in the Fluvial Setting of the New Madrid Zone*. U.S. Geological Survey Professional Paper 1504.
- Obermeier, S. F., G. S. Gohn, R. E. Weems, R. L. Gelinas, and M. Rubin. 1985. "Geologic Evidence for Recurrent Moderate to Large Earthquakes near Charleston, South Carolina." *Science*. Vol. 227. pp. 408-411.
- Odum, J. K., W. J. Stephenson, R. A. Williams, J. A. Devera, and J. R. Staub. 2002. "Near-Surface Faulting and Deformation Overlying the Commerce Geophysical Lineament in Southern Illinois." *Seismological Research Letters*. Vol. 73. No. 5. pp. 687-697.
- Odum, J. K., W. J. Stephenson, K. M. Shedlock, and T. L. Pratt. 1998. "Near-Surface Structural Model for Deformation Associated with the February 7, 1812, New Madrid, Missouri, Earthquake." *Geological Society of America Bulletin*. Vol. 110. No. 2, pp. 149-162.
- Osborne, E. Alabama Geological Survey, personal communication, February 8, 2005.
- Osborne, W. E., M. W. Szabo, T. L. Neathery, and C. W. Copeland, Jr. 1988. *Geologic Map of Alabama*. Geological Survey of Alabama Special Map 220. Scale 1:250,000 (5 sheets).
- Palmer, J. R., M. Shoemaker, D. Hoffman, N. L. Anderson, J. D. Vaughn, and R. W. Harrison. 1997. "Seismic Evidence of Quaternary Faulting in the Benton Hills Area Southeast Missouri." *Seismological Research Letters*. Vol. 68. No. 4. pp. 650-661.
- Parrish, S., and R. Van Arsdale. 2004. "Faulting along the Southeastern Margin of the Reelfoot Rift in Northwestern Tennessee Revealed in Deep Seismic-reflection Profiles." *Seismological Research Letters*. Vol. 75, No. 6, pp. 784-793.
- Physiographic Provinces of North Carolina. Available at: <http://gw.ehnr.state.nc.us/blue.htm>. Web site visited September 23, 2005.
- Potter, C. J., M. B. Goldhaber, P. C. Heigold, and J. A. Drahovzal. 1995. "Structure of the Reelfoot-Rough Creek Rift System, Fluorspar Area Fault Complex, and Hicks Dome, Southern Illinois, and Western Kentucky – New Constraints from Regional Seismic Reflection Data." In Shedlock, K. M., and A. C. Johnston, eds. *Investigations of the New Madrid Seismic Zone*. U.S. Geological Survey Professional Paper 1538Q, Q-1-Q-19. 1 folded plate.
- Powell, C. A., Center for Earthquake Research and Information, University of Memphis, personal communication, March 2, 2005.
- Powell, C. A., G. A. Bollinger, M. C. Chapman, M. S. Sobol, A. C. Johnston, and R. L. Wheeler. 1994. "A Seismotectonic Model for the 300-Kilometer-Long Eastern Tennessee Seismic Zone." *Science*. Vol. 264. pp. 686-688.
- Pratt, T. L., R. Culotta, E. C. Hauser, K. D. Nelson, L. Brown, S. Kaufman, J. Oliver, and W. Hinze. 1989. "Major Proterozoic Basement Features of the Eastern Midcontinent of North America Revealed by Recent COCORP Profiling." *Geology*. Vol. 17. pp. 505-509.

- Pujol, J., A. Johnston, J.-M. Chiu, and Y.-T. Yang. 1997. "Refinement of Thrust Faulting Models for the Central New Madrid Seismic Zone." *Engineering Geology*. Vol. 46. No. 3-4. pp. 281-298.
- Rajendran, C. P., and P. Talwani. 1993. "Paleoseismic Indicators near Bluffton, South Carolina: An Appraisal of Their Tectonic Implications." *Geology*. Vol. 21. No. 11. pp. 987-990.
- Rankin, D. W., A. A. Drake, Jr., L. Glover, III, R. Goldsmith, L. M. Hall, D. P. Murray, N. M. Ratcliffe, J. F. Read, D. T. Secor, Jr., and R. S. Stanley. 1989. "Pre-orogenic Terranes." In Hatcher, R. D., Jr., W. A. Thomas, and G. W. Viele, eds. *The Appalachian-Ouachita Orogen in the United States*. Boulder, Colorado: Geological Society of America, *The Geology of North America*. Vol. F-2. Chapter 2. pp. 7-100.
- Raymond, D. E. Alabama Geological Survey, personal communication, February 8, 2005.
- Raymond, Dorothy E., W. Osborne, W. Edward, Charles W. Copeland, and Thornton L. Neathery. 1988. *Alabama Stratigraphy*. Geological Survey of Alabama Circ. 140. 102 pp.
- Reinbold, D. J., and A. C. Johnston. 1987. *Historical Seismicity in the Southern Appalachian Seismic Zone*. U.S. Geological Survey Open-File Report 87-433. 858 pp.
- Richardson, R. M., and L. M. Reding. 1991. "North American Plate Dynamics." *Journal of Geophysical Research*. Vol. 96. pp. 12,201-12,223.
- Robinson, E. S., R. D. Law, and R. T. Williams. 2000. "Folding and Faulting of Plio-Pleistocene Sediments in Giles County, SW Virginia: 3) Seismic Refraction, Potential Fields, and Borehole Data." *Geological Society of America Abstracts with Program*. Vol. 32. No. 2. p. A-70.
- Robinson, E. S., S. Sayer, and R. D. Law. 1993. "A Seismic Refraction and Electrical Resistivity Survey of Faulted Alluvial Deposits in Giles County, VA." (Abs.) *EOS Transactions, American Geophysical Union*. Vol. 74. No. 16. p. 282.
- Russ, D. P. 1982. "Style and Significance of Surface Deformation in the Vicinity of New Madrid, Missouri." In McKeown, F. A., and L. C. Pakiser, eds. *Investigations of the New Madrid, Missouri, Earthquake Region*. U.S. Geological Survey Professional Paper 1236. pp. 95-114.
- Saikia, C. K., P. G. Somerville, H. K. Thio, N. F. Smith, A. Pitarka, and B. B. Woods. 1998. "Crustal Structure and Ground Motion Models in the Eastern and Central United States from National Seismographic Network Data." U.S. Nuclear Regulatory Commission NUREG/CR-6593. 156 pp.
- Saucier, R. T. 1991. "Geoarchaeological Evidence of Strong Prehistoric Earthquakes in the New Madrid (Missouri) Seismic Zone." *Geology*. Vol. 19. No. 4. pp. 296-298.
- Savy, J. B., W. Foxall, and N. Abrahamson. 2002. *Guidance for Performing Probabilistic Seismic Hazard Analysis for a Nuclear Plant Site: Example Application to the Southeastern United States: UCRL-ID-133494*. Prepared for the U.S. Nuclear Regulatory Commission. NUREG CR6607. 138 pp. plus Appendices A-G.
- Schruben, P. G., R. E. Arndt, and W. J. Bawiec. "Geology of the Conterminous United States at 1:2,500,000 Scale--A Digital Representation of the 1974 P. B. King and H. M. Beikman Map." USGS Digital Data Series 11, Release 2. Available at: <http://pubs.usgs.gov/dds/dds11>. Last modified: 22 August 2005. Web page visited 9/23/05.

- Schweig, E. S., and R. B. Van Arsdale. 1996. "Neotectonics of the Upper Mississippi Embayment." *Engineering Geology*. Vol. 45. No. 1-4. pp. 185-203.
- Schweig, E. S., and M. A. Ellis. 1994. "Reconciling Short Recurrence Intervals with Minor Deformation in the New Madrid Seismic Zone." *Science*. Vol. 264. pp. 1308-1311.
- Seeber, L., and J. G. Armbruster. 1991. *The NCEER-91 Earthquake Catalog: Improved Intensity-Based Magnitudes and Recurrence Relations for U.S. Earthquakes East of New Madrid*. National Center for Earthquake Engineering Research, NCEER-91-0021.
- Sexton, J. L., and P. B. Jones. 1986. "Evidence for Recurrent Faulting in the New Madrid Seismic Zone from Mini-Sosie High-Resolution Reflection Data." *Geophysics*. Vol. 51. No. 9. pp. 1760-1788.
- Sibol, M. S., G. A. Bollinger, and J. B. Birch. 1987. "Estimation of Magnitudes in Central and Eastern North America Using Intensity and Felt Area." *Bulletin of Seismological Society of America*. Vol. 77. No. 5. pp. 1635-1654.
- Smalley, R., Jr., M. A. Ellis, J. Paul, and R. B. Van Arsdale. 2005. "Space Geodetic Evidence for Rapid Strain Rates in the New Madrid Seismic Zone of Central USA." *Nature*. Vol. 435. pp. 1088-1090.
- Somerville, P., N. Collins, N. Abrahamson, R. Graves, and C. Saikia. 2001. *Ground Motion Attenuation Relations for the Central and Eastern United States*. Final Report to U.S. Geological Survey.
- Spotilla, J. Virginia Polytechnic Institute and State University, personal communication, November 21, 2003.
- SSHAC (Budnitz, R. J., G. Apostolakis, D. M. Boore, L. S. Cluff, K. J. Copersmith, C. A. Cornell, and P. A. Morris). 1997. *Recommendations for Probabilistic Seismic Hazard Analysis: Guidance on Uncertainty and Use of Experts*. Prepared for the U.S. Nuclear Regulatory Commission. NUREG/CR-6372. Washington, D.C.: U.S. Nuclear Regulatory Commission.
- Stephenson, W. J., J. K. Odum, R. A. Williams, T. L. Pratt, R. W. Harrison, and D. Hoffman. 1999. "Deformation and Quaternary Faulting in Southeast Missouri across the Commerce Geophysical Lineament." *Bulletin of the Seismological Society of America*. Vol. 89. pp. 140-155.
- Stepp, J. C. 1972. "Analysis of the Completeness of the Earthquake Hazard Sample in the Puget Sound Area and its Effect on the Statistical Estimates of Earthquake Hazard." *Proceedings of International Conference on Microzonation for Safer Construction and Research Applications*. Vol. 2. pp. 897-909.
- Stover, C. W., and J. L. Coffman. 1993. *Seismicity of the United States, 1568-1989 (Revised)*. U.S. Geological Survey Professional Paper 1527. 418 pp.
- Stover, C. W., G. Reagor, and S. T. Algermissen. 1984. *United States Earthquake Data File*. U.S. Geological Survey Open-File Report 84-225.
- Street, R. L. 1984. "Some Recent Lg Phase Displacement Spectral Densities and Their Implications with Respect to the Prediction of Ground Motions in eastern North America." *Bulletin of the Seismological Society of America*. Vol. 74. pp. 757-762.

- Street, R. L., G. A. Bollinger, and E. Woolery. 2002. "Blasting and Other Mining-related Activities in Kentucky: A Source of Earthquake Misidentification." *Seismological Research Letters*. Vol. 73. No. 5. pp. 739-750.
- Street, R. L., R. B. Hermann, and O. W. Nuttli. 1975. "Spectral Characteristics of the Lg Wave Generated by Central United States Earthquakes." *Geophysical Journal of the Royal Astronomical Society*. Vol. 41. pp. 51-63.
- Talwani, P. 2000. "Field Trip No. 1, Macroscopic Effects of the 1886 Charleston Earthquake." *Annual Meeting, Southeast Section, Geological Society of America, March 23-24, Charleston, South Carolina*.
- Talwani, P. 1999. "Fault Geometry and Earthquakes in Continental Interiors." *Tectonophysics*. Vol. 305. pp. 371-379.
- Talwani, P. 1982. "Internally Consistent Pattern of Seismicity near Charleston, South Carolina." *Geology*. Vol. 10. pp. 654-658.
- Talwani, P., and W. T. Schaeffer. 2001. "Recurrence Rates of Large Earthquakes in the South Carolina Coastal Plain Based on Paleoliquefaction Data." *Journal of Geophysical Research*. Vol. 106. No. B4, pp. 6621-6642.
- Talwani, P., D. C. Amick, and W. T. Schaeffer. 1999. *Paleoliquefaction Studies in the South Carolina Coastal Plain*. Report prepared for the Division of Engineering Technology, Office of Nuclear Regulatory Research, U.S. Nuclear Regulatory Commission, NUREG/CR-6619. 109 pp.
- Talwani, P., and J. Cox. 1985. "Paleoseismic Evidence for Recurrence of Earthquakes near Charleston, South Carolina." *Science*. Vol. 229. pp. 379-381.
- Tarr, A. C., P. Talwani, S. Rhea, D. Carver, and D. Amick. 1981. "Results of Recent South Carolina Seismological Studies." *Bulletin of the Seismological Society of America*. Vol. 71. No. 6. pp. 1883-1902.
- Taylor, K. B., R. B. Hermann, M. W. Hamburger, G. L. Pavlis, A. Johnston, C. Langer, and C. Lam. 1989. "The Southeastern Illinois Earthquake of 10 June 1987." *Seismological Research Letters*, Vol. 60. No. 3. pp. 101-110.
- Taylor, S. R. 1989. "Geophysical Framework of the Appalachians and Adjacent Greenville Province." In Pakiser, L. C., and W. D. Mooney. *Geophysical Framework of the Continental United States*. Boulder, Colorado: Geological Society of America Memoir 172. pp. 317-348.
- Thomas, W. A., University of Kentucky/Alabama Geological Survey, personal communication, February 8, 2005.
- Thomas, W. A. 2001. "Mushwad: Ductile Duplex in the Appalachian Thrust Belt in Alabama." *American Association of Petroleum Geologists Bulletin*, Vol. 85. pp. 1847-1869.
- Thomas, W. A. 1991. "The Appalachian-Ouachita Rifted Margin of Southeastern North America." *Geological Society of America Bulletin*. Vol. 103. pp. 215-431.

- Thomas, W. A. 1989a. "The Appalachian-Ouachita Orogen Beneath the Gulf Coastal Plain Between the Outcrops in the Appalachian and Ouachita Mountains." In Hatcher, R. D., Jr., W. A. Thomas, and G. W. Viele, eds. *The Appalachian-Ouachita Orogen in the United States*. Boulder, Colorado: Geological Society of America, *The Geology of North America*. Vol. F-2. Chapter 15. pp. 537-553.
- Thomas, W. A. (compiler). 1989b. "Tectonic Map of the Ouachita Orogen, and Cross Sections of the Appalachian-Ouachita Orogen Beneath the Gulf Coastal Plain." In Hatcher, R. D., Jr., W. A. Thomas, and G. W. Viele, eds. *The Appalachian-Ouachita Orogen in the United States*. Boulder, Colorado: Geological Society of America, *The Geology of North America*. Vol. F-2. Plate 9.
- Thomas, W. A. 1986. "Sequatchie Anticline, the Northwesternmost Structure of the Appalachian Fold-thrust Belt in Alabama." *Geological Society of America Centennial Field Guide – Southeastern Section*. pp. 177-80.
- Thomas, W. A. 1982. "Stratigraphy and Structure of the Appalachian Fold and Thrust Belt in Alabama." in W. A. Thomas and T. L. Neathery eds. "Appalachian Thrust Belt in Alabama: Tectonics and Sedimentation." *GSA Guidebook for Field Trip No. 13*. Vol. 24. pp. 55-66.
- Thomas, W. A., and G. Bayona. 2002. "Palinspastic Restoration of the Anniston Transverse Zone in the Appalachian Thrust Belt, Alabama." *Journal of Structural Geology*. Vol. 24. pp. 797-826.
- Thomas, W. A., T. M. Chowns, D. L. Daniels, T. L. Neathery, L. Glover, III, and R. J. Gleason. 1989. "The Subsurface Appalachians beneath the Atlantic and Gulf Coastal Plains." In Hatcher, R. D., Jr., W. A. Thomas, and G. W. Viele, eds. *The Appalachian-Ouachita Orogen in the United States*. Boulder, Colorado: Geological Society of America, *The Geology of North America*. Vol. F-2. Chapter 10. pp. 445-458.
- Thomas, W. A., and D. N. Bearce. 1969. "Sequatchie Anticline in North-Central Alabama." In Hooks, W. G., ed. *Seventh Annual Field Trip of the Alabama Geological Society, December 5-6, 1969*. Alabama Geological Survey. pp. 26-43.
- Thornbury, W. D. 1965. *Regional Geomorphology of the United States*. New York: John Wiley & Sons. 609 pp.
- Toro, G. R., and W. J. Silva. 2001. *Scenario Earthquakes for Saint Louis, MO, and Memphis, TN, and Seismic Hazard Maps for the Central United States Region Including the Effect of Site Conditions*. Final Technical Report prepared by Risk Engineering, Inc., Boulder, Colorado, under U.S. Geological Survey External Grant No. 1434-HQ-97-02981. January 10.
- Tuttle, M. 1993. *Implications for Tectonics, Paleoseismicity, and Ground Failure from Soft-Sediment Deformation in the Marked Tree Area of the New Madrid Seismic Zone*. Annual Report submitted to the U.S. Geological Survey under USGS External Project No. 14080001-G62001. 25 pp.
- Tuttle, M. P., M. Tuttle & Associates, personal communication, August 24, 2004.
- Tuttle, M. P., M. Tuttle & Associates, personal (electronic) communication. February 27, 2003.
- Tuttle, M. P. 2001a. "The Use of Liquefaction Features in Paleoseismology: Lessons Learned in the New Madrid Seismic Zone, Central United States." *Journal of Seismology*. Vol. 5. pp. 361-380.

- Tuttle, M. P. 2001b. "Towards a Paleoearthquake Chronology for the New Madrid Seismic Zone. Annual Report to the U.S. Geological Survey, USGS External Project No. 1434-99HZGR0022. 18 pp.
- Tuttle, M. P. 1999. *Late Holocene Earthquakes and their Implications for Earthquake Potential of the New Madrid Seismic Zone, Central United States*. Ph.D. Dissertation: University of Maryland. 250 pp.
- Tuttle, M. P., and E. S. Schweig. 2000. "The Earthquake Potential of the New Madrid Seismic Zone." *American Geophysical Union, EOS Transactions*. Vol. 81. No. 19. p. S308.
- Tuttle, M. P., and E. S. Schweig. 1996. "Recognizing and Dating Prehistoric Liquefaction Features: Lessons Learned in the New Madrid Seismic Zone, Central United States." *Journal of Geophysical Research*. Vol. 101. No. B3. pp. 6171-6178.
- Tuttle, M. P., E. S. Schweig III, J. Campbell, P. M. Thomas, J. D. Sims, and R. H. Lafferty III. 2005. "Evidence for New Madrid Earthquakes in AD 300 and 2350 B.C." *Seismological Research Letters*. Vol. 76. pp. 489-501.
- Tuttle, M. P., E. S. Schweig, J. D. Sims, R. H. Lafferty, L. W. Wolf, and M. C. Haynes. 2002. "The Earthquake Potential of the New Madrid Seismic Zone." *Bulletin of the Seismological Society of America*. Vol. 92. No. 6. pp. 2080-2089.
- Tuttle, M. P., E. S. Schweig, J. D. Sims, and R. H. Lafferty. 2001. "Recurrence of Clustered Major Earthquakes in the New Madrid Seismic Zone." *Seismological Research Letters*. Vol. 72. No. 2. pp. 265.
- Tuttle, M. P., and L. W. Wolf. 2003. *Towards a Paleoearthquake Chronology for the New Madrid Seismic Zone*. Progress Report submitted to the U.S. Geological Survey NEHRP. USGS External Project No. 1434-01HQGR0164. 36 pp.
- Tuttle, M. P., J. D. Sims, K. Dyer-Williams, R. H. Lafferty III, and E. S. Schweig III. 2000. *Dating of Liquefaction Features in the New Madrid Seismic Zone*. U.S. Nuclear Regulatory Commission Report NUREG/GR-0018. 42 pp. (plus appendices).
- Tuttle, M. P., J. Chester, R. Lafferty, K. Dyer-Williams, and R. Cande. 1999a. Paleoseismology Study Northwest of the New Madrid Seismic Zone. U. S. Nuclear Regulatory Commission Report NUREG/CR-5730, 96 pp. 1999a.
- Tuttle, M. P., J. Collier, L. W. Wolf, and R. H. Lafferty. 1999b. "New Evidence for a Large Earthquake in the New Madrid Seismic Zone between AD 1400 and 1670." *Geology*. Vol. 27. No. 9. pp. 771-774.
- Tuttle, M. P., R. H. Lafferty III, and E. S. Schweig III. 1998. *Dating of Liquefaction Features in the New Madrid Seismic Zone and Implications for Earthquake Hazard*. U. S. Nuclear Regulatory Commission Report NUREG/GR-0017. 77 pp. (plus appendices).
- U.S. Geological Survey. Water Resources NSDI Node, Physiographic divisions of the conterminous U.S. Available at: <http://water.usgs.gov/GIS/dsdl/physio.e00.gz>, <http://water.usgs.gov/GIS/metadata/usgswrd/XML/physio.xml>. Web site visited June 16, 2005.



- U.S. Geological Survey. "Community Internet Intensity Maps." Available at: [http://pasadena.wr.usgs.gov/shake/cus/STORE/Xteak/ciim\\_display.html](http://pasadena.wr.usgs.gov/shake/cus/STORE/Xteak/ciim_display.html). Last modified 8.17.2005. Web page visited June 12, 2005. U.S. Geological Survey. "Community Internet Intensity Maps." Available at: [Community http://pasadena.wr.usgs.gov/shake/cus/STORE/Xqnax\\_04/ciim\\_display.html](http://pasadena.wr.usgs.gov/shake/cus/STORE/Xqnax_04/ciim_display.html). Last modified 9.1.2005. Web site visited June 16, 2005.
- U.S.D.A., SCS. 1954. *Soil Survey: Jackson County, Alabama*. United States Department of Agriculture, Series 1941. No. 8.
- USNRC. 2005. "Safety Evaluation of Early Site Permit Application in the Matter of Dominion Nuclear North Anna, LLC, for the North Anna Early Site Permit Site." U.S. Nuclear Regulatory Commission, Washington, DC, June 16, 2005.
- USNRC. 2003a. *Regulatory Guide 1.132. Site Investigations for Foundations of Nuclear Power Plants. Revision 2*. October 2003.
- USNRC. 2003b. *Regulatory Guide 1.138. Laboratory Investigations of Soils and Rocks for Engineering Analysis and Design of Nuclear Power Plants. Revision 2*. December 2003.
- USNRC. 2003c. *Regulatory Guide 1.198. Procedures and Criteria for Assessing Seismic Soil Liquefaction at Nuclear Power Plant Sites*. November 2003.
- USNRC. 2002. "Update of the Risk-Informed Regulation Implementation Plan." SECY-02-0131. U.S. Nuclear Regulatory Commission, Washington, DC.
- USNRC. 2001. "Modified Reactor Safety Goal Policy Statement." SECY-01-0009. U.S. Nuclear Regulatory Commission, Washington, DC.
- USNRC. 1999. "White Paper on Risk-Informed, Performance-Based Regulation." SECY-98-144. U.S. Nuclear Regulatory Commission, Washington, DC.
- USNRC. 1998. "An Approach for Using Probabilistic Risk Assessment in Risk-Informed Decisions on Plant-Specific Changes to the Licensing Basis." Regulatory Guide 1.174. U.S. Nuclear Regulatory Commission, Washington, DC.
- USNRC. 1997. *Identification and Characterization of Seismic Sources and Determination of Safe Shutdown Earthquake Ground Motion*. Regulatory Guide 1.165, U.S. Nuclear Regulatory Commission, Washington, DC.
- USNRC. 1987. "Standard Review Plans and Associated Review Standards." *Standard Review Plan*. NUREG-0800. Office of Nuclear Reactor Regulation.
- USNRC. 1986. Safety Goals for the Operation of Nuclear Power Plants: Policy Statement. *Federal Register*. 10 CFR Part 50. Vol. 51. No. 149.
- USNRC. 1978. *Regulatory Guide 1.70. Standard Format and Content of Safety Analysis Reports for Nuclear Power Plants. Revision 3*. November 1978.
- Van Arsdale, R. B. 2000. "Displacement History and Slip Rate on the Reelfoot Fault of the New Madrid Seismic Zone." *Engineering Geology*. Vol. 55. pp. 219-226.

Van Arsdale, R. B., R. Cox, and J. Harris. 2002. *Investigation of Faulting Beneath the City of Memphis and Shelby County, Tennessee*. NEHRP Final report submitted to the U.S. Geological Survey. External Grant Number 02GQGR0053. 33 pp.

Van Arsdale, R. B., and A. Johnston. 1999. "Geological and Seismological Setting of the New Madrid Seismic Zone and the Wabash Valley Seismic Zone." Appendix A of Risk Engineering, Inc. 1999. *Updated Probabilistic Seismic Hazard Analysis for the Paducah Gaseous Diffusion Plant, Paducah, Kentucky*. Report prepared for Lockheed Martin Utility Systems, Inc., U.S. Nuclear Regulatory Commission Docket 07007001. April 26.

Van Arsdale, R. B., R. T. Cox, A. C. Johnston, W. J. Stephenson, and J. K. Odum. 1999. "Southeastern Extension of the Reelfoot Fault." *Seismological Research Letters*. Vol. 70. No. 3. pp. 348-359.

Van Schmus, W. R., M. E. Bickford, and A. Turek. 1996. "Proterozoic Geology of the East-Central Midcontinent Basement." In Van der Pluijm, B.A., and P.A. Catacosinos, eds. *Basement and Basins of Eastern North America*. Boulder, Colorado: Geological Society of America Special Paper 308. pp. 7-32.

Veneziano, D., and J. Van Dyck. 1985. *Analysis of Earthquake Catalogs for Incompleteness and Recurrence Rates: Seismic Hazard Methodology for Nuclear Facilities in the Eastern United States*. EPRI Research Project N. P101-29. EPRI/SOG Draft 85-1. Vol. 2, Appendix A. April 30.

Vlahovic, G., C. Powell, M. Chapman, and M. Sibol. 1998. "Joint Velocity Hypocenter-Velocity Inversion for the Eastern Tennessee Seismic Zone." *Journal of Geophysical Research*. Vol. 103. pp. 4879-4896.

Vlahovic, G., C. A. Powell, M. C. Chapman, and M. S. Sibol. 1996. "P and S Wave Velocity Structure and Hypocenter Locations on the Eastern Tennessee Seismic Zone." *Seismological Research Letters*. Vol. 67. No. 2. pp. 59.

Weems, R. E., and W. C. Lewis. 2002. "Structural and Tectonic Setting of the Charleston, South Carolina, Region—Evidence from the Tertiary Stratigraphic Record." *Geological Society of America Bulletin*. Vol. 114. No. 1. pp. 24-42.

Wells, D. L., and K. J. Coppersmith. 1994. "New Empirical Relationships Among Magnitude, Rupture Length, Rupture Width, Rupture Area, and Surface Displacement." *Bulletin of the Seismological Society of America*. Vol. 84. pp. 974-1002.

Wheeler, R. L. 1997. "Boundary Separating the Seismically Active Reelfoot Rift from the Sparsely Seismic Rough Creek Graben, Kentucky, and Illinois." *Seismological Research Letters*. Vol. 68. pp. 586-598.

Wheeler, R. L. 1996. "Earthquakes and the Southeastern Boundary of the Intact Iapetan Margin in Eastern North America." *Seismological Research Letters*. Vol. 67. No. 5. pp. 77-83.

Wheeler, R. L. 1995. "Earthquakes and the Cratonward Limit of Iapetan Faulting in Eastern North America." *Geology*. Vol. 23. No. 2. pp. 105-108.

Wheeler, R. L. 1994. "Northeast Boundary of Seismogenic Iapetan Faults Under the Appalachians." (Abs.) *Seismological Research Letters*. Vol. 65. No. 3/4. p. 231.

- Wheeler, R. L., S. Rhea, S. F. Diehl, J. A. Drahovzal, G. W. Bear, and M. L. Sargent. 1997. *Seismotectonic Map Showing Faults, Igneous Rocks, and Geophysical and Neotectonic Features in the Vicinity of the Lower Wabash Valley, Illinois, Indiana, and Kentucky*. U.S. Geological Survey Geologic Investigations Series I-2583-D.
- Wheeler, R. L., and G. A. Bollinger. 1984. "Seismicity and Suspect Terranes in the Southeastern United States." *Geology*. Vol. 12. pp. 323-326.
- Whisner, S. C., R. D. Hatcher, Jr., and J. W. Munsey. 2003. "Disturbed Sediments in the East Tennessee Seismic Zone: Evidence of Large Prehistoric Earthquakes in East Tennessee?" *Southeastern Geology*. Vol. 42. No. 2. pp. 1-16.
- Williams, H., and R. D. Hatcher, Jr. 1983. "Appalachian Suspect Terranes." In Hatcher, R.D., Jr., H. Williams, and I. Zietz, eds. *The Tectonics and Geophysics of Mountain Chains*. Geological Society of America Memoir 158. pp. 33-53.
- Williams, H., and R. D. Hatcher, Jr. 1982. "Suspect Terranes and Accretionary History of the Appalachian Orogen." *Geology*, Vol. 10. pp. 530-536.
- Williams, R. A., E. A. Luzietti, and D. L. Carver. 1995. "High-Resolution Seismic Imaging of Quaternary Faulting on the Crittenden County Fault Zone, New Madrid Seismic Zone, Northeastern Arkansas." *Seismological Research Letters*. Vol. 66. No. 3. pp. 42-57.
- Williams, R. T., E. S. Robinson, and R. D. Law. 2000. "Folding and Faulting of Plio-Pleistocene Sediments in Giles County, SW Virginia: 2) Ground-Penetrating Radar and Seismic Reflection Data." *Geological Society of America Abstracts with Program*. Vol. 32. No. 2. p. A-83.
- Wilson, C. W., Jr., and R. G. Stearns. 1958. "Structure of the Cumberland Plateau, Tennessee." *Geological Society of America Bulletin*. Vol. 69. pp. 1283-1296.
- Woods, B. B. 2003. *Revising U.S. Moment Catalog to Lower Magnitudes*. U.S. Geological Survey External Research Program Final Technical Report Award #01-HQ-GR-0158. 43 pp. July 11.
- Woolery, E. W., and R. Street. 2002. "Quaternary Fault Reactivation in the Fluorspar Area Fault Complex of Western Kentucky: Evidence from Shallow SH-Wave Reflection Profiles." *Seismological Research Letters*. Vol. 73. No. 5. pp. 628-639.
- Working Group on California Earthquake Probabilities. 2003. *Earthquake Probabilities in the San Francisco Bay Region: 2002-2031*. U.S. Geological Survey Open-File Report 03-214.
- Working Group on California Earthquake Probabilities. 1999. *Earthquake Probabilities in the San Francisco Bay Region: 2000 to 2030 - A Summary of Findings*. U.S. Geological Survey, Open File Report 99-517.
- Youd, T. L. et al. "Liquefaction Resistance of Soils: Summary Report from the 1996 NCEER and 1998 NCEER/NSF Workshops on Evaluation of Liquefaction Resistance of Soils." *Journal of Geotechnical and Geoenvironmental Engineering*. American Society of Civil Engineers. Vol. 127, No. 10. pp. 817-833. 2001.
- Youngs, R. R., F. H. Swan, and M. S. Power. 1988. "Use of Detailed Geologic Data in Regional PSHA: an Example from the Wasatch Front, Utah." In J.L. Von Thun, ed. *Earthquake Engineering and Soil Dynamics II – Recent Advances in Ground Motion Evaluation*. pp. 156-172.

Youngs, R. R., and K. J. Coppersmith. 1985. "Implications of Fault Slip Rates and Earthquake Recurrence Models to Probabilistic Hazard Estimates." *Bulletin of the Seismological Society of America*. Vol. 75. pp. 939-964.

Yule, D. E., and T. H. Grau. 2003. *Earthquake Event Report for the North Alabama 29 April 2003 MW - 4.6 Earthquake*. U.S. Army Engineer Research and Development Center, Geotechnical and Structures Laboratory, Vicksburg, Mississippi.

Zoback, M. L. 1992. "Stress Field Constraints on Intraplate Seismicity in Eastern North America." *Journal of Geophysical Research*. Vol. 97. No. B8. pp. 11,761-11,782.

Zoback, M. D., and M. L. Zoback. 1991. "Tectonic Stress Field of North America and Relative Plate Motions." In Slemmons, D. B., E. R. Engdahl, M. D. Zoback, and D. D. Blackwell, eds. *Neotectonics of North America: Geological Society of America, Decade Map*, Vol. 1. Chapter 19. pp. 339-366.

Zoback, M. L., and M. D. Zoback. 1989. "Tectonic Stress Field of the Continental United States." In Pakiser, L. C., and W. D. Mooney, eds. *Geophysical Framework of the Continental United States: Boulder, Colorado. Geological Society of America Memoir 172*. pp. 523-541.

Zoback, M. L., and M. D. Zoback. 1980. "State of Stress in the Continental United States." *Journal of Geophysical Research*. Vol. 85. pp. 6113-6156

**Appendix A. Borehole and Rock Core Logs,  
Piezometer Construction Logs, Photographs, Water Level Data**

**Appendix B. CPT Report**

**Appendix C. Technos Report**  
C1. March 18, 2005  
C2. August 19, 2005

## Appendix D. GeoVision Report



## Appendix E. Surveying Report

## Appendix F. Laboratory Data Report

## Appendix G. Photographs

## Appendix H. Slug Testing Memorandum

## Appendix I: Catalog Listing